RETROFIT OF REINFORCED CONCRETE MEMBERS USING ADVANCED COMPOSITE MATERIALS

A thesis
submitted in partial fulfilment
of the requirements for the Degree
of
Doctor of Philosophy in Civil Engineering
at the
University of Canterbury

by

Yung Chih Wang

University of Canterbury
Christchurch
New Zealand

February 2000

CONTENTS

ABSTRACT

Practical applications for the use of composite materials for retrofitting of reinforced concrete structural members of buildings and bridges were investigated in this research project. Carbon and glass advanced composite materials (CACM and GACM) saturated in an epoxy resin matrix were used to enhance their structural performance.

The following experimental work, supported by analytical work, was carried out in the investigation:

1. Use of Advanced Composite Materials (ACM) in bridge girders to increase the service load capacity. Eleven T-shape simply supported beams, representing half scale bridge girders, were tested under repeated cyclic and monotonic load conditions. CACM laminates bonded to the soffit of the beams were used to increase the service live load carrying capacity. In some test units the laminates were cut-off whereas in others the laminates were bonded to the whole span of the beam, except at the supports. Additional GACM U-strips were applied to the sides of some beams to improve the bond performance of the longitudinal laminate and to provide additional shear stiffness and strength. The side U-strips were anchored to the beam with glass fibre filaments. One beam was subjected to one million cycles in the service load range to study the fatigue behaviour of the retrofit scheme. The fatigue test showed the excellent behaviour that can be expected from well-detailed retrofit schemes incorporating carbon and glass fibre laminates. Design recommendations are proposed based on the results obtained from the tests and from analytical work.

2. Experimental work was conducted to investigate the seismic response of ACM-strengthened/retrofitted beams that present shear and bar curtailment deficiencies. Two full-scale T-section cantilever beams were built and tested under reversed cyclic loading. One unit was tested in its "as-built" condition until a flexure-shear failure developed at the curtailment point of the negative longitudinal reinforcement. The test unit was then repaired by applying GACM laminates across the top of the slab and to the sides of the beam in the damage

region. It was again re-tested under reversed cyclic loading. The other unit was retrofitted before testing in the same manner as the previous damaged unit and then subjected to reverse cyclic loading. A seismic assessment on the prototype unit was proposed to provide a simple evaluation on the beam with deficiencies in flexural design of T-beam, shear, and longitudinal bar curtailment. The tests show that the presence of a GACM laminate can successfully correct the deficiency by relocating the negative plastic hinges to occur in the beam at the column face. To ensure the adequate seismic performance of the retrofit scheme, shear deformations in the beams must be kept to a minimum to reduce the kinking effect and potential debonding of the ACM laminate.

3. The analytical and experimental study proposed a method for evaluating the short-term axial load strength of rectangular and square reinforced compression members confined with an ACM jacket and steel hoops. The results of this study can also be applied to the use of ACMs for column seismic retrofitting. Three 300 mm square and three 300 mm by 450 mm short reinforced columns were concentrically loaded first in tension, then in compression to failure. Either two or six layers of GACM jackets were applied to four of these columns. Two control units were tested in order to evaluate the enhancement of the axial load carrying capacity and to observe whether the ACM jackets were able to preclude premature buckling of the longitudinal reinforcement in the wrapped columns. The results clearly showed the efficiency of the jackets in enhancing the ultimate strain and strength of the columns. The jackets were also very effective in preventing longitudinal bar buckling from occurring. Designed equations in closed form were derived based on the calibration of the analytical model to provide a design of ACM-wrapped reinforced concrete column subjected to the concentric axial load.

ACKNOWLEDGEMENTS

I would like to express my profound gratitude to Dr. J.I. Restrepo and Professor R. Park, supervisors of this project, for their advice as well as encouragement. Appreciation is specially given to Dr. Restrepo for his never ending patience, invaluable instruction and his sincere friendship.

The financial supports provided by Contech Group Ltd. in New Zealand and partially by Composite Retrofit International in Canada are gratefully acknowledged. The helpful advice for English grammar correction received from Mr. R.W. Irwin, Managing Director of Contech Group Ltd., is very much appreciated.

Sincere thank is given to Professor M.P. Collins, at University of Toronto, for his advice on my experimental work and his support of the analytical programme, RESPONSE 2000.

The excellent assistance of the technical staff of the Department of Civil Engineering under the management of Messrs. G. Clarke, now retired, and D. MacPherson is acknowledged. Messrs. G.E. Hill, R. Allen, N. Dixon, N. Hickey, R. McConchie, J. Maley, P. Murphy, R. Newton and S. Toase are deeply appreciated for their technical assistance during testing.

Warm gratitude is given to Messrs. C.M. Lin and R. Presland, and Dr. F.J. Crisafulli who assisted in my experimental work. Other fellow post-graduate students who gave me many constructive discussions are also thanked.

I am particularly indebted to my wife for her taking care of our children and me without any complaint. Her prayers, love, encouragement and support always accompanied me to face the hardness and difficulty.

Finally, this undertaking could never have been achieved without the spiritual support from my Lord – Jesus Christ.

NOTATION

A = transformed section area.

A_c = area of concrete section measured to the centre line of the perimeter hoop.

A_{cc} = core concrete area, excluding area of the longitudinal steel.

$A_{cc,j}$ = core area of concrete confined by the ACM jacket.

A_{cj} = effective area of concrete confined by the ACM jacket.

A_{cjs} = effective area of concrete confined by both the ACM jacket and the steel hoop.

A_{cu} = unconfined concrete area.

A_e = area of effectively confined core concrete.

$A_{e,j}$ = the area of concrete effectively confined by the ACM jacket.

$A_{e,s}$ = the area of concrete effectively confined by the steel hoop.

A_p = cross section area of the ACM laminate.

$A_{p,cut}$ = cross section area of the ACM laminate being cut-off.

A_s = cross section area of the longitudinal steel reinforcement.

A_{sb} = cross section area of the steel reinforcement in the slab.

$A_{t,x}$ and $A_{t,y}$ = area of transverse steel reinforcement parallel to the x and y axis, respectively.

A_{vp} = area of external ACM strip bonded to the beam web.

$A_{vp,min}$ = minimum area of external ACM strip bonded to the beam web.

A_{vs} = area of transverse steel reinforcement in the beam.

A_{bx} = total area of the longitudinal steel reinforcement in the beam.

a = maximum aggregate size.

a_{nj} = length of the n-th side of the quadrilateral at the j-th measurement.

b = width of the beam.

b and h = sectional dimensions of the rectangular column.

b_p = width of the composite laminate bonded to the soffit of the beam.

b_f = width of the flange in the beam.

b_w = width of the web in the beam.

C = sectional compressive force due to bending moment reaction.

C' = sectional total compressive force due to bending moment and shear force reaction.

C_c = resultant concrete compressive force.

c = the depth measured from the sectional extreme compression fibre to the neutral axis.

c_v = maximum distance for the clear cover in transverse direction of the beam.

c_x = maximum distance for the clear cover in longitudinal direction of the beam.

D = overall column diameter.

D_c and D_c' = concrete diagonal compression force.

D_T and D_T' = concrete diagonal tension force.

d = effective depth of the section.

d_b = diameter of the longitudinal steel bar.

d_{bx} = diameter of the longitudinal steel bar in the beam.

d_i = a distance measured from the top concrete fibre to the centroid of steel bar in a layer i.

d_p = a distance measured from the top concrete fibre to the centroid of ACM laminate bonded to the soffit of the beam.

d_x and d_y = dimensions of the concrete core confined by perimeter steel hoops.

d_s = diameter of the steel hoop.

E_c = initial tangent modulus of concrete.

E_p = elastic modulus of ACM laminate.

E_{vp} = elastic modulus of the transverse ACM laminate.

E_s = elastic modulus of reinforcing steel.

E_{sec} = f'_{cc}/ε_{cc} in Popovics's equation.

e_v = tension shift caused by the diagonal tension cracking.

F = the measured load during testing.

F_l = the greater of the effective lateral confining pressures.

F_y = measured load at the onset of yielding of the beam.

F_u = the ultimate load at the failure of test beam.

f_c = concrete compressive stress.

f_{c0} = unconfined concrete compressive stress.

$f_{cc,j}$ = confined compressive stress of concrete confined by the ACM jacket.

$f_{cc,js}$ = confined compressive stress of concrete confined by both the ACM jacket and the steel hoop.

f_{cl} = the concrete tensile stress field.

f'_c = compressive strength of cylinder concrete.

f'_{c0} = unconfined concrete strength.

f'_{cc} = compressive strength of confined concrete.

$f'_{cc,j}$ = compressive strength of concrete confined by the ACM jacket.

$f'_{cc,js}$ = compressive strength of concrete confined by both the ACM jacket and the steel hoop.

f_{cr} = flexural tensile cracking strength of concrete.

f_j = stress in the ACM jacket.

f_l = lateral confining pressure onto the concrete.

f_l = the smaller of the effective lateral confining pressures.

f'_l = lateral confining strength onto the concrete.

$f_{l,jx}$ and $f_{l,jy}$ = lateral confining stress due to the confinement of ACM jacket in the x and y direction, respectively.

$f_{l,sx}$ and $f_{l,sy}$ = lateral confining stress due to the confinement of steel hoop in the x and y direction, respectively.

f_p = tensile stress in the ACM laminate.

f_{pu} = ultimate tensile stress of ACM laminate.

f_r = modulus of rupture of concrete.

f_s = stress in the steel reinforcement.

f_{sh} = stress in the steel hoop.

f_{sy} = yield strength of the longitudinal steel reinforcement.

f_{su} = ultimate strength of the longitudinal steel reinforcement.

f'_t = split tensile strength of the cylinder concrete.

f_{vp} = transverse stress of the external ACM stirrup bonded to the beam web.

f_{vpe} = effective transverse stress of the external ACM stirrup bonded to the beam web.

f_{vs} = transverse stress of internal steel stirrup in the beam.

f_{vsy} = yield strength of the internal steel stirrup.

f_{yh} = yield strength of the transverse steel reinforcement.

f_1 = principal concrete tensile stress field.

f_2 = principal concrete compressive stress field.

f_{2max} = maximum principal concrete compressive stress field.

h = overall depth of the beam section.

h_f = thickness of flange in the beam section.

h_{vp} = effective height of the external ACM stirrup bonded to the beam web.

I = moment of inertia.

I_e = effective moment of inertia.

I_g = moment of inertia of the gross concrete section.

jd = the level arm due to flexure.

k = coefficient for the shear degradation of the concrete.

= bond strength factor of the externally bonded ACM laminate.

k_c = concrete strength enhancement factor.

k_e = coefficient of concrete confining effectiveness.

K_{em} = measured initial stiffness of the beam.

K_{et} = theoretical initial stiffness of the beam.

l = beam length

l_e = effective beam length.

l_d = basic development length of the steel reinforcing bar.

l_{dp} = basic development length of the ACM laminate.

l_p = available development length of the ACM laminate.

M and M' = bending moment.

M_D = bending moment due to dead load.

M_i = ideal flexural strength.

M'_i = first-yield flexural strength.

M_L = bending moment due to live load.

M_n = nominal flexural strength.

M_u = required bending moment.

M_v = shifted bending moment due to the diagonal tension cracking.

M_y = moment at the onset of yielding.

N = axial force on the member.

N_p = equivalent axial force caused by the equivalent axial strain ε_x.

N_V = equivalent axial force due to shear.

N_{vp} = ACM component force corresponding to the force N_V.

N_{vs} = steel component force corresponding to the force N_V.

n = E_s / E_c, modulus of elasticity ratio.

P = applied load during testing.

P = axial compressive load.

P_c = axial compressive load carried by the concrete.

P_{cn} = nominal axial compressive strength carried by the concrete.

P_{c0} = axial compressive load carried by the unconfined concrete.

$P_{cc,j}$ = axial compressive load carried by the effective area of concrete confined by the ACM jacket.

$P_{cc,js}$ = axial compressive load carried by the effective area of concrete confined by both the ACM jacket and the steel hoop.

P_E = measured load.

P_L = tensile force of the ACM laminate.

P_n = calculated load capacity, due to bending moment, of the test beam.
= nominal axial compressive strength of a short reinforced concrete column.

P_s = axial compressive load carried by the longitudinal steel reinforcement in a column.

P_{sn} = nominal axial compressive strength carried by the longitudinal steel reinforcement in a column.

P_u = the design concentric axial load in a column.

R = $(\varepsilon_{cc}/\varepsilon_{c0} - 1)/(f'_{cc}/f'_{c0} - 1)$, ratio of strain increase to stress increase at the peak strength of confined concrete.

r = $E_c/(E_c-E_{sec})$ in Popovics's equation.
= radius of concrete column corner.

s = spacing between sets of hoops.
= spacing of internal steel stirrup in the beam.

s' = clear spacing between sets of hoops.

s_{mv} = crack spacing resulting from the crack control characteristic of the transverse reinforcement.

s_{mx} = crack spacing resulting from the crack control characteristic of the longitudinal reinforcement.

$s_{m\theta}$ = spacing of the diagonal crack in the concrete beam.

s_{vp} = spacing of external ACM stirrup in the beam.

T = sectional tensile force due to bending moment reaction.

T_p = ACM laminate force, due to bending moment, in a cross section of the beam.

T_s = total steel force, due to bending moment, in a cross section of the beam.

T_v = additional tension force caused by diagonal tension cracking.

T' = sectional resultant tensile force due to moment and shear.

T'_p = ACM component force of the resultant force T'.

T'_s = steel component force of the resultant force T'.

t_a = thickness of adhesive resin bonded to the soffit of the beam.

t_j = thickness of ACM jacket wrapped in the column.

t_p = thickness of ACM laminate bonded to the soffit of the beam.

t_{vp} = thickness of U-side ACM strip bonded to the beam side.

t_x and t_y = overall column section dimensions.

V = shear force.

V_c = shear strength carried by the concrete.

V_n = nominal shear strength.

V_p = shear strength carried by the external U-side ACM strip.

V_s = shear strength carried by the internal steel stirrup.

V_u = required shear force due to combined action of factored loads.

V_y = shear strength at the commencement of steel stirrup yielding.

v = shear stress.

v_{ci} = limited interface shear stress in the crack developed along the diagonal compression stress field.

v_n = nominal shear stress of concrete.

w'_{jx} and w'_{jy} = the width for the straight portion of the sides of the column.

w'_s = clear spacing between adjacent longitudinal bars restrained by transverse reinforcement.

w_{si} = centre-to-centre distance between longitudinal bars confined by transverse reinforcement in column.

w_{vp} = width of U-side ACM strip bonded to the beam web.

x = $\varepsilon_c/\varepsilon_{cc}$ in Popovics's equation.

x = longitudinal position of the beam, measured from the support.

x_i = the location of the i-th measured quadrilateral in the test beam.

z = the location of the slab steel bar, away from the edge of the beam part.

$\bar{y}$ = a distance of the centre of composite laminate to the centroid of the strengthened beam.

$\bar{y}_c$ = a distance of the resultant force C_c, measured from the neutral axis.

Δ = beam deflection.

Δ_y = beam deflection corresponding to the yielding force F_y.

$\Delta_{\phi j}$ = deformation due to flexure measured in j-th reading of the quadrilateral.

$\Delta_{\gamma j}$ = deformation due to shear measured in j-th reading of the quadrilateral.

Δh_j = height of the measured quadrilateral at the j-th reading.

ΔN_a = the differential horizontal force in the adhesive layer.

ΔN_p = the differential horizontal force in the ACM laminate.

ΔT_p = differential ACM laminate force due to the bending moment reaction.

$\Delta T'_p$ = differential ACM laminate force due to the bending moment and shear force reaction.

Δx = width of an analytical segment.

τ = interfacial bond stress between concrete and steel or ACM laminates.

τ_p = interfacial bond stress between concrete and ACM laminate.

$\bar{\tau}_p$ = average interfacial bond stress between concrete and ACM laminate in an analytical segment.

σ_L = stress in ACM laminate.

$\bar{\sigma}_{np}$ = average interfacial normal stress between concrete and ACM laminate in an analytical segment.

ε_a = axial strain of the loaded column.

ε_c = the concrete compressive strain.

ε'_c = the strain corresponding to the cylinder concrete strength f'_c.

ε_{c0} = the strain corresponding to the concrete compressive strength f'_{c0}.

ε_{cc} = the strain corresponding to the concrete compressive strength f'_{cc}.

ε_{ct} = the concrete strain in the extreme fibre of the cross section.

ε_{cr} = the tensile strain corresponding to the strength f_{cr}.

ε_{cu} = ultimate concrete strain.

ε_L = strain in ACM laminate.

ε_l = lateral strain in the axial loaded column.

ε_{max} = converted maximum strain from the reading of the gauged rosette.

ε_{min} = converted minimum strain from the reading of the gauged rosette.

ε_p = tensile strain in the ACM laminate.

ε_{pD} = the ACM laminate tensile strain corresponding to service dead load after retrofit.

ε_{pe} = effective tensile strain in the ACM laminate.

ε_{pu} = ultimate tensile strain of ACM laminate.

ε_{s} = the strain in the longitudinal steel reinforcement.

ε_{sD} = the longitudinal steel bar strain corresponding to service dead load after retrofit.

ε_{sh} = the steel strain at the commencement of strain hardening.

ε_{su} = ultimate strain of steel reinforcement.

ε_{sy} = yield strain of steel reinforcement.

ε_{s0} = the longitudinal steel bar residual strain during jacking up.

ε_{sD}' = the longitudinal steel bar strain corresponding to service dead load before retrofit.

ε_{t} = transverse strain, tension positive.

ε_{v} = volumetric strain of concrete column.

ε_{vpe} = effective transverse strain of external ACM stirrup.

ε_{x} = equivalent axial strain of the beam, tension positive.

ε_{1} = principal tensile concrete strain corresponding to f_1.

ε_{2} = principal compressive concrete strain corresponding to f_2, negative quantity.

$\varepsilon_{1,2,3}$ = measured strains obtained from the reading of the gauged rosette in the grid 1 to 3.

υ = Poisson's ratio of concrete.

υ_{t} = the tangential Poisson's ratio in a concentrically loaded column.

$\upsilon_{t,\,max}$ = a peak value of the tangential Poisson's ratio in a concentrically loaded column.

$\bar{\upsilon}$ = the effective Poisson's ratio in a concentrically loaded column.

μ_{Δ} = displacement ductility.

μ_{ϕ} = curvature ductility.

ϕ = the column strength reduction factor.

= curvature of the beam.

ϕ_{c} = the concrete strength reduction factor in a column.

ϕ_s = the steel strength reduction factor in a column.

ϕ_j = the curvature calculated by the measured quadrilateral at the j-th reading.

ϕ_m = maximum curvature.

ϕ_y = yield curvature.

ϕ'_y = first-yield curvature.

α = ratio of the shear stress to the maximum shear stress.

α_1 and α_2 = concrete strength enhancement factor.

β = converted angle from the reading of the gauged rosette.

γ_j = shear strain calculated by the measured quadrilateral at the j-th reading.

θ = concrete failure plane angle for the initial tangent to the arching profile due to the external confinement.

= fibre orientation in ACM laminate.

= angle of the inclination of the diagonal compression stress field.

θ_{nj} = angle of the quadrilateral set up in the test beam, where sub-index j is the reading sequence and n is the angle measured at the n-th corner of the quadrilateral.

ρ_{cc} = volumetric ratio of the longitudinal steel to the confined core concrete.

ρ_j, ρ_{jx}, ρ_{jy} = volumetric ratio of confining ACM jacket to the core concrete.

ρ_s, ρ_{sx}, ρ_{sy} = volumetric ratio of confining reinforcement to the core concrete.

ρ_v = transverse steel reinforcement ratio for the beam.

ρ_{vp} = transverse ACM strip ratio for the beam.

ρ_x and ρ_y = lateral steel ratio parallel to the x-axis and y-axis in rectangular column section, respectively.

ρ_w = steel reinforcement ratio for the beam.

ρ_x = longitudinal reinforcement ratio for the beam.

ω = width of the diagonal crack.

= uniform load.

ω_D = uniform dead load.

ω_L = uniform live load.

ABBREVIATIONS

ACM	= Advanced Composite Material
CACM	= Carbon-Fibre Advanced Composite Material
GACM	= Glass-Fibre Advanced Composite Material
FRP	= Fibre Reinforced Polymer Plate
CFRP	= Carbon-Fibre Reinforced Polymer Plate
GFRP	= Glass-Fibre Reinforced Polymer Plate
DEMEC	= Demountable Mechanical Gauges
MCFT	= Modified Compression Field Theory

CHAPTER 1

INTRODUCTION

1.1 General

In recent years repair and retrofit of existing structures have been among the most important challenges in structural engineering. The term retrofitting of reinforced concrete members has a broad meaning. This includes the increase of the load carrying capacity of structural members (strengthening) and the increase of the performance in structural members required to maintain the load carrying capacity during a strong earthquake (ductility).

The main reasons for retrofitting of reinforced concrete structures are:

- upgrading of resistance or stiffness to withstand increased load demand,
- increasing the strength and/or the ductility capacity of members in structures in seismically prone locations,
- eliminating structural deficiencies due to inadequate detailing such as the lack of sufficient transverse reinforcement or poor development of the longitudinal reinforcement,
- restoring the lost load carrying capacity in members subjected to corrosion of the reinforcement.

There are several options that can be used to retrofit or repair members of existing reinforced concrete structures. Among the most commonly used options are steel jacketing, active confinement by wire prestressing, jacketing with reinforced concrete and use of advanced composite materials. Nowadays, the application of advanced composite materials such as advanced composite material (ACM) laminates can be an economical way of achieving the desired level of performance for the retrofitted or repaired member. In the past two decades fibre advanced composite materials, which were originally developed for the aerospace and defence industries, have shown great potential for use in civil engineering. This innovative material made of fabric and

polymer matrix can be applied to conventional structures such as steel, concrete, and wood.

The general advantages of fibre composite laminates, where conventional materials such as steel plates cannot provide satisfactory service life, are high strength-to-weight ratio, excellent resistance to electrochemical corrosion, excellent low and high temperature performance, low-cost installation for any desired shape and surface texture and, for some materials, excellent performance under fatigue loading. The author believes the application of fibre advanced composite materials will lead to radical changes in construction methods, final forms and maintenance regimes for structures. This new approach is becoming increasingly important to enable extension of the service life of most structures into the 21st Century.

1.2 Research Evolution

This research project was sponsored by Contech Group Ltd. in New Zealand, who introduced Tyfo composite material to New Zealand in 1995 [F2, C5] and by Composite Retrofit International of Canada who is the international distributor of Tyfo. The main purpose of this project is to investigate the performance of retrofitted reinforced concrete members using the Tyfo composite system in the area of confinement of columns, enhancement of shear resistance and flexural strength of beams, and the bond characteristic between concrete and the composite material.

Three main areas, where advanced composite materials can be used, were investigated in the project.

The first part looked at the axial load carrying capacity increase of reinforced concrete columns confined with Tyfo fibreglass/epoxy jackets. This part is described in Chapter 8. At the beginning of this investigation research work in the effects of confinement on the axial load carrying capacity of columns had been limited to very small plain concrete prisms. This work and its theoretical back up constitute an original piece of study.

The second part looked at ways to enhance the flexural strength of beams with longitudinal bar curtailment deficiencies, which can lead to a premature flexure-shear failure and to a poor seismic response. Tyfo fibreglass/epoxy plates were adopted as the strengthening composite materials in the tests. The detailed description of this part is described in Chapter 5. With reference to the tests, an interesting topic was the extension of the care to study premature composite plate debonding. With regard to this part, the author is unaware of any previous investigation carried out anywhere else.

The third and final part was conducted on T-beams with the aim of increasing the live load carrying capacity. The strengthened beams were tested under repeated cyclic loading whereas one beam was tested for one million cycles in order to apply the test results into the retrofitting design of beams in building and bridge system. As a variant to the composite material used in the second test, carbonfibre/epoxy laminates were bonded to the soffit of the beams and fibreglass U-strips were placed on the beam sides to enhance the bond of the carbon laminate and to increase the shear strength of the beam. The detailed experiment can be referred to in Chapter 4. Previous research in this area has been confined to theoretical solutions using elastic theory or to laboratory work on small-scale rectangular beams. The experimental work carried out in this study presents alternative ways to detail the ACM laminates and to increase the shear strength of members. The experimental work is supported by comprehensive data collected in the tests. A general design philosophy is also proposed and justified by the development of a theoretical model and a simplification of it for use in a design office.

It is hoped that the information contained in this thesis will help in the task of implementing an effective building and bridge retrofit project in New Zealand and elsewhere.

1.3 Organisation

The reader should note that the layout of this report does not follow the chronological arrangement of the experimental programme. This report is divided into four parts.

Part I presented in Chapter 2 reviews the use of advanced composite materials in concrete structures. A literature review of the research is also made in this part.

Part II discusses the development of the analytical model and the experimental evidence to study the behaviour of reinforced concrete beams retrofitted with ACM laminates. Chapter 3 presents an analysis procedure to study the interface bond characteristic between concrete and ACM laminates and the failure mode of the beams strengthened with ACM laminates. Chapter 4 discusses a series of experimental work dealing with the use of ACM laminates for increasing the service live load in beams. Chapter 5 describes an experimental programme on the use of ACM laminates on beams with shear and bar curtailment deficiencies. Chapter 6 proposes a general design procedure for the beams retrofitted with external ACM laminates in the buildings and bridges.

Part III of the thesis covers a theoretical and experimental study on the retrofitting design of reinforced concrete columns subjected to axial compressive loads. Chapter 7 represents a theoretical analysis of concrete columns jacketed with ACM laminates. Chapter 8 develops an experimental study to validate the theoretical analysis and to verify the confinement effect using the ACM laminates. Chapter 9 provides an evaluation method for designing the retrofitting of axially loaded reinforced concrete columns using the confinement of ACM jackets.

Finally, Part IV contains the conclusions and contributions resulting from this investigation. Recommendations for future research are also included in this part.

PART I

REVIEW OF THE USE OF ADVANCED COMPOSITE MATERIALS IN CONCRETE STRUCTURES

CHAPTER 2

APPLICATION OF ADVANCED COMPOSITE MATERIAL LAMINATES TO CONCRETE STRUCTURES

There are several options that can be used to retrofit or repair members of existing reinforced concrete structures. Among the most commonly used options are steel jacketing, active confinement by wire prestressing, jacketing with reinforced concrete, and use of advanced composite material (ACM). Nowadays, the application of ACM can be an economical way of achieving the desired level of performance for the retrofitted or repaired member. In this chapter several ACM systems including the materials and technical review are described.

2.1 Fibre Composite Materials in the Construction Industry

Several types of fibre composite materials have been used to repair concrete members to either correct structural deficiencies or to enhance the service or ultimate loads. The following sections detail the most commonly used materials and the ways that they are applied to reinforced concrete members.

2.1.1 Advanced Composite Material Laminates

Advanced composite materials (ACMs) are composed of a fabric and a polymer resin. The fabric, comprised of a warp (0-degree orientation) and a weft (90-degree orientation) fibres, is manufactured predominately to a plain weave. Epoxy resin, a widely used polymer, is mixed and poured into the trough of an impregnator. A roll of continuous fabric is passed through the trough to saturate the fabric with a predetermined amount of resin. Then the saturated fabric matrix is cured at a temperature to form a ACM laminate.

Table 2.1 Comparison between E-glass, Aramid, and Carbon fibres [M3]

Criterion	Carbon	Aramid	E-glass
Tensile strength	very good	very good	very good
Compressive Strength	very good	inadequate	good
Modulus of elasticity	very good	good	adequate
Long term behaviour	very good	good	adequate
Fatigue behaviour	excellent	good	adequate
Alkaline resistance	very good	good	inadequate
Price	adequate	adequate	very good

The construction industry makes use of three main fibres, namely carbon, aramid, and E-glass. **Table 2.1** provides a qualitative list of the properties of the different fibres. The mechanical properties of the different fibre materials currently being considered for bridge and building applications differ widely in terms of ultimate stress and strain as well as elastic modulus. Nevertheless a common feature is that ACMs behave as linear elastic materials up to failure. The high modulus of elasticity and tensile strength rapidly decrease with increasing deviation angle between fibre orientation and loading direction, and the deformation characteristics become increasingly dominated by the properties of the resin. **Figure 2.1** shows the influence of the fibre orientation on the tensile properties for a typical ACM laminate. **Table 2.2** presents the main material properties for some of the fibres.

Table 2.2 Properties of Advanced Composite Materials [P6]

Material	Modulus of Elasticity, GPa	Ultimate Tensile Strength, MPa	Ultimate Strain, %
Fibre			
Carbon	160-270	1400-6800	1.0-2.5
Aramid (Kevlar 29)	62-83	2800	3.6-4.0
Glass	81	3400	4.9
Polyethylene	117	2600	3.5
Resin			
Epoxy	2.0-4.5	27-62	4-14
Vinylester	3.6	80	4

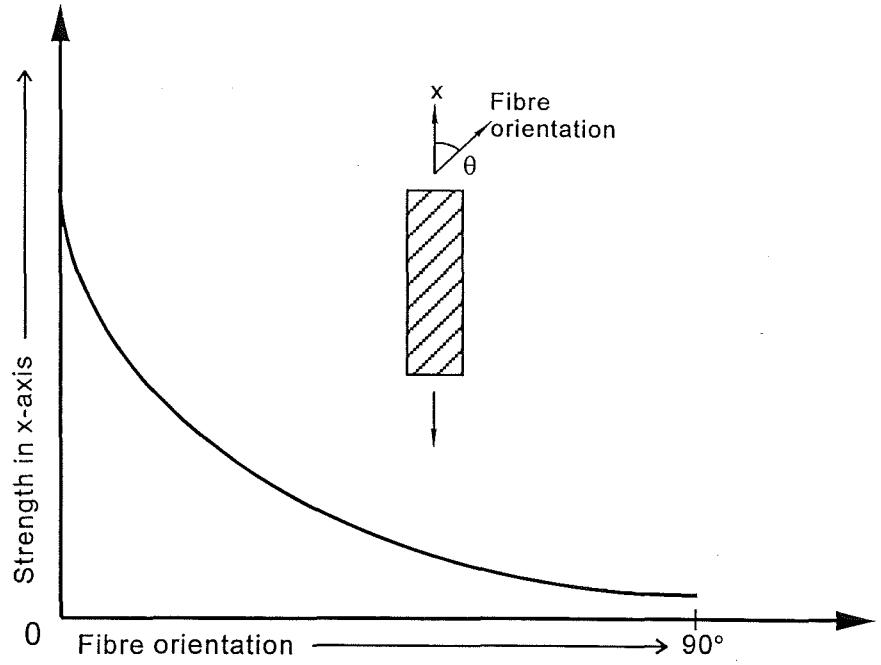

Figure 2.1 Tensile Characteristics for a ACM Laminate [P6]

2.1.2 Structural Adhesives

Of all the different categories of adhesives, epoxy adhesives are recognised to be the most appropriate for use to repair cracks in concrete, and to bond external reinforcement. Epoxy materials have certain attributes that can be useful in specific circumstances. Numerous types of epoxies with a wide range of mechanical properties are commercially available. It is very important to select a suitable epoxy for a particular application.

Epoxy resins are available in a range of viscosities, and will work with a number of hardeners or curing agents. When epoxy resins and hardeners or curing agents are mixed immediately according to an appropriate procedure they are capable of forming an adhesive with exceptional structural qualities. Factors contributing to the success of epoxy resin adhesives are good wetting characteristics, physical strength characteristics, chemical resistance, weatherability, electrical resistance, high temperature strength and stability, and good bond even to damp surfaces [M14]. However, the cost of epoxy resin adhesives is greater than of other commercial adhesives, such as polyesters and vinylesters.

Some disadvantages of epoxy used should be noted that

- Epoxies must be carefully processed to maintain moisture resistance.
- Cure time can be lengthy, especially under low temperature conditions.
- Some hardeners require special precautions in handling, and resin and some hardeners can cause skin reactions.

Until now research into the influence of epoxy resins on the bond strength of plated beams is limited. Saadatmanesh et al. [S2] recommended tough epoxies as more appropriate for the application of ACM laminated beams. Many other researchers [C7, G1, G2, M5, S5] have tested a range of epoxy resins through joint tests to establish their shear adhesion properties.

A difficulty encountered when bonding laminates to increase the stiffness and strength of reinforced concrete members is the large stress concentrations that develop at the end of the laminate. Ladner [L1] study the effect of the epoxy resin thickness between the reinforced concrete member and the steel plate in reducing the stress concentration. He found that the thickness of epoxy resin bed did not significantly affect the magnitude of the stress concentration and recommended using 1 to 2 mm thick beds.

2.1.3 Concrete Surface Preparation

The overall success and performance of patching materials applied to concrete surface is highly dependent on the quality of the cleaning and surface preparation performed. That is why the concrete surface preparation is an important factor concerning the application of ACMs to concrete structures if the enhancement of the structural performance of the repaired member relies on the bond to the laminate. In cases were the ACM is used in wraps to provide lateral confinement to the reinforced concrete member, bond between the member and the ACM is of little concern.

Concrete surfaces must be free of loose, weak, and unsound materials (including laitance) as well as any chemical contamination. The surface after roughing

should be kept as flat as possible. Most of methods for concrete surface preparation concerned in author's study are only related to mechanical abrasion, which are grinding, sandblasting, water-jetting, scraping, and scabbling. ACI 515.1R-79 or ASTM standard [C6] provided a general procedure for roughening, cleaning, and checking the concrete surface but not in a practical way. This is because the abrading extent can not be easily measured. Few researchers have reported the performance of concrete surface preparation [S4]. The results were restricted to the test condition offered by researchers. Meanwhile the effect of these surface preparation methods strictly depended on material properties, concrete strength, aggregate size, type of epoxy and ACM used, worker's operation skill, and construction environment, etc.

2.2 Reinforced Concrete Beams Strengthened with Steel and ACM Laminates

2.2.1 Previous Experimental Studies on Steel Plated Reinforced Concrete Beams

Since the early work in South Africa [F3] and in France [L2] in the mid-1960s, the technique of strengthening reinforced concrete members by bonding thin steel plates to their surface has been used in Belgium, France, Japan, Poland, South Africa, Switzerland, and in the United Kingdom for nearly three decades [J1]. This technique extended to ACM laminates as they became economically feasible in this decade. Consequently the research into the use of bonded steel plates is very relevant to the use of bonded ACM laminates and for this reason a literature survey on the research in this area was carried out.

MacDonald and Calder [M8] studied the behaviour of reinforced concrete I beams externally reinforced with steel plates bonded to their tension flanges. They tested a series of 3.5m long and 4.9m long beams under four-point loading. Results showed that the adhesive provided full composite action and that significant improvement in performance could be achieved in terms of crack control, stiffness, and ultimate load. Exposure tests were carried out on 0.5m long unreinforced concrete beams with steel plates bonded to one face. It was concluded that significant corrosion of the steel plate could take place during exposure to the environment. In addition, loss of bond strength at the steel/epoxy interface was observed, resulting from the corrosion

of the steel plate. The reduction in the overall strength of the beams was attributed to corrosion.

VanGermert and VandenBosch [V2] reported results of durability tests on concrete beams with epoxy-bonded external steel plates. They studied the effects of long-term exposure, fatigue, and temperature loading, concluding that the effects of atmospheric corrosion depend to a large extent on the preparation of the concrete and steel-plate surfaces and on the workmanship of the repair crew. Cyclic loading tests were performed on two 6m long simply supported beams. The beams were reinforced with a double layer of glued steel plates. The cross section of the beams was 300mm high by 250mm wide. The steel plates were 5 mm thick by 200 mm wide. The beams were tested under four-point loading and were subjected to cyclic loading resulting in a maximum stress of 40 MPa at the steel plates. Five hundred thousand cycles were applied to each beam at a rate of 30 cycles/min. The tests showed that no redistribution of stresses took place by deformation in the glue or by any failure of the glued connection. Also, full-scale temperature loading tests in the temperature range from -20 ℃ to +90℃ were conducted on specimens glued with EPICOL U epoxy adhesive. It was found that the cold-hardening epoxy glue had a poor thermal resistance. There was no decrease in the ultimate load for lower temperatures. However, at higher temperatures, the behaviour was different. At a temperature of about 60℃, the glue started to become weaker and more deformable. The epoxy joint was not able to transfer the shearing stresses from the steel plate to the concrete surface, and a crack propagated from the plate end into the concrete beam. At lower temperatures, the crack always began at the end of the plate and moved into the concrete. The performance of the cold-hardening epoxy joint was strongly reduced at high temperatures.

Swamy et al. [S6, S8] investigated the effect of glued steel plates on the first cracking load, cracking behaviour, deformation, serviceability, and ultimate strength of reinforced concrete beams. Forty beams were tested. All test beams had a rectangular cross section of 255 mm high by 155 mm wide. The beams were 2.5 m long. The tensile steel reinforcement of these beams consisted of 3-20 mm diameter bars. The beams were strengthened by applying steel plates, 1.5 mm, 3 mm, or 6 mm thick. In addition, the thickness of the epoxy resin bed was also varied to be 1.5 mm, 3 mm, or 6 mm thick.

The results indicated that the presence of the steel plates substantially increased the flexural stiffness, reduced the crack widths and the structural deformation at all load levels, and enhanced the ultimate load. Due to significant increase in the sectional stiffness, the serviceability load of the beams became higher.

These researchers also found that, in the region of the plate cut-off, the local bond stresses were considerably higher than those predicted by simple elastic theory and could result in premature debonding of the plates. Several measures to prevent premature plate debonding were studied. It was found that by providing mechanical anchorage to the plate ends the ultimate load capacity and mode of failure of the plated beam could be positively improved. The authors provided some simple design guidelines, like restricting the width to thickness ratio of the plates and neutral axis depth of the concrete sections, both to maintain ductility and to avoid premature debonding of the bonded plates.

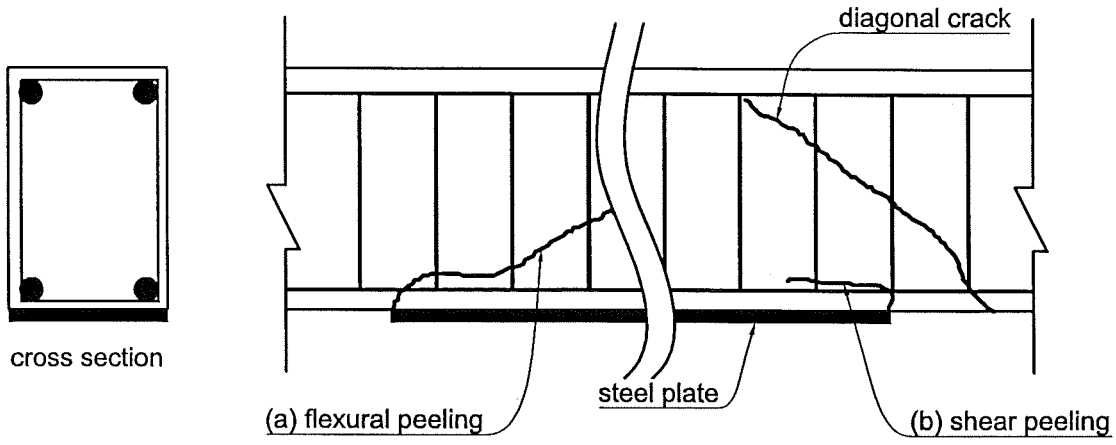

Figure 2.2 Failure Modes in a Steel-Plate-Bonded Beam [M6]

Oehlers [O1, O4] conducted a series of detailed studies on the failure mechanism of steel plated beams. Three identified failure mechanisms rationally categorised by him are referred to: (1) Flexural peeling, induced by increasing curvature, which is associated with a gradual separation of the plate as shown in **Figure 2.2(a)**; (2) shear peeling, induced by the formation of shear diagonal cracks, which are associated with rapid separation of the plate as illustrated in **Figure 2.2(b)**; and (3) a combination

of both flexural and shear peeling. According to test results, flexural and shear cracks, the bond stress along the bottom reinforcement, and aggregate interlock forces across peeling cracks play a potentially major part in the failure mechanism. He concluded that debonding could start at the plate ends owing to the stress concentrations caused by the discontinuity of the plate. Debonding could also occur between the plate ends due to a higher elastic shear flow stress at the plate/concrete interface.

2.2.2 Experimental Study on ACM Laminates Bonded to Reinforced Concrete Beams

Since 1982, carbon ACM laminates have been successfully applied to reinforced concrete beams by Meier et al. [M3]. He reported the use of thin carbon ACM laminates acting as flexural strengthening reinforcement for reinforced concrete beams. He suggested that ACM laminates could replace steel plates with overall cost savings emanating from the simplicity of the strengthening method because:

- they do not corrode,
- they are easy to handle in the construction site and can be bonded to the structure without expensive scaffolding,
- they are available on long lengths, therefore no joints are necessary,
- some ACMs show an outstanding fatigue behaviour.

Most of failure modes observed in the load tests carried out by Meier are shown in **Figure 2.3**.

Carbon ACM composites were successfully employed in loading tests for strengthening of concrete beams by Kaiser [K1]. He tested a series of 300 mm wide by 250 mm deep rectangular section and 2 m long reinforced concrete beams with different thickness of carbon ACM laminates applied to their soffit. The results showed the validity of strain compatibility hypothesis in the cross-section analysis. The development of an analytical model for composite laminate anchoring agreed with test results very well. Kaiser also investigated the fatigue behaviour of a beam strengthened with ACM laminates. The beam with the same dimension of previous static loading test

specimens was post-strengthened with a strip of 0.3×200mm of glass/carbon hybrid sheet without end laminate anchoring. The result depicted the hybrid sheet could still withstand after the fatigue failure of steel reinforcements. He studied the temperature effect over 100 freeze-thaw cycles from +25℃ to -25℃ on concrete beams strengthened with carbon ACM and found no adverse influence on the flexural capacity.

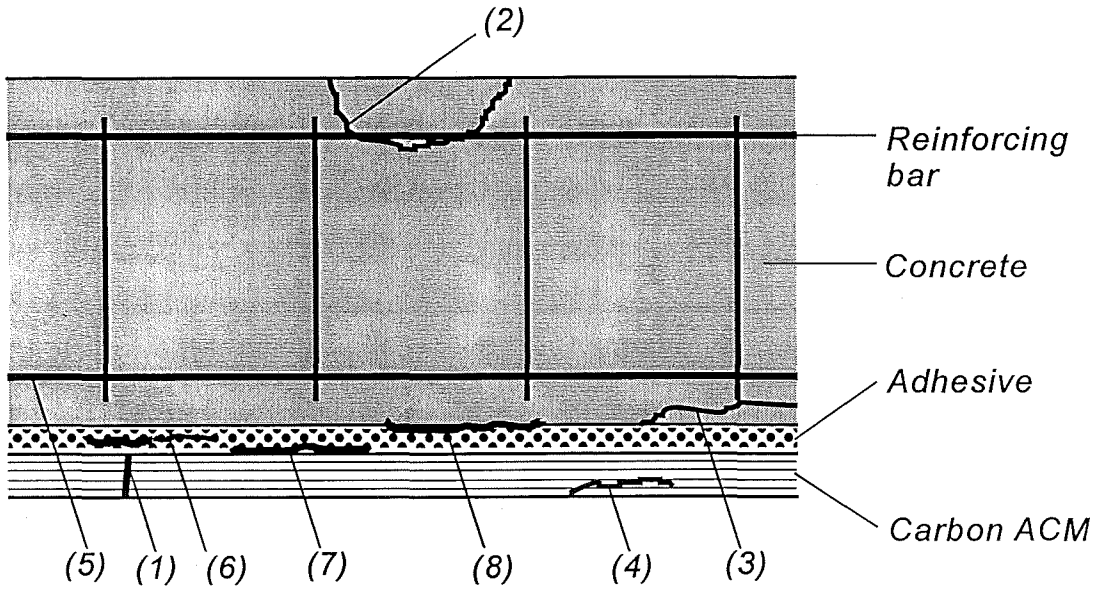

(1) tensile failure of the ACM sheet (2) concrete failure in the compressive zone
(3) continuous peeling off of ACM sheet due to an uneven concrete surface
(4) interlaminar shear within the ACM sheet (5) failure of the steel bars
(6) cohesive failure within the adhesive
(7) adhesive failure at the ACM/adhesive interface
(8) adhesive failure at the concrete/adhesive interface

Figure 2.3 Failure Modes in a Carbon ACM-Bonded Beam [M3]

Ritchie et al. [R5] used an interactive analysis procedure for predicting the stiffness and strength in bending of ACM laminated beams. He also tested a series of concrete beams strengthened with glass, carbon, and aramid ACM laminates. The analytical model was not verified completely by experimental testing owing to the lack of failures in the region of constant bending moment. However, for those that did, the model appeared to predict the flexural behaviour fairly accurately.

Saadatmanesh and Ehsani [S11] studied the static behaviour of reinforced

concrete beams with glass ACM laminates bonded to their tension zone. Their conclusions were:

1. The concrete surface preparation and the selection of the adhesive is of primary importance, and,
2. the strengthening technique is particularly effective for beams with relatively low steel reinforcement ratios.

Meier et al. [M3] performed fatigue test on a reinforced concrete T-beam with carbon ACM laminates applied to its soffit. The beam was tested under 6 point loading using more realistic fatigue load range (130 MPa to 260 MPa in steel bars) up to 10.7 million loading cycles to verify the excellent performance of carbon ACM in fatigue resistance. They also proposed a method for prestressing the strengthening laminates to increase the service load of the structure. Meier et al. point out that shear deformations between cracks in reinforced concrete members can cause premature debonding of ACM laminates that are applied to the top or bottom sides of the beam. This problem is illustrated in **Figure 2.4**. They also suggested ways to use ACM laminates to act as shear reinforcement and to effectively clamp the ends of the carbon ACM laminates, see **Figure 2.5**.

2.2.3 Concrete/ACM Interface Bond Strength

In the design of retrofit schemes incorporating ACM laminates for increasing the stiffness or the flexural strength of a reinforced concrete member, the concrete-to-ACM interface bond strength is one important design variable that needs to be considered. A literature survey of the research work conducted up to date is examined in this section.

The earliest study on the normal and bond shear stress distribution in a glued joint was published by Goland and Reissner [G3]. Their analysis led to a more general form of the differential equations describing the normal and bond shear stresses in joints in an elastic medium.

Research on the force transfer in epoxy bonded steel-to-concrete joints was

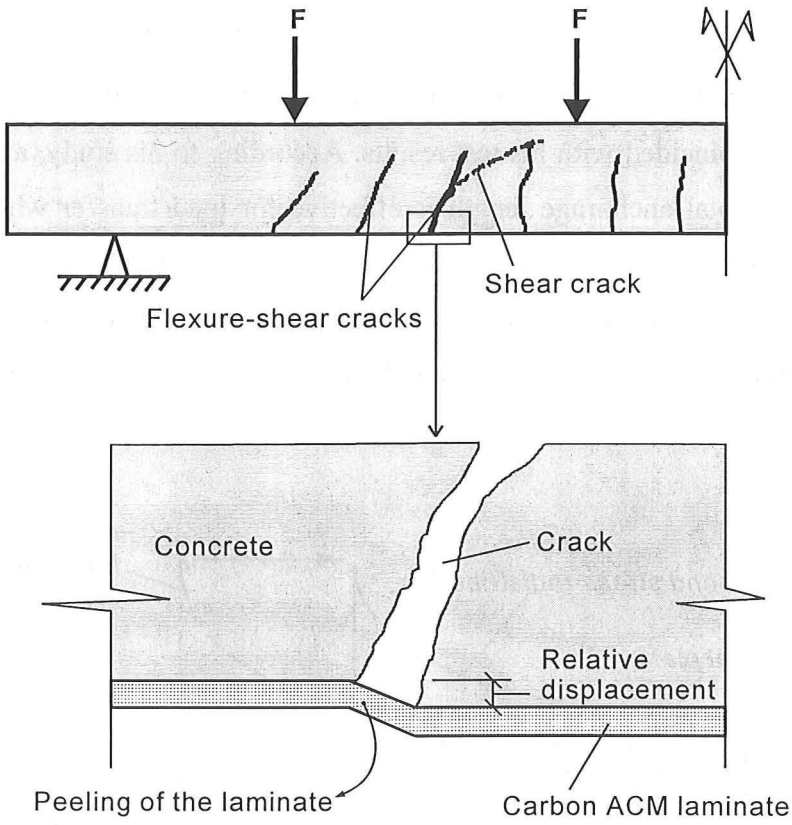

Figure 2.4 Carbon ACM Laminate Peel-off due to Shear Crack [M4]

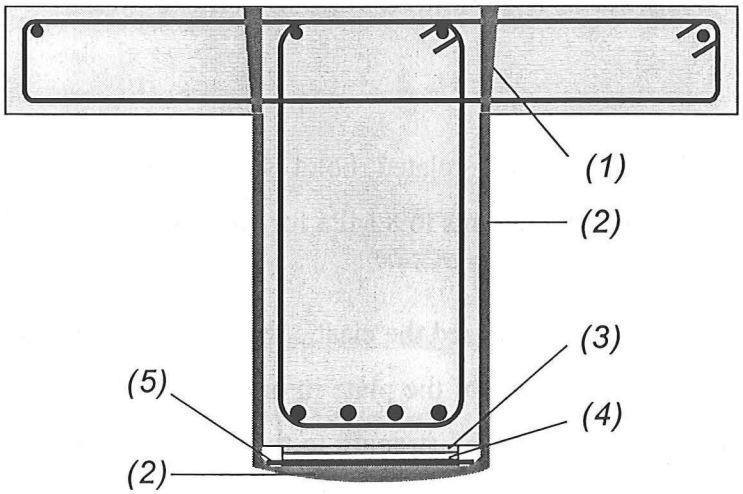

(1) anchorage zone (2) shear strengthening element
(3) adhesive (4) Carbon ACM laminate for flexural strengthening
(5) Carbon ACM plate for load distribution

Figure 2.5 Cross-Section of Beam with Shear Strengthening Arrangement [M3]

started by Bresson [B3, L2]. He set up a mathematical model to describe the behaviour of the joint loaded in the elastic region. Ladner [L1] derived the mathematical model and his model coincided with his test results. According to his study, a relatively small amount of the total anchorage length is effective for load transfer when all materials involved behave elastically. The total anchorage length will only be needed when, due to local failure of the bond, the peak value of the bond stress moves towards the unloaded end of the steel sheet. Thus, a redistribution of the bond stresses takes place as shown in **Figure 2.6**.

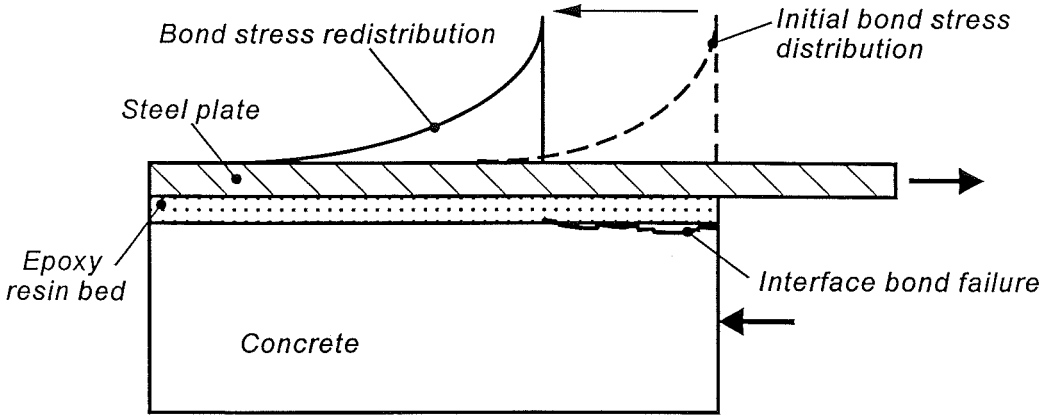

Figure 2.6 A Diagram in Explanation of Ladner Bond Stress Redistribution

Ranisch and Rostasy [R8] related bond strength to compressive strength, claiming that the bond strength amounts to 8 MPa for cube strength of 30MPa.

Swamy and Jones [S6, S8] used the elastic theory to study the steel-to-concrete bond stress concentration at the end of the plate in order to predict the load at the steel plate separation. They related the bond strength to the concrete cube strength, claiming that it varied from 6 to 8.3 MPa for cube strengths varying between 25 to 70 MPa. In a later study using large-scale beams, Swamy et al. related the bond strength to the tensile strength of concrete, rather than the compressive strength, claiming that the bond strength is equal to $\sqrt{2}$ times the tensile splitting strength of concrete. Since the split tensile strength is unlikely to exceed 4 to 5 MPa for normal concrete strength, this gives a bond strength of around 6 to 7 MPa. They found that the peak interface bond stress

determined experimentally had a value of 2τ, where τ is the bond stress derived using elastic theory.

An analytical solution using partial interaction theory was developed by Roberts [R6] for predicting the shear and normal stress concentrations in adhesive joints. Roberts concluded that the shear and normal stress concentrations in the adhesive layer at the ends of steel plates could be reduced significantly by using a more flexible adhesive, by reducing the thickness of the steel plate, and by terminating the steel plate as close to the beam supports as possible. He also stated that failure of epoxy-bonded steel plates is likely to be occur at the bond stresses between 3 to 5 MPa combined with the interface normal stresses between 1 to 2 MPa.

Kaiser [K1] modified Ladner's model from elastically linear stress distribution on bonded steel plates to a linear and non-linear stress distribution behaviour on carbon ACM laminates, as shown in **Figure 2.7**. His study was focussed on finding a way to calculate the anchorage length of carbon ACM laminates used for increasing the flexural strength of beams. The laminate stresses as a function of the laminate thickness for a given anchoring length at ultimate anchoring loads as theoretically calculated by him are depicted in **Figure 2.8**. It is noted that bond stress value of 8 MPa was obtained from his theoretical and experimental study on carbon ACM-to-concrete bond. However, the influence of the concrete strength is neglected in the analytical model. The concrete strength adopted in his model is valid for a cube strength of 40 MPa. If the concrete strength is different, a lower bond stress value could be expected.

Sarif et al. [S10] carried out tests on double overlap ACM laminate-to-concrete specimens in which it was found that the maximum sustainable interface shear stress was 3.5 to 4 MPa, with failure occurring in the concrete in all cases.

Using some simple tests to calculate the interface characteristics between adhesive and concrete, Arduini et al. [A7, A8] concluded that the bond strength of the ACM laminate to the adhesive interface was about 3 times the bond strength of concrete-to-adhesive interface. As a result the ACM laminate-to-concrete bond strength was controlled by failure at the concrete-to-adhesive interface. They recommended using a bond strength of 5 MPa for concrete cylinder cube compressive strengths of

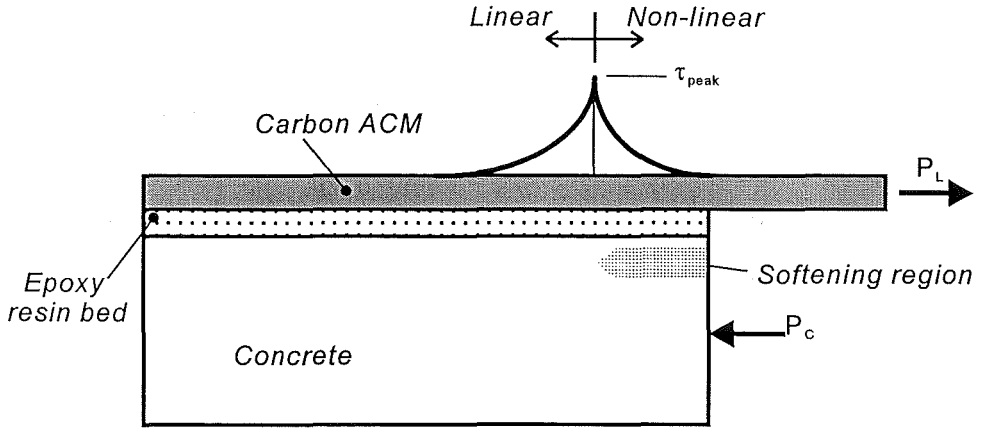

Figure 2.7 Linear and Non-linear Bond Stress Distribution on a Carbon ACM Laminate Anchor [K1]

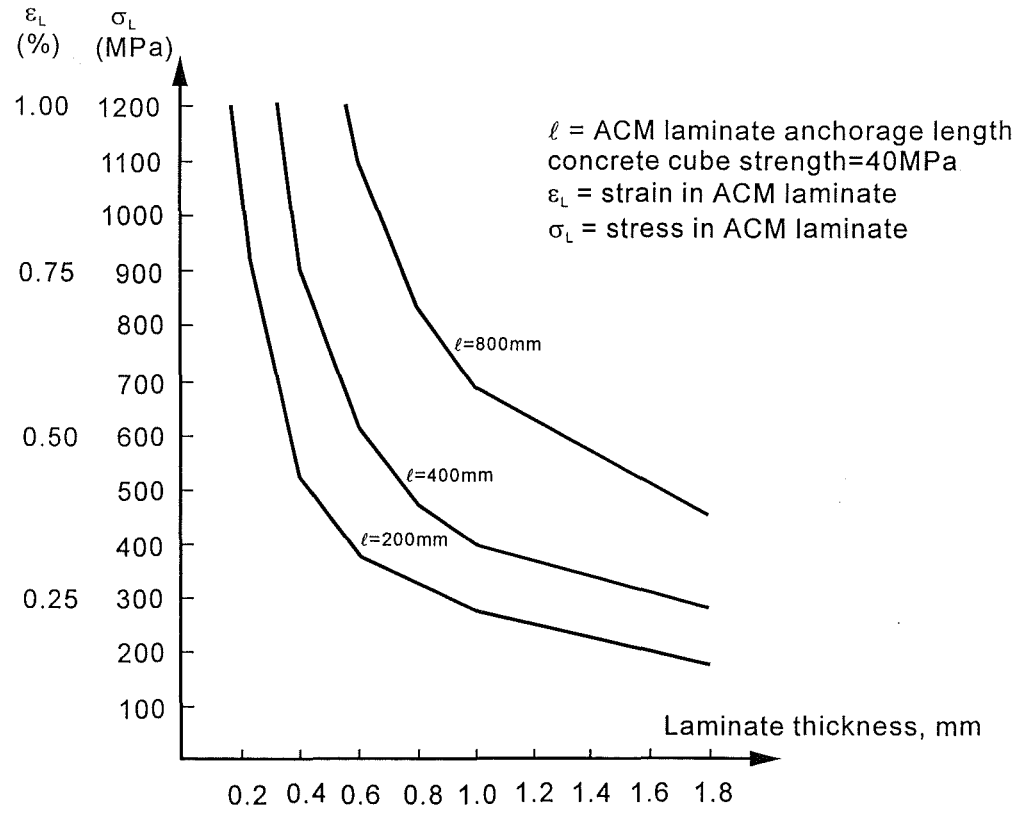

Figure 2.8 Anchorage Length for ACM Laminates Bonded to Reinforced Concrete Beams [K1]

around 30 MPa.

Quantrill et al. [Q1, Q2] performed shear pull-off tests using glass ACM laminates bonded with 1mm thick adhesive to a concrete prism of 65 MPa cube compressive strength. These test results gave an average bond strength of 6.4 MPa. When a 2mm thick adhesive layer was used, the average bond strength was 5.8 MPa. Failure occurred in all cases within the concrete adjacent to the bondline.

2.2.4 Analysis and Design Aspects on Externally Plated Concrete Beams

Swamy and Jones [S8] proposed that stresses near the end of steel plates could be assessed using the following procedures:

1. Carry out an elastic analysis of the beam section to determine the neutral axis depth and the second moment of area of the transformed section.
2. Use conventional elastic theory to determine the horizontal shear stress in beams to obtain the interface shear stress at the plate end:

$$\tau = \frac{VA\bar{y}}{Ib_p} \tag{2.1}$$

where

V is the maximum shear due to ultimate loading,

A is the transformed area of the plate,

$\bar{y}$ is the distance from the neutral axis to the centroid of the plate,

I is the transformed second moment of area of the section,

b_p is the width of plate.

3. The peak interface shear stress will be approximately twice the value obtained above.
4. The ultimate interface bond strength is approximately $\sqrt{2}$ times the tensile strength of concrete.
5. Use a factor of safety against failure is given by the ratio of the ultimate interface bond strength to the calculated horizontal shear stress.

Swamy and Jones [S6] suggested that for externally bonded flexural reinforcement, peeling failure of the plate would not occur if the width-to-thickness ratio was not less than 50.

Oehlers [O1-O4] studied the flexural and shear peeling stresses in reinforced concrete beams strengthened with epoxy-bonded steel plates. He conducted tests to determine the failure mechanism of steel plated beams. The various debonding failure modes were categorised rationally. He determined the interaction between flexural and shear peeling experimentally and suggested empirical equations for the design of steel bonded plates.

Oehlers found that debonding at the plate ends due to shear forces is not influenced by the presence of stirrups and depends on the formation of the diagonal shear crack as measured by the shear strength of the unplated structure without stirrups.

Saadatmanesh and Ehsani [S11] reported results from the study of reinforced concrete beams with glass ACM sheets bonded to their tension zone. They performed a parametric study to examine the effect of different design material properties and quantities on the strength of the retrofitted beams. The results indicated that the flexural strength of RC beams can be significantly increased by gluing glass ACM laminates to the tension face. In addition, the epoxy-bonded laminates improved the cracking behaviour of the beams by delaying the formation of visible cracks and reducing crack widths at higher load levels.

Triantafillou and Plevris [T5] used the strain compatibility method and an analytical method, concepts of fracture mechanics, and a model for the ACM peeling-off mechanism to provide a comprehensive study of the short-term flexural behaviour of reinforced concrete beams strengthened with externally bonded ACM laminates. They produced diagrams showing the beam designs for which each failure mechanism is dominant, examined the effect of ACM laminates on the ductility and stiffness of strengthened component, and gave results of four-point bending tests confirming the analysis.

Arduini and Nanni [A9] performed a discrete element analysis to simulate their experimental works. The analytical model proposed took into account the mechanical properties of constituent materials and the characteristics of the concrete-to-ACM interface. The resultant forces at both ends of each discrete element were then provided to determine the maximum bond stresses of the interface between ACM laminate and concrete, using a concept of the triangular-shape stress distribution in an analytical element as represented in Eq.2.2.

$$\tau_{a,\max} = \frac{2(\Delta N_p + \Delta N_a)}{bD_x} \tag{2.2a}$$

$$\sigma_{a,\max} = \left[\Delta N_p (t_a + \frac{t_p}{2}) + \Delta N_a \frac{t_a}{2} \right] \frac{6}{bD_x^2} \tag{2.2b}$$

where $\tau_{a,max}$ and $\sigma_{a,max}$ are the shear stress and normal stress at the concrete-to-adhesive interface. ΔN_p and ΔN_a are the differential horizontal force in the ACM laminate and adhesive. t_p and t_a are the thickness of ACM laminate and adhesive. b is the beam width and D_x is the length of analytical element, respectively.

The analysis carried out by Aduini et al. was also compared by a numerical solution using non-linear finite element analysis. These two analytical methods show good agreement with the experiments. They concluded that the type of ACM, the laminate thickness, and the bonded length produce different types of failure modes as **Figure 2.9**. The advantage of using their proposed model to predict the strengthened beams is the tendency of the bond stress distribution of the interface between concrete and ACM laminate can be quickly detected. However, the analytical model did not consider the effect of the concrete diagonal shear cracking. This will result in the fact that the realistic bond stress distribution of the ACM laminate bonded to the soffit of beams may not be obtained.

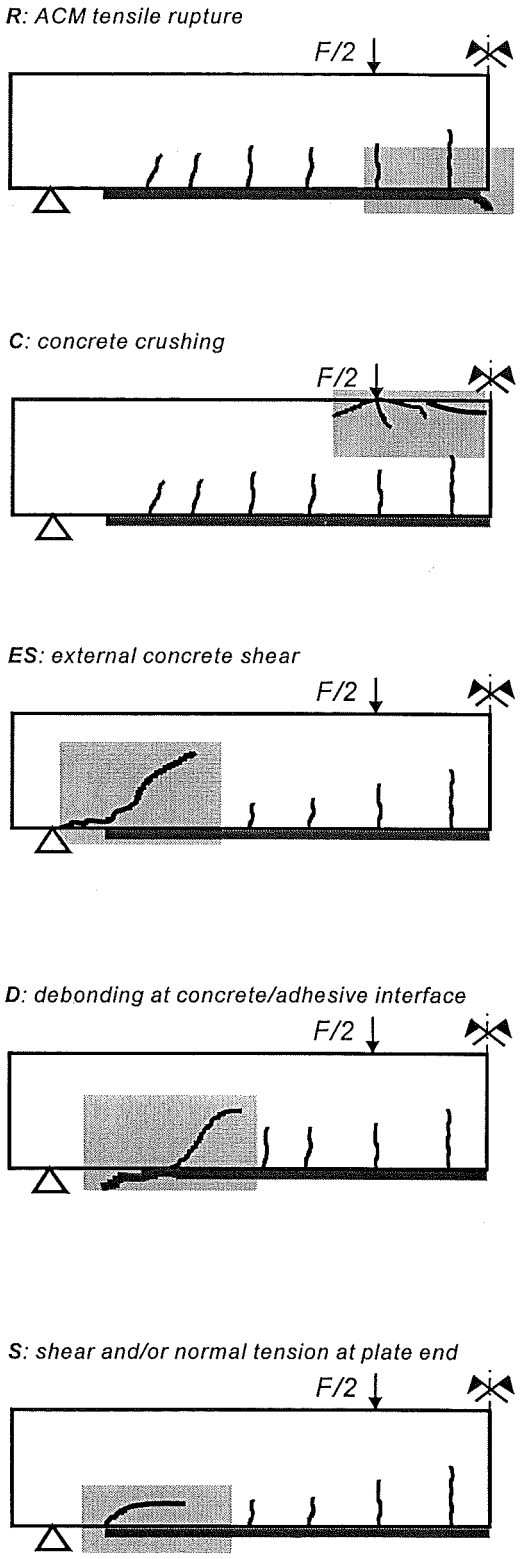

Figure 2.9 Typical Failure Mechanisms of RC Beams Strengthened with Externally Bonded ACM Laminates [A9]

2.3 Reinforced Concrete Columns Confined with ACM

Research work has indicated that by increasing the confinement in the potential plastic regions of columns results in an increase in the compressive strength of the core concrete and ultimate compression strain and hence ductility [P3].

Recent technological developments in the area of fibre composite materials have resulted in a cost reduction, to the extent that composite materials can now be readily used in the construction industry. ACM may be used to provide cost efficient solutions over traditional techniques. For instance, ACM jackets applied to the perimeter of reinforced concrete columns may be used to confine the concrete and enhance its compressive strength. ACM jackets may also provide restraint against buckling of the longitudinal column bars, which may be very advantageous in columns of older buildings located in seismic regions because, very often, the hoops are widely spaced and are unable to provide an effective restraint.

Since use of fibre composites for confinement of concrete is relatively new, theoretical work in this area is restricted to models that were originally developed for transverse steel reinforcement. Therefore, the theory of concrete confinement is mainly described using such models.

2.3.1 Confined Concrete Model

Research in the area of axial compression strength enhancement in reinforced concrete columns was reported as early as 1928 with triaxial load tests on concrete cylinders subjected to active fluid pressure [R9]. This research was followed by concentrically loaded full scale tests on circular columns with spiral steel reinforcement providing passive confining pressure [R10]. Classic confining equations are in the following form:

$$f'_{cc} = f'_{c0} + 4.1 f_l \tag{2.3}$$

and

$$\varepsilon_{cc} = \varepsilon_{c0}(1+20.5\frac{f_l}{f'_{c0}}) \tag{2.4}$$

where f'_{cc} and ε_{cc} are the maximum concrete stress and the corresponding strain, respectively. Term f_l is the lateral active pressure. Terms f'_{c0} and ε_{c0} are unconfined concrete strength and corresponding strain, respectively.

Passive confinement of the concrete by means of transverse steel reinforcement has been the subject of significant research in the past two decades, particularly in seismic prone regions, where the concrete confinement is required to increase the deformation capacity in those critical regions of a structure. Comprehensive research work in this area has been carried out at the University of Canterbury [P1, M10, L3].

Mander et al. [M10, M11] proposed a unified stress-strain approach for confined concrete applicable to members with circular and rectangular cross sections. The stress-strain model is illustrated in **Figure 2.10** and is based on an equation suggested by Popovics [P8]. For a slow strain rate and monotonic loading, the longitudinal compressive concrete stress f_c is given by

$$f_c = \frac{f'_{cc}\, xr}{r-1+x^r} \tag{2.5}$$

where f'_{cc} is the compressive strength of confined concrete, given by Eq.2.19,

$$x = \frac{\varepsilon_c}{\varepsilon_{cc}} \tag{2.6}$$

where ε_c is the longitudinal compressive strain,

$$\varepsilon_{cc} = \varepsilon_{c0}\left[1+R\left(\frac{f'_{cc}}{f'_{c0}}-1\right)\right] \tag{2.7}$$

where R is a constant, f'_{c0} and ε_{c0} are the unconfined concrete strength and

corresponding strain, respectively. In general, ε_{c0}=0.002 can be assumed. Mander et al. proposed a value of R = 5,

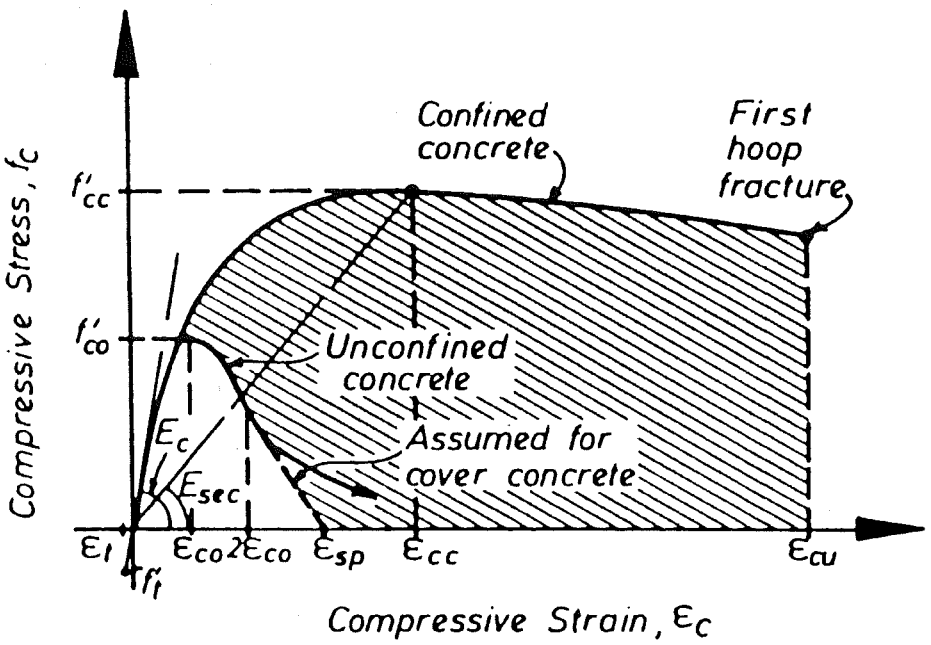

Figure 2.10 Stress-Strain Model for Monotonic Loading of Confined and Unconfined Concrete [M11]

$$r = \frac{E_c}{E_c - E_{\text{sec}}} \tag{2.8}$$

where E_c is the initial tangent modulus of concrete, which gives $E_c = 4730\sqrt{f'_{c0}}$ MPa for normal-weight concrete, and E_{sec} is the secant modulus of confined concrete at peak stress given by

$$E_{\text{sec}} = \frac{f'_{cc}}{\varepsilon_{cc}} \tag{2.9}$$

To define the stress-strain behaviour of the unconfined concrete, the Popovics equation represented in Eq.2.5 is used by replacing f'_{cc} by f'_{co}.

2.3.2 Effectively Confined Concrete Core

An approach similar to the one used by Sheikh and Uzumeri [S12, S13] was adopted by Mander et al. [M11] to determine the effective lateral confining pressure on the concrete section. The maximum transverse pressure from the confining steel can only be exerted effectively on that part of the concrete core where the confining stress has fully developed due to arching action. **Figure 2.11(a)** and **(b)** shows the arching action that is assumed to occur between the levels of transverse circular and rectangular hoop reinforcement. The critical section occurs midway between layers of transverse reinforcement. To enable the critical core area to be quantified, many researchers have assumed that arching action produces a boundary between the confined concrete and the unconfined concrete which is parabolic in shape [D2]. **Figure 2.12** shows the basic geometric properties of the unconfined region if arching occurs over a length, w, and begins and ends with an angle θ from the x-axis.

Sheikh and Uzumeri [S13] tested columns with square cross sections with various numbers of longitudinal bars and various configurations of transverse steel. They assumed parabolic arching which takes place between the centre-lines of the ties. Therefore, a reduction factor, λ, which can be used to take into account the reduction in the area of the effectively confined core because of arching between ties, can be calculated as

$$\lambda = \frac{\left(d_x - \frac{s}{2}\tan\theta\right)\left(d_y - \frac{s}{2}\tan\theta\right)}{d_x d_y} \qquad (2.10)$$

where d_x and d_y are the core dimensions measured to the centre-line of the peripheral spiral. They also assumed, that at the level of a transverse tie, arching action takes place between the centre-lines of longitudinal bars that are supported by transverse ties as shown in **Figure 2.11(b)**. At the level of the ties, the decrease in the effectively confined core due to each arch is $(w_{si}^2 \tan\theta)/6$ where w_{si} is the centre-to-centre distance between longitudinal bars. They calculated a second reduction factor, λ_1, as

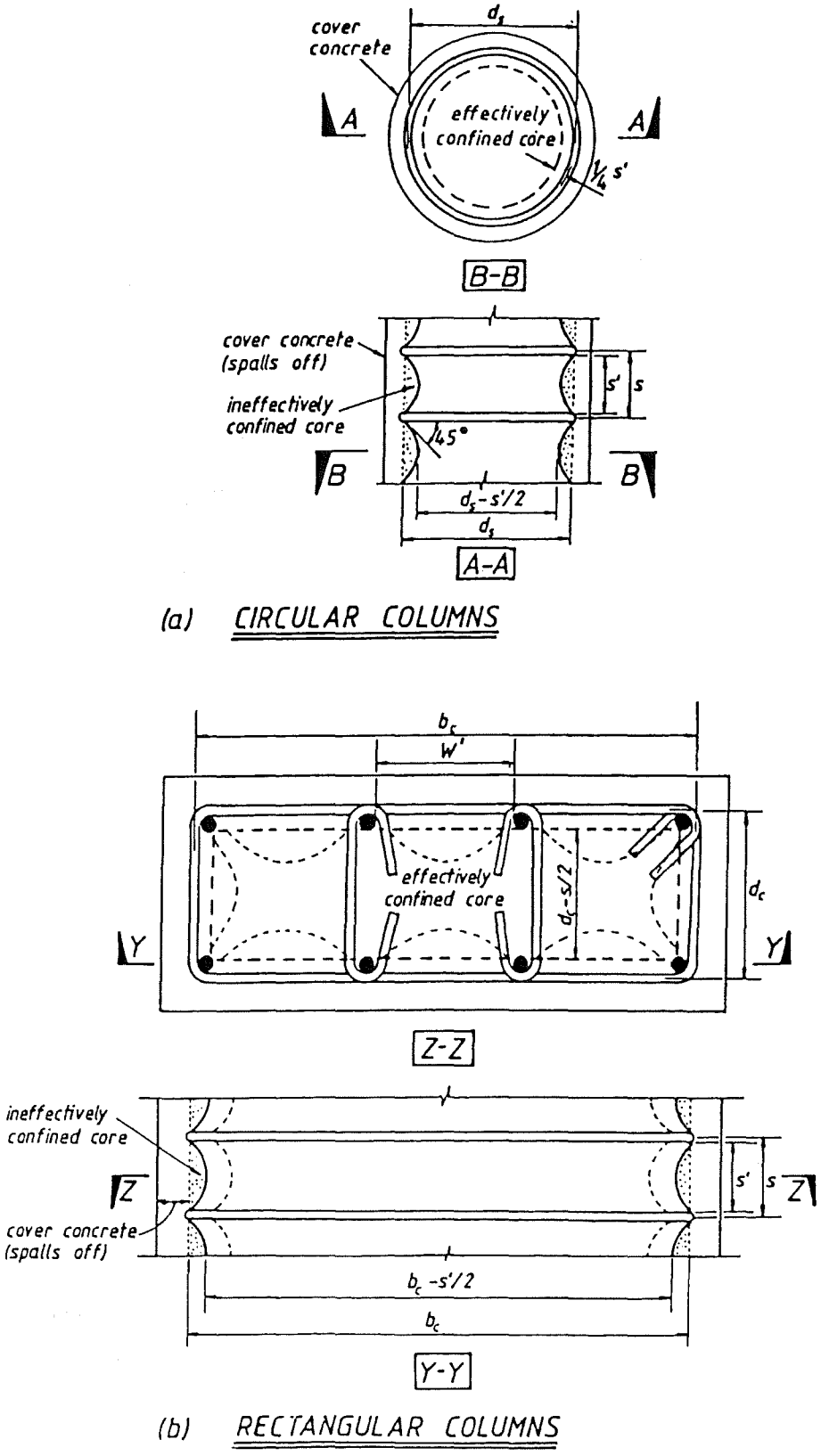

Figure 2.11 Assumed Arching Mechanism between Hoops [M10]

$$\lambda_1 = 1 - \frac{\sum_{i=0}^{n} \frac{w_{si}^2}{6} \tan\theta}{d_x d_y} \tag{2.11}$$

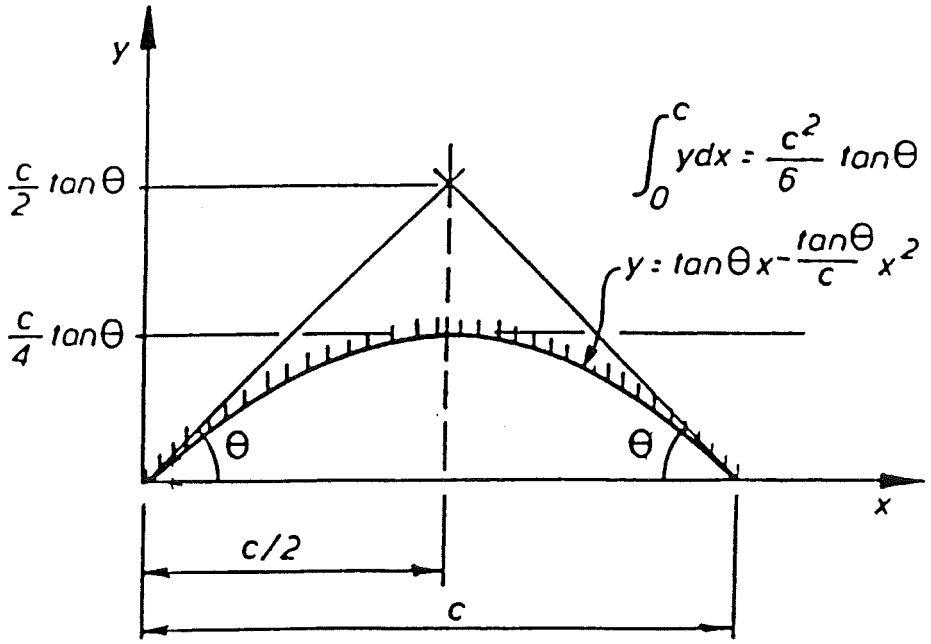

Figure 2.12 Section Properties of a Parabola [D2]

The area of the effectively confined core is then found by

$$A_e = \lambda\lambda_1 A_c \tag{2.12}$$

where A_c is the area within the centre line of the perimeter spiral or hoop. Sheikh and Uzumeri did regressional analysis to find the best value for θ and recommended that all arching action begins at an angle of 45 degrees.

Mander et al. [M11] assumed the same core dimensions and a similar arching mechanism as Sheikh and Uzumeri but they assumed that arching takes place between the clear spacing of reinforcements. The effectively confined core for circular hoops is shown in **Figure 2.11(a)** and is given by

$$A_e = \frac{\pi d_s^2}{4}\left(1 - \frac{0.5s'}{d_s}\right)^2 \tag{2.13}$$

where d_s is diameter of transverse hoop bar, and s' is clear spacing between hoops bars.

2.3.3 Effective Lateral Confining Pressure

Mander et al. assumed that the area of the confined concrete is the area of the concrete within the centre lines of the perimeter hoop, A_{cc}. That is, $A_e < A_{cc}$. Then, the effective lateral confining pressure is given by

$$f'_l = k_e f_l \tag{2.14}$$

where f_l is lateral pressure from the transverse reinforcement, assumed to be uniformly distributed over the surface of the concrete core, and the confining effectiveness coefficient k_e is represented by

$$k_e = \frac{A_e}{A_{cc}} \tag{2.15}$$

and

$$A_{cc} = A_c(1 - \rho_{cc}) \tag{2.16}$$

where ρ_{cc} is the ratio of area of longitudinal reinforcement to area of core of section, and A_c is area of core of section enclosed by the centre lines of the perimeter hoop. The area of effectively confined core, A_e, can be evaluated according to the previous description.

Therefore, the effective lateral confining stress on the concrete is obtained as,

for the confinement of a column with circular cross section:

$$f'_l = \frac{1}{2} k_e \rho_s f_{yh} \tag{2.17a}$$

and

$$\rho_s = \frac{4A_{sp}}{d_s s} \tag{2.17b}$$

where, ρ_s is volumetric ratio of confining reinforcement to core concrete, given in Eq.2.17b. A_{sp} is the area of spiral bar and d_s is the diameter of spiral.

For the confinement of a column with rectangular cross section in x-axis and y-axis:

$$f'_{lx} = k_e \rho_x f_{yh} \quad \text{in x-axis} \tag{2.18a}$$

$$f'_{ly} = k_e \rho_y f_{yh} \quad \text{in y-axis} \tag{2.18b}$$

and

$$\rho_x = \frac{A_{sx}}{sd_c} \tag{2.18c}$$

$$\rho_y = \frac{A_{sy}}{sb_c} \tag{2.18d}$$

where, ρ_x and ρ_y are the lateral steel ratio parallel to the x-axis and y-axis, respectively. f_{yh} is yield strength of transverse reinforcement. A_{sx} and A_{sy} are the total area of transverse bars running in the x and y directions, respectively.

2.3.4 Compressive Strength of Confined Concrete

To determine the confined compressive strength f'_{cc}, a constitutive model involving a specified ultimate strength surface for multiaxial compressive stresses is used. Mander et al. developed a model based on an ultimate surface model proposed by William and Warnke [W1] and calibrated by Elwi and Murray [E1] using the data from Schickert and Winkler [S1].

By assuming tension is positive, the minor, intermediate, and major principal stresses for a point on the failure surface corresponds to the confined concrete compressive strength, f'_{cc}, the smaller confining stress, f'_{l2}, and the larger confining stress, f'_{l1}. The general solution of the multiaxial failure criterion in terms of the two confining stresses is shown in **Figure 2.13**.

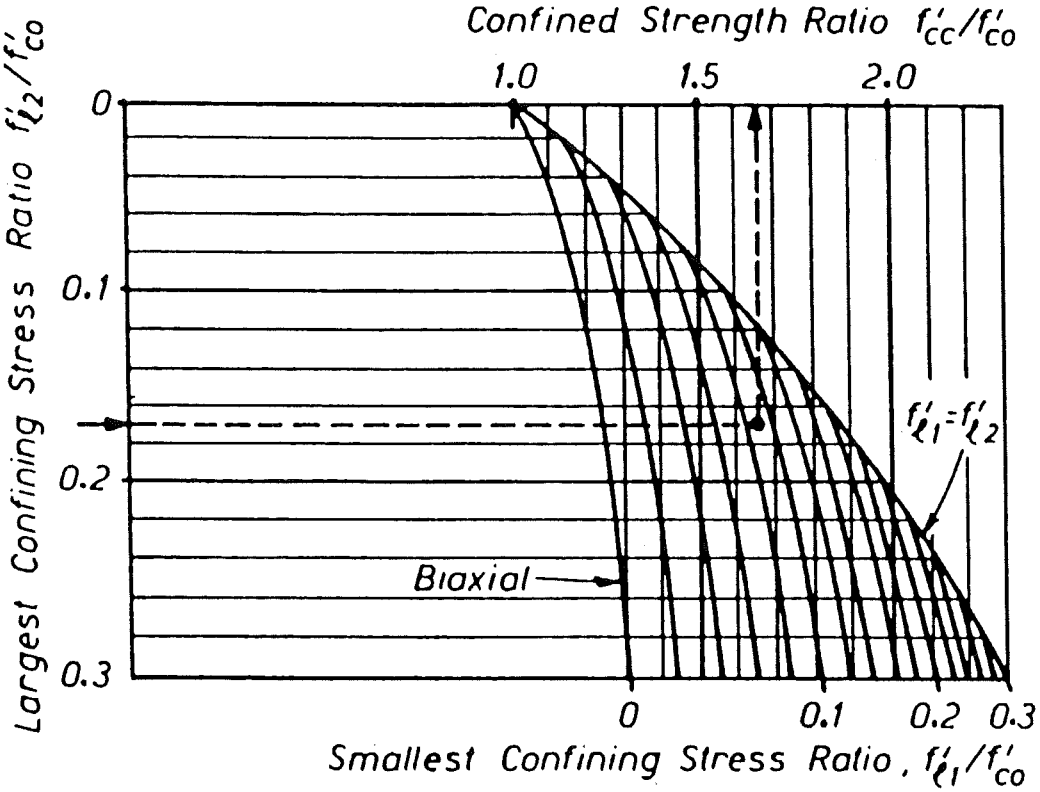

Figure 2.13 Confined Strength Determination from Lateral Confining Stresses for Rectangular Sections [M11]

In the case where the two confining stresses are equal, the closed-form solution for the confined concrete strength is given as

$$f'_{cc} = f'_{c0}\left(-1.254+2.254\sqrt{1+\frac{7.94f'_l}{f'_{c0}}}-2\frac{f'_l}{f'_{c0}}\right) \qquad (2.19)$$

where f'_{c0} is unconfined concrete compressive strength, and f'_l is given by Eq.2.17 for circular confined section or Eq.2.18 for square confined section.

2.3.5 Previous Investigations into Concrete Columns Retrofitted with ACM Jackets

ACM jackets confine the concrete column similarly to steel jackets. The jacket restrains the longitudinal reinforcement from buckling. The enhancement of ultimate concrete compressive strain permits higher plastic rotations and thus increases the curvature ductility capacity of the critical section in a column. Jackets manufactured using composite materials have been proved to significantly enhance the performance of reinforced concrete columns subjected to seismic loading [P9].

Design of ACM jackets for retrofitting of existing columns requires analytical tools that predict the confining strength of the concrete core. Limited research has been carried out to evaluate the confinement effectiveness of ACM jackets, taking into account the mechanics of fibre composites as well as the triaxial state of stresses in concrete core.

Katsumata et al. [K2] tested ten one-quarter scale column specimens with 200 mm square cross sections. The columns were strengthened with carbon fibre jackets before testing. They were tested under cyclic lateral loads and under constant axial loads. It was concluded that the jackets enhanced seismic performance. In particular, the ultimate displacement and energy dissipation capacity increased approximately linearly in accordance with carbon fibre volumetric ratio.

Saadatmanesh et al. [S14] adopted the concrete confining model proposed by Mander et al. [M11] to predict the strength and ductility of concrete columns externally confined by means of high-strength fibre composite straps. A parametric study was conducted to examine the effects of various design parameters such as concrete compressive strength, thickness and spacing of straps, and type of strap. The analytical results indicate that the strength and ductility of concrete columns can be significantly increased by wrapping high-strength fibre composite straps around the columns.

Rochette et al. [R4] used an incremental finite element approach to evaluate the response of fibre-wrapped square columns subjected to axial load. They modeled concrete as an elastic-perfectly plastic material, and adopted the Drucker-Prager failure

criterion. Their model, although it compares favorably with their own test results, does not provide a simple tool for the practitioner.

Restrepo and DeVino [R3] discussed a theoretical approach for finding the concentric load carrying capacity of rectangular reinforced concrete columns strengthened with an elastic jacket. They based their study on the model proposed by Mander et al. [M11] but assumed that the unconfined concrete, which cannot spall off the column, behaves as an elasto-plastic material. Analytical equations are derived to determine the capacity of axially loaded reinforced concrete columns which are confined by a combination of steel hoops and by composite jackets applied to the perimeter of the columns. It was shown that composite materials could be used for confining rectangular reinforced concrete columns.

SEQAD [S15] performed a series of axial compression tests on square concrete prisms wrapped with different thickness of high-strength fibreglass/epoxy jackets to investigate the influence of jacket thickness on concrete compressive stress-strain characteristics. The dimension of the square-section concrete prism is 207 mm square x 610 mm high. The nominal concrete strength of the concrete prisms is 35 MPa (5000 psi). The volumetric ratio of jacket, ρ_j, applied to concrete prisms was varied from 0.025 to 0.1, expressed as

$$\rho_j = 2t_j \frac{b+h}{bh} \tag{2.20}$$

where t_j is jacket thickness, and b, h are cross-section dimension. They concluded that the axially confined peak stress and corresponding strain are related only to the volumetric ratio of jacket and the jacket transverse strain for all test prisms wrapped with jackets is independent of jacket thickness at axial peak stress, kept as approximately constant as 0.002. Based on their test results, they proposed empirical equations referred as to Richart et al. [R9] shown in Eq.2.3 and Eq.2.4, given as

$$f'_{cc} = f'_{c0}(1+2\rho_j) \tag{2.21}$$

$$\varepsilon_{cc} = 0.002(1+9\rho_j) \tag{2.22}$$

Note that, for normal-strength concrete columns, a volumetric ratio of $\rho_j = 0.10$ satisfies the confinement requirement for columns with high axial load in accordance with ACI 318 Design Standard [A12]. That is after initial spalling of cover concrete the load capacity of the column remains higher than that of the column with unconfined gross section.

Mirmiran et al.[M12, M13] made a series of uniaxial compression tests on concrete-filled ACM tubes. The test specimens are 152.5 mm diameter x 305 mm high concrete cylinders. A comparison of test data with available confinement models indicates that while they produce acceptable results for steel-encased concrete, they overestimate the strength of ACM-encased concrete. This is attributed to their inability in estimating the dilatancy of confined concrete. They determined the volumetric strain ε_v and the tangential Poisson's ratio υ_t for ACM-wrapped concrete columns. The equations for these parameters are given as

$$\varepsilon_v = \varepsilon_a + 2\varepsilon_l \tag{2.23}$$

$$\upsilon_t = \frac{\Delta\varepsilon_l}{\Delta\varepsilon_a} = \frac{\varepsilon_{\ln ew} - \varepsilon_{lold}}{\varepsilon_{anew} - \varepsilon_{aold}} \tag{2.24}$$

where ε_a is the axial strain and ε_l is the lateral strain. Tensile strains are considered negative. Then they concluded that an effective confinement with fibre composites, unlike steel jackets, can reduce the dilation tendency of concrete, as it reverses the direction of volumetric strains.

Samaan and Mirmrian et al. [S17] extended their previous research into developing a model to predict the complete bilinear stress-strain response of ACM-confined circular column in both axial and lateral directions. The model is based on the test results to find the correlation between the dilation rate of concrete and the hoop stiffness of restraining member. The parameters of the model are directly related to the material properties of the ACM jacket and concrete core. According to these researches, the predicted stress-strain curves compare well with the results of their study as well as with tests conducted by others. However, it is doubtable whether their proposed

empirical equations for evaluating the relationship of concrete expansion between longitudinal and transverse direction can be applied to the prediction of general behaviour of concrete or not.

PART II

RETROFIT OF REINFORCED CONCRETE BEAMS

CHAPTER 3

ANALYTICAL STUDY OF RC BEAMS WITH EXTERNALLY BONDED ADVANCED COMPOSITE MATERIAL LAMINATES

3.1 Introduction

In this chapter a model for the analysis of ACM laminates externally bonded to beams is developed. Tee section reinforced concrete beams with carbon ACM laminates bonded to their soffit and glass ACM laminates applied to their sides are analysed. Chapter 4 includes test results used to calibrate the proposed model.

The model presented in this chapter builds upon the segmental model developed by Arduini and Nanni [A8, A9]. The improvements found in the latter model relate to consideration of the effects caused by diagonal tension cracking and refinement in the numerical evaluation of the bond and normal stresses. Moment-curvature analysis is extensively used in the proposed model. The following assumptions are used:

- Plane sections remain plane under bending,
- The tensile strength of concrete is ignored,
- Perfect bond exists between composite laminate and concrete beam,
- The presence of the adhesive layer between the composite laminate and the reinforced concrete beam is ignored.

The analytical procedure is summarised in schematic form in **Figure 3.1**. The main steps and assumptions made in the procedure are described in the following sections.

3.2 Material Properties

The stress-strain relationship of reinforcing steel is assumed to be tri-linear as

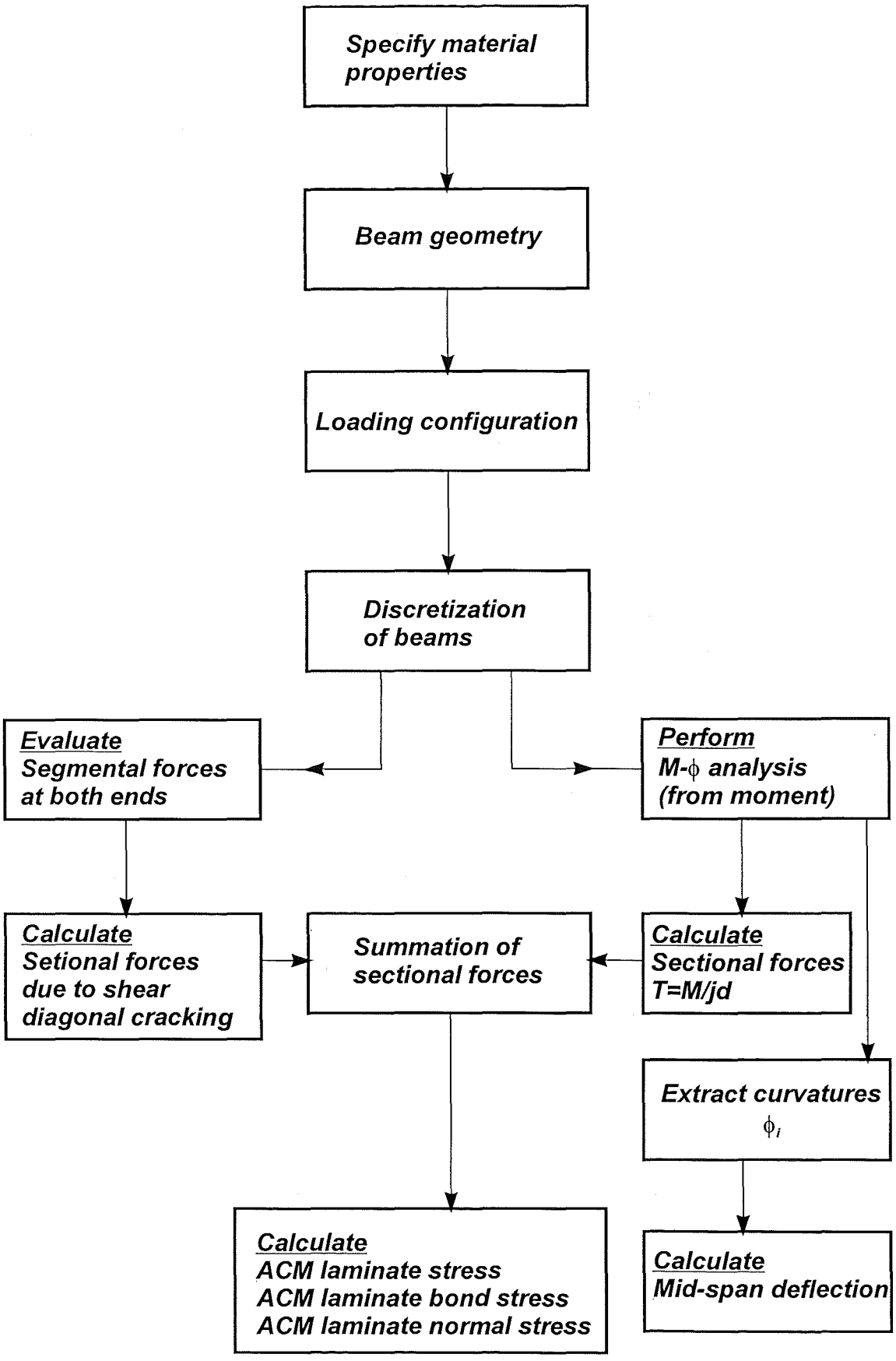

Figure 3.1 Segmental Analysis of Beams Reinforced with Flexural ACM Laminate

shown in **Figure 3.2(a)**.

Hongnestad's parabola to idealise the stress-strain relationship for concrete is used. **Figure 3.2(b)** depicts the stress-strain curve of concrete [C4], where f'_c is concrete cylinder compressive strength, E_c is the initial tangent modulus of concrete, which gives $E_c = 4730\sqrt{f'_c}$ MPa for normal-weight concrete, f_{cr} is the direct tensile cracking strength, and ε_{cr} is the strain corresponding to the stress f_{cr}. Normally the strain ε'_c at maximum concrete compressive strength is assumed equal to 0.2% and the maximum strain ε_{cu} is 0.3%. Note that the presence of confining reinforcement in beams is unlikely to significantly affect the load-deflection response. For this reason the simple parabolic representation of the stress-strain behaviour has been adopted in the study.

In general the ACM laminates behave in a linear elastic manner up to failure. A wide range of composites with different mechanical properties is available. **Figure 3.2(c)** illustrates two composite laminates, carbon ACM and glass ACM, which were used in the analytical study. The relevant properties are f_{pu1} = 600 MPa with E_{p1} = 60 GPa for carbon ACM, and f_{pu2} = 320 MPa with E_{p2} = 20 GPa for glass ACM, where f_{pu} and E_p are the ultimate strength and the modulus of elasticity of the laminates, respectively.

3.3 Section Analysis

The strains and stresses in the ACM laminate, steel longitudinal reinforcement, and concrete, as well as curvature, are calculated using an incremental deformation technique described in this section. For convenience of calculations, the strain in the extreme fibre of the concrete ε_{ct} is increased in increments to generate the moment-curvature relationships.

Figure 3.3 shows the strains and stresses across the depth of a typical T-beam section with a composite laminate bonded to the tension face of the beam. The strain in the extreme fibre of the beam, ε_{ct}, is increased until failure is reached. It is assumed that failure is reached when either the concrete strain reaches ε_{cu}=0.003 or the composite laminate reaches its ultimate tensile strain. The strains in the reinforcing bars in the

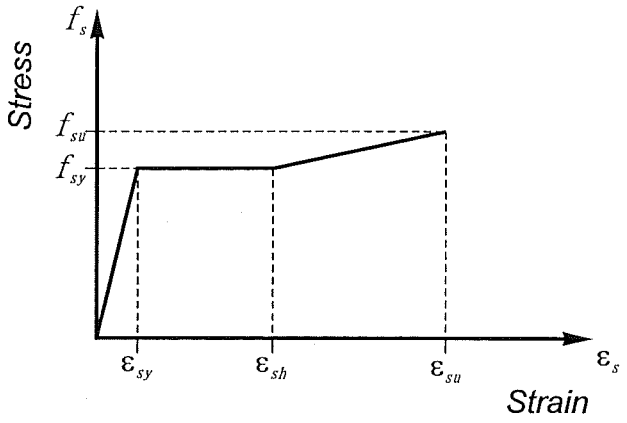

(a) Tri-linear Steel Model

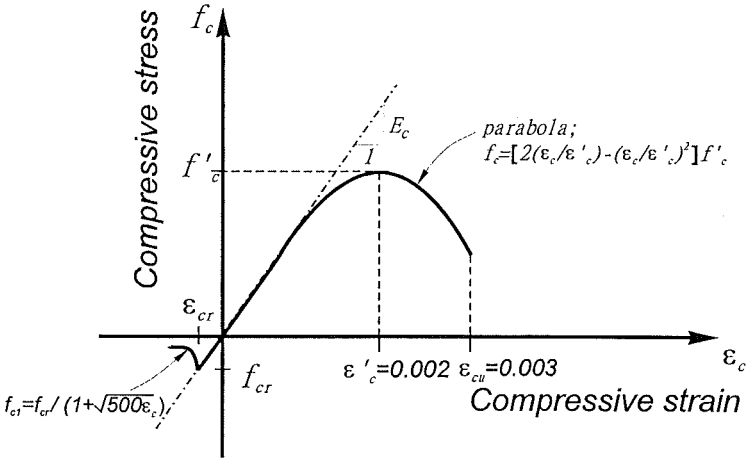

(b) Concrete Model

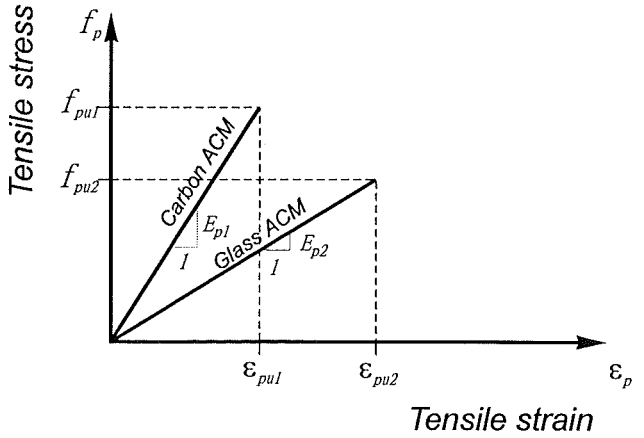

(c) ACM

Figure 3.2 Idealised Material Stress-Strain Curves

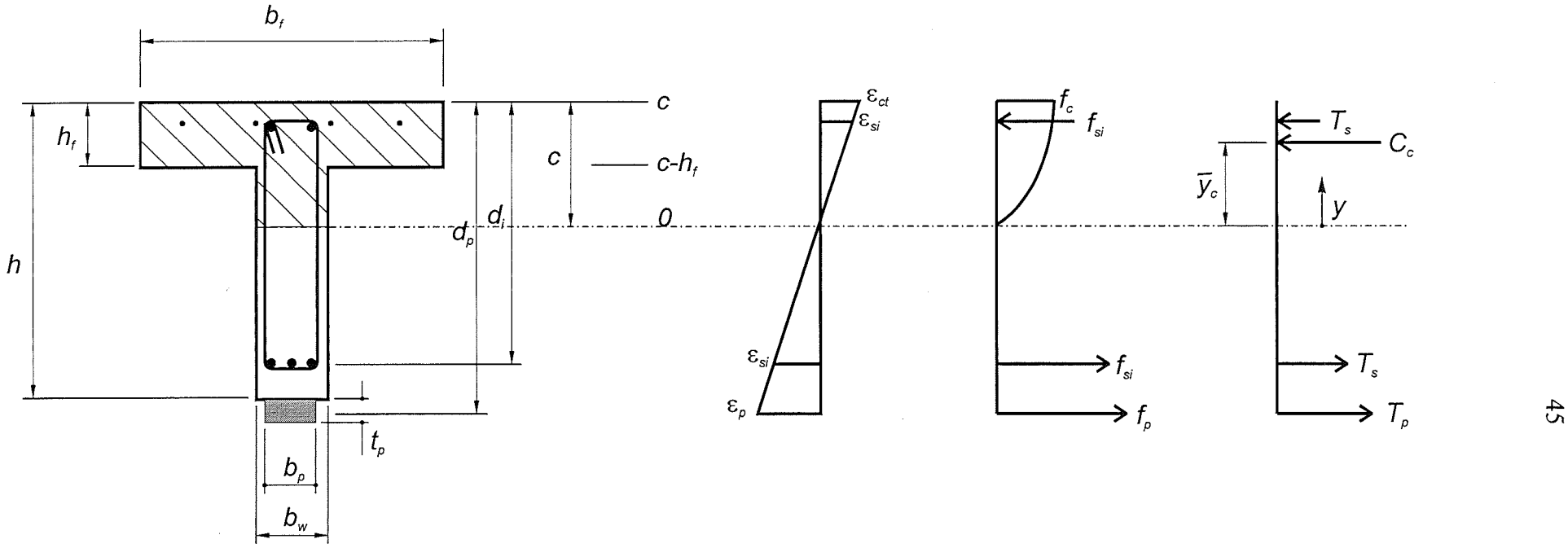

Figure 3.3 Flexural Strain, Stress, and Force Diagrams across Depth of a T-beam Section

composite laminate are calculated in terms of ε_{ct} using strain compatibility,

$$\varepsilon_{si} = \varepsilon_{ct}\frac{c - d_i}{c} \tag{3.1}$$

$$\varepsilon_{p} = \varepsilon_{ct}\frac{c - d_p}{c} \tag{3.2}$$

where ε_{si} is the strain in steel rebar at level i, c is the distance to neutral axis measured from top concrete fibre, d_i is the distance from top concrete fibre to centroid of steel rebar in layer i, ε_p is the strain in composite laminate, and d_p is the distance from top concrete fibre to centroid of the composite laminate.

The reinforcing steel stresses f_{si} and the ACM laminate stress f_p corresponding to strains ε_{si} and ε_p are found from the stress-strain curves for steel and ACM material as shown in **Figure 3.2(a) and (c)**.

$$f_{si} = E_s\varepsilon_{si}\text{ , if } \varepsilon_{si} \le \varepsilon_{sy} \tag{3.3a}$$

$$f_{si} = f_{sy}\text{ , if } \varepsilon_{sy} < \varepsilon_{si} \le \varepsilon_{sh} \tag{3.3b}$$

$$f_{si} = f_{sy} + \frac{\varepsilon_{si} - \varepsilon_{sh}}{\varepsilon_{su} - \varepsilon_{sh}}(f_{su} - f_{sy})\text{ , if } \varepsilon_{sh} < \varepsilon_{si} \le \varepsilon_{su} \tag{3.3c}$$

and

$$f_p = E_p\varepsilon_p \tag{3.4}$$

where E_s is modulus of elasticity of steel, E_p is modulus of elasticity of the composite laminate, ε_{sy} is the yield strain of steel, f_{sy} is the yield stress of steel, ε_{sh} is the steel strain at the commencement of strain-hardening, ε_{su} is the ultimate steel strain, and f_{su} is the ultimate steel stress, as is also depicted in **Figure 3.2(a)**.

The steel force T_s, and the ACM laminate force T_p are found by multiplying the stresses by their corresponding areas and the laminate stress by laminate area, respectively.

$$T_s = \Sigma f_{si} A_{si} \tag{3.5}$$

$$T_p = f_p A_p \tag{3.6}$$

where A_{si} is total area of steel in layer i, and A_p is the cross section area of the composite laminate.

The distribution of concrete stresses in the compression zone is found from the stress-strain curve of concrete shown in **Figure 3.2(b)**. The parabolic shape of concrete stress-strain relationship in compression proposed by Hognestad [C4] is expressed as follows:

$$f_c(\varepsilon_c) = f_c^{'}\left[2\frac{\varepsilon_c}{\varepsilon_c^{'}} - \left(\frac{\varepsilon_c}{\varepsilon_c^{'}}\right)^2\right] \tag{3.7}$$

where $f_c(\varepsilon_c)$ is concrete compressive stress, and ε_c is concrete compressive strain.

As mentioned in the assumption, the tensile stress of the concrete is neglected in the bending analysis. Hence the magnitude of the concrete compressive force is given by Eq.3.8.

$$C_c = \int_0^{c-h_f} f_c b_w dy + \int_{c-h_f}^{c} f_c b_f dy \tag{3.8}$$

The location of the resultant force C_c is represented by,

$$m_c = \int_0^{c-h_f} f_c b_w y dy + \int_{c-h_f}^{c} f_c b_f y dy \tag{3.9}$$

$$\overline{y_c} = \frac{m_c}{C_c} \tag{3.10}$$

It is noted that b_w and $c\text{-}h_f$ can be set to zero in Eqs.3.8 and 3.9 when the neutral axis falls within the thickness of the flange, which is same as the case of rectangular

section with a constant width of b_f.

The location of the neutral axis c is obtained from the equilibrium of internal forces as given by Eq.3.11. Eq.3.11 is solved iteratively until equilibrium of forces across the depth of the cross section is satisfied.

$$C_c + T_s + T_p = 0 \tag{3.11}$$

The internal moment of resistance is obtained by summing the moments of resulting from internal forces about an axis.

$$M = C_c \overline{y_c} + \sum_{i=1}^{n} f_{si} A_{si} (d_i - c) + f_p A_p (d_p - c) \tag{3.12}$$

The curvature, by definition, is equal to

$$\phi = \frac{\varepsilon_{ct}}{c} \tag{3.13}$$

3.4 Evaluation of the Additional Tensile Forces in the Beam Resulting from Diagonal Tension Cracking

Since the early days of research into reinforced concrete members, it was recognised that upon the development of diagonal tension cracking, a truss model could explain, with some degree of satisfaction, the reason why the forces in the reinforcement in tension are not proportional to the bending moment acting there [M9]. A disadvantage of truss models is that they are unable to provide an insight into the transition of beam to truss behaviour. That is, the development of the additional tensile forces in the tension reinforcement cannot be predicted with truss models. The most accurate and rational method that can describe this transition is the Modified Compression Field Theory (MCFT) developed by Collins and Mitchell [C4].

In the MCFT, reinforced concrete is treated as a composite material with its own

stress-strain characteristics. Equilibrium, compatibility, and constitutive relationships are formulated in terms of average stress and average strain. Variability in the angle of inclination of the diagonal compression stress field and strain-softening in the response are considered. The MCFT can be applied to the analysis of reinforced concrete beams subjected to shear, moment, and axial load at any loading level, including beams which are reinforced in flexure and shear with elastic materials as ACM laminates. Hence, the MCFT is implemented in this study as part of the refined analytical model for the prediction of the behaviour of ACM composite beam at any load level. Although too complex for regular use in the design, the procedure has its ability to provide a rational method in analysis.

The procedure for predicting the response using the MCFT of a beam with a ACM laminate applied to its soffit and loaded in shear and bending moment is described below. Following the calculation steps, many variables will be mainly explained in the segmental model with ACM laminates as **Figure 3.4** shows. The calculation steps are,

(1) Guess a principal strain, ε_1.

(2) Guess the inclination, θ, of the diagonal compression stress field.

(3) Calculate the diagonal crack width, ω,

$$s_{mx} = 2c_x + \frac{d_{bx}}{10\rho_x} \tag{3.14a}$$

$$\rho_x = \frac{A_{sx}}{b_w h} \tag{3.14b}$$

$$s_{mv} = 2\left(c_v + \frac{s}{10}\right) + \frac{d_{bv}}{10\rho_v} \tag{3.14c}$$

$$\rho_v = \frac{A_{vs}}{b_w s} \tag{3.14d}$$

$$s_{m\theta} = \frac{1}{\frac{\sin\theta}{s_{mx}} + \frac{\cos\theta}{s_{mv}}} \tag{3.15}$$

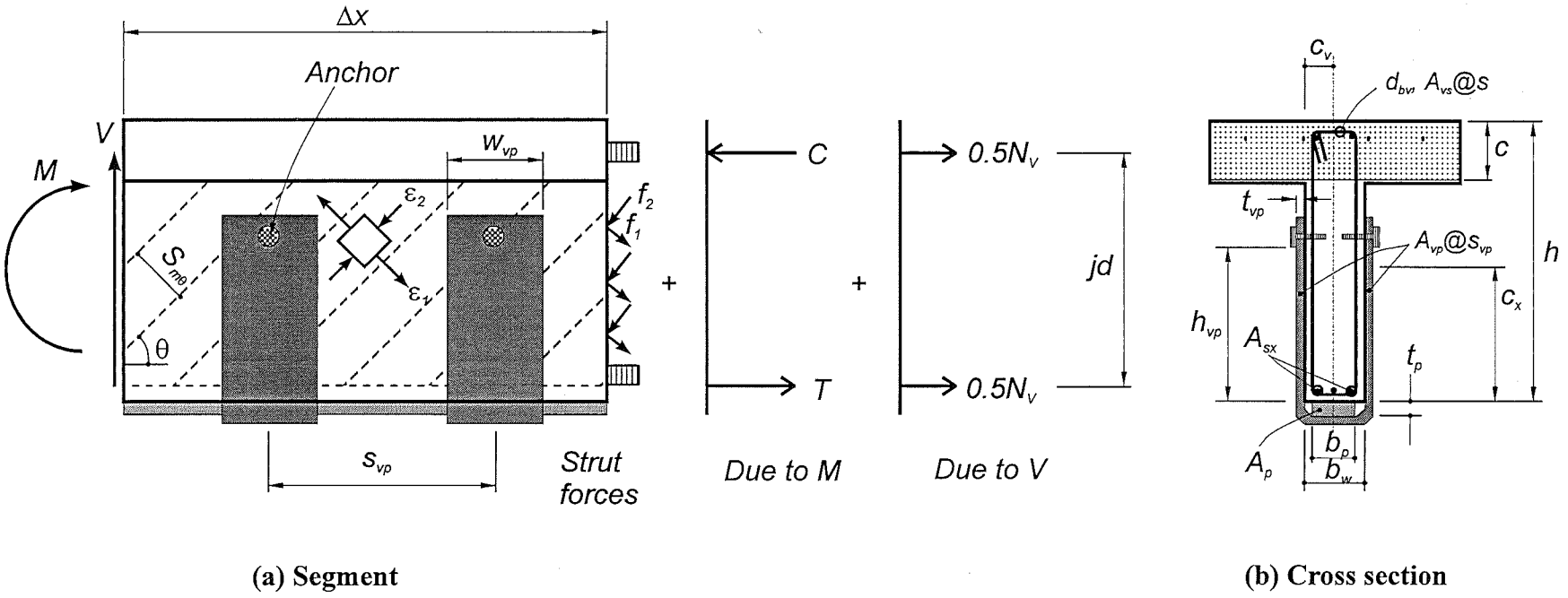

(a) Segment **(b) Cross section**

Figure 3.4 MCFT Model for Beams with ACM Laminates

$$\omega = \varepsilon_1 s_{m\theta} \tag{3.16}$$

where, s_{mx} and s_{mv} are the crack spacings resulting from the crack control characteristics of the longitudinal and transverse reinforcement, respectively. Variables c_x and c_v are the maximum distance for clear cover in longitudinal and transverse direction (see **Figure 3.4(b)**).

(4) Estimate a value for transverse strain ε_t and check the stress in steel stirrup f_{vs} and in the ACM stirrup f_{vp}.

$$f_{vs} = E_s \varepsilon_t \le f_{vsy} \tag{3.17}$$

$$f_{vp} = E_p \varepsilon_t \le f_{vpe} \tag{3.18}$$

where f_{vsy} is yield stress in the steel stirrup and f_{vpe} is effective stress in the ACM stirrup.

(5) Calculate principal tensile stress f_1,

$$f_1 = E_c \varepsilon_1 \text{ for } \varepsilon_1 \le \varepsilon_{cr} \tag{3.19a}$$

$$f_1 = \frac{f_{cr}}{1+\sqrt{500\varepsilon_1}} \text{ for } \varepsilon_1 > \varepsilon_{cr} \tag{3.19a}$$

or

$$f_1 = v_{ci} \tan\theta + \frac{A_{vs}}{s b_w}\left(f_{vsy} - f_{vs}\right) + \frac{A_{vp}}{s_{vp} b_w}\left(f_{vpe} - f_{vp}\right) \tag{3.20a}$$

$$v_{ci} = \frac{0.18\sqrt{f_c'}}{0.3 + \frac{24\omega}{a+16}} \tag{3.20b}$$

whichever is less and

where v_{ci} is the interface shear stress in cracks developed along the diagonal compression stress field. Variable a is the maximum aggregate size, which is assumed here to be 20mm in the case of normal reinforced concrete.

(6) Calculate the resulting shear force, V,

$$V = f_1 b_w jd \cot\theta + \frac{A_{vs} f_{vs}}{s} jd \cot\theta + \frac{A_{vp} f_{vp}}{s_{vp}} h_{vp} \cot\theta \tag{3.21}$$

where jd is flexural level arm and h_{vp} is the effective height of the ACM stirrups (see **Figure 3.4(b)**).

(7) Calculate the principal concrete compressive stress, f_2,

$$v = \frac{V}{b_w jd} \tag{3.22}$$

$$f_2 = (\tan\theta + \cot\theta)v - f_1 \tag{3.23}$$

(8) Calculate the strength of the diagonal compression stress field,

$$f_2 = f_{2\max}\left[2\left(\frac{\varepsilon_2}{\varepsilon'_c}\right) - \left(\frac{\varepsilon_2}{\varepsilon'_c}\right)^2\right] \tag{3.24a}$$

$$\text{where, } \frac{f_{2\max}}{f'_c} = \frac{1}{0.8 + 170\varepsilon_1} \le 1.0 \tag{3.24b}$$

(9) Check if $f_2 \le f_{2max}$. If it is not, the solution is not possible. Return to step (1) and try a smaller value for ε_1.

(10) Calculate the following strains.

$$\varepsilon_2 = \varepsilon'_c\left(1 - \sqrt{1 - f_2 / f_{2\max}}\right) \tag{3.25}$$

$$\varepsilon_x = \frac{\varepsilon_1 \tan^2\theta + \varepsilon_2}{1 + \tan^2\theta} \tag{3.26}$$

$$\varepsilon_t = \frac{\varepsilon_1 + \varepsilon_2 \tan^2\theta}{1 + \tan^2\theta} \tag{3.27a}$$

$$\gamma = 2(\varepsilon_x - \varepsilon_2)\cot\theta \tag{3.27b}$$

where, γ is the shear strain in the web. Variables ε_1 and ε_2 are the principal concrete tensile and compressive strain. Variables ε_x and ε_t are the longitudinal and transverse strain in the beam, respectively.

(11) Calculate the stresses f_{vs} and f_{vp} corresponding to the strains calculated in Step (10), and check with the estimate of ε_t, f_{vs}, and f_{vp} in Step (4). If necessary, revise the estimate and return to Step (5).

(12) Use Eq.3.28 to determine an equivalent axial force N_p caused by an equivalent axial strain ε_x, found by setting at the level of jd/2 in the sectional strain distribution that corresponds to a given moment (see **Figure 3.5**).

$$0.5N_p = E_s\varepsilon_x A_s + E_p\varepsilon_x A_p \tag{3.28}$$

where A_s is area of the longitudinal tensile steel reinforcement and A_p is cross section area of the longitudinal tensile ACM reinforcement.

(13) In the case of a member subjected only to moment and shear, the resulting internal axial force N must be zero. Thus,

$$N = N_p - V\cot\theta + f_1 b_w jd \tag{3.29}$$

If Eq. 3.29 is not satisfied, a new estimate of θ is required and a new iteration must be carried out from Step (3).

3.5 Section Forces

Once the iterative procedure discussed in the previous section converges, the section forces can be computed. With reference to **Figure 3.6**, the resulting section forces of an analytical segment can be estimated as below.

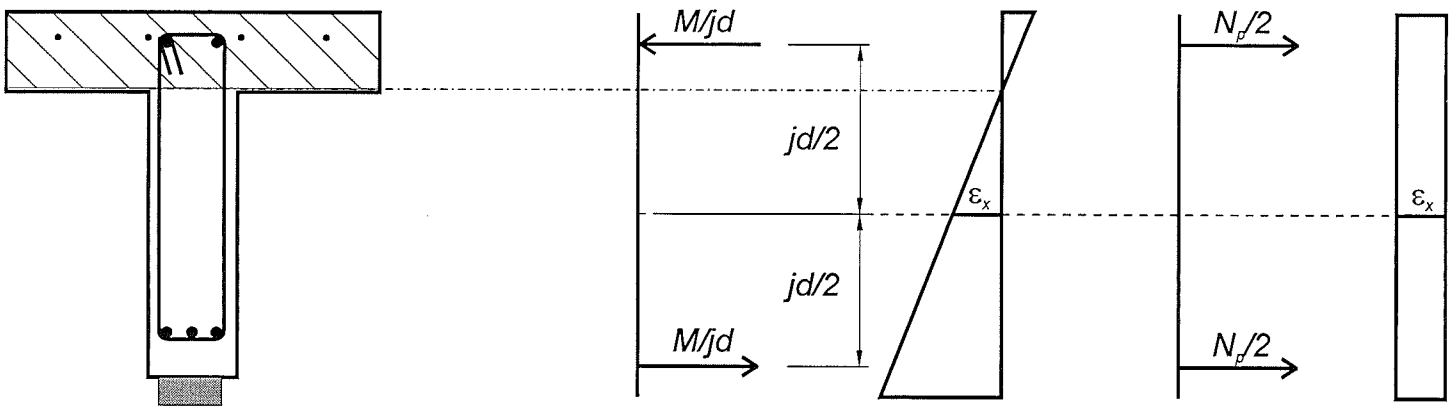

(a) cross section

(b) forces and strain due to moment M

(c) forces and strain due to equivalent axial force N_p

Figure 3.5 Comparison of Forces and Strains due to Moment and Its Equivalent Axial Force

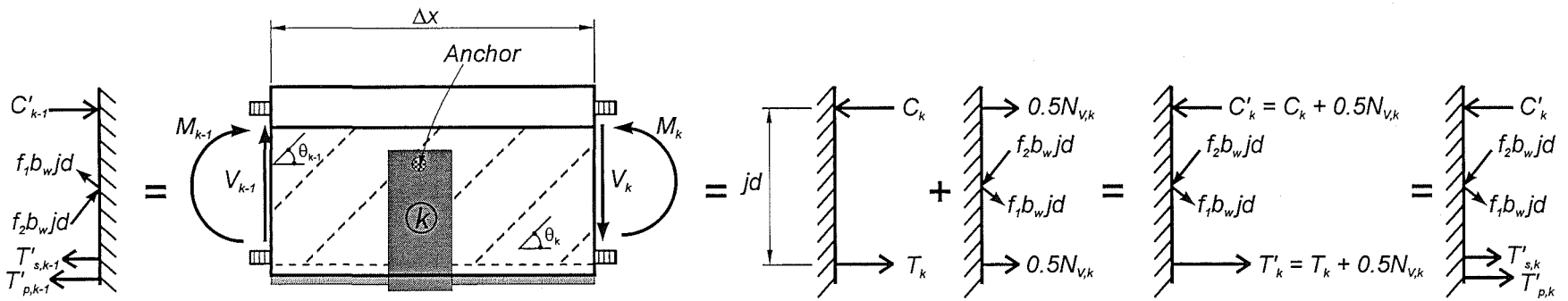

(a) Segment k **(b) Due to M_k** **(c) Due to V_k** **(d) Total resultant forces** **(e) Tensile component forces**

Figure 3.6 Diagrams for the Components of Resultant Sectional Forces

$$C_k = T_k = \frac{M_k}{jd_k} \tag{3.30}$$

$$N_{V,k} = f_2 b_w jd \cos\theta_k - f_1 b_w jd \cos\theta_k \tag{3.31}$$

where T_k and C_k are the sectional forces, resulting from bending, in tensile and compressive chord respectively. f_1 is the tensile stress resulting from the diagonal tension field and f_2 is the compression stress resulting from the diagonal compression stress field. $N_{v,k}$ is the equivalent axial force due to shear. At joint k-1, the sectional forces are the same as the above equations by substituting sub-index k for k-1.

In **Figure 3.6(d)**, the total resultant force in tensile chord T'_k can be obtained.

$$\begin{aligned} T'_k &= T_k + 0.5N_{v,k} \\ &= \frac{M_k}{jd_k} + 0.5\left(f_2 b_w jd \cos\theta_k - f_1 b_w jd \cos\theta_k\right) \end{aligned} \tag{3.32}$$

The total resultant forces in tensile chord, T'_k, can further be divided into two component forces in tension given in Eq.3.33 (see **Figure 3.6(e)**).

$$T'_k = T'_{s,k} + T'_{p,k} \tag{3.33}$$

where $T'_{s,k}$ and $T'_{p,k}$ are the steel and ACM component forces of the reinforcement in the tensile chord. The relationship of these individual tensile forces can also be represented as:

$$T'_{s,k} = T_{s,k} + 0.5N_{vs,k} \le f_{su} A_s \tag{3.34a}$$

$$T'_{p,k} = T_{p,k} + 0.5N_{vp,k} \le f_{pu} A_p \tag{3.34b}$$

where $T_{s,k}$ and $T_{p,k}$, are the tensile forces resulting bending moment only. $N_{vs,k}$ and $N_{vp,k}$ are the equivalent axial forces resulting from the diagonal stress field carrying the shear force. These forces are given by

$$T_{p,k} = E_p \varepsilon_p A_p \tag{3.35a}$$

$$\begin{aligned} T_{s,k} &= T_k - T_{p,k} \\ &= \frac{M_k}{jd_k} - E_p \varepsilon_p A_p \end{aligned} \tag{3.35b}$$

$$N_{vp,k} = N_{v,k} \frac{T_{p,k}}{T_k} \tag{3.36a}$$

$$N_{vs,k} = N_{v,k} \frac{T_{s,k}}{T_k} \tag{3.36b}$$

Note that the individual resultant tensile forces given by Eq.3.35 are needed to evaluate the concrete-to-ACM laminate interface bond stresses.

3.6 ACM/Concrete Bond Stresses

The actual distribution of the concrete-to-ACM laminate interface bond stress follows an exponential form as mentioned in the previous chapter [L1, K1]. A trapezoidal shaped bond stress distribution at the adhesive-concrete interface is assumed in each segment. The appropriate explanation in deriving the concrete-to-ACM interface bond stresses may be determined in relation to **Figure 3.7**. In each segment, the ACM laminate forces at both ends are obtained previously and then a mean bond stress in the segment can be evaluated. Thus the differential laminate force in each segment is represented as,

$$\begin{aligned} \Delta T_{p,k} &= T'_{p,k} - T'_{p,k-1} \\ &= \frac{\tau_{p,k-1} + \tau_{p,k}}{2} \times \Delta x \times b_p \end{aligned} \tag{3.37a}$$

Although the actual bond stresses, $\tau_{p,k-1}$ and $\tau_{p,k}$, at both ends of each segment can not be achieved in the analytical method, a mean value of bond stress in a segment is computed as depicted in **Figure 3.7(b)** and **(c)**.

$$\bar{\tau}_{p,k} = \frac{\tau_{p,k-1} + \tau_{p,k}}{2} \tag{3.37b}$$

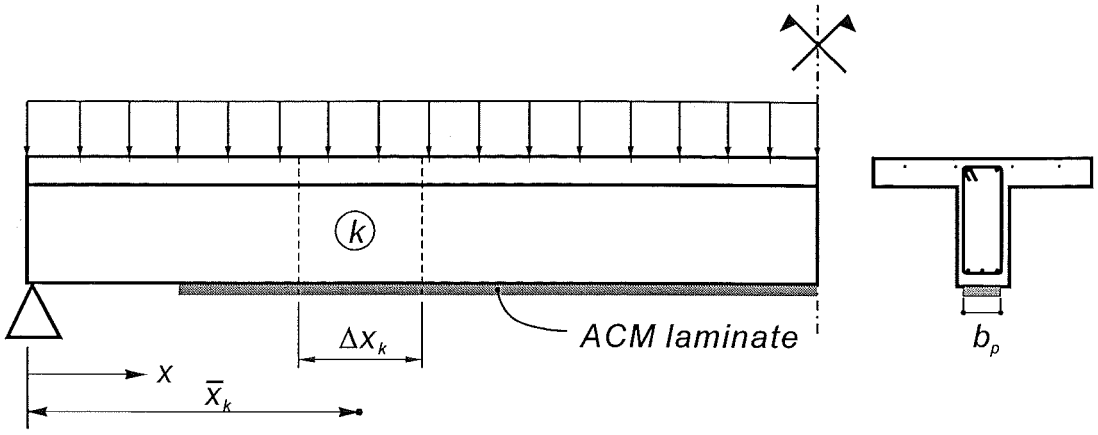

(a) Analytical beam

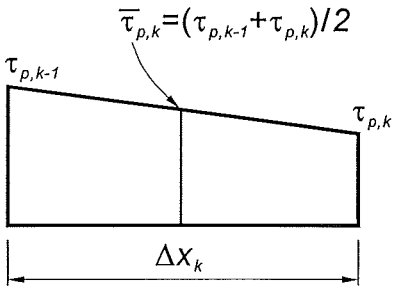

(b) Assumed bond stress distribution in a segment

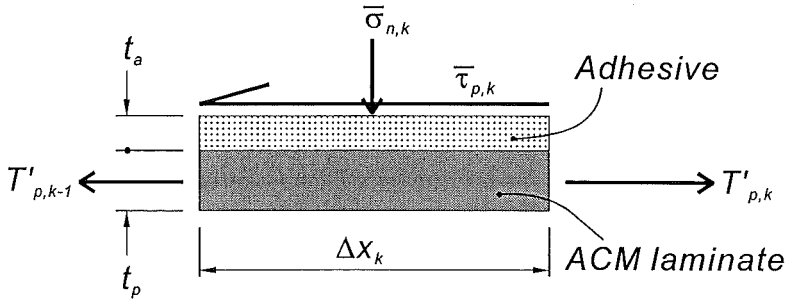

(c) Internal stresses acting on ACM laminate

Figure 3.7 ACM Bond Stress Distribution in the Analytical Segment Model

Replacing Eq.3.37a by Eq.3.37b, the mean laminate bond stress in each segment can be determined as,

$$\bar{\tau}_{p,k} = \frac{T'_{p,k} - T'_{p,k-1}}{b_p \Delta x} \tag{3.38}$$

Similarly, the tensile stress normal to the same interface is also assumed to be linear at the both ends of the segment. The mean normal bond stress acting on the ACM laminate of each segment is evaluated as,

$$\bar{\sigma}_{np,k} = \left[\left(T'_{p,k} - T'_{p,k-1} \right) \left(t_a + \frac{t_p}{2} \right) \right] \frac{6}{b_p \Delta x^2} \tag{3.39}$$

where, t_p and t_a are the thicknesses of the ACM laminate and adhesive respectively and b_p is the width of ACM laminate.

3.7 Calculation of Beam Deformation

In the analysis presented above, the relationships for the concrete-to-ACM interface behaviour were derived. It is of further interest to calculate the beam deformation for a given loading configuration and support system. In a uniformly loaded, simply supported beam with a span of *l*, the deflection at mid-span can be expressed by Eq.3.40. This is basically derived using the first moment area method under the curvature diagram.

$$\Delta = \int_0^{0.5l} \phi x dx \tag{3.40}$$

In order to find the deflection it is convenient to perform the integration numerically. Eq.3.40 can be approximated by a summation of discrete terms [C4],

$$\Delta = \sum_{k=1}^{n} \left(\frac{\phi_{k-1} x_{k-1} + \phi_k x_k}{2} \right) \Delta x_k \tag{3.41}$$

where x_k is the location of the beam measured from the support, and Δx_k is the length of a given segment k. For the first segment 1 where the support is located, curvature ϕ_0 and location x_0 become zero. In the computation of beam deformation for a simple-supported beam, small slopes are assumed, neglecting the difference between curved and straight infinitesimal lengths. Also the effects of shear are disregarded as it is assumed that the deformation due to shear is relatively small in comparison with that due to flexure.

3.8 Parametric Analysis

To investigate the influential factors on the result of the analytical model, a parametric analysis on case studies was conducted. The analysis was performed to evaluate the sensitivity of the model to the width of the segments, the effect of loading configuration, and the layout of the ACM laminates. In addition the proposed model was compared with the model developed by Arduini and Nanni [A9]. A Tee-section simple supported beam with 5m long was chosen for conducting the case studies. The beam is shown in **Figure 3.8(a)**. The materials given in Section 3.2 were adopted in the analysis. **Figure 3.8(b)** illustrates the case studies analysed.

3.8.1 Comparison of Analytical Results between Two Models

This section compares the results obtained with the model proposed in this study and that proposed by Arduini and Nanni [A9]. In the latter mode the influence of diagonal tension cracking due to shear is not considered.

In the following discussion, the Arduini and Nanni is referred to as the M segment model (the segment model considering the effect of bending) whereas the model proposed in this study is referred to as the MV segment model (the segment model considering the effect of bending and shear). The differences of the analytical results between these two models can be seen in **Figure 3.9**. Case 3 shown in **Figure 3.8(b)** is

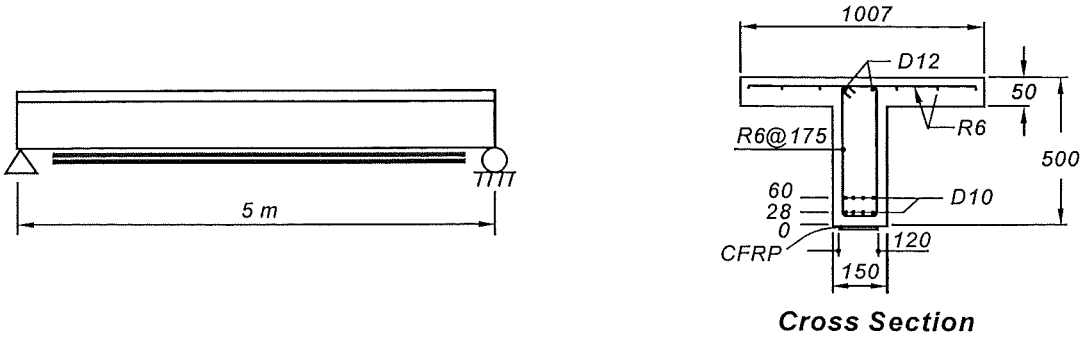

(a) Details of Simple Supported Tee Beam

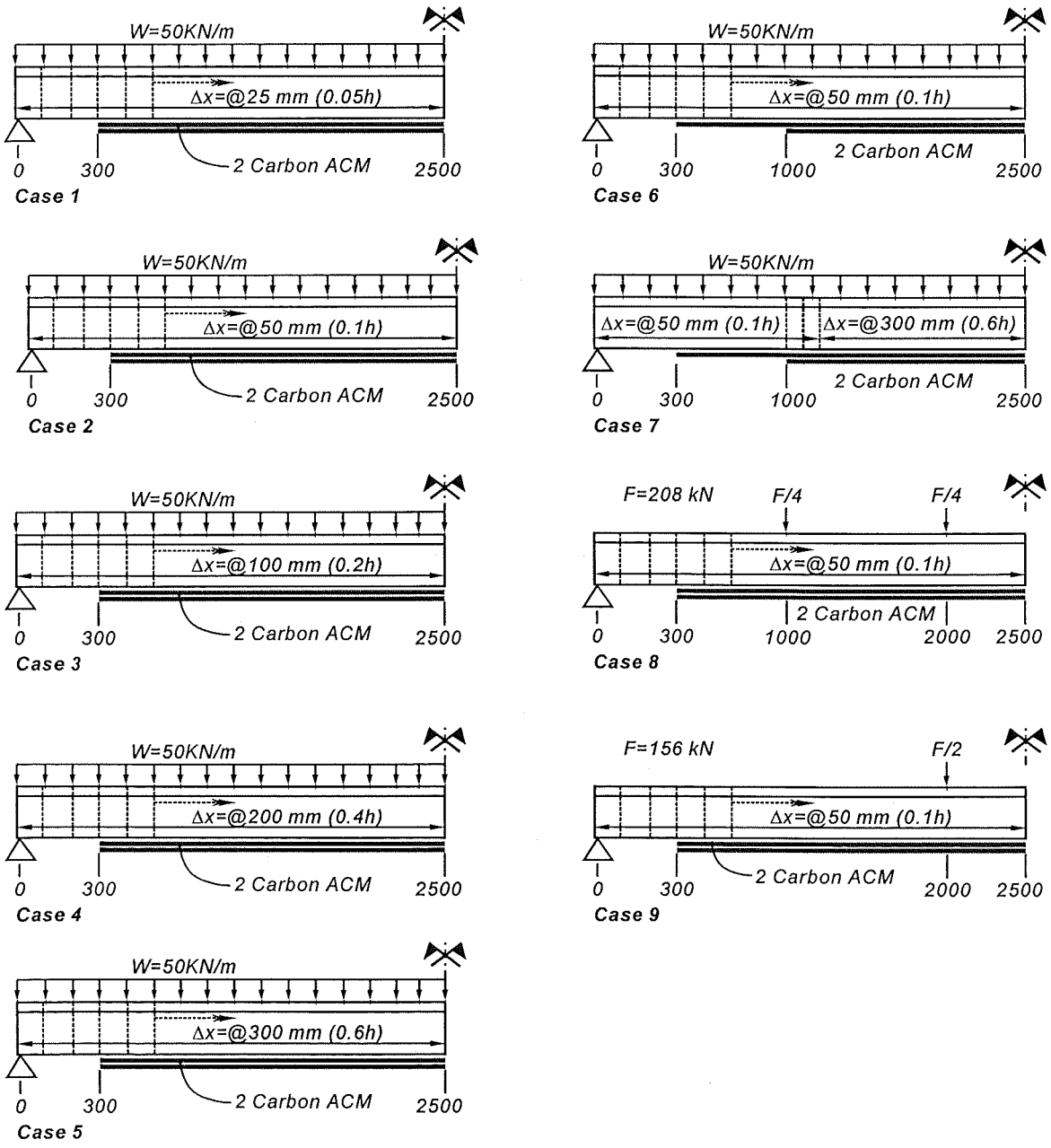

(b) Case Studies in the Segmental Analysis

Figure 3.8 Case Studies

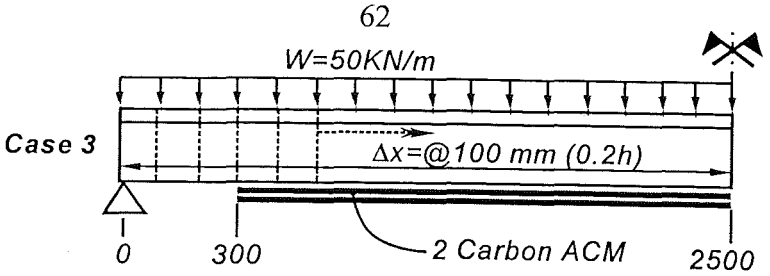

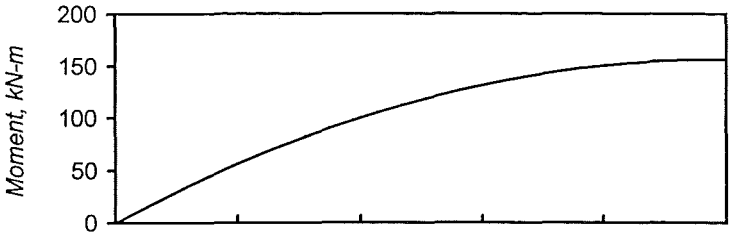

(a) Bending Moment Diagram

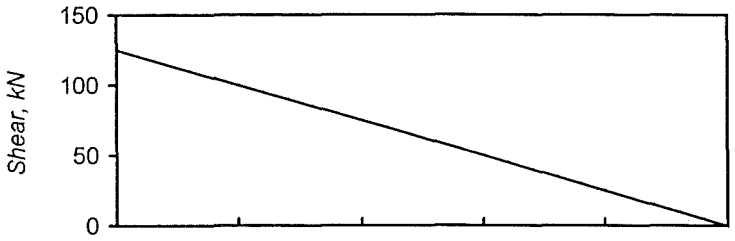

(b) Shear Force Diagram

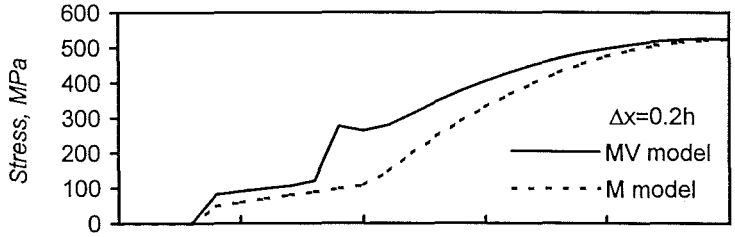

(c) Carbon ACM Stress Distribution (f_{pu}=600 MPa)

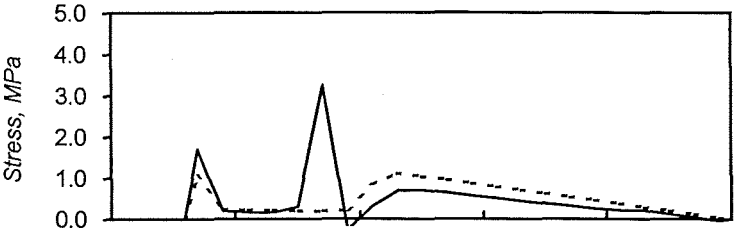

(d) Interface Bond Stress Distribution

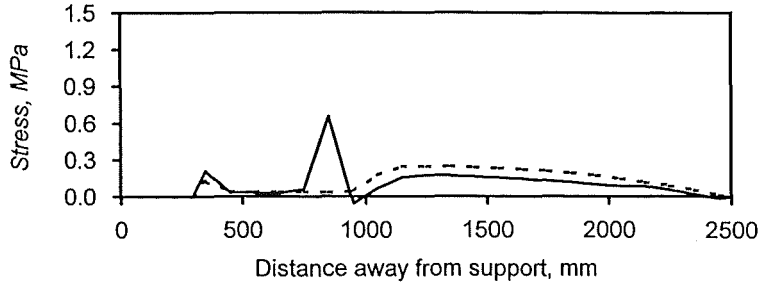

(e) Interface Normal Stress Distribution

Figure 3.9 Comparison between the M and MV Models

chosen for the study. It is clear in **Figure 3.9(c)** that the ACM laminate stress calculated by the MV model is always equal or greater than that predicted by M model. This is because the so called tension shift effect due to diagonal shear cracking [P1] is accounted for in the MV model. It is concluded that the results of the MV model are more realistic than those in the M model. Near the carbon ACM laminate end, located in zone of higher shear, the interface bond shear and normal stresses calculated by the MV model is more realistic than that calculated by the M model.

When the interface bond stress between concrete and ACM laminate is calculated, the concept of mean stress in each segment as represented in Eq.3.38 and Eq.3.39 is used for both analytical models. Note that original evaluation of the laminate bond stress proposed in M model (see Eq.2.2) is different from the value determined by Eq.3.38. This is because the bond stress obtained in Eq.2.2 overestimated the real laminate bond behaviour and the concept of the triangular type of bond stress distribution in each segment is not correct. In **Figure 3.9(d) and (e)**, the calculated laminate bond stresses, resulting from MV model, in shear and normal direction are larger in the zone of higher shear. The highest laminate bond stress estimated is 1.1 MPa resulting from M model and 3.2 MPa resulting from MV model, respectively. If the bond strength is 3.0 MPa, the failure modes analysed by the both models are totally different. That is, the failure analysed by M model could be the carbon ACM laminate rupture at beam mid-span whereas the failure conducted by MV model could be the laminate debonding. Thus the analysis conducted by M model may cause an unrealistic result.

3.8.2 Effect of the Segment Length

To observe the effect caused by the length of a discrete segment, a beam was partitioned with segments varying from 0.05h to 0.6h in length. Cases 1 to 5, shown in **Figure 3.8**, were selected for conducting the parametric study. The results were attained using the MV segment model only.

A numerical limitation of the segmental model, also observed by Arduini and Nanni [A9], is the lack of convergence towards the peak bond stress in the laminate-to-concrete interface at the laminate ends only. The effect of this computational problem is that bond stress failure can not be predicted using any existing failure theory.

Nevertheless, the significance of the method relies in the capability of indicating the stress concentration in relative terms. For a parametric study the model can be used to show the effect of several variables. This study will be discussed below.

Cases 1 to 5 are the beams represented by segments with 25 mm, 50 mm, 100 mm, 200 mm, and 300 mm, which correspond to 0.05 to 0.6 of the overall beam depth, respectively. **Figure 3.10** shows the results of stress distribution in the carbon ACM laminate and the interface bond stresses. The stress distribution in the carbon ACM laminate is not sensitive to the length of the segment. However, the interface stress varies depending on the length of the segment. This is because the bond stress and normal stress between the concrete and the carbon ACM laminate were calculated assuming a linear variation of the longitudinal tensile stress in the segment, see Eq.3.38 and Eq.3.39. This situation can be explained by a concept of average stress calculated in a given segment length. If a smaller segment length, such as $\Delta x = 0.05h$, is considered, a more pronounced local peak stress is obtained. On the other hand, the longer the segment length chosen, the more closer to an average stress in the segment is obtained. Also, the laminate force is determined using an approximate, not exact, solution in dealing with bending moment and shear diagonal cracking. Thus the differential laminate force, $T'_{p,k}$-$T'_{p,k-1}$, represented in Eq.3.38 and Eq.3.39 becomes insensitive and causes the calculated laminate bond stress and normal stress to be very sensitive to the segment length. However, the tendency of the bond stress distribution is not influenced by the segment length.

Since the segment length affects the analytical result of the laminate bond stress, special attention must be given to the choice of appropriate segment widths for a reasonable analysis. The sensitivity analysis carried out suggests that a beam can be separated in segments with lengths varying between 0.1h and 0.6h. Smaller length segments are required for at least a distance 0.2h from the ACM cut-off points and for a zone of higher shear, 60% of maximum shear, if the bond stress concentration is to be observed. An example was selected by a more complicated condition of the beam with curtailed carbon ACM laminates as presented in Cases 6 and 7 of **Figure 3.8**. The beam in case 6 was analysed with equal segment lengths of 0.1h over the span while the beam in case 7 was represented by 0.1h long segments ranging from the beam end to the ACM laminate cut-off point and by 0.6h long segments elsewhere. **Figure 3.11** shows the results of Cases 6 and 7 are nearly identical. The modelling of beams with the

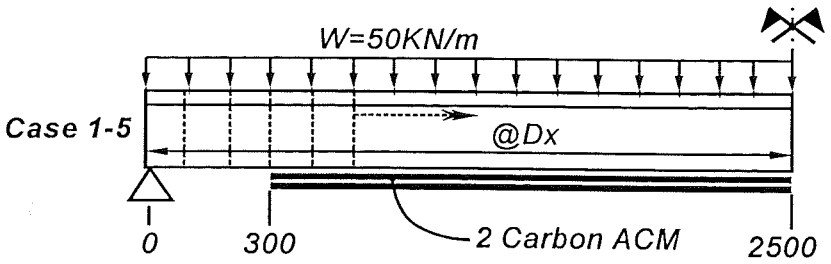

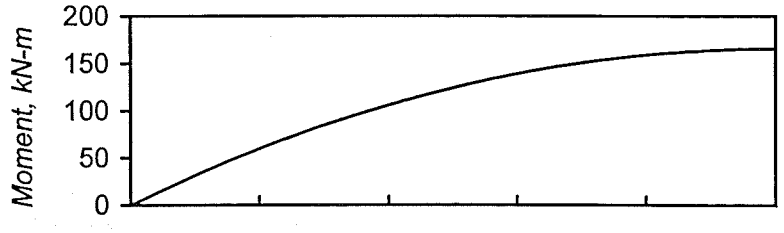

(a) Bending Moment Diagram

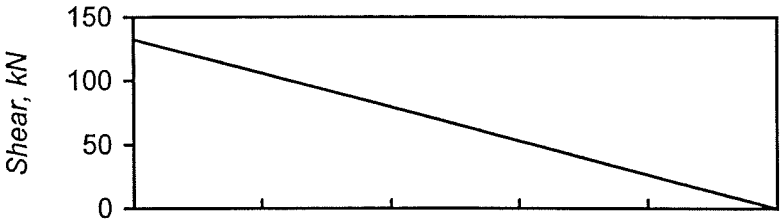

(b) Shear Force Diagram

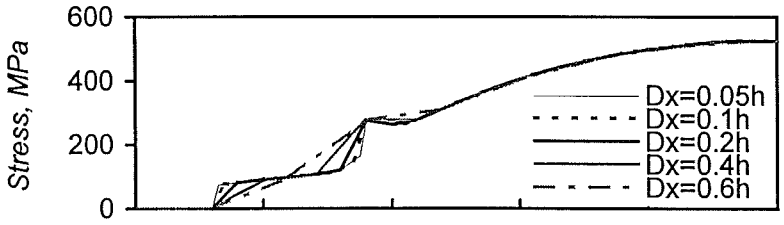

(c) Carbon ACM Stress Distribution (f_{pu}=600 MPa)

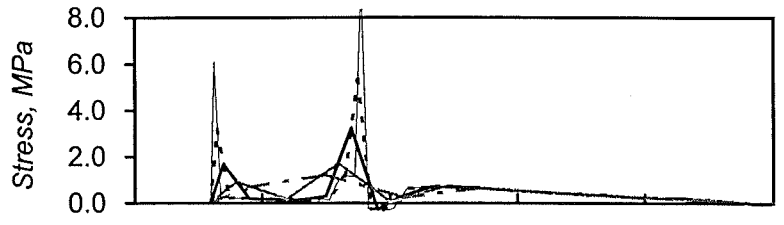

(d) Interface Bond Stress Distribution

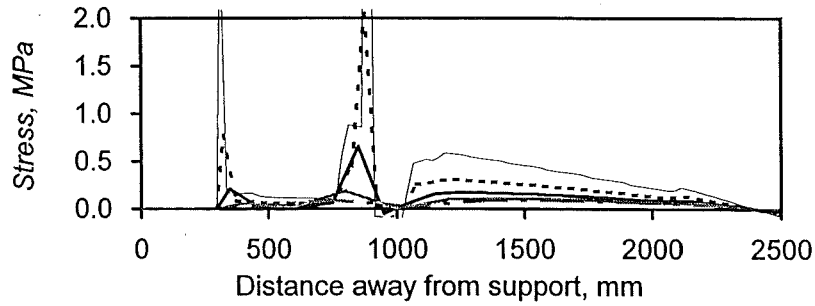

(e) Interface Normal Stress Distribution

Figure 3.10 Comparison among These Different Widths

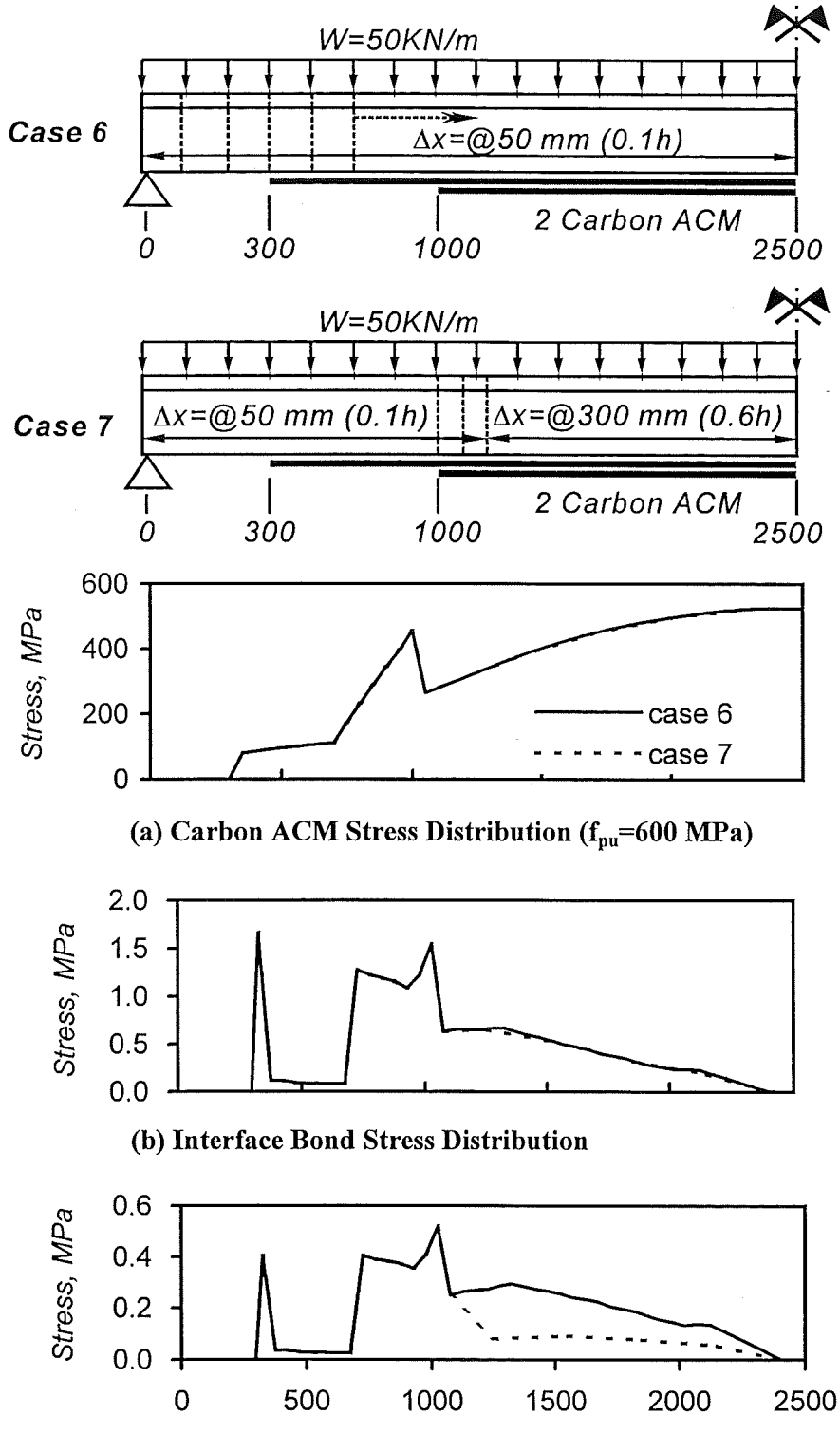

(a) Carbon ACM Stress Distribution (f_{pu}=600 MPa)

(b) Interface Bond Stress Distribution

(c) Interface Normal Stress Distribution

Figure 3.11 Comparison of Results between Cases 6 and 7

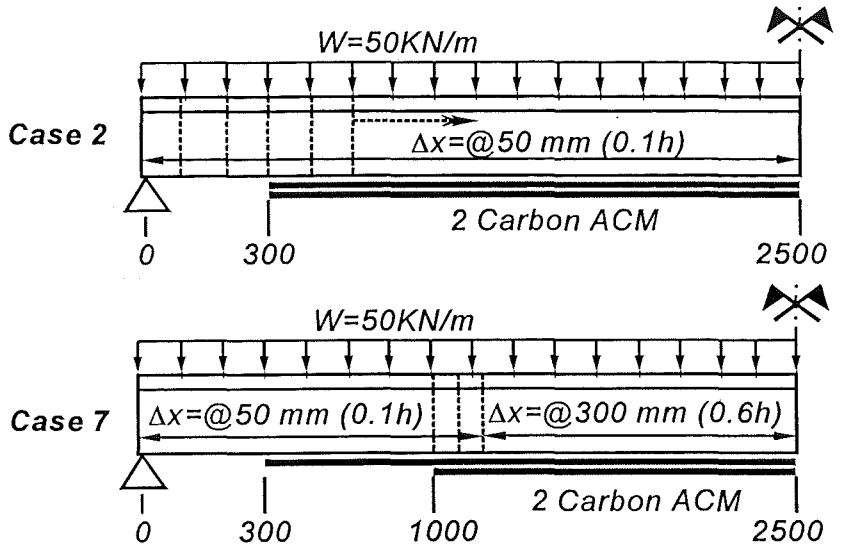

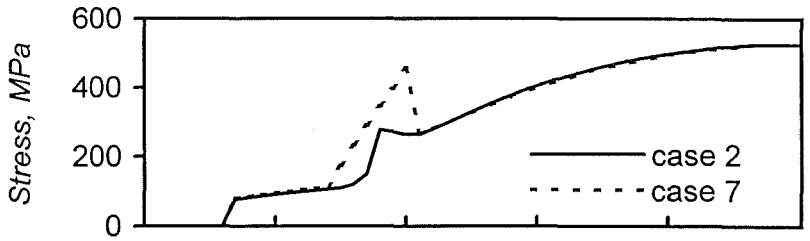

(a) Carbon ACM Stress Distribution (f_{pu}=600 MPa)

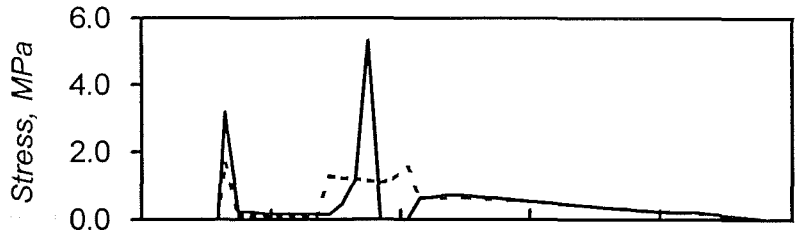

(b) Interface Bond Stress Distribution

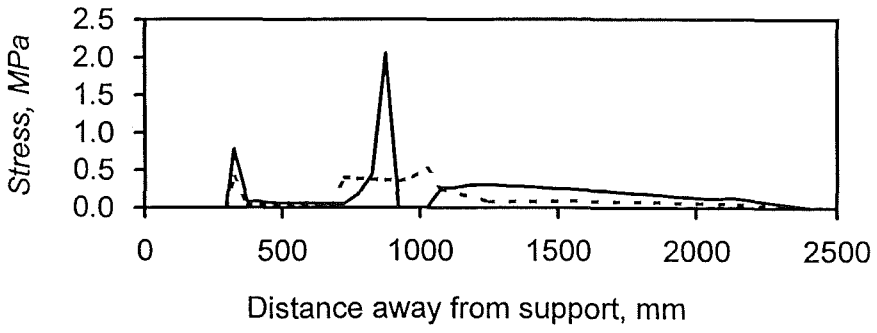

(c) Interface Normal Stress Distribution

Figure 3.12 Comparison of Analytical Results between Beams with Continuous and Staggered Carbon ACM Laminates

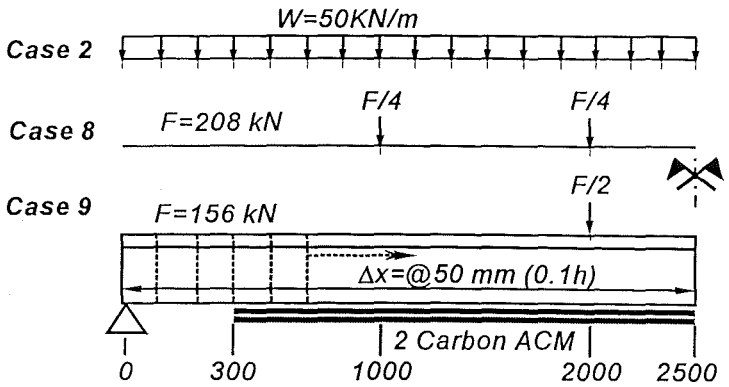

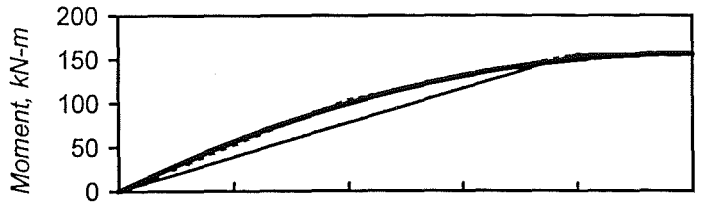

(a) Bending Moment Diagram

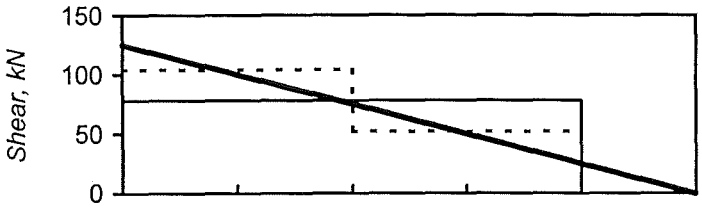

(b) Shear Force Diagram

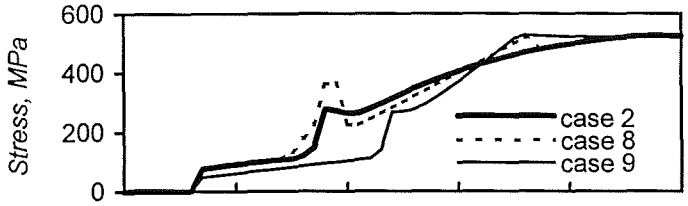

(c) Carbon ACM Stress Distribution (f_{pu}=600 MPa)

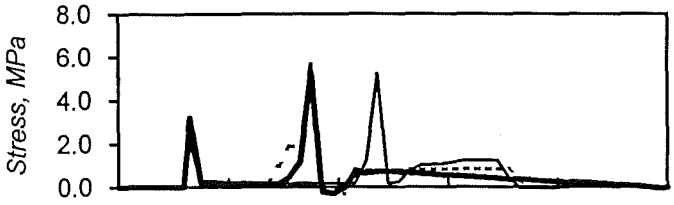

(d) Interface Bond Stress Distribution

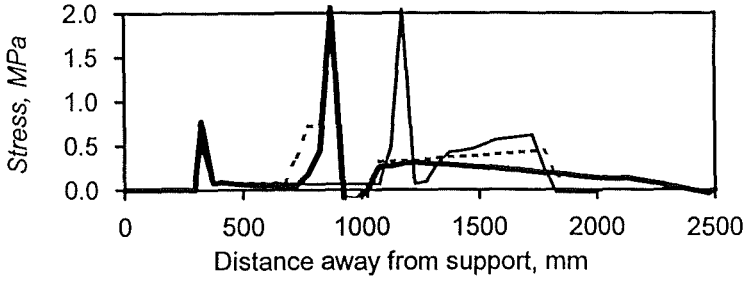

(e) Interface Normal Stress Distribution

Figure 3.13 Effect of Type of Loading

arrangement used for Case 7 will be adopted later on for the analysis of the beams tested in this programme.

3.8.3 Beams with Staggered Carbon ACM Plates

An economical way to use carbon ACM laminates is to curtail them when they are not needed to resist flexure. **Figure 3.12** compares the cases where the laminates are curtailed and when they are not.

The analytical model indicates that the interface bond and normal stresses are concentrated at the strip ends, a position where diagonal cracking occurs, and at the cut-off point. The stress concentrations at the laminate ends and in the vicinity of the diagonal cracking of the beam with full carbon ACM laminates (Case 2) are much higher than those stresses developed when the laminates are cut-off (Case 7). In the analytical cases the composite beam with full length carbon ACM laminates, Case 2, would fail by the laminate debonding whereas the beam with staggered carbon ACM laminates, Case 7, could develop its full strength with the carbon ACM laminate rupture at the beam mid-span. Consequently, in some cases it can be concluded that staggered carbon ACM laminates can be used more efficiently than laminates bonded throughout the beam span.

3.8.4 Influence on Loading Types

The sensitivity of the model to the types of loading on a beam was also studied. The beam in Case 2 shown in **Figure 3.8** has a uniform distributed load. Case 8 and 9 are loaded at 6 and 4 points, respectively. Note that the model is capable of handling both continuous as well as discrete loading patterns. **Figure 3.13** depicts the small difference in stresses between Case 2 and Case 8, which supports the premise that beams loaded at 6 points can represent quite accurately uniformly distributed loading in an actual experiment.

3.9 Conclusions

The analytical discrete segment model presented in this chapter takes into account a reasonably approximate solution using a traditional moment curvature analysis for bending moment and a rational modified compression field theory for shear diagonal cracking. The analytical beams can be rectangular or tee sections externally reinforced with epoxy-bonded fibre composite laminates. A parametric study is performed to investigate the sensitivity of the model. The conclusions made are:

1. The proposed model, using discrete segment analysis and considering the effect of bending moment and shear diagonal tension cracking in each segment, is used to analyse the beams bonded with ACM laminates to their soffit and sides. This allows simulation of the failure of the strengthened beams in a more practical manner than other analytical models.

2. The sensitivity analysis carried out suggests that the beam can be discretized in segments with lengths varying between 0.1h and 0.6h. Smaller length segments are required for at least a distance 0.2h from the ACM cut-off points and for a zone of higher shear, 60% of maximum shear, if the bond stress concentration is to be observed.

3. In some cases, the beams strengthened with staggered ACM laminates can be used more efficiently than the beams bonded with ACM laminates over the length of the beam span.

4. To simulate a uniform distributed loading in a beam, the choice of loading patterns in a test programme is very important. This may lead to unrealistic test results if an adequate loading type is not used in an actual experiment. According to the results of the parametric study, beams loaded at 6 points represent more accurately uniformly distributed loading than beams loaded at 4 points.

5. Additional experimental work represented in the next chapter can be carried out to verify the analytical method.

CHAPTER 4

EXPERIMENTAL STUDY ON THE BEHAVIOUR OF RC BEAMS WITH BONDED ACM LAMINATES

4.1 Introduction

This chapter describes an experimental programme on the behaviour of reinforced concrete T-beams retrofitted with ACM laminates to soffits and sides. The prototype specimens include beams with both continuous and curtailed bottom longitudinal steel reinforcement. Three test series were performed in the experimental programme, namely Series-A, Series-B and Series-C. Series-A tests are related to the flexural strengthening of reinforced concrete beams. Series-B tests include beams strengthened for both shear and flexure. Series-C includes a test to study the fatigue behaviour of a retrofitted reinforced concrete beam. The theoretical model developed in Chapter 3 is also verified by comparing predicted and measured results.

4.2 Test Specimens

4.2.1 Beam Selection

To simulate existing structures with poor concrete quality and reinforcing steel typical of older bridge girders, 20 MPa concrete compressive strength and Grade 300 reinforcing steel were chosen for prototype test beams. A 5m long simply supported T-beam represents a 1/2 to 2/3 scale beam of small span cast-in-place reinforced concrete bridges in New Zealand. In the prototype beams, two types of reinforcing arrangement were studied: Beams type BT1 and Beams type BT2, see **Figure 4.1**. Beams type BT1 had continuous bottom longitudinal reinforcement with 2 layers of 4-D10 bars while Beams type BT2 had 2-D10 bars cut-off at a distance of 850 mm from the beam ends. These types of beams had identical vertical load carrying capacity because the bar curtailment has no effect on the capacity when tested in their "as-built" condition and

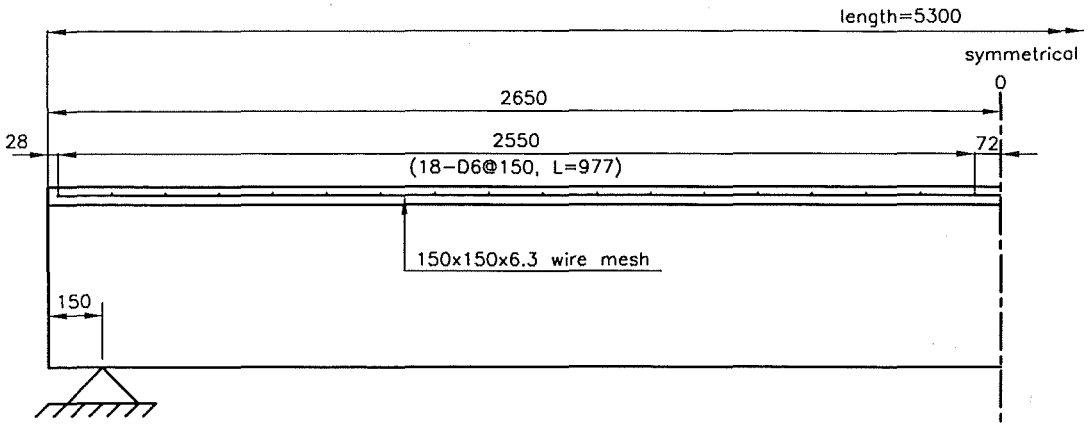

(a) Slab bar (D6 wire mesh) arrangement for unit BT1 & BT2

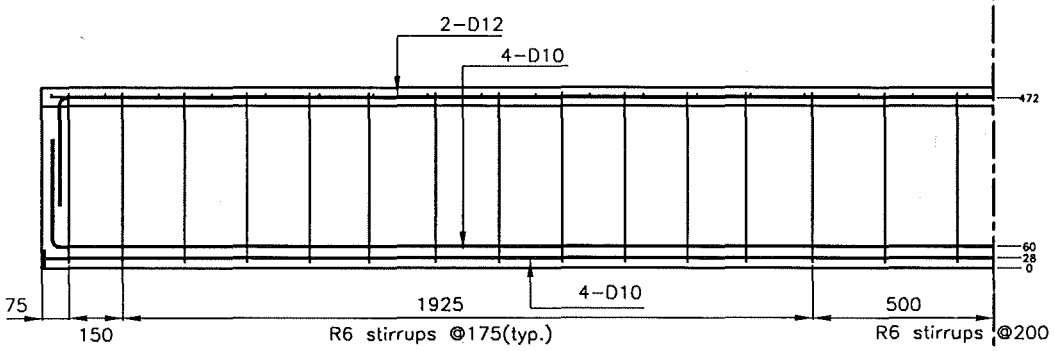

(b) Beam bar and stirrup arrangement for unit BT1

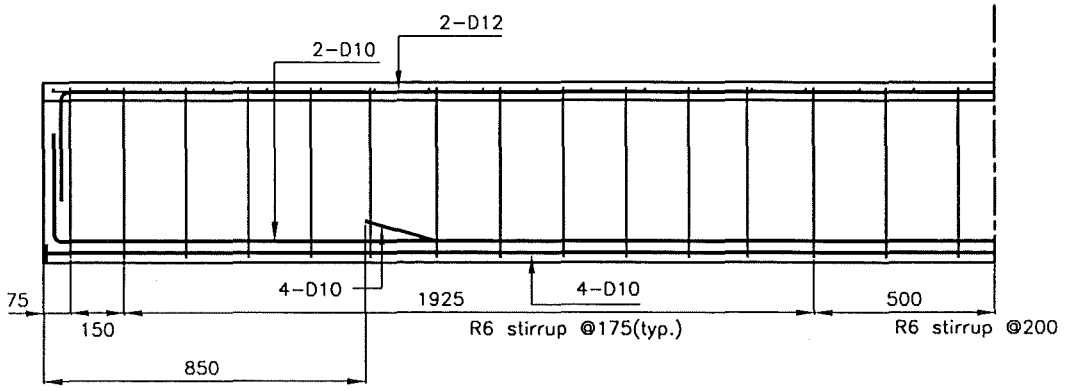

(c) Beam bar and stirrup arrangement for unit BT2

Figure 4.1 Reinforcing Arrangement of Prototype Beams

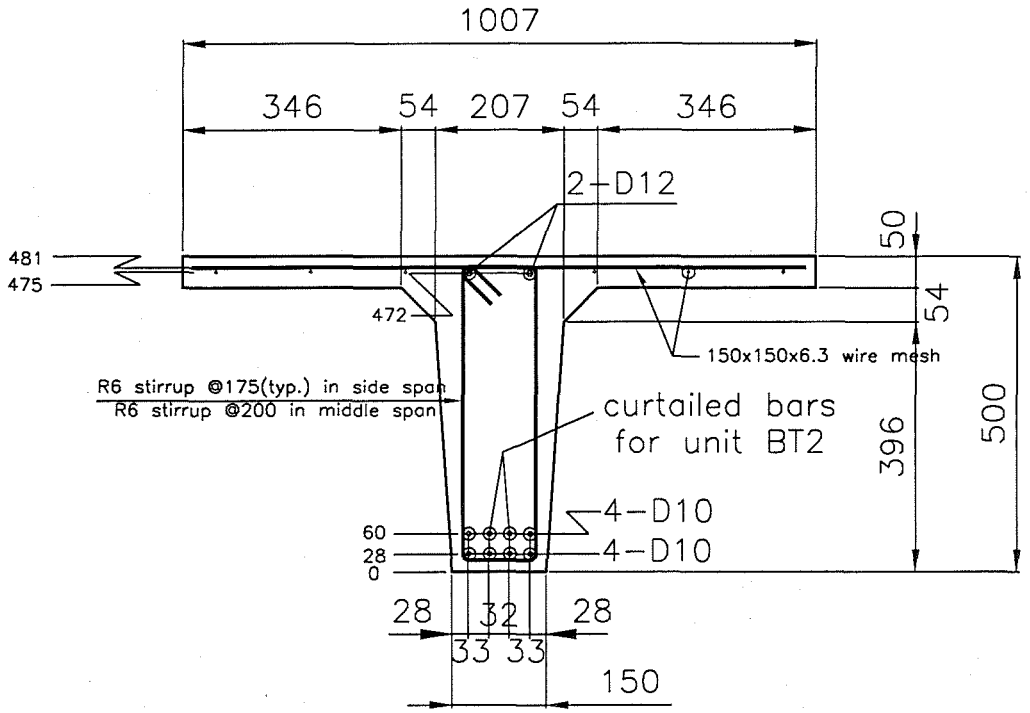

(d) Section Detail of Units BT1 and BT2

Figure 4.1 Reinforcing Arrangement of Prototype Beams (Cont.)

under the load arrangement chosen.

4.2.2 Description of Series of Tests

The design concept for the retrofit was to raise the service live load carrying capacity while ensuring a controlled failure at the ultimate limit state. As a result, the preferred failure mode was by flexure at the region of maximum bending moment. Other failure modes were considered undesirable. In some tests it was necessary to accept failures other than flexure to obtain a proper calibration of the theoretical model discussed in Chapter 3.

Figure 4.2 shows complete details of the ACM laminates applied to the beams. Carbon ACM (CACM) laminates were applied to the soffit of the beams. Glass ACM (GACM) U-strips were applied to some beams to increase the shear strength of the beam and to provide a clamping action to the CACM laminates to avoid premature delamination. The GACM strips were anchored in the web of the beam, using fibreglass, multifilament anchors embedded in an epoxy-filled hole in the concrete. Note that part of this test was to observe the performance of the anchors, which were located in a region of tension in the beam web.

Series-A test looked at the general behaviour of RC beams externally strengthened with CACM laminates bonded to their soffit. The performance of these beams can be compared with the results of the theoretical model discussed in Chapter 3. Six beams were tested as part of this series. **Figure 4.2(a)** shows details of the extent of the ACM reinforcement bonded to the beams. All units except Unit F1 had three CACM laminates bonded to the beam's soffit. Unit F1 had only one layer of CACM laminate. The main variable in the tests of beams with three layers of CACM laminates, was the laminate layout. The purpose of different laminate arrangement in this series was to investigate the interface bond behaviour between concrete and the CACM laminate. Units F2 and F3 were strengthened with full-length CACM laminates whereas Units F4 to F6 had staggered CACM laminates. One important aspect is that the staggered CACM laminates are applied to the tensile face of the reinforced concrete beams not only for eliminating the bond stress concentration at the laminate ends but also for material-cost savings.

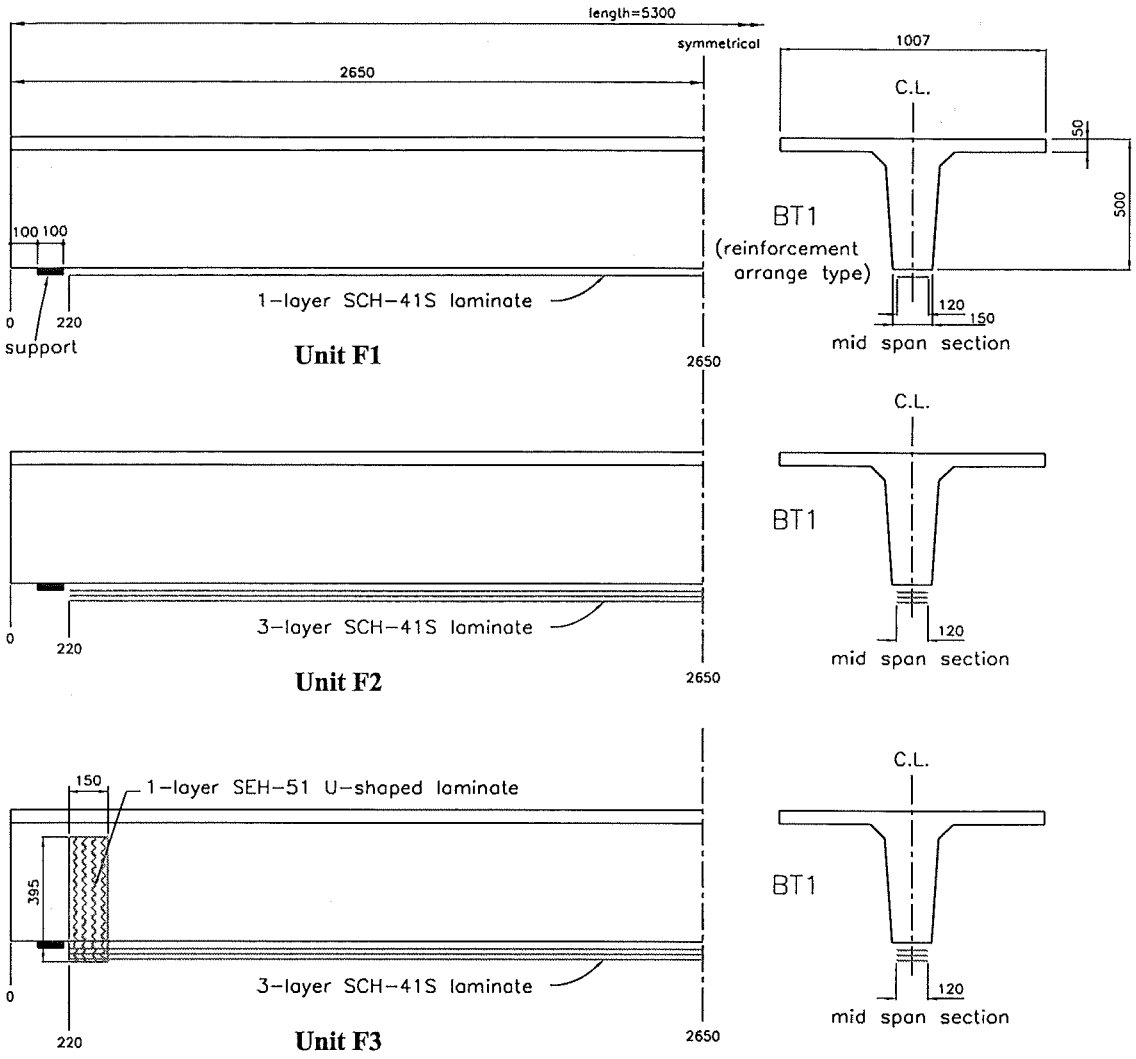

Note:
The thickness of 1-layer SCH-41S laminate is 1.00mm.
The thickness of 1-layer SEH-51 laminate is 1.27mm.

(a) Series-A

Figure 4.2 Arrangement of the CACM Laminates in the Test Units

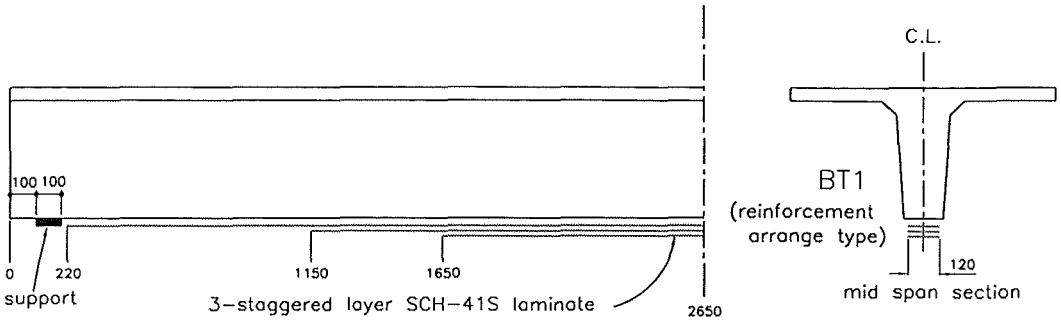

Unit F4

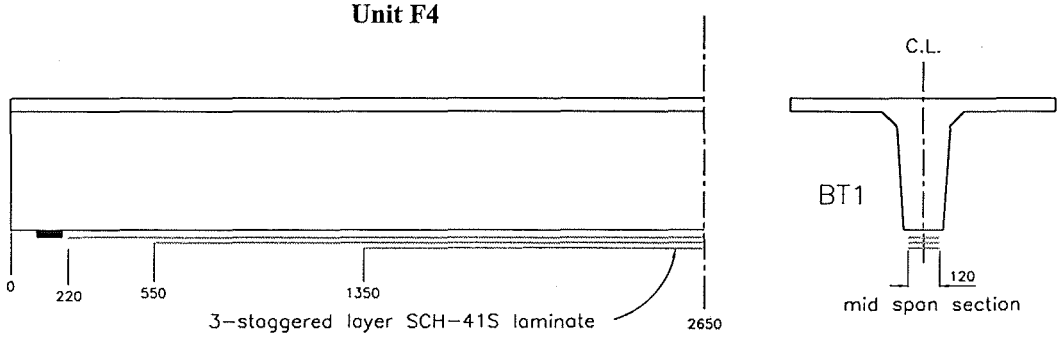

Unit F5

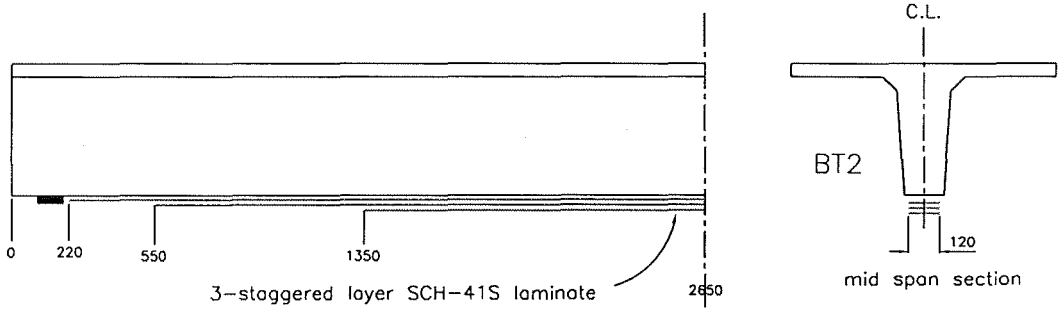

Unit F6

Note:
The thickness of 1-layer SCH-41S laminate is 1.00mm.
The thickness of 1-layer SEH-51 laminate is 1.27mm.

(a) Series-A (Cont.)

Figure 4.2 Arrangement of the CACM Laminates in the Test Units (Cont.)

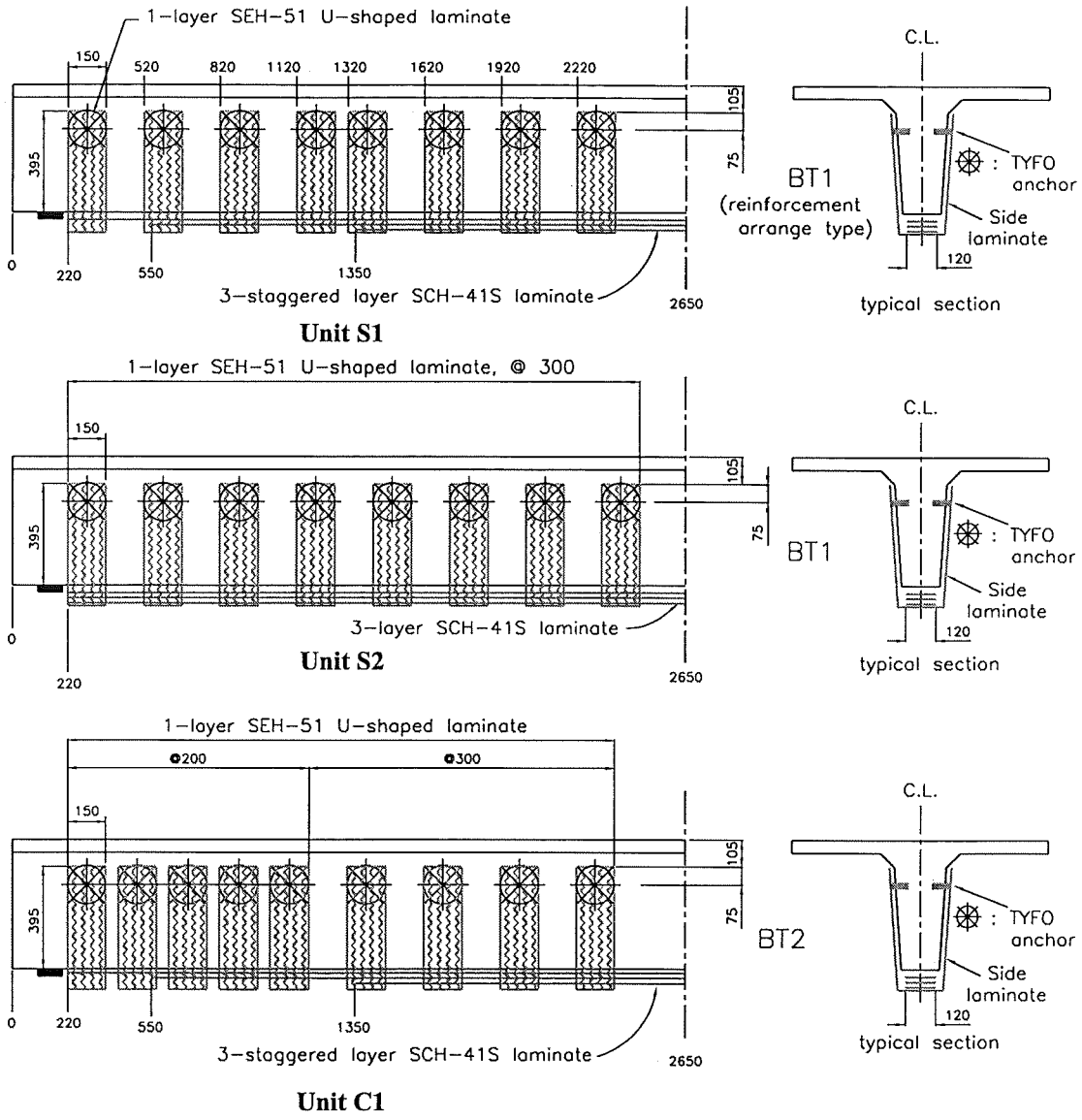

Note:
The thickness of 1-layer SCH-41S laminate is 1.00mm.
The thickness of 1-layer SEH-51 laminate is 1.27mm.

(b) Series-B

Figure 4.2 Arrangement of the CACM Laminates in the Test Units (Cont.)

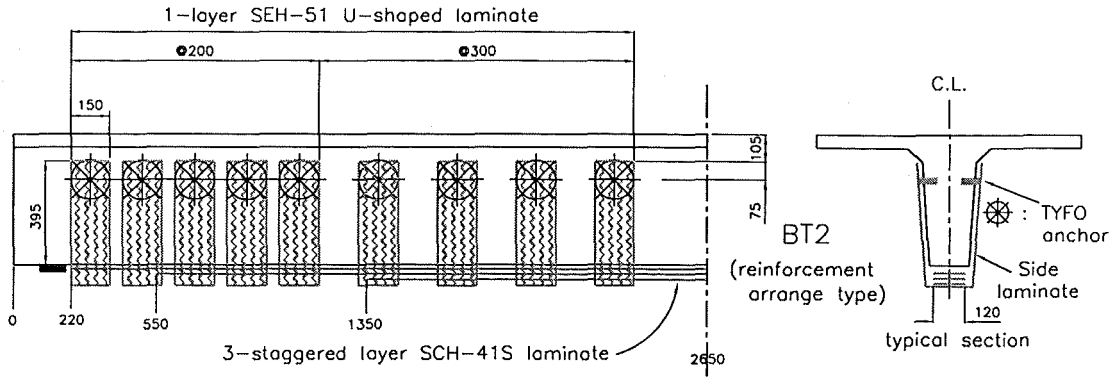

Unit C2

(c) Series-C - Fatigue Loading Test

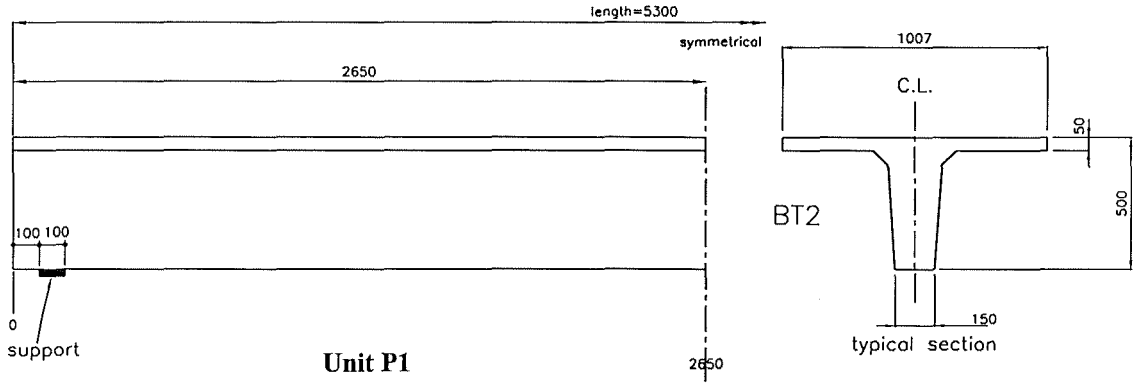

Unit P1

Note:
The thickness of 1-layer SCH-41S laminate is 1.00mm.
The thickness of 1-layer SEH-51 laminate is 1.27mm.

(d) Benchmark Test Unit

Figure 4.2 Arrangement of the CACM Laminates in the Test Units (Cont.)

The design of the 3-layer CACM laminates was based on principles of strain compatibility similar to the design of conventionally reinforced concrete beams. Note in **Figure 4.2(a)** that Units F2 and F3 are similar. However, F3 has GACM U-strips bonded to the longitudinal CACM laminate ends. The aim of the GACM U-strip was to prevent the premature end laminate debonding that was theoretically predicted for Unit F2. Units F4 and F5 had the continuous longitudinal steel reinforcing arrangement but the CACM laminates were cut-off differently. Units F6 and F5 had the same CACM laminate arrangement but the longitudinal reinforcement in Unit F6 was curtailed (see reinforcement arrangement BT2 in **Figure 4.1**).

Series-B units were designed considering both flexural and shear strengthening with CACM laminates and GACM U-strips. **Figure 4.2(b)** shows details of the extent of the ACM laminates and strips in the three units tested in this series. The measured and analytical results obtained in the Series-A test were considered in the retrofit scheme for these test units. The ends at both sides of the U-strips are anchored with Tyfo glass-fibre strands, a proprietary anchoring system. The design consideration of the Tyfo anchor is based on the cross section aspect ratio, described in Section 6.2.3.2. Units S1 and F5, Units S2 and F2, and Units C1 and F6 were identical except for the addition of the GACM U-strips in Units S1, S2, and C1.

It was considered that presence of the GACM U-strips would enhance the shear strength of the beams. The side strips were 150 mm wide by 1.27 mm thick GACM laminates. Research work carried out by Beukel [B4] had concluded that stirrups of partial height, that is, not anchored in the concrete compressive region above the neutral axis depth, increased the shear strength in beams. This assumption was to be proven in the tests in this series. To account for the presence of these wraps the nominal shear strength of the beams, V_n, was computed by modifying the nominal shear strength given by the New Zealand Concrete Structures Standard, NZS 3101: 1995 [N4, B4],

$$V_n = (0.07 + 10\rho_w)\sqrt{f_c'}\, b_w d + \frac{A_{vs} f_{vsy}}{s} d + \frac{A_{vp} f_{vpe}}{s_{vp}} h_{vp} \qquad (4.1)$$

where, ρ_w is the tensile steel reinforcement ratio which shall not be taken greater than 0.013 and d is the beam effective depth. The other variables in Eq.4.1 are shown in **Figure 3.4** and are described in Section 3.4. The right hand term in Eq.4.1 has been derived assuming a 45 degree inclined crack crossing the U-strips. The effective transverse stress in the U-strips, f_{vpe} (= ε_{vpe} E_p), was determined assuming 0.4% effective transverse strain, ε_{vpe} as proposed by Priestley et al. [P6].

The test unit in Series-C, see **Figure 4.2(c)**, was conducted to study the fatigue behaviour of the ACM laminate. This unit was identical to Unit C1.

The prototype Unit P1, see **Figure 4.2(d)**, was tested using the beam BT2 to represent the original or "as-built" beam behaviour.

4.3 Construction of the Test Units

4.3.1 Beams

The construction of all beams was carried out in a precast concrete yard using standard steel moulds. Prior to casting of the concrete, steel studs for measuring longitudinal steel strains were tack-welded to the sides of one bottom longitudinal reinforcing bar. **Figure 4.3** shows the beam cages in the yard during the placement of the concrete.

The fresh concrete was placed in the steel moulds and mechanically vibrated. The maximum aggregate size of the concrete was 19 mm and the slump of the fresh concrete ranged between 80 mm and 120 mm. Test cylinders 200 mm high x 100 mm diameter were cast and vibrated on a vibrating table. The cylinders were cured in the same condition as the test units. All the test units were cured with wet sacking for 7 days after removal from the moulds and set aside until the ACM laminates were bonded.

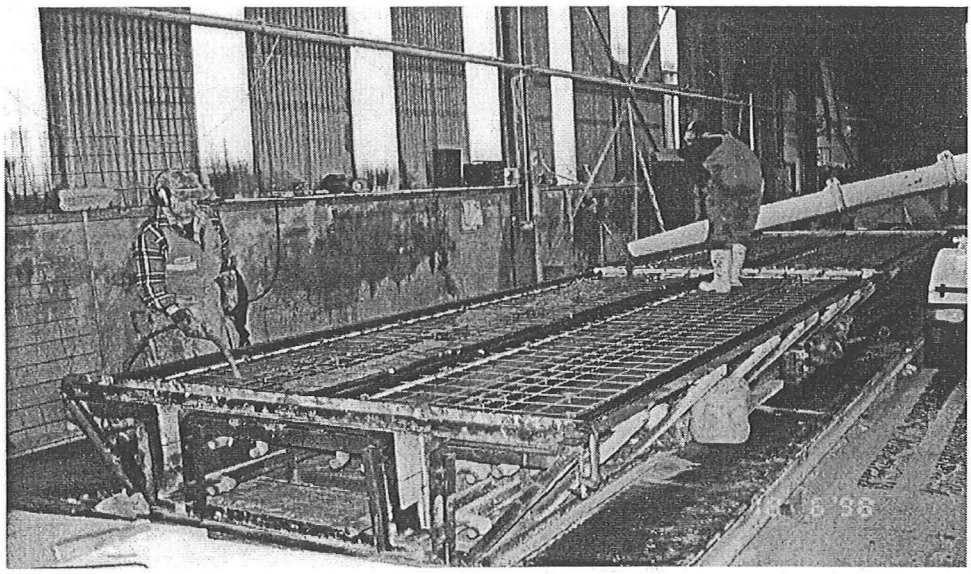

Figure 4.3 Casting of the Fresh Concrete

4.3.2 Application of the ACM Laminates

The carbon and glass ACM laminates used in the tests were those of the TYFO Fibrwrap System, provided by FYFE Co. Ltd. in the USA. Two types of unidirectional ACMs were used. SCH-41S carbon fibre laminate was used for flexural strengthening, and SEH-51 glass fibre laminate was used for shear strength enhancement. The laminates were applied to the test units when the concrete was at least 28 days old. The procedure used is described below:

(1) Before bonding the ACM laminates, the concrete surface in the specimens was mechanically roughened. The surface in Units F1 to F5 was scabbled (see **Figure 4.4(a)**) whereas dry sandblasting was employed in Units F6, S1, S2, C1, and C2 (see **Figure 4.4(b)**).

It is believed that the overall effect of the two roughening methods on the concrete-to-ACM laminate interface bond strength is very similar. However, sandblasting is more practical if a large amount of roughening is required.

After the concrete was prepared a survey on the amplitude of roughened

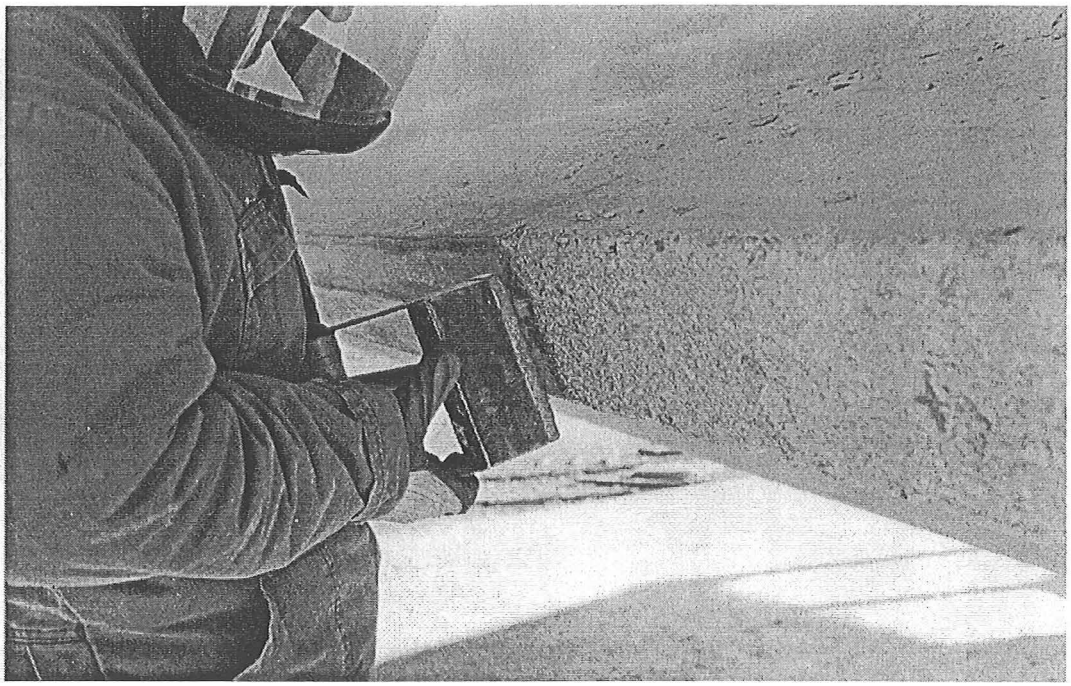

(a) Scrubbing

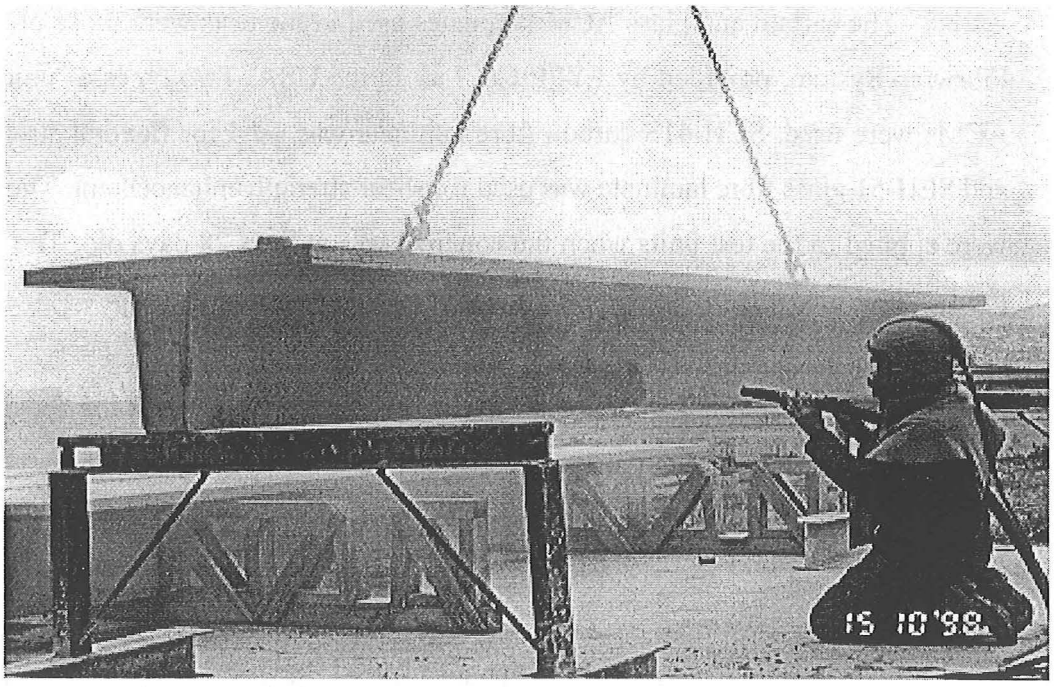

(b) Dry Sandblasting

Figure 4.4 Concrete Surface Preparation

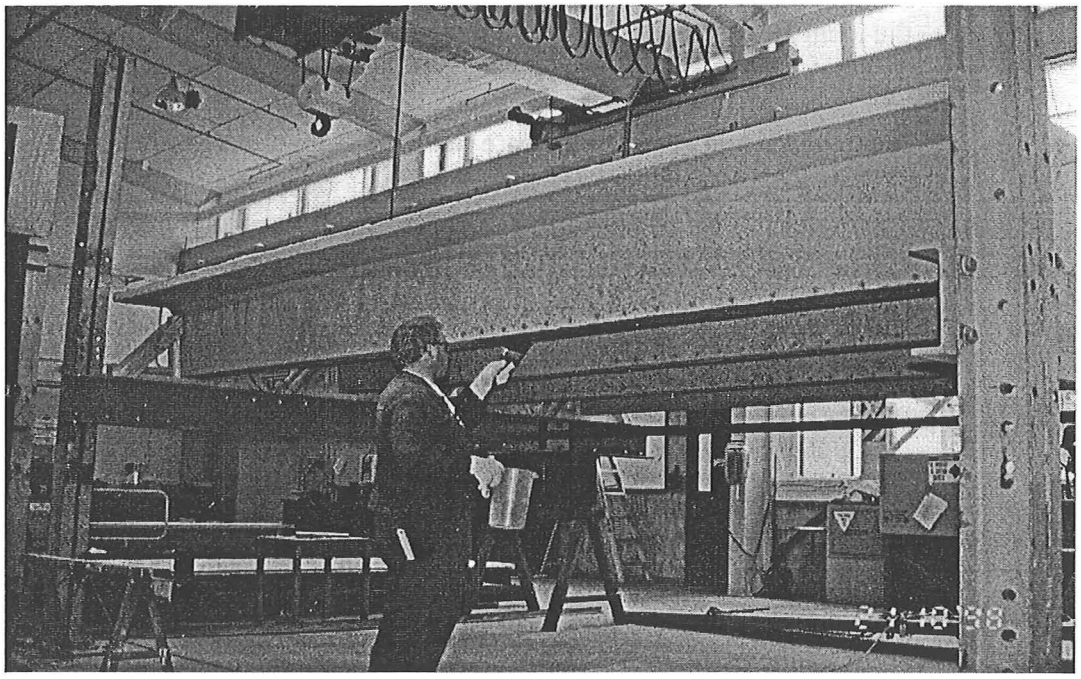

(a) Prime epoxy coating

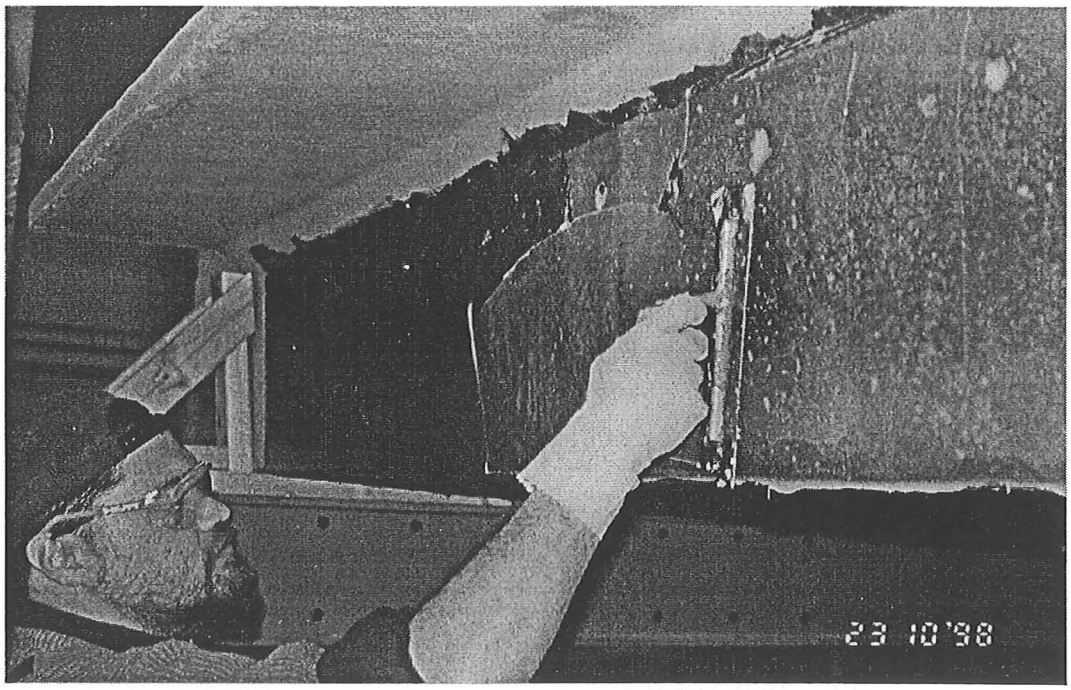

(b) Applying epoxy adhesive

Figure 4.5 Application of Adhesives to Concrete Surface

concrete surface was performed. According to the manufacturer's specifications, the ideal amplitude should range between 1 and 2 mm.

(2) Sharp edges and protrusions were removed from the concrete surface.

(3) Dust and debris on the concrete surface was removed using an oil-free high-pressure air gun.

(4) Primer epoxy coating was applied to the concrete surface (see **Figure 4.5(a)**).

The epoxy coating is made from TYFO^{TM} WS, which is a combination of the standard TYFO^{TM} S epoxy with a special fumed silica (Cab-O-Sil) thickener added to the A component of TYFO^{TM} S epoxy. The epoxy coating can be used to fill surface voids in the concrete of up to 76mm in diameter and 25mm deep. It is cured for few hours until it becomes "tacky".

(5) A 2 mm (approx.) thick TYFO^{TM} WS epoxy paste adhesive was applied to the previous epoxy coated surface before application of ACM laminates, as shown in **Figure 4.5(b)**. The epoxy was left for few hours as specified in the manufacturer's instructions.

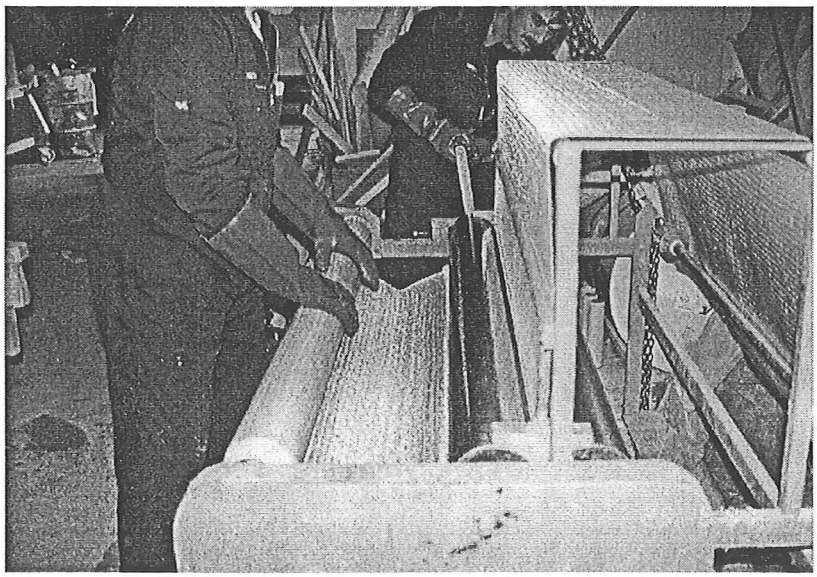

Figure 4.6 Saturating the ACM Laminates on Site

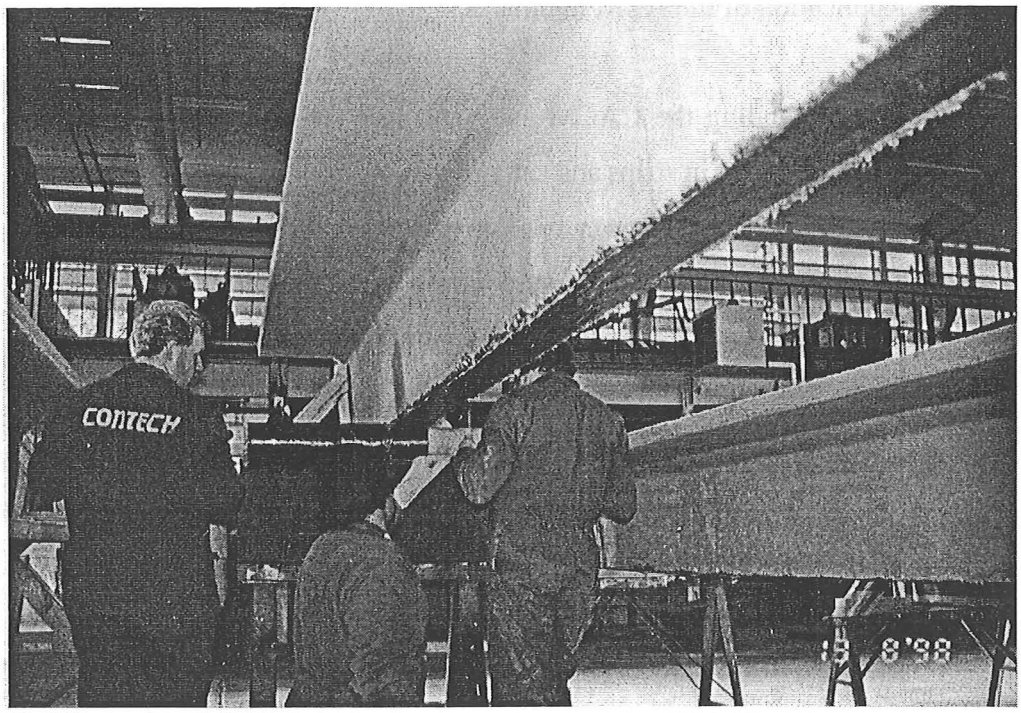

(a) Application of Carbon ACM Laminates

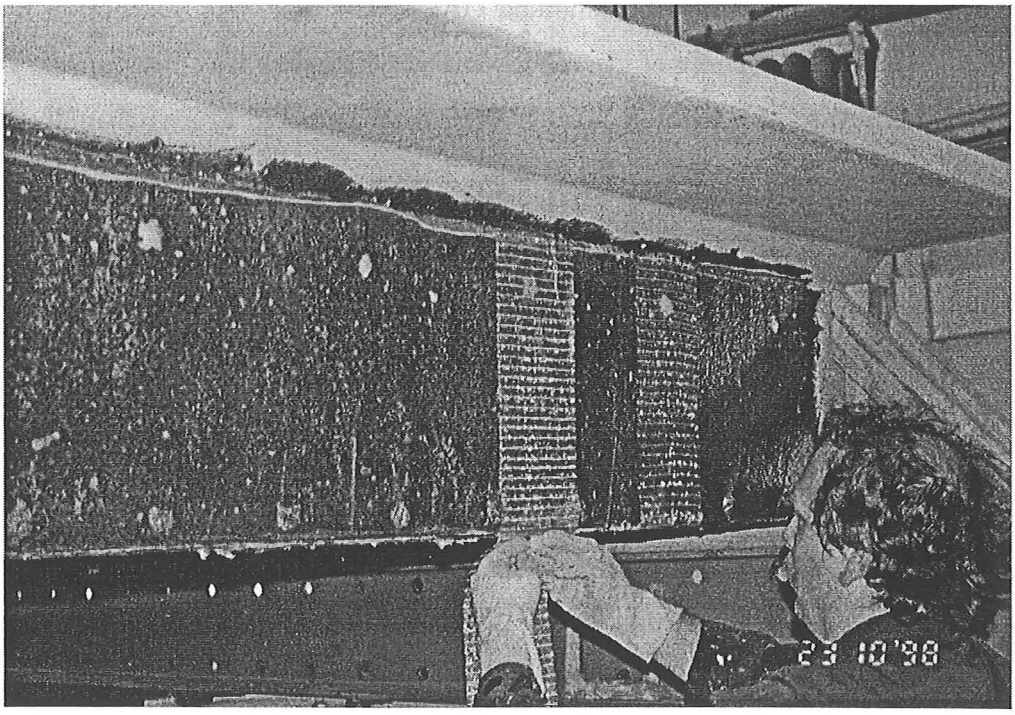

(b) Application of Glass ACM U-Strips

Figure 4.7 Attaching the ACM Laminates to Concrete Surface

(6) Application of the ACM laminates.

Before bonding the CACM laminates and GACM strips, the cloth-like fabric sheets were cut in strips and saturated in TYFO™ S epoxy resin. It can be seen in **Figure 4.6** that the epoxy resin is mixed on site, poured into the trough of the saturator and a roll of the strip fabric is passed through. The saturated ACM laminates were then applied to the member as specified.

The application of saturated CACM laminates to the soffit of the test beams is shown in **Figure 4.7(a)**. Then the saturated GACM U-strips were glued to the desired position as illustrated in **Figure 4.7(b)**. TYFO™ Fibr-Anchor was used to fasten the free ends of the U-strips. The function of TYFO™ Fibr-Anchors is similar to the action of dowel reinforcement to provide a mechanical connection between GACM strips and the concrete to avoid delamination of the strip. According to the construction specification of TYFO Anchors, 14 mm diameter and 80 mm deep holes were drilled at both ends of U-strips before Step 4 was carried out. After the saturated GACM U-strips were attached to the desired position, a bundle of glassfibres mixed with epoxy was inserted into the drilled holes, see **Figure 4.8**. Special care must be taken to avoid small air bubbles inside the saturated ACM sheets.

(7) The system was cured at a control temperature of 15℃ or above for at least 2 weeks.

4.4 Material Properties

With each test beam, three 100 mm diameter and 200 mm high concrete cylinders were cast. Six additional cylinders were made each time concrete was placed. Six cylinders were cured in a fog room and tested at 28 days to determine the concrete compressive strength f'_c, and the split tensile strength f'_t. The remaining cylinders were cured alongside the beam. **Table 4.1** shows the concrete properties of all test units.

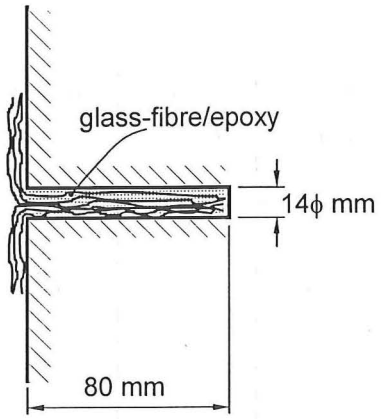

(a) Anchor Details

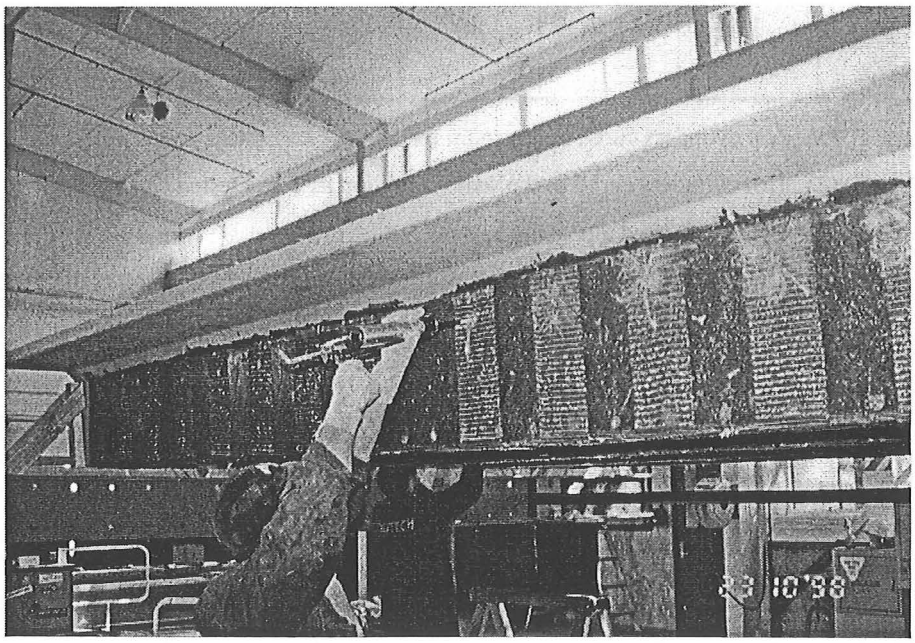

(b) Installation

Figure 4.8 TYFO Fibr-Anchors

Table 4.1 Concrete Properties

Batch No.	f'_c [1] (MPa)	f'_t [2] (MPa)	Slump (mm)	Beam Type	Unit No.	Age at Test (days)	f'_c [3] at Test (MPa)
1	18	1.8	120	BT1	F2	89	18
					F3	93	17
					F4	98	18
					F5	105	18
2	18	2.0	120	BT2	P1	47	19
					F6	135	19
					C1	143	19
					C2 start [4]	162	19
					C2 end [4]	225	19
3	19	1.7	80	BT1	F1	63	20
					S1	121	20
					S2	125	20

Notes: (1) Test cylinders cured in fog room for 28 days and tested on the 28th day.

(2) Test cylinders cured as the same condition as 1 and tested on the 28th day.

(3) Cylinders cured alongside beams.

(4) The concrete strength is measured at start and end of testing on Unit C2.

Table 4.2 Mechanical Properties of Reinforcing Steel of Test Units

Bar [1]	A_s (mm^2)	f_{sy} (MPa)	E_s (GPa)	ε_{sh} [2] (%)	ε_{su} (%)	f_{su} (MPa)
D12	113.1	316	197	3.2	27	470
D10	78.5	325	192	3.2	28	458
R6	28.3	365	203	1.2	13	504
wire-mesh R6	28.3	609	-	-	-	666

Notes: (1) D: deformed bar, R: plain round bar

(2) The strain at the commencement of strain hardening.

Reinforcing steel bars were cut from each batch and tensile tests were performed to obtain the stress-strain behaviour. Average results from these tests are given in **Table 4.2**. A minimum of three samples were taken from each batch and in no case did the yield stress of any individual bar exceeded 5% of the average for the batch.

The ACM laminate mechanical properties were measured in accordance with ASTM D 3039 [A2]. Three samples were taken from the carbon and glass ACM laminates used. The mean strength and modulus were determined from the measured results. The test results of ACM samples are given in **Table 4.3**. The SCH-41S fabric is a unidirectional stitched carbon fibre. The SEH-51 fabric is a woven glass fibre reinforced mainly in one direction. Aramid fibres are provided in the fabric at 90 degrees and are used mainly for quality control during the application of the epoxy-saturated laminate.

Table 4.3 ACM Properties

Type	Test Unit	Test sample dimension			Mean values	
		thickness (mm)	width (mm)	length (mm)	f_{pu} (MPa)	E_p (GPa)
Carbon ACM (SCH-41S)	F1 to F5	2.00[1] (two plies)	25	350	658	65.0
Carbon ACM (SCH-41S)	F6, S1, S2, C1, C2	2.00[1] (two plies)	25	350	609	63.5
Glass ACM (SEH-51)	All	2.54[2] (two plies)	25	300	374	19.8

Notes: (1) Based on a nominal ply thickness of 1.00 mm

(2) Based on a nominal ply thickness of 1.27 mm

4.5 Loading System

All the test beams are subjected to six-point loading to closely simulate uniform loading. **Figure 4.9** shows the test arrangement and **Figure 4.10** shows a beam during

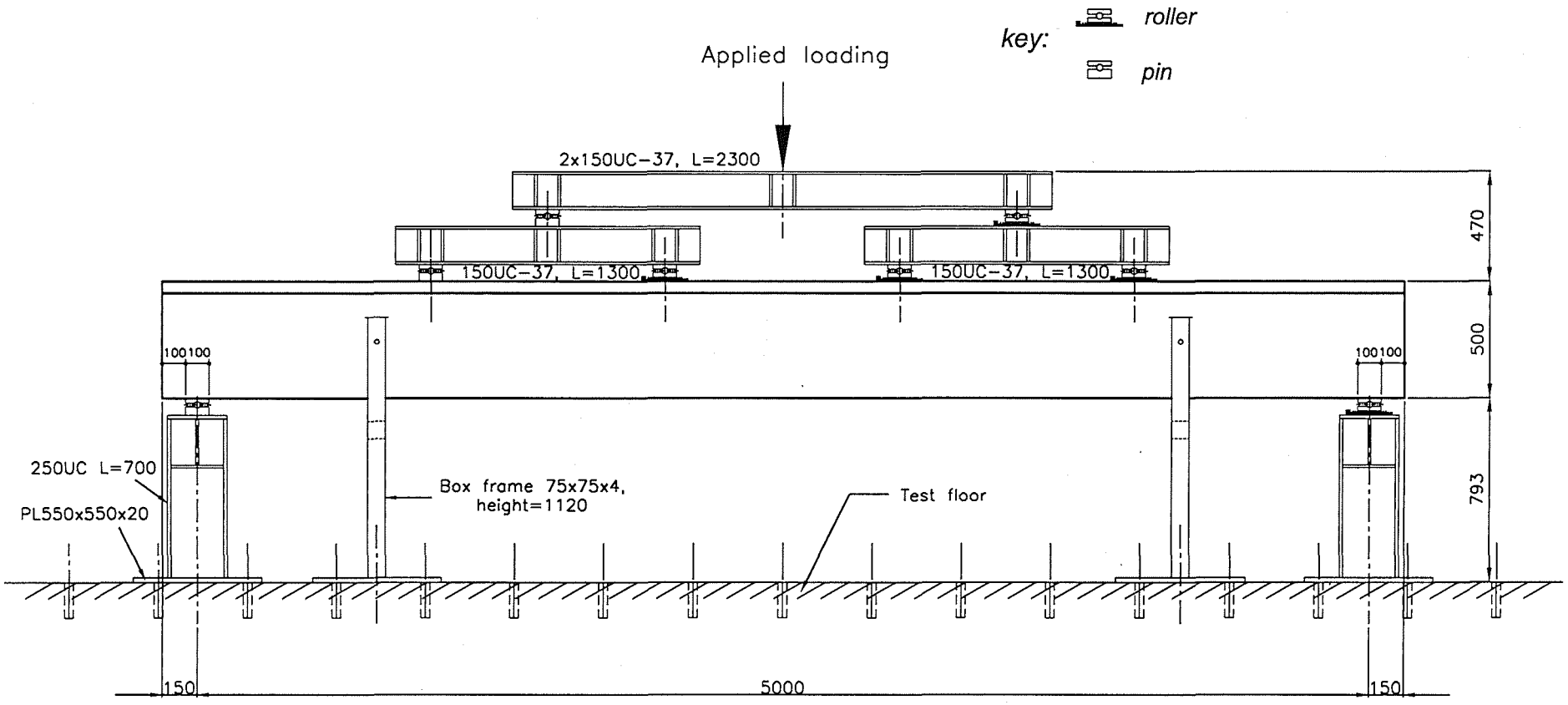

Figure 4.9 Six Point Loading Test Arrangement

testing.

Except for the benchmark beam, Unit P1, all units were subjected to relatively low level repeated loading, facilitated by using a home-made servo-control unit to drive a single 250 kN capacity hydraulic actuator. The loading frequency was 12 cycles per minute. Then, monotonic loading was applied to all units to induce failure. A 1500 kN capacity hydraulic centrehole ram was used for this part of the test.

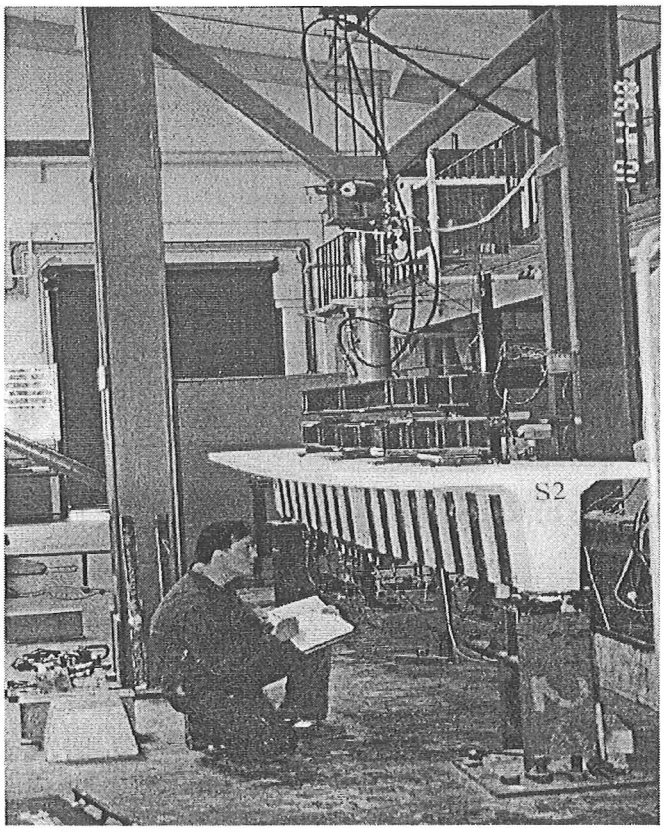

Figure 4.10 Test Set-up for ACM Bonded Beam

4.6 Test Sequence

Figure 4.11 shows the test sequence applied to the beams. Unit P1 was quasi-statically tested under monotonic loading (see **Figure 4.11(a)**).

The repeated loading shown in **Figure 4.11(b)** was applied to Units F1 to F6,

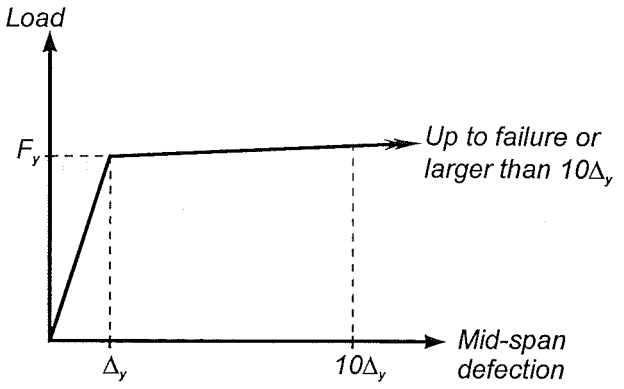

(a) Monotonic Loading for Unit P1

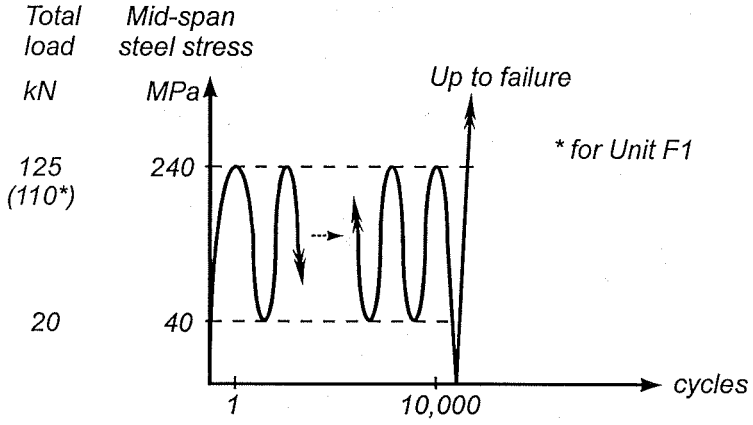

(b) Repeated Loading for Units F1~F6, S1, S2, C1

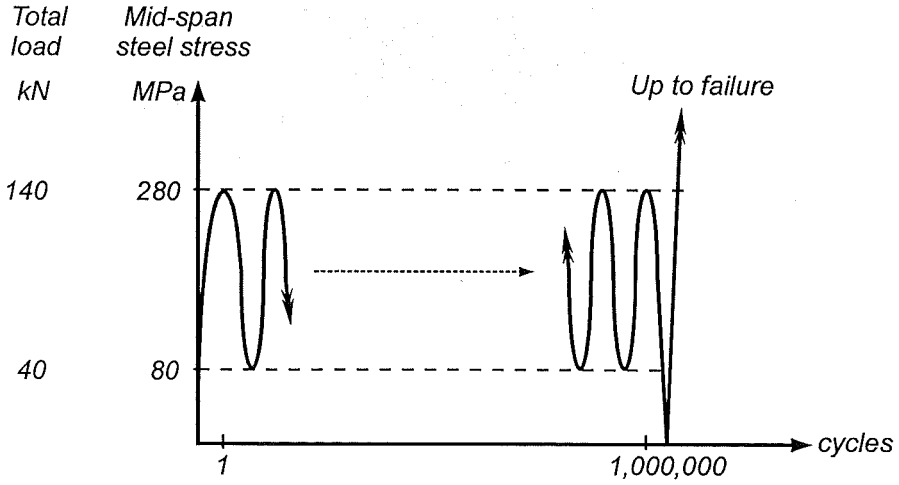

(c) Fatigue Loading for Unit C2

Figure 4.11 Loading Sequences in Test Units

Units S1 and S2, and Unit C1. These beams were subjected to ten thousand cycles. The load in the actuator was set to induce maximum and minimum stresses in the reinforcing steel of 240 and 40 MPa, respectively. That is, a stress range of 200 MPa. Then quasi-static monotonic loading was applied up to failure.

Unit C2 was subjected to over a million cycles of repeated loading (see **Figure 4.11(c)**). The amplitude of the load in these cycles was controlled by a stress range in the reinforcing steel of 200 MPa with maximum and minimum stresses of 280 MPa and 80 MPa, respectively. Quasi-static monotonic loading to failure was applied to the beam after the repeated loading test had ended.

4.7 Instrumentation

The load applied by the single hydraulic actuator was monitored by a strain gauged load cell. Two load cells with capacities of 250 kN and 1300 kN were used. The smallest capacity load cell was fitted to the actuator in the repeated loading test whereas the other load cell was fitted to the 1500 kN capacity hydraulic ram.

Linear potentiometers with 200 mm travel were used to measure the deflection at mid span of the beams. These transducers are suitable for measuring displacement and have an electrical DC voltage output directly proportional to the position of the moving rod. For the long-term measurements of Unit C2, two dial gauges were added to the deflection measurement as a back-up measure.

Demountable mechanical gauges (DEMEC) were employed to measure the strains in the ACM laminates as well as in the concrete. The gauge lengths used were 102 and 204 mm. The resolution of the 102 and 204 mm gauge length DEMEC gauges is 20×10^{-6} and 10×10^{-6} mm/mm, respectively. ACM and reinforcing steel strains were measured with electrically strain gauged clip gauges. These gauges were manufactured in the Department of Civil Engineering following a University of Auckland design. Clip gauges were typically used with gauge lengths ranging between 100 and 200 mm. **Figure 4.12** illustrates the clip gauges during calibration and during the strain measurement of CACM laminates.

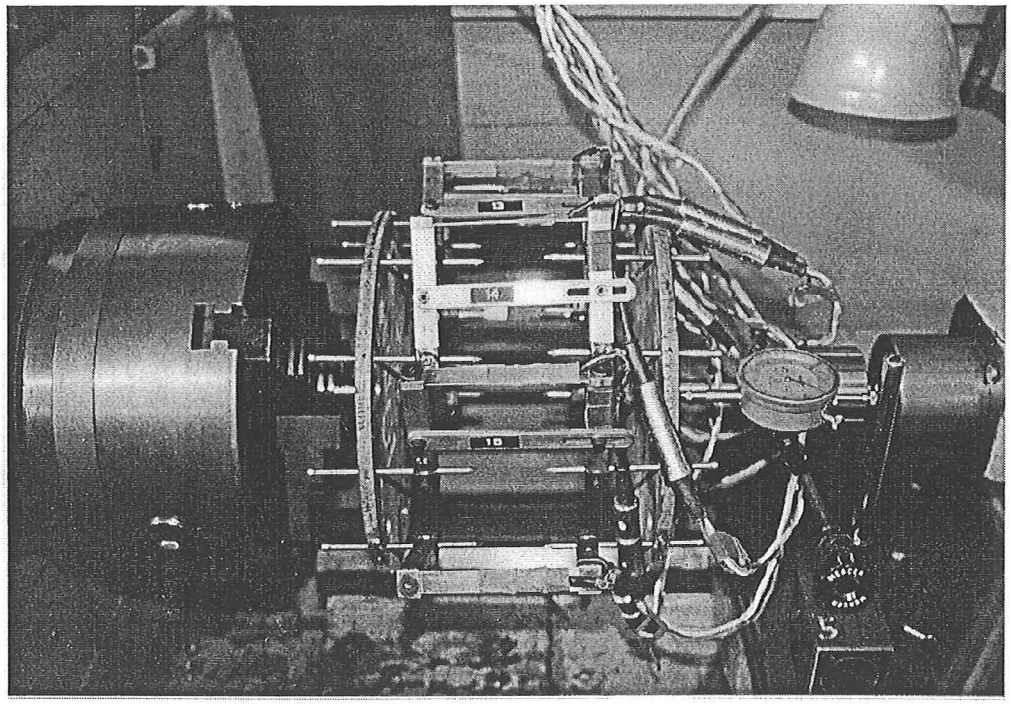

(a) Calibration

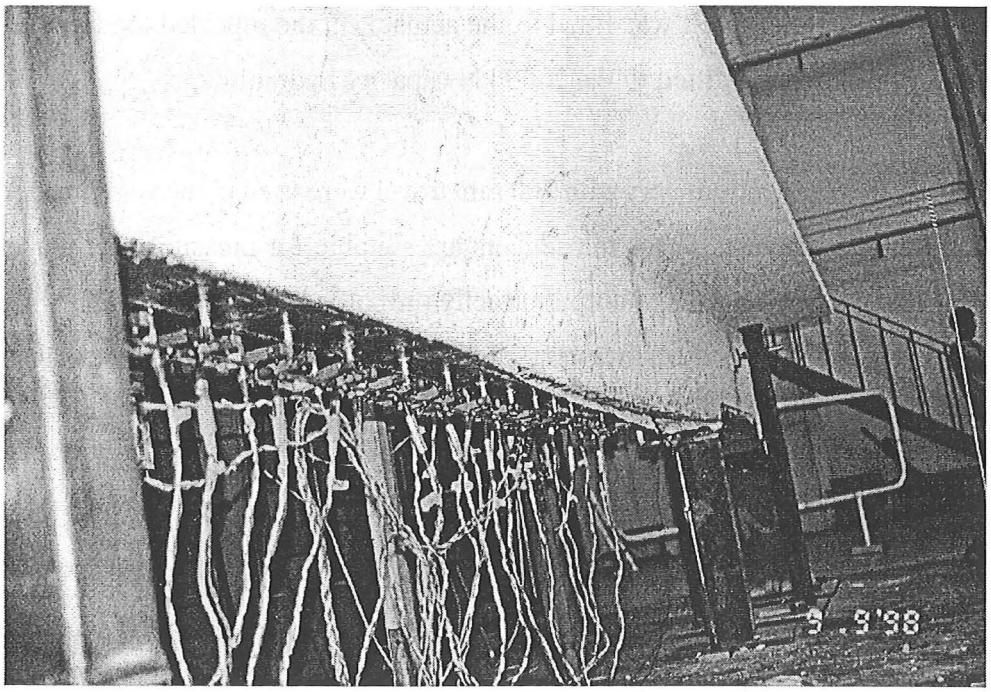

(b) Measurement

Figure 4.12 View of Clip Gauges Used in the Test Programme

Figure 4.13 shows the instrumentation arrangement for all test units. The strain on the CACM laminate was measured using DEMEC and clip gauges for Units F1 to F6, Units S1 and S2, and Unit C1. The reason for measuring the CACM strain with two types of gauges is that clip gauges can continuously monitor strains as a test progress whereas DEMEC gauges can only provide discrete but very accurate strain readings. The strain on the CACM laminates and GACM strips and the reinforcing steel in Unit C2 was measured only with DEMEC gauges due to the long-term measurement stability of this device.

4.8 Concrete Surface Measurement after Mechanical Abrading

Two mechanical abrading methods, scabbling and sandblasting, were employed in the test programme. The concrete surface in Unit F1 to Unit F5 was scabbled while the surface in Unit F6 and Series-B and Series-C Units was sandblasted.

The amplitude of the scabbled concrete surface was measured using a vernier as illustrated in **Figure 4.14(a)**. This measurement was performed choosing few typical points. The average amplitude of about 3 mm was obtained. However the vernier measurement could not easily measure the typical smaller amplitude obtained from sandblasting. Hence, a more accurate measurement of the concrete roughness was devised using a dial gauge as shown in **Figure 4.14(b)**. The gauge was installed in a circular steel cylinder with a hole inside for inserting the tip of the dial gauge into it. A 0.5 mm diameter needle was fixed in the end of the dial gauge tip to allow the smaller amplitude measurement. The results in the dial gauge measurement are plotted in **Figure 4.15**. It is shown that about 2.0 mm amplitude in average is obtained.

4.9 Test Results

4.9.1 Test Results on the Prototype Beam Unit P1

Figure 4.16 shows the relationship between applied load and measured mid-

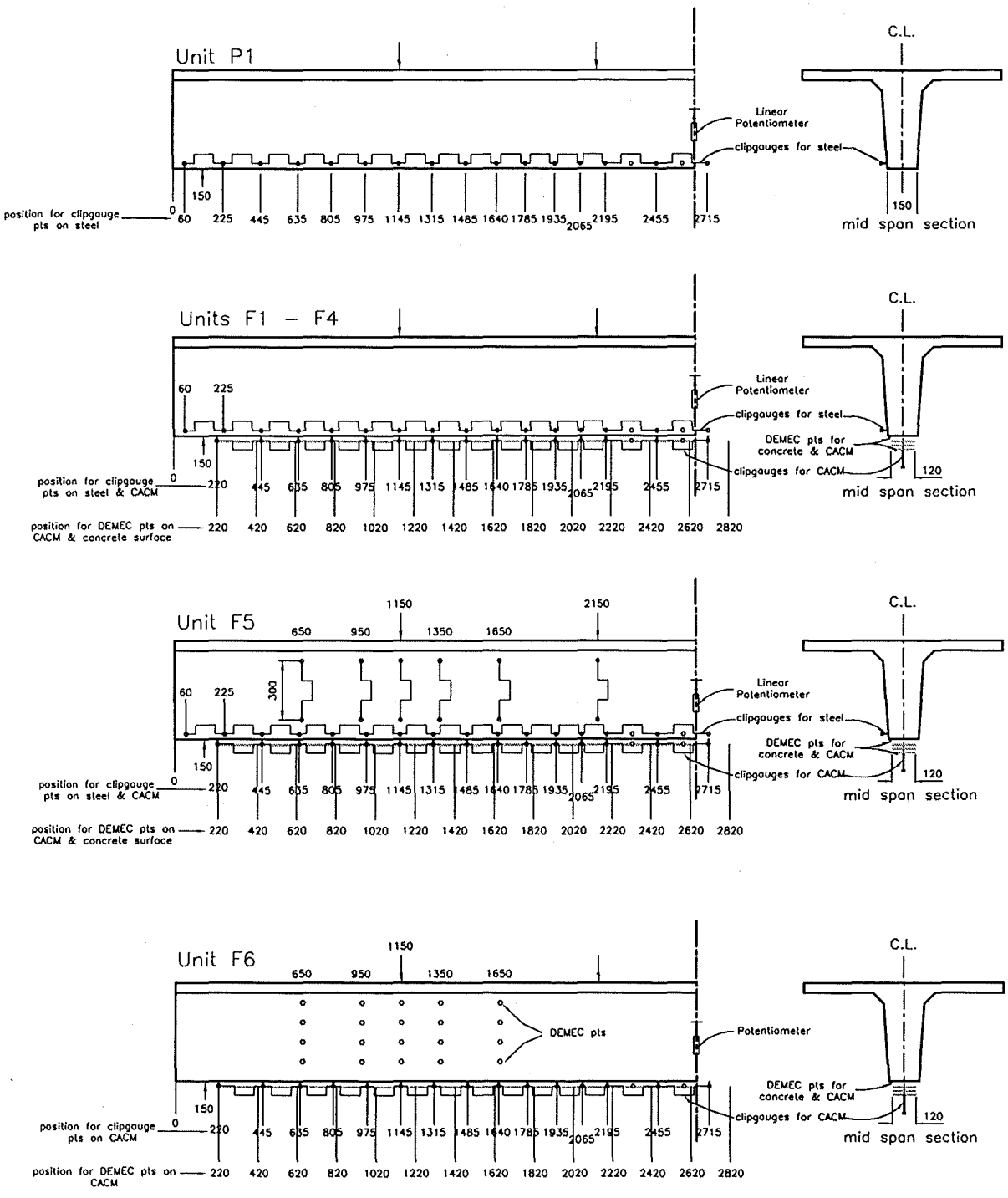

Figure 4.13 Instrumentation

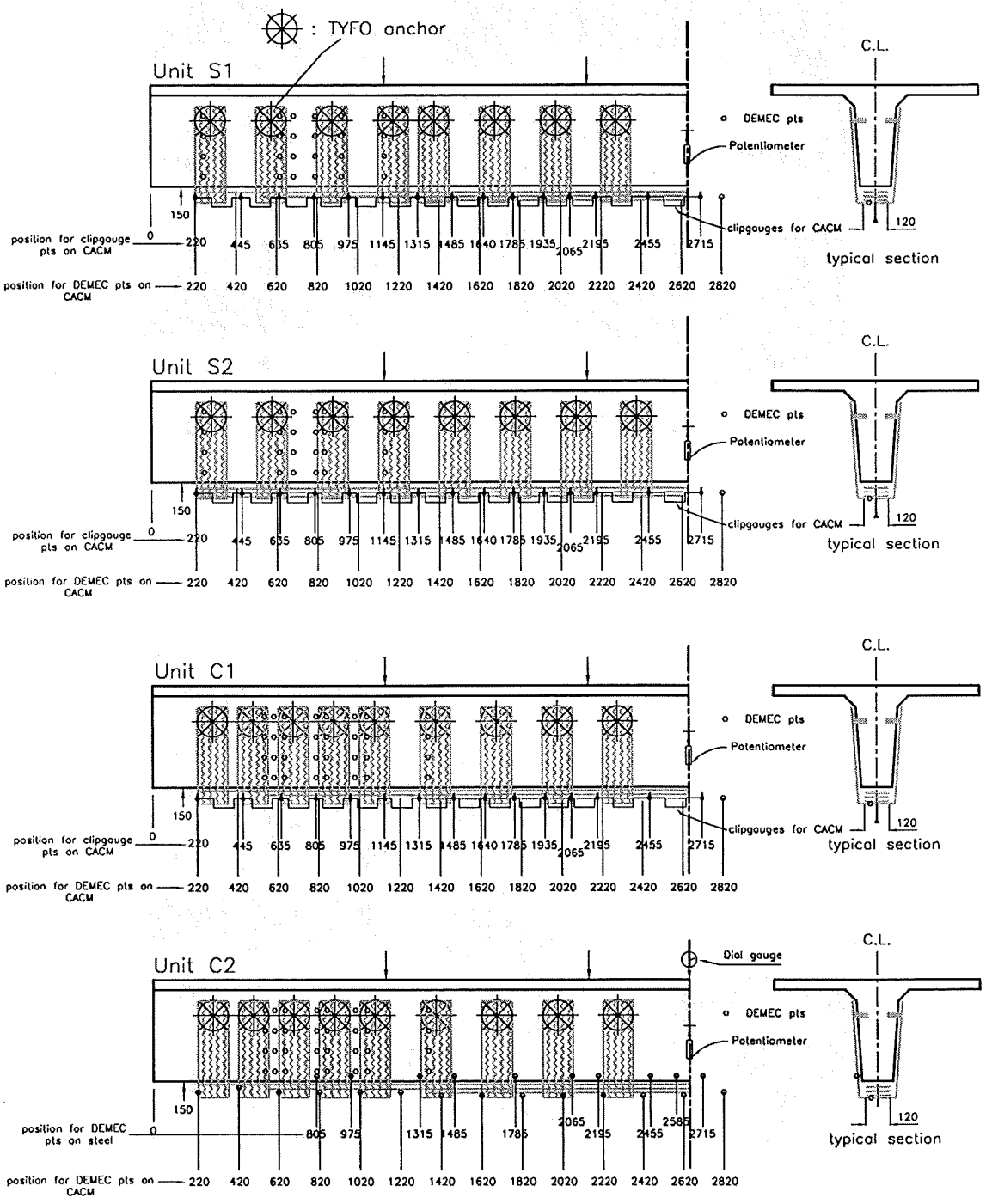

Figure 4.13 Instrumentation (Cont.)

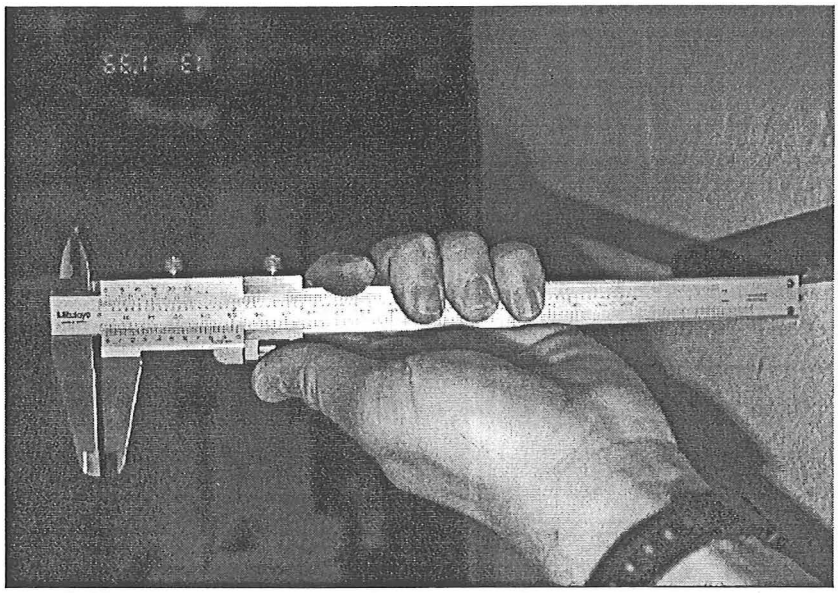

(a) Using a Vernier

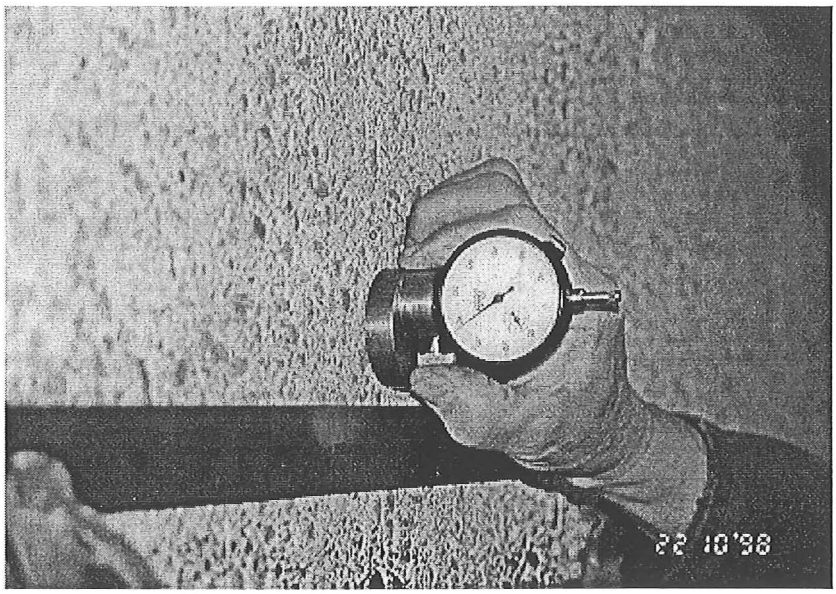

(b) Using a Dial Gauge

Figure 4.14 Measurement of the Concrete Surface Roughness

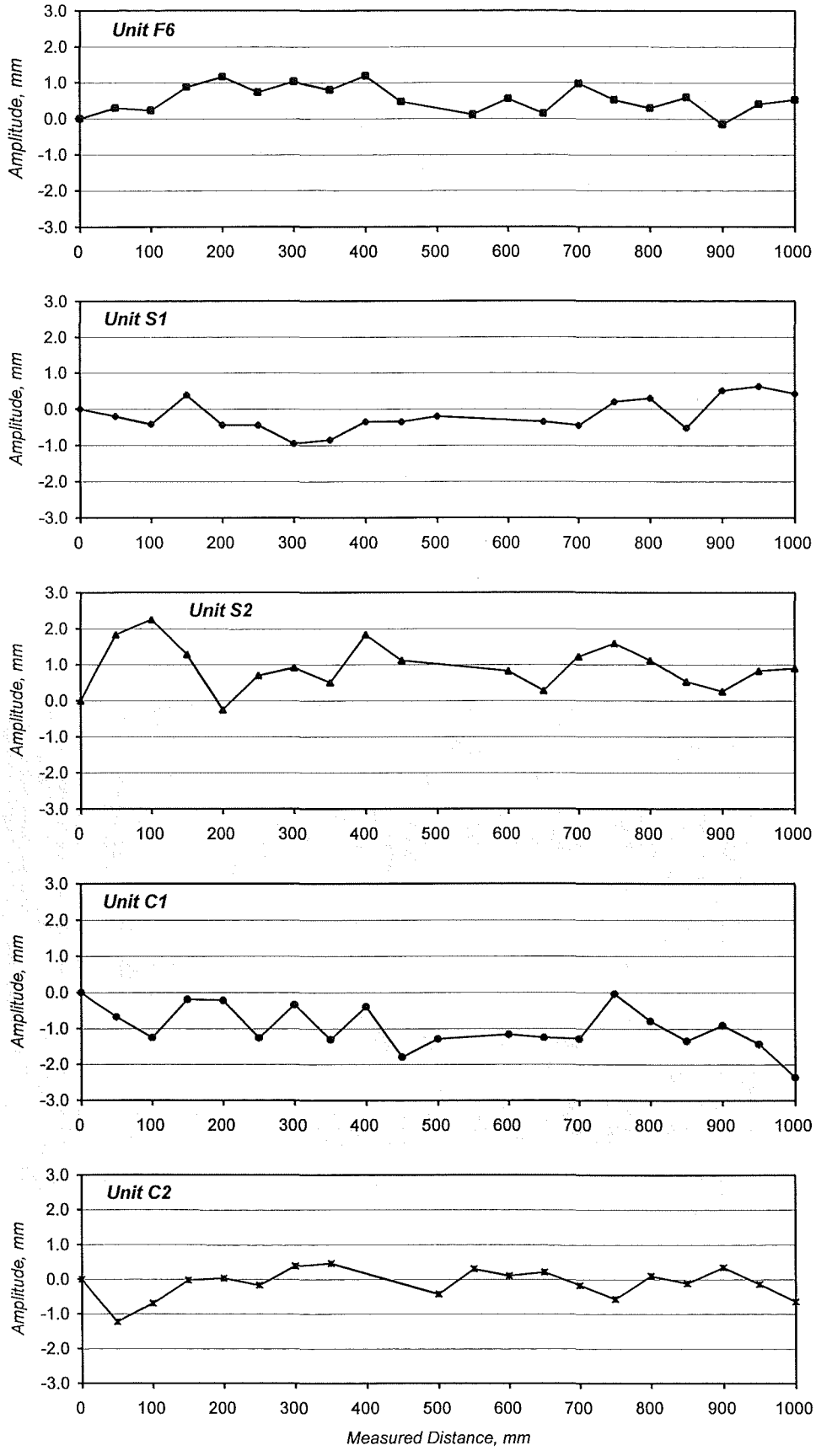

Figure 4.15 Measured Concrete Surface Roughness Prepared by Sandblasting

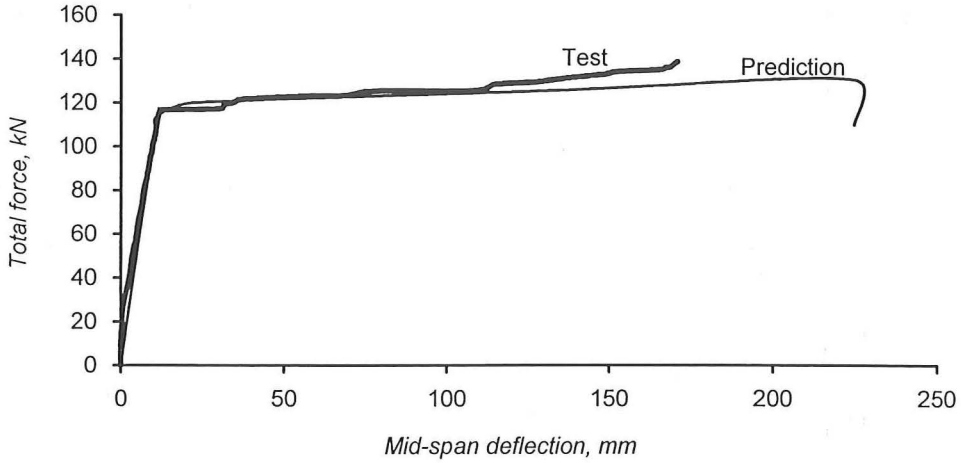

(a) Load versus Midspan Deflection

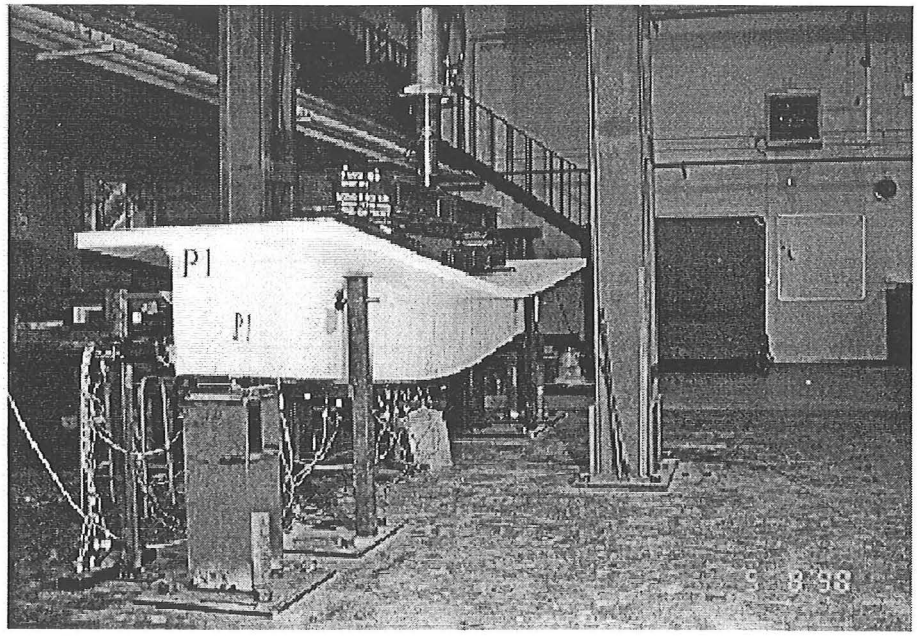

(b) View of Unit P1 at the End of the Test

Figure 4.16 Unit P1

span deflection and the unit at the end of the test. The prediction was also performed assuming the strain compatibility and force equilibrium over the depth of the beam section as described in Section 3.3. The prediction agrees with the measurement very well, as expected. **Figure 4.16(b)** shows that the beam tested showed very ductile behaviour as expected in the original design. Note that the test was halted when the mid-span deflection reached 171mm, far beyond 10 times the first yield deflection of 10.2mm. The load was still being sustained when the test ended.

Figure 4.17 depicts the crack pattern of Unit P1 at the end of test. The width of the main flexural cracks in mid-span becomes wider as the curvature increases and plastic deformation takes place in the central region of the beam span. Many small cracks in the beam bottom merged in the beam web above the bottom longitudinal reinforcement forming a main wide crack. The main cracks bifurcated at these ends near the neutral axis depth. Large plasticity was observed to occur at mid-span where the flexural cracks became up to over 6 mm wide at the end of the test.

It was observed that about 45-degree diagonal cracks developed at the vicinity of rebar cut-off points. These cracks remained small and did not affect overall response.

4.9.2 Test Results on Series-A Units

4.9.2.1 General Behaviour

During the repeated loading cycles, the load and mid-span deflection were recorded against time as depicted in **Figure 4.18**. The applied loading was very stable due to the servo control system. The mid-span deflection had a small tendency to increase as the cyclic loading history progressed. The difference of the mid-span deflection between the first cycle and the last cycle at maximum load ranged from 0.4 mm to 1.1 mm. **Table 4.4** shows the maximum and minimum load applied to the units during the repeated loading test as well as the difference of the mid-span deflections between the beginning and end of the test. The difference in deflection at the beginning and the end of the repeated loading was possibly caused by shear deformations developed during the gradual opening of diagonal cracks. The gradual opening of these cracks was monitored

Unit P1
Beam Type: BT2
Failure load, F=139kN
Central deflection=171mm
Failure mode: flexural failure

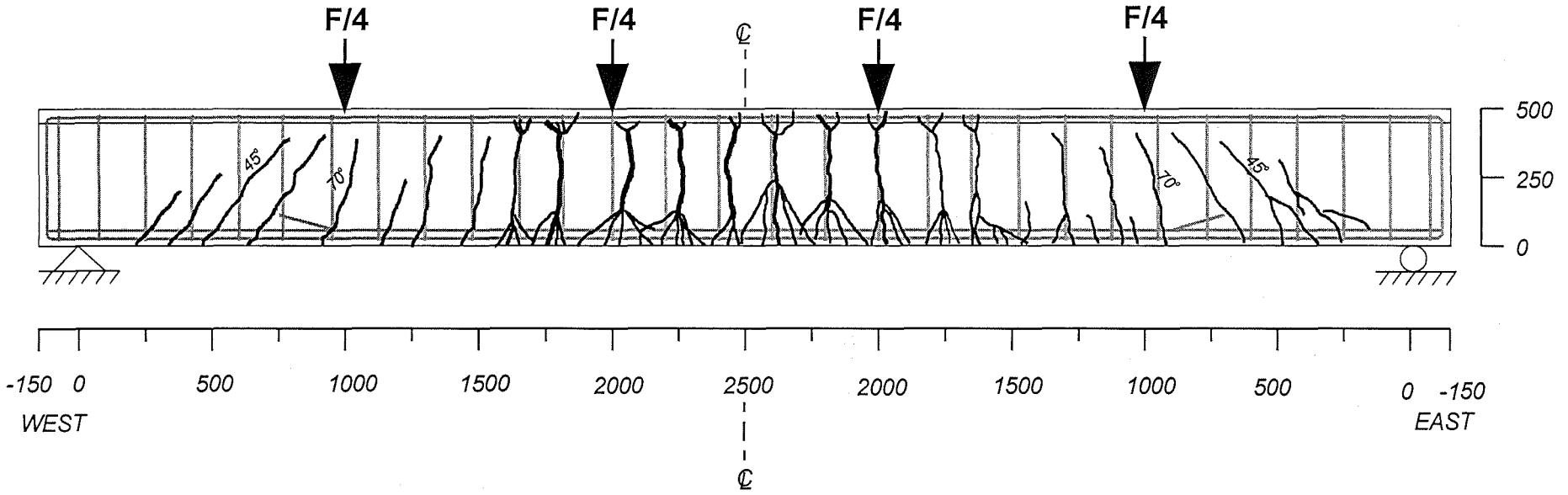

Figure 4.17 Crack Pattern of Unit P1 at the End of Test

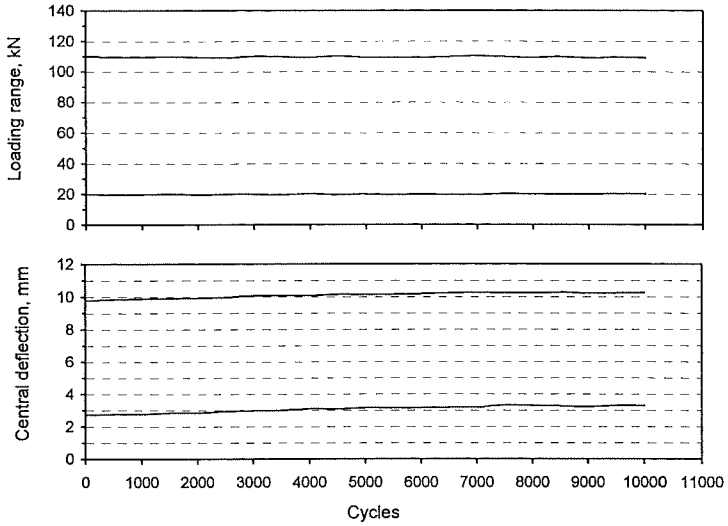

(a) Unit F1

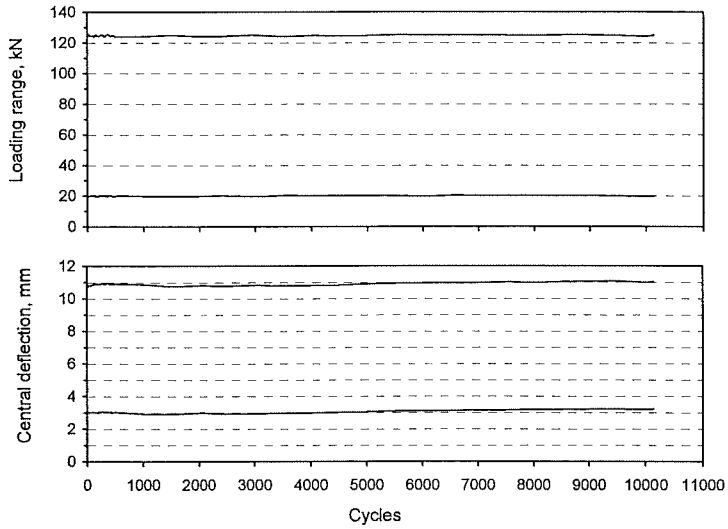

(b) Unit F2

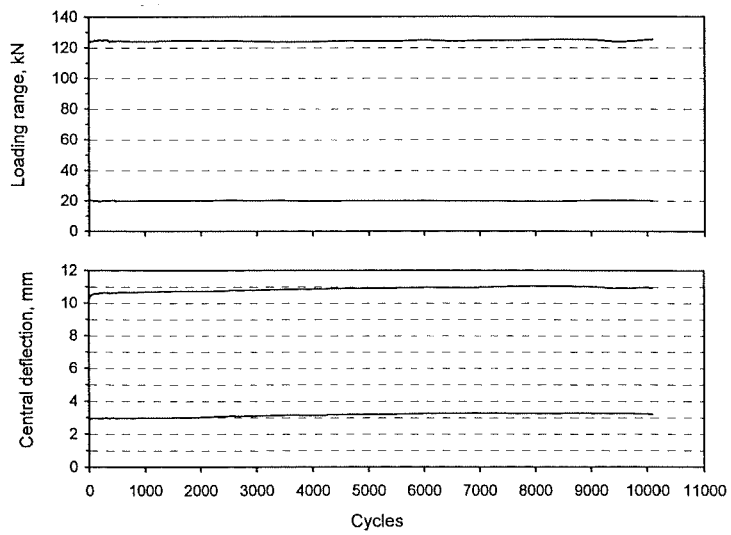

(c) Unit F3

Figure 4.18 Load and Deflection History Measured During Repeated Loading Cycles for Series-A Units

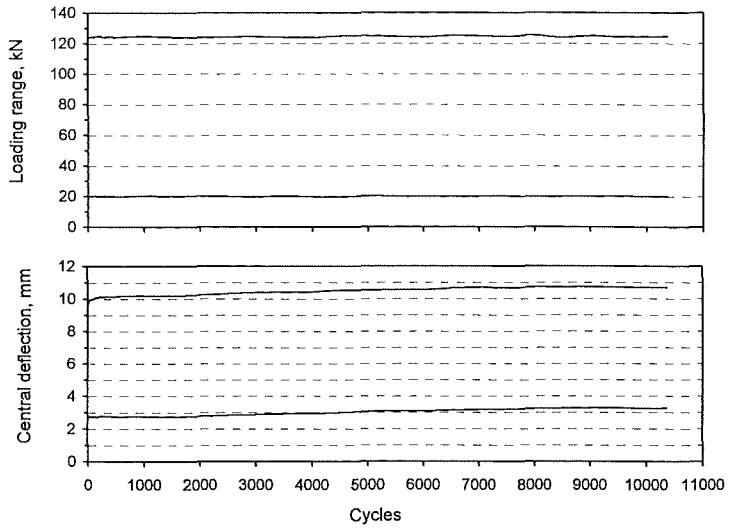

(d) Unit F4

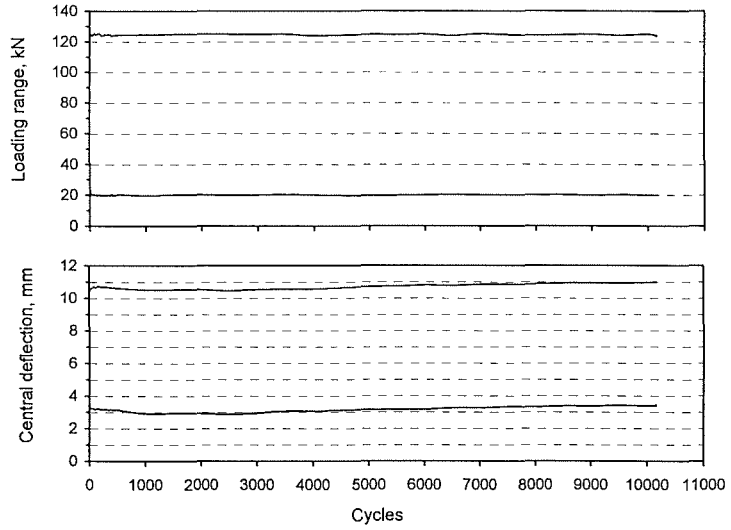

(e) Unit F5

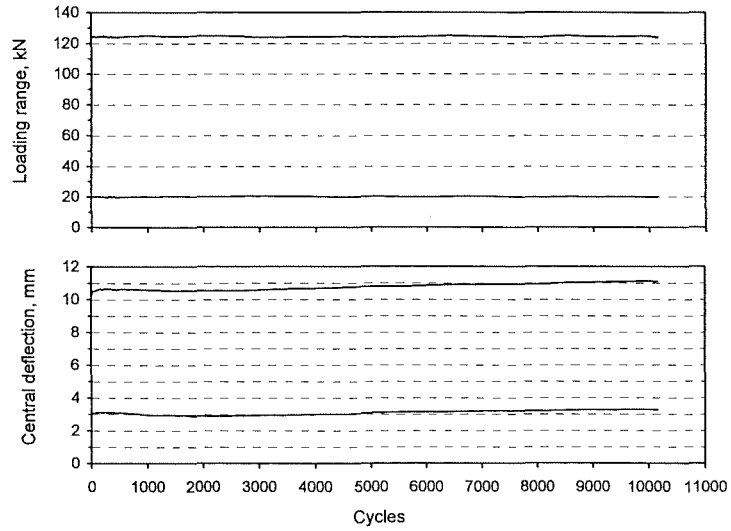

(f) Unit F6

Figure 4.18 Load and Deflection History Measured During Repeated Loading Cycles for Series-A Units (Cont.)

both macro and microscopically using a crack microscope.

Figure 4.19 depicts the crack pattern recorded at the end of the tests of Units F1 to F6. The development of cracking at different loading stages was monitored in all Units but Units F1 and F2. At the stage of repeated loading, new diagonal cracks developed at the highest shear zone in Units F3 to F6. The development of diagonal cracks caused the deflection increase during repeated loading cycle as mentioned previously. The diagonal cracks at the highest shear zone were found to begin as soon as in the first 100 cycles of repeated loading.

Table 4.4 The Difference of Mid-Span Deflection due to the Cyclic Effect of Repeated Loading for Test Series-A Units

Unit		F1	F2	F3	F4	F5	F6
Beam type		BT1	BT1	BT1	BT1	BT1	BT2
No. of Carbon ACM Laminates		1	3	3	3	3	3
Extent of laminates		full length	full length	full length	staggered	staggered	staggered
max. load (kN)		110	125	125	125	125	125
min. load (kN)		20	20	20	20	20	20
$\Delta_{10,000}$-Δ_1 (mm)	at max. load	0.4	0.9	0.5	1.1	1.2	0.7
	at min. load	0.6	0.1	0.2	0.4	0.1	0.3

Notes: Δ_1 = the mid-span deflection measured at first cycle of max. repeated loading.

$\Delta_{10,000}$ = the mid-span deflection measured at last cycle of max. repeated loading.

The crack widths in the region of pure bending moment were measured at the peak load. This load theoretically induced a maximum stress of $0.75f_{sy}$ (240 MPa) in the longitudinal reinforcement. **Table 4.5** shows the magnitude of the crack widths in the first and last cycle of repeated cyclic loading. It was observed that the number of flexural

Unit F1
Beam Type: BT1
Failure load, F=180kN
Central Deflection=54mm
Failure mode: CACM laminate rupture at central span

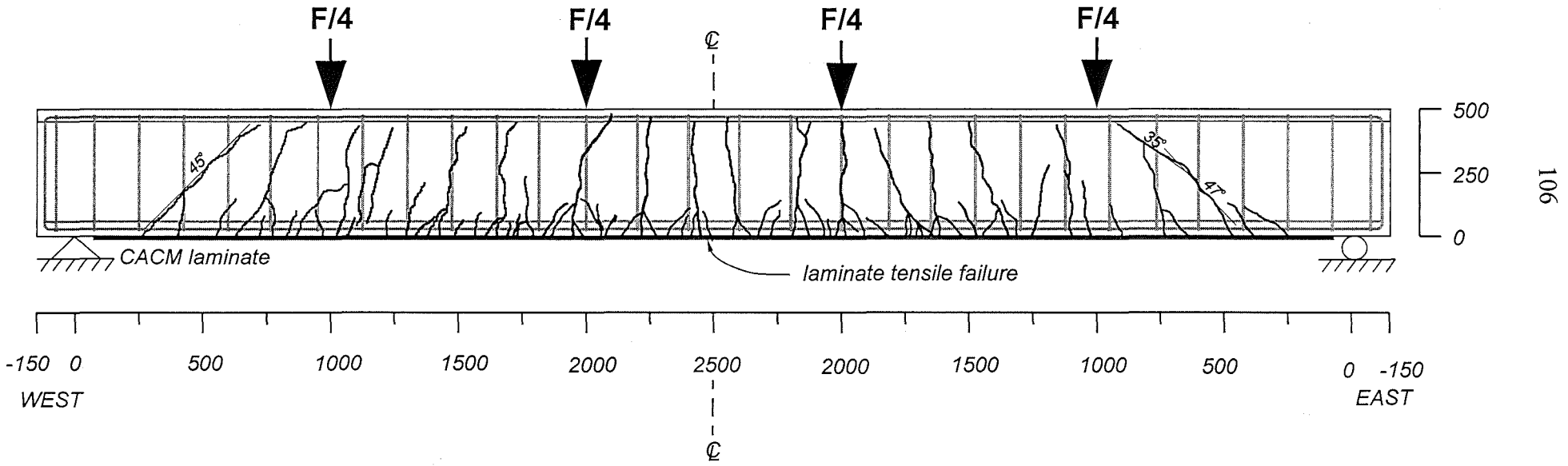

(a) Unit F1

Figure 4.19 Crack Pattern of Test Series-A Units at the End of Test

Unit F2
Beam Type: BT1
Failure load, F=239kN
Central deflection=48mm
Failure mode: CACM laminate end peel-off at east side

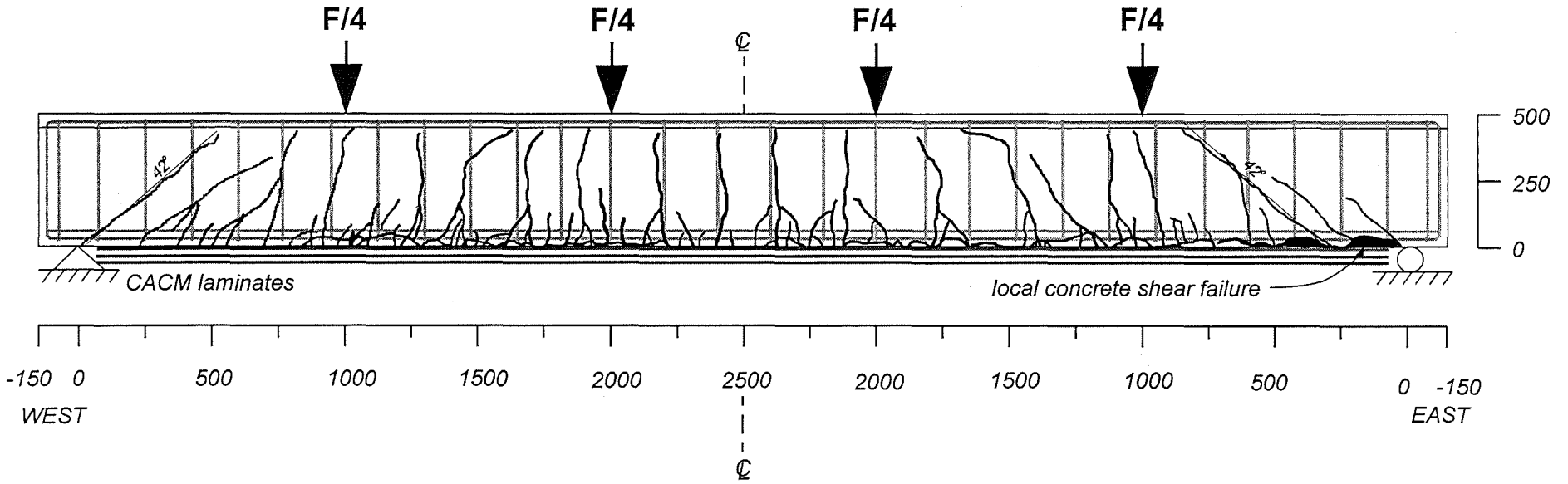

(b) Unit F2

Figure 4.19 Crack Pattern of Test Series-A Units at the End of Test (Cont.)

Unit F3
Beam Type: BT1
Failure load, F=236kN
Central deflection=48mm
Failure mode: CACM laminate peel-off due to shear distortion at 700mm away from east support

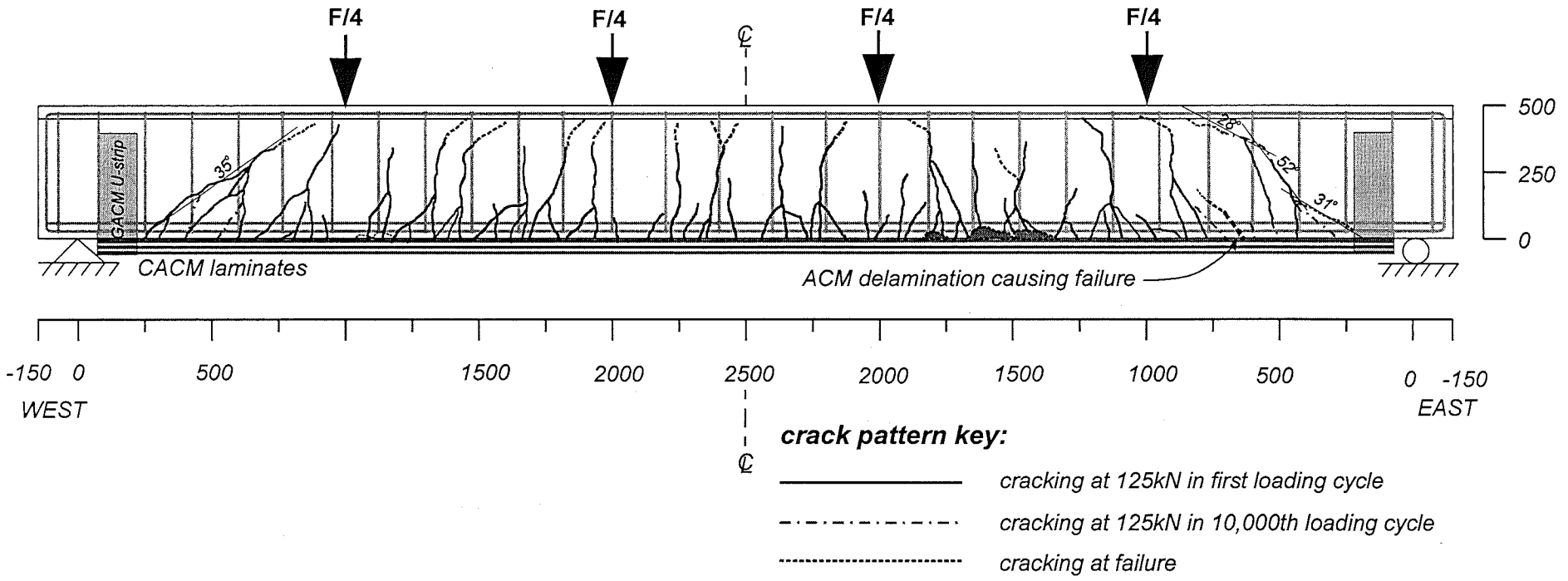

(c) Unit F3

Figure 4.19 Crack Pattern of Test Series-A Units at the End of Test (Cont.)

Unit F4
Beam Type: BT1
Failure load, F=202kN
Central deflection=35mm
Failure mode: CACM delamination starting at 1.5 m away from west support

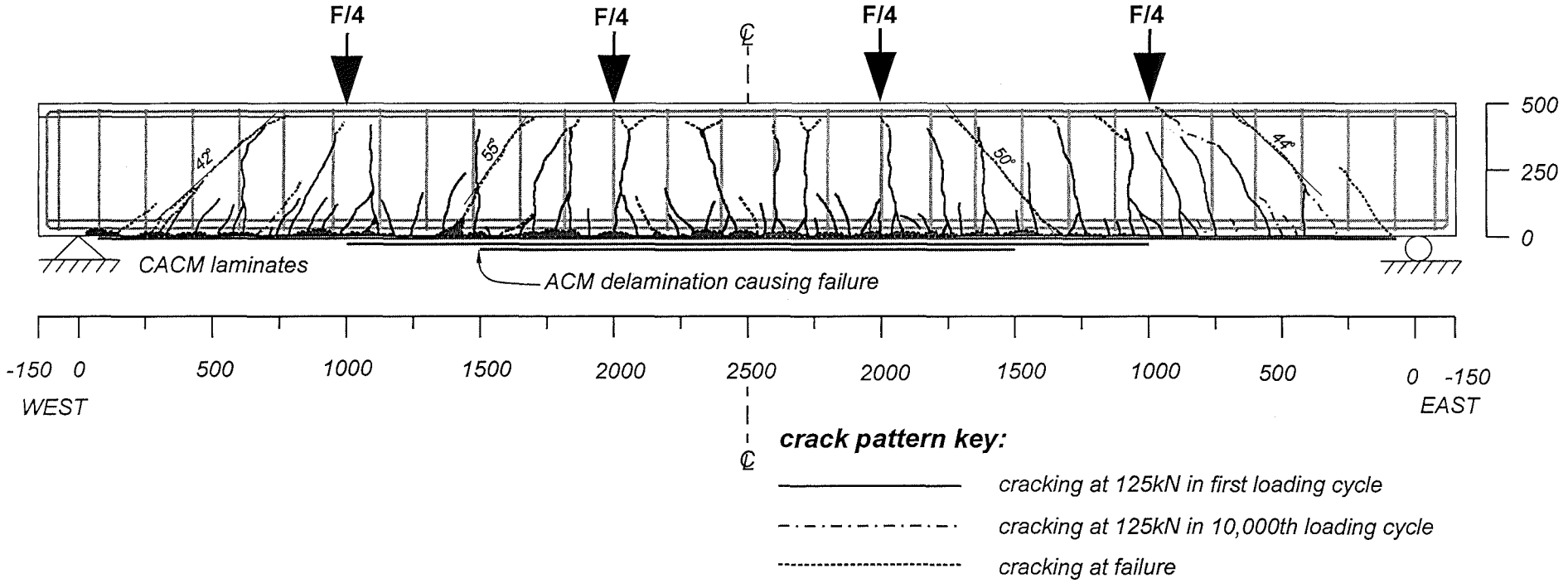

(d) Unit F4

Figure 4.19 Crack Pattern of Test Series-A Units at the End of Test (Cont.)

Unit F5
Beam Type: BT1
Failure load, F=238kN
Central deflection=48mm
Failure mode: CACM delamination starting at 1.2 m away from east support

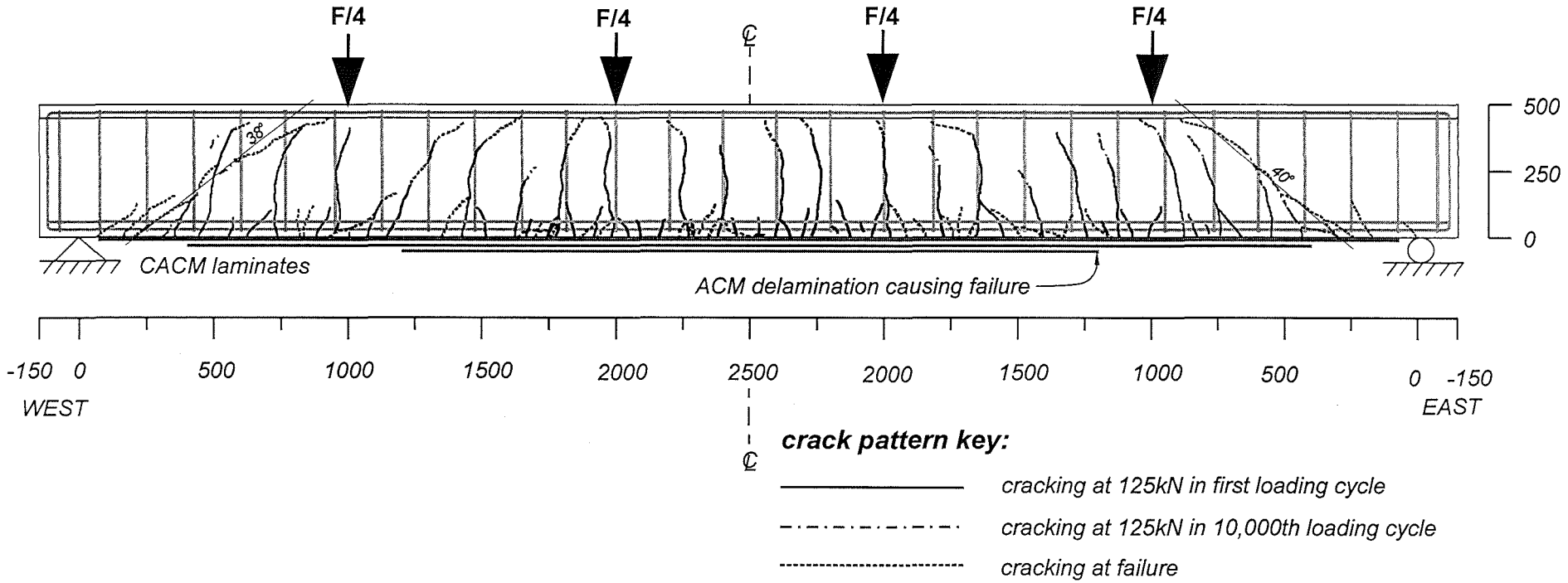

(e) Unit F5

Figure 4.19 Crack Pattern of Test Series-A Units at the End of Test (Cont.)

Unit F6
Beam Type: BT2
Failure load, F=220kN
Central deflection=45mm
Failure mode: CACM delamination starting 1.2 m away from east support

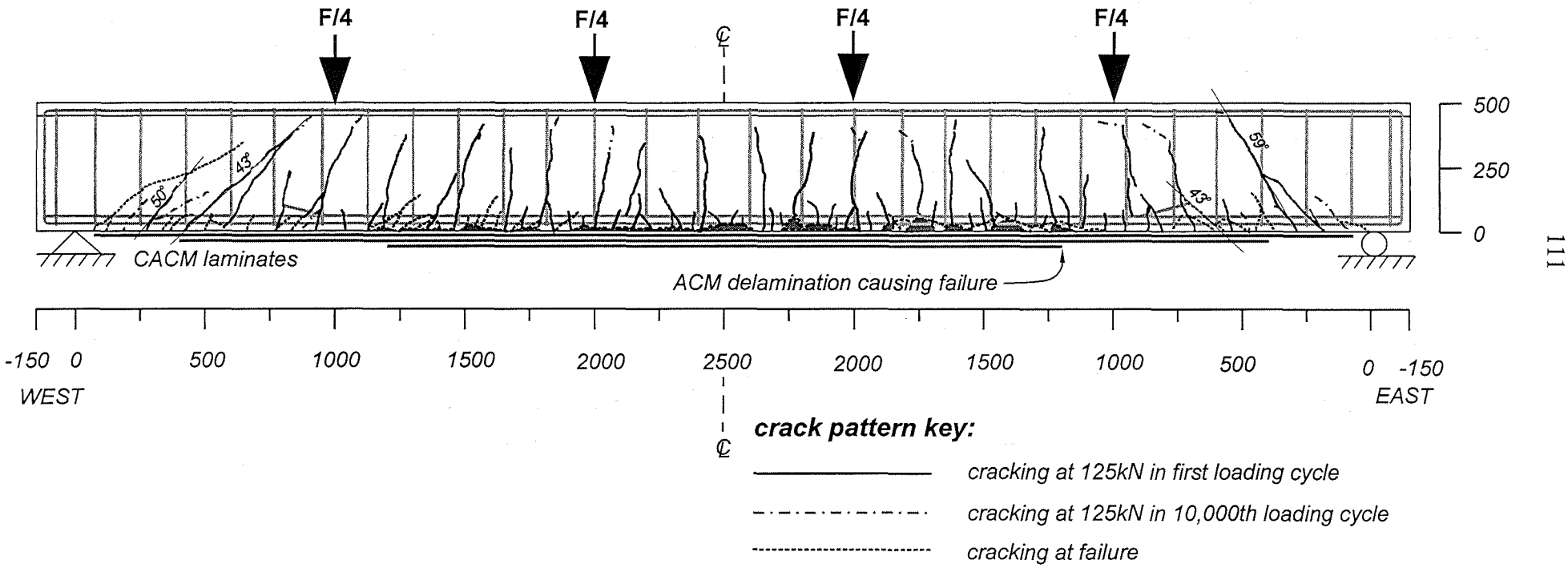

(f) Unit F6

Figure 4.19 Crack Pattern of Test Series-A Units at the End of Test (Cont.)

Table 4.5 Flexural Crack Width in the Region of Pure Bending Moment for Series-A Units

Unit	Cycle	Load (kN)	Crack width (mm), measured level = 50mm away from beam bottom face																			Σ
			No.1	No.2	No.3	No.4	No.5	No.6	No.7	No.8	No.9	No.10	No.11	No.12	No.13	No.14	No.15	No.16	No.17	No.18	No.19	No.20	
P1	1st	110	0.12	0.08	0.10	1.10	0.12	0.04	0.06	0.06	0.10												1.78
F1	1st	115	0.05	0.04	0.04	0.04	0.06	0.04	0.06	0.04	0.04	0.06	0.04	0.05	0.02	0.02	0.06	0.08	0.06	0.02	0.04	0.04	0.90
	10000th	115										0.06	0.04	0.05	0.02	0.02							
F2	1st	125	0.01	0.02	0.04	0.04	0.04	0.04	0.03	0.04	0.04	0.02	0.02	0.02	0.04	0.01	0.03	0.04	0.02	0.02			0.52
	10000th	125									0.04						0.03						
F3	1st	125	0.02	0.02	0.04	0.08	0.02	0.02	0.06	0.02	0.04	0.04	0.04	0.06	0.04	0.04	0.04	0.02					0.60
	10000th	125			0.04	0.10					0.04			0.06	0.04			0.04					
F4	1st	125	0.02	0.02	0.02	0.04	0.04	0.04	0.01	0.04	0.04	0.06	0.04	0.06	0.06	0.06	0.02	0.02	0.04	0.05	0.06		0.74
	10000th	125		0.02						0.04						0.06			0.04				
F5	1st	125	0.12	0.04	0.06	0.06	0.05	0.04	0.06	0.04	0.04	0.10	0.10	0.02	0.04	0.04	0.06						0.87
	10000th	125	0.14			0.06			0.06			0.10	0.10										
F6	1st	125	0.04	0.04	0.04	0.02	0.02	0.06	0.02	0.10	0.01	0.04	0.10	0.02	0.02	0.16	0.08	0.04	0.02	0.04			0.87
	10000th	125		0.04			0.08	0.08		0.10			0.08			0.14							

cracks in Units F1 to F6 was about twice of that observed in Unit P1. **Table 4.5** is conclusive in that the crack widths in beams with bonded CACM laminates were approximately half or less of that in the prototype beam. This trend implies that the serviceability performance in the reinforced concrete beams strengthened with CACM laminates bonded to their soffit is better than that in the prototype beam due to the large number of well distributed fine cracks.

Table 4.6 Measured Stiffness and Failure Load of Test Series-A Units

Unit	ACM laminates	$F'_{y,t}$ (1) (kN)	Δ_m (2) (mm)	$F'_{y,t} / \Delta_m$ (3) (kN/mm)	Stiffness (4) ratio	F_u (5) (kN)
P1	-	100	9.6	10.4	1.00	139
F1	1	110	9.4	11.7	1.13	180
F2	3	125	10.2	12.3	1.18	239
F3	3	125	10.1	12.4	1.19	236
F4	3	125	9.6	13.0	1.25	202
F5	3	125	10.0	12.5	1.20	238
F6	3	125	10.4	12.0	1.15	220

Notes: (1) $F'_{y,t}$ = theoretical load corresponding to a stress of $0.75f_{sy}$ (240 MPa) in the longitudinal reinforcing steel.

(2) Δ_m = mid-span deflection corresponding to $F'_{y,t}$.

(3) Measured stiffness of the test unit.

(4) Ratio between the stiffness in a unit and the stiffness of Unit P1.

(5) F_u = failure load of the test unit at the end of test.

Figure 4.20 plots the applied vertical load versus the observed mid-span deflection for the test units in Series-A. The observed behaviour in the service load range is also shown in **Figure 4.20**. The response of prototype beam is also plotted in these figures for comparison. The stiffness in the service load range and failure loads at the test units are shown in **Table 4.6**. The stiffness was defined as the ratio between the service load corresponding to the three quarters of the yield stress in the lower layer of beam

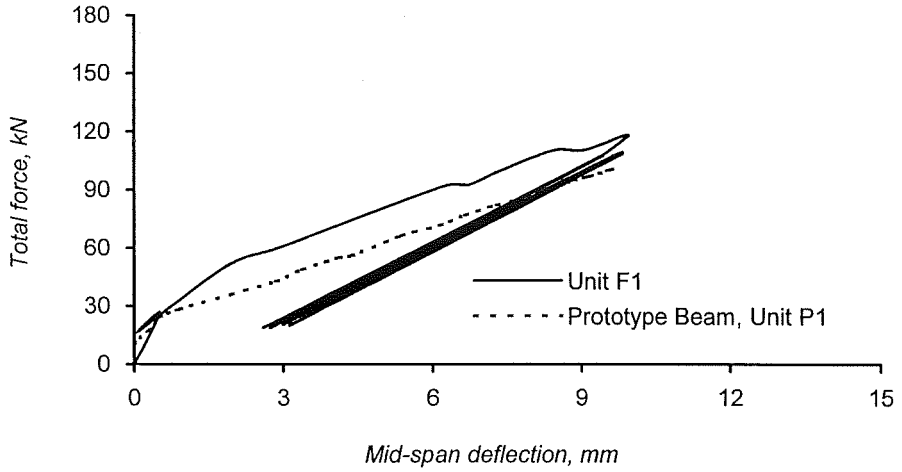

Response in the Service Load Range

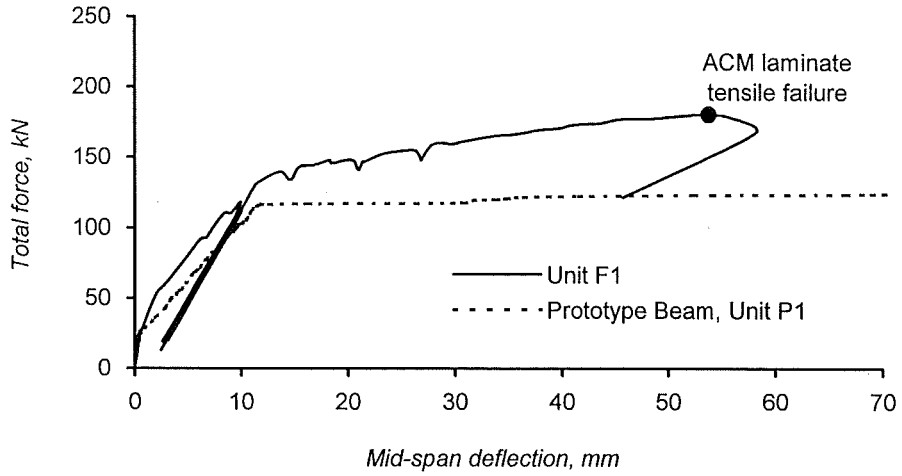

Total Response

(a) Unit F1

Figure 4.20 Vertical Load versus Mid-span Deflection for Series-A Units

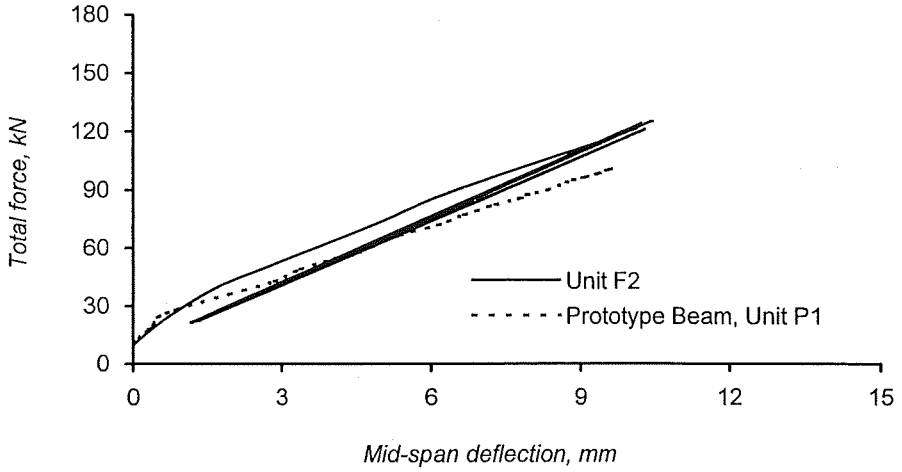

Response in the Service Load Range

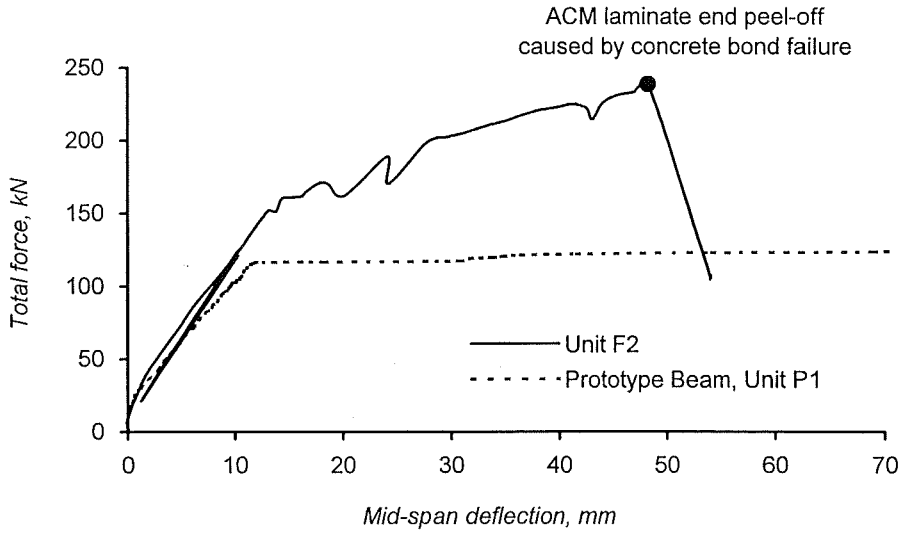

Total Response

(b) Unit F2

Figure 4.20 Vertical Load versus Mid-span Deflection for Series-A Units (Cont.)

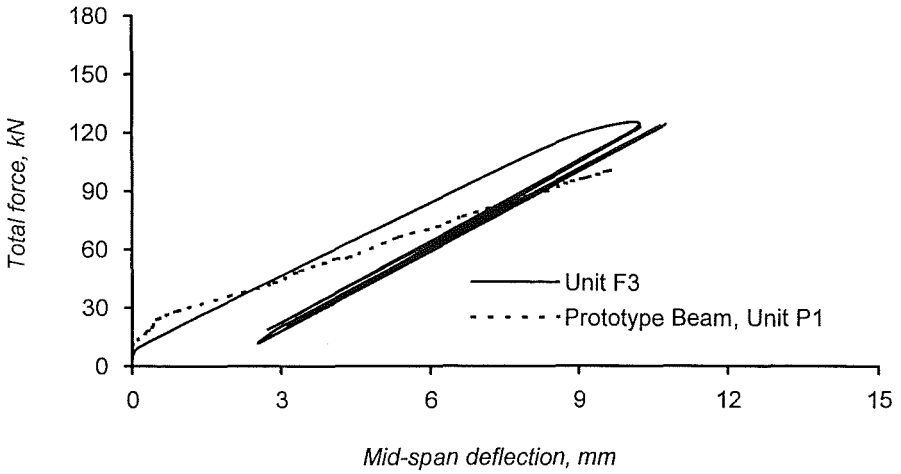

Response in the Service Load Range

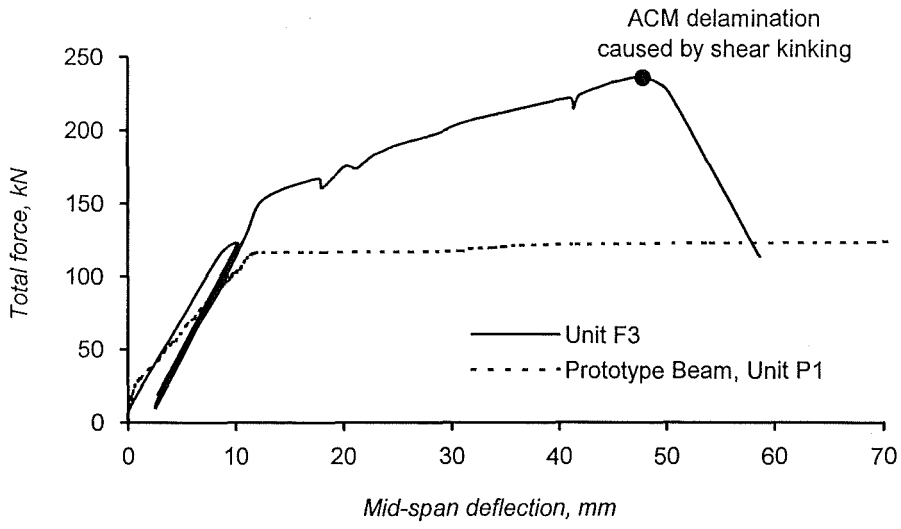

Total Response

(c) Unit F3

Figure 4.20 Vertical Load versus Mid-span Deflection for Series-A Units (Cont.)

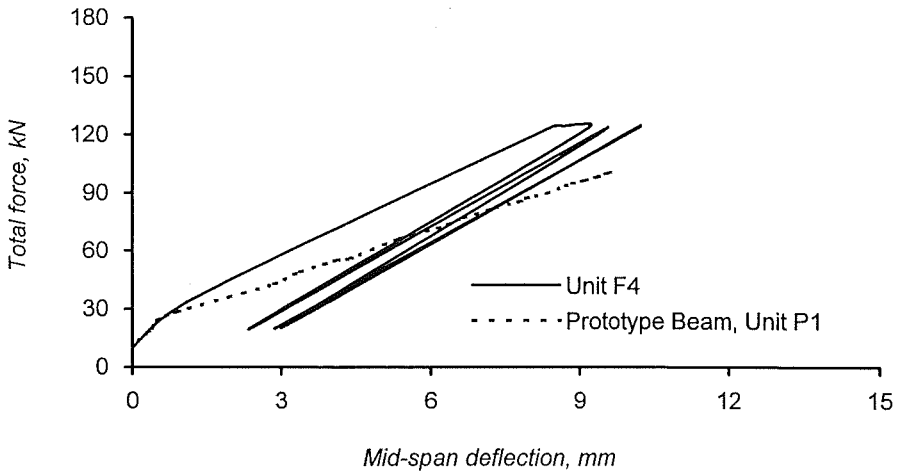

Response in the Service Load Range

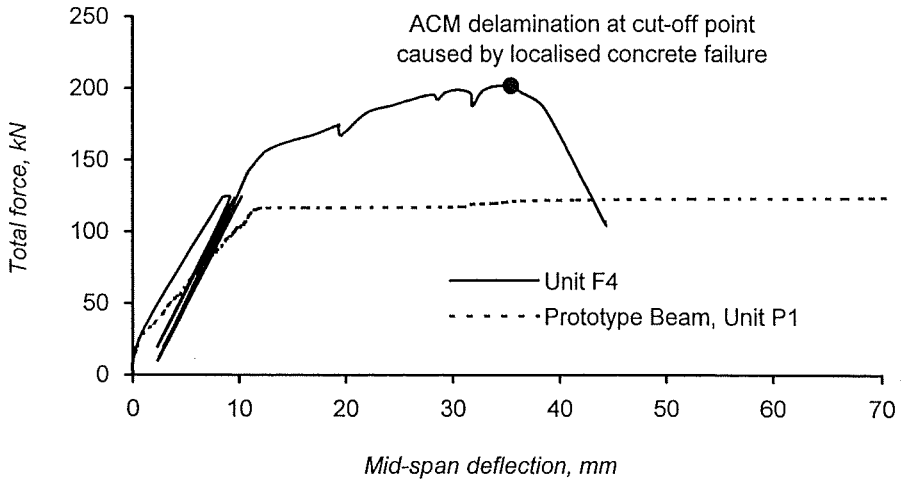

Total Response

(d) Unit F4

Figure 4.20 Vertical Load versus Mid-span Deflection for Series-A Units (Cont.)

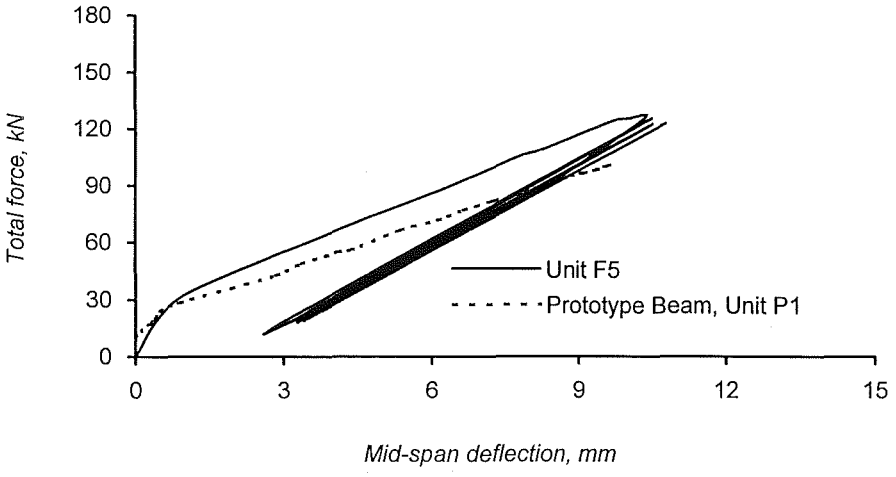

Response in the Service Load Range

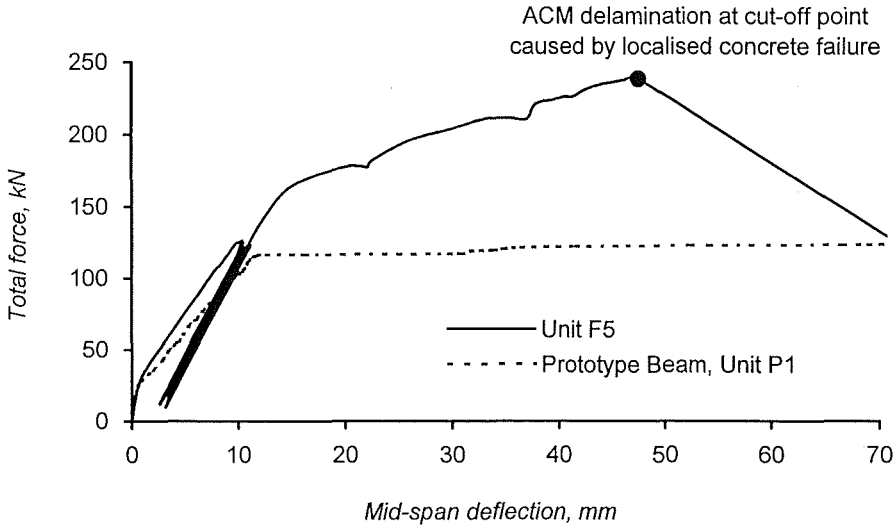

Total Response

(e) Unit F5

Figure 4.20 Vertical Load versus Mid-span Deflection for Series-A Units (Cont.)

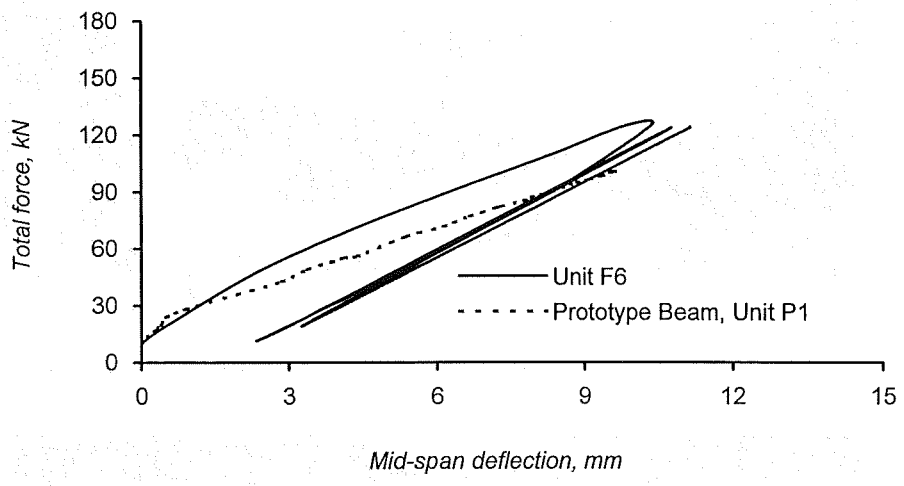

Response in the Service Load Range

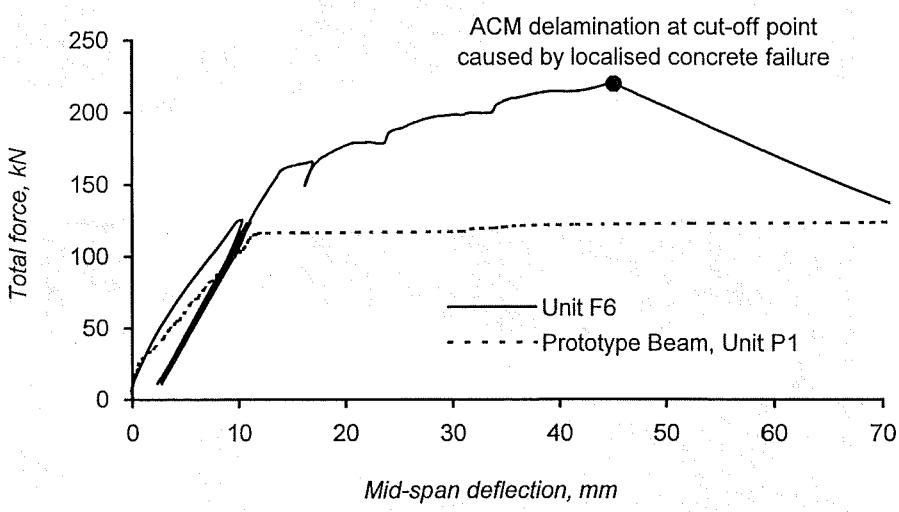

Total Response

(f) Unit F6

Figure 4.20 Vertical Load versus Mid-span Deflection for Series-A Units (Cont.)

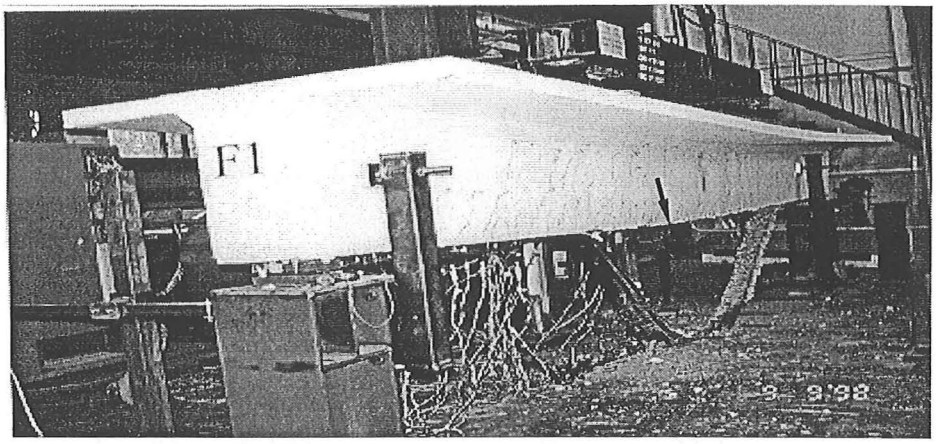

(a) Unit F1 with CACM Laminate Rupture at Mid-span

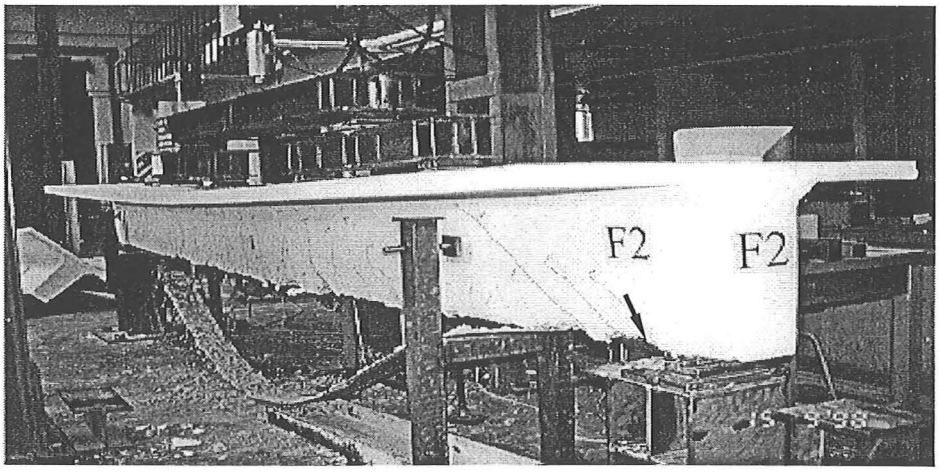

(b) Unit F2 with CACM Laminate End Peel-off at East Side

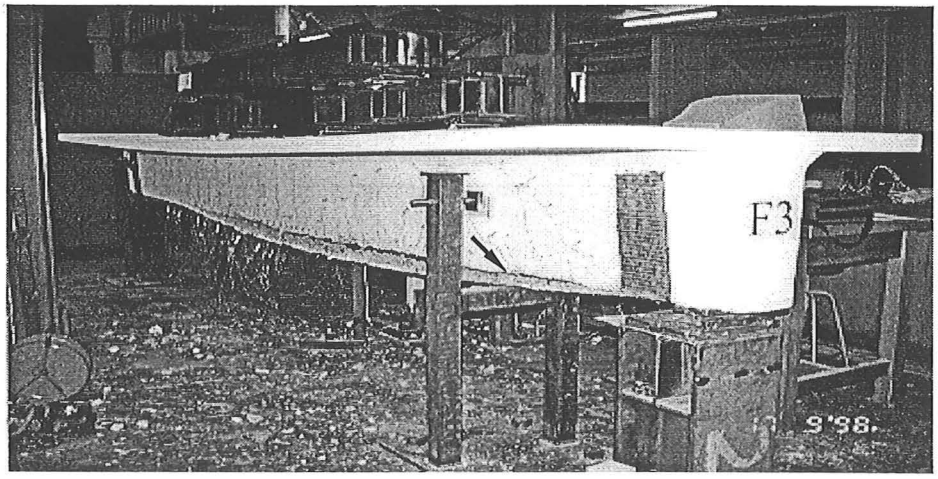

(c) Unit F3 with CACM Delamination due to Shear Distortion at East Side

Figure 4.21 Failure Mode of Test Series-A Units

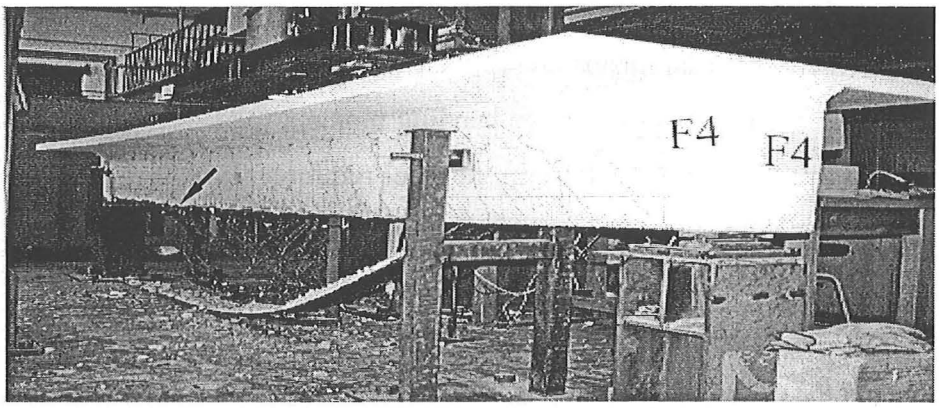

(d) Unit F4 with CACM Delamination Starting at 1.5 m away from West Support

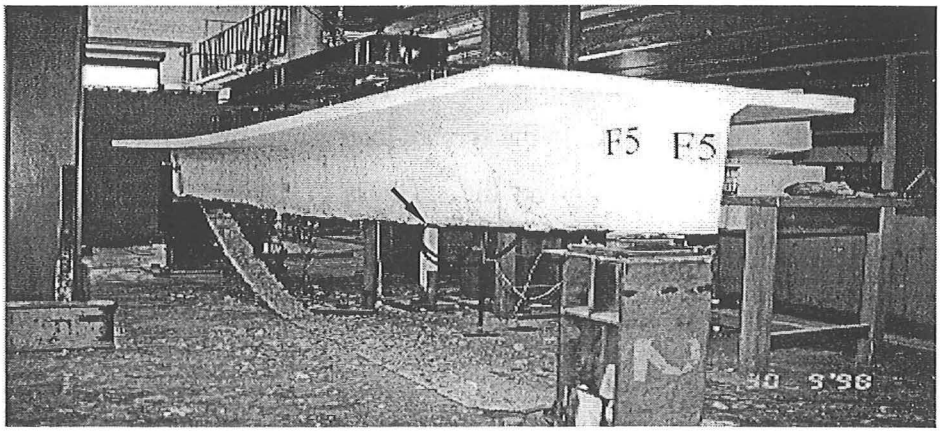

(e) Unit F5 with CACM Delamination Starting at 1.2 m away from East Support

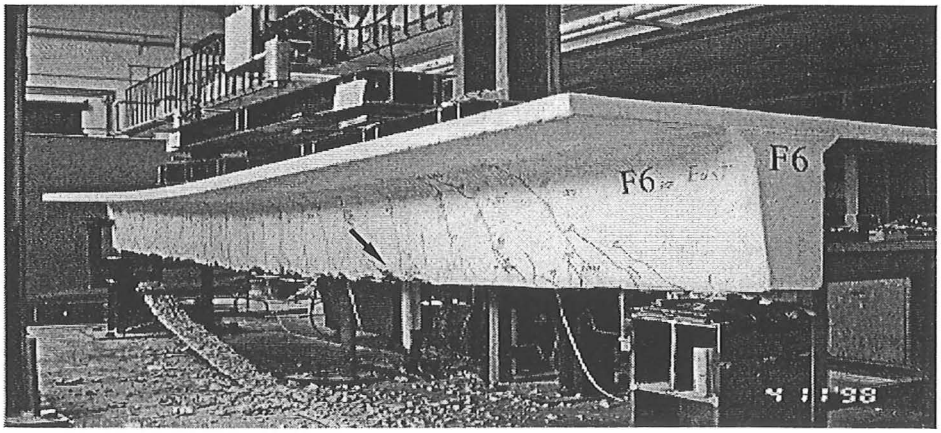

(f) Unit F6 with CACM Delamination Starting at 1.2 m away from East Support

Figure 4.21 Failure Mode of Test Series-A Units (Cont.)

longitudinal bars ($0.75f_{sy}$ = 240 MPa) and the mid-span deflection measured at this load. It can be referred from **Table 4.6** that both the service load and the stiffness of the beams increase when ACM laminates are applied to the beams to resist flexure. Note that in flanged beams subjected to positive bending moment the service load is nearly always controlled by the allowable stress in the steel reinforcement. The service load increase can be theoretically derived as will be discussed in Chapter 6.

A description of the behaviour observed during the testing of the Series-A Units is given in the following paragraphs.

Unit F1

Unit F1 was retrofitted with a full-length only one CACM laminate bonded to its tension face, see **Figure 4.2(a)**. In the service load range, the stiffness of the strengthened beam increased, which is 13% over the stiffness of the prototype Unit P1 (see **Figure 4.20(a)** and **Table 4.6**). The number of flexural cracks at mid-span was about twice of that observed in the prototype unit but their width was significant smaller, see **Table 4.5**.

This unit was loaded until a tensile failure in the CACM laminate occurred at mid-span. **Figure 4.20(b)** plots the overall response of the unit. Failure was always announced far in advance by creaking sounds coming from the laminate. Also the mode of failure of this unit conformed to the design philosophy proposed in Section 4.2.2. The crack pattern for Unit F1 was similar to that observed in Unit P1, compare **Figures 4.17** and **4.19(a)**. A view of Unit F1 after failure occurred is shown in **Figure 4.21(a)**.

Unit F2

Unit F2 was retrofitted with three full-length CACM laminates bonded to its tension side, see **Figure 4.2(a)**. The stiffness of this unit at the first cycle of the repeated loading stage was 18% greater than that measured in Units P1 as **Table 4.6** shows. This implied the service load enhancement could be achieved when the externally bonded ACM laminate is used. The eighteen flexural cracks that developed in the first cycle of the repeated loading at the mid-span were similar to those observed in Unit F1. However, the total crack width is smaller than that measured in Unit F1, see **Table 4.5**. This is

because the initial stiffness of the beam Unit F2 is higher that that of Unit F1.

Unit F2 failed at a load equal to 239 kN, which is below the theoretical load of 268 kN required to cause the tensile failure in the CACM laminate at the beam mid-span. The crack patterns at the end of the test were different from those observed in Unit F1, see **Figure 4.19(b)**. Failure in this beam was due to peeling of the laminate caused by a localised concrete shear failure at the concrete-to-CACM laminate interface at the east end of the laminates, see **Figures 4.19(b)** and **4.21(b)**. The inclination of diagonal cracks at the high shear zone were 42 degrees, which are slightly flatter than those measured in Unit F1.

Unit F3

Unit F3 was identical to Unit F2 except for additional GACM U-strips bonded to the ends of the full-length CACM laminates, see **Figure 4.2(a)**. The U-strips were placed to prevent the localised concrete shear failure that occurred at the end of the CACM laminates in Unit F2. However, as can be seen by comparing **Figures 4.20(b)** and **(c)**, the behaviour for both units was nearly identical. The total crack width depicted in **Table 4.5** and the initial stiffness shown in **Table 4.6** show a nearly identical behaviour for Units F2 and F3 at the service load range.

Although the U-strips bonded to Unit F3 were able to hamper the CACM laminates from peeling off at the ends, delamination occurred at a distance of about 700 mm away from the east end, see **Figure 4.19(c)**. Delamination occurred at about the same ultimate load as the laminate peel-off in Unit F2. As will be shown in Section 4.9.2.4, beam shear distortion, which developed as a result of the beam shear strength and capacity being very close, induced premature delamination of the laminates. The crack pattern at the end of the test of Units F2 and F3 are very similar, see **Figures 4.19 (b)** and **(c)**.

Unit F4

Unit F4 had three staggered CACM laminates bonded to the tension side, see **Figure 4.2(a)**. The vertical force versus mid-span deflection of this beam is shown in

Figure 4.20(d). The observed response in the service load range indicates that staggering of the CACM laminates had no effect on the stiffness of this unit. In fact, the stiffness was slightly higher than that of Units F2 and F3, see **Table 4.6**. This is certainly a statistical error as first principles indicate that the stiffness would tend to slightly decrease when staggering the laminates. The total crack width measured in the first cycle of the repeated loading stage was smaller than that observed in Unit P1 but larger than that observed in Units F2 and F3, see **Table 4.5**. It can be said that the performance of the beam retrofitted with staggered ACM laminates at the service load range is similar to that of beam retrofitted with full-length ACM laminates.

Failure of this unit occurred at 202 kN, which was the lowest among the Series-A Units. **Figures 4.19(d)** and **4.21(d)** show the crack pattern and the beam at the end of the test. Cut-off points of the CACM laminates were deliberately designed short in order to observe a potential failure in their region. Such failure enabled the calibration of the model described in Chapter 3. A discussion of the predicted and measured behaviour is presented in Section 4.9.2.4.

Unit F5

Unit F5 had three staggered CACM laminates. The laminates were well developed and as a result the cut-off points were further away from mid-span than the cut-off points in the laminates in Unit F4. It can be observed in **Figure 4.20(e)** that the vertical load versus mid-span deflection behaviour at the service load range is very similar to that recorded in Units F2 to F4. The total crack width measured in the region of constant bending moment was larger than that measured in Units F2 to F4, see **Table 4.5**. **Table 4.6** shows that the stiffness of this unit is comparatively similar to the stiffness in Units F2 to F4.

The failure load obtained at the ultimate load stage was 238 kN, which was similar to the ultimate load in Units F2 and F3 and greater than that of Unit F4. Failure in this unit occurred at the cut-off point of the 2-to-3-layer laminate at a distance of 1.2 m away from the east support. **Figures 4.19(e)** and **4.21(e)** show the extent of cracking and the unit at the end of the test. Localised concrete shear failure occurring in the highly stressed laminates at the cut-off point, was the main reason for causing failure in this unit.

Unit F6

Units F6 and F5 had the same CACM laminate layout. The only difference among these two units was the layout of the beam longitudinal steel reinforcement. In Unit F5 the longitudinal steel reinforcement was continuous whereas 2 D10 bars were cut-off in Unit F6, compare **Figures 4.1(b)** and **(c)**. This test was carried out to show that the longitudinal reinforcing steel layout in a beam needs to be considered when designing a retrofit scheme involving ACM laminates.

Figure 4.20(f) shows the measured vertical load-midspan deflection of Unit F6. In the load service range this unit showed stiffness lower than all the other units retrofitted with three CACM laminates. A reason for this could have been the larger shearing deformations that developed at the beam bar cut-off points. The unit failed at a vertical load of 220 kN, which is lower than the ultimate load recorded for Unit F5. The beam bar cut-off accelerated the effect of localised concrete shear failure occurred in the concrete adjacent to the laminates. The laminates had been stressed even higher than those in Unit F5 because they had to supply the additional tensile that was being carried by the curtailed beam bars. **Figures 4.19(f)** and **4.20(f)** show the crack pattern of this unit and the beam at the end of the test.

The total crack width measured in the region of constant bending moment was same as that measured in Unit F5, see **Table 4.5**. **Table 4.6** depicts that the stiffness of the unit was measured lower than that of Unit F5. It is believed the curtailment of the steel reinforcement in Unit F6 reduces the stiffness of the beam.

4.9.2.2 Discussion of the Failure Mechanisms

Figure 4.21 shows each of Series-A units at the end of the tests. Unit F1 was loaded up until tensile rupture of the CACM laminate occurred in the region of maximum bending moment at mid-span. This behaviour is ideal as failure and deformation capacity are predictable. As soon as the internal longitudinal steel bars reach yielding, the CACM laminate mainly contributes to an additional increase in load. The ultimate displacement and load can be found using strain compatibility and the Hooke-Bernoulli assumption of

plane before bending remains plane after bending.

According to the analytical study on Unit F2, a very high concentrated bond stress develops in the CACM laminate ends. This stress concentration causes the laminate to peel off. According to the observations taken during testing, Unit F2 failed in an abrupt manner as the CACM laminate peeled off. This failure mode can be observed in **Figure 4.21(b)**. A thick concrete layer broke away from the beam and remained bonded to the laminate.

The use of GACM U-strips to both ends of the CACM laminates in Unit F3 prevented the carbon laminate from peeling off. **Figure 4.22** presents a series of time-sequence photographs taken near to and at failure. These series photographs explain the debonding failure mode due to the shear kinking proposed by Meier and Kaiser [M4], see **Figure 2.4**. **Figure 4.22** clearly illustrates that the CACM delamination begins in a flexure-shear crack at 700mm away from the eastern support, see **Figures 4.22(b)** and **(c)**, and then the laminate separates quickly due to the shear kinking effect, see **Figure 4.22(d)**. Finally the whole CACM laminates completely debonded over the entire beam, see **Figures 4.22(e)** and **(f)**.

Units F4, F5 and F6 had a very similar failure mode of CACM delamination. The delamination started at the 2-to-3 layer CACM laminate cut-off point, see **Figures 4.23(a)** and **4.24(b)**. In the loading increment prior to failure, many flatter inclined cracks developed at the cut-off point, see **Figure 4.25**. The load causing the flat cracks at the laminate cut-off point was 190kN for Unit F4 and 200kN for Units F5 and F6. Failure in the laminate-to-concrete interface originated because of a combination of reasons. At the cut-off points the tensile forces in the laminates are large because of the sudden termination of the laminate and because of the additional demand caused by the diagonal compression field, or truss effect. This effect is clearly seen by comparing the M and MV models shown in **Figure 3.9**. In addition the applied shear force is approaching the shear strength of the beams, as will be shown in Section 4.9.2.4. This implies that shear distortion is relatively high in this region. Such distortion induces localised concrete shear stresses at the concrete-to-laminate interface.

The failure modes observed in the Series-A test are sketched in **Figure 4.26**. The

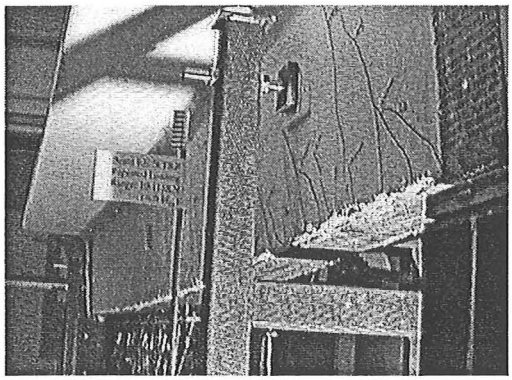

(a) at 220kN,
T=0.0 second

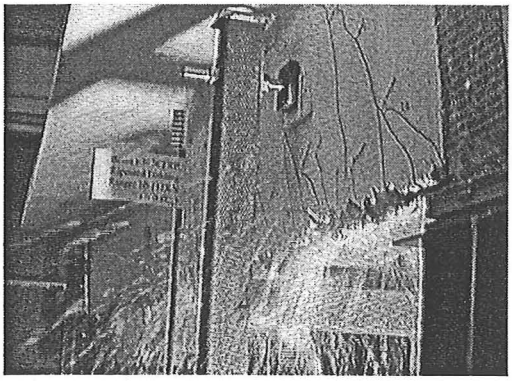

(d) at CACM Delamination,
T=6.7 seconds

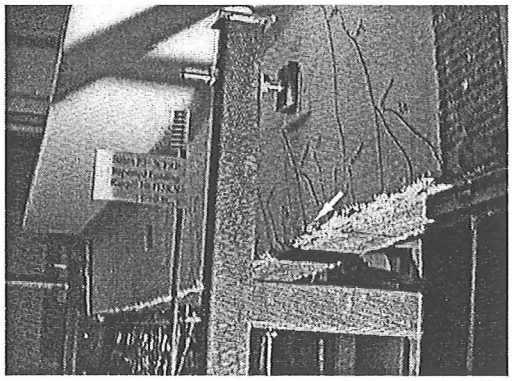

(b) at 230kN,
T=4.0 seconds

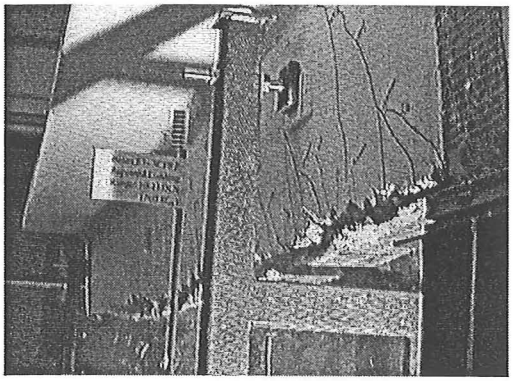

(e) after Delamination,
T=8.0 seconds

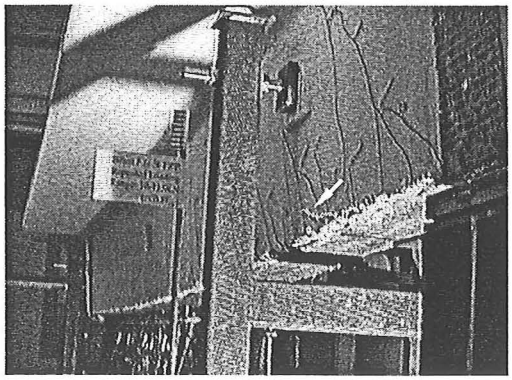

(c) at Ultimate Load 236kN,
T=6.0 seconds

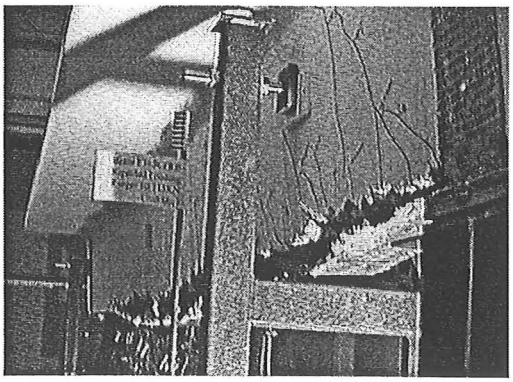

(f) End of Test

Figure 4.22 Unit F3 at Various Instants During Loading near and at Failure

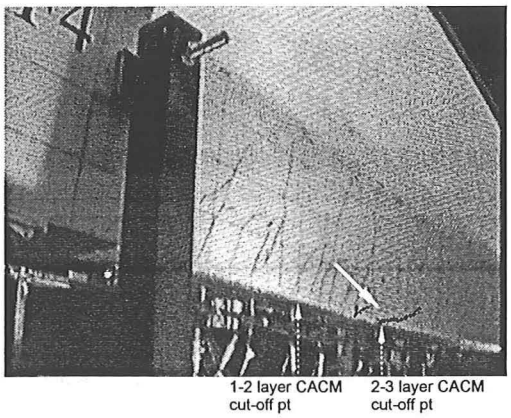

(a) at 190kN

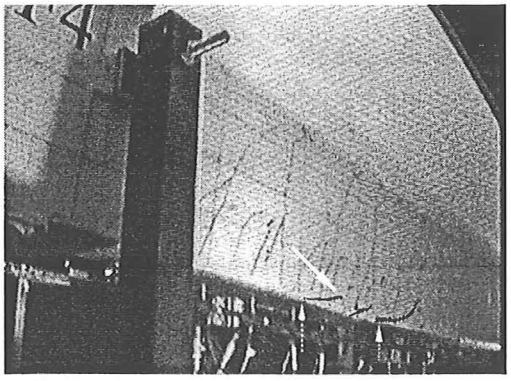

(b) at Ultimate Load 202kN during Delamination, T=0.0 second

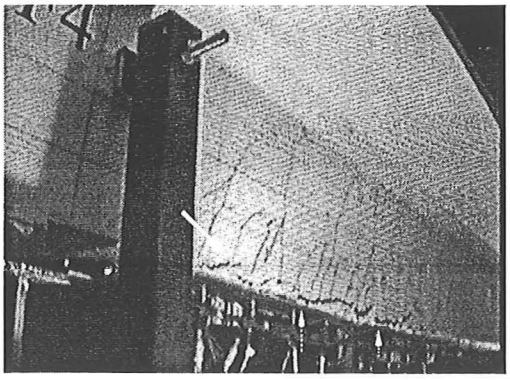

(c) at Ultimate Load 202kN during Delamination , T=8.0 seconds

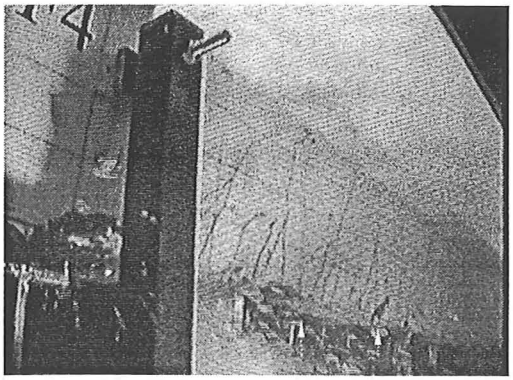

(d) at T=10.0 seconds

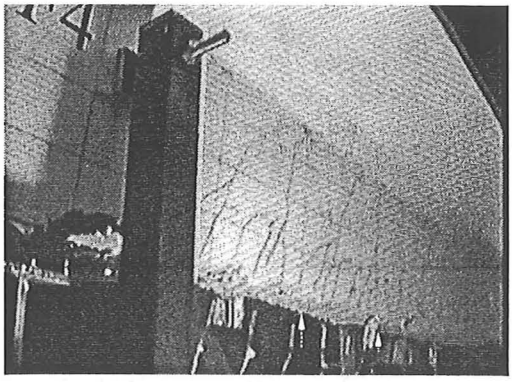

(e) End of Test

Figure 4.23 Unit F4 at Various Instants During Loading near and at Failure

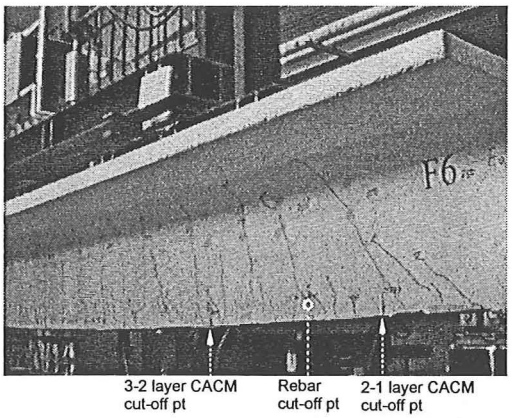

(a) at 180kN

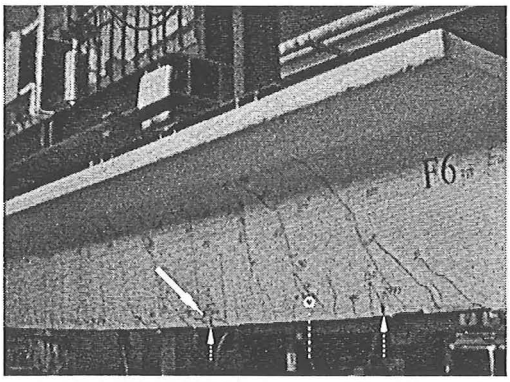

(b) at 190kN

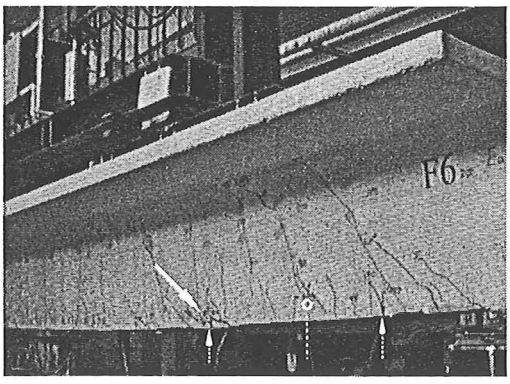

(c) at 200kN

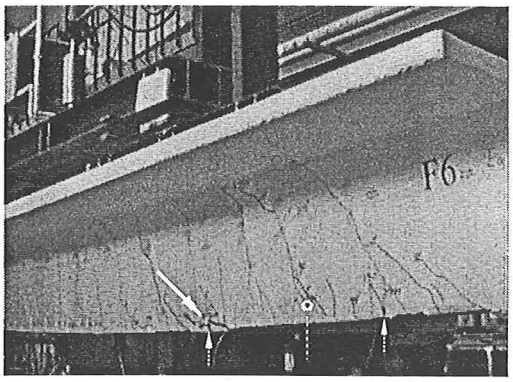

(d) at Ultimate Load 220kN,
T=0.0 second

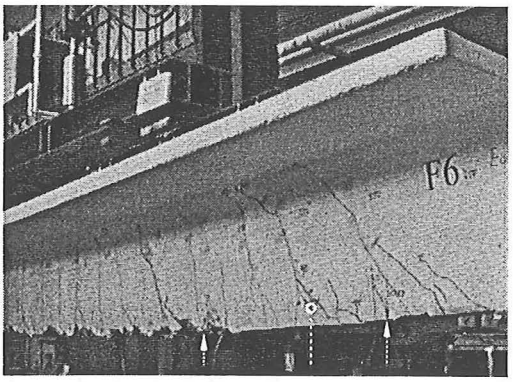

(e) at CACM Delamination,
T=0.6 second
End of Test

Figure 4.24 Unit F6 at Various Instants During Loading near and at Failure

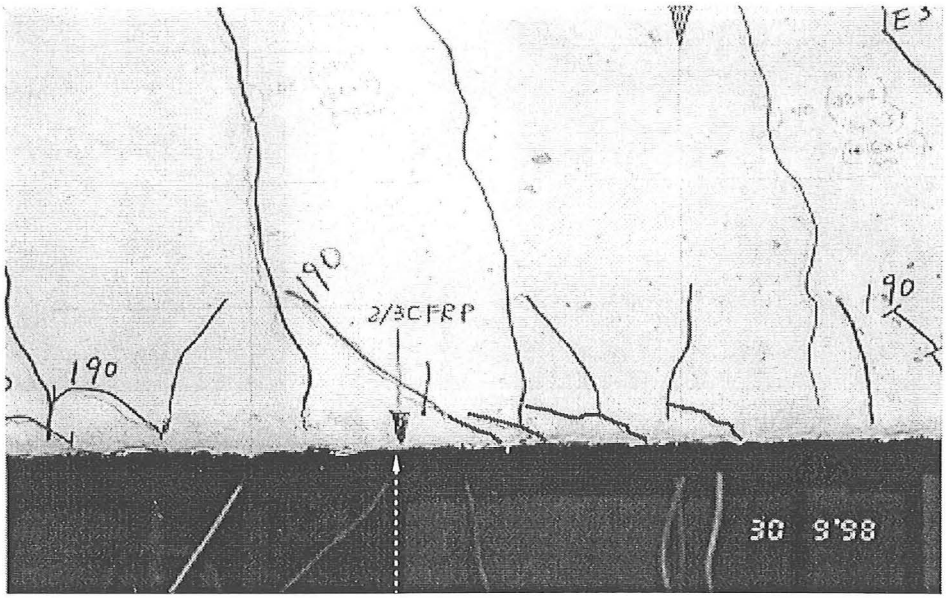

3-2 layer CACM
cut-off pt.

(a) Unit F5, at Eastern Side, 200kN

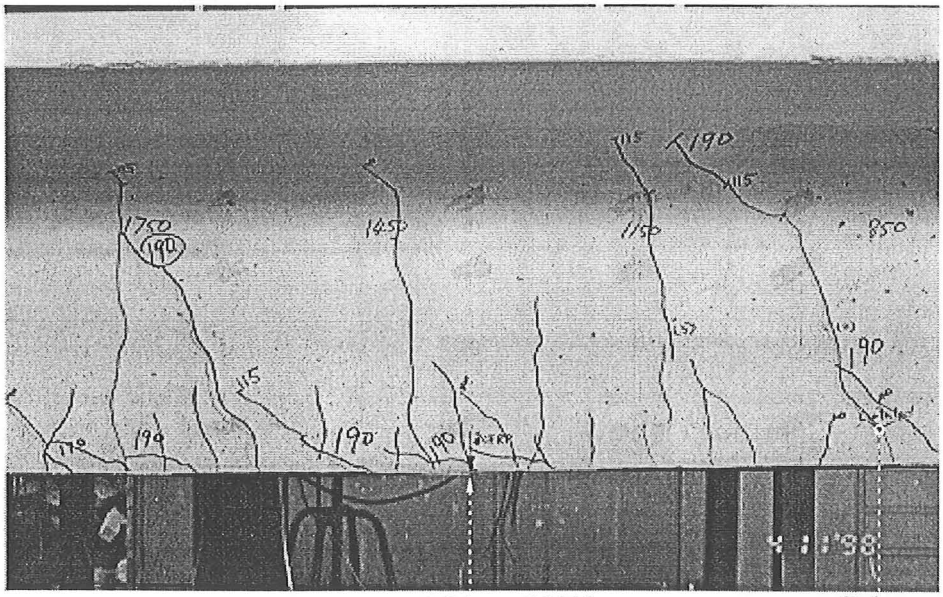

3-2 layer CACM
cut-off pt.

Rebar
cut-off pt.

(b) Unit F6, at Eastern Side, 200kN

Figure 4.25 The Local Crack Pattern Developed at the CACM Cut-off Point

F: CACM tensile rupture at mid span

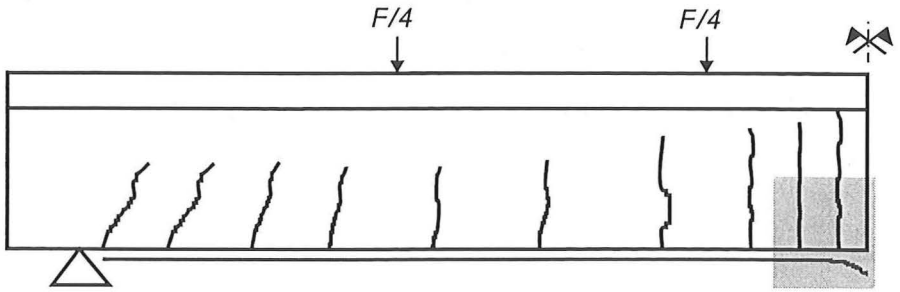

DE: CACM laminate end peel-off

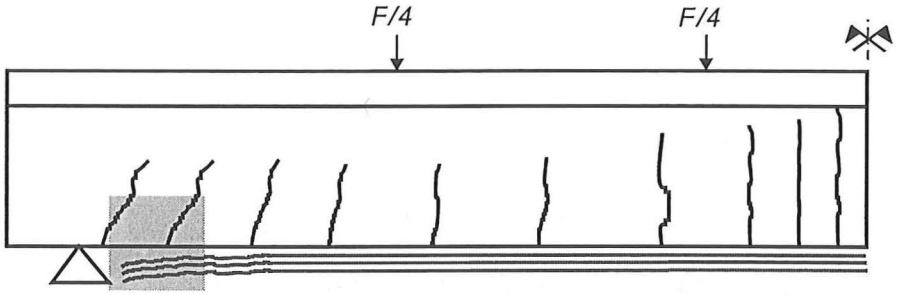

DS: CACM debonding due to shear kinking

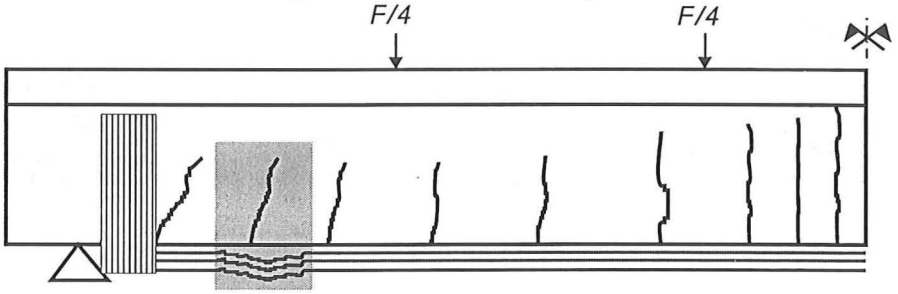

DC: CACM debonding due to localised concrete failure at the laminate cut-off point

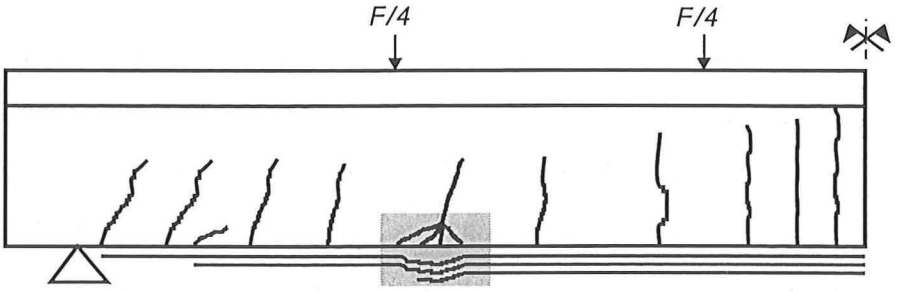

Figure 4.26 Failure Mechanisms Observed in Series-A Units

shaded area represents the triggered failure mechanism of the beam. It is worth mentioning that the CACM delamination for all test beams occurred within the concrete cover, between longitudinal steel bars and the laminate as **Figure 4.27** shows. This type of delamination is the result of good concrete surface preparation and adequate epoxy adhesive for the laminate bonding.

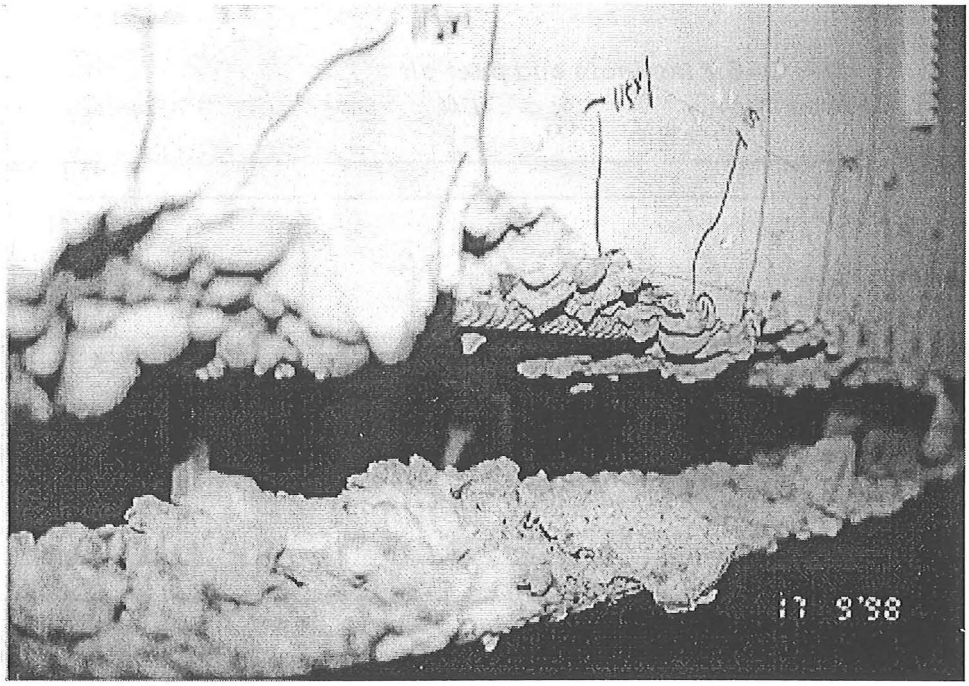

Figure 4.27 Detail of ACM Laminate Debonding

4.9.2.3 Concrete Surface and ACM Laminate Longitudinal Strains

The strain on the extreme bottom fibre of concrete surface and CACM laminate was measured by DEMEC gauge to verify the relationship of strain compatibility between concrete and ACM laminate. The arrangement of DEMEC gauge on the beam bottom of concrete and CACM laminate is shown in **Figure 4.13**. Only Units F1 to F5 were instrumented and the data collected is presented and discussed below.

The analytical model described in Chapter 3 assumed perfect bond between the concrete and the ACM laminate. Such assumption needs to be experimentally verified to

give validity to the proposed model. **Figure 4.28** shows the longitudinal strains measured in CACM laminate and concrete bottom surface. Strain measurements shown in **Figure 4.28** were chosen as close to ultimate load of each beam as possible. It is clear in **Figure 4.28** that the longitudinal strain in the concrete surface and the ACM laminate are very similar. In conclusion, the test results confirm that the assumption of no slip between ACM laminate and concrete is adequate for analysis.

4.9.2.4 Comparison with Analytical Results

The prediction of Series-A units is performed using the analytical model proposed in Chapter 3. The test beams were modelled with the segment arrangement in **Figure 3.8**. **Figure 4.29** shows the predicted and measured vertical load versus mid-span deflection relationship for Units F1 to F6. **Figures 4.30** to **4.35** shows the predicted and measured distribution of forces and stresses along the beam span for these units. In these figures, the term F_u is the ultimate load obtained in the test or/and analysis. The strain $\varepsilon_{pmax,\ @2\text{-layer}}$, for example, is the maximum ACM laminate strain that occurs in the interval reinforced with two ACM laminates. ε_{pmax} is the maximum laminate strain that occurs at the beam mid-span. M is the bending moment and V is the shear force due to the applied load, respectively. M_V is the shifted bending moment that accounts for the effects of diagonal cracking, see Section 3.8.1, and M_n is the nominal bending moment strength. V_y and V_n are the shear strength causing the stirrup yielding and the nominal shear capacity. The shear strengths are evaluated using the modified compression field theory (MCFT) as discussed in Chapter 3 and the code design equation specified in NZS 3101 [N4] as mentioned in Eq.4.1. The development length of the ACM laminate, needed for calculating the nominal flexural strength envelope M_n in **Figures 4.30(a)** to **4.35(a)**, was given as

$$l_{dp} = \frac{f_{pu} t_p b_p}{k\sqrt{f'_c}\, b_w} \tag{4.2}$$

where f_{pu} is the tensile strength of the laminate, t_p is the laminate thickness, k is a bond strength factor, and f'_c is the concrete compressive strength. Eq.4.2 represents a general derivation for the laminate width b_p not equal to the beam web width b_w, as can be referred

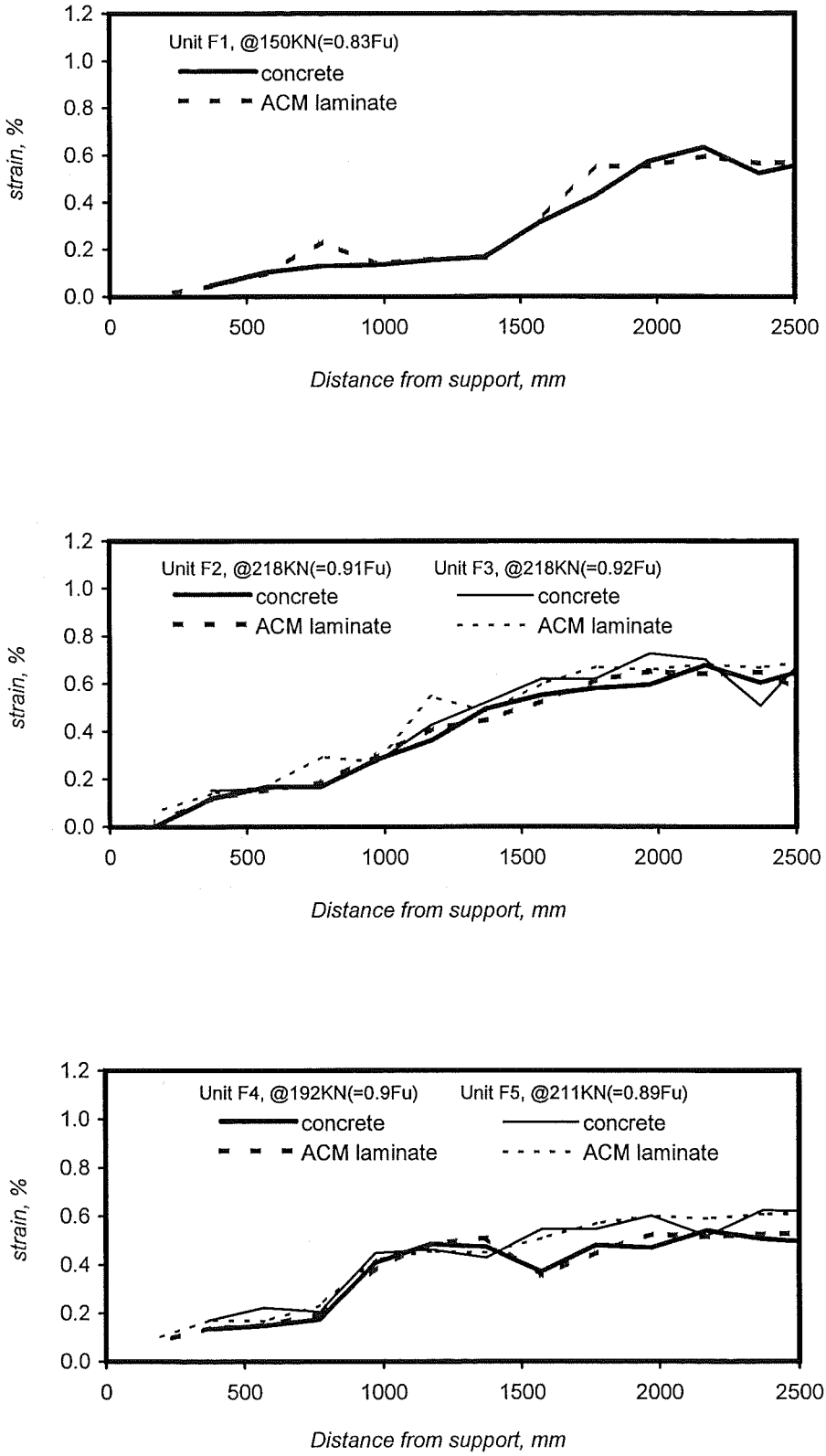

Figure 4.28 Concrete and ACM Laminate Longitudinal Strain Profile Measured at the Bottom Face of the Beam

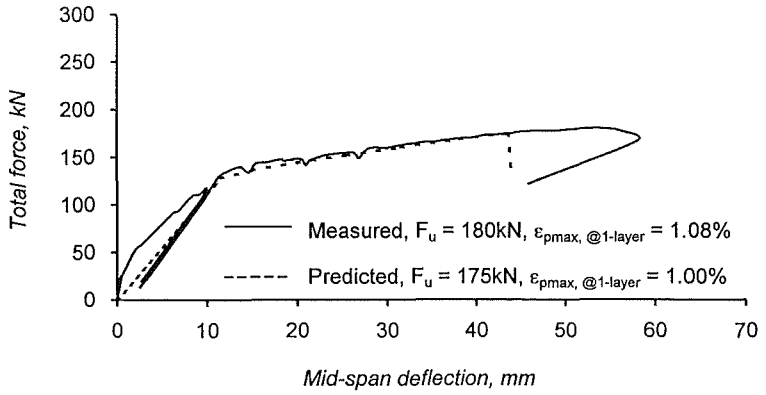

(a) Unit F1

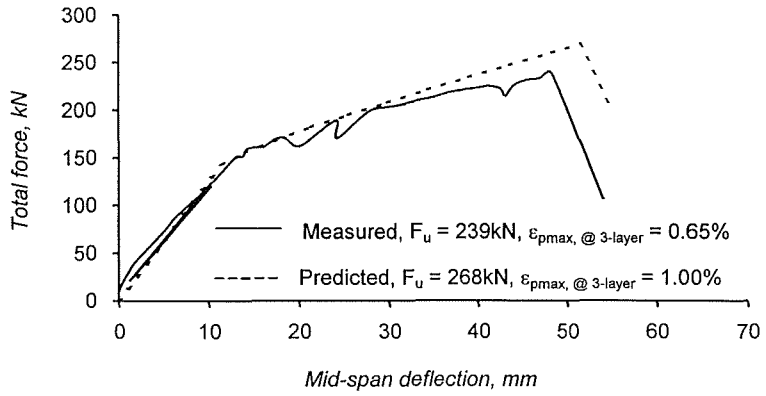

(b) Unit F2

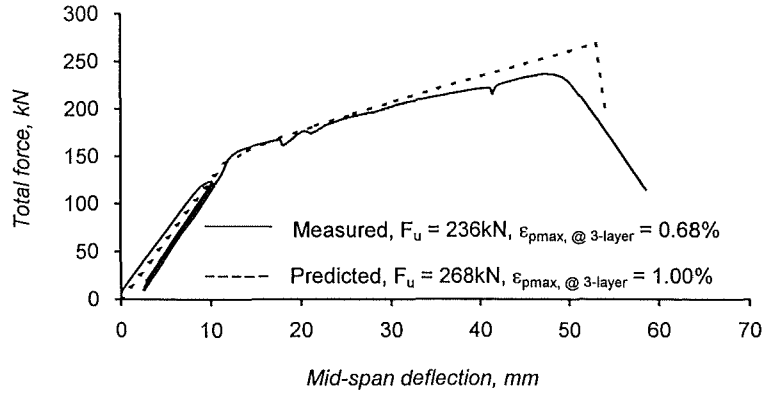

(c) Unit F3

Figure 4.29 Comparison of Load v.s. Deflection between Test and Prediction for Series-A Units

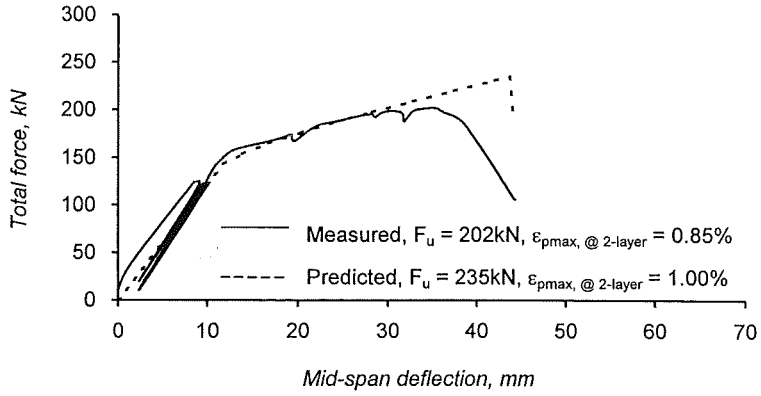

(d) Unit F4

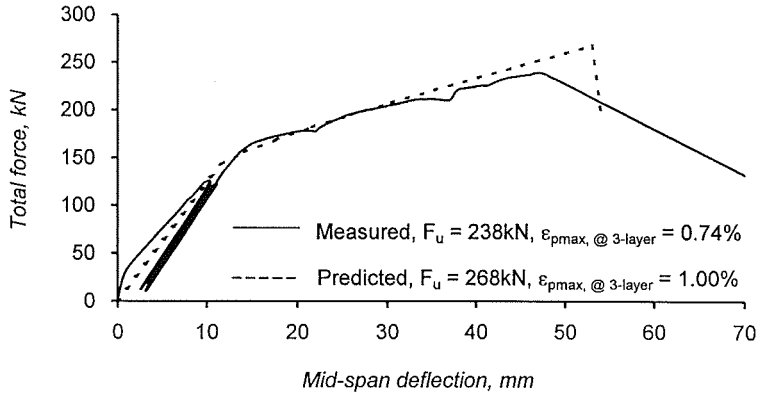

(e) Unit F5

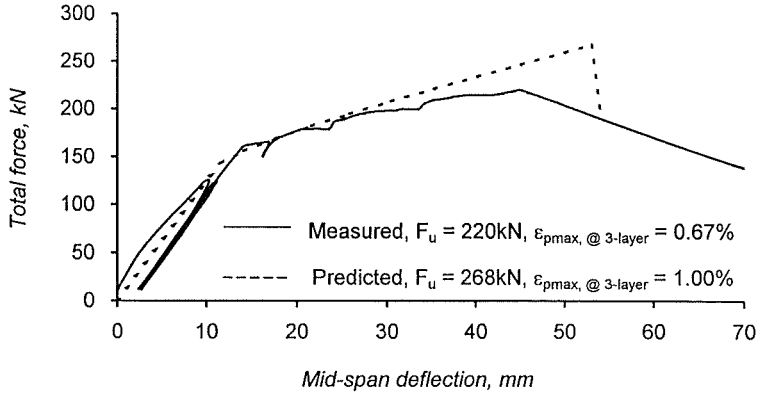

(f) Unit F6

Figure 4.29 Comparison of Load v.s. Deflection between Test and Prediction for Series-A Units (Cont.)

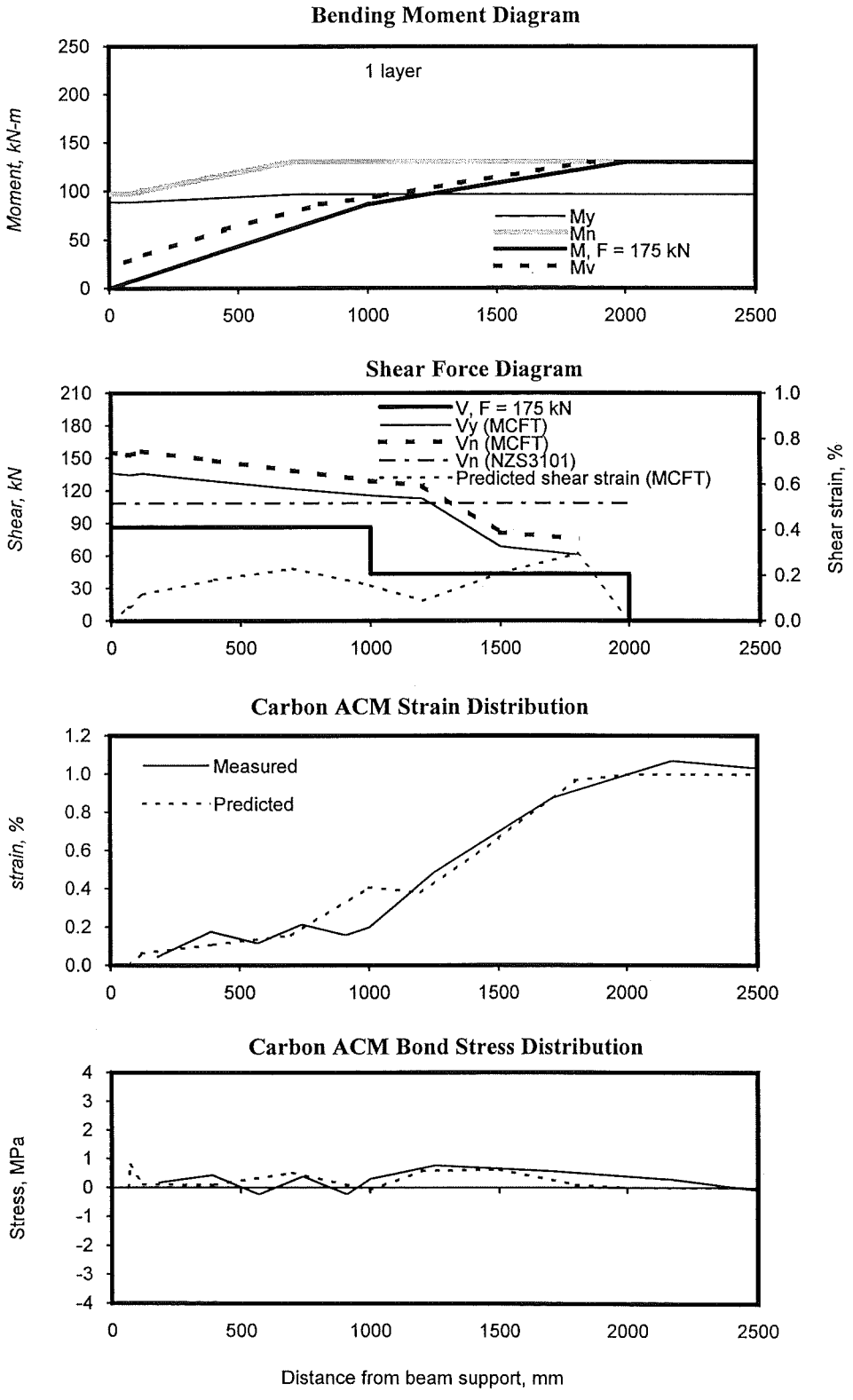

Figure 4.30 Prediction and Measurement on the Bond Behaviour of the Carbon ACM Laminate for Unit F1 near the Ultimate Load

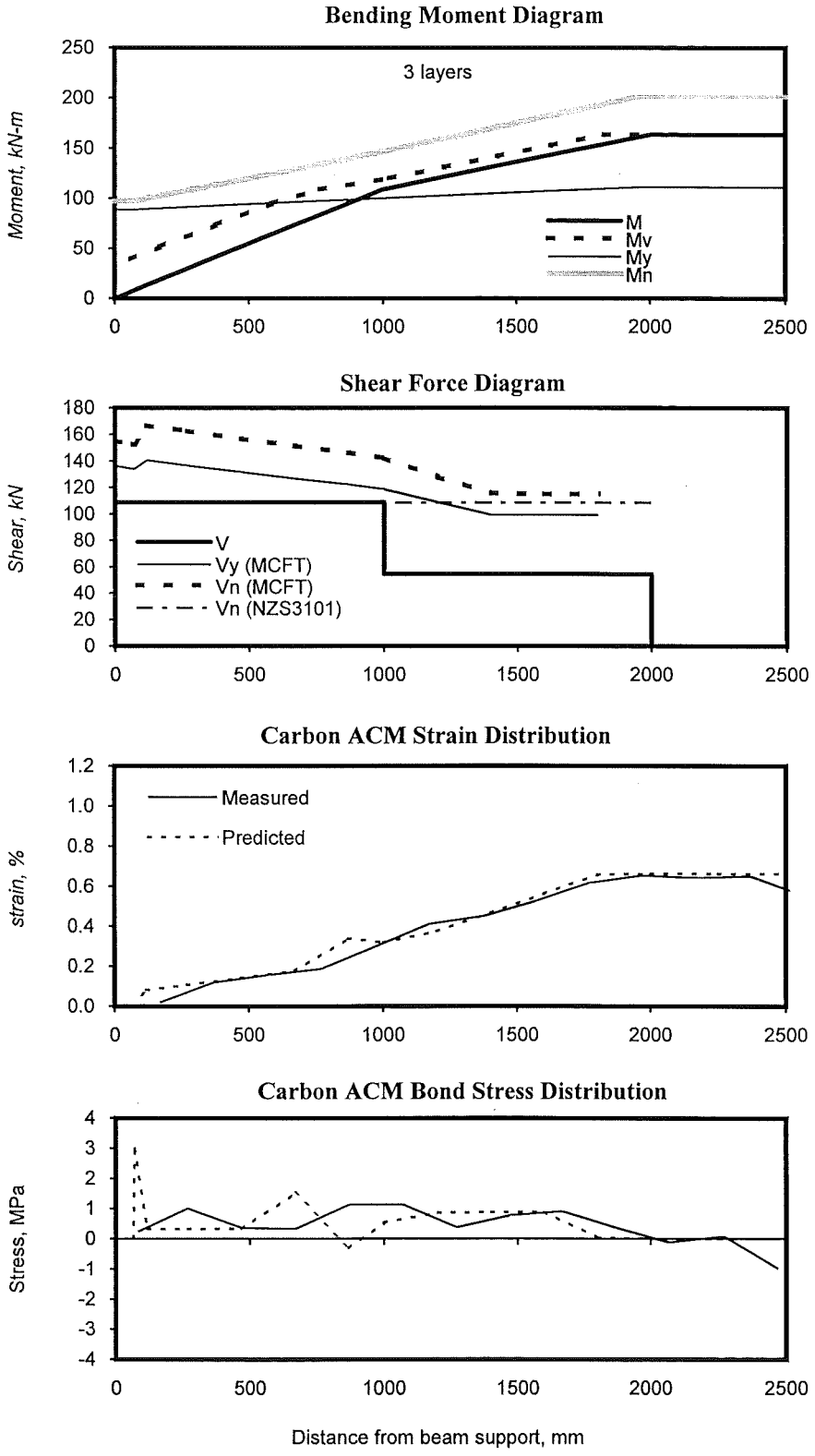

(a) at F = 218 kN

Figure 4.31 Prediction and Measurement on the Bond Behaviour of the Carbon ACM Laminate for Unit F2

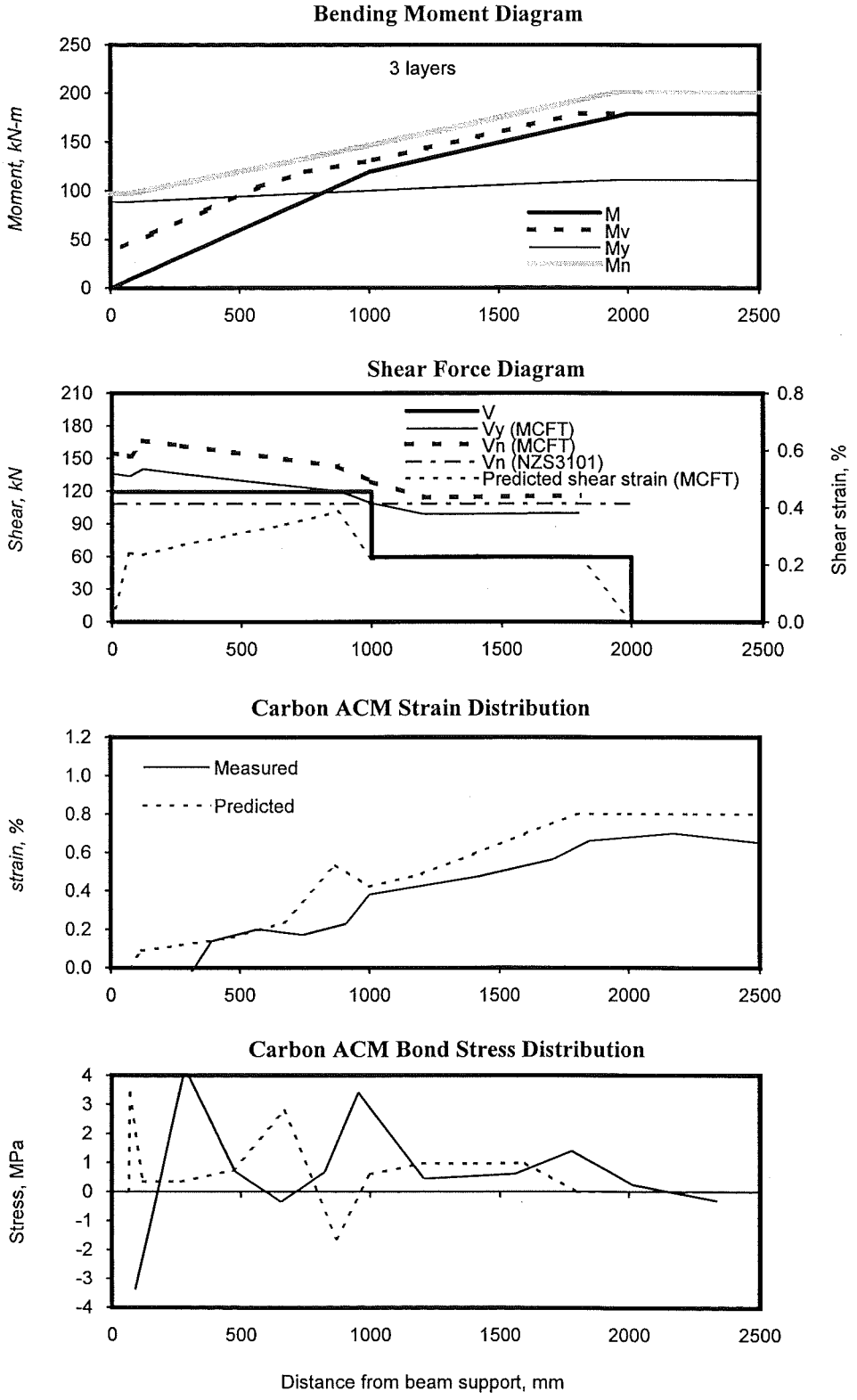

(b) at Ultimate Load, F = 239 kN

Figure 4.31 Prediction and Measurement on the Bond Behaviour of the Carbon ACM Laminate for Unit F2 (Cont.)

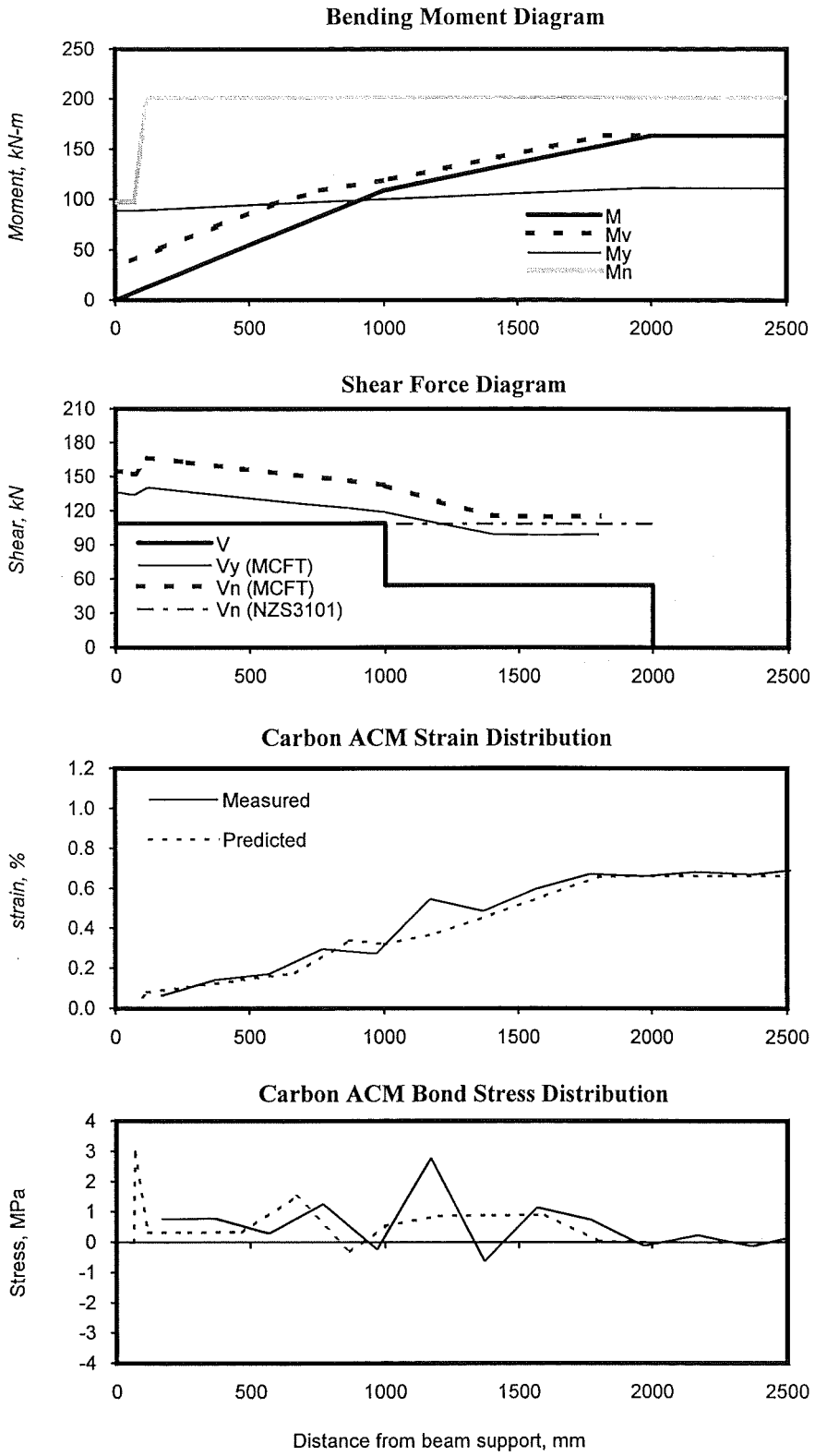

(a) at F = 218 kN

Figure 4.32 Prediction and Measurement on the Bond Behaviour of the Carbon ACM Laminate for Unit F3

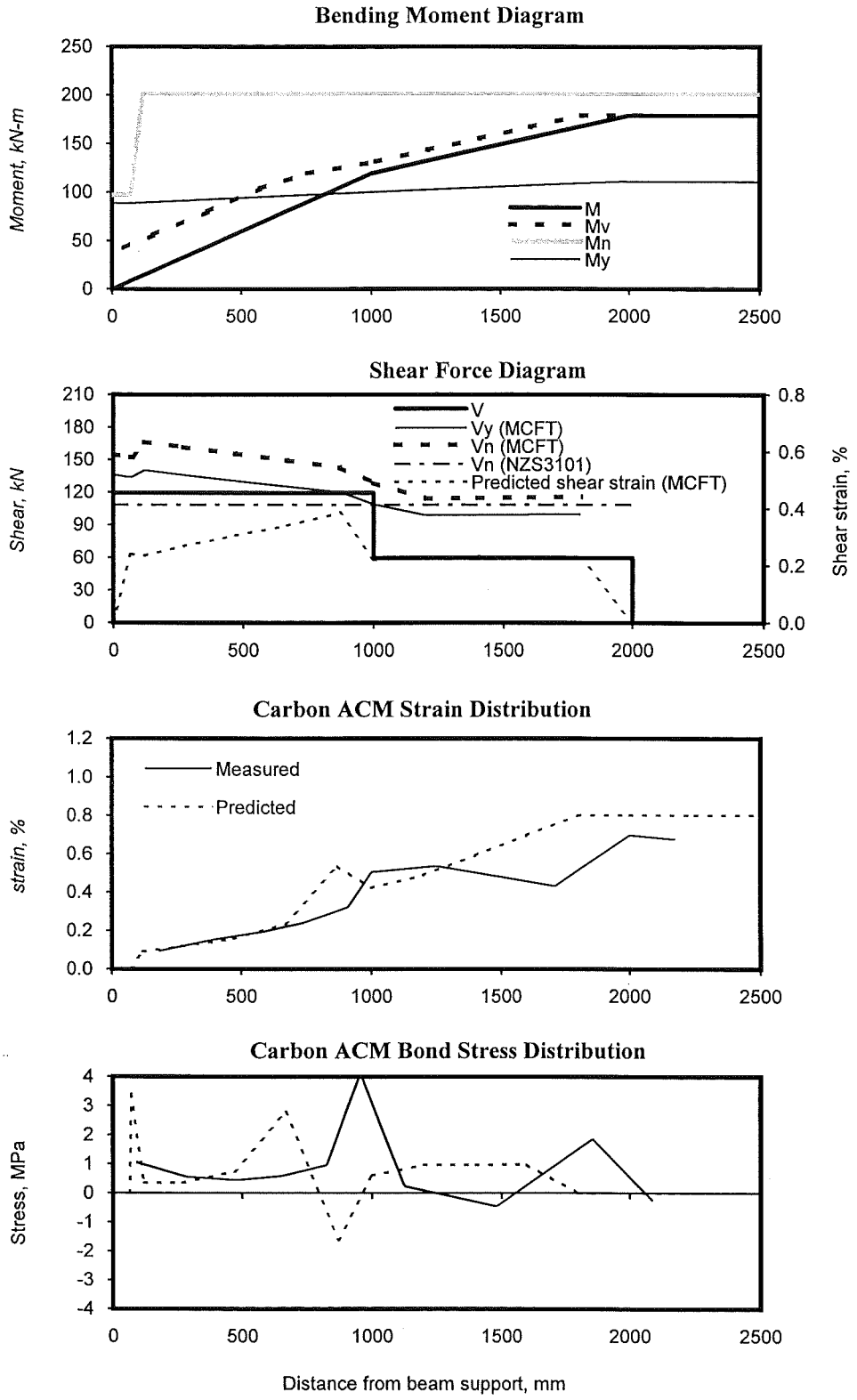

(b) at Ultimate Load, F = 236 kN

Figure 4.32 Prediction and Measurement on the Bond Behaviour of the Carbon ACM Laminate for Unit F3 (Cont.)

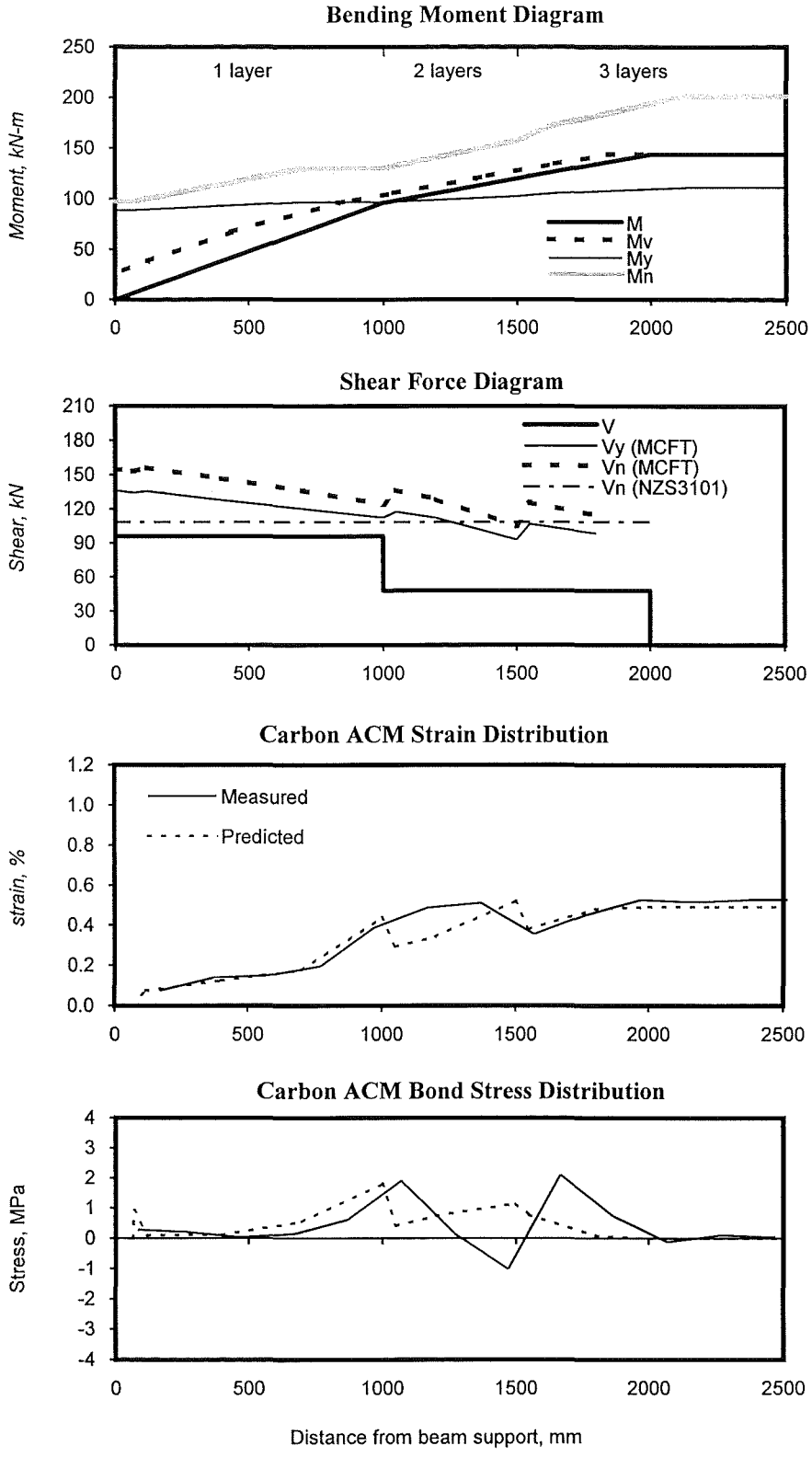

(a) at F = 192 kN

Figure 4.33 Prediction and Measurement on the Bond Behaviour of the Carbon ACM Laminate for Unit F4

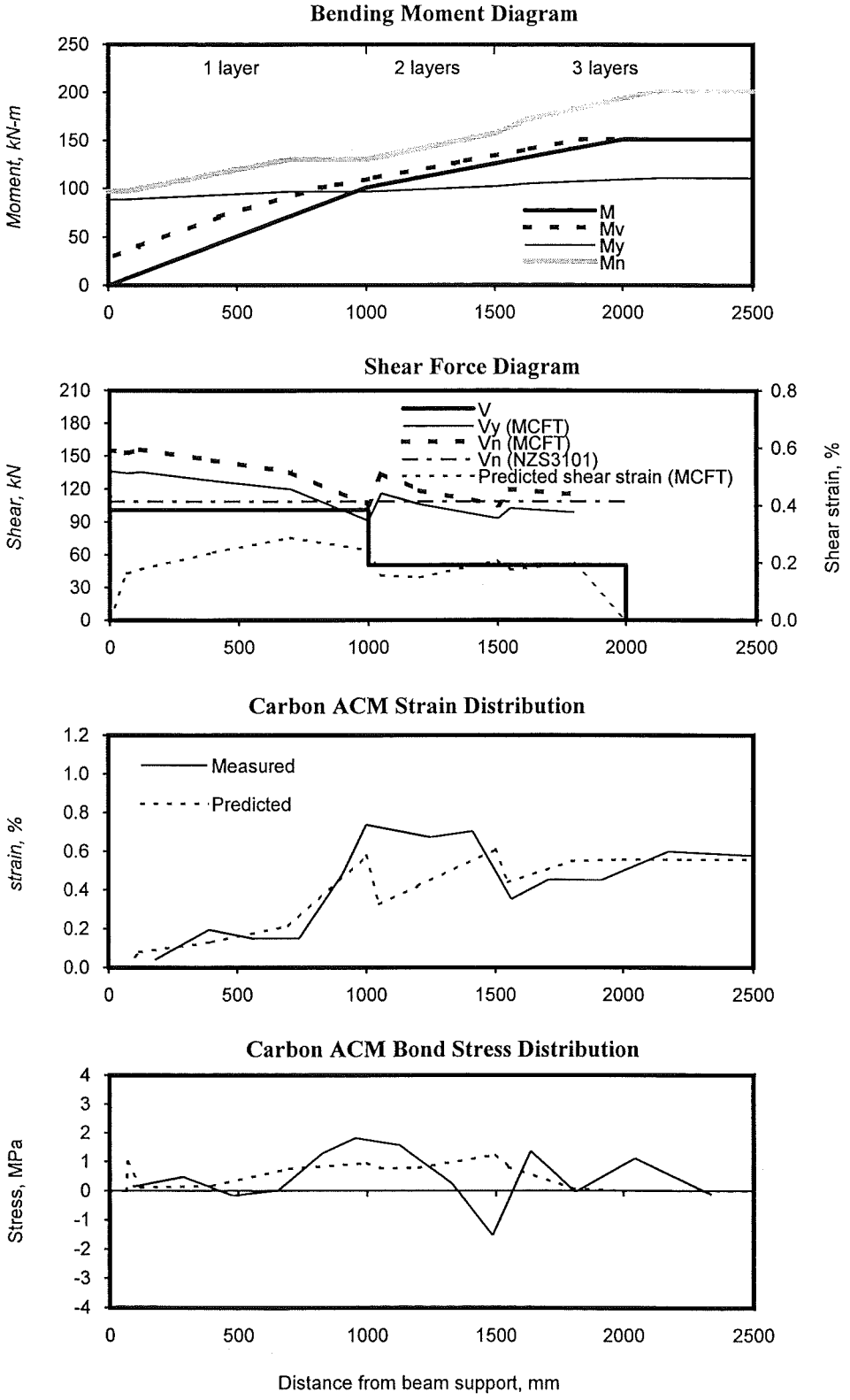

(b) at Ultimate Load, F = 202 kN

Figure 4.33 Prediction and Measurement on the Bond Behaviour of the Carbon ACM Laminate for Unit F4 (Cont.)

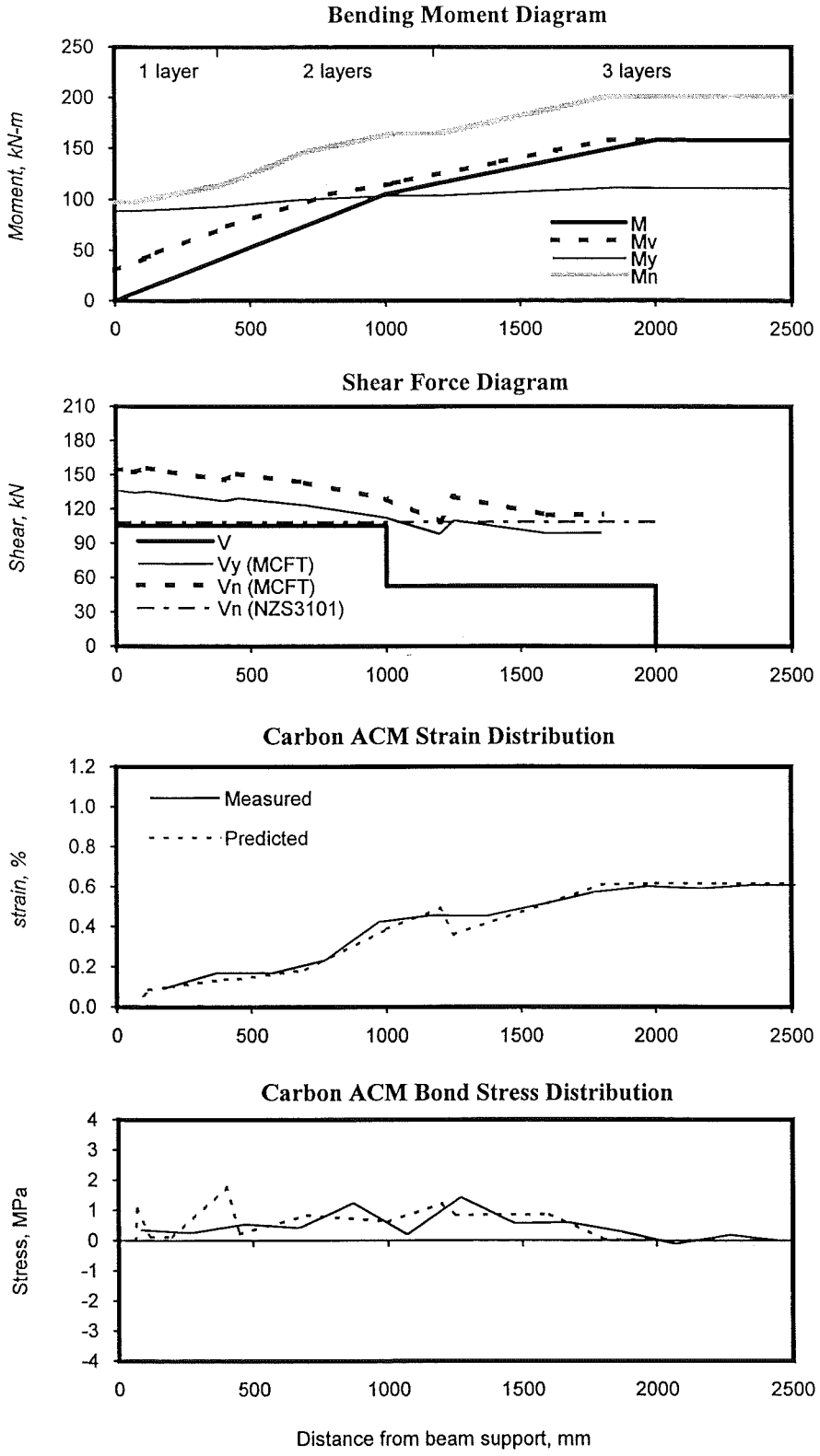

(a) at F = 211 kN

Figure 4.34 Prediction and Measurement on the Bond Behaviour of the Carbon ACM Laminate for Unit F5

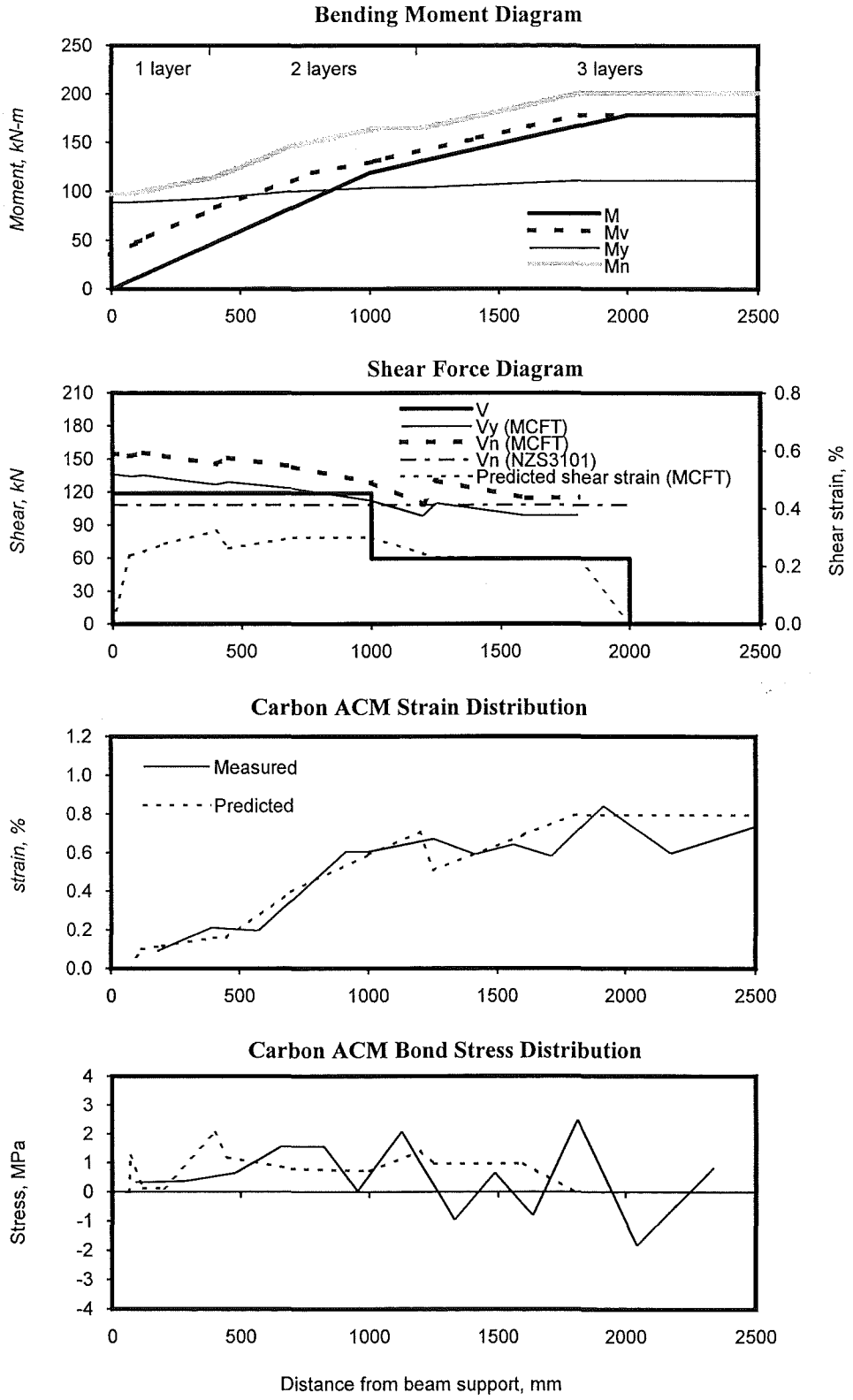

(b) at Ultimate Load, F = 238 kN

Figure 4.34 Prediction and Measurement on the Bond Behaviour of the Carbon ACM Laminate for Unit F5 (Cont.)

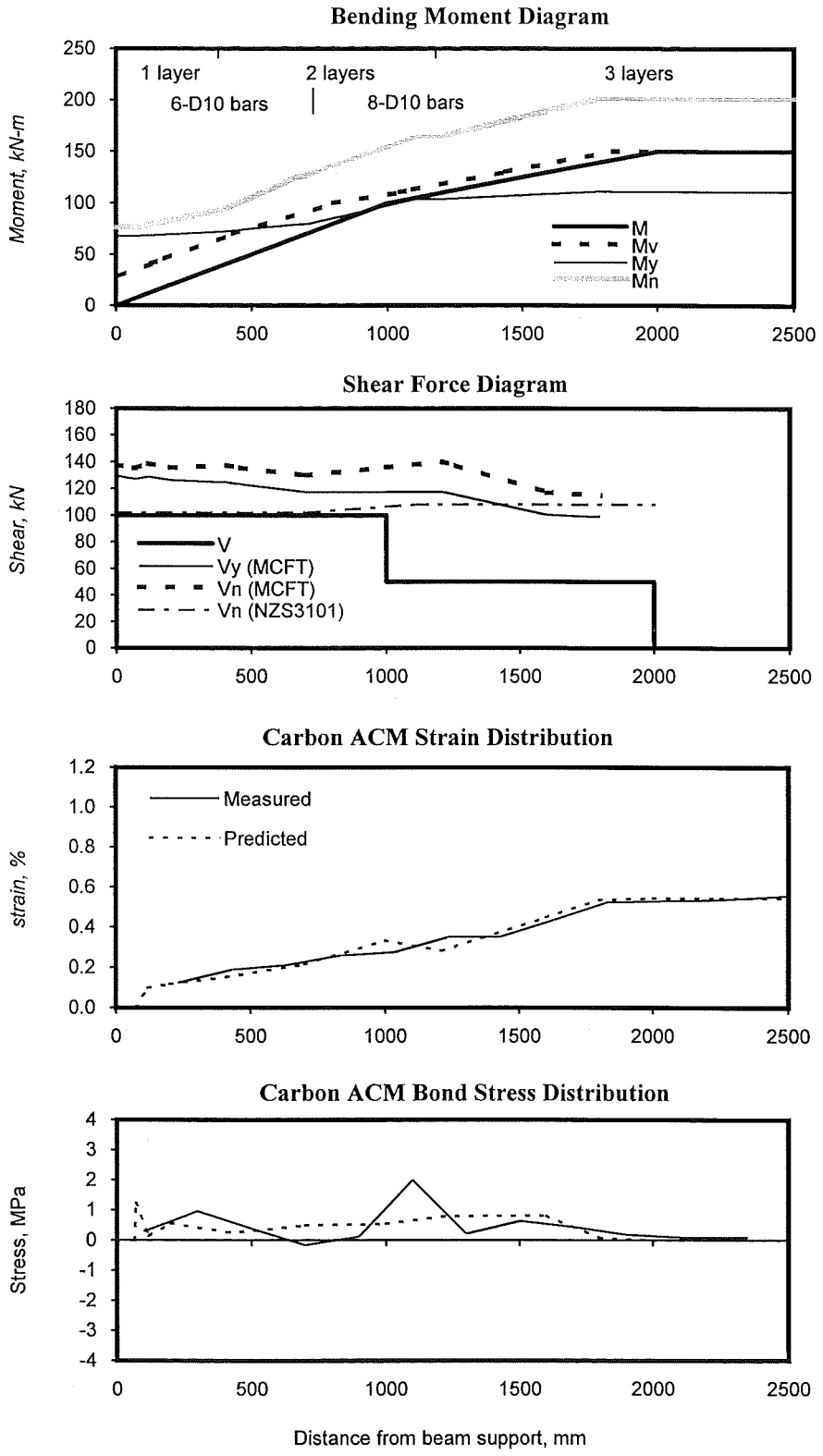

(a) at F = 200 kN

Figure 4.35 Prediction and Measurement on the Bond Behaviour of the Carbon ACM Laminate for Unit F6

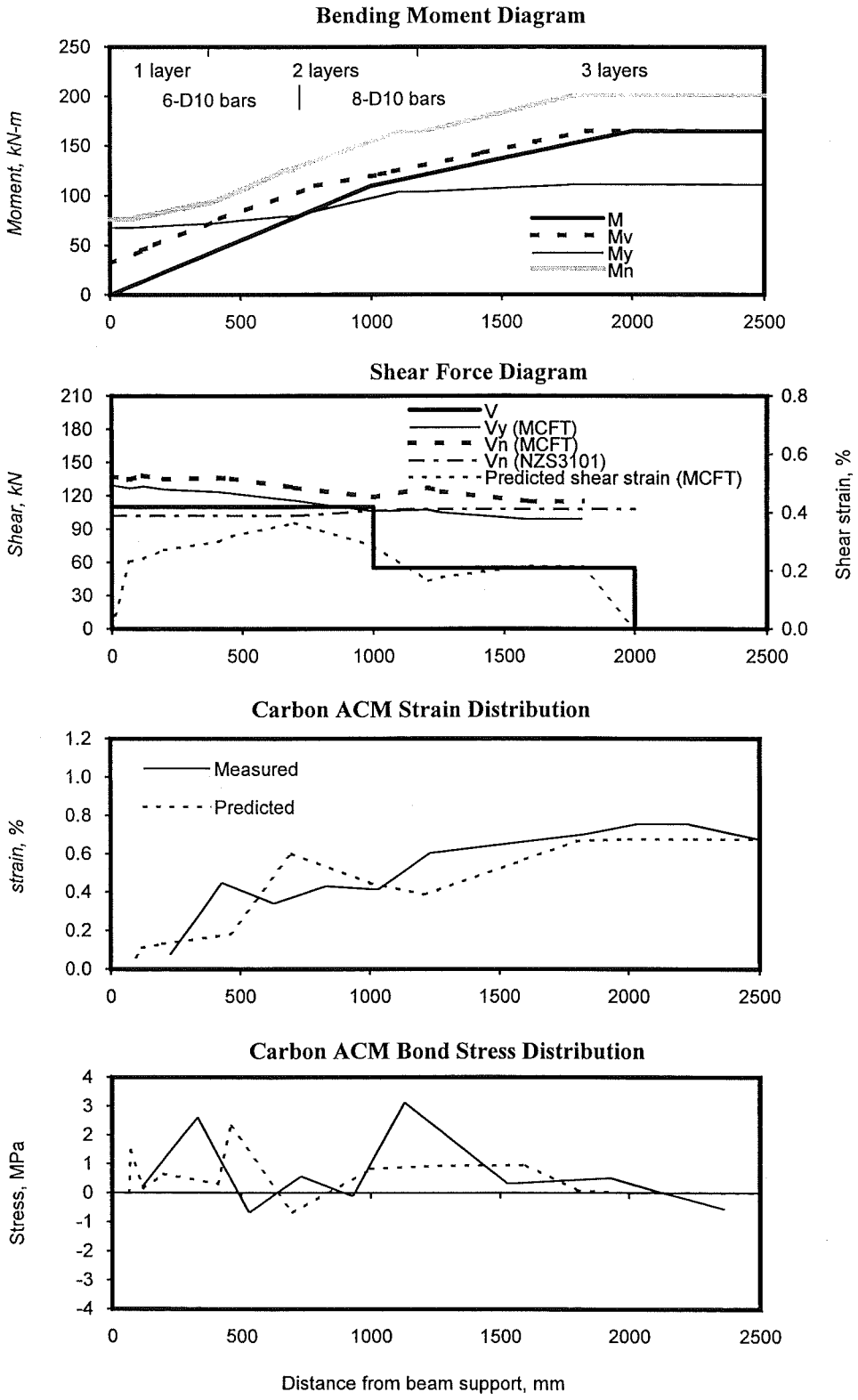

(b) at Ultimate Load, F = 220 kN

Figure 4.35 Prediction and Measurement on the Bond Behaviour of the Carbon ACM Laminate for Unit F6 (Cont.)

as in **Figure 3.3(a)**. Note the bond strength factor k = 0.2 was adopted in the prediction. The detailed evaluation of the laminate development length will be carried out and discussed in Chapter 6.

Prediction of the Response of Unit F1

The theoretical shear strain predicted for Unit F1 by the analytical model using the principal strains is shown together with the shear force diagram. It is evident from this figure that the magnitude of the shear strain at a given section depends on the shear force acting there as well as on the longitudinal strain induced by bending. This is clear, for example, in the beam segment from 1 to 2 m away from the left support, the shear force is constant in this interval but the bending moment decreases towards the support. The shear strain is a maximum in this interval near the section with maximum bending moment, while it generally decreases as the bending moment decreases.

Also shown in **Figure 4.30** are the predicted and measured laminate longitudinal strains. The analytical model predicts very well the measured response except in the distributed region where the vertical load is applied at 1 m from the support. At this location the model tends to overpredict the longitudinal strain. This response validates the assumptions made for the analytical model in Chapter 3 and shows that the modified compression field theory can be employed to analyse these types of structural members. The ACM laminate bond stress distribution plotted in **Figure 4.30** shows good agreement between the test data and that predicted by the model. Note that good agreement is very difficult to obtain, as bond stresses are very sensitive to the resolution of the clip gauges and the gauge length.

Prediction of the Response of Units F2 to F6

The measured and predicted vertical load versus mid-span deflection response of these units is illustrated in **Figures 4.29(b)** to **(f)**. The predicted and measured responses agree very well, perhaps with the exception of the response in the low load levels of elastic response. This error is due to the fact that the effect of the tensile response of concrete in flexure was ignored in the model. However the initial stiffness coincides very well with the secant stiffness of the member at a load level approaching the elastic limit.

Figures 4.31 to **4.35** shows the response of the Units F2 to F6 at two different load levels, including one very close to failure. The prediction of the carbon laminate strain distribution in the load below ultimate in these units, see **Figures 4.31(a)** to **4.35(a)**, is excellent, confirming that the assumptions made for the theoretical model are very reasonable. The prediction of the bond stress is not so good but this can be expected as bond is influenced by the force gradient. This gradient can be subjected to large experimental errors.

At ultimate load the measured and predicted strain and bond stress distribution is less accurate, see **Figures 4.31(b)** to **35(b)**. This is due to two main reasons. The strain readings at this load level were taken from the less accurate clip gauges while in the lower load levels the strains shown were taken from manual DEMEC readings. In the load levels approaching ultimate DEMEC readings were suspended to avoid an unnecessary risk to the technician as failure was imminent. Another reason for the discrepancy is that at ultimate load, very flat diagonal cracks developed in the concrete cover between the laminate and the longitudinal reinforcement in the critical locations. It is believed that bond stress redistribution could have occurred there. By comparing shear force diagrams in these figures at ultimate load, the shear forces due to the applied loads are greater than the nominal shear strengths. This indicates the delamination failures of these units, F2 to F6, are mainly caused by the shear kinking due to the commencement of the large shear distortion.

4.9.3 Test Results on Series-B Units

4.9.3.1 General Behaviour

In this test series, the performance of reinforced concrete tee beams strengthened with CACM laminates bonded to their soffit for flexural strength enhancement and with GACM U-strips bonded to their sides for shear strength enhancement was investigated. Test Series-B compared three units, namely Units S1, S2 and C1. The beam type for Units S1 and S2 is BT1 and that for Unit C1 is BT2, see **Figure 4.1**. General details of the retrofit scheme in Series-B Units are depicted in **Figure 4.2(b)**. These beams were designed following the design procedure described in Chapter 6 for beams requiring

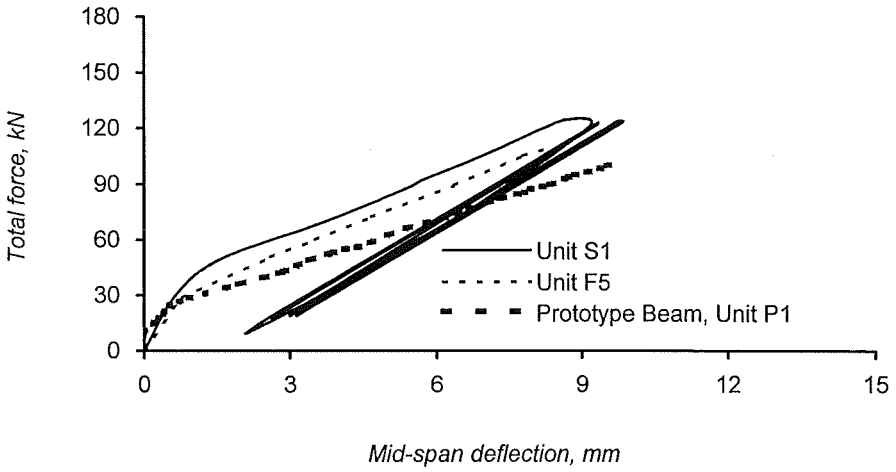

Response in the Service Load Range

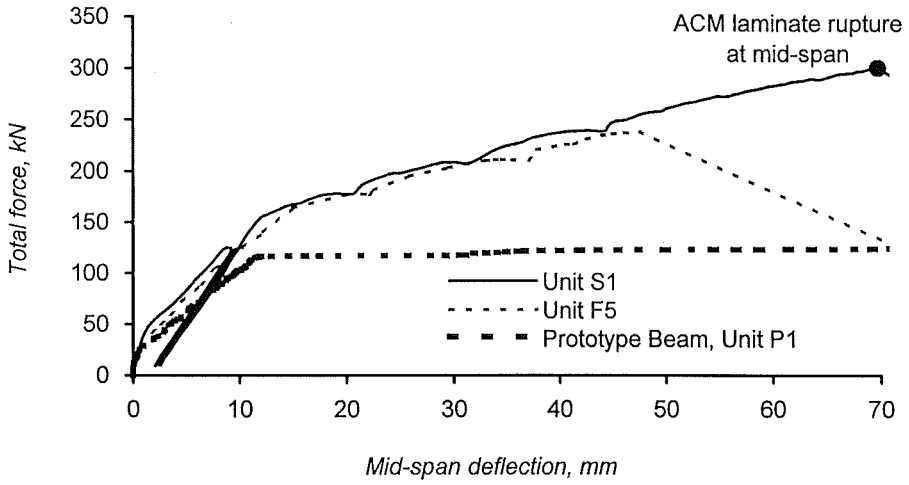

Total Response

(a) Unit S1

Figure 4.36 Vertical Load versus Mid-span Deflection for Series-B Units

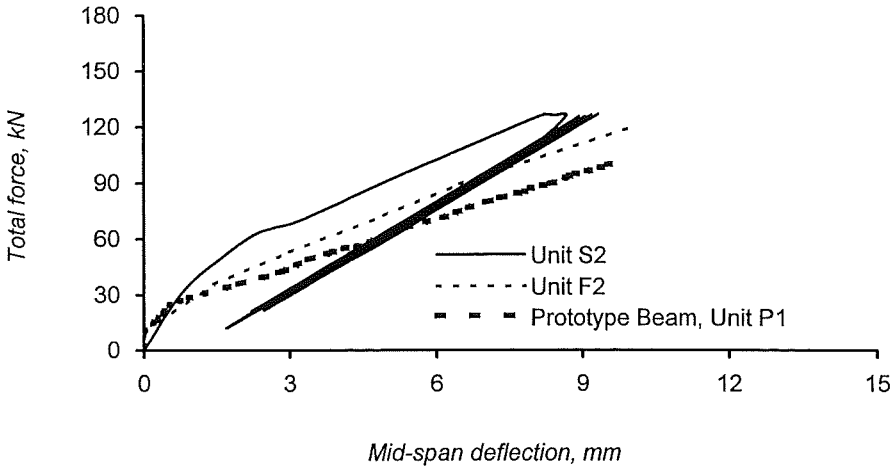

Response in the Service Load Range

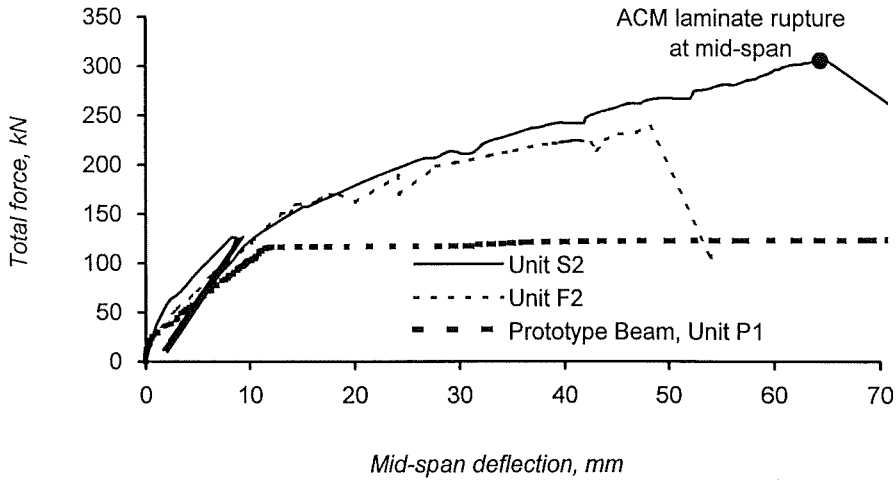

Total Response

(b) Unit S2

Figure 4.36 Vertical Load versus Mid-span Deflection for Series-B Units (Cont.)

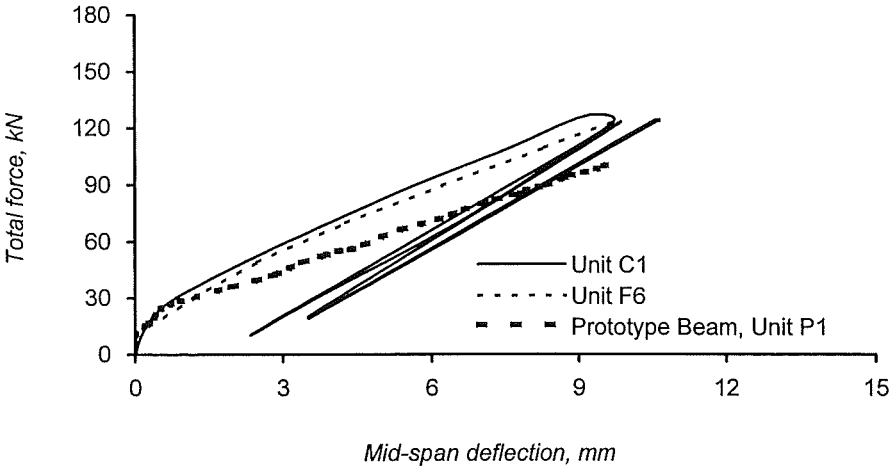

Response in the Service Load Range

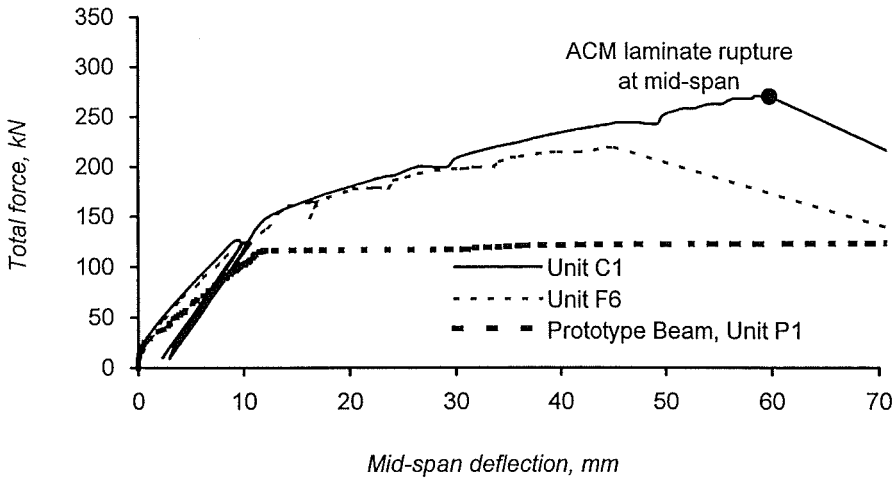

Total Response

(c) Unit C1

Figure 4.36 Vertical Load versus Mid-span Deflection for Series-B Units (Cont.)

service live load enhancement. Equation 4.1 was used to design the beam for shear enhancement. A strain in the GACM strips equal to 0.4% was used in Eq.4.1 as proposed by Priestley et al. [P6]. Following the behaviour observed during the testing of the beams discussed in Chapter 5, the U-strips were all anchored at their ends. A proprietary glass/epoxy anchor was used for this purpose.

Table 4.7 Measured Stiffness and Failure Load of Test Series-B Units

Unit	$F'_{y,t}$ (1) (kN)	Δ_m (2) (mm)	$F'_{y,t} / \Delta_m$ (3) (kN/mm)	stiffness (4) ratio	F_u (5) (kN)	ε_{pu} (6) (%)
P1	100	9.6	10.4	1.00	139	-
S1	125	9.2	13.6	1.31	300	1.19
S2	125	8.4	14.9	1.43	306	1.25
C1	125	9.7	12.9	1.24	270	1.02

Notes: (1) $F'_{y,t}$ = theoretical load corresponding to a stress of $0.75f_{sy}$ (240 MPa) in the longitudinal reinforcing steel.

(2) Δ_m = mid-span deflection corresponding to $F'_{y,t}$.

(3) Measured stiffness of the test unit.

(4) Ratio between the stiffness in a unit and the stiffness of Unit P1.

(5) F_u = failure load of the test unit at the end of test.

(6) ε_{pu} = measured CACM laminate strain corresponding to F_u at mid-span of the beam.

Figure 4.36 shows the applied vertical load versus the observed mid-span deflection for the test units in Series-B. The response in the service load range is also shown in this figure. The response of the prototype beam, Unit P1, is also plotted in these figures for comparison. The measured initial stiffness determined in the service load range as well as the failure loads are given in **Table 4.7**. The definition of the initial stiffness is the same as Series-A units. The failure mode and the crack pattern for each unit at the end of the test are illustrated in **Figures 4.37** and **4.38**, respectively.

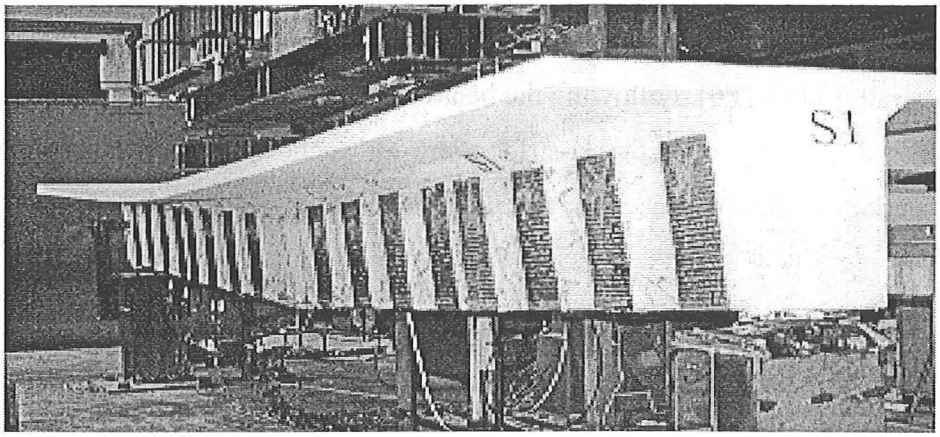

(a) Unit S1

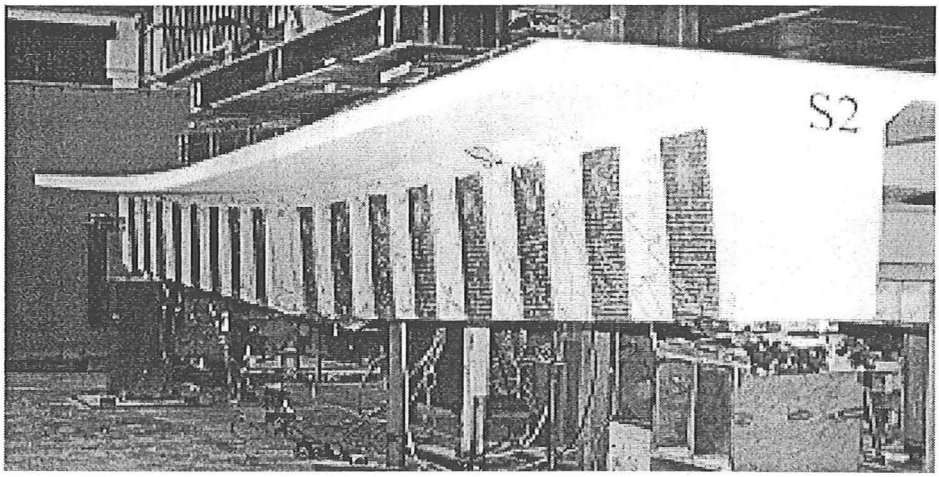

(b) Unit S2

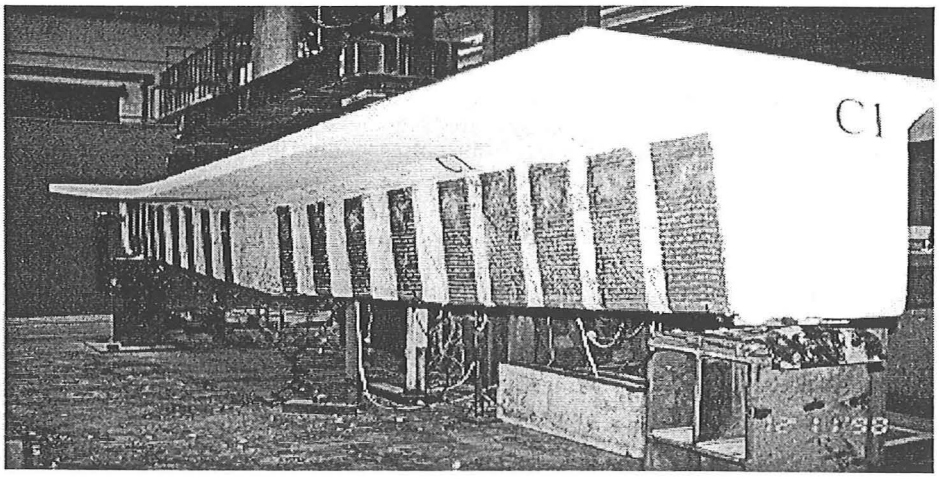

(c) Unit C1

Figure 4.37 Failure Mode of Test Series-B Units

Unit S1
Beam Type: BT1
Failure load, F=300kN
Central deflection=70mm
Failure mode: Carbon ACM laminate rupture at central span

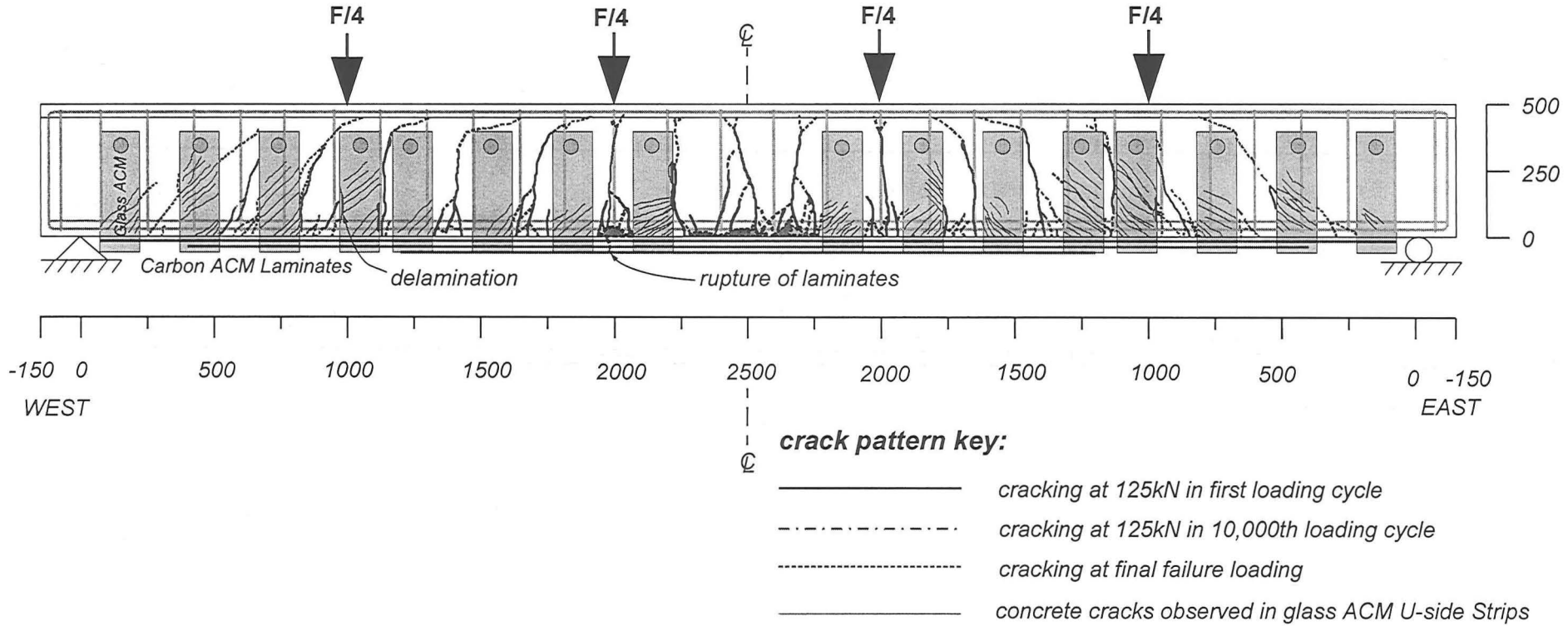

(a) Unit S1

Figure 4.38 Crack Pattern of Test Series-B Units at the End of Test

Unit S2
Beam Type: BT1
Failure load, F=306kN
Central deflection=65mm
Failure mode: Carbon ACM laminate rupture at central span

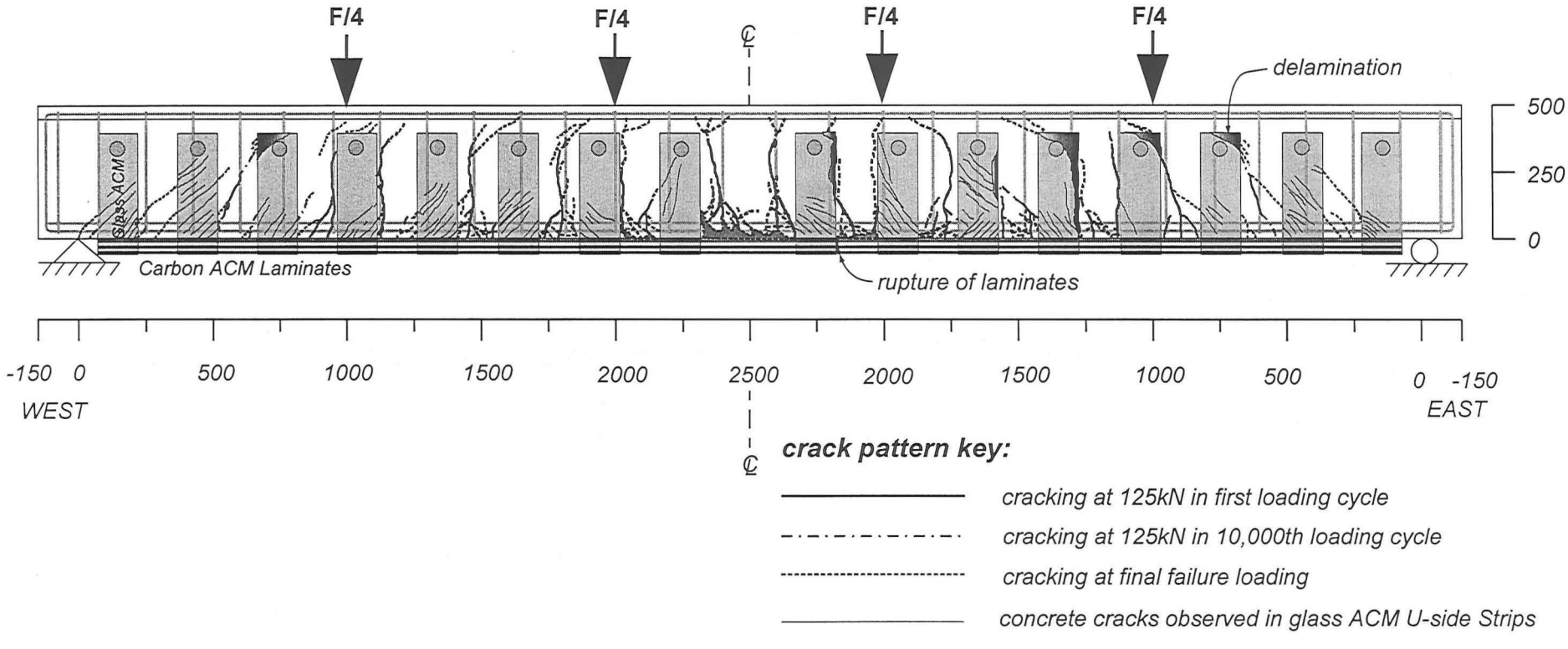

(b) Unit S2

Figure 4.38 Crack Pattern of Test Series-B Units at the End of Test (Cont.)

Unit C1
Beam Type: BT2
Failure load, F=270kN
Central deflection=60mm
Failure mode: Carbon ACM laminate rupture at central span

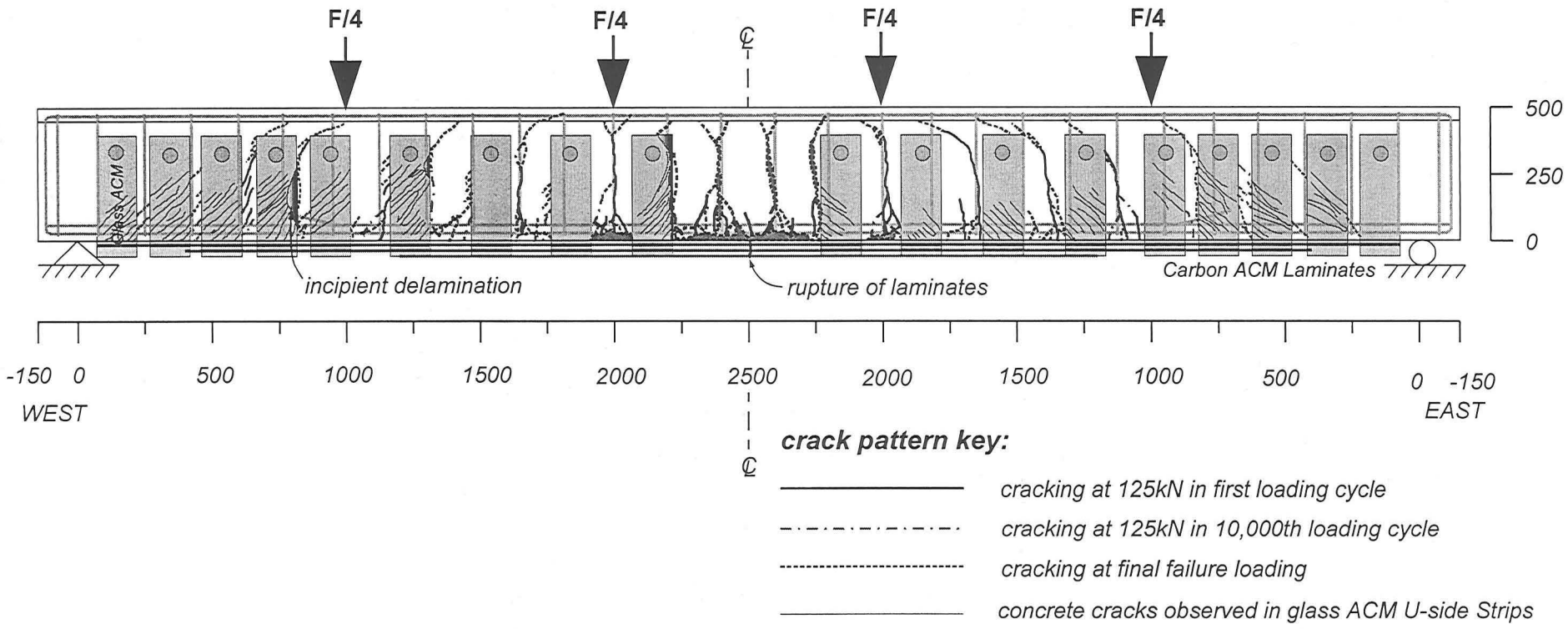

(c) Unit C1

Figure 4.38 Crack Pattern of Test Series-B Units at the End of Test (Cont.)

Unit S1

Unit S1 was identical to Unit F5 except for the additional GACM U-strips. At the service load range, the initial stiffness observed in Unit S1 was 31% greater than that measured in Unit P1 and 11% greater than the stiffness of Unit F5, see **Tables 4.6** and **4.7**. The difference in stiffness between Units S1 and F5 is mainly due to reduction in the beam shear distortion caused by the presence of the GACM U-strips in Unit S1.

The full vertical load versus mid-span deflection response is depicted in **Figure 4.36(a)**. Unit S1 was loaded up until a tensile rupture of the CACM laminate occurred at mid-span. The measured ultimate load was 300 kN, which is more than twice the ultimate load measured in Unit P1. The measured ultimate tensile strain of the CACM laminate that ruptured was 1.19%, see **Table 4.7**, higher than the ultimate strain of 1% measured in the tensile tests of isolated coupons.

Figure 4.37(a) shows a view of Unit S1 at the end of the test. The large mid-span rotation in the beam is due to the rupture of the CACM laminate. **Figure 4.38(a)** shows the cracking pattern in this unit. During the test, all the U-strips were tapped to check for delamination. The bond to the concrete appeared in excellent condition. Only at one location a GACM U-strip was found to show incipient delamination around an edge, see **Figure 4.38(a)**. It was also evident that few wide cracks which developed in the concrete between U-strips of the beam were developed into many fine cracks when passing through the U-strips. The test provided clear evidence that the U-strips with the fibreglass anchors were able to carry a large shear force and to reduce the shear distortion. Furthermore, the development of the bond between CACM laminate and concrete was also enhanced by the additional anchors of the U-strips because bond slip or delamination of the ACM was not found to occur during testing.

Unit S2

Unit S2 was identical to Unit F2 except for the additional GACM U-strips.

At the service load range the stiffness observed in Unit S2 was 43% greater than that measured in Unit P1 and 21% greater than that measured in Unit F2, see **Tables 4.6**

and **4.7**. This effect is due to the contribution of the GACM U-strips as mentioned in Unit S1. Also, a higher initial stiffness than Unit S1 was obtained due to the 3-layered full-length CACM laminates over the beam length.

The complete vertical load versus mid-span deflection response of Unit S2 is shown in **Figure 4.36(b)**. The measured ultimate load was 306 kN. Unit S1 failed when the CACM laminate ruptured at mid-span after reaching a tensile strain of 1.25%.

Figure 4.37(b) shows a view of Unit S2 at the end of the test. The concentration of damage at mid-span is evident in this figure. **Figure 4.38(b)** depicts the crack pattern of this unit. Some delamination of the U-strips was observed to have occurred during the final stages of the test. However, the presence of the anchors very effectively prevented complete delamination from occurring.

Unit C1

Unit C1 was identical to Unit S1 except for the longitudinal steel bars curtailed in the former unit. The condition for the curtailment carried out to the steel reinforcement and the carbon ACM laminate in Unit C1 represents the worst case among the Series-B units.

At the service load range, see **Figure 4.36(c)**, the degradation of the stiffness due to the cyclic loading effect was more pronounced than that observed in Units S1 and S2. The initial stiffness measured was 24% greater than that measured in Unit P1 but lower than that measured in Units S1 and S2, see **Table 4.7**.

The failure mode of Unit C1 was the same as Units S1 and S2, which is that tensile rupture occurred in the CACM laminate at the mid-span, see **Figure 4.37(c)**. The ultimate load and the maximum ACM laminate strain corresponding to the failure load were 270 kN and 1.02%, respectively. The overall response of the load versus mid-span deflection was very similar to the response observed for Units S1 and S2.

The crack pattern which developed in the concrete and in the ACM U-strips in the beams was very similar, compare **Figures 4.38(a)** to **(c)**. More fine diagonal cracks

occurred in the U-strips at the high shear region. This may be due to the larger additional shear distortion caused by the curtailment of the steel bars. At the end of test, incipient peeling from the edge of ACM U-strips was observed. However, this did not affect the behaviour of shear resistance of the U-strip. Also, the delamination of the CACM did not occur in Unit C1.

4.9.3.2 Crack Width Development During the Repeated Cyclic Loading Range

Table 4.8 gives the flexural crack widths measured in the Series-B Units during repeated cyclic loading. The Series-A beams with the same CACM laminate arrangement as Series-B units are also depicted in the table for comparison. The total crack width in pure bending moment region for Series-B units is very similar to the Series-A beams except Units C1 and F6. The crack width of Unit C1 is slightly larger than that of Unit F6 at the first cycle of the repeated loading. This will be discussed later.

Table 4.9 shows the measurement of the crack widths of diagonal cracks in the high shear zone is performed during the repeated loading cycles. It can be observed that the growth of crack width in Series-A Units is much wider than that in Series-B Units. The fact responsible for this phenomenon is that the U-strip did hamper the growth in the diagonal shear crack and caused finer cracks than those in beams without the U-strips. This scenario was clearly observed in the comparison between Units C1 and F6. Due to no external U-strips located in the vicinity of the steel bar curtailment, Unit F6 developed wider diagonal cracks in the bar curtailed region than Unit C1 especially during the last cycle of the repeated loading. Thus, the accumulated growth in the diagonal crack width reduces the growth in flexural crack width. That is the reason why the flexural crack width measured in F6 is smaller than that measured in Unit C1.

4.9.3.3 Transverse Strains on Concrete and Glass ACM U-strips

To determine the shear strength contributed by the ACM strips bonded to sides of the beam, it was necessary to quantify the effective strain of the side strip. In the design of the test beams, the maximum effective strain of ACM U-strips was assumed to be not more than 0.4 %.

Table 4.8 Flexural Crack Width in Pure Bending Region for Series-B Units

Unit	cycle	Load (kN)	Flexural crack width in pure bending area, measured level=50mm from beam bottom face (mm)																		Σ
			No.1	No.2	No.3	No.4	No.5	No.6	No.7	No.8	No.9	No.10	No.11	No.12	No.13	No.14	No.15	No.16	No.17	No.18	
S1	1st	125	0.14	0.02	0.12	0.04	0.02	0.12	0.12	0.04	0.02	0.14									0.78
S1	10000th	125	0.20	0.02	0.08	0.06	0.02	0.14	0.10	0.06	0.02	0.18									0.88
F5	1st	125	0.12	0.04	0.06	0.06	0.05	0.04	0.06	0.04	0.04	0.10	0.10	0.02	0.04	0.04	0.06				0.87
S2	1st	125	0.06	0.18	0.02	0.16	0.04	0.08													0.54
S2	10000th	125	0.04	0.16	0.02	0.14	0.04	0.08													0.48
F2	1st	125	0.01	0.02	0.04	0.04	0.04	0.04	0.03	0.04	0.04	0.02	0.02	0.02	0.04	0.01	0.03	0.04	0.02	0.02	0.52
C1	1st	125	0.16	0.04	0.04	0.10	0.06	0.04	0.02	0.12	0.06	0.04	0.16	0.04	0.16						1.04
C1	10000th	125	0.16	0.04	0.04	0.10	0.02	0.02	0.02	0.10	0.06	0.02	0.16	0.04	0.14						0.92
F6	1st	125	0.04	0.04	0.04	0.02	0.02	0.06	0.02	0.10	0.01	0.04	0.10	0.02	0.02	0.16	0.08	0.04	0.02	0.04	0.87

Table 4.9 Diagonal Crack Width in Shear Zone for Series-A and Series-B Units

Unit	cycle	Load	Western Side, mm				Eastern Side, mm				max. $\delta\omega$[2]
			high shear, 0~1.0 m[1]		low shear, 1.0~2.0 m[1]		low shear, 1.0~2.0 m[1]		high shear, 0~1.0 m[1]		
		(KN)	No.1	No.2	No.1	No.2	No.2	No.1	No.2	No.1	,mm
S1	1st	125	0.04	0.02	0.10		0.08	0.10			
S1	10000th	125	0.04	0.06	0.10		0.08	0.08		0.06	0.04
F5	1st	125	0.02	0.10	0.08	0.06	0.10	0.08	0.10	0.02	
F5	10000th	125	0.01	0.20	0.08	0.06	0.16	0.08	0.12	0.06	0.10
S2	1st	125	0.04		0.08	0.06	0.06	0.10		0.06	
S2	10000th	125	0.06		0.10	0.06	0.06	0.10		0.04	0.02
C1	1st	125	0.08		0.12	0.10	0.14	0.14		0.12	
C1	10000th	125	0.12		0.14	0.10	0.12	0.16		0.14	0.04
F6	1st	125	0.06	0.20	0.01	0.16		0.30	0.08	0.30	
F6	10000th	125	0.32	0.12	0.01	0.16		0.44	0.16	0.44	0.26

Notes: (1) The distance in different shear zone, which is counted from the beam support of each side.

(2) The maximum variation of diagonal crack width between first cyclic loading and 10,000th cyclic loading.

Figure 4.39 shows the transverse strain measured on concrete and GACM U-strips. In general, the concrete strain is larger than that on the ACM strip. This is because many fine shear cracks are spread over the ACM U-strip. Note that the measured effective transverse strain for Series-B units was performed using DEMEC gauges. Thus, the measured loads were lower than the ultimate loads. From the measured results, the maximum transverse strain measured on the ACM U-strip was about 0.45%, obtained from Unit C1 near the failure load. It is believed the effective transverse strain of 0.4% used for design is appropriate.

4.9.3.4 Comparison between the Predicted and Measured Response of Units S1, S2 and C1

Figure 4.40 compares the measured and predicted load-deflection response of Units S1, S2 and C1. There is excellent agreement between the theoretical and observed response. Note that the theoretical ultimate load and deflection are underestimated as an ultimate longitudinal strain of 1% was used in the analysis for the laminates. The ultimate strains observed in the tests vary from 1.02% to 1.25%.

Figure 4.41 shows the analytical results in Series-B units at ultimate load. The bending moment diagram includes the applied bending moment, the shifted bending moment that accounts for the effects of diagonal tension cracking and the nominal flexural strength envelope. Also shown is the shear force diagram including the applied shear force and the nominal shear strength envelopes. The nominal shear strength envelopes are plotted for two cases: one disregarding the presence of the U-strips and the other one considering the U-strips as fully effective over the entire beam depth. Both envelopes were calculated using the modified compression field theory that accounts for longitudinal and transverse strain compatibility. These two envelopes can be considered as lower and upper cases as partial height strips may not be fully effective in transferring shear. Moreover, the nominal shear strength calculated using Eq.4.1 and disregarding the U-strips is also shown in the shear force diagram. **Figure 4.41** also shows the predicted and measured laminate longitudinal strain and bond stress distribution.

The lower bound shear strengths calculated by MCFT and by Eq.4.1 with $A_{vp} = 0$ show that a shear failure would have taken place at a lower load if the ACM U-strips had

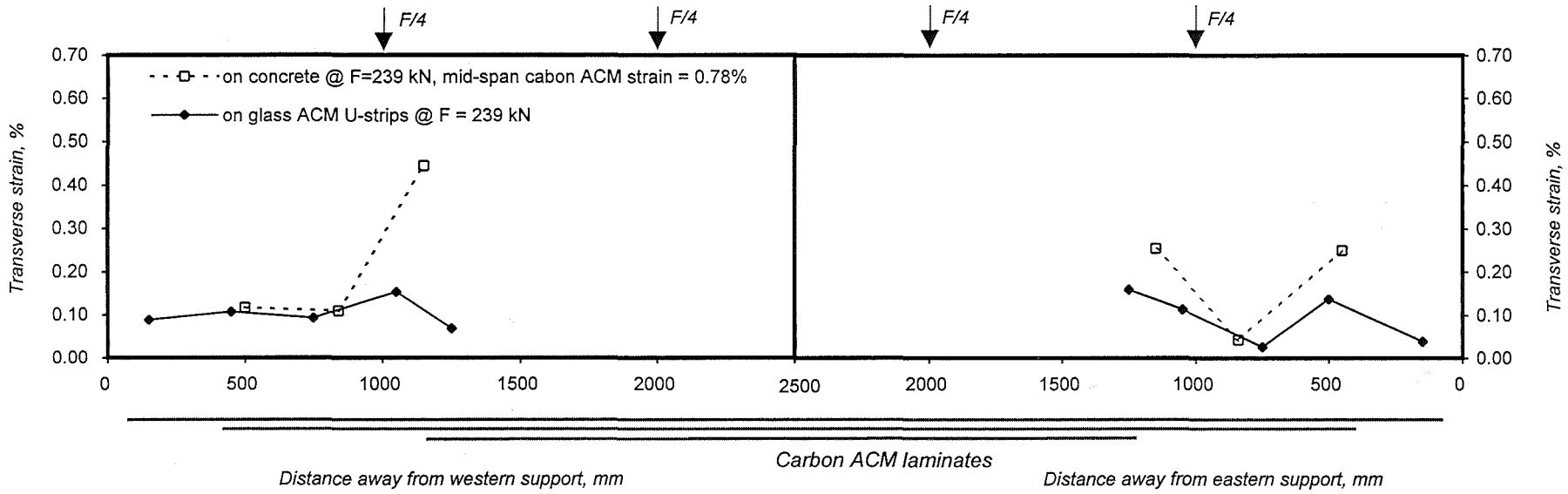

(a) Unit S1

Figure 4.39 Transverse Strain Measured on Concrete and Glass ACM U-Strips for Series-B Units

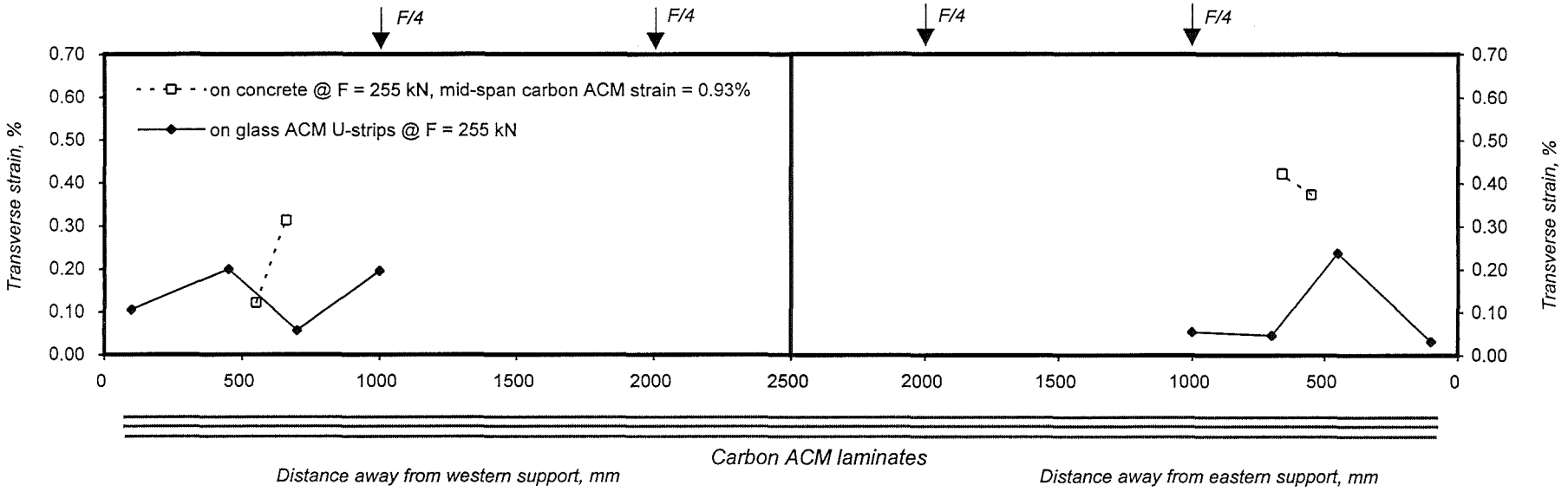

(b) Unit S2

Figure 4.39 Transverse Strain Measured on Concrete and Glass ACM U-Strips for Series-B Units (Cont.)

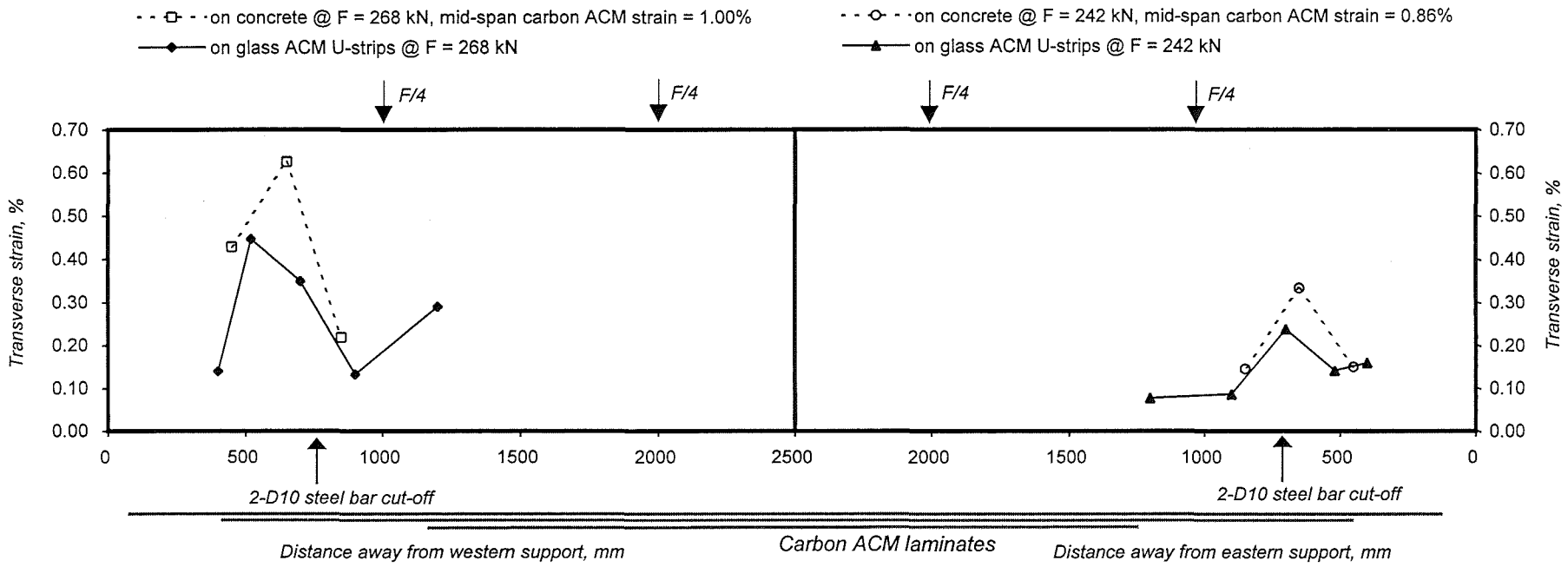

(c) Unit C1

Figure 4.39 Transverse Strain Measured on Concrete and Glass ACM U-Strips for Series-B Units (Cont.)

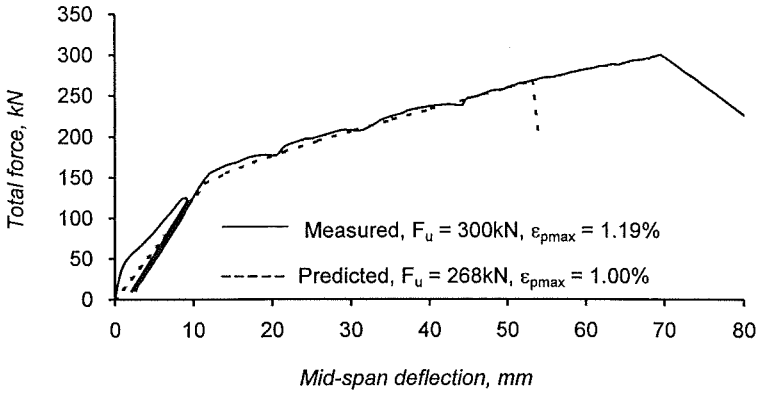

(a) Unit S1

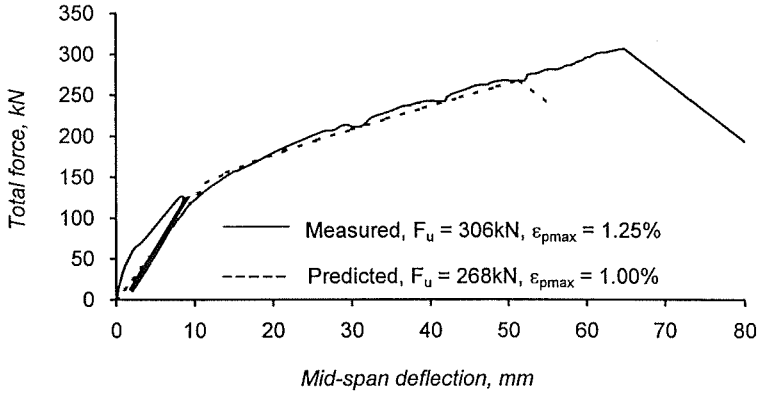

(b) Unit S2

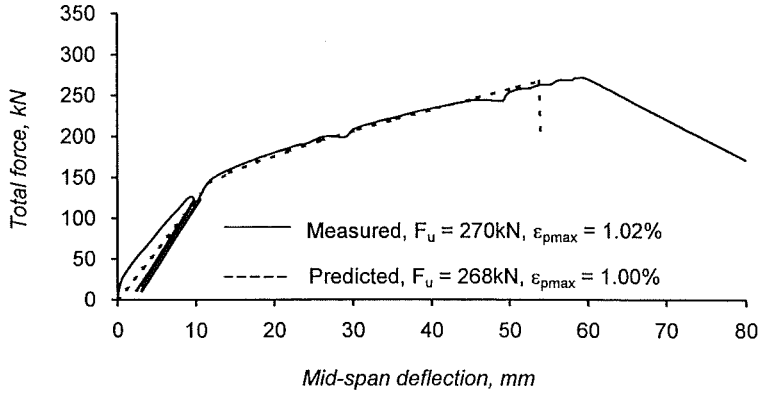

(c) Unit C1

Figure 4.40 Comparison of Load v.s. Deflection between Test and Prediction for Series-B Units

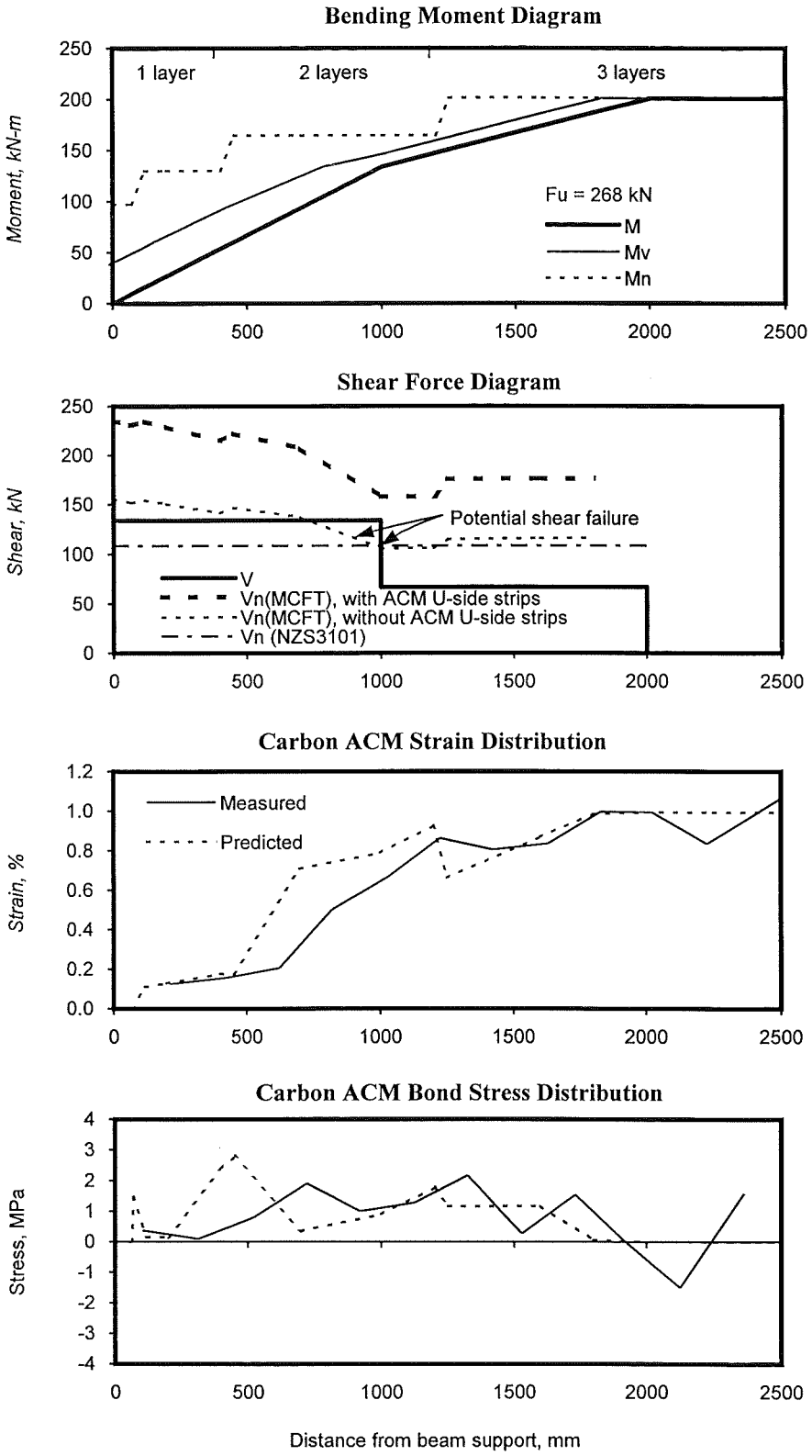

(a) Unit S1

Figure 4.41 Analysis on Series-B Units at Ultimate Load

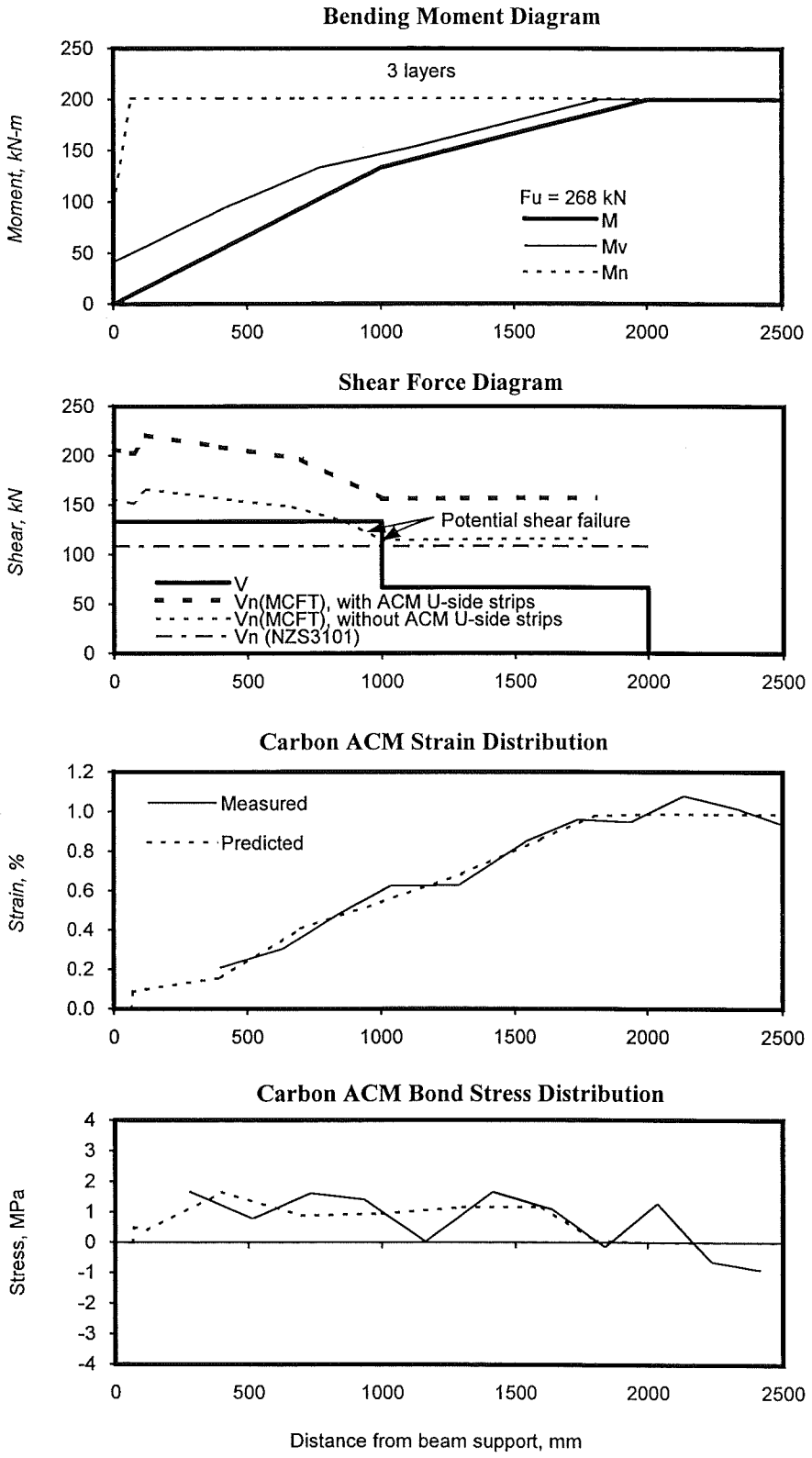

(b) Unit S2

Figure 4.41 Analysis on Series-B Units at Ultimate Load (Cont.)

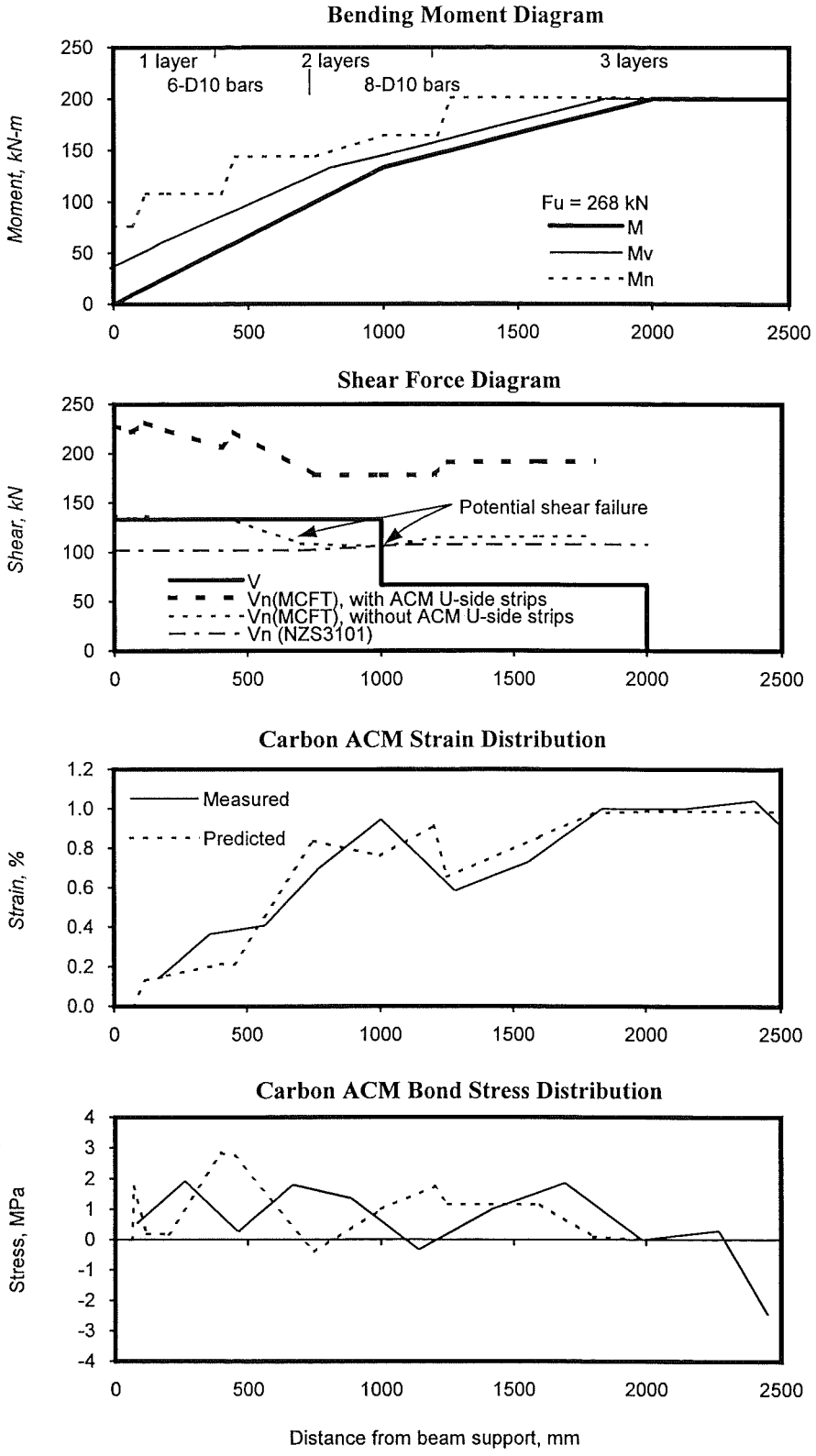

(c) Unit C1

Figure 4.41 Analysis on Series-B Units at Ultimate Load (Cont.)

not contributed to the shear strength of the beams, see **Figures 4.41(a)** to **(c)**. According to the shear strength envelopes determined using MCFT, Units S1 and C1 would have failed in shear at approximately 1m from the supports at an applied load of 215 kN whereas Unit S2 would have failed in shear at the same location at vertical load of 230 kN if the ACM U-strips had not been provided as the shear resistance of the beams. The upper bound strength computed from the MCFT, assuming full contribution of the U-strips, shows that the shear strength of the units is greater than the demand in all. As far as the laminate longitudinal strain and bond stress distribution the analytical model agrees quite well, particularly for Units S2 and C1, with the observed measurements, see **Figures 4.41(a)** to **(c)**.

In summary it can be said that the MCFT model discussed in Chapter 3 can describe very well the behaviour of beams with bonded ACM laminates applied to resist bending and shear. Furthermore, the increase of shear strength due to the presence of ACM U-strips of partial height was evident.

The fibreglass Tyfo-anchors were very effective in preventing delamination of the U-strips. As some delamination took place on the edges of some strips, it can be said that the anchors are fully effective in 120 mm wide strips.

4.9.4 Test Results on Series-C Unit

4.9.4.1 General

This test was performed to observe the effect of fatigue loading on the beam retrofitted with ACM laminates for flexure and shear. Unit C2 was identical to Unit C1. This unit was subjected to over a million cycles inducing a stress range of 200 MPa in the beam longitudinal reinforcing steel and then a monotonic load was applied up to failure.

All strain measurements on steel reinforcement, CACM laminates, and GACM U-strips were obtained using DEMEC gauges. The deflection of the beam was measured using a dial gauge to ensure stable readings during cyclic loading. Except for the steel bar fracture due to the fatigue caused by the cyclic loading, the response of load-deflection observed in Unit C2 is very similar to that observed in Unit C1 as described in the

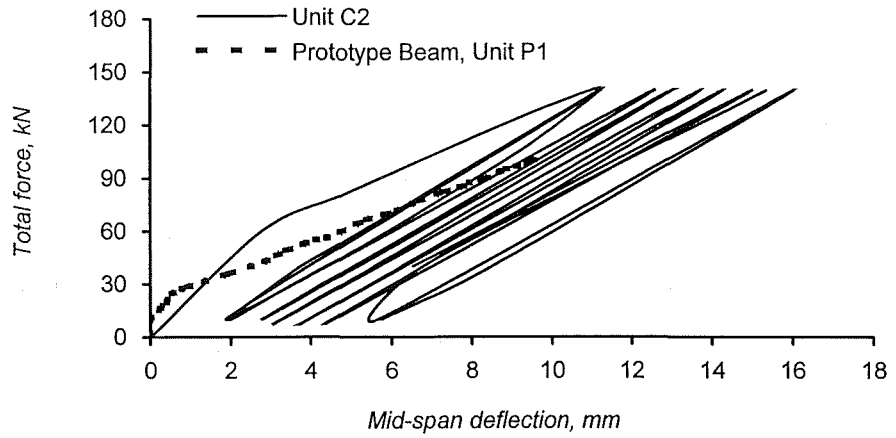

(a) Response in the Service Load Range

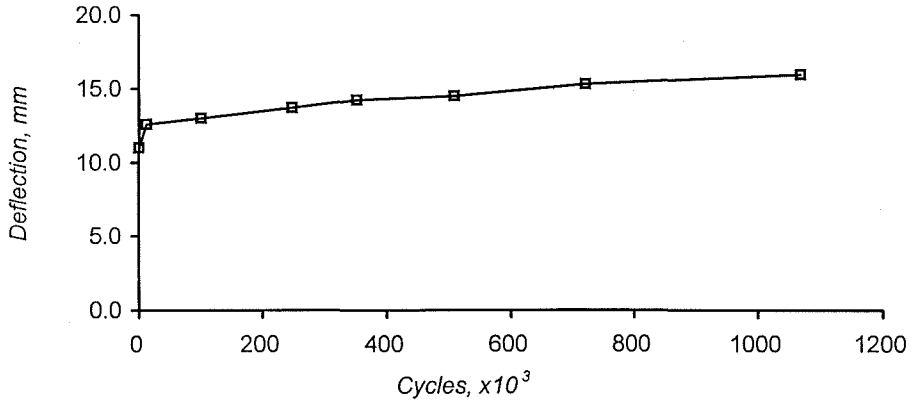

(b) Mid-span Deflection Growth at Peak Load

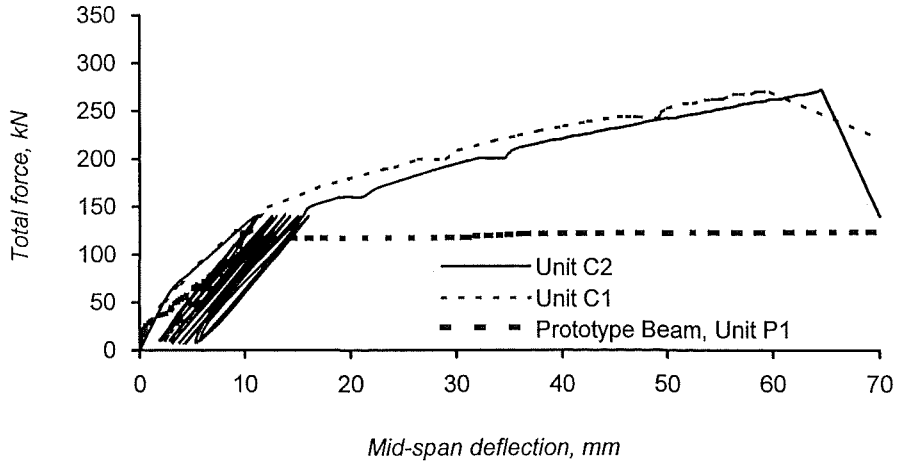

(c) Total Response

Figure 4.42 Vertical Load versus Mid-span Deflection for Series-C Unit C2

following sections.

4.9.4.2 Test Results - Service Load Range

Figure 4.42(a) shows the vertical load and mid-span deflection relationship measured for Unit C2 in the service load range. The mid-span deflection gradually increased with the number of the repeated cycles, see **Figure 4.42(b)**. The beam stiffness and the carbon laminate strain at mid-span can be seen in **Table 4.10** for different stages during this part of the test. It is believed that stiffness degradation and the growth in the ACM laminate strain were caused by both the gradual development of shear distortion and the fracturing of a reinforcing bar in the midspan region.

Table 4.10 Measured Stiffness of Test Series-C Unit C2

Cycles	$F'_{y,t}$ [(1)] (kN)	Δ_m [(2)] (mm)	$F'_{y,t} / \Delta_m$ [(3)] (kN/mm)	ε_p [(4)] (%)
1	140	11.0	12.7	0.15
12,250	140	12.6	11.1	0.17
100,296	140	13.0	10.8	0.17
247,322	140	13.7	10.2	0.18
351,503	140	14.2	9.9	0.19
508,540	140	14.5	9.7	0.20
721,047	140	15.3	9.2	0.21
1,067,852	140	16.0	8.8	0.22

Notes: (1) $F'_{y,t}$ = theoretical load corresponding to a stress of $0.875f_{sy}$ (280 MPa) in the longitudinal reinforcing steel.

(2) Δ_m = mid-span deflection corresponding to $F'_{y,t}$.

(3) Measured stiffness of the test unit.

(4) ε_p = measured CACM strain at mid-span, corresponding to $F'_{y,t}$.

Figure 4.43 shows the growth in strain measured in the steel reinforcement and the CACM laminate. The erratic strain distribution in the steel reinforcement at mid-span

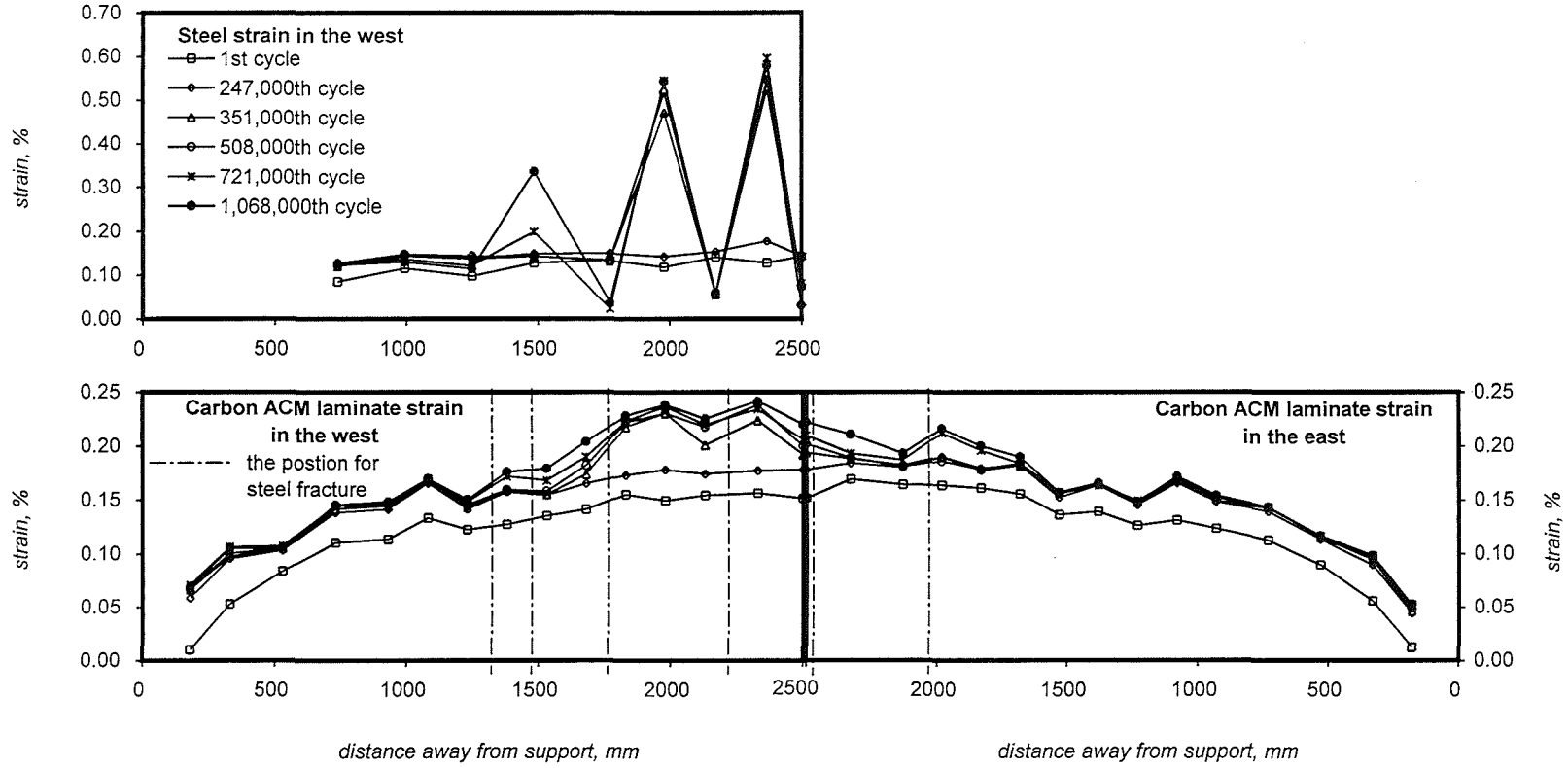

Figure 4.43 Strain Distribution in Steel Reinforcement and Carbon ACM Laminate of Unit C2 during Cyclic Loading

of the beam occurred after 350,000 cycles and was due to fracture of the only bar that had been tack-welded for fixing the clip gauges on the west side of the beam. This bar also fractured at several other locations as the test progressed. The CACM laminate provided strength lost by the ruptured steel bar. It is shown that the tendency of CACM strain distribution in the east is different from that in the west after 350,000 cycles. This is because beam bar fracture at the welded points took place.

The crack width measured during the cyclic loading is illustrated in **Figure 4.44**. The flexural cracks are measured in the pure bending zone and diagonal cracks are surveyed on the concrete surface in the shear span. It is clear that some flexural crack widths increased after the fracture of the steel bar beyond 350,000 cycles. The growth in width of the diagonal cracks was reasonably constant after the first 10,000 cycles and very stable after 350,000 cycles. A similar trend is shown by the transverse strain measured in the concrete surface and GACM U-strips, see **Figure 4.45**. A check of the condition of Unit C2 at the end of the repeated cycles showed no delamination of the U-strips and no signs of distress anywhere in the beam but in those localised regions where fracturing of a D10 bar was suspected. This test is conclusive in that the interface between concrete and ACM laminate is not affected by the fatigue loading.

4.9.4.3 Test Results - Ultimate Limit State

Figure 4.42(c) depicts the overall vertical load versus mid-span deflection response of Unit C2. The load-deflection curves measured in Units P1 and C1 are also plotted for comparison. It is clear that the behaviour for Units C1 and C2 at the ultimate limit state is nearly the same.

The failure mode and behaviour of Unit C2 was also similar to Unit C1. At the ultimate state, tensile rupture of the CACM laminate occurred at mid-span. **Figure 4.46(a)** shows Unit C2 at the end of the test. **Figure 4.46(b)** illustrates the failure point where the CACM laminate and the bottom steel bar fractured.

The crack pattern at the end of the test is sketched in **Figure 4.47**. The fracture points of the steel reinforcement are also shown in this figure. No delamination in the GACM U-strips was found in this unit.

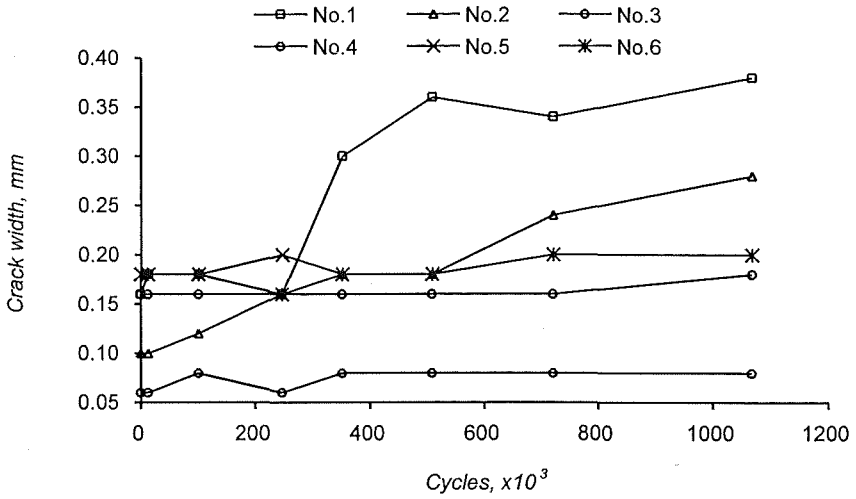

(a) Flexural Crack Width in the Pure Bending Zone

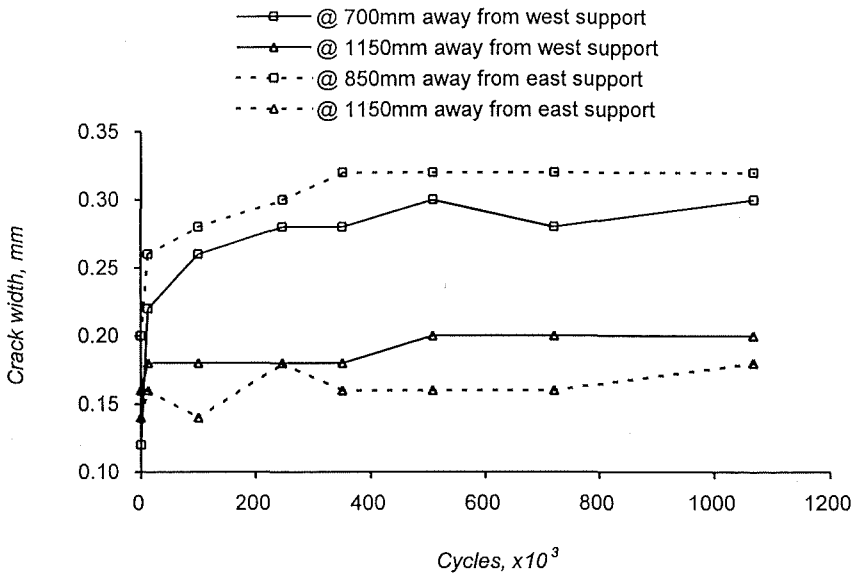

(b) Diagonal Crack Widths in High Shear Zone

Figure 4.44 Unit C2 Crack Width Measured at Peak Load

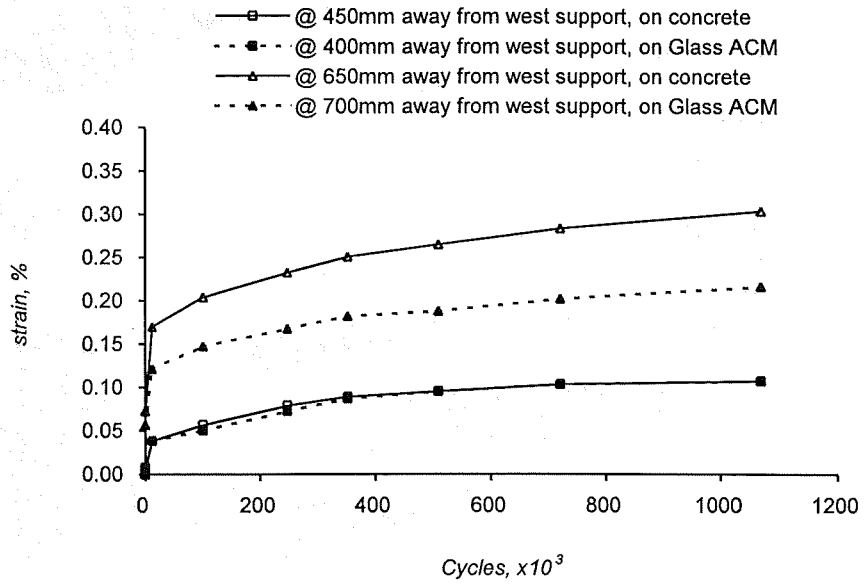

(a) Transverse Strain in the West Side

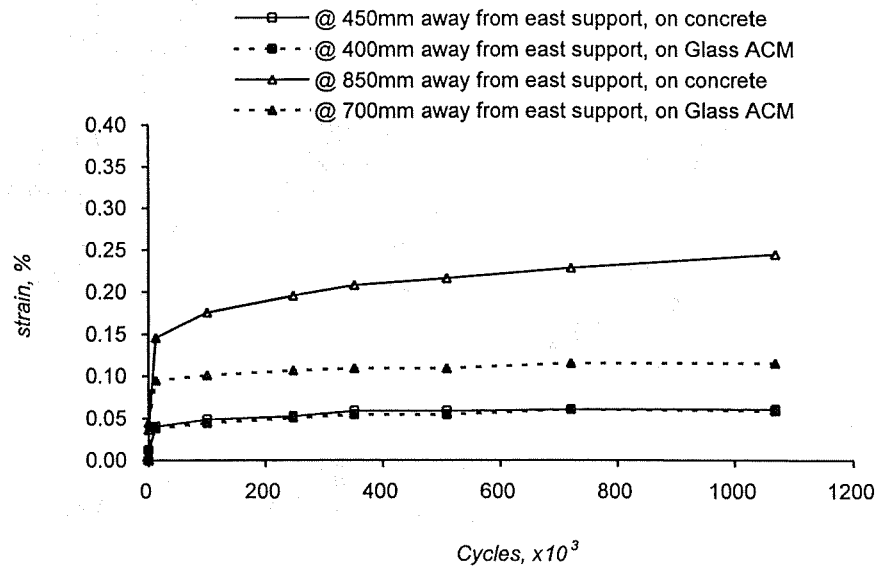

(b) Transverse Strain in the East Side

Figure 4.45 Transverse Strain Measured on Concrete and Glass ACM U-Strips of Unit C2 at Peak Load

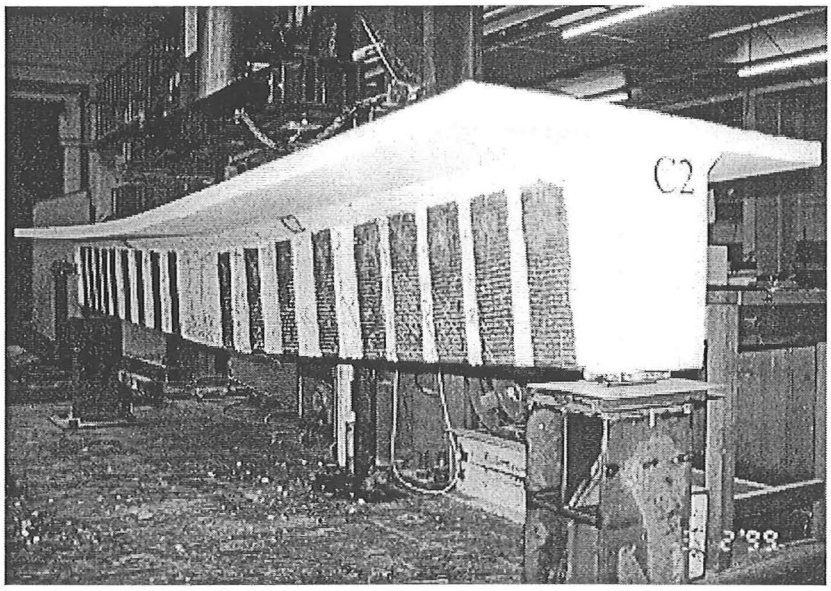

(a) Carbon ACM Tensile Rupture at Mid-span

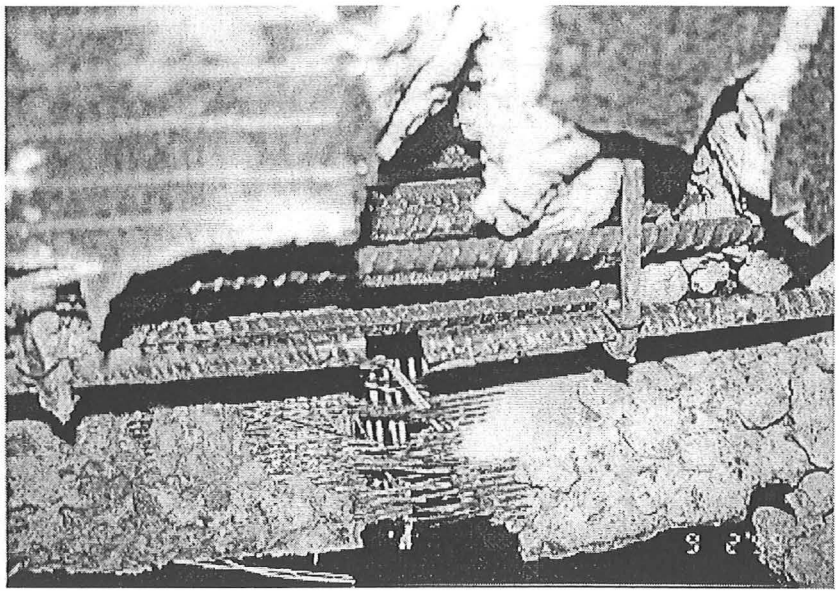

(b) Detail in the Position of Carbon ACM Rupture

Figure 4.46 Failure Mode of Unit C2

Unit C2
Beam Type: BT2
Failure load, F=272kN
Central deflection=65mm
Failure mode: Carbon ACM laminate rupture at mid-span

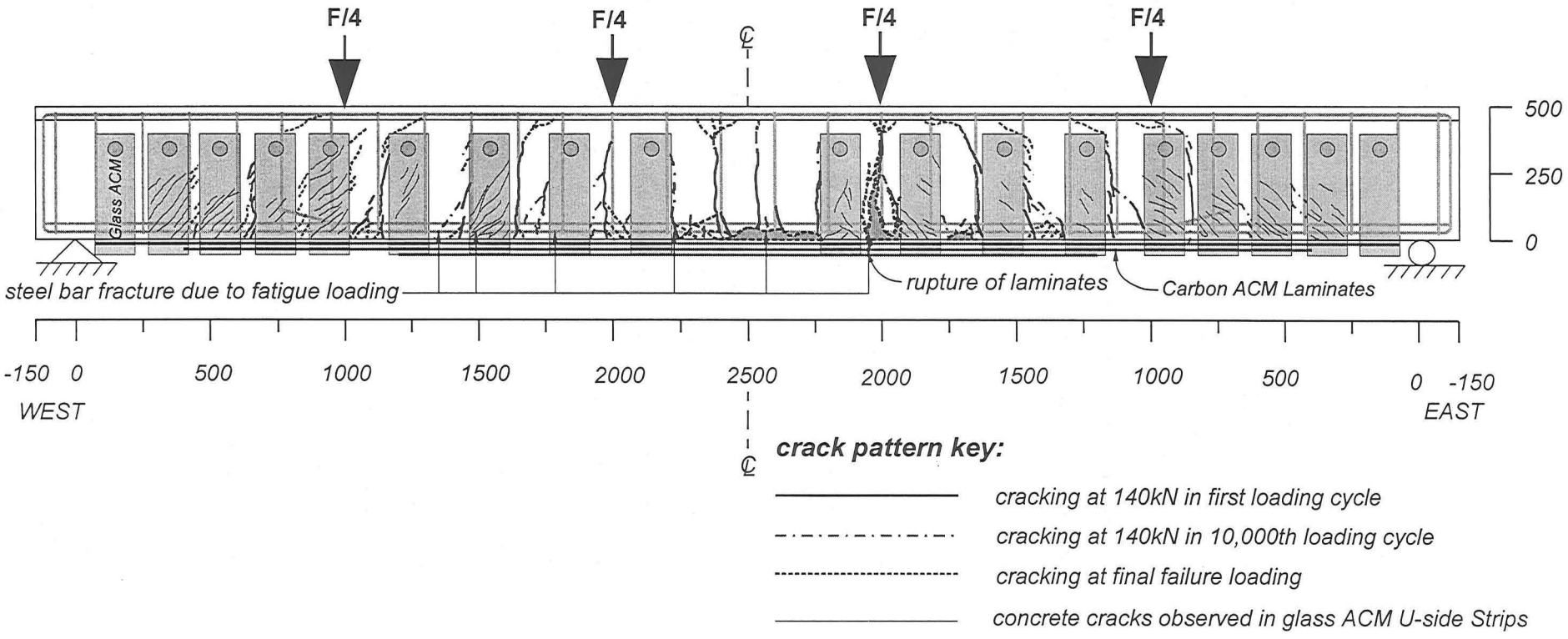

Figure 4.47 Crack Pattern of Test Series-C Unit C2 at the End of Test

4.10 Conclusions

This chapter presented the experimental and the analytical results. The conclusions made are:

1. The concrete surface preparation in the test was conducted using two mechanical abrading methods; scabbling and sandblasting. In general the interface bond strength between concrete and ACM laminate for two mechanical methods did not show obvious differences. The use of the dial gauge measurement method to quantify the quality control of the roughened concrete surface is preferable. The average amplitude of the roughened concrete surface attained in the test programme is 3 mm for scabbling and 2 mm for sandblasting.

2. The results of strain measurements on bottom concrete faces and carbon ACM laminates indicate that the assumption of no slip between the concrete surface and ACM laminate described in the theoretical study is acceptable.

3. It is found in the comparison between test and analysis on the beams strengthened with carbon ACM laminates bonded to their soffits that there is a very strong interaction between ACM delamination and shear capacity of the beams. This interaction has proven that the ACM laminate will separate suddenly due to the commencement of shear kinking when the shear applied is near the beam shear strength.

4. The prediction performed using the previous proposed analytical segment model, as mentioned in Chapter 3, correlated very well to the test results. The analytical model can be used to study the strength and failure mode of reinforced concrete beams strengthened with full-length or staggered ACM laminates bonded to their soffit and sides.

5. The beams with staggered carbon ACM laminates were studied with a view to cost savings and practical application. In engineering terms, the beams with full-length ACM laminates bonded to their soffit and the beams with staggered ACM laminates behave in a similar manner at service load range and even at

ultimate limit state. However, special attention must be given to the manner of the design of the curtailment of ACM laminate which is bonded to the beam tension face.

6. Attention must be paid in the prototype beam with curtailed steel reinforcement, to the fact that the flexure-shear crack in the vicinity of steel bar cut-off can cause the shear strength of the beam to be lower and thus influence the response of a beam retrofitted with ACM laminates.

7. A large number of finer flexural cracks were observed in the beams retrofitted with longitudinal ACM laminates applied to the soffit of the beams.

8. Glass ACM U-strips with fibre-anchors were used in the shear enhancement of Series-B units. These strips improve the bond strength of the ACM laminates bonded to the soffit of the beams. The ACM laminate tensile rupture was attained in all Series-B beams whereas delamination of the carbon ACM laminate occurred in the Series-A units, except Unit F1, which is the same as the failure mode of Series-B units. According to test results in Series-B Units, the highest measured transverse shear strain in the glass ACM U-strip was 0.45 %. Hence 0.4% effective transverse strain can be used for the design of glass ACM U-strips with mechanical anchors. The fibreglass Tyfo-anchors used in the test were very effective in preventing delamination of the U-strips. As some delamination took place on the edges of a number of strips it can therefore be concluded that the anchors are fully effective in conjunction with 120 mm wide strips.

9. The test results of a Series-C Unit subjected to one million cycles of repeated loading shows that the behaviour of the beam strengthened with carbon and glass ACM laminates resembles the behaviour of the same type of beam subjected to the monotonic loading at service load range. In addition, the carbon ACM laminates sustained the load when the steel bar fractured due to fatigue. The test result shows that the bonded epoxy/ACM laminate can withstand a better resistance to fatigue loading than the steel reinforcement.

CHAPTER 5

FIBREGLASS/EPOXY ACM FOR THE SEISMIC UPGRADING OF REINFORCED CONCRETE BEAMS WITH SHEAR AND BAR CURTAILMENT DEFICIENCIES

5.1 Introduction

For many years structural engineers have designed building structures in seismically prone regions of the world for lateral loads that are significantly less than those required to ensure elastic response. As a result, critical regions of the lateral load resisting elements are expected to undergo inelastic excursions and to dissipate energy. If these structures are to perform adequately their critical regions must be detailed for ductility. While the concept of inelastic response was known since the late 1950s, reinforced concrete building codes began to incorporate ductility requirements for seismic design in the 1970s only. The American Concrete Institute building code, ACI 318-71 [A11], following the San Fernando Earthquake of 1971, introduced seismic design recommendations by requiring the detailing for ductility of those regions in the earthquake resisting structural system assumed to be critical. The main recommendations to ensure ductile response were the use of closely spaced transverse reinforcement at the beam and column ends. In the 1970s the ACI 318-71 building code became accepted as a model code for seismic design in many parts of the world.

It is known now that buildings designed according to ACI 318-71 may not perform adequately during strong earthquakes. Recent earthquakes and experimental work have shown that shear failures, premature longitudinal bar buckling, and lap splices are some of the most common deficiencies found in structures designed with this code. Composite materials have been shown to be able to successfully correct most of these deficiencies [P6]. Also the reinforcing bar curtailment designed using the earlier code may result in another deficiency which promotes potential brittle shear failure. This will be discussed in the chapter.

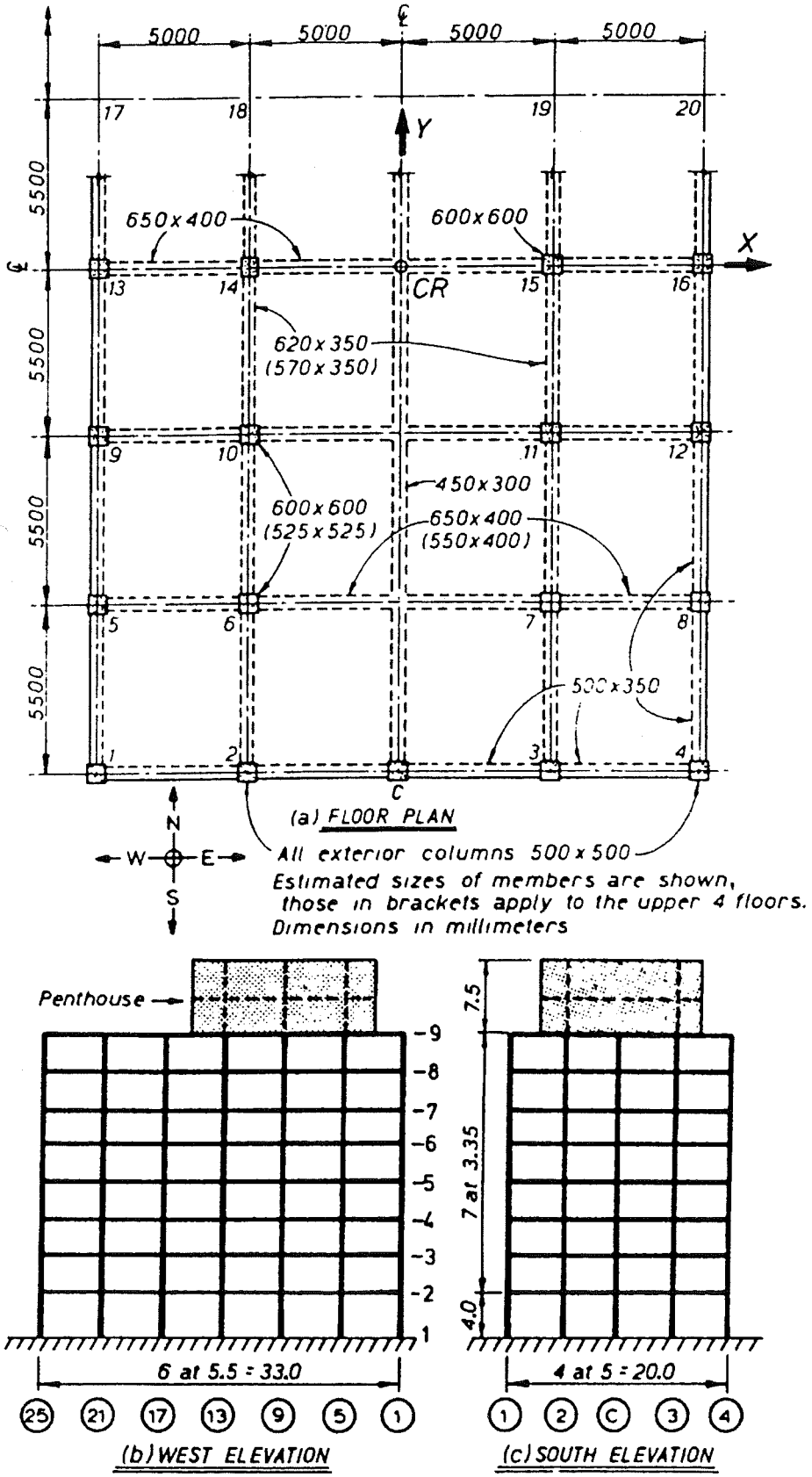

Figure 5.1 Framing System of an Eight-storey Building [P4]

This chapter summarises a simple assessment method and a related experimental programme to evaluate the effectiveness of glassfibre/epoxy (glass ACM) laminates in retrofitting and repairing reinforced concrete beams with bar curtailment deficiencies leading to flexure-shear failures. The test programme is looking at ways to assess the seismic behaviour of flanged beams designed according to older codes and to find ways to correct the potential deficiencies using glass ACM laminates.

5.2 Description of the Test Units

The eight-storey building shown in **Figure 5.1** was designed following the seismic design recommendations contained in the ACI 318-71 building code. The primary earthquake resisting system of the building was formed by a grid of moment resisting frames spaced at 5.5 m and 5.0 m in two orthogonal directions. The slab was designed to transfer gravity loading in two-way action. The lateral force coefficient for the design of the building for seismic induced forces was 0.09.

A simple assessment of the structure in an upper storey, mentioned later, indicated that negative plastic hinges would not form at the beam ends as could be expected, due to the presence of the slab reinforcement and to the curtailment of the longitudinal reinforcement in the beam. A prototype beam of this kind was chosen to conduct the experimental programme in this part of the study. The beam flange width and slab thickness were 960 mm and 120 mm, respectively. The overall depth of the beam was 550 mm and the web was 350 mm wide. Complete reinforcing details are depicted in **Figure 5.2**. The concrete strength was chosen to be 20 MPa to simulate a worst case scenario in construction.

In the test programme, two identical full-scale beam subassemblies were built and tested under reversed cyclic loading conditions simulating seismic loading. Three tests were performed in the two units as follow:

Test Unit T1 – Stage 1	To test and observe the seismic performance of the as-built unit.
Test Unit T1 - Stage 2	To repair the beam in the damaged region and

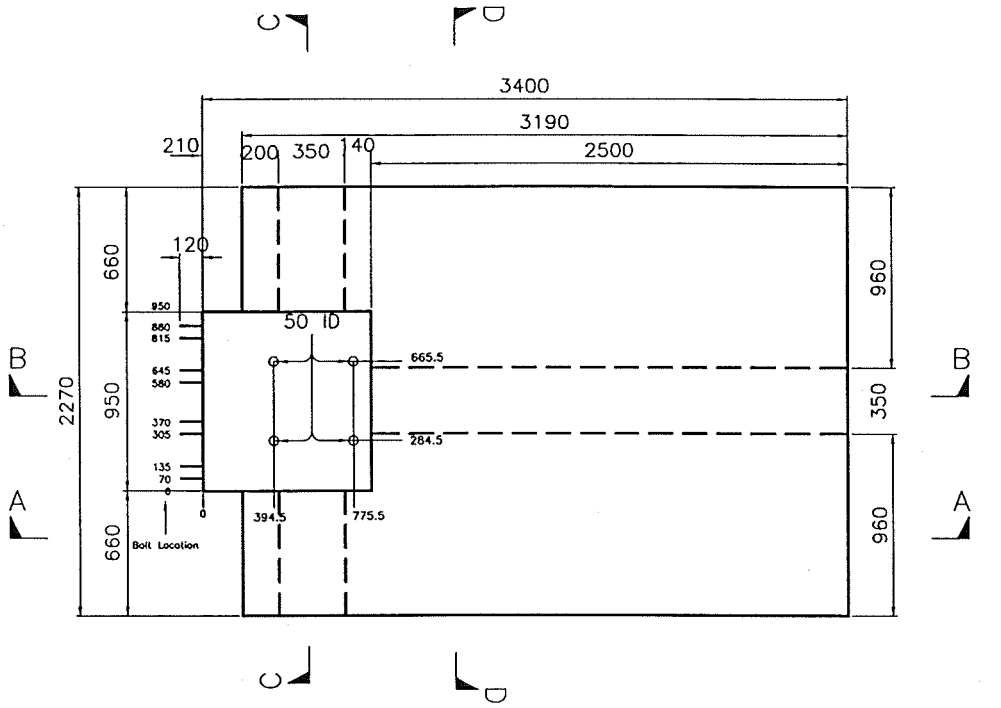

Plan View

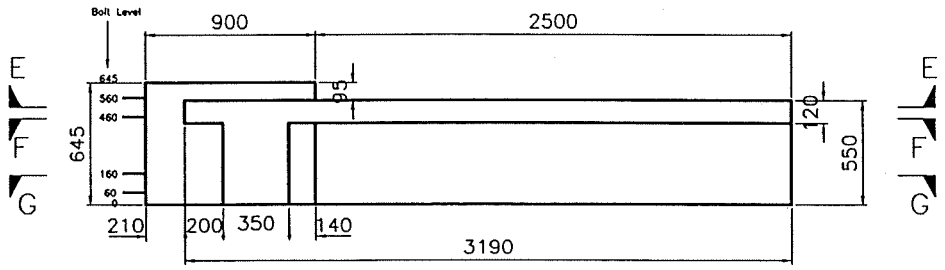

Elevation

Figure 5.2 Reinforcing Details of Units T1 and T2

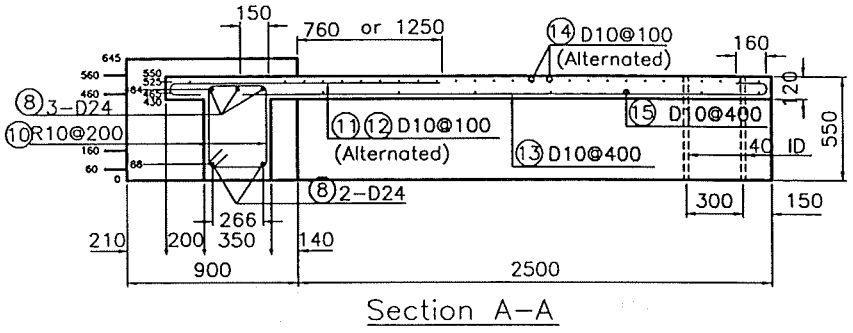

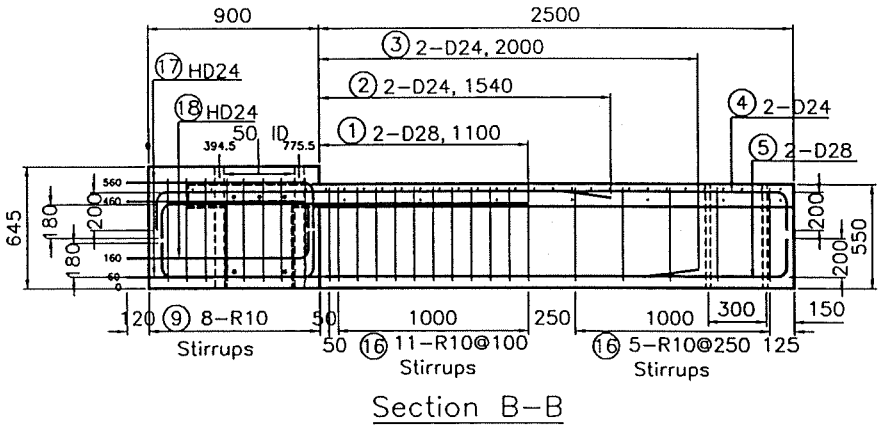

Figure 5.2 Reinforcing Details of Units T1 and T2 (Cont.)

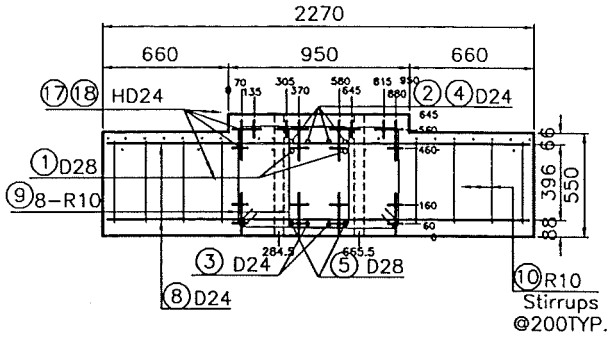

Section C–C

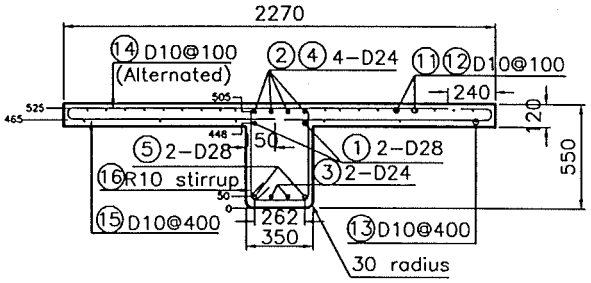

Section D–D

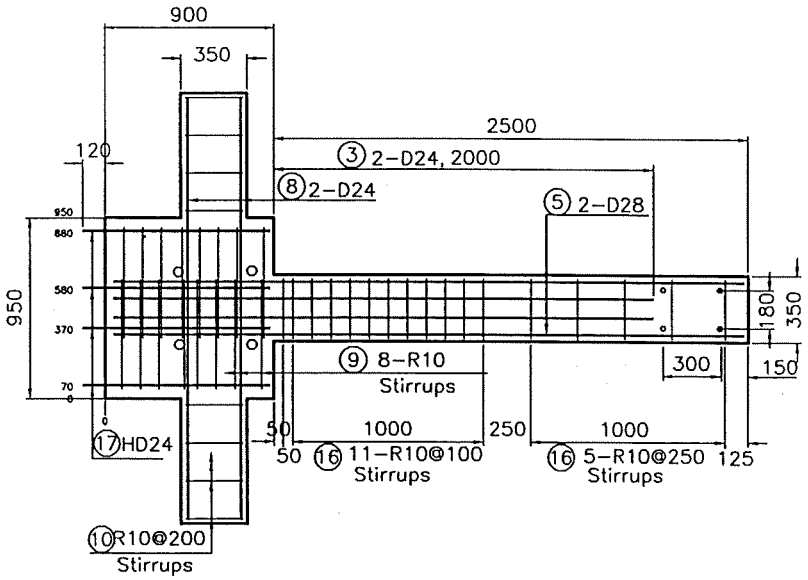

Section G–G

Figure 5.2 Reinforcing Details of Units T1 and T2 (Cont.)

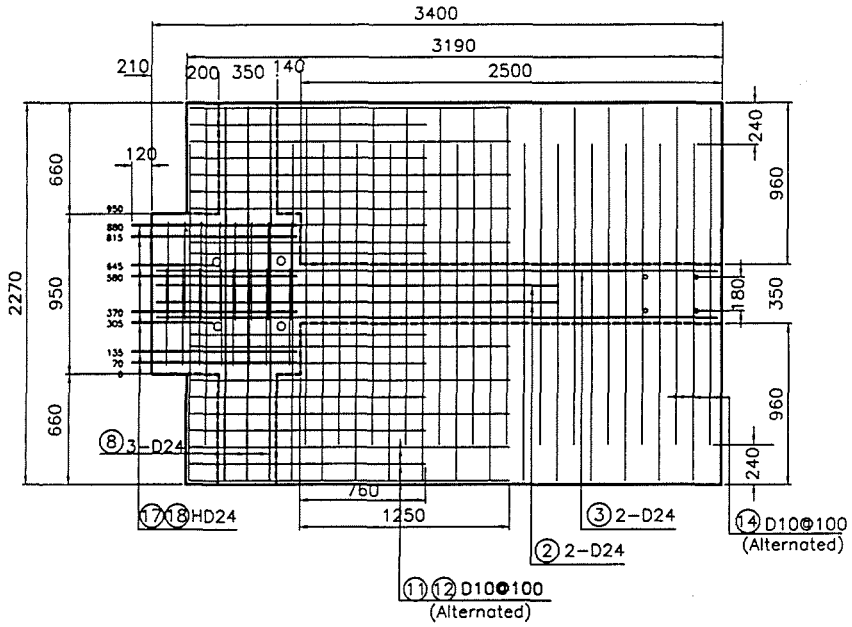

Section E–E Top Slab Bars

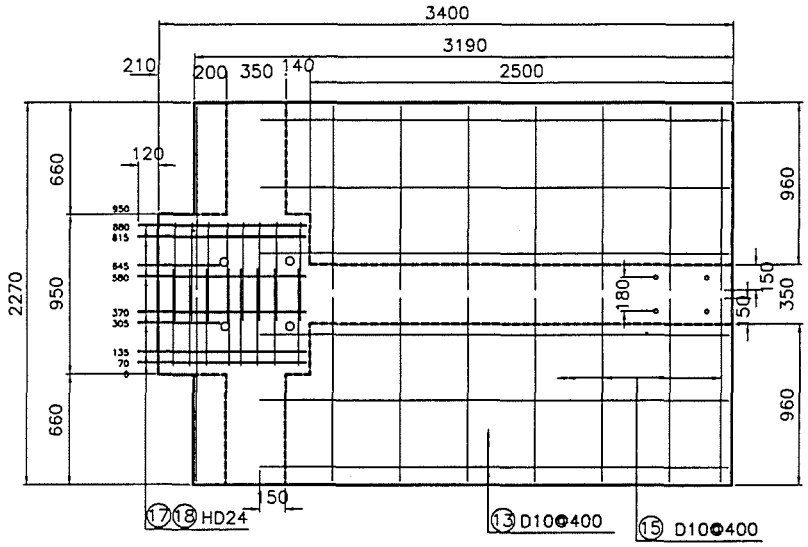

Section F–F Bottom Slab Bars

Figure 5.2 Reinforcing Details of Units T1 and T2 (Cont.)

	resume testing.
Test Unit T2	To retrofit the beam before testing. Test and observe the seismic performance of the retrofitted unit.

5.3 Specimen Fabrication

Reinforcing steel cages were fabricated to meet a construction tolerance of about ± 5 mm. The formwork for the specimens was manufactured using 19 mm plywood sheets. The moulds were stiffened with timber battens, steel angles, and brackets. The moulds were undercoated and oiled before concreting.

Prior to casting concrete, strain gauges and steel studs for the clip gauges were attached or welded to the steel reinforcement. The cages then were fixed in position within the moulds using 25 mm spacer blocks. **Figure 5.3** shows the test specimen before placing the concrete.

The two test units were cast using concrete in different pours. The maximum aggregate size was 20 mm and the slump measured during casting concrete ranged between 100 mm and 130 mm. Test cylinders 200 mm high by 100 mm diameter were cast and vibrated on a vibrating table. The cylinders were cured in the same condition as the test units. The two units were cured using wet sacking for 7 days and were stripped and left to dry indoors.

5.4 ACM Laminate Application

The flexural/shear strength deficiency found in the units was corrected using TYFO S fibrwrap fibreglass/epoxy laminates. **Figure 5.4** illustrates details of the repair work with the glass ACM laminates applied to the top of the beam. The criterion for the design of the laminate is discussed in Section 5.8.3.2. In addition, glass ACM U-shaped strips were applied to sides of the beam to improve the shear resistance. These strips were not anchored at their ends.

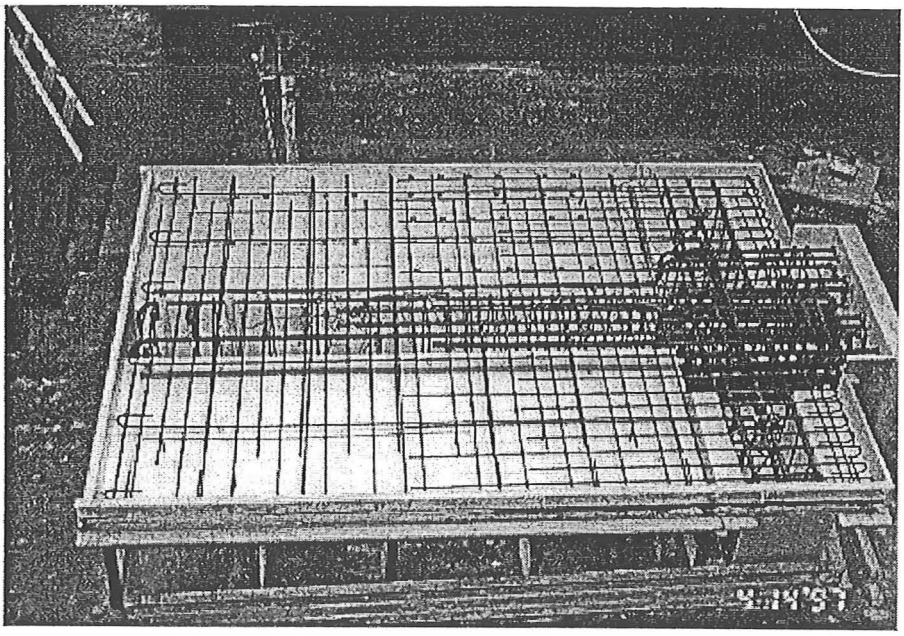

Figure 5.3 Details of Test Specimen Prior to Casting of the Concrete

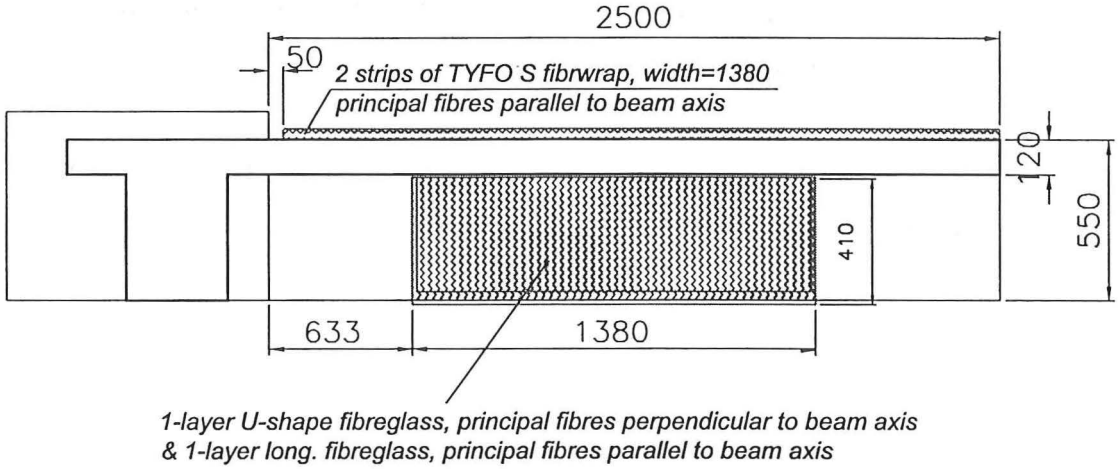

Note: The thickness of 1-layer TYFO S fibrwrap is 1.27 mm.

Figure 5.4 Retrofit Scheme of Test Units

As mentioned in earlier, the as-built beam, Unit T1, was loaded until a flexure-shear failure developed. Then, the damaged unit T1 was repaired with following procedure:

1. Injecting a low viscosity epoxy resin to the main cracks, as shown in **Figure 5.5(a)**.

2. The concrete surface where the glass ACM laminates were to be applied was ground to remove any laitance and then cleaned with an oil-free air pressure, see **Figure 5.5(b)**.

3. A thick layer of epoxy adhesive, TYFO WS, was applied to the concrete surface before the application of saturated glass ACM laminates, see **Figure 5.5(c)** and **(d)**.

4. Saturating the glass ACM laminates in site, see **Figure 4.6**.

5. Applying two 1.38 m wide layers of TYFO S fibrwrap on the top of slab, see **Figure 5.5(e)**, and applying TYFO S fibrwrap on the sides of the beam at the damaged region, see **Figure 5.5(f)**.

Unit T2 was retrofitted in the same manner as unit T1, except that epoxy resin injection, as per Step 1, was not needed.

5.5 Material Properties

5.5.1 Concrete

The measured properties of the concrete cast in the units are given in **Table 5.1**. The concrete compressive strength at the day of testing was measured using 100 mm diameter by 200 mm high cylinders.

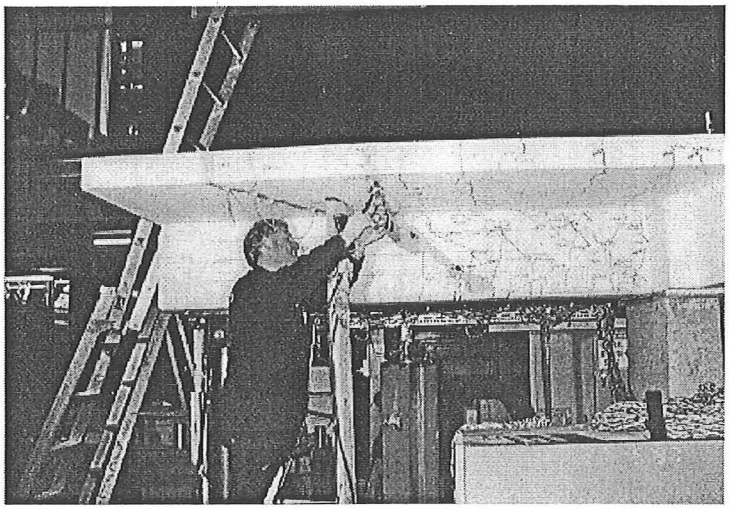

(a) Epoxy Injecting to Main Cracks

(b) The Concrete Surface after Grinding

(c) Application of the TYFO WS Epoxy Resin on the Sides of the Beam

Figure 5.5 Sequence of Repairing on Damaged Unit T1

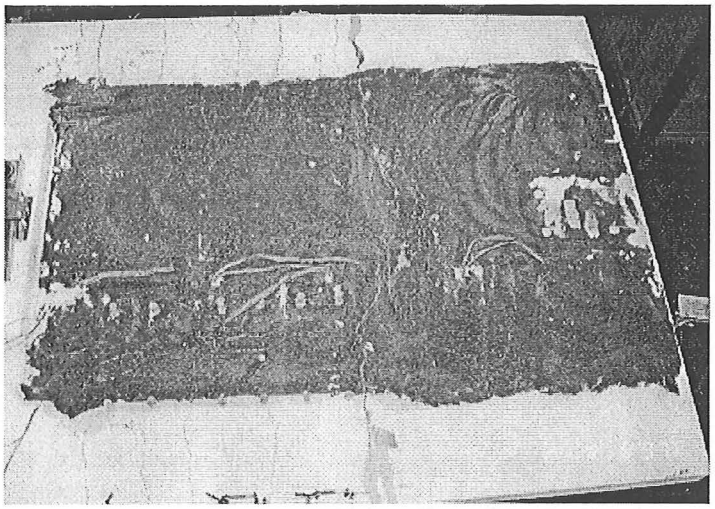

(d) Application of the Epoxy Resin on the Top of Slab

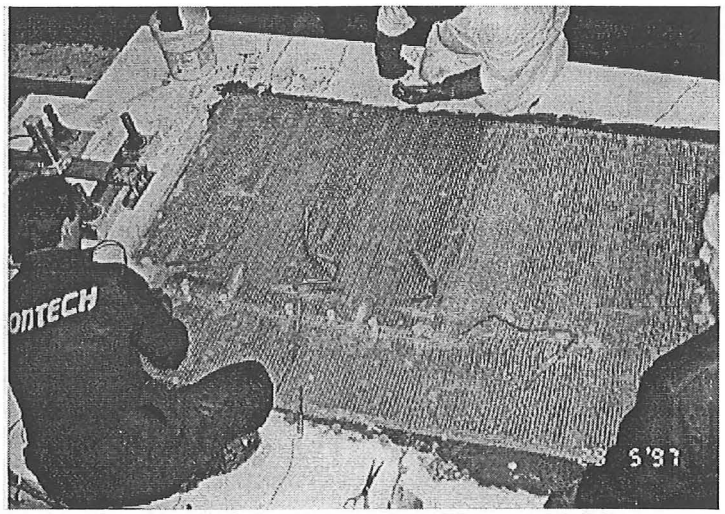

(e) Application of the Saturated Glass ACM Laminates on the Top of the Slab

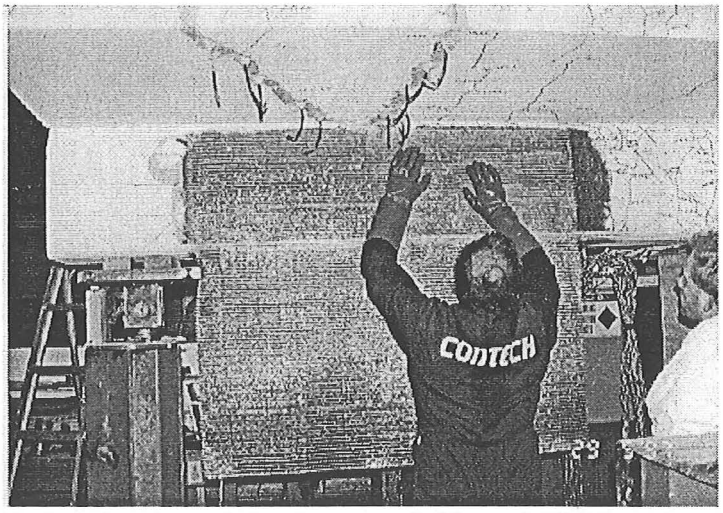

(f) Application of the Saturated Glass ACM Laminates on the Sides of the Beam

Figure 5.5 Sequence of Repairing on Damaged Unit T1 (Cont.)

Table 5.1 Concrete Properties

Unit	Slump (mm)	F'_c [1] (MPa)	Age at Test (days)
T1	100	24	62
T2	120	18	95

Note: (1) Average of six cylinders

Table 5.2 Mechanical Properties of Reinforcing Steel of Test Units[1]

Reinforcing type [2]	A_s (mm^2)	f_{sy} (MPa)	E_s (GPa)	ε_{sh} (%)	ε_{su} (%)	f_{su} (MPa)
D28	618.5	316	198	1.8	12	454
D24	452.4	320	200	2.1	24	475
D10	78.5	316	212	2.7	22	464
R10	78.5	354	201	-	-	469

Notes: (1) Average of three tests

(2) D: deformed bar, R: plain round bar

Table 5.3 Glass ACM Properties[1]

Type	Test sample dimension			Mean values	
	Thickness (mm)	width (mm)	length (mm)	Tensile Strength (MPa)	Modulus (GPa)
TYFO SHE-51	2.54[2]	25	350	387	18.7

Notes: (1) Test on three coupons carried out in accordance with ASTM 3039D

(2) Two plies of fibreglass laminates were adopted. A nominal ply thickness is 1.27 mm.

5.5.2 Steel Reinforcement

Grade 300 with a 5 percentile lower characteristic yield strength of 300 MPa reinforcing steel was used to build the cages at the units. The mechanical properties of the bars is given in **Table 5.2**.

5.5.3 Glass ACM Laminates

The mechanical properties of the TYFO S SEH-51 laminates were measured in accordance with the general specification of ASTM D 3039 [A2]. Three samples were taken from the ACM laminates used, and mean values of strength and modulus were determined from the measured results. The mechanical properties are given in **Table 5.3**.

5.6 Instrumentation

Figure 5.6 shows the instrumentation layout in the units. Strain gauges, clip gauges, linear potentiometers, DEMEC gauges, load cells, and an inclinometer were employed in the tests. Those gauges except the inclinometer were described in detail in Section 4.7.

The inclinometer, Tokyo Sokki KB-1 AB, see **Figure 5.7**, can detect a maximum rotation of one degree with a sensitivity of 0.883 mV/V. The component of beam end deflection due to the rotation of column stub was measured with the inclinometer and then deducted from the total measured deflection.

Linear potentiometers placed quadrilaterally on the web side of the beam enabled the average shear and flexural deformation of each "gauged region" to be estimated [D1]. **Figure 5.8** depicts the average flexural and shear distortion components captured by this arrangement of linear potentiometers. From geometry, the following relationships can be established:

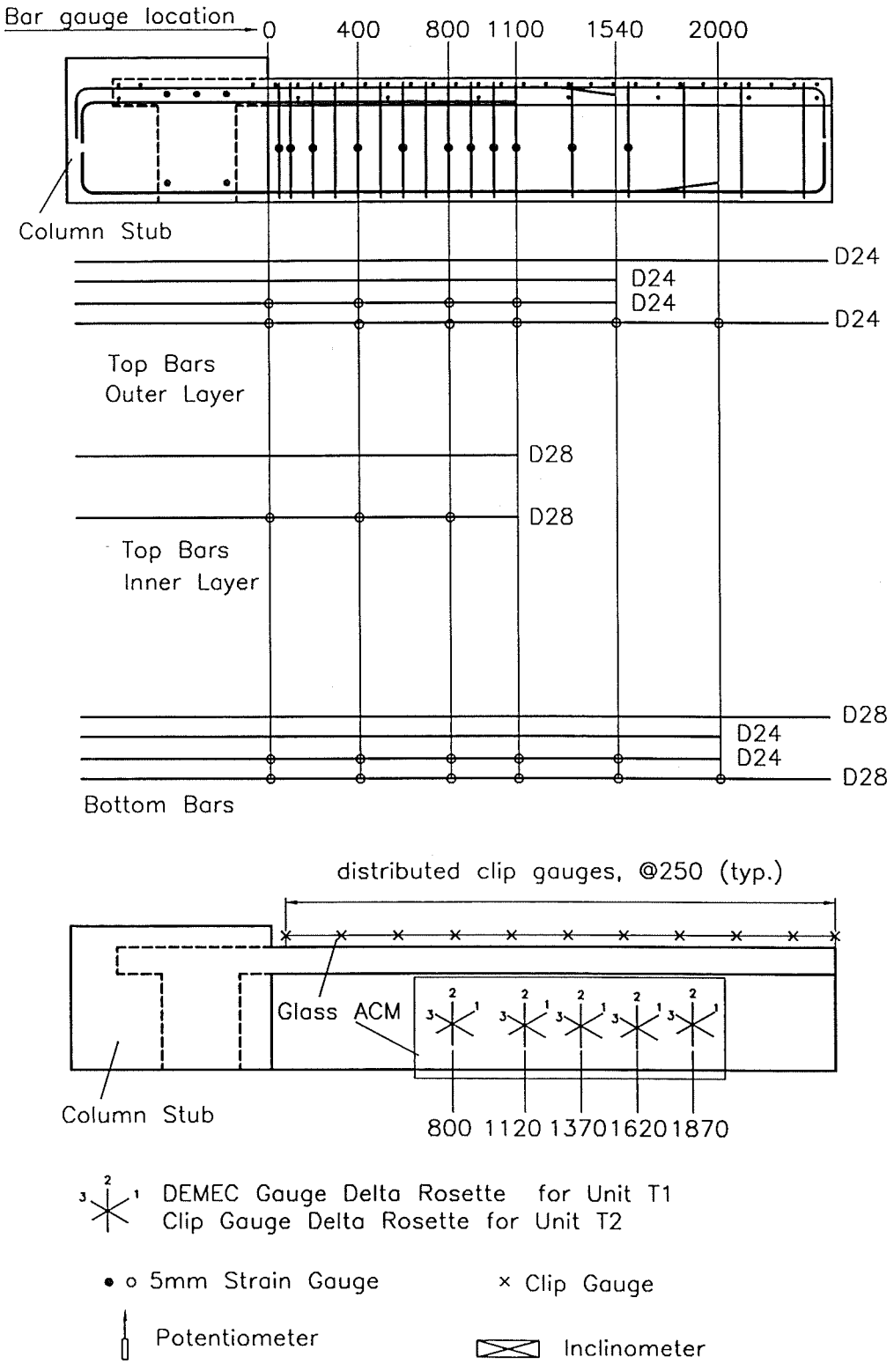

Figure 5.6 Instrumentation Arrangement of test Units T1 and T2

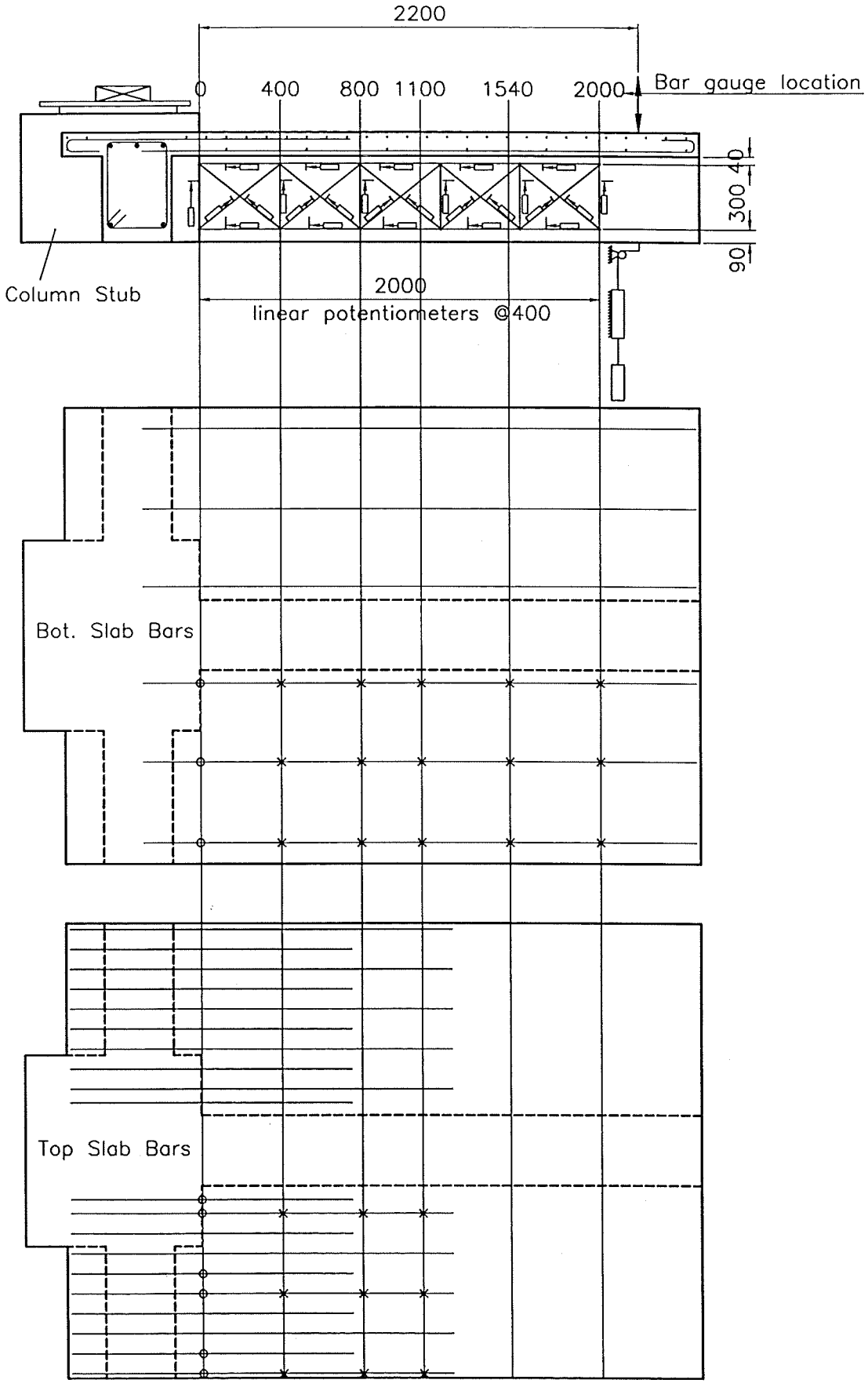

Figure 5.6 Instrumentation Arrangement of test Units T1 and T2 (Cont.)

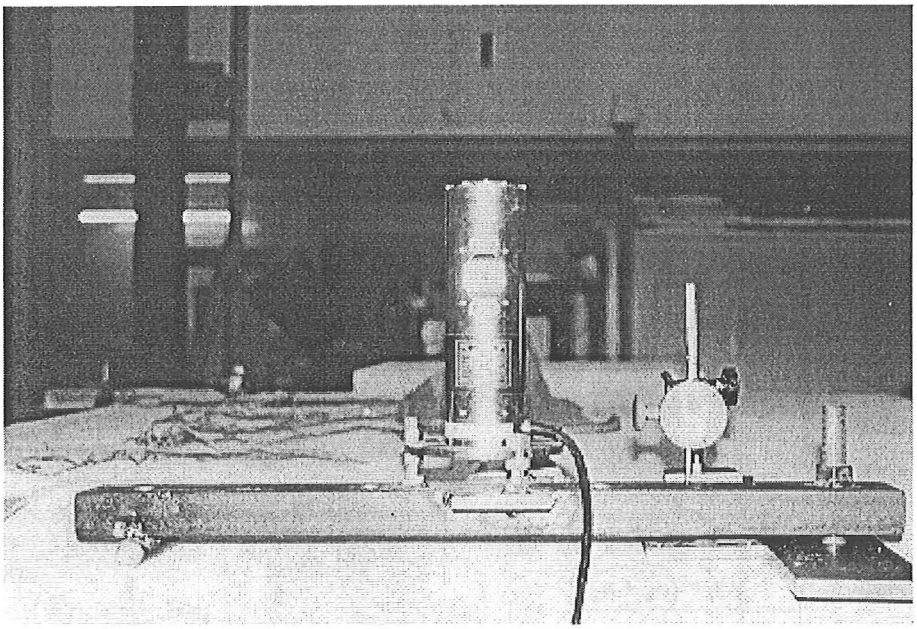

Figure 5.7 Inclinometer Used in the Test

$$\cos\theta_{1j} = \frac{a_{1j}^2 + a_{4j}^2 - a_{5j}^2}{2a_{1j}a_{4j}} \tag{5.1a}$$

$$\cos\theta_{2j} = \frac{a_{2j}^2 + a_{1j}^2 - a_{6j}^2}{2a_{2j}a_{1j}} \tag{5.1b}$$

$$\cos\theta_{3j} = \frac{a_{3j}^2 + a_{2j}^2 - a_{5j}^2}{2a_{3j}a_{2j}} \tag{5.1c}$$

$$\cos\theta_{4j} = \frac{a_{4j}^2 + a_{3j}^2 - a_{6j}^2}{2a_{4j}a_{3j}} \tag{5.1d}$$

The sum of these angles is compared to 360 degrees and adjustment is made by scaling each so that they total this amount. The curvature is calculated as

$$\phi_j = 0.5\left(-\theta_{11} + \theta_{1j} - \theta_{21} + \theta_{2j} + \theta_{31} - \theta_{3j} + \theta_{41} - \theta_{4j}\right) / \Delta h_j \tag{5.2}$$

The shear strain is calculated as

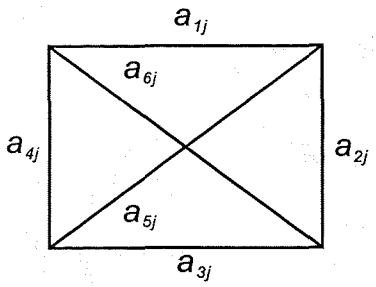

(a) Sides and diagonals

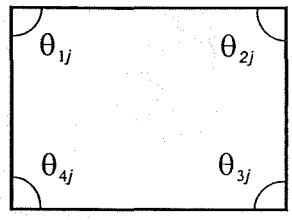

(b) Angles

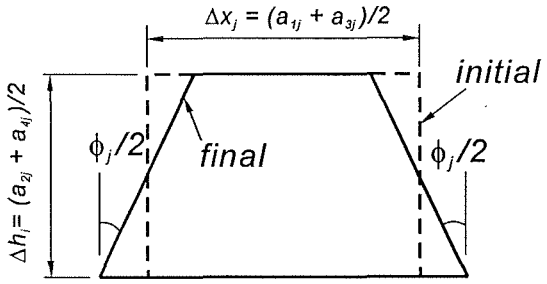

(c) Curvature

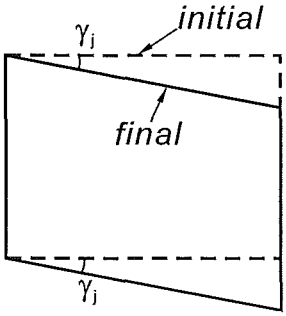

(d) Shear strain

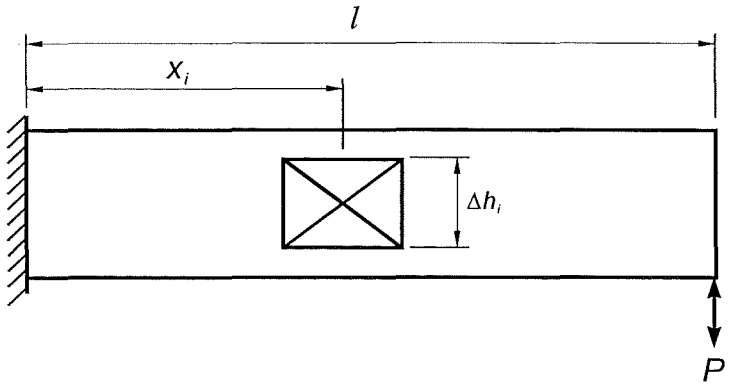

(e) Deformation calculation

Figure 5.8 Notation for Quadrilateral

$$\gamma_j = 0.25\left(\theta_{11} - \theta_{1j} - \theta_{21} + \theta_{2j} + \theta_{31} - \theta_{3j} - \theta_{41} + \theta_{4j}\right) \tag{5.3}$$

As shown in **Figure 5.8(e)**, the deformation due to flexure and shear in each quadrilateral, $\Delta_{\phi j}$ and $\Delta_{\gamma j}$, is calculated as

$$\Delta_{\phi j} = \phi_j \Delta h_j \left(l - x_i\right) \tag{5.4a}$$

$$\Delta_{\gamma j} = \gamma_j \Delta h_j \tag{5.4b}$$

The measurement of the glass ACM laminate strain on top of slab and side of beam web is carried out. It is noted that the principal strain and angle calculated from the measured strain is performed using a gauged rosette, see **Figure 5.6**. Three grids of DEMEC or clip gauge points are constructed in a fixed geometrical configuration for making these measurements. The geometry of rosette used in the test is called delta rosette that grid 1 is usually selected to be the reference axis and the remaining two grids, 2 and 3, are oriented at 60 degree and 120 degree angles. The transformation relationships can be solved to yield the principal strains and their directions based on the three measured strains as shown below:

$$\varepsilon_{\max} = \frac{\left(\varepsilon_1 + \varepsilon_2 + \varepsilon_3\right)}{3} + \frac{\sqrt{2}}{3}\sqrt{\left(\varepsilon_1 - \varepsilon_2\right)^2 + \left(\varepsilon_2 - \varepsilon_3\right)^2 + \left(\varepsilon_1 - \varepsilon_3\right)^2} \tag{5.5a}$$

$$\varepsilon_{\min} = \frac{\left(\varepsilon_1 + \varepsilon_2 + \varepsilon_3\right)}{3} - \frac{\sqrt{2}}{3}\sqrt{\left(\varepsilon_1 - \varepsilon_2\right)^2 + \left(\varepsilon_2 - \varepsilon_3\right)^2 + \left(\varepsilon_1 - \varepsilon_3\right)^2} \tag{5.5b}$$

$$\beta = \frac{1}{2}\tan^{-1}\left[\frac{\sqrt{3}\left(\varepsilon_2 - \varepsilon_3\right)}{\left(\varepsilon_1 - \varepsilon_2\right) + \left(\varepsilon_1 - \varepsilon_3\right)}\right] \tag{5.5c}$$

where, β is the angle from grid 1 to the nearer principal axis.

5.7 Test Arrangement

Figure 5.9(a) shows the test set-up. Since the interface bond between the glass ACM laminate and the concrete surface was considered critical, care was taken to

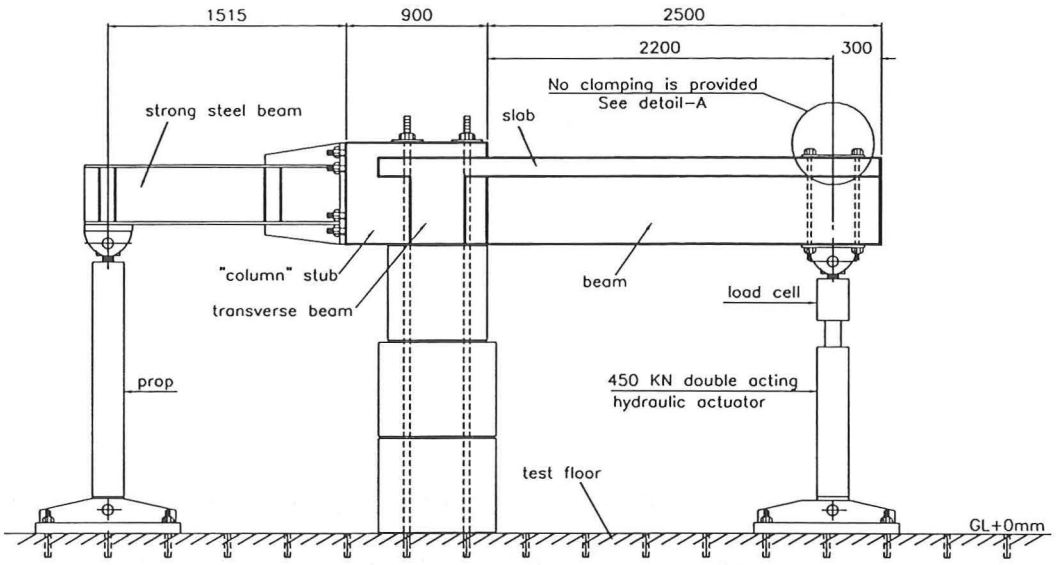

(a) Loading Rig

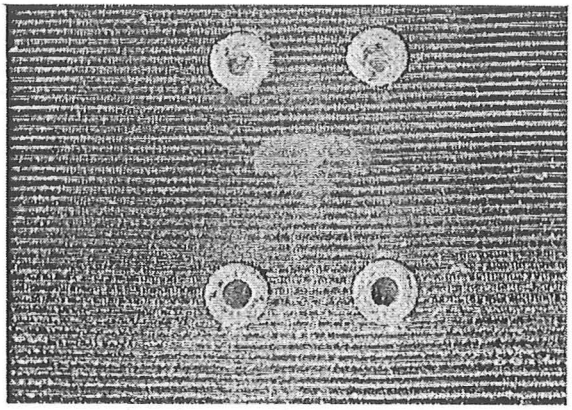

Before steel cap installation

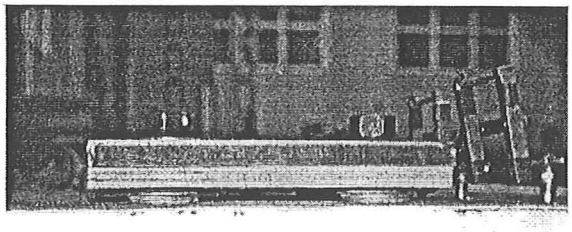

Washers and ply wood insert between steel cap and glass ACM laminate

(b) Detail-A

Figure 5.9 Test Set-up

ensure that the steel plate at the point of application of downward loading would transfer the load directly onto the beam without clamping the glass ACM laminate, see **Figure 5.9(b)**.

The position of the hydraulic actuator at the beam end emulated reasonably well the boundary conditions in the bay of the frame in a 7th storey of the building as **Figure 5.10** illustrates.

Figure 5.11(a) plots the test regime. Load controlled cycles were initially imposed to the units to find the secant stiffness and vertical displacement at 75% of the estimated capacity of the unit, see **Figure 5.11(b)**. Displacement controlled cycles were applied to the units when loaded beyond the elastic range. The cycles were controlled in terms of the displacement ductility, μ_{Δ}, which is defined as the ratio between the applied vertical displacement, Δ, and the vertical displacement at first yield, Δ_y. The vertical displacement at first yield is defined here as 4/3 times the vertical displacement observed in the load controlled cycles to 75% of the capacity of the unit, P_n [P4]. Vertical displacements were measured at the point of application of loading with any component of vertical displacement due to the rigid body rotation of the column stub being removed.

For experiments on reinforced concrete structures, especially in seismic tests, it is also important to estimate the initial stiffness of the test member. The measured initial stiffness of the test specimen K_{em} is then given by

$$K_{em} = \frac{P_n}{\Delta_y} \tag{5.6}$$

The drift is also used as an index for the level of displacement imposed on the test specimens, which ratio can be obtained by dividing the vertical free-end deflection by the structural length.

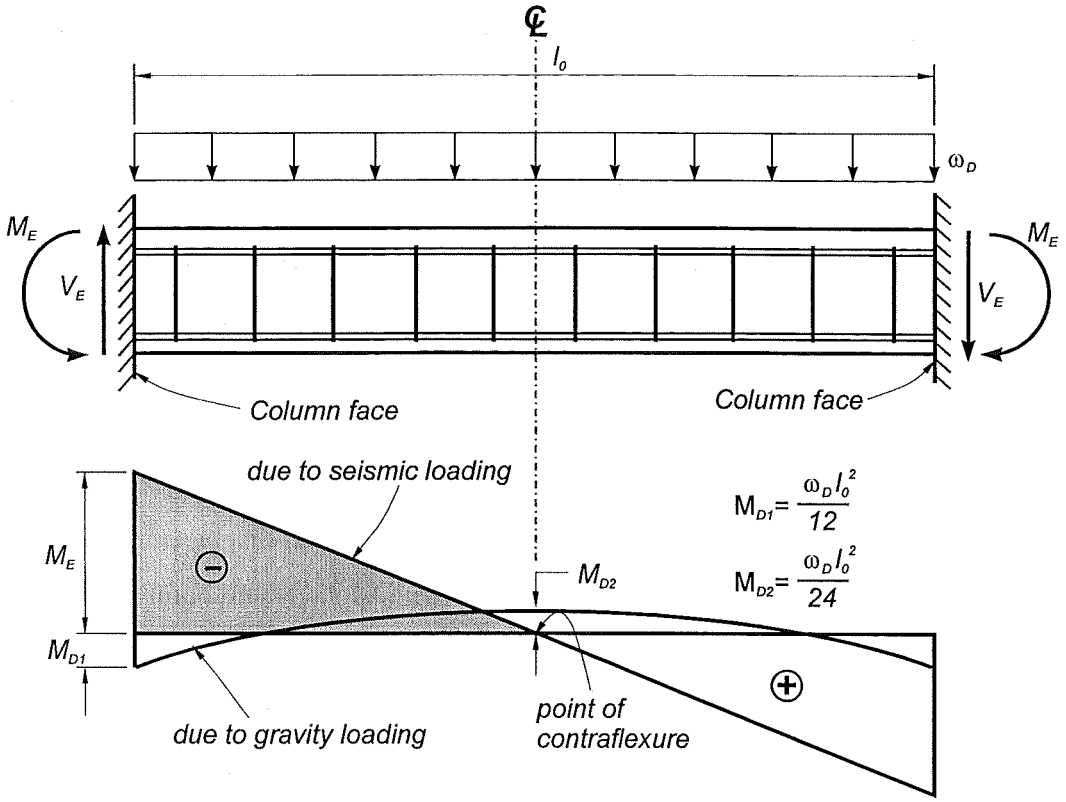

(a) Prototype Beam

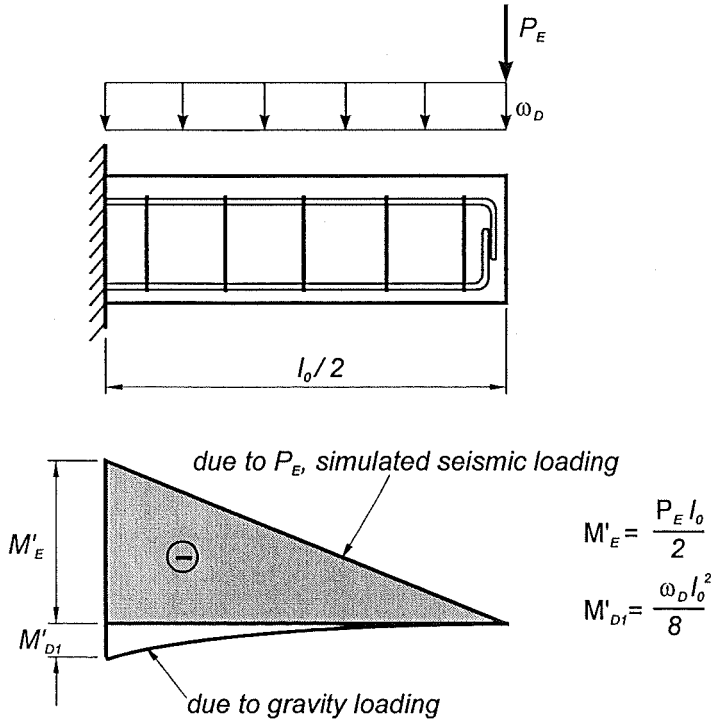

(b) Subassembly

Figure 5.10 Comparison between Actual Frame and Test Units

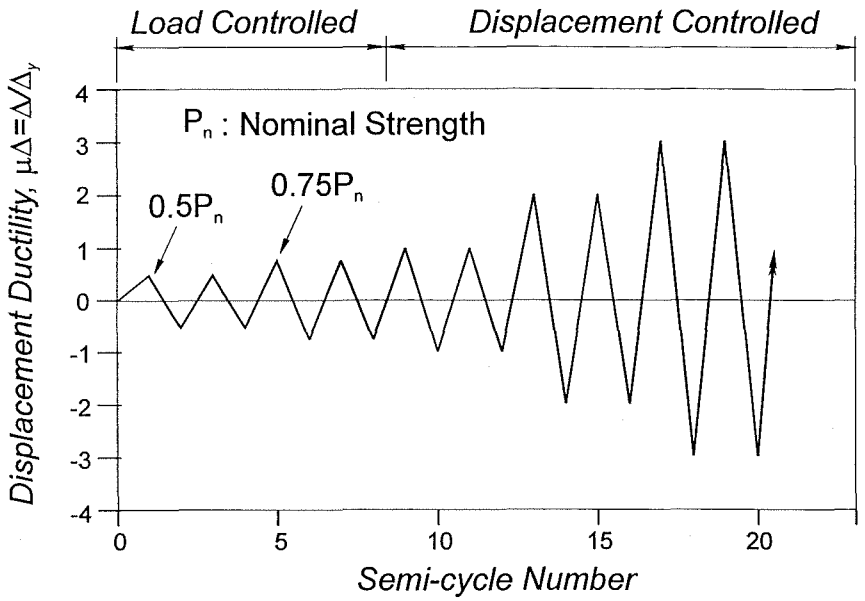

(a) Test Regime

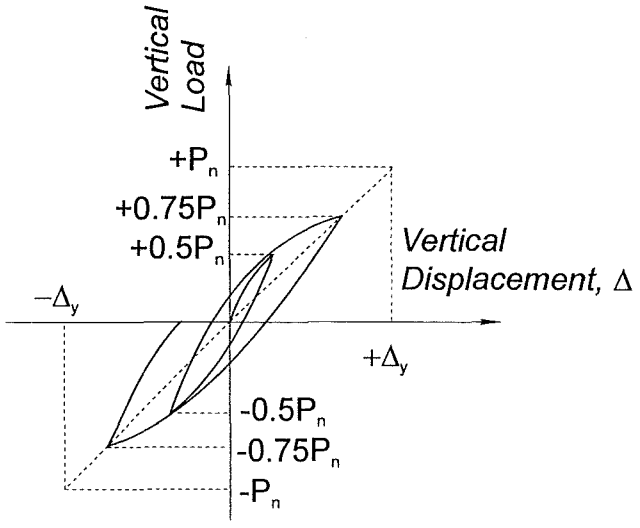

(b) Definition of first yield displacement

Figure 5.11 Test Sequence

5.8 Seismic Assessment of Existing Reinforced Concrete Beams and Structural Upgrading

This section deals with the assessment of the capacity of reinforced concrete beams which may have poor development of the longitudinal reinforcement. The method developed in Chapter 3 could be used to carry out such assessment as it can provide the full response of the member. However, in practice the full response is not needed. A simple method using variable angle trusses can be employed very efficiently. The method consists in computing the nominal flexural strength envelope of the member. The applied bending moment cannot be compared directly with the flexural strength envelope as a result of the diagonal tension cracking or truss effect. However, if the bending moment is shifted, both capacity and demand can be compared. This method will be illustrated in the following section.

5.8.1 Nominal Flexural Strength Envelope

The first step in the assessment is to complete the nominal strength envelope of the member. This envelope can be plotted by finding the nominal flexural strengths of different sections along the member.

In the process of calculating the flexural strength at a given section, allowances should be made to consider the effects caused by the development length of a bar from the cut-off point and to the presence of a shear lag in the slab. A simple way to account for these two effects is to compute the effective area of tension reinforcement in the section. **Figure 5.12** shows this criteria. **Figure 5.12(a)** illustrates that for a bar inside a beam, a fraction of the reinforcement area should be considered for a distance equal to the development length from the cut-off point. **Figure 5.12(b)** shows the case of a slab bar. In addition to the reduction in effectiveness caused by the development length from the cut-off point, the effectiveness of the bar is reduced due to the shear lag. The shear lag effect, considered here equal to a distance z, is computed assuming a 45 degree angle.

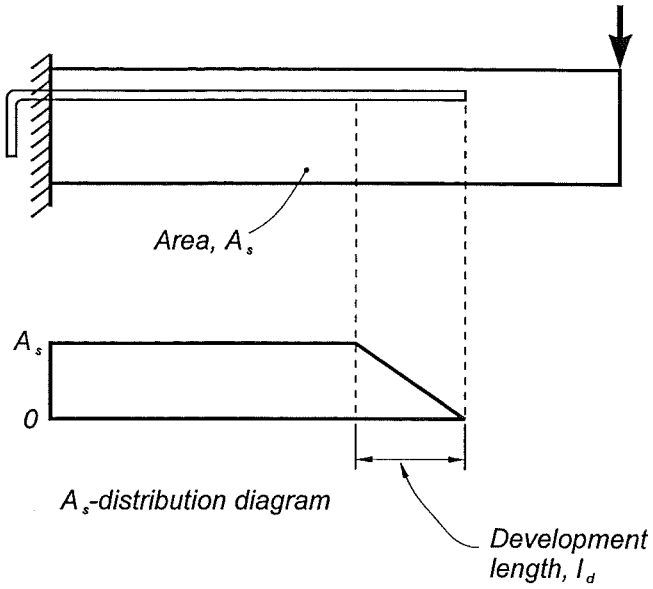

(a) Beam Bars

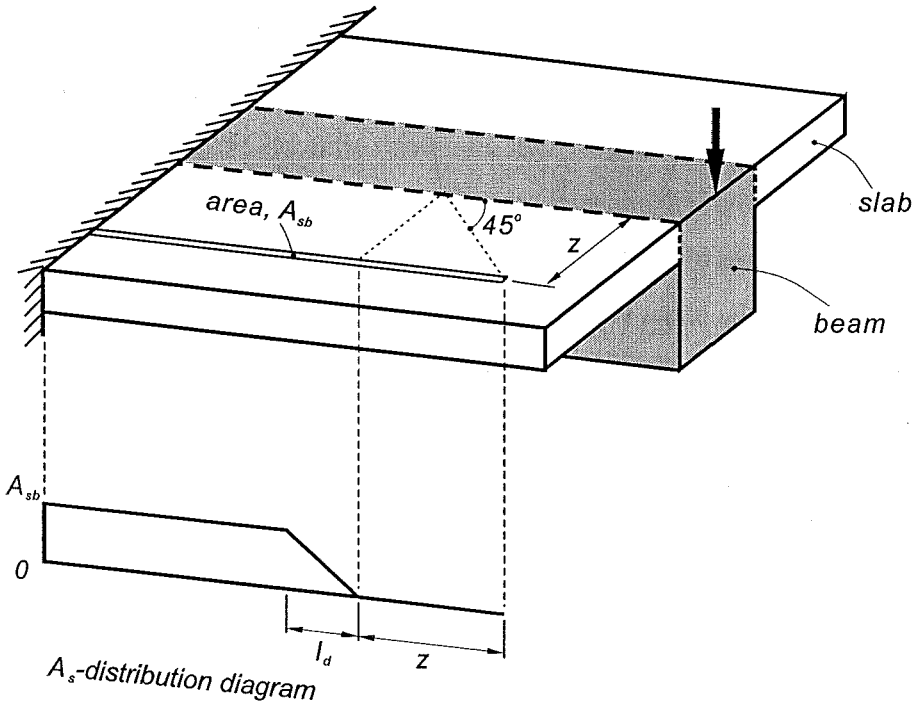

(b) Slab Bars

Figure 5.12 Calculation of Reinforcing Steel Area in Tension

5.8.2 Shear Strength Analysis

5.8.2.1 Shear Strength of Beams

The shear strength of beams with rectangular stirrups and externally bonded glass ACM side strips can be obtained revising from Eq. 4.1, as given in Eq. 5.7.

$$\begin{aligned} V_n &= V_c + V_s + V_p \\ &= k\sqrt{f'_c}\, b_w d + \frac{A_{vs} f_{vsy}}{s} d + \frac{A_{vp} f_{vpe}}{s_{vp}} h_{vp} \end{aligned} \tag{5.7}$$

where V_c is the nominal shear strength carried by the concrete mechanism and k is taken varies according to the curvature ductility imposed in the section. It is noted that the strength taken by concrete part shown in Eq.5.7 is different from that given by Eq.4.1. This is because in the non-seismic provisions of NZS 3101:1995 [N4], k is given as (0.07+10 ρ_w) for beams as seen in Eq. 4.1. NZS 3101:1995 requires that k determined be not more than 0.2, nor less than 0.08. On the basis of test results, both Hakuto et al. [H1] and Priestley [P7] suggest that k = 0.2 could be assumed for beams without plastic hinging. V_p is the shear strength sustained by the U-shape glass ACM strips externally bonded to sides of the beam. The area of glass ACM shear reinforcement A_{vp} is the total thickness of the sheet (usually $2t_{vp}$, the thickness of the glass ACM sheets on both sides of the beam) times the width of the shear glass ACM strip w_{vp}. If continuous sheets are used, the width of the strip, w_{vp}, and the spacing of the strips, s_{vp}, should be equal. The above equation assumes that the critical diagonal tension crack is inclined at 45 degrees to the longitudinal axis of the beam.

5.8.2.2 Degradation of Shear Strength of Beams

The degradation of the shear strength in plastic hinge regions is due to the reduction of the concrete nominal shear stress resisted by the concrete mechanism, mainly due to the loss of aggregate interlock. The nominal shear stress v_c reduces with increase in curvature ductility. **Figure 5.13** shows the degradation of the nominal shear stress proposed by Priestley [P7] and Hakuto et al. [H1]. In this figure, factor k varies

from 0.2 to a residual factor of 0.05.

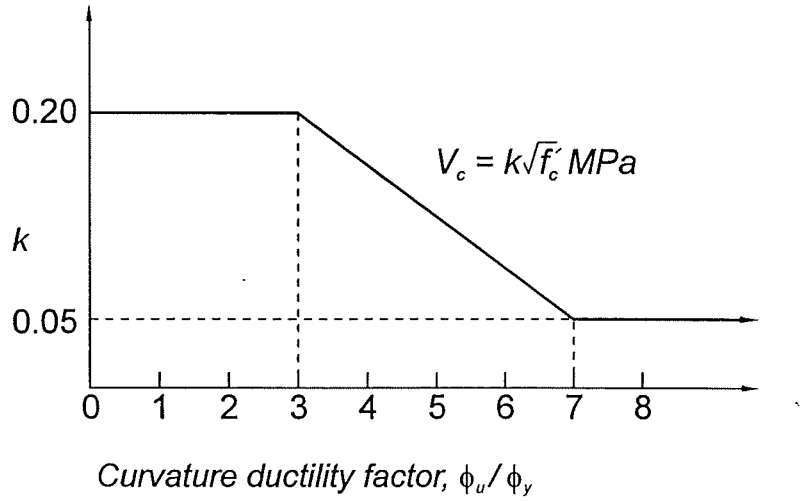

Figure 5.13 Degradation of Nominal Shear Stress Resisted by the Concrete [P7]

5.8.2.3 Tension Shift

It has long been recognised that in cracked reinforced concrete beams, the tension force in the longitudinal reinforcement can not be directly estimated from the M/jd diagram [P1, R2]. This is due to the interaction between flexure and shear after diagonal cracking. **Figure 5.14** illustrates the concept for deriving the additional tension force T_v in beam longitudinal reinforcement and the "tension" shift e_v [P1] caused by diagonal tension cracking for a beam idealised as a truss with parallel chords in which the diagonal compression field is inclined at an angle θ. The derivation of the following equations is given by Restrepo et al. [R2].

$$T_v = \frac{V}{2\tan\theta} \tag{5.8a}$$

$$e_v = \frac{jd}{2\tan\theta} \tag{5.8b}$$

It is proposed that the angle of inclination of the diagonal compression field at the ultimate limit state is

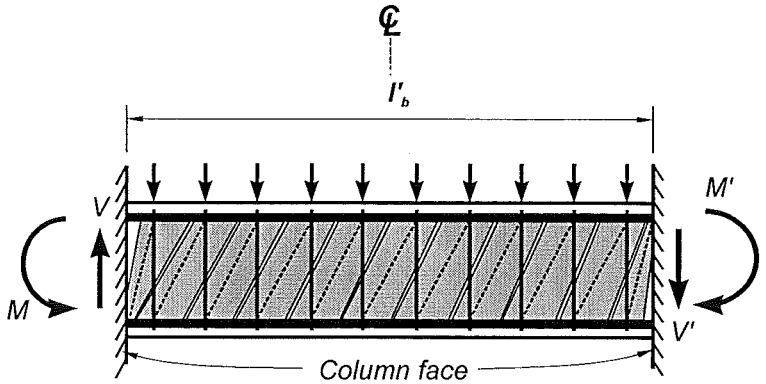

(a) Beam of a frame and assumed truss model

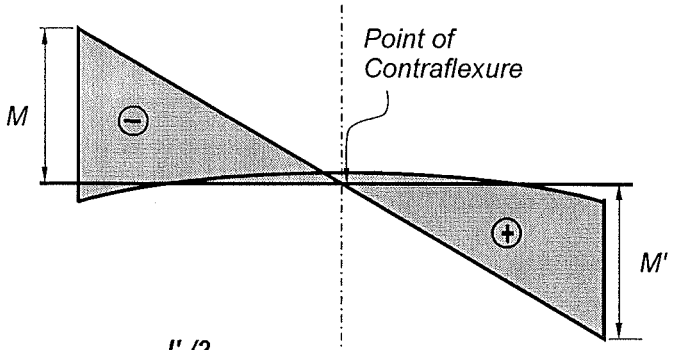

(b) Bending moment diagram

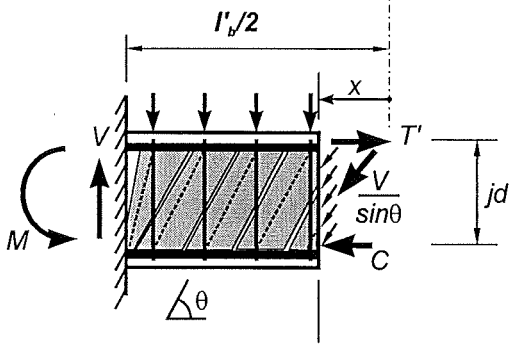

(c) Free body diagram

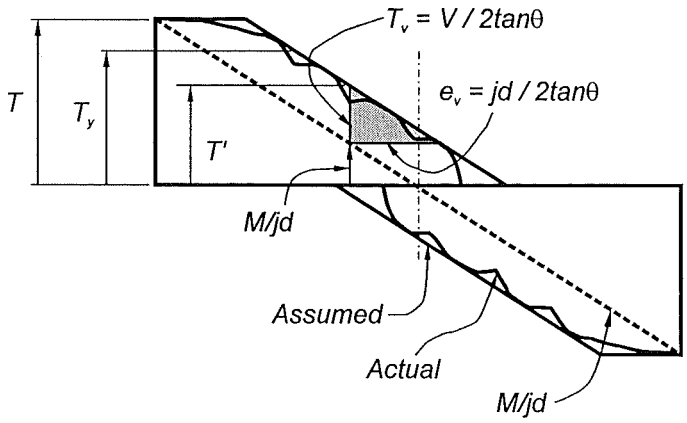

(d) Tensile force diagram

Figure 5.14 Tension Shift Concept [R2]

$$\tan\theta = \frac{jdA_{vs}f_{vsy}}{s(V - V_c)} \tag{5.9}$$

where V_c can be obtained using $0.05\sqrt{f'_c}b_w d$.

5.8.3 Assessment Results

5.8.3.1 Prototype Reinforced Concrete Beam

Figure 5.15 shows the assessment results in the prototype beam Unit T1 in both loading directions. The bending moment M due to the applied point P is depicted by the dashed line whereas the shifted moment M_v considering the tension shift effect is represented by the thicker solid line in the same diagram. The solid line M_v is to present an actual moment distribution when the diagonal cracks have been commenced in the beam. The nominal strength envelope is also plotted. The comparison of the nominal strength envelope with the shifted moment will determine the location where a hinge will occur and the capacity of the beam.

It can be seen in **Figure 5.15** that the plastic hinges in the positive loading direction will develop at the column face when the load reaches 179 kN as desired. Nevertheless, in the negative loading direction, a hinge will develop at 1310 mm from the column face and not at the face itself when the load reaches 190 kN. As a result, the diagonal crack will occur and the location in the vicinity of the bar curtailment could lead to the flexure-shear failure, as this region is not detailed for ductility to allow the development of a plastic hinge.

Figure 5.16 shows a different trend for the response of the beam under negative bending moment if the slab reinforcement is not taken into account. It shows the plastic hinges in the negative loading direction may start from the column face and spread over the beam to the bar cut-off point. The behaviour of the beam without considering the slab bar contribution in the negative loading direction is completely different from the actual response mentioned above.

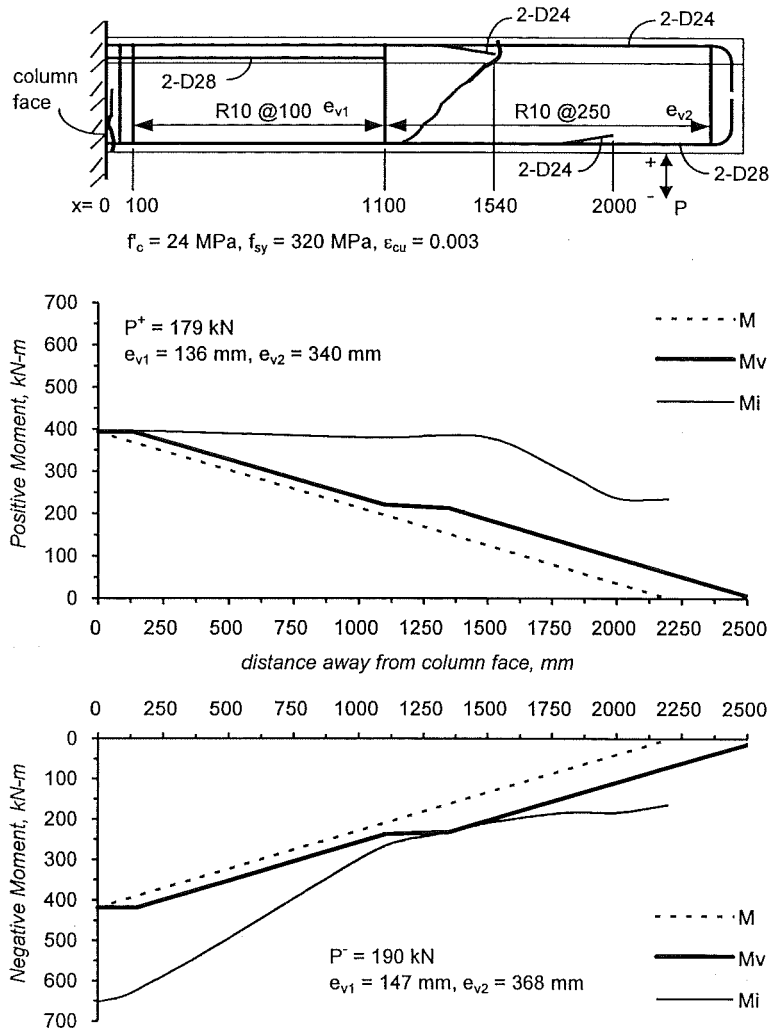

(a) Bending Moment Diagrams

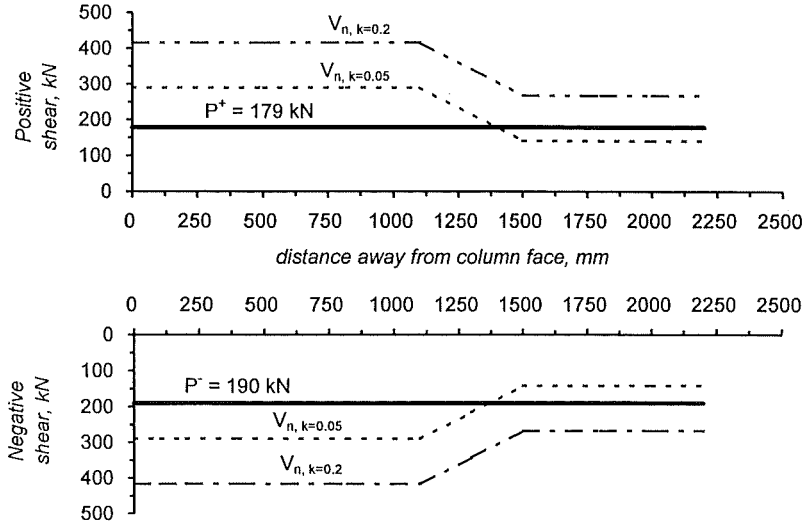

(b) Shear Force Diagrams

Figure 5.15 Seismic Assessment Results in Prototype Beam, Considering Slab Contribution

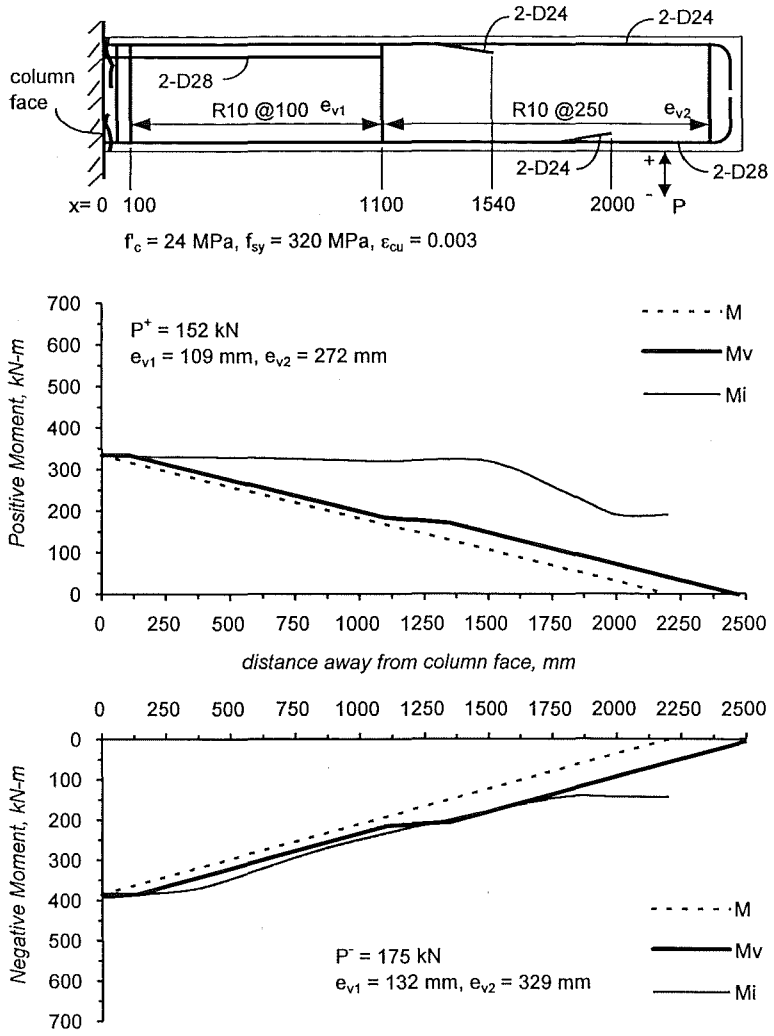

(a) Bending Moment Diagrams

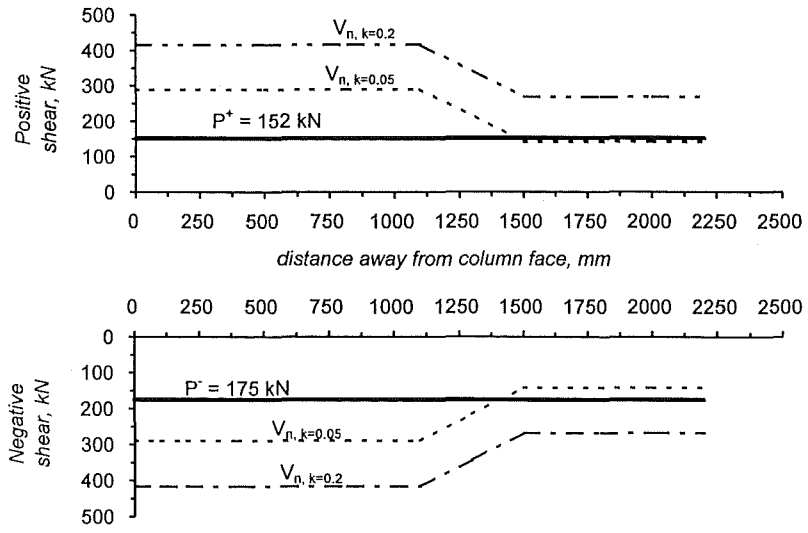

(b) Shear Force Diagrams

Figure 5.16 Seismic Assessment Results in Prototype Beam without Slab Contribution

Hence, an aspect ignored in the ACI 318-71 building code is the participation of the slab longitudinal reinforcement toward the negative flexural strength of flanged beams of moment resisting frames designed to provide the earthquake resistance. It can be speculated that this practice was considered conservatively as it was believed that the slab contribution increased the negative flexural strength of the beam and increased the lateral load resistance of the building and, as a result, decreased the ductility demand in the critical regions. The main problem when ignoring the participation of the slab reinforcement is that the curtailment of the beam reinforcement and the transverse reinforcement provided for shear resistance may be inadequate, as proven above.

Nowadays, modern codes require that the contribution of the reinforcement in cast-in-place concrete solid slabs be assessed and be accounted for in design [P4, N4]. It can be shown that, especially in the upper floors of buildings where the slab contribution is more significant in relative terms, the critical region for the development of a negative plastic hinge may not occur at the beam ends but at a distance away towards mid span of the beam. A represented diagram can be seen in **Figure 5.17**. The relocation of the critical region implies that plasticity will develop where no special detailing for ductility has been provided. Such beams may fail in a rather brittle manner and at a load less than that required to attain the flexural strength when accounting for the longitudinal reinforcement of the beam alone.

5.8.3.2 Repaired/Retrofitted Reinforced Concrete Beam

It has been realised from the previous assessment on the prototype beam that if the beam behaviour is to be enhanced, the performance of the flexural and shear strengths under negative loading direction around the bar curtailment region needs to be increased to prevent a brittle failure at this location. The retrofit concept is to make this weak region strong enough to ensure the formation of a negative plastic hinge in the beam at the column face where closely space hoops had been provided to ensure ductile response.

The repair/retrofit work was done by providing additional passive negative flexural resistance to the beam throughout its length, except at the column face. The

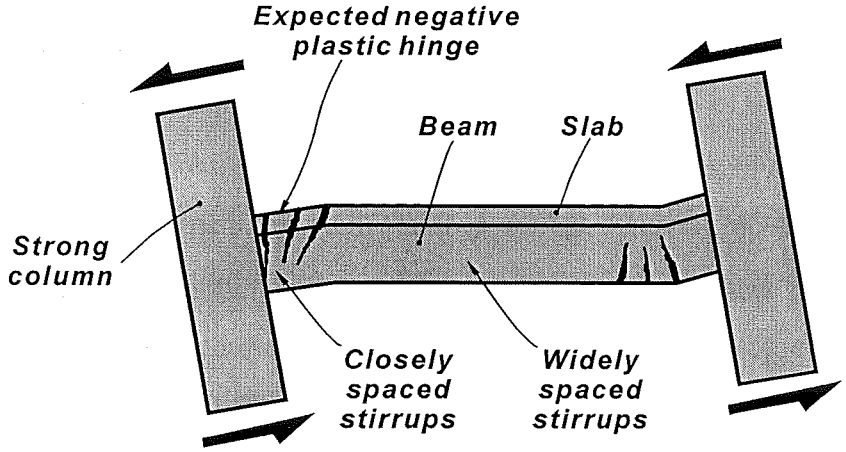

(a) Assumed behaviour

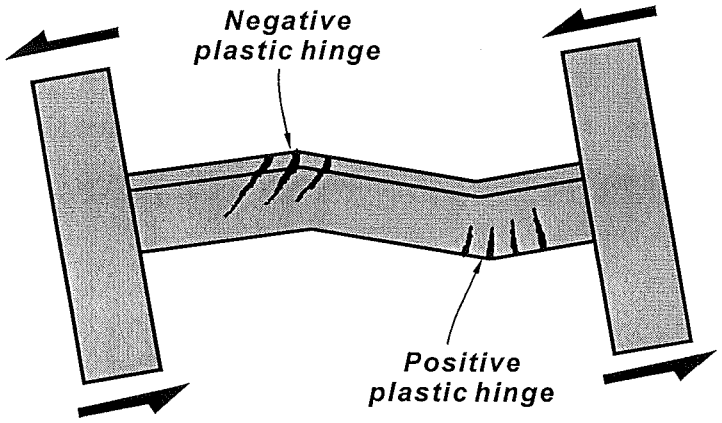

(b) Actual behaviour

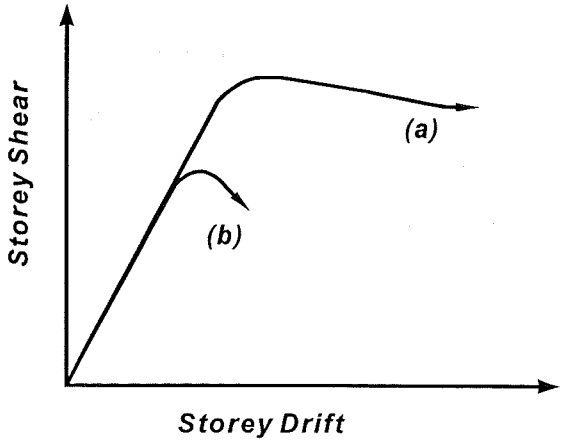

(c) Response

Figure 5.17 Influence of the Slab on the Seismic Performance of Frames Designed to Older Codes

strength deficit was found by modelling the beam as variable angle truss as shown in the solid line of **Figure 5.18(a)**. Consideration was given during the design of the repair/retrofit scheme to limiting the longitudinal tensile strain in the fibreglass/epoxy laminate bonded to the slab to ε_p = 0.4 %, and also to limiting the average bond stress between the glass ACM laminate and the concrete to be less than $0.17\sqrt{f'_c}$ [MPa]. The tensile strain limit was chosen to avoid premature deterioration of the shear strength mechanism in the beam where the longitudinal reinforcement had been cut-off. The average bond stress limit was selected to avoid premature delamination of the laminate.

The U-shape fibreglass laminates were designed to control the width of the diagonal cracks and, hence, to delay the loss of the shear transfer mechanism through aggregate interlock. The shear capacity was expected to be enhanced by the U-shape glass ACM bonded to the critical region of the beam as illustrated in **Figure 5.18(b)**. Thus the shear-flexure failure will be prevented when the maximum load is reached, and the plastic hinge will form at the column face.

5.9 Test Results

The test beams, Prototype Unit T1, Repaired Unit T1, and Retrofitted Unit T2 were tested under the reversed cyclic quasi-static loading regime shown in **Figure 5.11**. This loading regime has commonly been used to simulate the effects of earthquake loading. During the test, different types of data collected consisted of applied load vs free-end displacement, strains in the beam and slab longitudinal reinforcement, strains in the stirrups, beam deformation due to curvature and shear distortion determined from the quadrilaterals built up by the linear potentiometers, strain distribution on the top of fibreglass/epoxy strips, and principal strains calculated from the rosettes located on the sides of the U-shaped fibreglass. The crack pattern was also recorded throughout the tests.

It is noted that the results with a negative symbol described in the following, represent the values obtained when subjected to negative moment and a positive symbol means the results obtained due to positive moment.

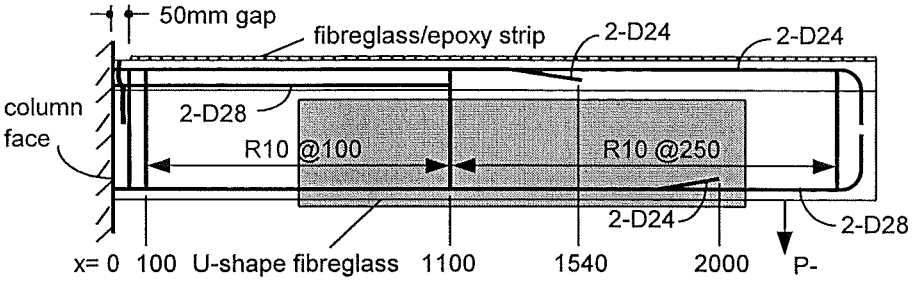

f'_c = 24 MPa, f_{sy} = 320 MPa, ε_{cu} = 0.003, ε_{ju} = 0.004

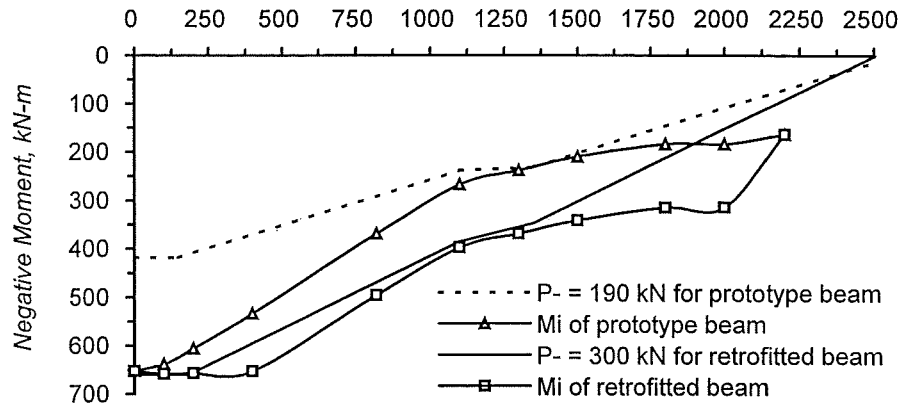

(a) Bending Moment Diagrams

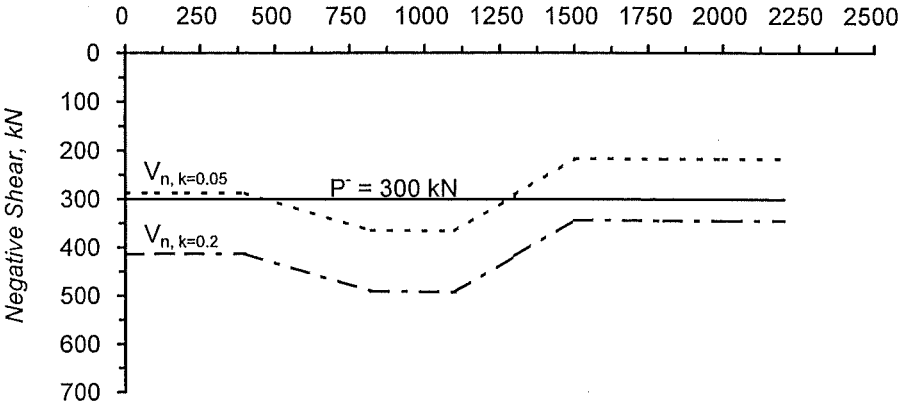

(b) Shear Force Diagrams

Figure 5.18 Assessment of the Capacity of the Repaired/Retrofitted Units Loaded under Negative Bending Moment

5.9.1 General Behaviour

Prototype Unit T1

Figure 5.19 shows the hysteric response of all test units. The predicted capacity P_n calculated based on the section at the column face was also plotted. In order to compare the predicted values with the test results, the small influence of gravity loading on the predicted capacity was removed.

Prototype Unit T1 behaved as expected when loaded upwards. A positive plastic hinge formed in the beam at the column face and extensive yielding of the beam bottom longitudinal reinforcement, described later, was observed in this region. The measured and predicted capacity agreed very well, as anticipated.

Under downward loading, cracking in the beam extended from the column face to near the point of application of loading. When the beam was pushed into the inelastic range, a large diagonal crack inclined at 42 degrees to the horizontal opened up at 1.3 m from the column face. The extent of cracking at the end of the test is shown in **Figure 5.20(a)**. It is apparent in **Figure 5.19(a)** that the negative flexural strength, calculated at the face of the column and considering the slab reinforcement, was not attained. At -1% drift angle the main diagonal crack was 4.8 mm wide and the capacity of the beam had begun to drop due to an imminent flexure-shear failure. The failure scenario can be seen in **Figure 5.21**.

This drift angle and the associated damage were considered to be the limit at which a satisfactory repair scheme could be carried out in a structure. Consequently, the test was halted and the repair work conducted.

Repaired Unit T1 and Retrofitted Unit T2

The damaged unit T1 was then repaired as described in Section 5.4. Unit T2 was also retrofitted in the same manner as Unit T1. The hysteric response of the Repaired Unit T1 and Retrofitted Unit T2 can be compared with the response of

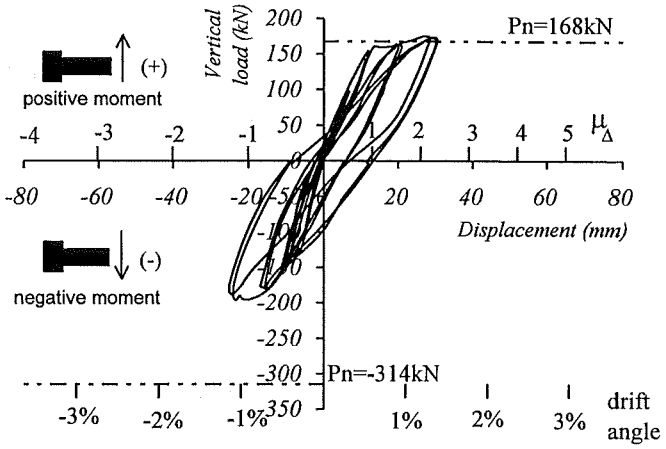

(a) Prototype Unit T1

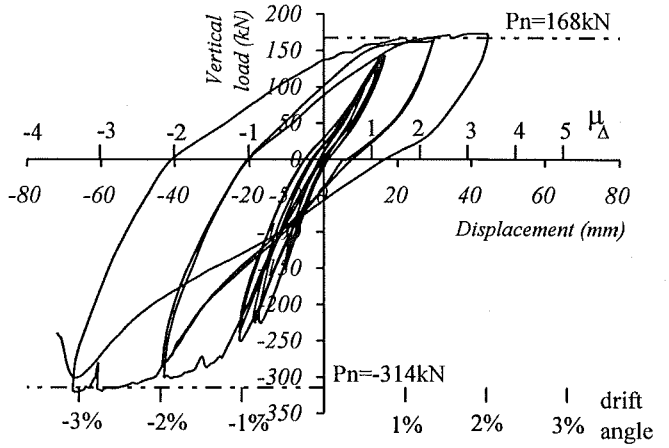

(b) Repaired Unit T1

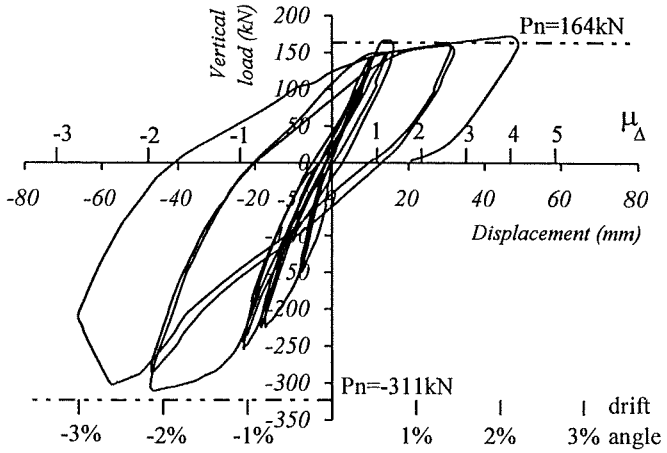

(c) Retrofitted Unit T2

Figure 5.19 Measured Hysteretic Response

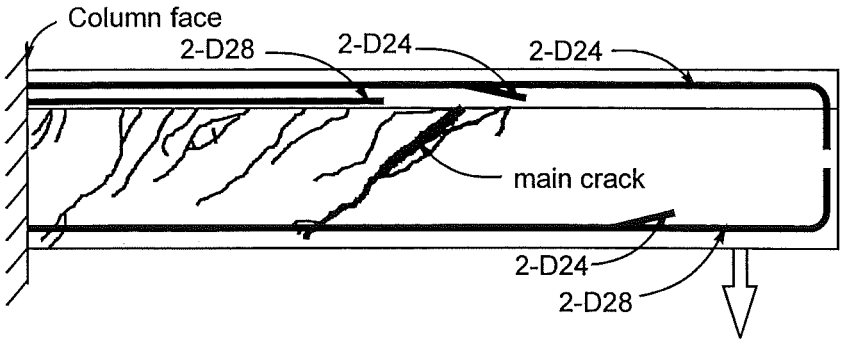

(a) Prototype Unit T1

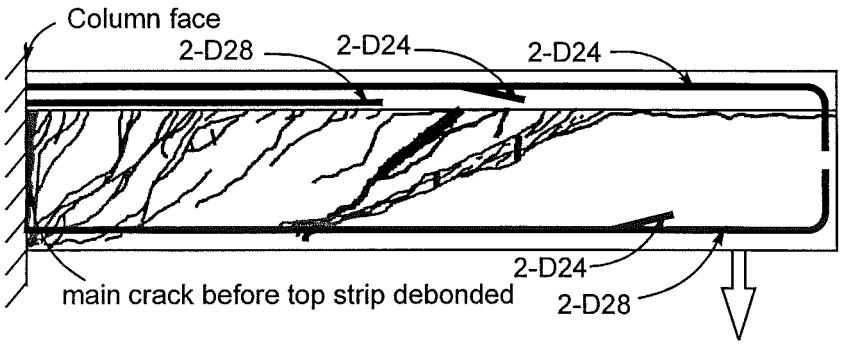

(b) Repaired Unit T1

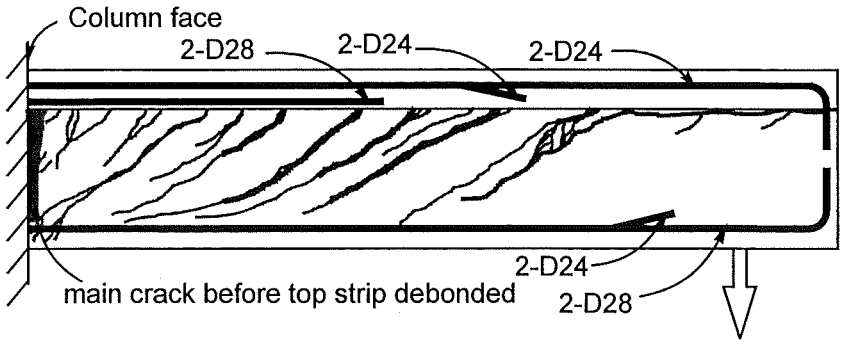

(c) Retrofitted Unit T2

Figure 5.20 Crack Pattern Developed in the Test Units When Loaded Downwards

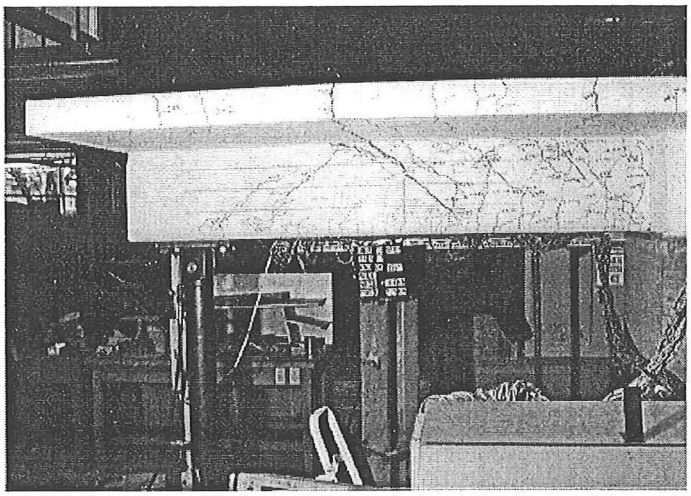

(a) View from side of beam

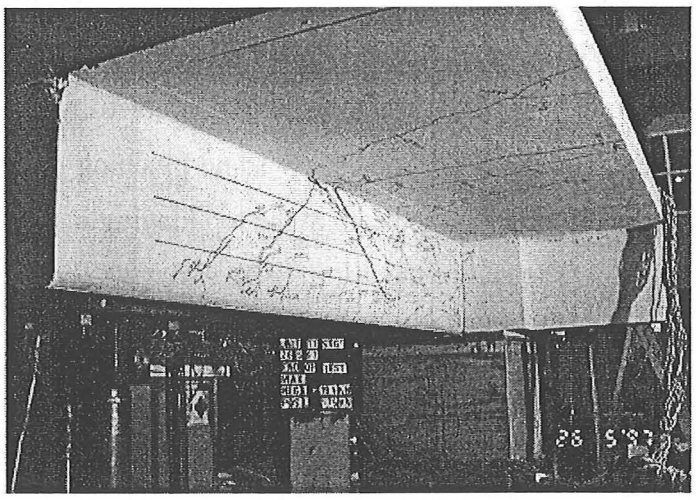

(b) View from bottom of beam

(c) View from top of slab

Figure 5.21 View of Unit T1 at the End of Test

Prototype Unit T1 in **Figure 5.19**. It is evident that the laminate bonded to the slab was very effective in forcing a negative plastic hinge to develop in the beam at the column face. The significant strength increase under negative loading is due to the contribution of the slab reinforcement.

Cracking due to negative loading in these two tests was more distributed than in the first test, see **Figure 5.20**. The major cracks occurred in the beams at the column face. In these two tests delamination of the three-sided fibreglass/epoxy strips commenced from the top in the region where the beam top longitudinal reinforcement had been cut-off and slowly propagated downwards and sideways. The delamination pattern in side strips of Repaired Unit T1 was displayed in **Figure 5.22**. This suggests that side strips bonded to the web of reinforced concrete beams without anchors to U-strip top edges are not a reliable way to enhance the shear strength of a beam. Both units reached two cycles to -2% drift angle at a displacement ductility μ_Δ = -2 with minimum strength degradation. The hysteric loops show some pinching due to the formation of diagonal cracks that developed in the beam at the top longitudinal bar cut-off points, see **Figure 5.20(b) and (c)**. The end of the test in these two units occurred in the cycles to a displacement ductility μ_Δ = -3 at -3% drift angle when reaching the peak displacement the top glass ACM laminates suddenly peeled off as shown in **Figure 5.23**. The delamination of the laminate was induced by the kinking effect caused by the large shear distortion in the beam bar curtailed region at 1.3 m from the column face after the side strips were rendered ineffective.

5.9.2 Initial Stiffness

In the test the theoretical initial stiffness is calculated and compared with the value obtained from the test results. The theoretically initial stiffness of test beams can be obtained using Eq.5.10.

$$K_{et} = \frac{3E_c I_e}{l_e^3} \tag{5.10}$$

where l_e is the effective length of the test beam, E_c is the elastic modulus of concrete, and I_e is the effective moment of inertia. In term of design effort, it is practical to use an

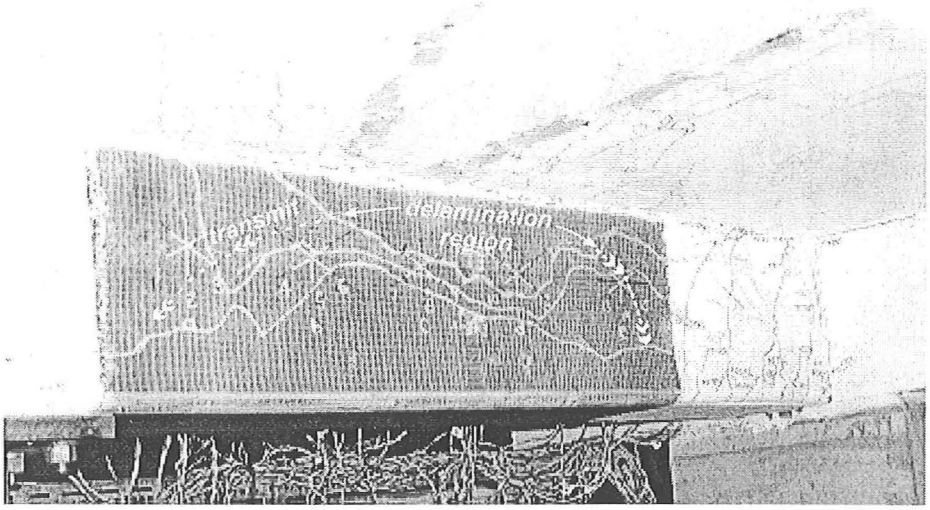

Figure 5.22 Delamination of U-shaped ACM Strip in Repaired Unit T1

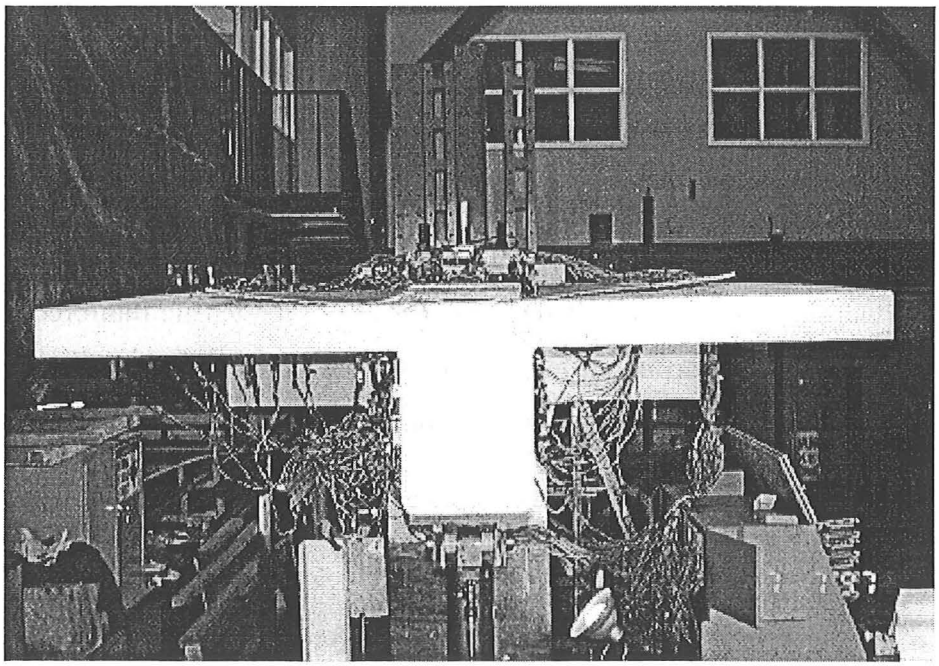

Figure 5.23 Plate Separation of Top ACM Laminate in Retrofitted Unit T2

approximate value in evaluating the effective moment of inertia. To compare with test results, two of evaluation methods were adopted in the calculation of effective moment of inertia of T-section beam. One is from Paulay and Priestley [P4] as given in Eq.5.11.

$$I_{e1} = 0.35 I_g \tag{5.11}$$

where I_g is the moment of inertia of gross concrete section, neglecting the reinforcement contribution.

The other evaluation on the effective moment inertia is considered assuming only the contribution of tensile reinforcement as presented in Eq.5.12.

$$I_{e2} = nA_s(d-c)^2 \tag{5.12}$$

where n is modulus of elasticity ratio ($=E_s/E_c$), A_s is area of tension reinforcement, d is effective depth, and c is distance from compression face of section to neutral axis when the section is loaded to first yield of tensile reinforcement.

Table 5.4 shows the results in the measured and calculated initial stiffness. It is apparent the estimation of initial stiffness considering only the contribution of tensile steel reinforcement, is closer to the measured value. The initial stiffness was calculated using the effective moment of inertia estimated from Eq. 5.11 and seems overestimated. It implies that the initial stiffness strongly correlates to the tensile reinforcement in the section. For an estimation of stiffness of reinforced concrete section, the calculated effective moment inertia using Eq. 5.12 is recommended.

5.9.3 Moment and Shear Deformation

Figure 5.24 displays the history of flexural rotation and shear deformation at different measured quadrilaterals. **Figure 5.25** shows the deformation components due to flexure and shear in the beams. The distance depicted in the figures is taken from the column face. It is exhibited in Prototype Unit T1 that the obvious variation in flexural rotation appeared when the loop reached the first cycle to μ_Δ=-0.8, in the range located

Table 5.4 Calculated and Measured Initial Stiffness of Test Units

Uint	Loading Direction	n	A_s[1] (mm^2)	d[2] (mm)	c[2] (mm)	I_g (mm^4)	I_{e1}[3] (mm^4)	I_{e2}[3] (mm^4)	K_{et1}[4] (kN/mm)	K_{et2}[4] (kN/mm)	P_n (kN)	Δ_y (mm)	K_{em} (kN/mm)
Prototype Unit T1	Positive	8.63	1232	500	96	$9.977x10^9$	$3.492x10^9$	$1.735x10^9$	22.8	11.3	168	13.0	12.9
	Negative	8.63	4650	489	247	$9.977x10^9$	$3.492x10^9$	$2.350x10^9$	22.8	15.3	314	20.1	15.6
Retrofitted Unit T2	Positive	9.97	1232	500	101	$9.977x10^9$	$3.492x10^9$	$1.955x10^9$	19.7	11.1	164	11.7	14.0
	Negative	9.97	4650	489	258	$9.977x10^9$	$3.492x10^9$	$2.474x10^9$	19.7	14.0	311	23.9	13.0

Notes:

1. The area of steel reinforcements is considered at the column face.
2. These values are calculated assuming first yield of tensile reinforcements in the balance of the sectional forces.
3. The values are determined using Eq. 5.11 and Eq. 5.12, respectively.
4. The theoretical stiffness is obtained from the results of I_{e1} and I_{e2}.

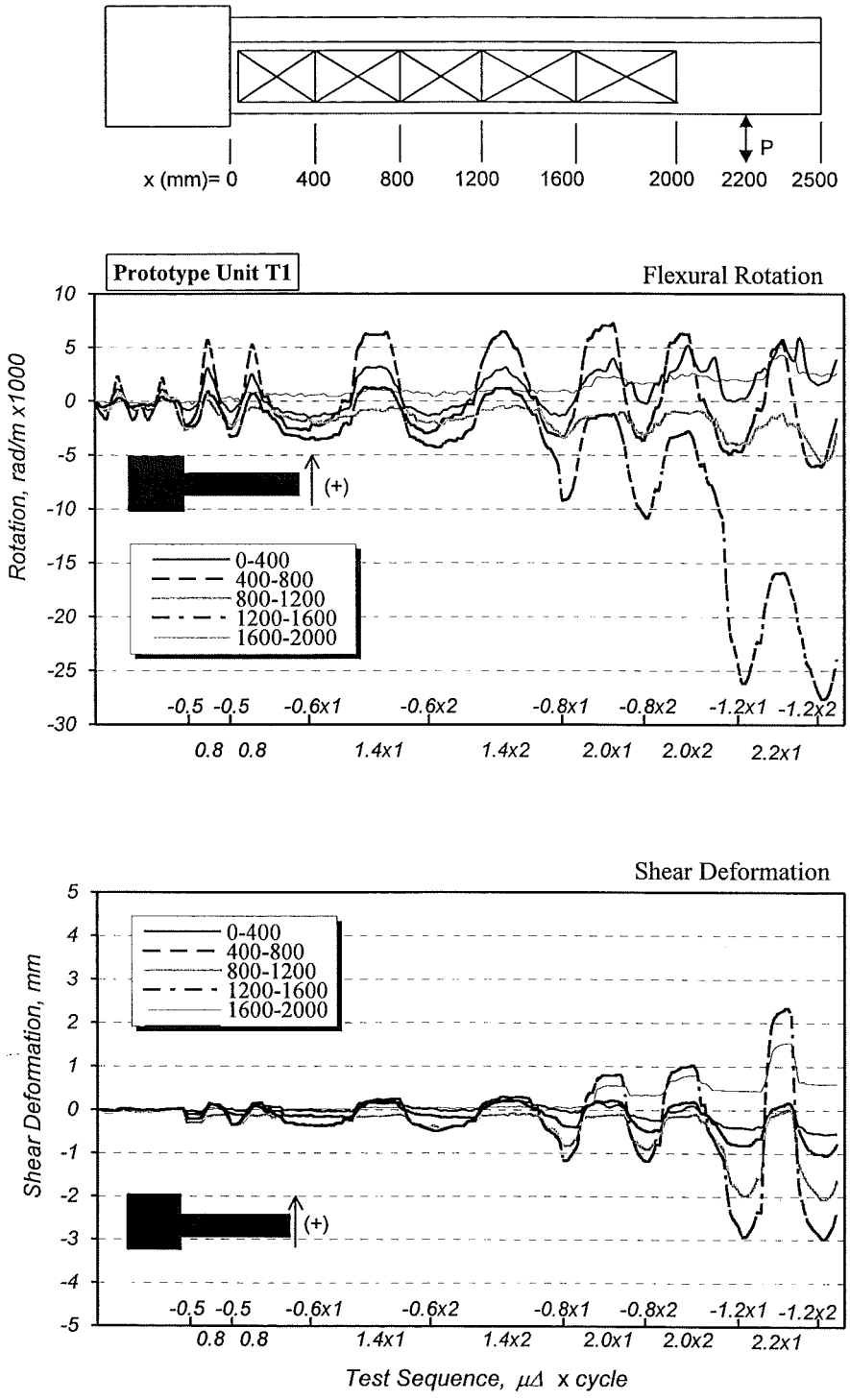

(a) Prototype Unit T1

Figure 5.24 Sequence of Flexural Rotation and Shear Deformation

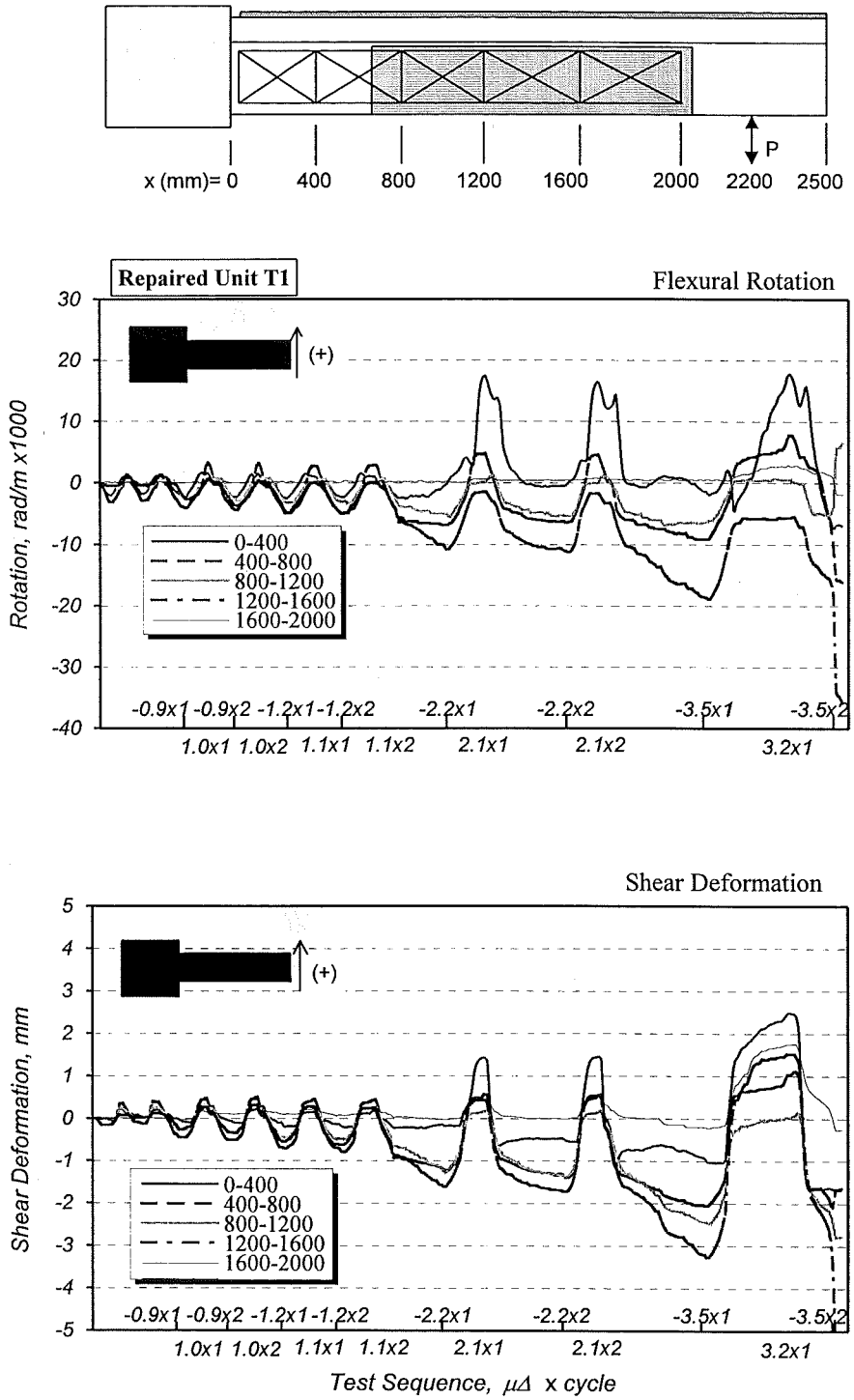

(b) Repaired Unit T1

Figure 5.24 Sequence of Flexural Rotation and Shear Deformation (Cont.)

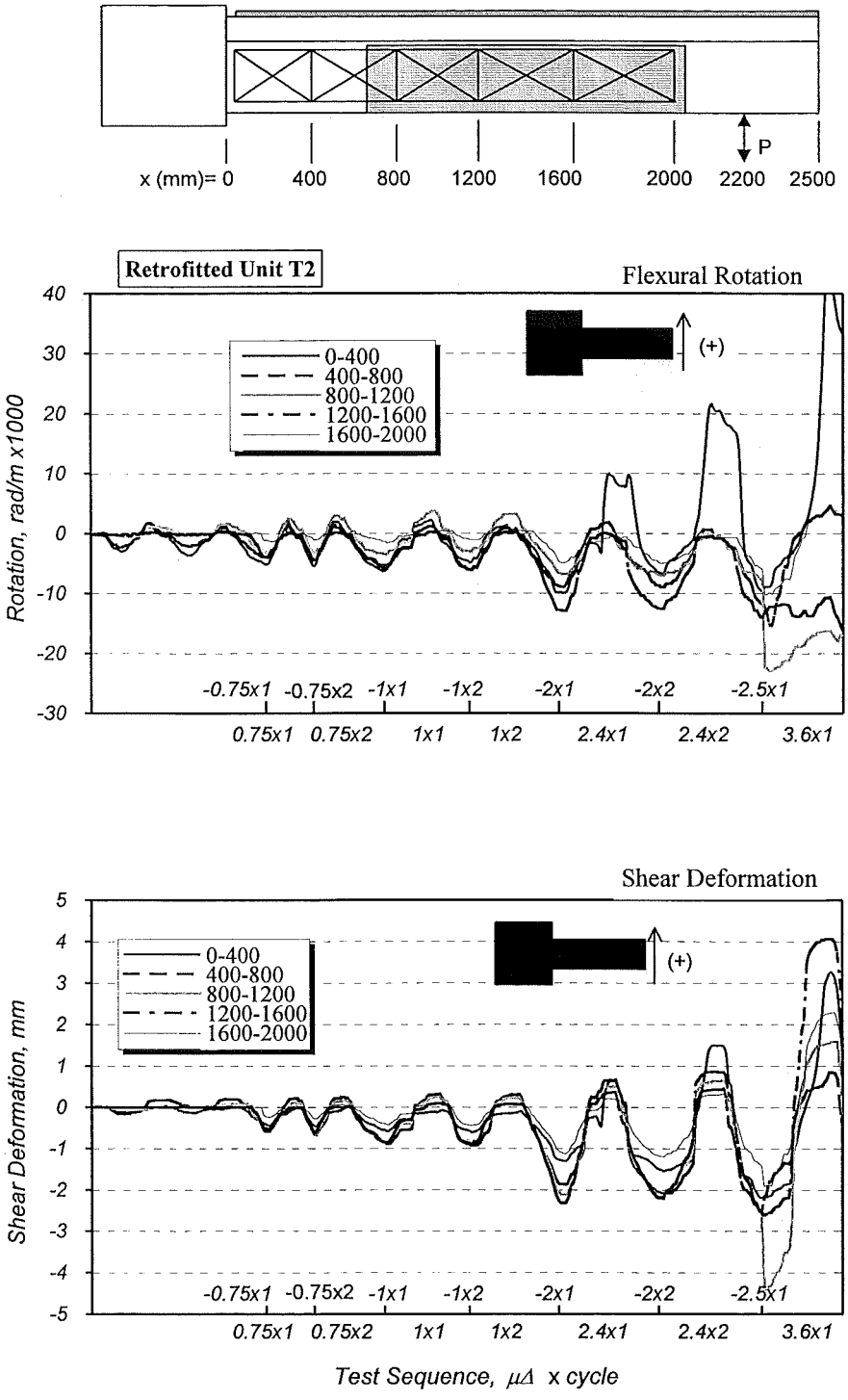

(c) Retrofitted Unit T2

Figure 5.24 Sequence of Flexural Rotation and Shear Deformation (Cont.)

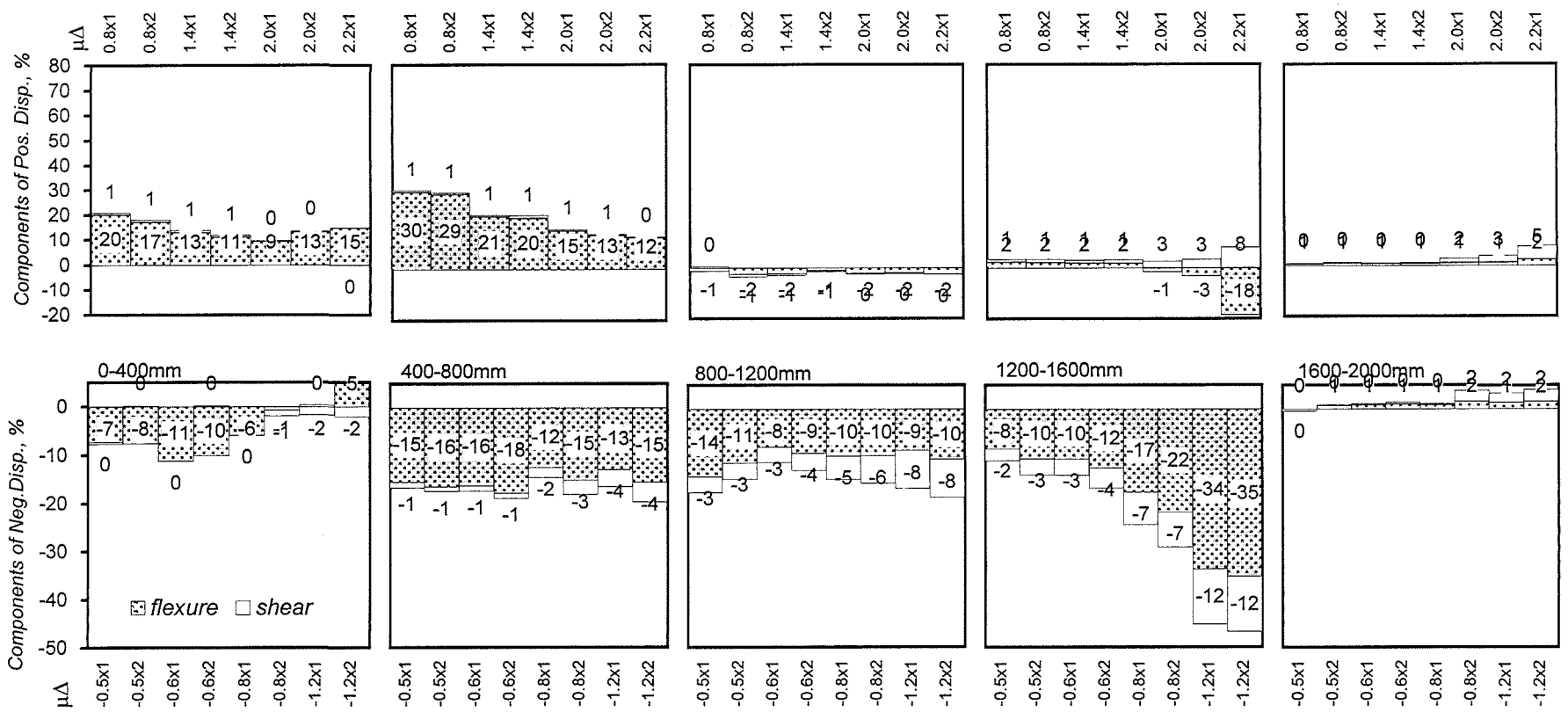

(a) Prototype Unit T1

Figure 5.25 Deformation Components due to Flexure and Shear, Expressing as a Percentage of Total Deformation

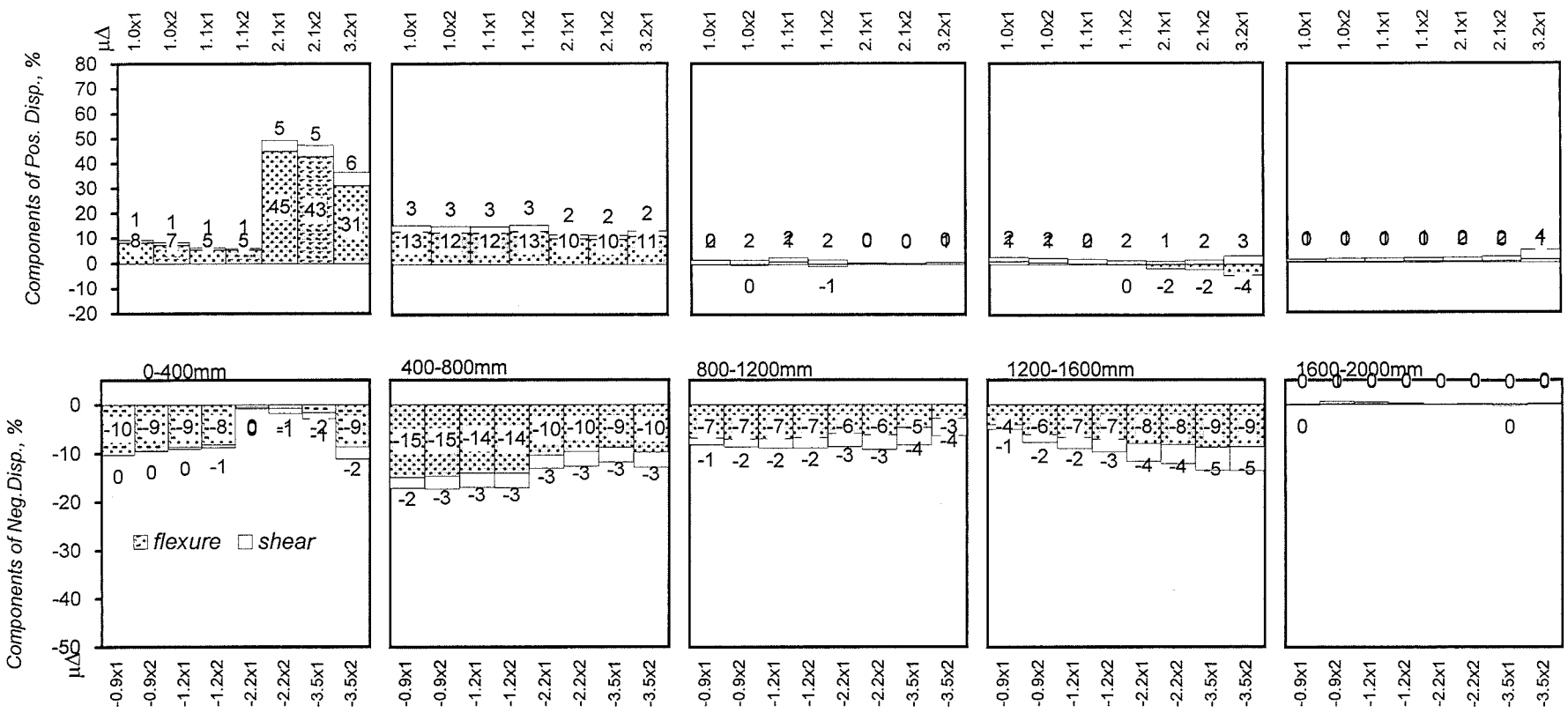

(b) Repaired Unit T1

Figure 5.25 Deformation Components due to Flexure and Shear, Expressing as a Percentage of Total Deformation (Cont.)

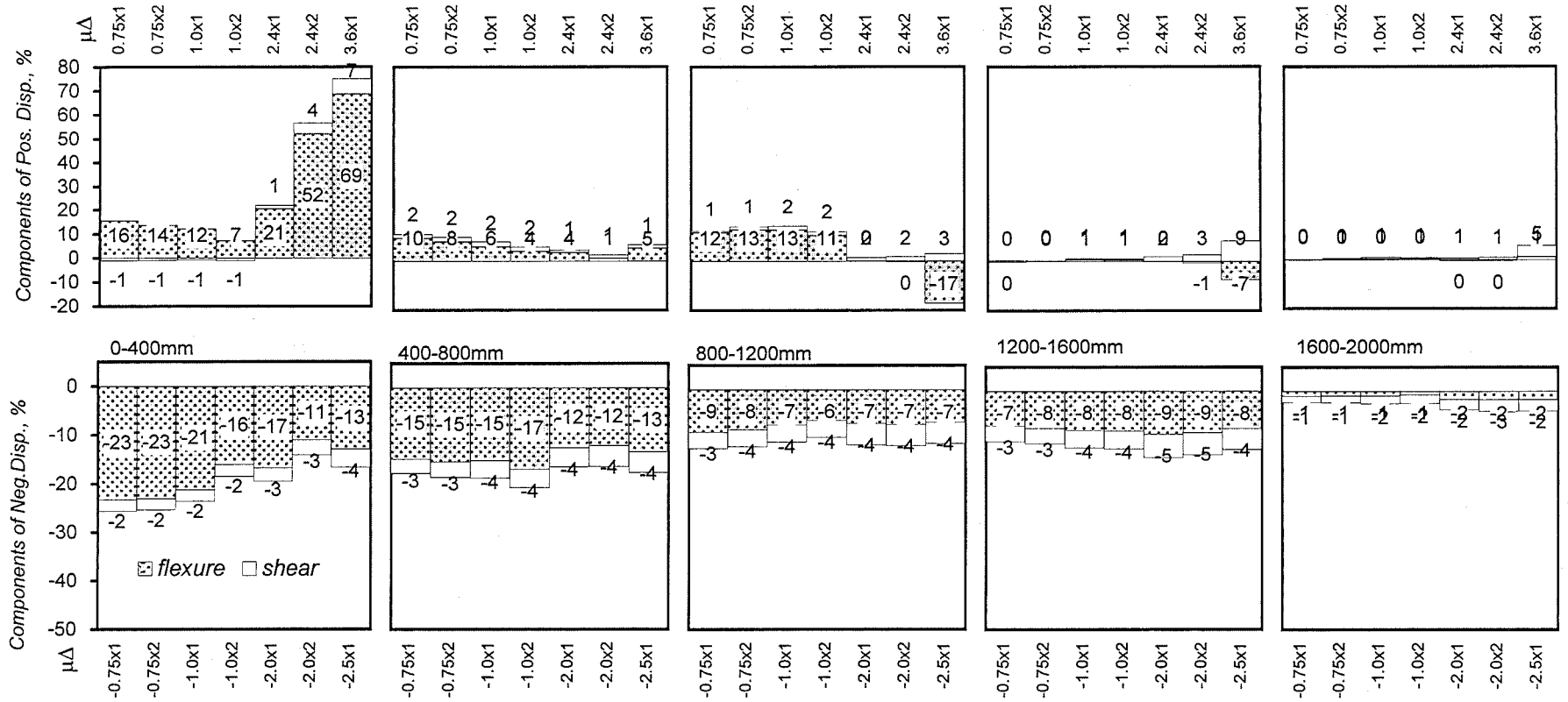

(c) Retrofitted Unit T2

Figure 5.25 Deformation Components due to Flexure and Shear, Expressing as a Percentage of Total Deformation (Cont.)

1200 to 1600mm away from column face, where the main diagonal crack developed. The shear deformation in the zone becomes larger at the same time. It is believed that the reinforcement in the region where the main diagonal crack has developed will yield first when the load is continuously applied and the shear deformation becomes larger soon after the curvature in the main diagonal crack starts increasing. This is evidenced in **Figure 5.25(a)** where most of deformations are concentrated in the deficient zone. In the positive loading of the prototype unit, the deformation due mostly to flexure occurred adjacent to the column face.

The cyclic loop of flexural and shear deformation for repaired or retrofitted unit is different from that of prototype unit, see **Figure 5.24**. In the negative loading of the repaired/retrofitted units as shown in **Figure 5.25(b)** and **(c)**, the deformation due to flexure and shear spread over the beam. This is based on the fact that the local flexural and shear strengths in the deficient zone were enhanced by the fibreglass/epoxy laminates bonded to the beam top and sides.

The components of the free-end displacement at each cyclic peak loading are shown in **Figure 5.26**. These components, flexural and shear deformation, were estimated following the method described in Section 5.6, expressed as a percentage of the total structural displacement. The top part of these figures displays the results of the loading cycles in the positive direction while the bottom part shows the components of the loading cycles in the negative direction. It is noted that the unaccounted component is determined by deducting the deformations due to flexure and shear from the total structural displacement. This component may be caused by the deformation due to fix-end rotation developed at the column face, where the tensile reinforcement were anchored into the column face after the steel reinforcement yielded. It can be seen in the negative loading that the repaired/retrofitted units have the same behaviour in keeping a similar amount of the percentage of deformation due to flexure and shear from the beginning to the end of loading cycle. However, in the prototype unit, the percentage due to flexure and shear grew in the inelastic cycle to $\mu_\Delta = -1.2$.

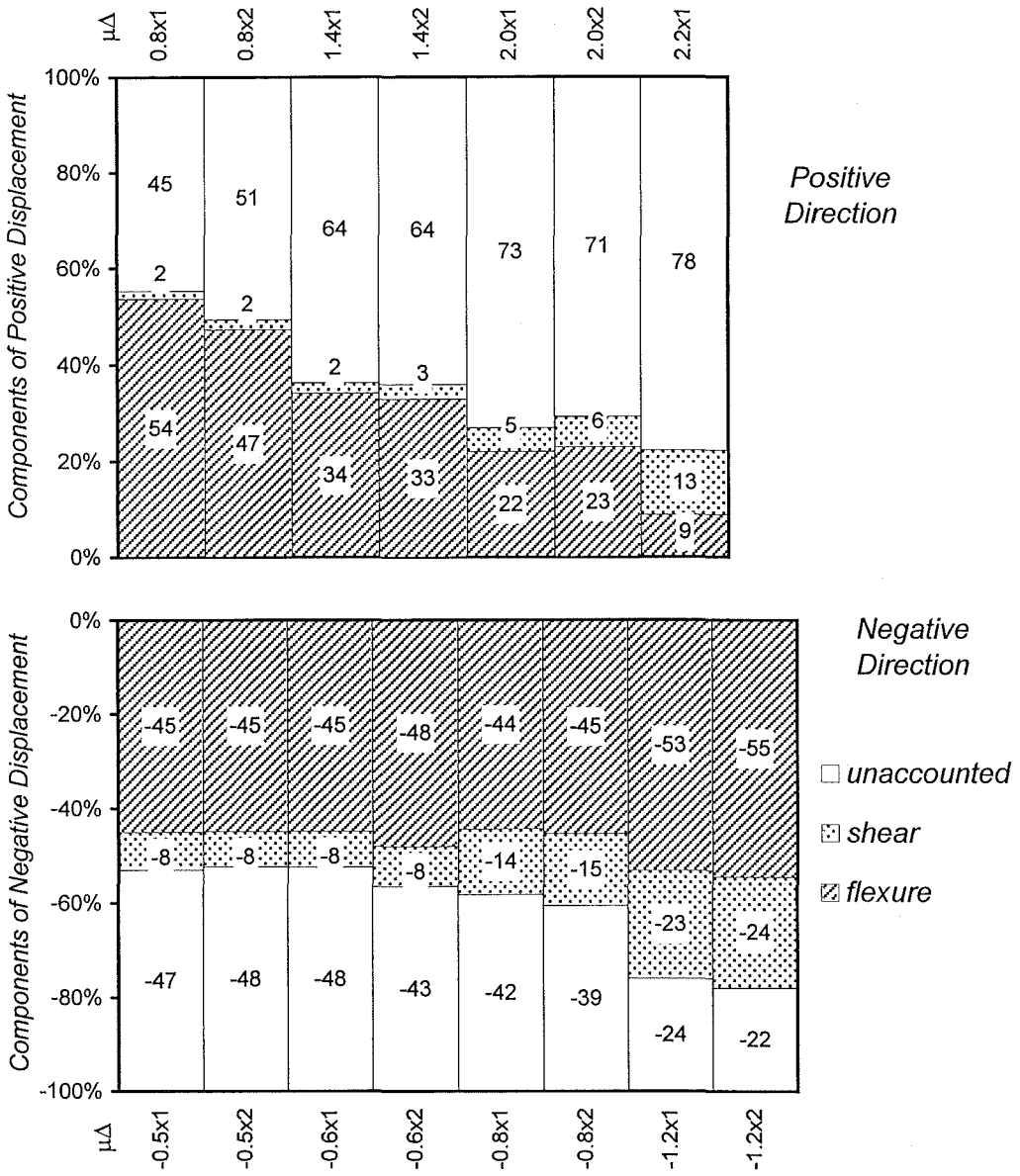

(a) Prototype Unit T1

Figure 5.26 Components of Free-end Displacement at Each Peak Loading

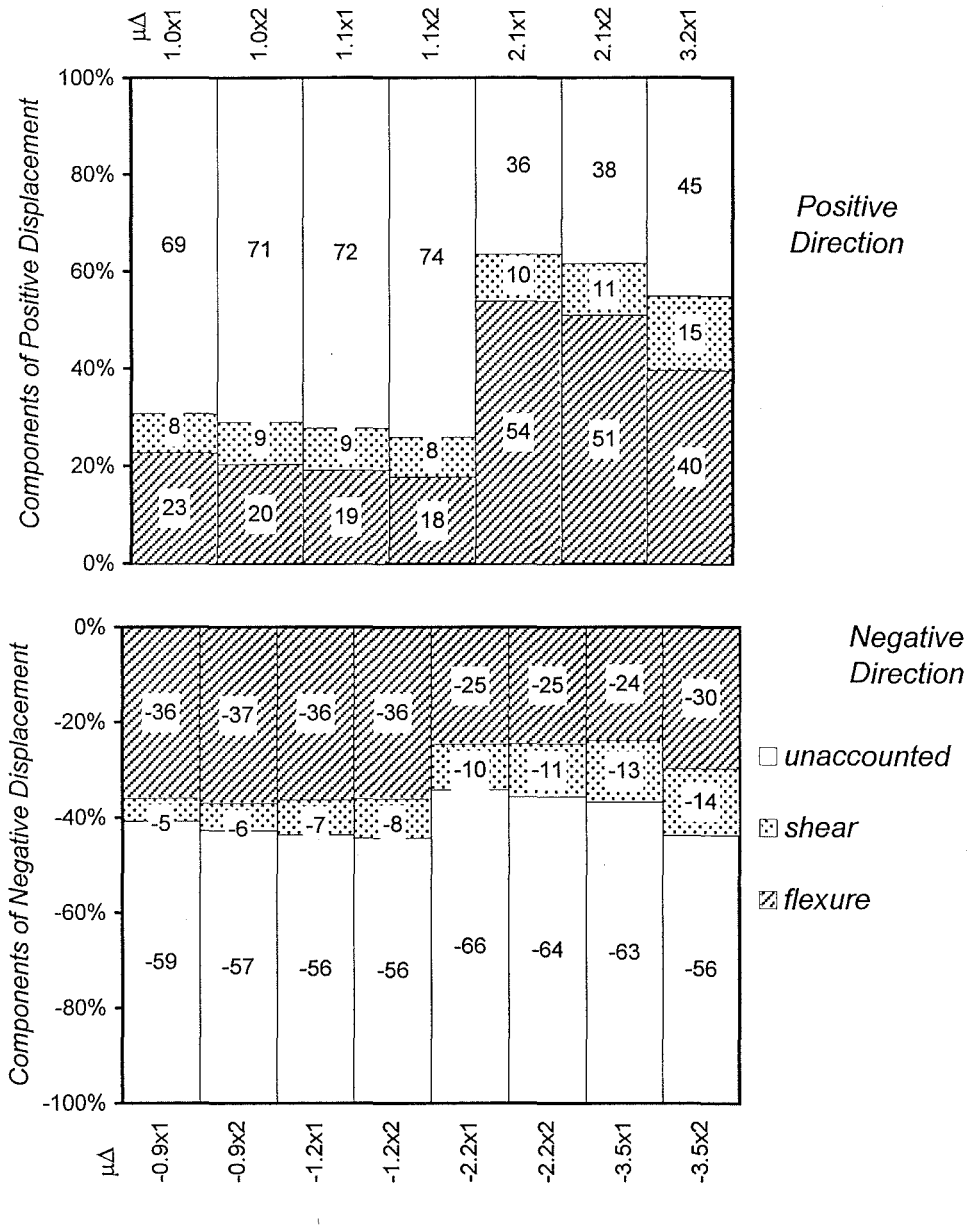

(b) Repaired Unit T1

Figure 5.26 Components of Free-end Displacement at Each Peak Loading (Cont.)

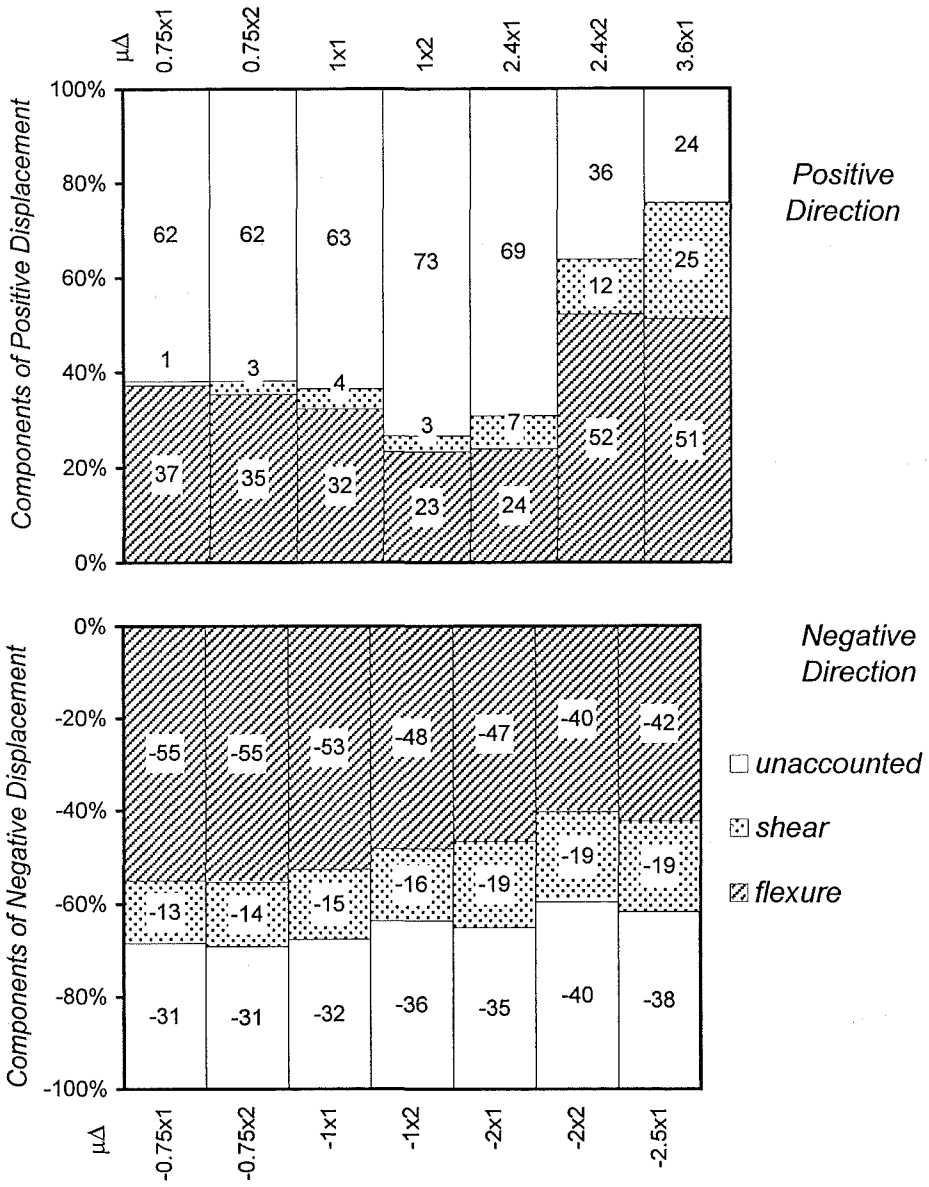

(c) Retrofitted Unit T2

Figure 5.26 Components of Free-end Displacement at Each Peak Loading (Cont.)

5.9.4 Strain of Steel Reinforcing Bars

The measured results of the strain in the beam and slab longitudinal reinforcement and in the steel stirrups are shown from **Figures 5.27** to **5.30**. The purpose of these selected figures is to observe the response of the reinforcement in some critical regions.

In the positive loading cycles for all test units, the bottom beam reinforcement was loaded to yielding at the range adjacent to the column face as depicted in **Figure 5.27**. The figure of Retrofitted Unit T2 is not plotted due to malfunctioning of the datalogger equipment when reading the bottom bar strains during testing.

In the Prototype Unit T1, as illustrated in **Figures 5.28(a)** to **5.29(a)**, the beam and slab top longitudinal reinforcement remained elastic at the column face but yielded in the region adjacent to the large diagonal crack, which is about 1300 mm away from the column face. Note that there are no closely spaced stirrups in this part of the beam. Further downward cycles resulted in extensive yielding of the stirrups, seen in **Figure 5.30(a)**, and crushing of the concrete in this region of the beam.

In repaired/retrofitted units, see **Figure 5.28**, the beam top reinforcement yielded at the section closer to column face instead of in the region where the beam bars were curtailed. The slab reinforcement was observed to yield across the full flange width in a yield line passing through the column face, as shown in **Figure 5.29**. This was confirmed as the previous assessment capacity P_n accounting for all the slab longitudinal reinforcement agreed very well with the measured load. However, in the repaired/retrofitted units, yielding of the bars also took place at the deficient region when the cyclic loading reached $\mu_\Delta = -2$. This is because the U-shape side glass ACM strips without anchors to the top edges is delaminated at the deficient region and the large diagonal crack again commences at the shear deficient region when the loading is applied to the higher ductility cycle. A large stirrup strain measured in the deficient region of the retrofitted unit at the end of displacement cycle indicated that a larger shear deformation occurred in the vicinity of the beam bar cut-off points. This shear deformation forced the fibreglass/epoxy laminates on the top of slab to delaminate as in the beams of Series-A described in Chapter 5.

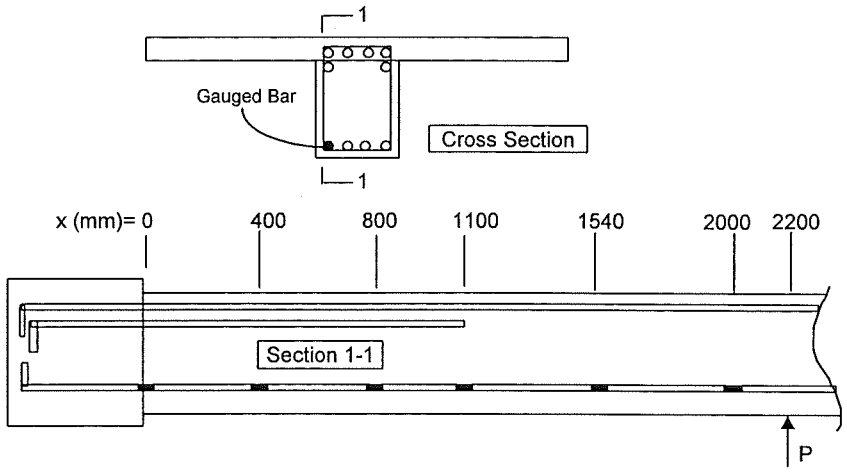

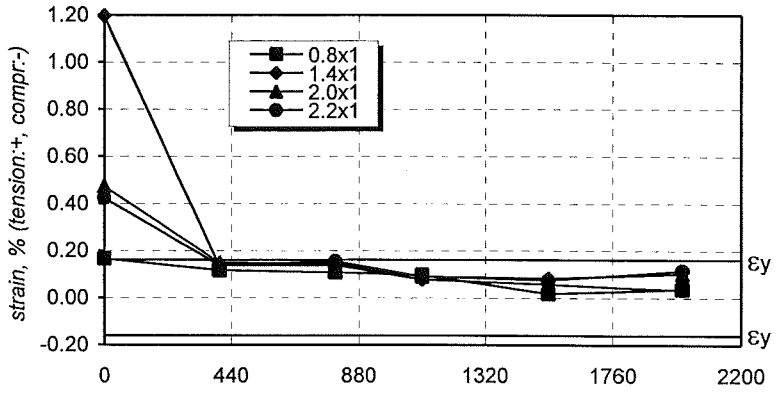

(a) Prototype Unit T1

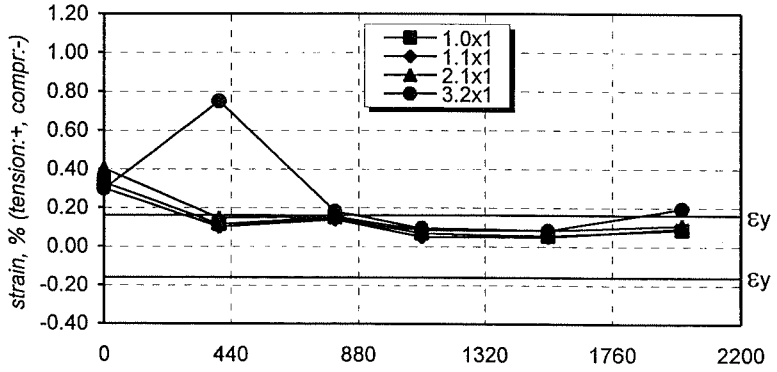

(b) Repaired Unit T1

Figure 5.27 Strain Distribution on Bottom Beam Bar at Positive Loading Cycles

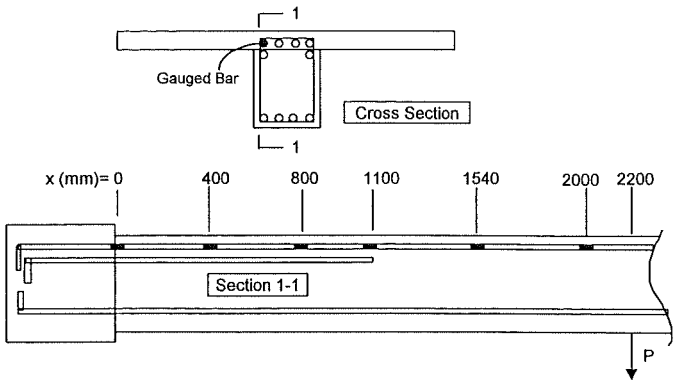

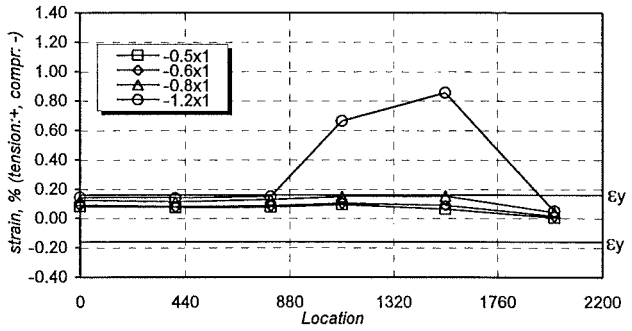

(a) Prototype Unit T1

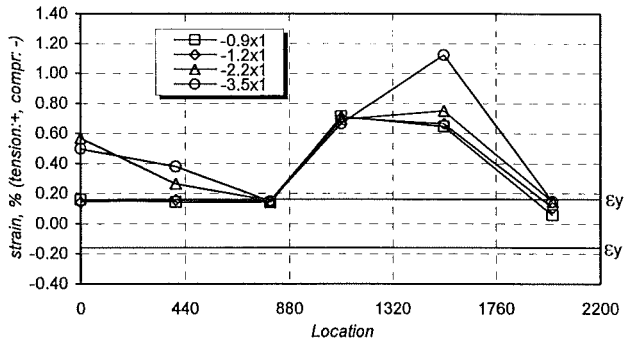

(b) Repaired Unit T1

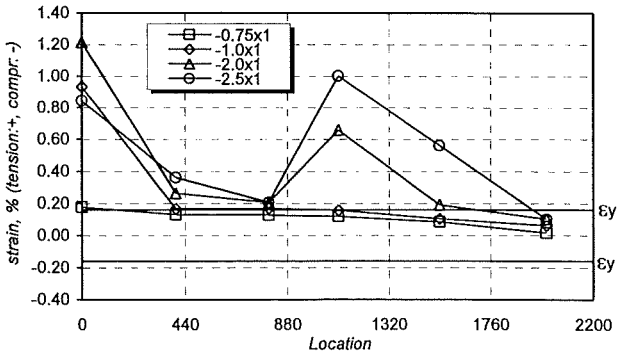

(c) Retrofitted Unit T2

Figure 5.28 Strain Distribution on Top Beam Bar at Negative Loading Cycles

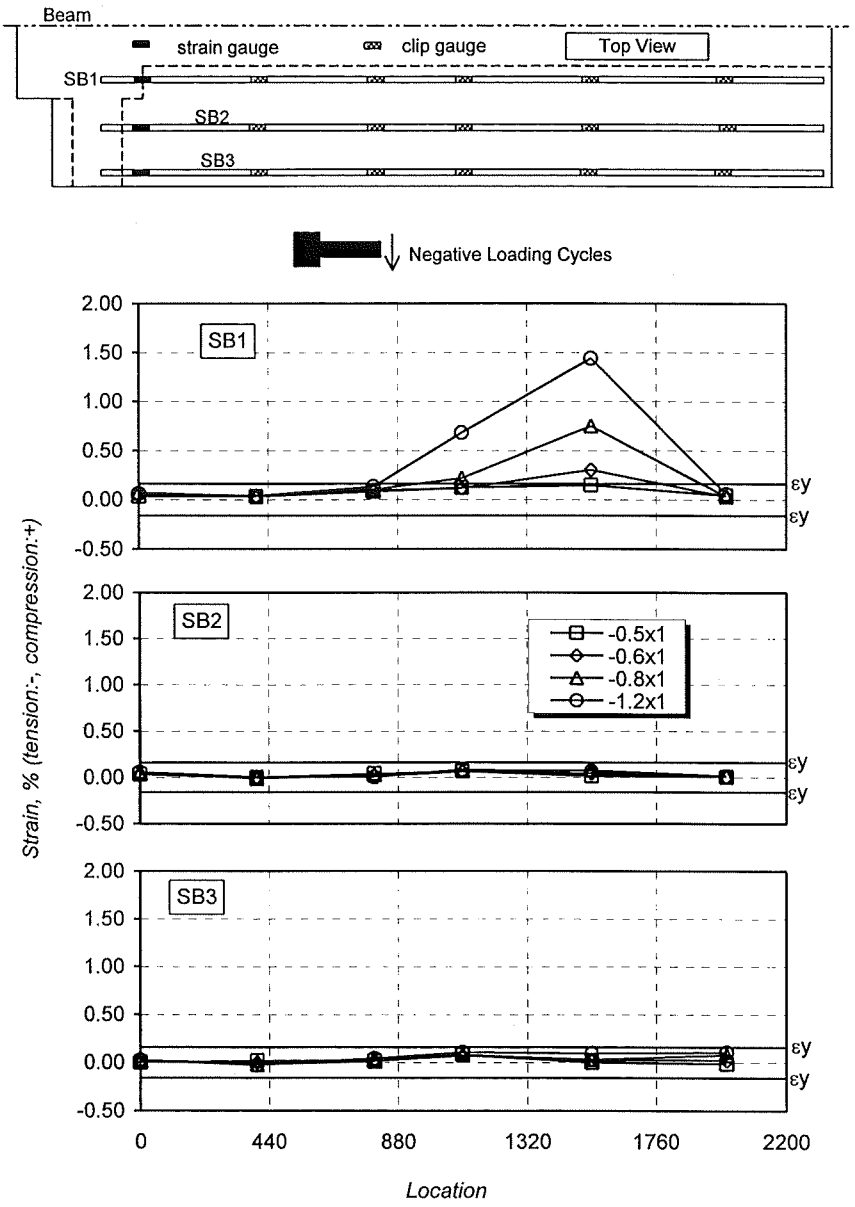

(a) Prototype Unit T1

Figure 5.29 Strain Distribution on Bottom Slab Bars at Negative Loading Cycles

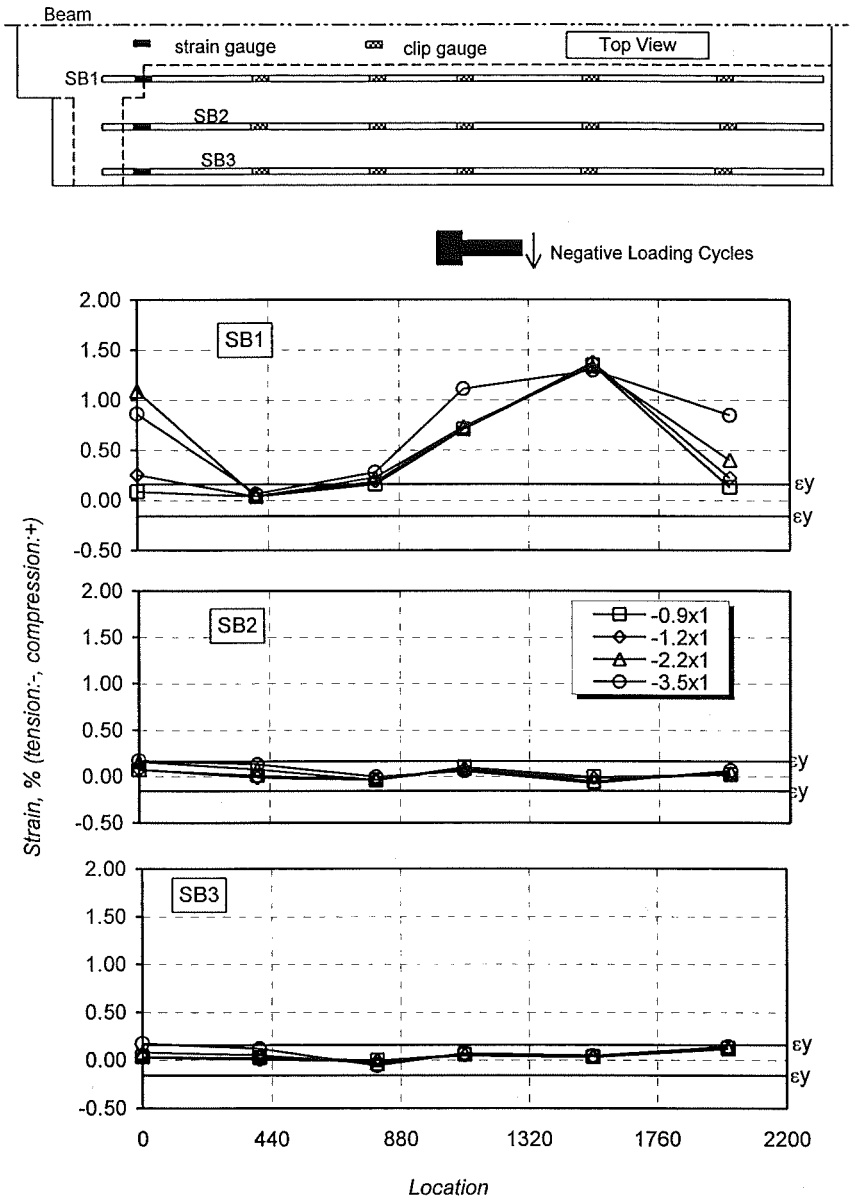

(b) Repaired Unit T1

Figure 5.29 Strain Distribution on Bottom Slab Bars at Negative Loading Cycles (Cont.)

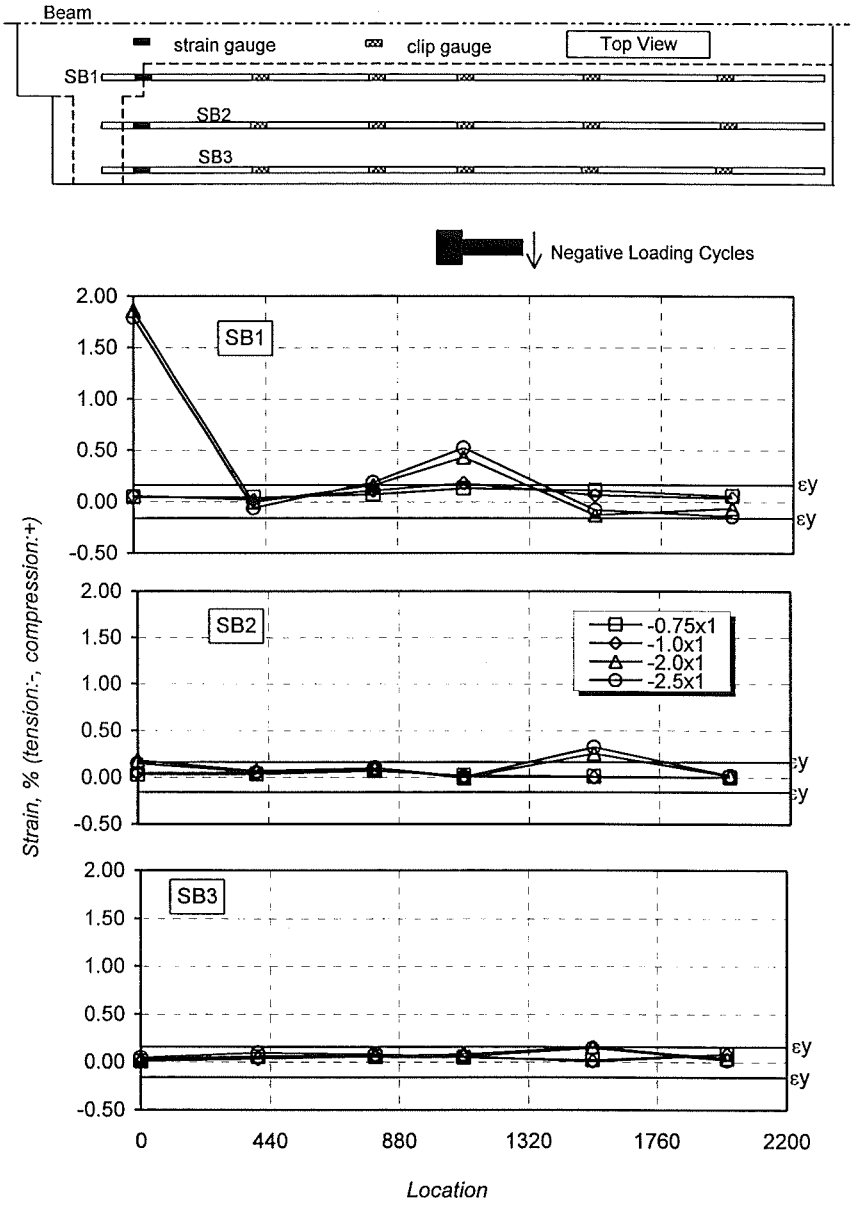

(c) Retrofitted Unit T2

Figure 5.29 Strain Distribution on Bottom Slab Bars at Negative Loading Cycles (Cont.)

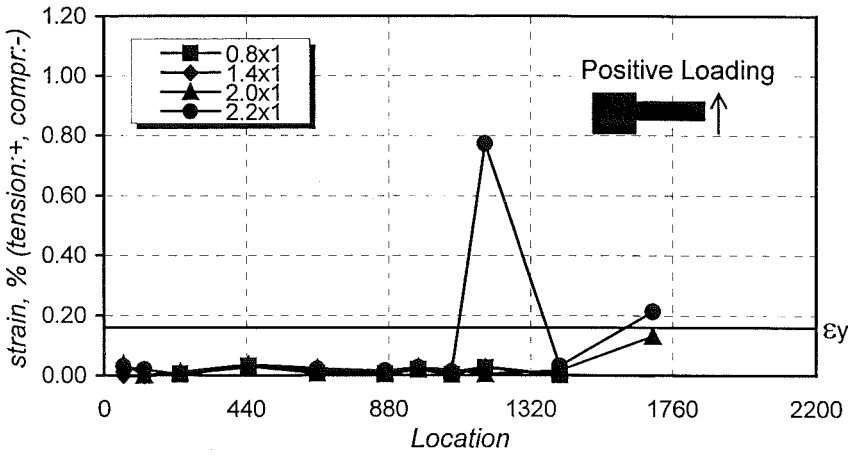

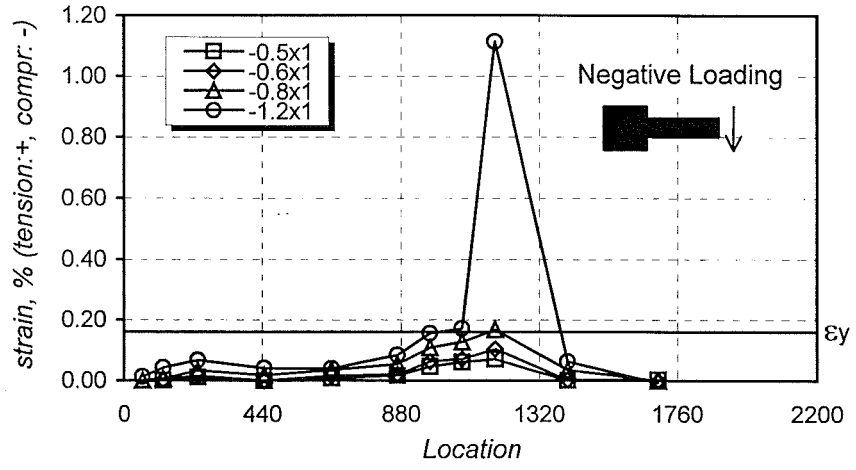

(a) Prototype Unit T1

Figure 5.30 Strain in Steel Stirrups

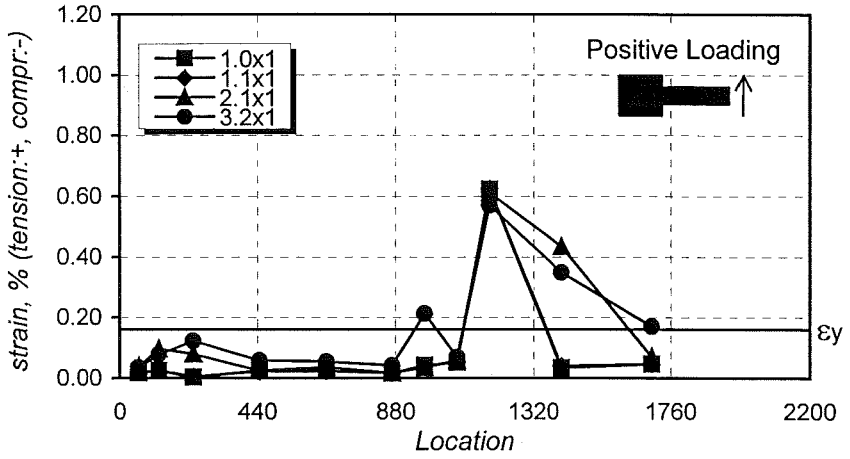

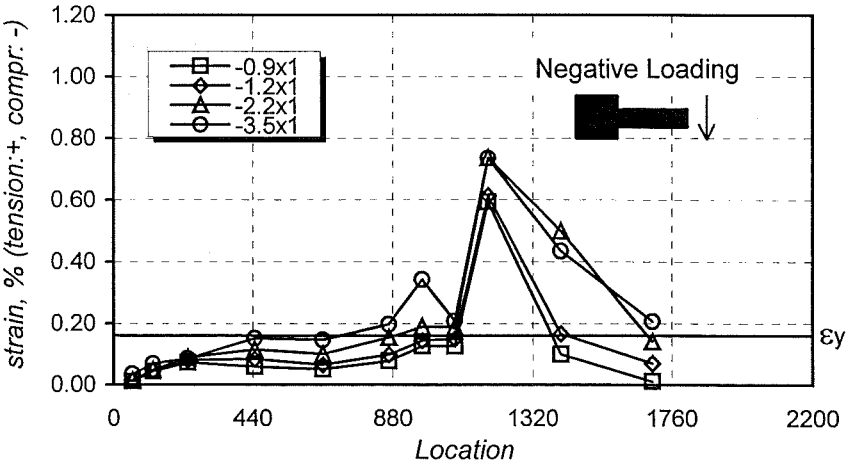

(b) Repaired Unit T1

Figure 5.30 Strain in Steel Stirrups (Cont.)

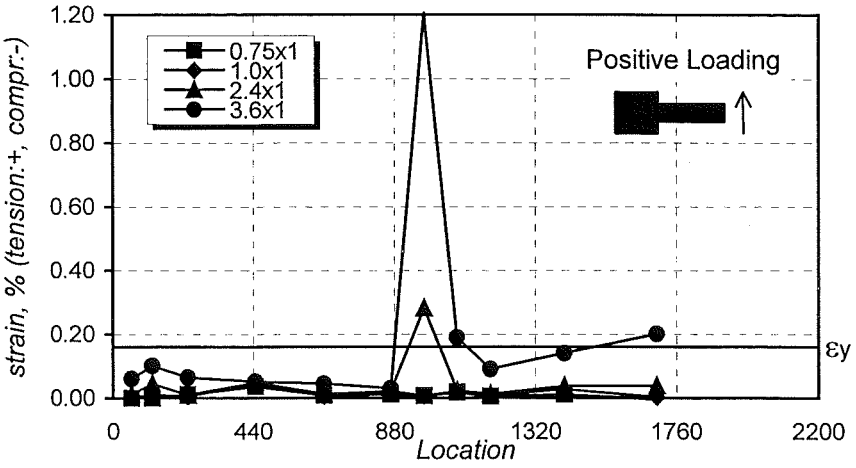

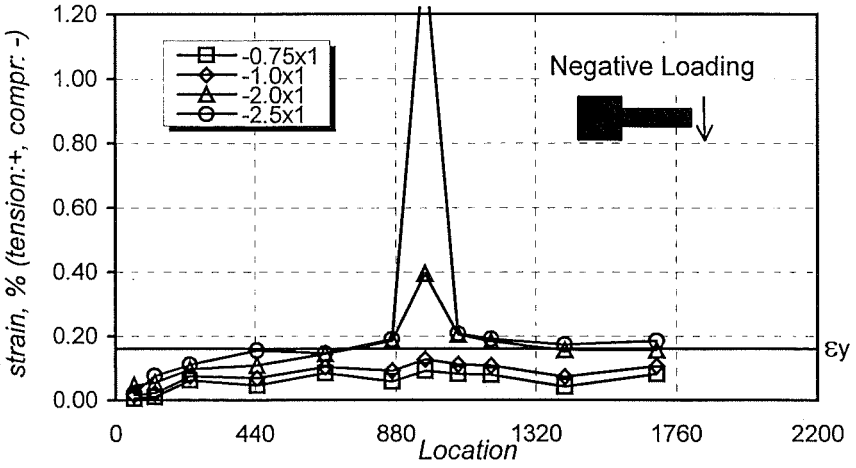

(c) Retrofitted Unit T2

Figure 5.30 Strain in Steel Stirrups (Cont.)

5.9.5 Strain on the U-shaped Plates

The debonding pattern of U-shape strips for both repaired and retrofitted units was very similar. Delamination commenced from the end of the strips in the region where the beam top longitudinal reinforcement had been cut-off and slowly propagated downwards and sideways. **Figure 5.31** shows the history of the measured U-shape strip strain in the transverse direction. The debonding occurred when the strain did not show any cyclic variation. After debonding, the strain measured was not reliable and is not shown here. It was found in both tests that most of measured strains become unreliable when the cycle reached to $\mu_{\Delta} = -1.0$.

Since the reliable reading could not be obtained in the inelastic loading range, the principal strain and its inclination were limited to elastic response. A selected result in Repaired Unit T1, measured by DEMEC gauge delta rosette, is shown in **Figure 5.32**. It can be observed that, up to about 250 kN in the elastic range, the maximum principal strain and its inclination to the beam axis are approximately 0.3% and 50 degrees respectively. The effective transverse strain in the U-shaped side glass ACM strip reached only 0.15 %, after which the strips began to debond. The effective transverse strain for the design of side glass ACM strips was 0.4%. This suggests that the U-shape strips should be anchored if they are to provide shear enhancement. Anchoring of the side strips was incorporated with success to the beams in the test programme discussed in Chapter 4.

5.9.6 Strain Distribution on Longitudinal Fibreglass/Epoxy Plates

Figures 5.33 and **5.34** depict the strain profile of the glass ACM laminate bonded to the slab for Repaired Unit T1 and Retrofitted Unit T2 respectively. The local laminate bond stress was also determined assuming the uniform bond stress distribution between two measured points as given by Eq. 3.38. The laminate strain measurement in Repaired Unit T1 shows that fluctuating reading occurred adjacent to both laminate ends after inelastic loading cycles, see **Figure 5.33(a)**. This is because the clip gauge is easily influenced by the previous flexural cracks developed in the test on the prototype unit. However, the measurement in Retrofitted Unit T2 (see **Figure 5.34(a)**) shows

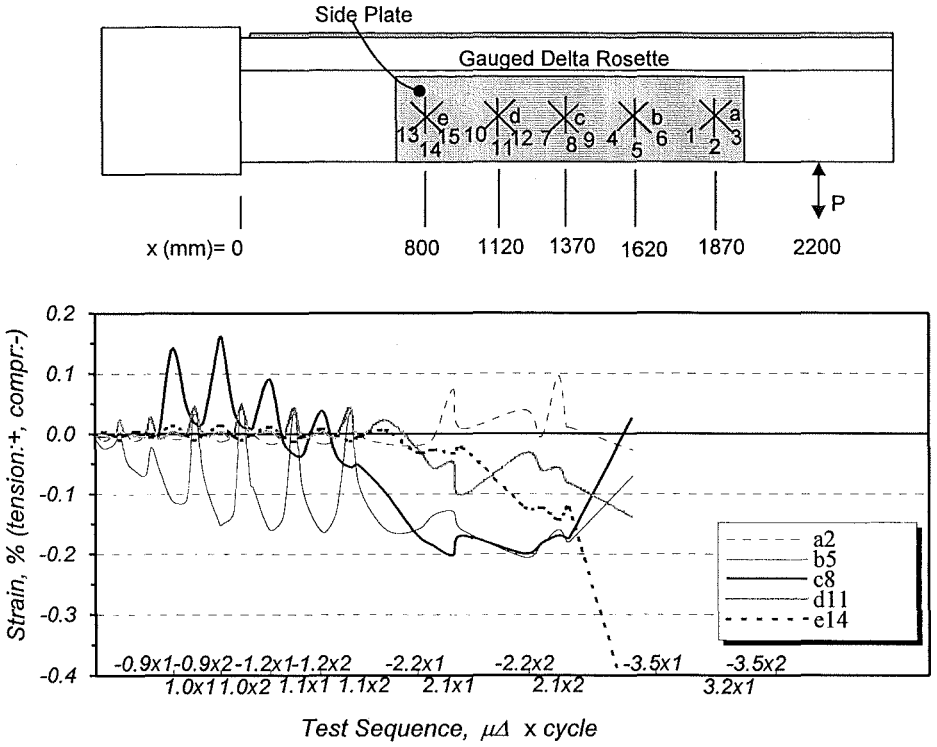

(a) Repaired Unit T1

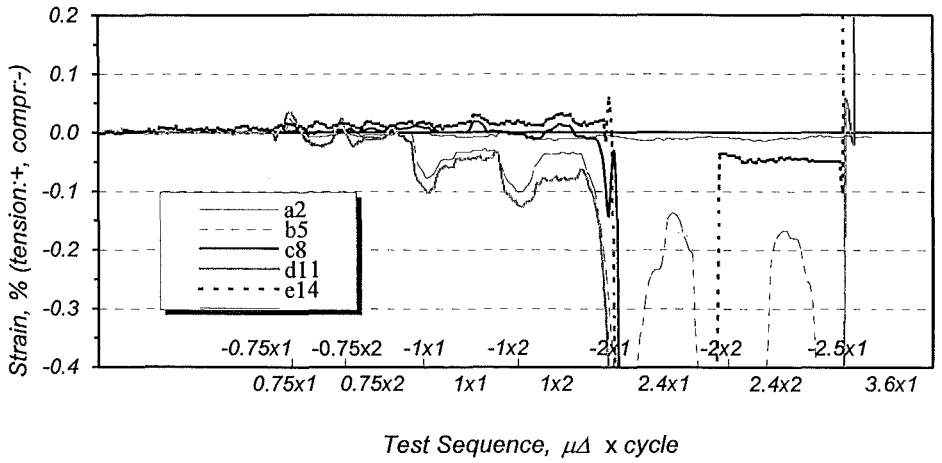

(b) Retrofitted Unit T2

Figure 5.31 History of the Strain of U-shape Side Plates in the Direction of the Main Fibres

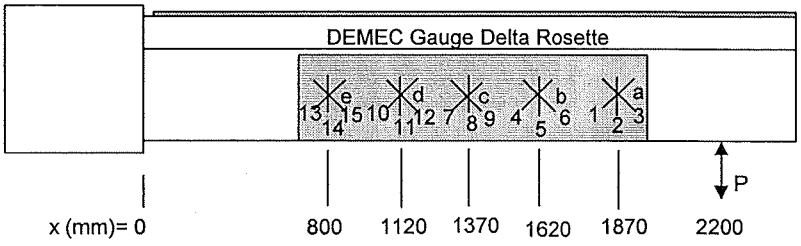

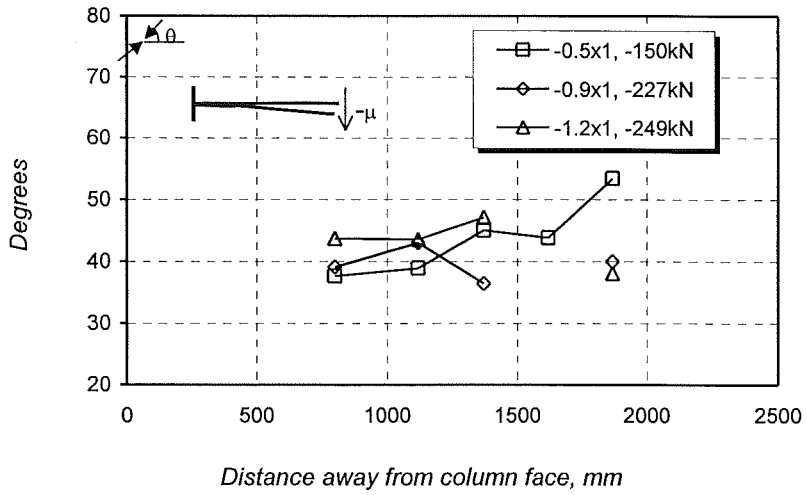

Figure 5.32 Inclination of Principal Compressive Strain on U-shape ACM Strip of Repaired Unit T1

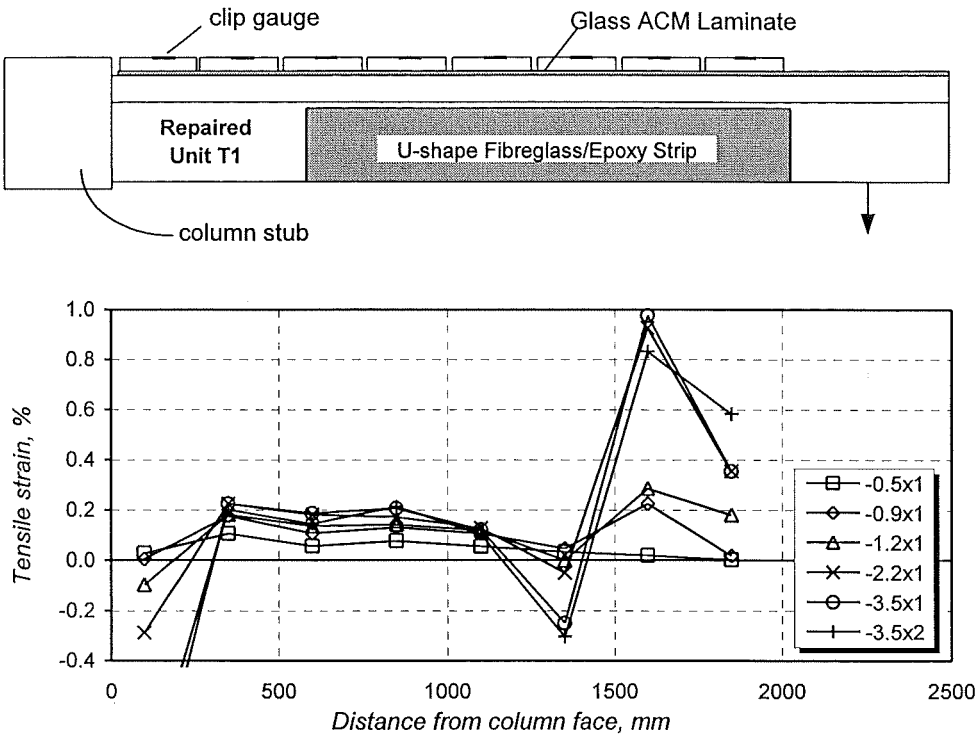

(a) Measured Strain

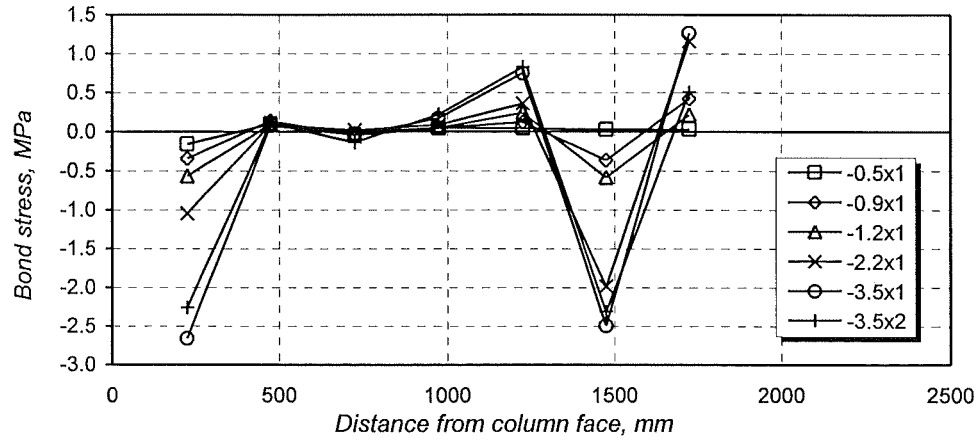

(b) ACM Bond Stress

Figure 5.33 Longitudinal Strains and Bond Stresses in the ACM Laminate Bonded to the Slab for Repaired Unit T1

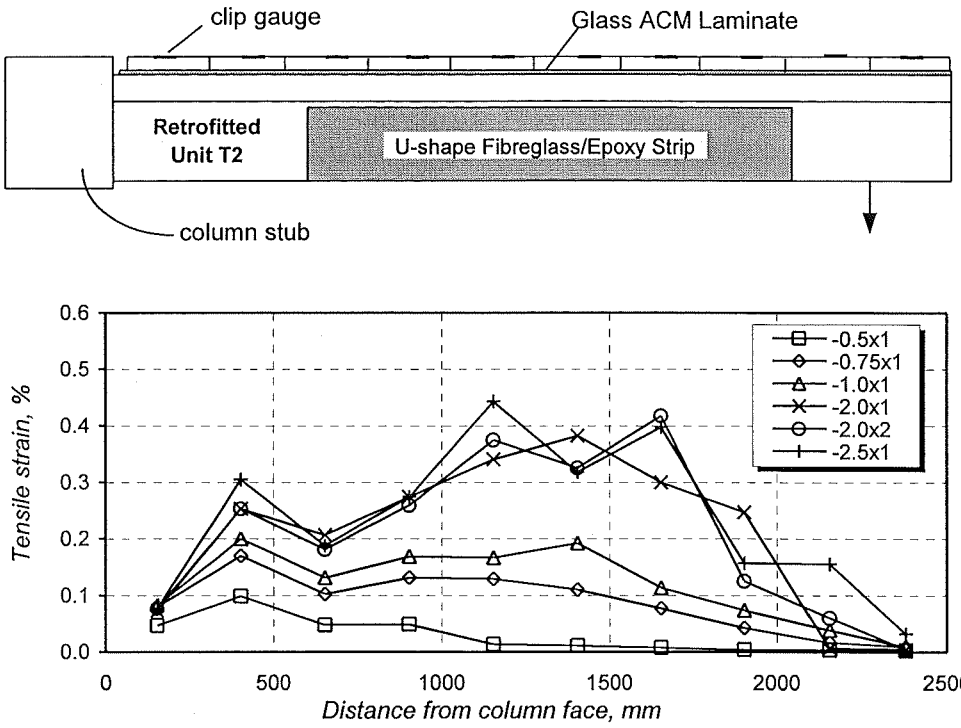

(a) Measured Strain

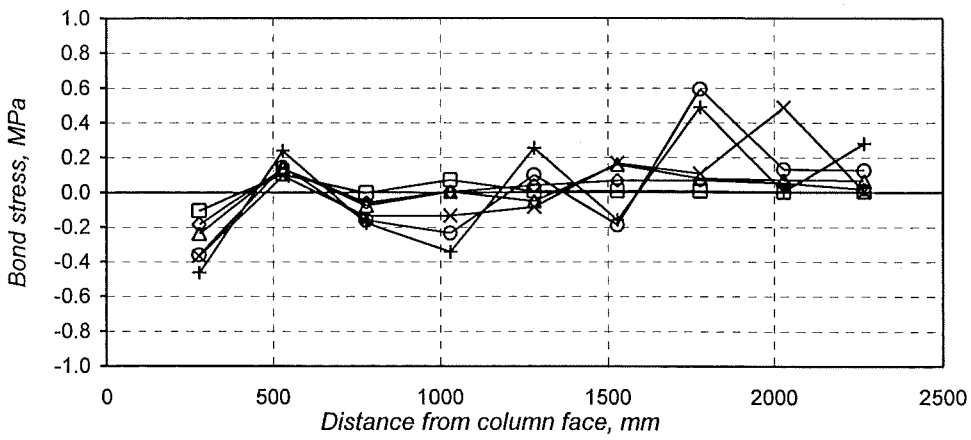

(b) ACM Bond Stress

Figure 5.34 Longitudinal Strains and Bond Stresses in the ACM Laminate Bonded to the Slab for Retrofitted Unit T2

stable and reasonable values, which could be used for study.

In **Figure 5.34**, it is apparent that the observed behaviour of the glass ACM laminate compares very well with the limiting design strain of 0.4% chosen for the retrofit. The maximum strain gradient occurred in the glass ACM laminates between 1.7 to 2.5 m from the column face and the local bond stress was obtained as low as 0.6 MPa in maximum, see **Figure 5.34(b)**. The average bond stress in this region was about $0.07\sqrt{f'_c}$ [MPa] and is the value associated with the bond failure observed in the tests. From such a low bond stress observed, it is concluded that the main factor for the delamination of the laminates was the large shear distortion that occurred in the beam after the delamination of the U-shaped strips.

5.10 Conclusions

1. The experimental programme carried out in this research indicates conclusively that under some circumstances, the critical region in beams of moment resisting frames designed for earthquake resistance and designed with older code provisions, may form negative plastic hinges in apparently unexpected regions. This is due to the effect that the slab reinforcement has in the overall seismic response of the frame. This deficiency may result in an unexpected flexure-shear failure of the beam at a remote critical location, such as the region of the curtailment of longitudinal reinforcement.

2. A simple evaluation of existing reinforced concrete beams with longitudinal bar curtailments can be carried out using a concept of tension shift adopting a variable angle truss model to identify the failure mechanism.

3. The design of flexural enhancement, which ensures that a strain limit of 0.4% imposed on the glass ACM laminate, may be used to enhance the flexural strength at the bar cut-off points.

4. U-shaped strips bonded to the sides of a beam are ineffective in resisting shear unless they are properly anchored at their ends. The loss of the side strips caused shear distortion of the beam and led to kinking and delamination of the longitudinal glass ACM laminate at larger shear angles.

CHAPTER 6

DESIGN RECOMMENDATIONS FOR PART II

6.1 Introduction

Chapters 4 and 5 described experimental programmes on the use of ACM laminates to improve the performance of beams both at the service and ultimate limit state for two different loading conditions. Chapter 4 focused on the live load increase in beams, particularly bridge girders whereas Chapter 5 focussed on the use of ACM laminates to relocate the plastic hinges in beams of seismic resistant frames and avoid a premature flexure-shear failure caused by poor development of the longitudinal reinforcement.

This chapter is endeavoured to provide simple design recommendations that can be used in a design office.

6.2 Design Recommendations for Live Load Increase in Beams

6.2.1 Design Philosophy

The design concept for the retrofit of beams is to raise the service live load carrying capacity. CACM laminates are recommended for use of flexural reinforcement where low amplitude cycle repeated loading needs to be considered. This is because CACM laminates have excellent fatigue properties as was demonstrated by the test on Unit C2, see Section 4.9.4.

6.2.2 Serviceability Limit State

Figure 6.1 shows the curvature diagrams at the critical region of a bridge girder at different loading stages prior, during and after bonding the CACM laminates. The curvature due to dead load alone before application of the laminate, see line (a) in **Figure**

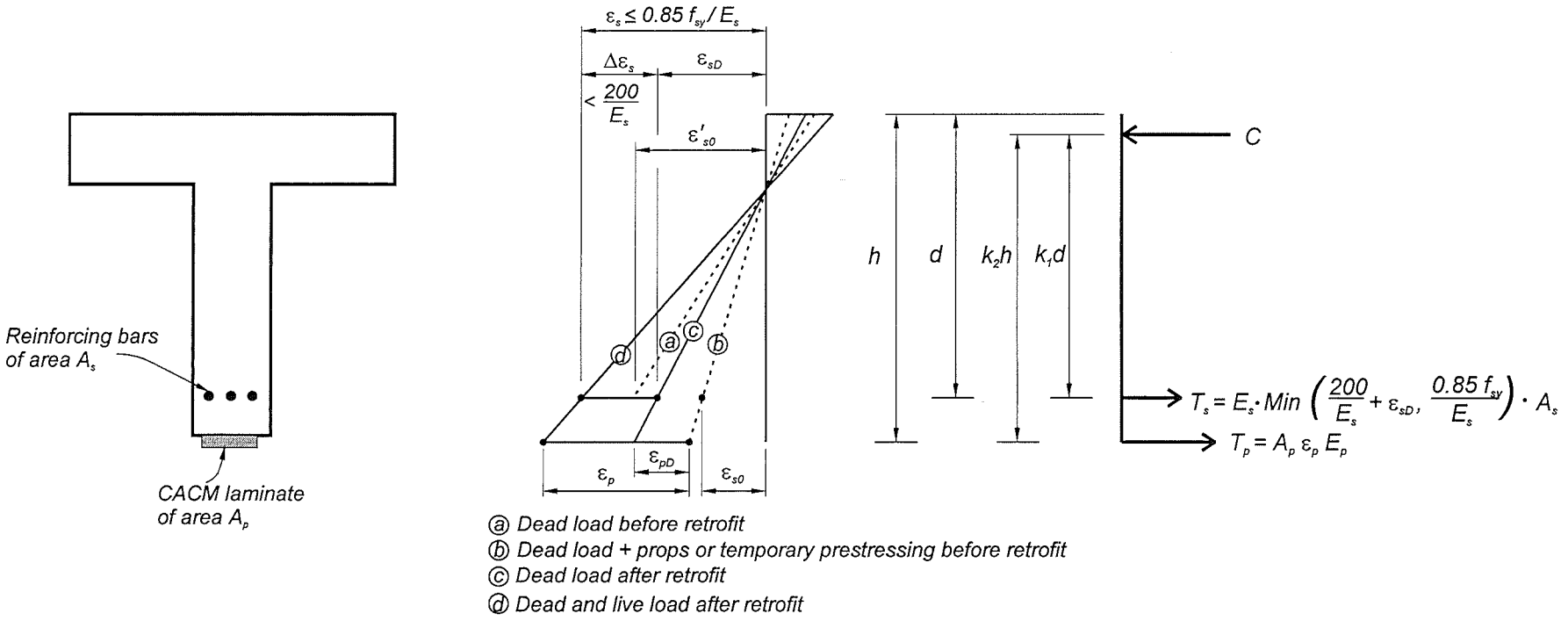

(a) Beam Cross Section

(b) Curvature Diagrams at Different Stages

(c) Sectional Forces due to Service Dead and Live Load Acting Together

Figure 6.1 Section Behaviour Before and Immediately After Retrofit

6.1(b), can be established theoretically by accounting for shrinkage and creep effects. In bridge girders an increase in the service live load is either controlled by the allowable stress range in the reinforcing steel or by the absolute tensile stress in the longitudinal reinforcement. The allowable stress limit in the concrete seldom controls the design in simply supported T-beams and will not be considered in this study.

To obtain the maximum service live load, the beam can either be prestressed or jacked up to reduce the stress in the longitudinal reinforcement prior to bonding of CACM laminates. **Figure 6.2** depicts the reduction of the bending moment caused by jacking a girder during the retrofit operation. As the bending moment is reduced, the curvature in the critical region will also decrease, see line (b) in **Figure 6.1(b)**. An alternative method which involves prestressing of the laminate before bonding it to the concrete has been used in Switzerland [M3]. This method is not discussed in this study.

The first step in the design for flexure at the service limit state is to ensure that the stress in the longitudinal reinforcing steel when the service dead and live loads act together will be less than $0.85f_{sy}$ and that in addition for deformed bars the stress range will not exceed 200 MPa. The stress range is defined as the stress difference caused by dead load alone and combined dead and live loads. Note that 200 MPa stress range is the value currently allowed by the New Zealand Concrete Structures Standard for non-prestressed deformed bars [N4]. These two limits are shown in **Figure 6.1(b)** for clarity.

The second step is to obtain the tensile strain at the depth of the beam at the location of the centroid of the ACM laminate. This can easily be obtained from the curvature distribution, as shown in **Figure 6.1(b)**.

The internal forces at the critical region due to service dead and live load acting together are shown in **Figure 6.1(c)**. If it is assumed that $k_1 d / k_2 h = d / h$, $(\varepsilon_{sD} - \varepsilon_{so}) / \varepsilon_{pD} = d/h$ and that $k_1 = 0.9$ then the following procedure for establishing the cross section area of the CACM laminate, A_p, can be derived using strain compatibility principles,

$$A_p = \frac{\frac{d}{h}\left(M / 0.9d - A_s E_s \varepsilon_s\right)}{E_p \varepsilon_p} \qquad (6.1a)$$

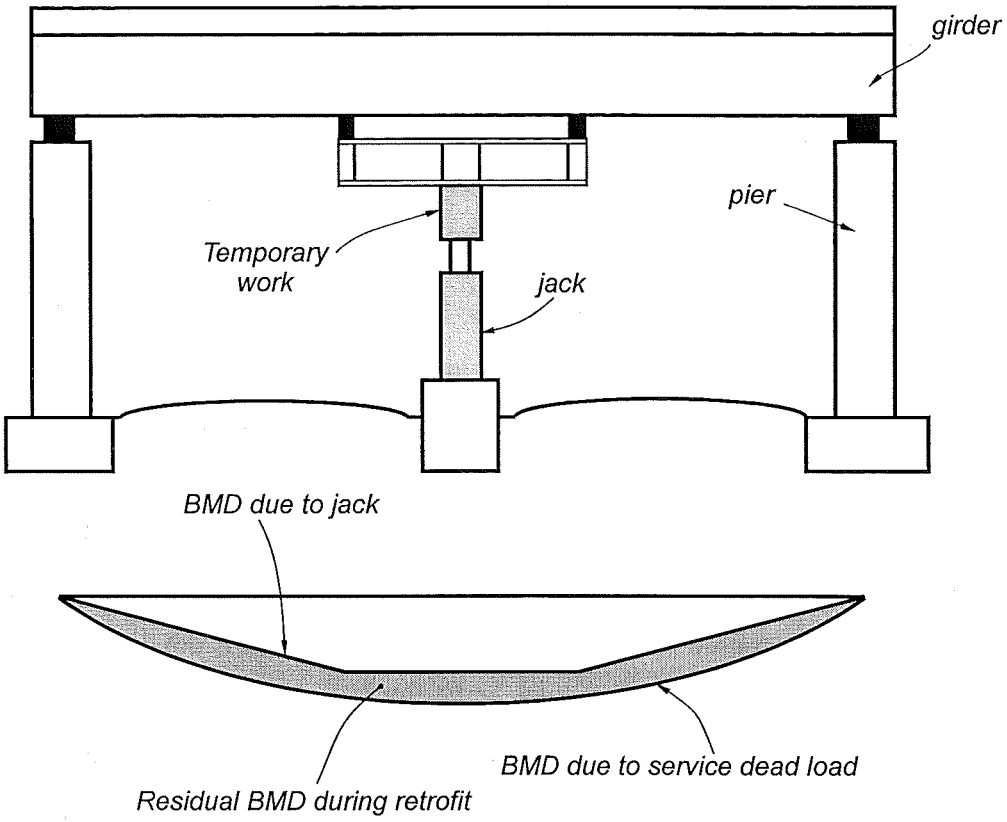

Figure 6.2 Jacking-up Technique to Optimise the Use of CACM Laminates

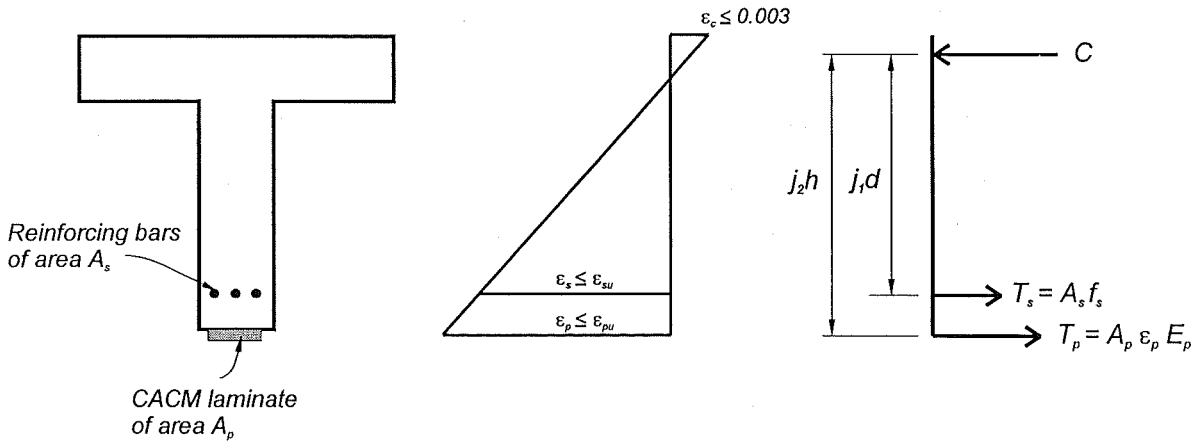

(a) Beam Cross Section **(b) Strain profile at the Ultimate Limit State** **(c) Sectional Forces**

Figure 6.3 Strain Profile and Sectional Forces at Ultimate Load

where

$$\varepsilon_{sD} = \frac{\varepsilon'_{s0} + (h/d)^2 \frac{E_p A_p}{E_s A_s} \varepsilon_{s0}}{1 + (h/d)^2 \frac{E_p A_p}{E_s A_s}} \tag{6.1b}$$

$$\varepsilon_s = Min\left(0.001 + \varepsilon_{sD}, \frac{0.85 f_{sy}}{E_s}\right) \tag{6.1c}$$

$$\varepsilon_p = \varepsilon_{pD} + (\varepsilon_s - \varepsilon_{sD})\frac{h}{d} \tag{6.1d}$$

and

$$\varepsilon_{pD} = (\varepsilon_{sD} - \varepsilon_{s0})\frac{h}{d} \tag{6.1e}$$

where, M_D is the moment due to service dead load, M is the moment due to service dead and live loads, E_s is elastic modulus of the steel reinforcement, and E_p is elastic modulus of the ACM laminate. The remaining variables are defined in **Figure 6.1**.

Note that Eq. 6.1a is only closed form when $\varepsilon_{s0}' = \varepsilon_{s0}$, that is, when the laminates are applied to the girder and the girder is not jacked up or temporarily prestressed. In any other case an iterative method needs to be employed to solve Eq. 6.1a for A_p.

6.2.3 Ultimate Limit State

Any retrofit design scheme has to ensure that the dependable strength of the retrofitted beam is equal or greater than the design action. In some cases, particularly in the case of bridge girders where large load factors are used in design, the area of laminates can be greater than that required by serviceability limit state.

6.2.3.1 Design for Flexure

In the design for flexure the following inequality must be satisfied:

$$\phi M_n \geq M_u \tag{6.2}$$

where ϕ is the strength reduction factor for flexure, M_n is the nominal flexural strength and M_u is the required bending moment obtained from the structural analysis using factored dead and live loads. The flexural strength of the beam is associated with the rupture of the CACM laminates at the 5 percentile lower characteristic ultimate tensile strain, f_{pu}. Such a value should be provided by the manufacturer of the laminate.

The nominal flexural strength is evaluated using strain compatibility principles. The force distribution in the critical section at the ultimate flexural strength is shown in **Figure 6.3**. The nominal bending moment is found by taking moments about the position of the resultant compressive force C. Note that the strain in the extreme fibre in compression may be such that $\varepsilon_c < 0.003$ when the ultimate tensile strain of the CACM laminate is reached. As a result, the equivalent rectangular compressive stress block recommended by design standard can not be used. Another possibility is that a compressive failure can develop as the concrete reaches the ultimate compressive strain before the CACM laminate reaches the ultimate tensile strain. In this case the ultimate tensile strength of the CACM laminate can not be used to evaluate the nominal flexural strength. The best way to check the nominal flexural strength is to evaluate it by using a moment-curvature computer program that can easily check the position of the neutral axis depth and the ultimate strains in each of the three materials involved. Such programs are readily available [C4].

6.2.3.2 Design for Shear

In the design for shear the following inequality must always be satisfied:

$$\phi V_n \geq V_u \tag{6.3}$$

where V_n is the nominal shear strength and V_u is the required shear force due to the combination of factored dead and live loads.

Figure 6.4 presents a flow chart with the different steps required for a shear design. Let V_u be the required shear force obtained from the structural analysis using factored loads, b_w the width of the web of the beam and d the effective beam depth, conservatively measured to the centroid of the longitudinal beam reinforcing steel. The possibility exists that V_u / b_wd is such that a diagonal compressive failure will occur before the flexural strength can develop. In this case the live load cannot be increased fully and the cross sectional area of the CACM laminates has to be reduced to avoid such failure mode. It is believed that a design controlled by diagonal compressive failure in some rare cases only.

It is not unusual to find in practice that the shear strength provided by the transverse steel and concrete mechanisms is insufficient to meet the new demand. Consequently, there is a need to increase the shear strength of the beam.

The use of U-side Glass ACM (GACM) strips, see **Figure 6.5(a)**, is a practical way to provide an increase in the shear strength in a T-beam, as it was demonstrated in the tests described in Chapter 4. The strips act over the height of the beam where the diagonal cracks are wide. **Figure 6.6** shows how the diagonal compression field in the beam web suddenly changes direction when the partial height strips transfer shear across the diagonal cracks. The U-strips need to be properly anchored at their ends. This can be achieved by using glass filaments embedded in an dust-free roughened epoxy-filled hole or by using a threaded rod crossing the entire web and anchored at the end of the strips as close as practicable to the underside of the flange. It should be pointed out here that the experimental work conducted in this study showed excellent effectiveness of the glass anchors in thin-web beams. It was observed during the experimental work discussed in Chapter 4 that proprietary TYFO glass anchors could effectively clamp a 120 mm wide by 1.27 mm thick GACM strip designed to carry an effective tensile stress of 80 MPa. The effectiveness of the glass anchors can not directly be extrapolated to applications in wide web beams at this stage as a potential for a local shear failure leading to pull-out of the anchor may exist in these type of beams. It is suggested that rods crossing the full beam web and anchored at the beam sides be used in beams with a cross section aspect

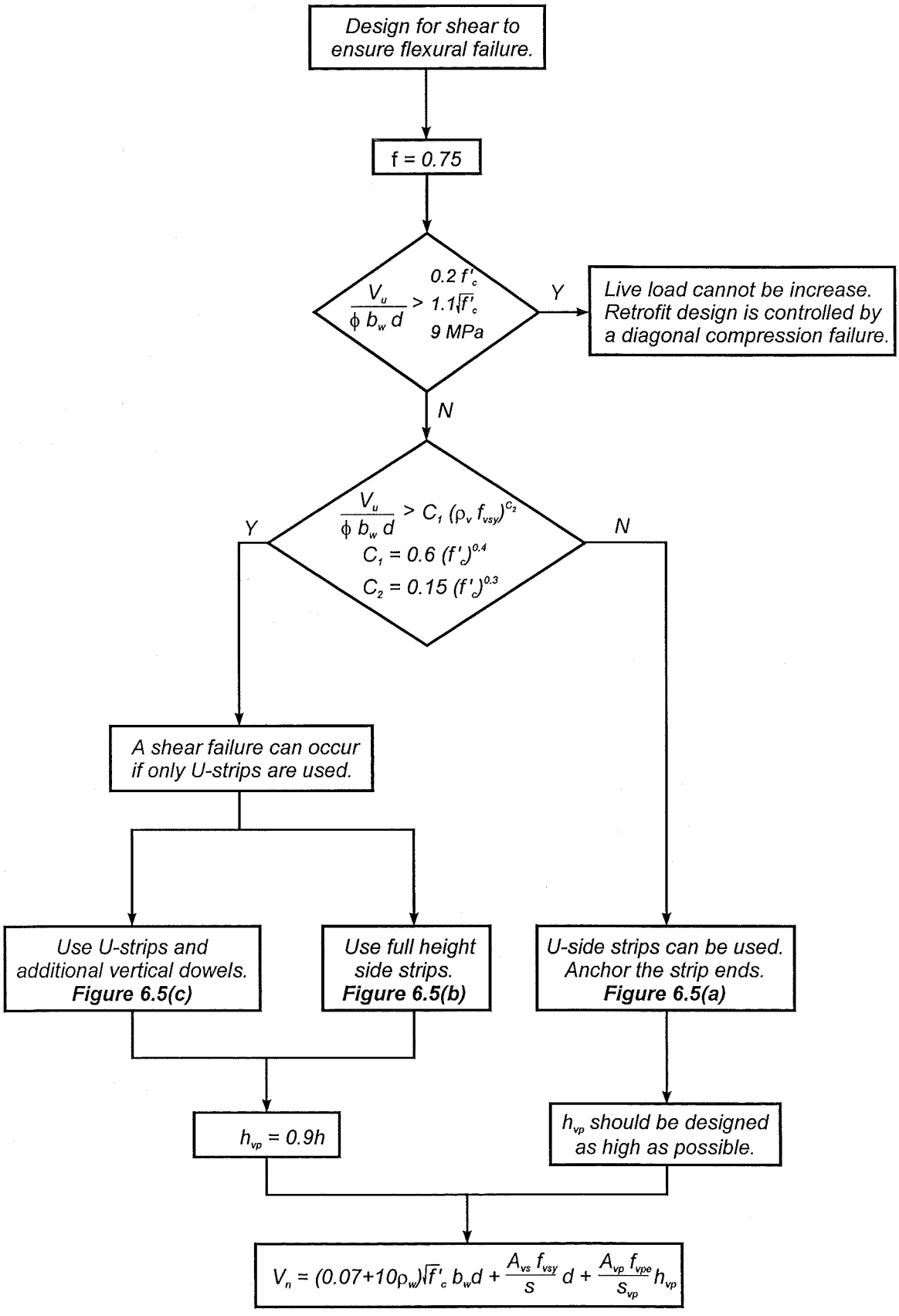

Figure 6.4 Design Flowchart for Beam Shear Enhancement

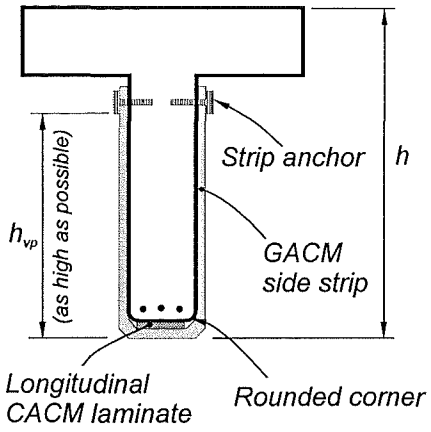

(a) U-side Strip

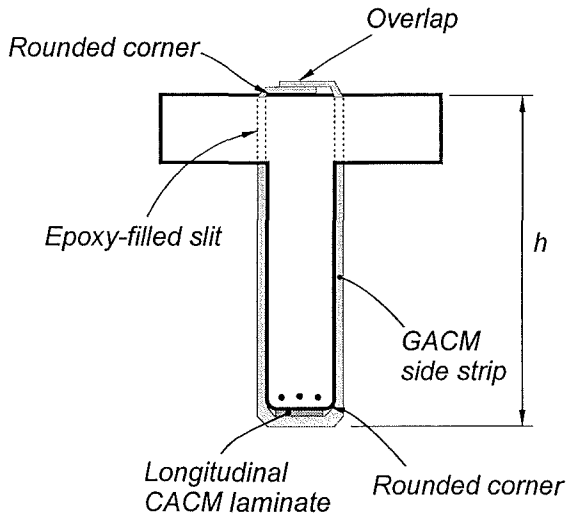

(b) Full Height Strip

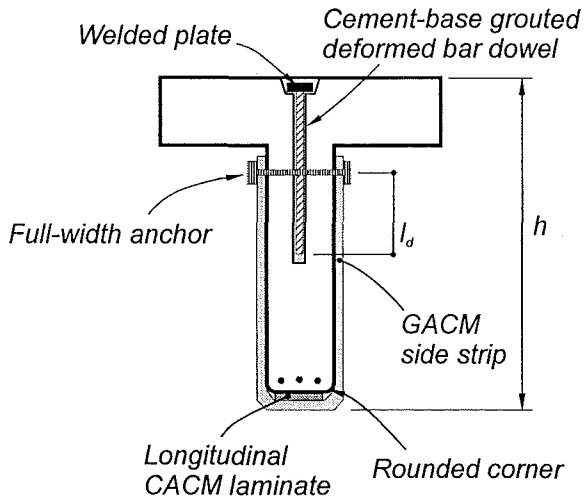

(c) U-side Strip and Additional Vertical Dowel

Figure 6.5 Detailing of GACM Side Strips for Shear Strength

ratio $b_w/d > 3/4$ until further research is carried out.

The shear strength provided by the three mechanisms, namely the concrete, the transverse steel reinforcement and the GACM strips is given by Eq.4.1, which is reproduced here for convenience

$$V_n = (0.07 + 10\rho_w)\sqrt{f_c'}\, b_w d + \frac{A_{vs} f_{vsy}}{s} d + \frac{A_{vp} f_{vpe}}{s_{vp}} h_{vp} \qquad (6.4)$$

where, ρ_w is the tensile steel reinforcement ratio which shall not be taken greater than 0.013, b_w is the width of the beam web, d is the beam effective depth and h_{vp} is the effective height of the ACM U-strip. The variables A_{vs}, f_{vsy} and s are the area, yield strength and spacing of the steel stirrups, respectively. The term A_{vp}, f_{vpe} and s_{vp} are the area, effective stress and spacing of the ACM U-strips, respectively.

The U-side strips should be designed for a stress corresponding to $\varepsilon_{vpe} = 0.004$. This value was observed in the experimental programme described in Chapter 4 and has also been recommended for the shear strengthening of columns [P6]. In the case of strips anchored with either glass anchors or rods, a 120 mm wide strip should be effectively clamped by the anchoring system. The centre-to-centre spacing of the U-side strips should be less than h/2 as following conventional reinforced concrete design recommendations.

When undertaking a shear strength enhancement design incorporating U-strips, the possibility of a shear failure developing in the web between the flange and the end of the strips should be investigated. The check for this failure mode is clearly shown in the flow chart shown in **Figure 6.4**.

In composite construction the use of the shear friction concept is recommended for the design of the shear reinforcement crossing the potential horizontal failure plane. The use of this concept is simple to use. For assessment purposes the shear friction concept can result in very low estimates of the shear strength as this concept tends to be quite conservative, particularly when the clamping pressure is low [C4, W2, M15]. Take

for example the T-beams in Series-B and C described in Chapter 4. A potential shear failure could develop above the end of the U-side strips as shown in **Figure 6.6**. The potential failure plane is crossed by 2 legged 6 mm diameter stirrups with f_{vsy} = 365 MPa spaced at 175 mm. The transverse reinforcement can induce a clamping uniform distributed force equal to 118 N/mm. An assessment of the shear strength in accordance with the shear friction concept using μ = 1.4 shows that the shear force of 74 kN is required to induce such failure. The shear force in all these units at the development of a flexural failure ranged between 135 and 153 kN. This approach resulted in a conservative estimation of the shear strength of the retrofitted beams in Series-B and C as no signs of failure of this type where observed in any of the tests. The conservatism of the shear friction approach has been discussed by many researchers [M15, S18, W2, C4]. However, the simplicity of the method and its physical concept are such that design standards have retained it.

Walraven et al. [W2] discussed the physical mechanism that resists shear across a crack. They proposed, based on a statistical analysis, the following equation for evaluating the 5 percentile lower characteristic shear strength:

$$v_n = C_1 \left(\rho_v f_{vsy}\right)^{C_2} \tag{6.5a}$$

where

$$\rho_v = \frac{A_{vs}}{b_w s} \tag{6.5b}$$

$$C_1 = 0.6 f_c'^{\,0.4} \tag{6.5c}$$

and

$$C_2 = 0.15 f_c'^{\,0.3} \tag{6.5d}$$

The equation proposed by these researchers showed excellent correlation with

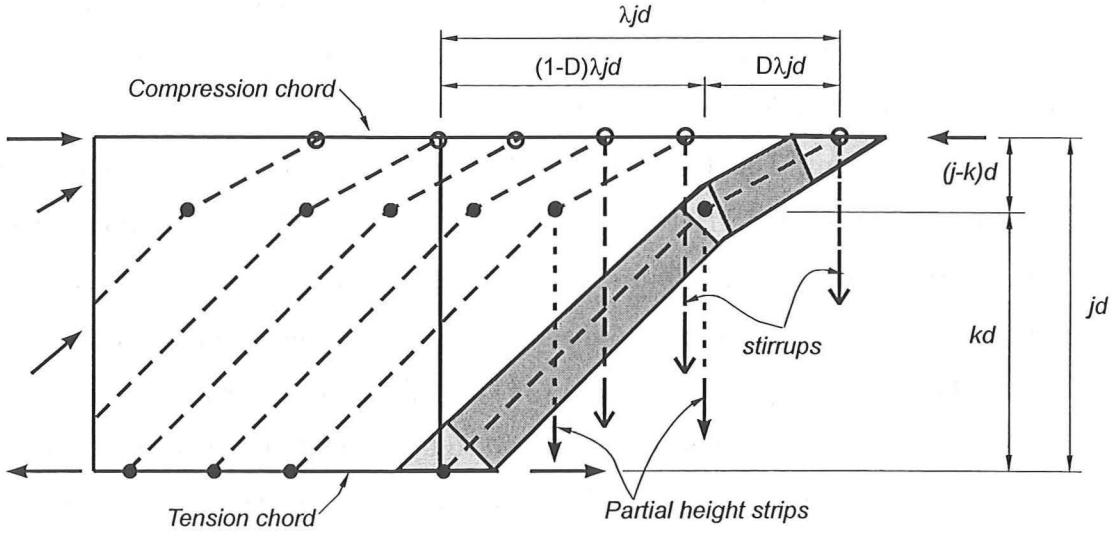

(a) Analogous Truss

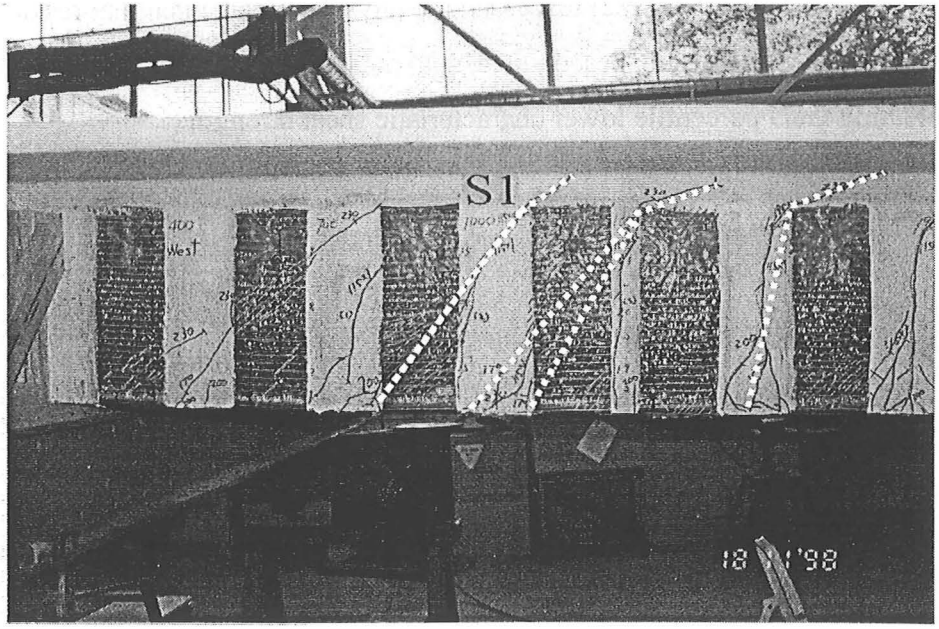

(b) Observation of Truss Mechanism Shown in White Dashed Lines, Unit S1 at the End of the Test

Figure 6.6 Truss Mechanism Illustrating the Shear Force Transfer through Partial Height ACM Strips

measured data and a coefficient of variation of 10% [W2].

The shear force predicted for the T-beams in Series-B and C according to Eq. 6.5 is 167 kN, which indicates that a shear failure developing in the beam web below the flange and above the end of the U-side strips was not expected to occur.

In this study it is recommended that the shear strength of the beam web above the end of the U-strips and below the flange be conservatively evaluated as

$$V_n = v_n b_w d \tag{6.6}$$

where v_n is given by Eq. 6.5a.

Two possible solutions are proposed here in the case that Eq. 6.6 predicts a shear strength lower than the expected demand. These solutions are shown in **Figure 6.5**. The first solution, shown in **Figure 6.5(b)** is to slit the flange, pass the U-strips across the slit and wrap them on top of the slab. The second solution is to use the U-side strips, anchor them with transverse rods anchored at both sides and to grout a vertical deformed reinforcement that crosses the failure plane and is developed beyond the transverse rod anchoring the side strips.

6.2.3.3 Development of the Laminates

The experimental work carried out in T-beams and described in Chapter 4 was conclusive in that the assumptions of longitudinal and transverse strain compatibility and that of perfect bond between bonded ACM laminates and the concrete are valid. This implies that the bond stress distribution between a laminate and the concrete can be determined by accounting for the effects of diagonal tension cracking of the concrete. The experimental work also showed the bond strength at the laminate-to-concrete surface interface was never critical as failure leading to delamination always took place in the concrete itself.

Figure 6.7 shows a free body diagram of a small element in a diagonally cracked

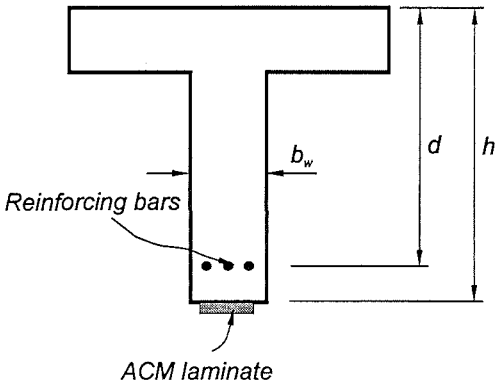

(a) Beam Cross Section

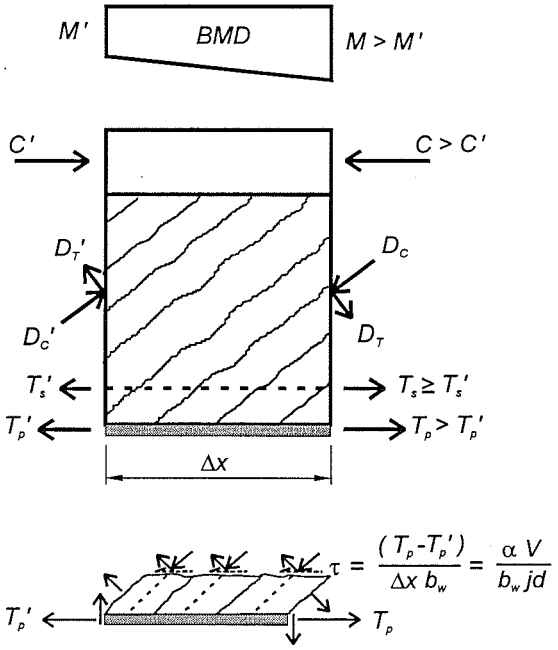

(b) Bond Stress in a Small Element

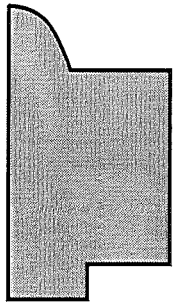

(c) Shear Stress Distribution when $T_s > T_s'$

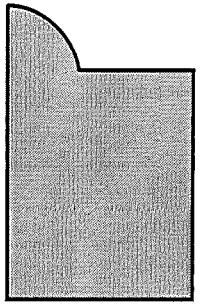

(d) Shear Stress Distribution when $T_s = T_s'$

Figure 6.7 Definition of Bond Stress

reinforced concrete T-beam in a region of combined bending moment and shear force. The beam has been retrofitted with bonded ACM laminates at the soffit. The bond stress in the concrete between the laminate and the horizontal longitudinal steel reinforcement can be determined as shown in **Figure 6.7(b)**. Unlike conventional reinforced concrete members with continuous reinforcing bars, in members retrofitted with continuous ACM laminates, the maximum bond stress does not necessarily occur in the region of maximum shear force. This is because the bond stress can be greater in a region of lower shear force where the reinforcing steel bars yield. This is clearly indicated by comparing the shear stress distributions shown in **Figures 6.7(c)** and **(d)**. The magnitude of the shear stress in the region between the laminate and the bars is equal to the bond stress.

When the steel reinforcing bars are stressed within the elastic limit the bar forces at either side of the element shown in **Figure 6.7(b)** are such that $T_s > T'_s$. As the ACM laminate is always elastic it is always expected in a region of combined bending moment and shear force that $T_p > T'_p$. As a result both the ACM laminate and the bars contribute to the change in bending moment in the element and hence, the shear stress diagram looks like that shown in **Figure 6.7(c)**. When the bars yield $T_s = T'_s$ the steel reinforcing bars cannot contribute to the change in bending moment in the element. Consequently, all the change in bending moment is due to the force difference in the ACM laminate at either side of the element. This results in the shear stress distribution shown in **Figure 6.7(d)** and in large bond stresses in the concrete between the laminate and the reinforcing bars.

The example shown in **Figure 6.8** illustrates the variation of bond stress in a simply supported weightless T-beam when loaded at midspan with a point load. It is evident that despite the shear force being constant along the beam span, the bond stress in the concrete between the laminate and the steel reinforcing bars is not constant. The maximum bond stress occurs in the length of the beam where the reinforcing bars are required to yield from points A-A' due to flexure, and longitudinal and transverse strain compatibility. Note that at the laminate ends some bond stress concentration is also expected to occur.

The bond stress distribution above ACM laminates in beams loaded at the ultimate limit state can be more complex than the distribution obtained for the beam shown in **Figure 6.8**. As an example, **Figure 6.9** illustrates the complex distribution of

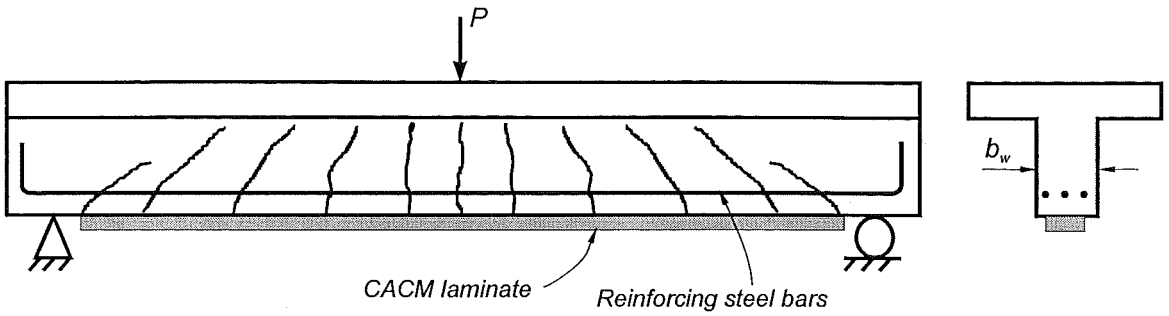

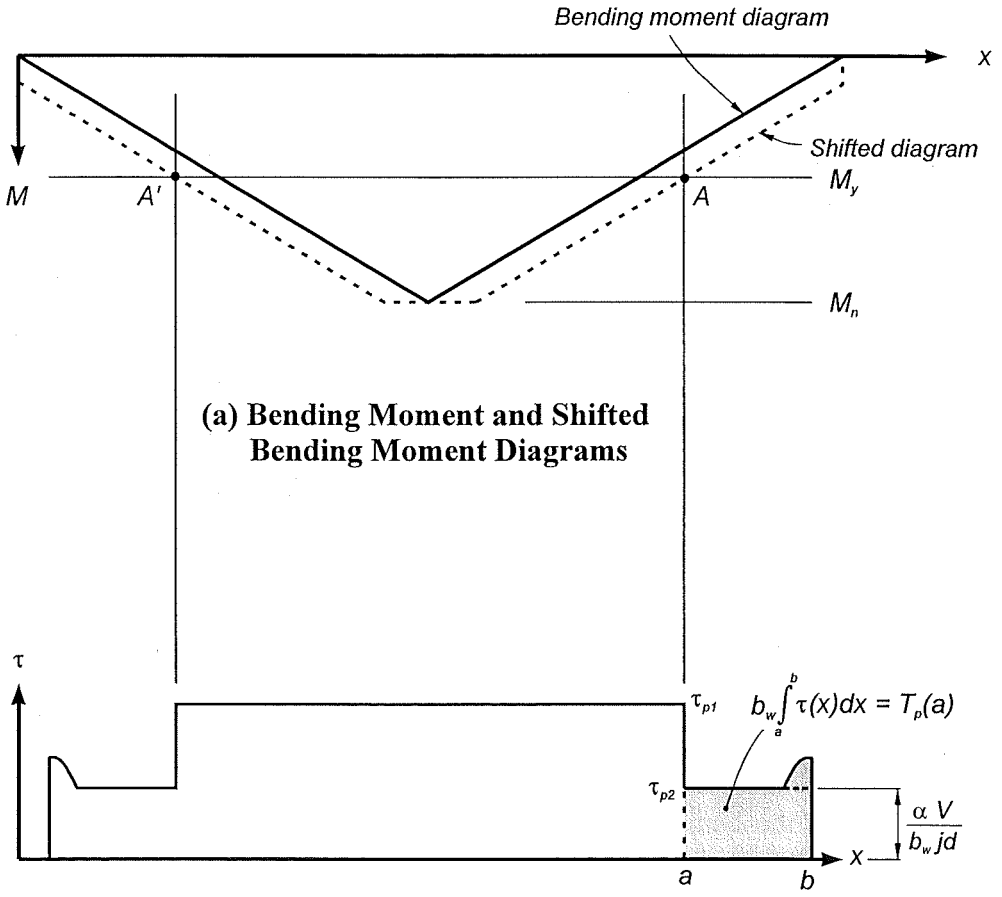

(a) Bending Moment and Shifted Bending Moment Diagrams

(b) CACM Laminate Bond Stress Distribution

Figure 6.8 An Example for Evaluation of CACM Laminate Bond Stress

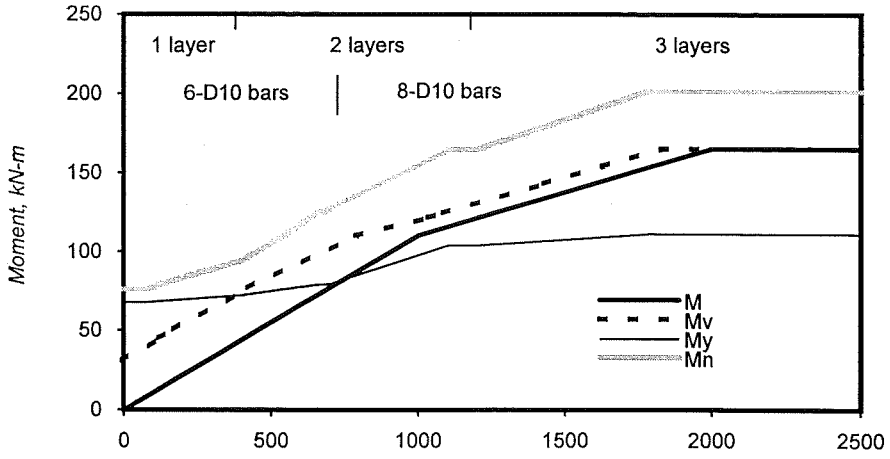

(a) Bending Moment and Shifted Moment Diagrams

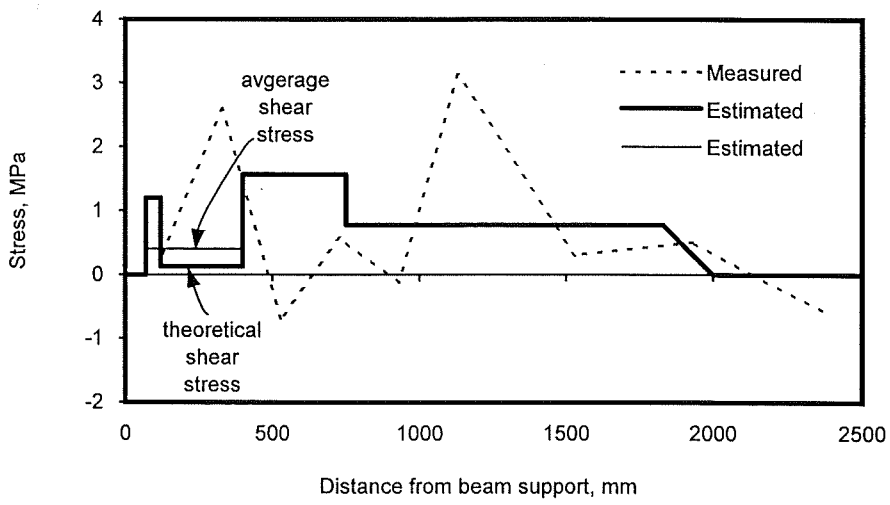

(b) Bond Stress Distribution

Figure 6.9 Estimated Concrete Bond Stress Distribution in Unit F6 when Loaded Close to Failure, F = 220 kN

bond stress near ultimate load, derived using the concept shown in **Figure 6.7**, of Unit F6 tested as part of Series-A in the experimental programme described in Chapter 4. The bond stress distribution can, close to ultimate load when bond failure is imminent, change significantly as the diagonal compression field that develops in the concrete above the laminate changes direction and redistributes these stresses. The beam shown in **Figure 6.8** shows clearly the concept of bond stress concentration at the laminate ends. The bond stress distribution can be determined according to the mechanistic approach shown in **Figure 6.8**. This bond stress is shown in this figure as $\frac{\alpha V}{b_w jd}$. Nonetheless, the bond distribution is such that the area under the bond stress diagram between points a and b in **Figure 6.8** must equal the laminate tensile force at section a, $T_p(a)$. Stress concentration is expected to develop at the laminate ends when the integral of the theoretical bond distribution $\frac{\alpha V}{b_w jd}(x_b - x_a)b_w$ is less than $T_p(a)$.

The use of the bond stress concept in design leads to tedious operations and a false sense of accuracy because bond redistribution cannot easily be considered in designing and the concentration of stress at the laminate ends cannot be assessed accurately, see **Figure 6.9**. A simple approach that makes use of average bond stresses is proposed in this study. It consists of using the development length concept briefly discussed in Section 4.9.2.4.

In the concept developed in Section 4.9.2.4 it was assumed that bond failure in a laminate always occurs in the concrete rather than in between laminates or at the concrete-to-laminate interface. The proposed basic development length equation based on this criterion is reproduced here for convenience:

$$l_{dp} = \frac{f_{pu} t_p b_p}{k\sqrt{f_c'}\, b_w} \qquad (6.7)$$

where f_{pu} is the tensile strength of the laminate, t_p is the laminate thickness, k is a bond strength factor, f'_c is the concrete compressive strength and b_w is the width of beam web. In the test presented in Chapter 4, k = 0.2 was adopted. However, it is recommended k =

0.17 can be used as a lower limit for design. Factor $0.17\sqrt{f_c'}$ can be interpreted as an average bond stress.

It is proposed here that development of the laminates follows the same principles as the development of steel longitudinal reinforcement in beams recommended by design standards. That is, the laminates must be extended a distance $l_{dp} + l'$ from the point where they are required for full strength or l' from the point where, according to the bending moment design envelope, they are not required to resist flexure. Term l' is the greater between the overall beam depth, h, and one-sixteenth of the beam span.

The experimental work discussed in Chapter 4 showed conclusively that U-side strips can effectively reduce the development length of a laminate. This is because less reliance is placed on the tensile strength of concrete to provide bond resistance. Hence, the development length of a laminate of a group of laminates can be smaller than the basic development length given by Eq. 6.7 if the laminates are clamped with U-side strips. The amount of transverse reinforcement in the way of U-side strips can be evaluated using the modified shear friction concept proposed by Walraven et al. [W2] and shown in Eq. 6.5a. This is achieved by substituting the shear stress v_n in this equation by:

$$v_n = 0.17\sqrt{f_c'}\,\frac{l_{dp}}{l_p} \tag{6.8}$$

In other words, Eq. 6.8 suggests that bond stresses increase in proportion to the ratio of the basic development length l_{dp} associated with an average bond stress of $0.17\sqrt{f_c'}$ to the available development length l_p.

Replacing Eq. 6.8 into Eq. 6.5a, making $f_{vsy} = f_{vpe}$ and solving for ρ_{vp}, we obtain:

$$\rho_{vp} = \frac{1}{f_{vpe}}\left(0.17\sqrt{f_c'}\,\frac{l_{dp}}{l_p} \times \frac{1}{C_1}\right)^{1/C_2} \tag{6.9a}$$

and

$$A_{vp} = \rho_{vp} b_w s_{vp} \tag{6.9b}$$

Term l_{dp} is the basic development length and term l_p is the available development length for the ACM laminate, respectively. Coefficients C_1 and C_2 can be referred to Eqs. 6.5c and 6.5d. The effective transverse stress for the ACM U-strip, $f_{vpe} = 0.004E_{vp}$, is recommended. Then, the number of U-side strips for bond strength enhancement of the longitudinal ACM laminate is obtained using the relationship of Eq. 6.9. The design procedure for the ACM laminate bond enhancement using the ACM U-side strip is shown in **Figure 6.10**.

It is also recommended that minimum transverse reinforcement in the way of U-side strips anchored below the flange in T-beams be provided at the cut-off points. This is to prevent accidental debonding at this region. In lieu of any test data, it is suggested that the minimum U-side strip be designed to resist, at the development of a tensile strain of the U-side strip equal to 0.004, one-twentieth of the ultimate tensile force of the longitudinal laminates being cut-off. This concept is mathematically expressed below,

$$A_{vp,\min} = \frac{A_{p,cut} f_{pu}}{20 \times 0.004 E_{vp}} \tag{6.10}$$

where, $A_{vp,\min}$ is the minimum cross section area of the U-side strip bonded at the cut-off point of the longitudinal laminate, $A_{p,cut}$ is the area of the longitudinal laminate being cut-off, f_{pu} is the ultimate tensile strength of the longitudinal ACM laminate and E_{vp} is the elastic modulus of the ACM U-side strip.

6.2.4 Design Example

The service live load is to be increased on a two-lane bridge. The bridge has simply supported 12.8 m long spans as shown in **Figure 6.11**. The girders are spaced 2.5 m apart. The deck of the bridge is 200 mm thick. General reinforcing details of the bridge are shown in **Figure 6.11.** The measured material properties are f_{sy} = 290 MPa for the longitudinal reinforcement, f_{vsy} = 272 MPa for the transverse reinforcement and f_c' = 45

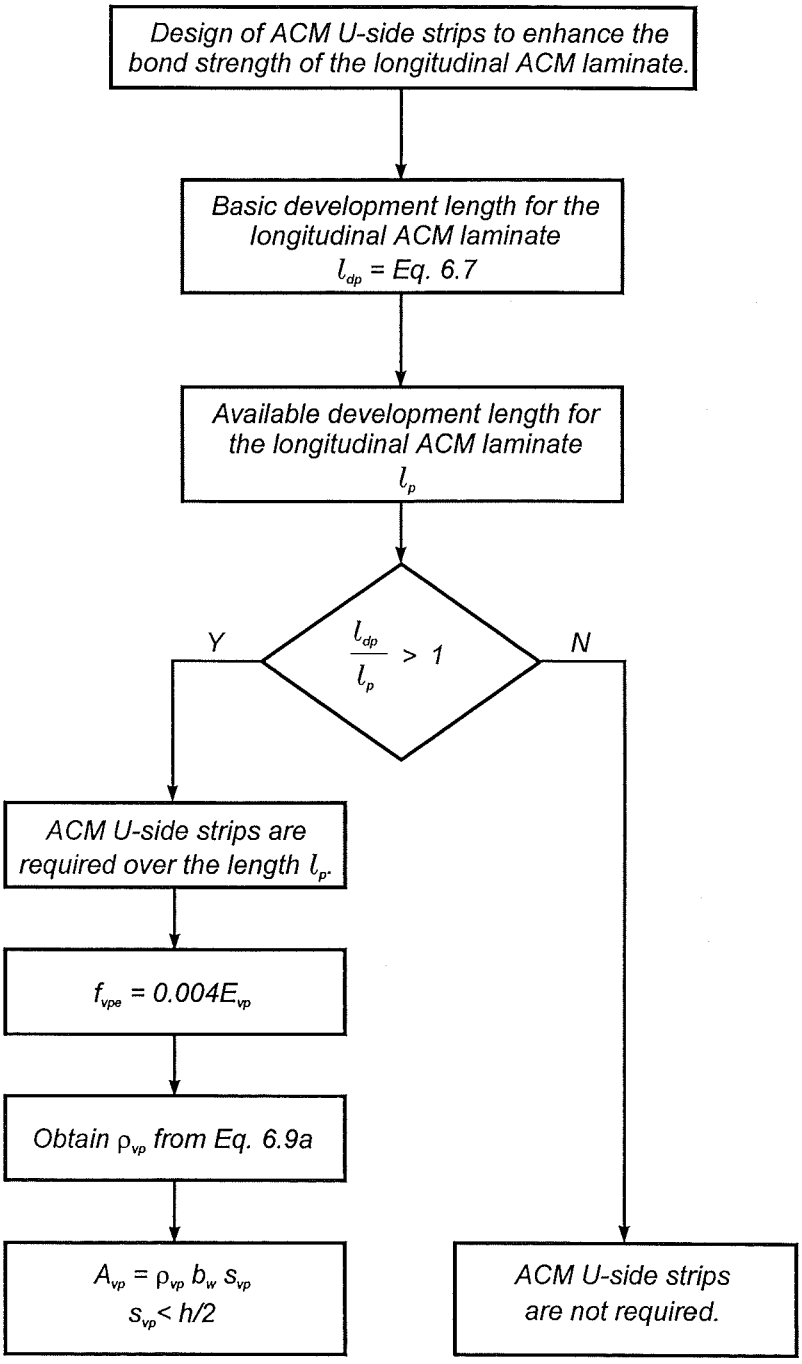

Figure 6.10 Design Flowchart for the Bond Strength Enhancement of the Longitudinal ACM Laminate

MPa. Unidirectional CACM laminates with E_p = 63 GPa and f_{pu} = 630 MPa and GACM strips with E_{vp} = 20 GPa and f_{vpu} = 400 MPa will be bonded to the soffit and the sides of the beam to retrofit the bridge. The service and ultimate design actions obtained from the structural analysis for the upgraded bridge are:

Service dead load bending moment: M_D = 380 kN-m
Service live load + impact bending moment: $M_{L\&I}$ = 1.25 MN-m
Ultimate bending moment: M_u = 3.22 MN-m
Ultimate shear force: V_u = 500 kN

Strength reduction factors for flexure and shear for the retrofit are to be taken equal to 0.85 and 0.75, respectively.

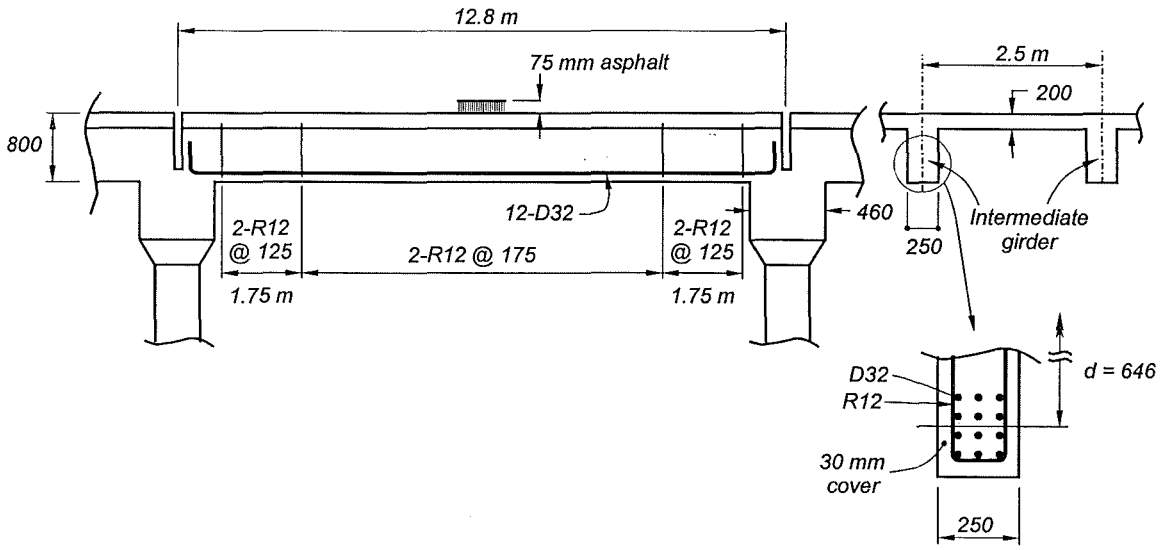

Figure 6.11 General Reinforcing Details of the Two Lane Bridge

Solution

(1) Design for Flexure

Use 220 mm wide CACM laminates bonded to the soffit of the beam. The girder is to be jacked up for applying the CACM laminate with some of upward dead load so that $\varepsilon_{s0} = 0.0001$, see **Figure 6.1(b)**.

Calculation of area of laminates required at the ultimate limit state

Dependable bending moment provided by the reinforcing steel, using d = 646 mm.

$$\phi M_{ns} = 1.43 \text{ MN-m}$$

Bending moment shortfall to be provided by the laminates.

$$\phi M_{np} = 3.22 - 1.43 = 1.79 \text{ MN-m}$$
$$\text{for } \phi = 0.85,\ M_{np} = 2.11 \text{ MN-m}$$

Using strain compatibility, it can be found that the ultimate tensile strain of the laminate controls the design and the amount required is $A_{pl} = 4{,}186 \text{ mm}^2$. Note that the strain ε_{s0} caused by the girder jack-up does not affect the calculation result at the ultimate limit state.

Calculation of area of laminates required at the service limit state

Service load bending moment, $M = M_D + M_{L\&I} = 1.63$ MN-m

A strain compatibility analysis, including long term effects, shows that the tensile strain in the longitudinal reinforcement due to service dead load is $\varepsilon'_{so} = 0.00038$.

Find the area of laminates with $\varepsilon_{s0} = 0.0001$. Adopting Eq. 6.1 and using trial and error, we obtain:

$$\varepsilon_{sD} = 0.000323 \qquad \text{Eq. 6.1b}$$

$$\varepsilon_{pD} = 0.000276 \qquad \text{Eq. 6.1e}$$

$$\varepsilon_{s} = 0.001233 \qquad \text{Eq. 6.1c}$$

$$\varepsilon_{p} = 0.001127 \qquad \text{Eq. 6.1d}$$

and

$$A_{p2} = 5{,}157 \text{ mm}^2 \qquad \text{Eq. 6.1a}$$

Therefore, the design for flexure is controlled by the service load requirement since $A_{p2} > A_{p1}$. Then, $A_p = \text{Max}\,(A_{p1}, A_{p2}) = 5{,}157 \text{ mm}^2$.

Use 23-220 mm wide by 1.04 thick SCH-41 CACM laminates.

(2) Development of the CACM Laminates

The basic development length of the CACM laminate is

$$l_{dp} = \frac{630 \times 1.04 \times 220}{0.17\sqrt{45} \times 250} = 506 \text{ mm} \qquad \text{Eq. 6.7}$$

and the basic development length for three, five and six laminates is 1.52, 2.53 and 3.04 m, respectively.

The laminates are to be extended a distance h = 800 mm or $l/16$ (l = 12.8 m) = 800 mm, whichever is greater, for the point where they are no longer required to resist flexure or l_{dp} + h for the point where is required for full strength. **Figure 6.12** shows the layout of the laminates. As the available anchorage length l_p for the five innermost is less than the basic development length l_{dp}, see **Figure 6.12**, U-side strips are required to enhance the anchorage condition. Therefore, refer the design flowchart presented in **Figure 6.10**,

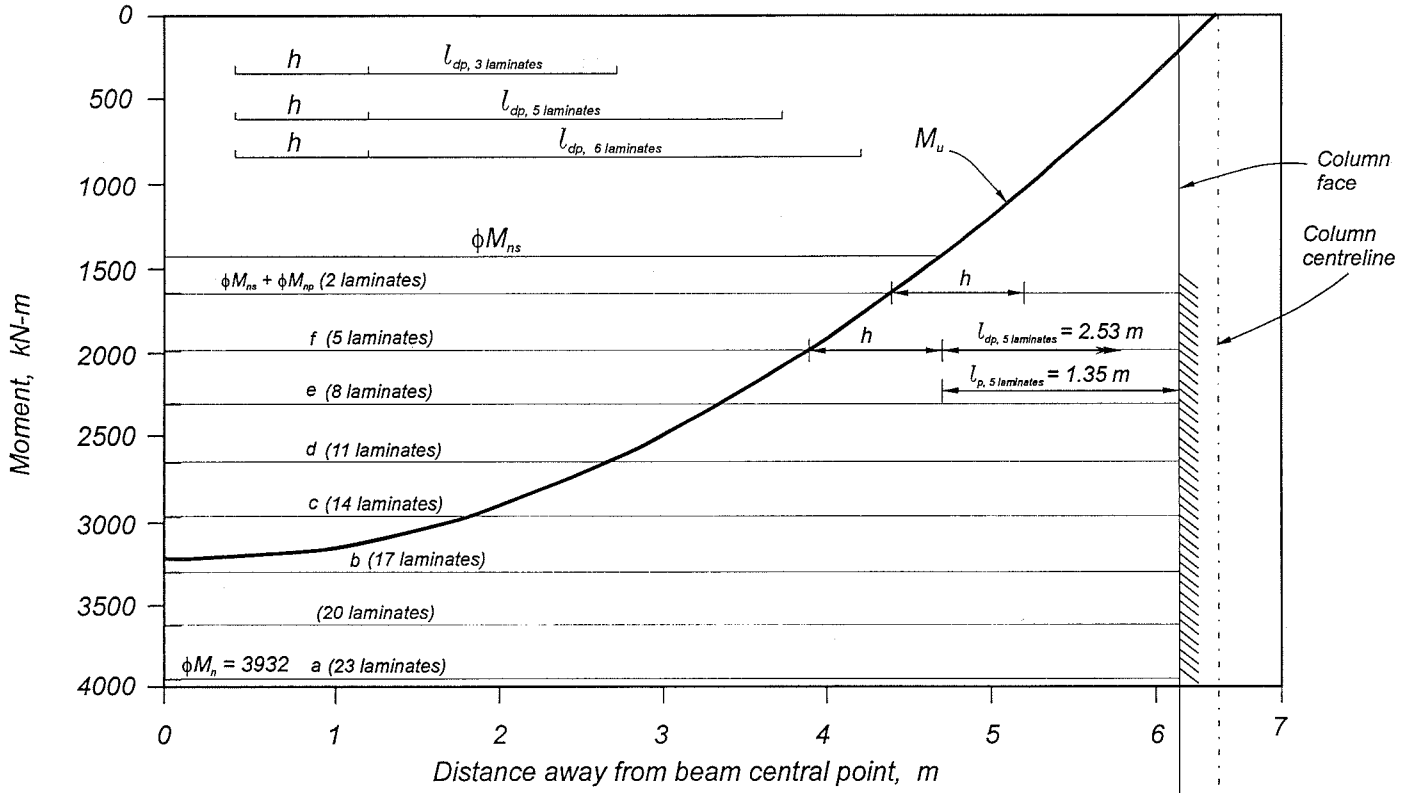

(a) Design Bending Moment Diagram

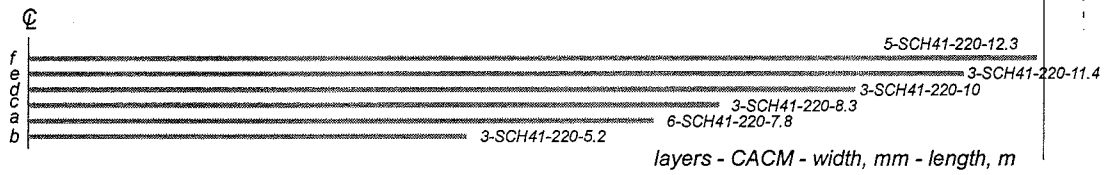

(b) Laminate Layout

Figure 6.12 Design of Staggered CACM Laminates

$l_{dp} = 2.53$ m for five CACM laminates

$l_p = 1.35$ m

$\frac{l_{dp}}{l_p} = 1.87 > 1$, U-side strips are required

Then, $f_{vpe} = 80$ MPa, $C_1 = 2.75$ and $C_2 = 0.47$ obtained from Eqs. 6.5c and 6.5d.

$\rho_{vp} = 0.00731$ Eq. 6.9a

Try using 120 mm wide by 1.27 mm thick GACM U-side strips and solve s_{vp}.

$s_{vp1} = 167$ mm $< h/2$ √

The GACM U-side strip added at the CACM laminate cut-off points should be checked. Therefore, design for the cut-off points of three and six laminates, the minimum area of the U-side strip can be obtained from Eq. 6.10 as

$$A_{vp1,\min} = \frac{3 \times 1.04 \times 220 \times 630}{20 \times 0.004 \times 20000} = 270 \text{ mm}^2 \text{ for 3-laminate cut-off}$$

and

$$A_{vp2,\min} = 541 \text{ mm}^2 \text{ for 6-laminate cut-off}$$

Thus, use 120 mm wide by 1.27 mm thick (single layer) GACM U-side strips at the cut-off points of three laminates as $A_{vp} = 305$ mm$^2 > A_{vp1,\min}$ and use 120 mm wide by 2.54 mm thick (double layers) GACM U-side strips at the cut-off points of six and five laminates as $A_{vp} = 610$ mm$^2 > A_{vp2,\min}$.

(3) Design for Shear

Only the shear design in the region of the beam where stirrups are spaced at 125 mm apart is discussed in this example.

So, check for a diagonal compression failure,

$$\frac{V_u}{\phi b_w d} = 4.1\,\text{MPa} \;<\; 9\,\text{MPa} \qquad \surd$$

$$= 0.092 f_c' \;<\; 0.2 f_c' \qquad \surd$$

$$= 0.62\sqrt{f_c'} \;<\; 1.1\sqrt{f_c'} \qquad \surd$$

The nominal shear strength provided by the concrete and transverse steel mechanisms only is obtained from Eq. 6.3:

$$V_n = 614\ \text{kN and } \phi V_n = 460\ \text{kN} < V_u = 500\ \text{kN}$$

Thus, GACM U-side strips are required to increase the shear resistance. So, check whether it is possible to use partial height U-side strips:

from Eq. 6.5, using $\rho_v = 0.00904$, $v_n = 4.2$ MPa
and from Eq. 6.6, $V_n = 678$ kN and $\phi V_n = 509\ \text{kN} > V_u = 500$ kN $\surd$

Hence U-side strips can be anchored immediately below the deck of the bridge.

The area of U-side strips is obtained from Eqs. 6.3 and 6.4

$$\phi \frac{A_{vp} f_{vpe}}{s_{vp}} h_{vp} = (500 - 460) \times 10^3$$

For GACM strips with $E_{vp} = 20$ GPa, the design stress corresponding to $\varepsilon_{vpe} = 0.004$ is $f_{vpe} = 80$ MPa. Try using 120 mm wide by 1.27 mm thick GACM strips with $h_{vp} = 550$ mm. Solving above equations for s_{vp}.

$$s_{vp2} = 251\ \text{mm} \;<\; h/2 \qquad \surd$$

Thus, the design of U-side strips is governed by the development of CACM

laminates as $s_{vp} = \text{Min}\ (s_{vp1}, s_{vp2}) = 167$ mm

Finally, use 120 mm wide by 1.27 mm thick (single layer) GACM U-side strips at 165 mm centre-to-centre. Anchor the strip ends using glass anchor filaments, see **Figure 6.13**.

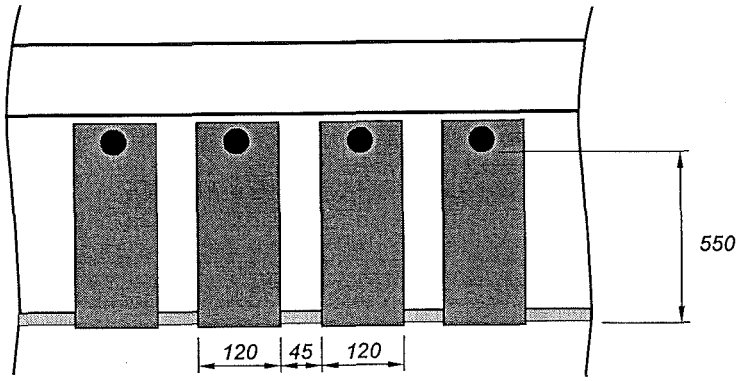

Figure 6.13 Arrangement of GACM U-Side Strips

6.3 Seismic Retrofit of Beams with Longitudinal Bar Cut-off Deficiencies

The design concept for beams forming part of a lateral load resisting frame and showing longitudinal bar anchorage deficiencies leading to a potential flexure-shear failure in a region of the beam not detailed for ductility is to force the plastic hinge to develop at the column face. Section 5.8 discussed a method for assessing the lateral load resistance of a beam. The method can be used to determine the location where plastic hinges are likely to form, particularly for negative plastic hinges that may form in a beam away from the column faces. This is most common in older buildings as a result of the presence of slab reinforcement and of poor development of the longitudinal reinforcement in the beam.

To shift a negative plastic hinge from the deficient region to the beam end it is necessary to increase both the flexural and shear strength there. The strength enhancement can be achieved by either using GACM or CACM longitudinal laminates

and U-side strips. The flexural strength deficiency in this region should be evaluated using capacity design principles [P1, P4, P6]. This involves the evaluation of the most likely flexural strengths that will develop in the positive and shifted negative plastic hinges in the beam span.

To avoid excessive shear deformations in the strengthened region, it is proposed here that the longitudinal strain in the laminate be equal or less than 0.004 and using the same procedure described in Section 6.2.3.1. The development of the laminates should follow the same principles discussed in previous section. The deficient region should also be checked for shear. The shear force demand should be evaluated from the most likely flexural strengths that will develop in the negative and shifted positive plastic hinges, thus following capacity design requirements. U-side strips should be provided according to Section 6.2.3.2 if required.

6.4 Conclusions

This chapter presents a design approach for reinforced concrete beams strengthened with externally bonded ACM laminates. The method proposed can be used to incorporate staggered ACM laminates in the retrofit.

One important factor associated in the design is that not only the ultimate limit state but also the serviceability limit state should be satisfied in the design of retrofit schemes for bridges. This is because the design of the longitudinal laminates may be governed by the serviceability limit state requirements.

Design recommendations for both the serviceability and ultimate limit states are developed in this chapter. The recommendations given here discuss the design for flexure, shear and the development of the laminates.

The design concept for beams forming part of a lateral load-resisting frame and showing longitudinal bar anchorage deficiencies leading to a potential flexure-shear failure in a region of the beam not detailed for ductility is mentioned. To shift the plastic hinge from the deficient region to the beam end it is necessary to increase both the

flexural and shear strength of the beam. Therefore, the strength enhancement in both flexure and shear can be achieved by either using GACM or CACM longitudinal laminates and U-side strips.

Finally, a design example is discussed to show the application of the simple design method.

PART III

RETROFIT OF REINFORCED CONCRETE COLUMNS

CHAPTER 7

THEORETICAL ANALYSIS OF CONCRETE COLUMNS CONFINED BY FIBRE COMPOSITES

7.1 General

Strengthening of reinforced concrete columns subjected to high axial load ratio levels is a challenge a structural engineer often faces. Low concrete strengths combined with poor site curing conditions may result in axial load ratios in individual columns of multi-storey buildings being much higher than those that were anticipated during design.

There are several ways to enhance the axial load capacity of columns with strength deficiencies. One of them is through passive confinement of the concrete. As the ultimate load is approached, the concrete in the column dilates and exerts pressure on the confining element. This interaction leads to a triaxial state of stress in the concrete core of the column that results in an increase of the ultimate compressive strength of the concrete. Thus, the axial load carrying capacity of the column is also increased. Confinement of the concrete also substantially increases the deformation capacity of reinforced concrete columns, changing their mode of failure from brittle to ductile.

This chapter presents equations for monotonic compression loading to determine the stress-strain relationship of reinforced concrete columns subjected to axial compression. The analytical method revises the recommendations proposed by Restrepo and DeVino [R3] to evaluate the axial load carrying capacity of short reinforced concrete rectangular columns account for the dual confinement effect provided by an external ACM jacket and internal steel hoops. The objective of this analytical study is to provide predictions to the experiments conducted in Chapter 8 and to propose design recommendations, described in Chapter 9, for use in practice.

7.2 Evaluation of the Axial Compressive Load – Axial Deformation Response

Figure 7.1 shows a cross section of a reinforced concrete rectangular column that is confined by an external jacket and by internal reinforcing steel hoops. The jacket confines the column core introducing pressure through the rounded corners. It is assumed that the jacket is reinforced only in one direction and is applied to the column to act as confining reinforcement. The reinforcing steel hoops introduce the confining pressure at the nodes between hoops and the column longitudinal reinforcements. In the concrete confined by ACM jacket, arching action occurs in the horizontal direction only, whereas in the concrete confined by steel hoops, arching action occurs in two directions. It should be noted that when both sources of confinement are present, a large area of the concrete core may be confined by both the jacket and the reinforcing steel hoops.

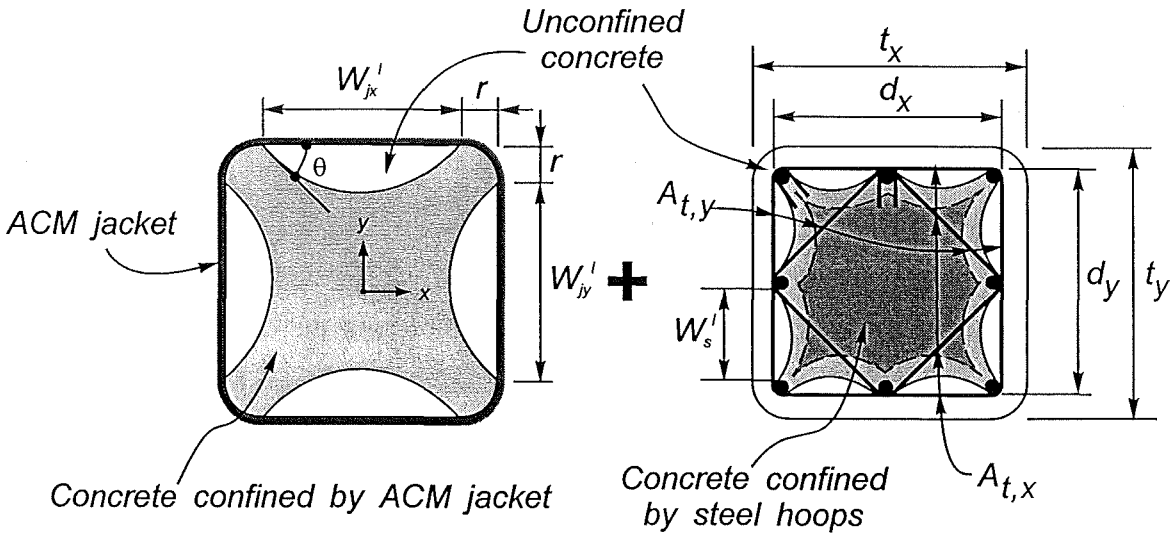

Figure 7.1 Dual Confinement Effect on a Rectangular Column with a ACM Jacket and Internal Steel Hoops

The concentric compressive load of a short reinforced concrete column, P, is given by

$$P = P_c + P_s \tag{7.1a}$$

where

$$P_s = f_s A_s \tag{7.1b}$$

and

$$\begin{aligned} P_c &= P_{c0} + P_{cc,j} + P_{cc,js} \\ &= f_{c0} A_{cu} + f_{cc,j} A_{cj} + f_{cc,js} A_{cjs} \end{aligned} \tag{7.1c}$$

where P_c and P_s are the compressive loads carried by the concrete and the longitudinal reinforcing bars, respectively. A_s is the area of longitudinal reinforcement and f_s is the compressive stress in longitudinal reinforcement.

To evaluate the compressive stress of longitudinal reinforcement in the column, the monotonic stress-strain model of reinforcing steel, proposed by Dodd and Restrepo [D3], is adopted. This model can be used to convert a given history of column axial strain in compression into the compressive stress-strain relationship of longitudinal reinforcement. Thus, it is assumed that the strain in the concrete of the column is equal to the strain in the longitudinal reinforcement. However, for the purpose of design the steel in compression can be assumed to be a simple model that behaves as an elasto-plastic material. Therefore $f_s \leq f_{sy}$, where f_{sy} is yield strength of longitudinal reinforcement.

The compressive load carried by the concrete, P_c, results from the loads sustained by three distinct regions. In Eq.7.1c, P_{c0} is the load carried by the unconfined concrete area, A_{cu}, and f_{c0} is the compressive stress of unconfined concrete. $P_{cc,j}$ is the load carried by the effective area of concrete confined by the ACM jacket, A_{cj}, and $f_{cc,j}$ is the compressive stress of concrete confined by the ACM jacket. $P_{cc,js}$ is the load carried by the effective area of concrete confined by both the ACM jacket and the steel hoops, A_{cjs}, and $f_{cc,js}$ is the corresponding stress. Hence, the entire uniaxial stress-strain relationship for a concentrically loaded column wrapped with an ACM jacket can be obtained if the stress-strain relationships for each of the region and for the reinforcing steel are known.

The short term compressive strength of concrete in columns with significant confinement can be determined analytically using refined models. In the analytical study,

f_{c0}, $f_{cc,j}$, and $f_{cc,js}$ are evaluated using a stress-strain model proposed by Mander et al. [M10]. A general approach to calculate a stress-strain relationship for confined concrete has been described in Section 2.3.1.

The area of effective confining core confined by the steel hoops and a jacket can be found considering parabolic arching which takes place between two steel hoops in vertical direction and between two longitudinal bars restrained by the hoops in the transverse direction. The evaluation method proposed by Sheikh and Uzumeri [S13] and refined by Mander et al. [M11] is adopted here. These areas of effective confining core are given by the following expressions,

$$A_{cu} = A_{cc,j} - A_{e,j} \tag{7.2}$$

$$A_{cj} = A_{e,j} - A_{e,s} \tag{7.3}$$

$$A_{cjs} = A_{e,s} \tag{7.4}$$

where $A_{cc,j}$ is the area of concrete confined by the jacket, $A_{e,j}$ is the area of concrete effectively confined by the jacket, and $A_{e,s}$ is the area of concrete effectively confined by the steel hoops.

In the case of a rectangular column, the above areas, $A_{cc,j}$, $A_{e,j}$, and $A_{e,s}$, are given by,

$$A_{cc,j} = t_x t_y - A_s - (4r^2 - \pi r^2) \tag{7.5}$$

$$A_{e,j} = t_x t_y - \frac{w'^{\,2}_{jx} + w'^{\,2}_{jy}}{3} \tan\theta - A_s - (4r^2 - \pi r^2) \tag{7.6}$$

$$A_{e,s} = \left(d_x d_y - \sum \frac{w'^{\,2}_{s}}{6} \right) \left(1 - 0.5 \frac{s'}{d_x} \right) \left(1 - 0.5 \frac{s'}{d_y} \right) \tag{7.7}$$

Figure 7.1 defines the variables used in above equations. The term s' is the clear distance between consecutive sets of steel hoops. It is assumed that the core area confined by the internal steel hoops is restrained within the area confined by the external jacket. Angle θ in Eq.7.6 can be derived using experimental work. Also, the area of concrete effectively

confined by the jacket, $A_{e,j}$, is limited by $w'_{jx} < 2w'_{jy}$ when the longer side is w'_{jx} or by $w'_{jy} < 2w'_{jx}$ when the longer side is w'_{jy}.

In the case of a circular column, see **Figure 7.2**,

$$A_{cc,j} = A_{e,j} = \frac{\pi D^2}{4} - A_s \tag{7.8}$$

$$A_{e,s} = \frac{\pi d_s^2}{4}\left(1 - 0.5\frac{s'}{d_s}\right)^2 \tag{7.9}$$

where D is overall column diameter and d_s is the diameter of steel hoops. It can be seen that $A_{cc,j} = A_{e,j}$ makes $A_{cu} = 0$ and consequently the confined effectiveness of circular column is greater than that for a rectangular column.

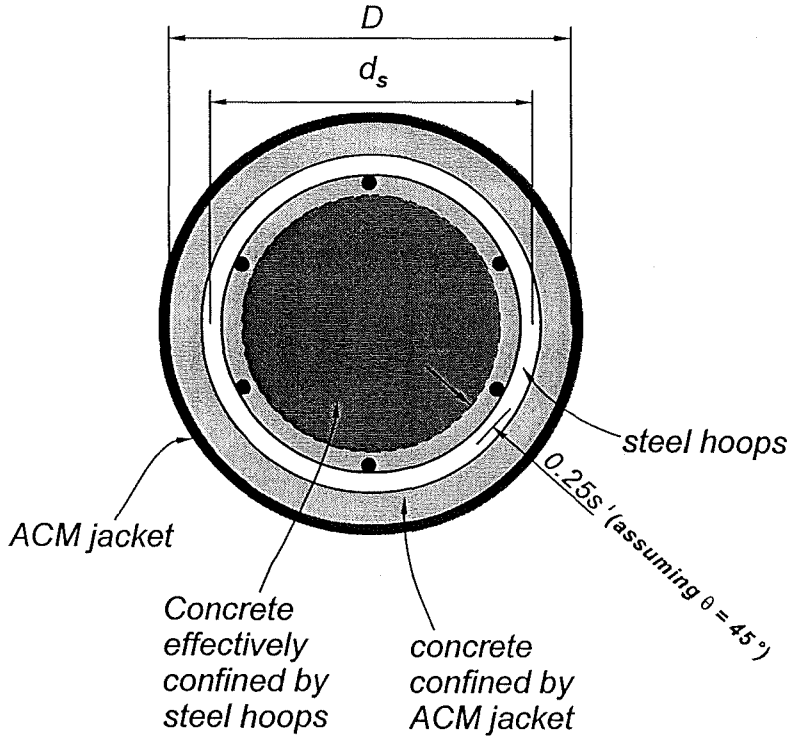

Figure 7.2 Dual Confinement Effect on a Circular Column with a ACM Jacket and Internal Steel Hoops

7.3 Compressive Strength of Confined Concrete

The compressive strength of confined concrete, f'_{cc}, is given by,

$$f'_{cc} = k_c f'_c \tag{7.10}$$

in which f'_c is the cylinder concrete compressive strength and k_c is the concrete strength enhancement factor. Factor k_c depends on the biaxial state of stresses induced by the lateral confining pressures. This factor is given by,

$$k_c = \alpha_1 \alpha_2 \tag{7.11}$$

where α_1 is a strength enhancement factor that considers the concrete to be subjected to a triaxial stress state with bi-equal confining stresses and α_2 is a reduction factor that considers any deviation from the bi-equal confining stress concept.

Therefore, α_1 is same as the expression proposed by Mander et al. [M11], and shown in Eq. 2.19, is repeated here for convenience,

$$\alpha_1 = 1.25\left(1.8\sqrt{1+7.94\frac{F_l}{f'_c}} - 1.6\frac{F_l}{f'_c} - 1\right) \tag{7.12a}$$

For α_2 Mander et al. proposed an iterative solution, see **Figure 2.13**. It is proposed here that this factor can be calculated with the following closed form equation,

$$\alpha_2 = \left[1.4\frac{f_l}{F_l} - 0.6\left(\frac{f_l}{F_l}\right)^2 - 0.8\right]\sqrt{\frac{F_l}{f'_c}} + 1 \tag{7.12b}$$

In the above equations, F_l and f_l are the maximum and minimum confining lateral stresses, respectively.

7.4 Evaluation of the Dual Lateral Confining Pressure

To calculate the concrete strength enhancement factors, see Eq.7.12, the lateral confining pressure must be found. The evaluation of the lateral confining pressure due to an elastic jacket and internal reinforcing steel hoops for rectangular and circular columns is derived below.

7.4.1 Confinement Provided by the ACM Jacket Only

Rectangular Columns

The lateral confining stresses induced by ACM jacket in the x and y directions, $f_{l,jx}$ and $f_{l,jy}$, are,

$$f_{l,jx} = \rho_{jx} f_j \tag{7.13a}$$

$$f_{l,jy} = \rho_{jy} f_j \tag{7.13b}$$

where f_j is the stress in the jacket. The reinforcement ratios ρ_{jx} and ρ_{jy} are defined as,

$$\rho_{jx} = 2\frac{t_j}{t_y} \tag{7.14a}$$

$$\rho_{jy} = 2\frac{t_j}{t_x} \tag{7.14b}$$

where t_j is the nominal jacket thickness and t_x and t_y are the overall column cross section dimensions.

Circular Columns

The lateral confining stress induced by the jacket, $f_{l,j}$, is,

$$f_{l,j} = \rho_j f_j \tag{7.15}$$

where f_j is the stress in the jacket. The confinement reinforcement ratio ρ_j is defined as,

$$\rho_j = 4\frac{t_j}{D} \tag{7.16}$$

where t_j is the nominal jacket thickness and D is the overall column diameter.

7.4.2 Confinement Provided by the Transverse Steel Hoops Only

Rectangular Columns

The lateral confining stresses induced by the steel hoops in the x and y directions, $f_{l,sx}$ and $f_{l,sy}$, are,

$$f_{l,sx} = \rho_{sx} f_{sh} \tag{7.17a}$$

$$f_{l,sy} = \rho_{sy} f_{sh} \tag{7.17b}$$

where f_{sh} is the stress in the hoops.

The confinement reinforcement ratio ρ_{sx} and ρ_{sy} are defined as,

$$\rho_{sx} = \frac{A_{t,x}}{sd_y} \tag{7.18a}$$

$$\rho_{sy} = \frac{A_{t,y}}{sd_x} \tag{7.18b}$$

in which d_x and d_y are the distances between the centre lines of the perimeter hoop in the x and y directions, respectively. $A_{t,x}$ and $A_{t,y}$ are areas of transverse steel reinforcement parallel to the x and y-axis, respectively. s is the spacing between sets of hoops.

Circular Columns

The lateral confining stress induced by the steel hoops, $f_{l,s}$, is,

$$f_{l,s} = \rho_s f_{sh} \tag{7.19}$$

The reinforcement ratio ρ_s is defined as,

$$\rho_s = 4\frac{A_b}{sd_s} \tag{7.20}$$

where A_b is the area of steel hoops and d_s is the hoop diameter.

7.4.3 Combined Confinement due to the ACM Jacket and the Transverse Steel Hoops

The lateral confining stress acting upon area $A_{cc,j}$ due to both confining materials is equal to,

$$f_l = f_{l,s} + f_{l,j} \tag{7.21}$$

Then, the confined concrete compressive strength of the area of the column solely confined by the jacket, $f'_{cc,j}$ is found substituting Eq.7.13 or Eq.7.15 into Eq.7.10 or Eq.7.11 for rectangular and circular columns, respectively. Furthermore, the confined concrete compressive strength of the area of the column confined by the jacket and the transverse steel reinforcement, $f'_{cc,js}$ is found substituting Eq.7.21 into Eq.7.10 or Eq.7.11 for rectangular and circular columns, respectively.

7.5 Analytical Procedure

The prediction of the complete response of a concentrically loaded column confined with steel hoops and a ACM jacket can be computed with the following procedure:

(1) Give a longitudinal strain, ε_a.

(2) Evaluate a moderate lateral strain, ε_l.

It is assumed that the lateral strain in the concrete surface of the column and the strain in the jacket are compatible. No bond slip in the interface between concrete and composite material is considered. A relationship between longitudinal and lateral strain is obtained through a model refined using an experimental work. This is because microcracking develops when the axial load level nearly reaches the unconfined concrete strength and concrete dilation becomes significant. Moreover, the dilation ratio, the ratio of lateral strain to longitudinal strain, varies depending on the concrete strength, the applied axial load level, and the stiffness of confining material used. Such relationship is discussed in Chapter 8.

(3) Calculate the lateral stresses of the steel hoops, f_{sh}, and the ACM jacket, f_j, as,

$$f_{sh} = E_s \varepsilon_l \leq f_{yh} \tag{7.22}$$

$$f_j = E_p \varepsilon_l \leq f_{pu} \tag{7.23}$$

where E_s and E_p are the elastic modulus of steel and the ACM, respectively. f_{yh} is the yield strength of steel and f_{pu} is the ultimate strength of the ACM.

(4) Calculate the lateral confining pressure provided by the jacket and by the steel hoops from Eq.7.13 or Eq.7.15 for the jacket and from Eq.7.17 or Eq.7.19 for the steel hoops.

(5) Combine the lateral confining pressure due to the jacket and the steel hoops using Eq.7.21.

(6) The compressive strengths of confined concrete due to the confinement of the jacket, $f'_{cc,j}$, and the confinement of both the jacket and the steel hoops, $f'_{cc,js}$, can be obtained using Eq.7.10.

(7) Calculate the axial compressive stresses due to unconfined concrete, f_{c0}, confined concrete provided by the jacket, $f_{cc,j}$, and confined concrete provided by both the jacket and the steel hoops, $f_{cc,js}$.

To calculate these compressive stresses at a given axial strain, ε_a, Eqs.2.5 to 2.9 are used.

(8) Calculate concrete components of the axial load, P_{c0}, $P_{cc,j}$, and $P_{cc,js}$, resulting from the different concrete cores, A_{cu}, A_{cj}, and A_{cjs}, from Eqs.7.1 to 7.9. Then the compressive load carried by the concrete of the column, P_c represented in Eq. 7.1c, can be obtained.

(9) Determine the stress in the longitudinal reinforcing steel f_s corresponding to the longitudinal strain ε_a by using a theoretical stress-strain model. The compressive load carried by the longitudinal reinforcing bars P_s is obtained from Eq.7.1b.

(10) The concentrically compressive load of a short reinforced concrete column P at the given strain ε_a is calculated. Return to Step 1 and proceed with another value for ε_a.

7.6 Conclusion

This chapter discusses a theoretical approach for evaluating the enhancement of the axial compression load of column by means of advanced composite material jackets.

The proposed model builds upon an approach used for evaluating the compressive strength of concrete columns confined by steel hoops only. This original model was proposed by Mander et al. [M10, M11]. The proposed analytical model develops closed-form equations that can be used by hand calculation to determine the concentric load versus longitudinal strain of the strengthened reinforced concrete columns.

The model requires a relationship between the transverse and longitudinal strains as well as the extent of arching of the concrete that define the regions subjected to different lateral confinement. These parameters are discussed in Chapter 8.

CHAPTER 8

TESTS ON CONCENTRICALLY LOADED REINFORCED CONCRETE COLUMNS CONFINED WITH FIBREGLASS/EPOXY JACKETS

8.1 Introduction

Although fibreglass/epoxy jackets have been shown in flexural tests to enhance ductility capacity of both circular and rectangular columns, limited data is available on the behaviour of columns loaded under concentric compression. In some cases, columns are found to have low concrete compressive strengths, which result in a high axial load ratio. The capacity of such columns can be enhanced by means of passive confinement of the column through the use of an external jacket. In addition, the behaviour of concentrically loaded columns, retrofitted with an external jacket, allows the identification mechanism of passive confinement and the calibration of a suitable, yet simple, theoretical model such as that discussed in the previous chapter. The proposed model requires a relationship between transverse and longitudinal strain as well as the extent of arching of the concrete.

In order to obtain the relationship required by the proposed analytical model, a test programme was established to examine the axial stress-strain characteristics of rectangular reinforced concrete columns confined by steel hoops and by a ACM jacket.

8.2 Objectives

The main objectives of this investigation are:

(i) to provide experimental validation to the analytical approach described in the previous chapter,

(ii) to propose a design method to determine the axial load carrying capacity of

concentrically loaded short reinforced concrete columns confined by a ACM jacket and by internal steel hoops,

(iii) to provide experimental evidence of the ACM jacket in precluding buckling of the longitudinal column bars.

8.3 Description of the Test Units

Figure 8.1 depicts general reinforcement details of the test units. As it can be seen, two test series of 900 mm high columns were built and tested. The first series, Series CS, consisted of 300 mm square columns whereas the second series, Series CR, comprised 300 mm deep by 450 mm wide rectangular columns.

The longitudinal reinforcing steel ratio for the columns was 1.5%. The longitudinal bars were Grade 430 reinforcement, with a lower 5 percentile characteristic yield strength of 430 MPa. Grade 300 - 10 mm diameter reinforcing steel hoops and ties, with a lower 5 percentile characteristic yield strength of 300 MPa, were spaced at 180 mm apart to simulate old construction or construction in non-seismic regions. With such hoop spacing premature buckling of the longitudinal bars was expected to occur upon a strain reversal from a tensile strain excursion beyond the elastic range.

Each of the series comprised three columns. In each series, the first column was left unwrapped to act as a control specimen (Columns CS0 and CR0). Two and six glass ACM wraps (TYFO S Fibrwrap) were applied to the second and third columns (Columns CS2 and CR2, and, Columns CS6 and CR6).

8.4 Construction of the Test Units

After tying the reinforcing cages, the longitudinal bars were welded to the end plates with a full penetration weld to ensure they could yield in tension. The corners of the column moulds were rounded to 30 mm radius. This radius was considered to be more achievable in small columns of buildings and was much smaller than that recommended

for bridge columns [S16]. Thus, one aspect to be carefully observed during the tests was the potential knife edge effect of the smaller radius on the jackets.

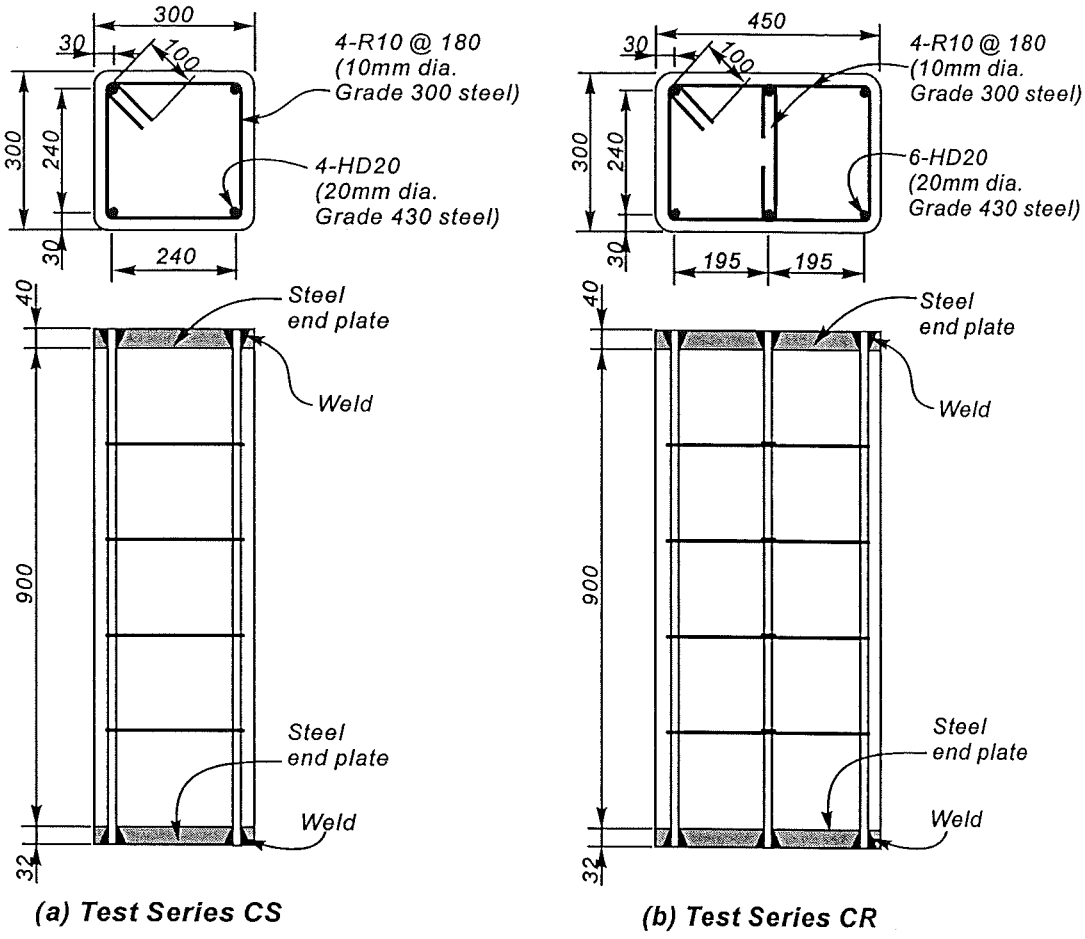

Figure 8.1 General Reinforcing Details of the Test Units

All columns were cast upright through a hole left in the upper steel plate. The fresh concrete was provided by a commercial ready-mix concrete supplier. The maximum aggregate size was 20 mm and the slump of 140 mm was measured prior to pouring concrete. The specified concrete cylinder compressive strength was 20 MPa. Test cylinders, 100 mm diameter by 200 mm high, were cast in standard steel moulds.

The columns were stripped off the moulds one day after being cast. A curing compound was applied to the columns 16 hours after removing the moulds. Twelve concrete cylinders were treated similarly to the columns whereas three cylinders were cured in a fog room. The first set of cylinders are more representative of the outer column

shell while the fog cured cylinders are more typical of the strength in the column core. It should be noted that most of the remedial work for enhancing the axial load carrying capacity of columns using jackets will generally come from columns that have not received good initial curing conditions.

8.5 ACM Jacket Application

The ACM jacketing was carried out using TYFO S Fibrwrap System. TYFO S Fibrwrap System consists of a SEH-51 fabric saturated in a two part epoxy resin, TYFO A and B. The 1.27 mm nominally thick wraps were applied when the columns had an age of two weeks. As shown in **Figure 8.2**, the surface of the columns was smoothed and then an epoxy coat was spread to the surface of the column. The method of application consisted of applying the continuous epoxy-saturated fabric until the specified number of wraps were achieved. The final wrap overlapped 150 mm the beginning of first wrap. The jackets were left curing at 18-20 degree Celsius for at least two weeks before testing. **Figure 8.3** summarises the installation of the jackets.

Note in **Figure 8.3** that a 20 mm gap was left at the column's mid-height to emulate the boundary conditions of actual columns when the wrap is butted or ended at the beam or foundation faces. The end plates and the jackets were connected using a 150 mm long TYFO S Fibrwrap perimeter strip with the main fibres oriented along the column axis. This was done to ensure that yielding of the column bars would occur away from the end regions.

8.6 Instrumentation

Figure 8.4 illustrates the instrumentation of the columns for determining longitudinal and transverse strains. The longitudinal strain was monitored by four 30 mm travel linear potentiometers with a 450 mm gauge length. The lateral strain was manually measured using DEMEC gauges in the test units with jackets only. The axial load was monitored using a load cell. **Figure 8.5** shows the measurement during testing.

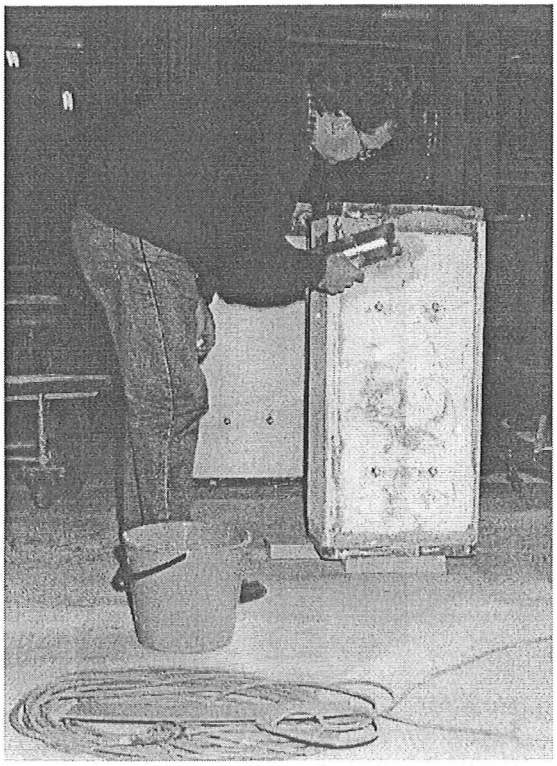

(a) Spreading Epoxy Adhesives

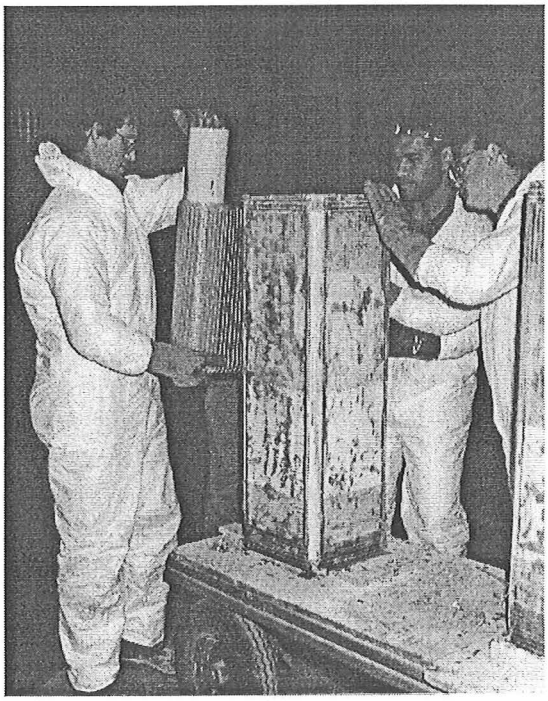

(b)Applying Epoxy-Saturated Fibreglass Jackets

Figure 8.2 Application of Fibreglass/Epoxy Jackets to a Test Column

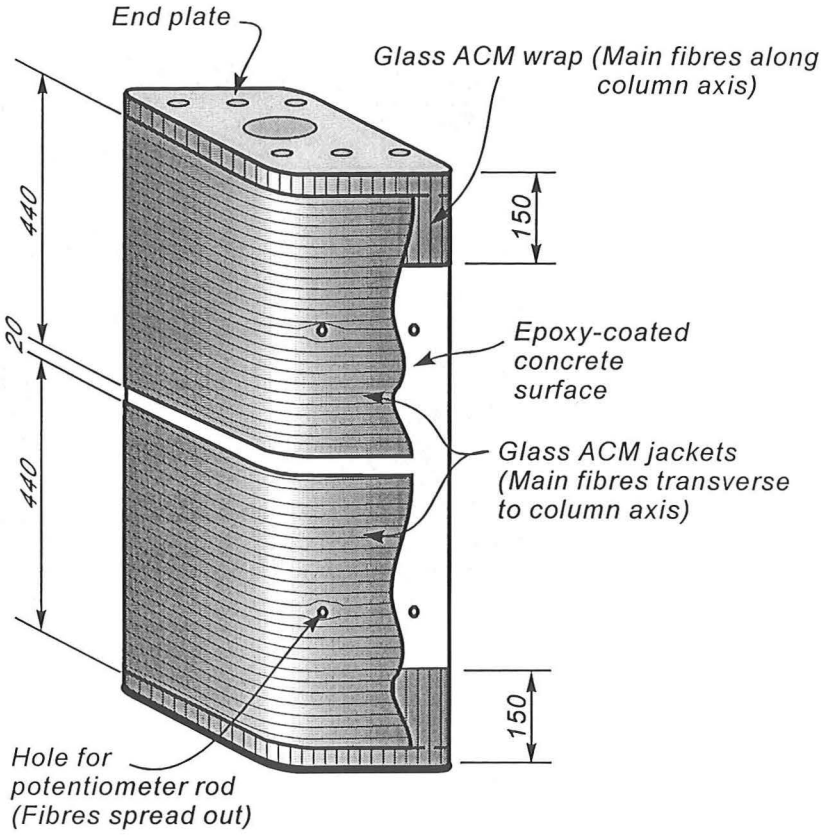

Figure 8.3 Detailed Arrangement of Glass ACM Jackets

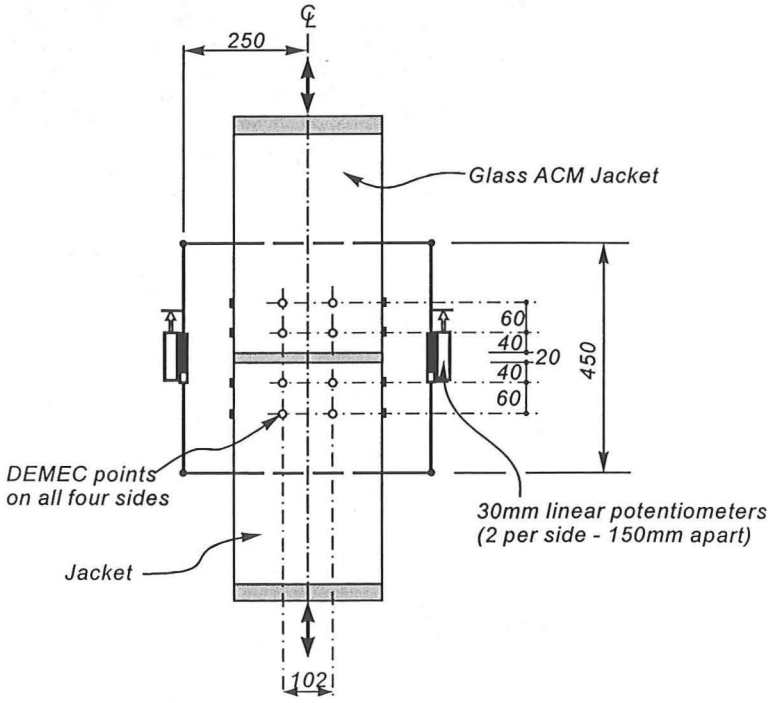

Figure 8.4 Instrumentation of the Test Units

8.7 Loading System and Test Regime

Concentric tension and compression loading was applied by a 10 MN capacity DARTEC electro-hydraulic universal testing machine. The columns were bolted to grips with spherical bearings. The axial load was applied in small increments at a strain rate of about 0.00001 mm/mm per second. **Figure 8.6** shows the general test set-up.

There were three types of test histories applied to the columns,

(i) For test units CS0 and CR0 with no wrapping (see **Figure 8.7(a)**):

- compressive loading corresponding to a strain of 0.2% for determining the average concrete compressive strength,
- tensile loading corresponding to -0.5% strain to simulate a tensile excursion in a severe earthquake and encourage premature buckling of the column longitudinal bars upon reversing of the load,
- Unload the tensile load and apply compression up to failure.

(ii) For test units CS2 and CR2 with 2 wraps (see **Figure 8.7(b)**):

- for Unit CS2 only, compressive loading to 0.2% strain,
- tensile loading corresponding to -0.5% strain to simulate a tensile excursion,
- unloading from tension and then loading in compression up to failure to evaluate the effectiveness of the jackets in preventing premature bar buckling, to evaluate the increase of the concentric strength and to observe the mode of failure of the columns.

(iii) For test units CS6 and CR6 with 6 wraps (see **Figure 8.7(c)**):

Figure 8.5 Measurement of Longitudinal and Lateral Strain

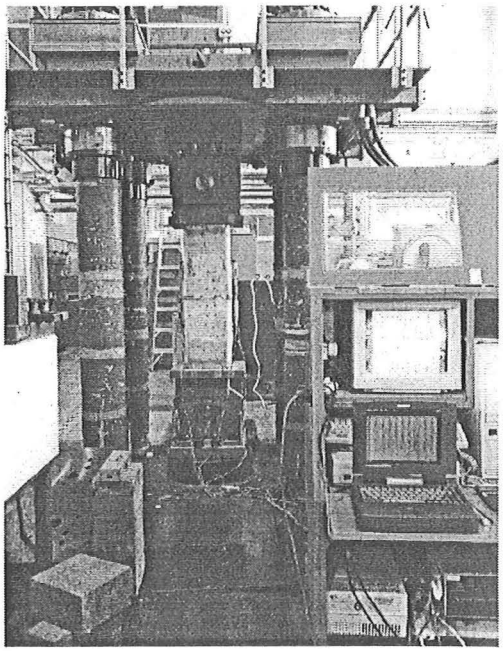

Figure 8.6 Test Set-up

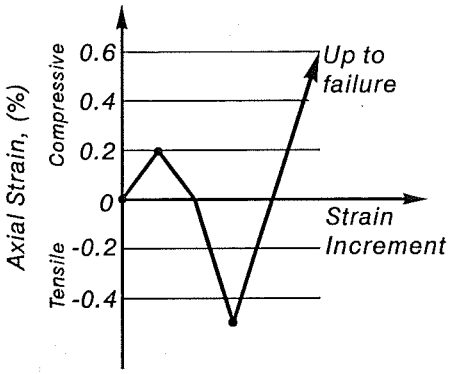

(a) Units CS0 and CR0

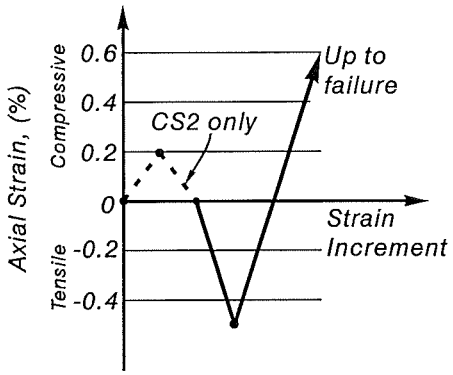

(b) Units CS2 and CR2

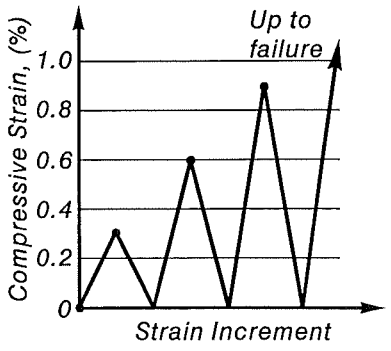

(c) Units CS6 and CR6

Figure 8.7 Test History Applied to the Columns

- tested in compression with unloading and reloading cycles at 0.3, 0.6 and 0.9% and then monotonic loading in compression up to failure to evaluate the strength enhancement and to observe the mode of failure.

8.8 Material Properties

Tables 8.1 to **8.3** presents the main mechanical properties of the reinforcing steel, the concrete and the TYFO S Fibrwrap jacket. Of particular interest is the concrete compressive strength, which showed large differences according to the curing method. The average concrete compressive strength derived from the tests on Columns CS0 and CR0 lie between the two values obtained from the cylinder tests, suggesting a variation of the strength within the member.

8.9 Test Results

Experimental results of the test columns are presented in **Figure 8.8** to **8.13**. In these figures there are three graphs which show:

(a) Experimental axial load versus axial strain. The overall response of cyclic loading according to the test history described in **Figure 8.7** is plotted in the individual figure.

(b) The monotonic loading response of axial compressive load versus axial compressive strain and its components of the axial load carried by confined concrete core and longitudinal reinforcement, respectively.

The purpose of these figures is to demonstrate how the loads carried by concrete core and reinforcing steel bars are decomposed from the total measured load. The longitudinal reinforcement force was found using the stress-strain model for reinforcing steel developed by Dodd and Restrepo [D3] except beyond buckling of the bars.

Table 8.1 Mechanical Properties of the Reinforcing Steel

Bar	A_s (mm^2)	E_s (GPa)	f_{sy} (MPa)	f_{su} (MPa)	ε_{sh} (%)	ε_{su} (%)
R10	28.5	230	305	434	1.50	19.0
HD20	314.2	200	439	592	1.17	6.67

Table 8.2 Concrete Compressive Strength

Type of Test	Curing Method	No. of Tests	Age (days)	f'_c (MPa)
Concrete[1] Cylinder	Fog Room	3	28	19.5
Concrete[1] Cylinder	Curing Compound	2	32	12.7
Concrete[1] Cylinder	Curing Compound	2	42	13.5
Column[2] CS0	Curing Compound	1	39	18.9
Column[2] CR0	Curing Compound	1	35	18.9

Notes: (1) Tests on 100 mm diameter by 200 mm high cylinders

(2) At a compressive strain of 0.2%

Table 8.3 Mechanical Properties[1] of TYFO S Fibrwrap at 0°

Thickness (mm)	Width (mm)	Length (mm)	E_p (GPa)	f_{pu}[2] (MPa)	ε_{pu} (%)
2.54 (two plies)	25	300	20.5	375	2.0

Notes: (1) Test on two coupons carried out in accordance with ASTM 3039D

(2) Based on a nominal ply thickness of 1.27 mm

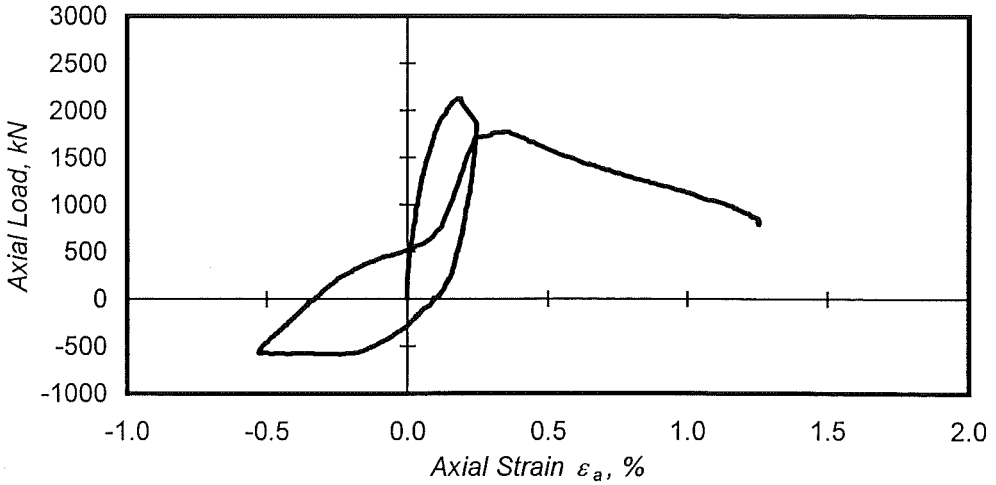

(a) Overall Response

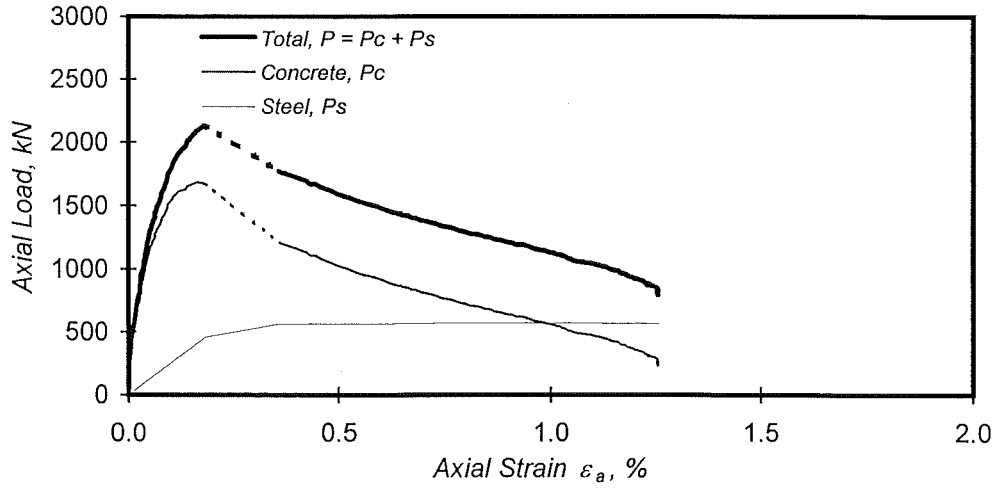

(b) Monotonic Loading Components

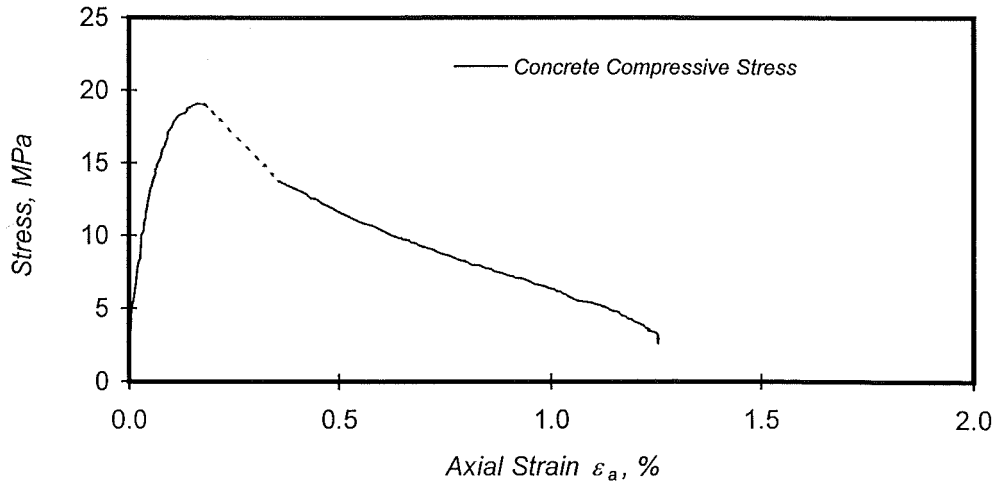

(c) Stress-Strain Relationship

Figure 8.8 Experimental Results of Unit CS0

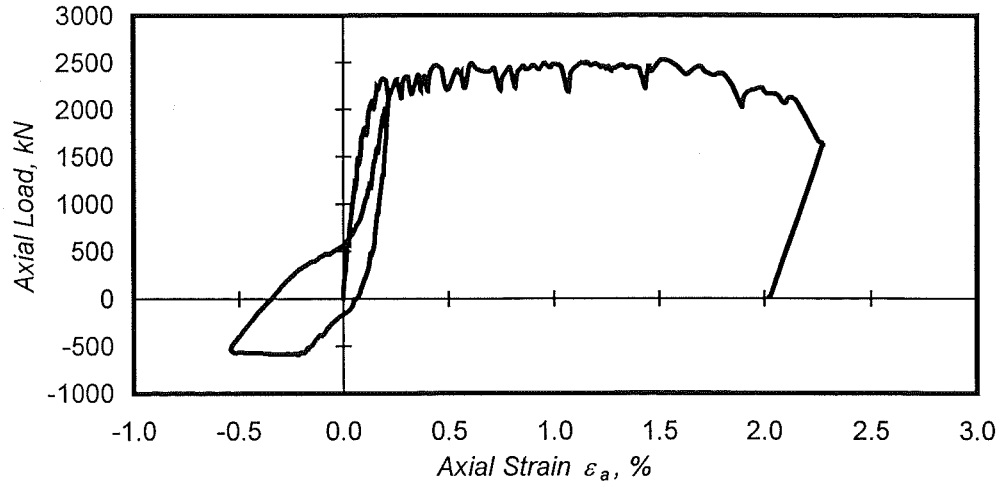

(a) Overall Response

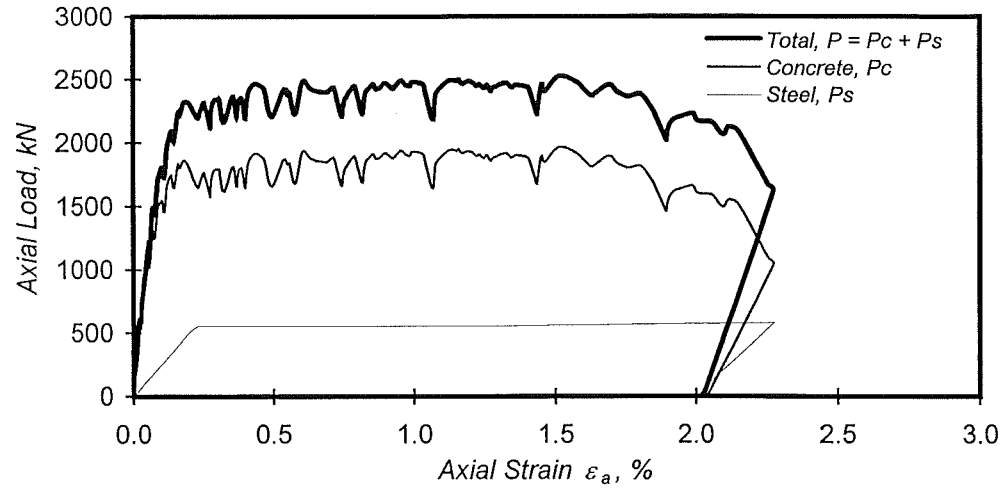

(b) Monotonic Loading Components

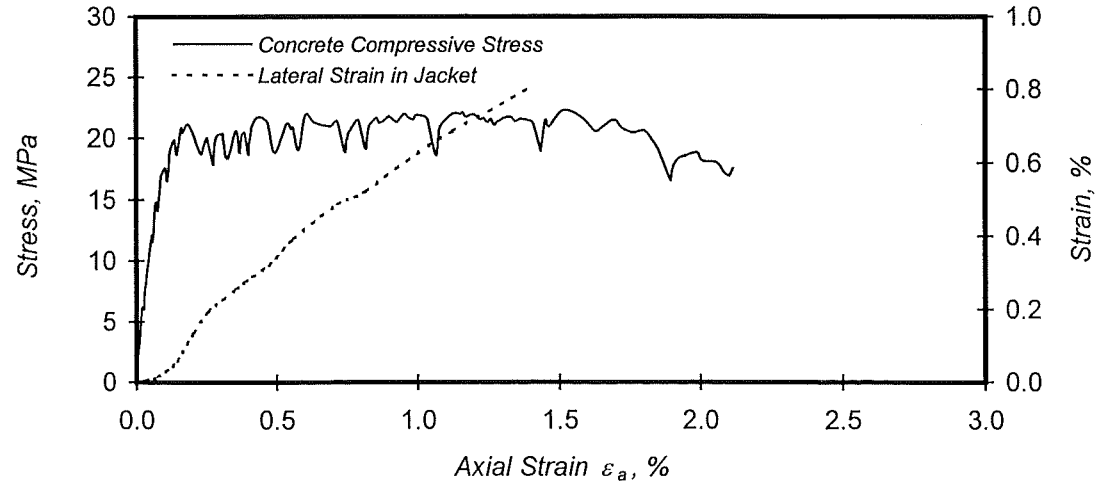

(c) Stress-Strain Relationship

Figure 8.9 Experimental Results of Unit CS2

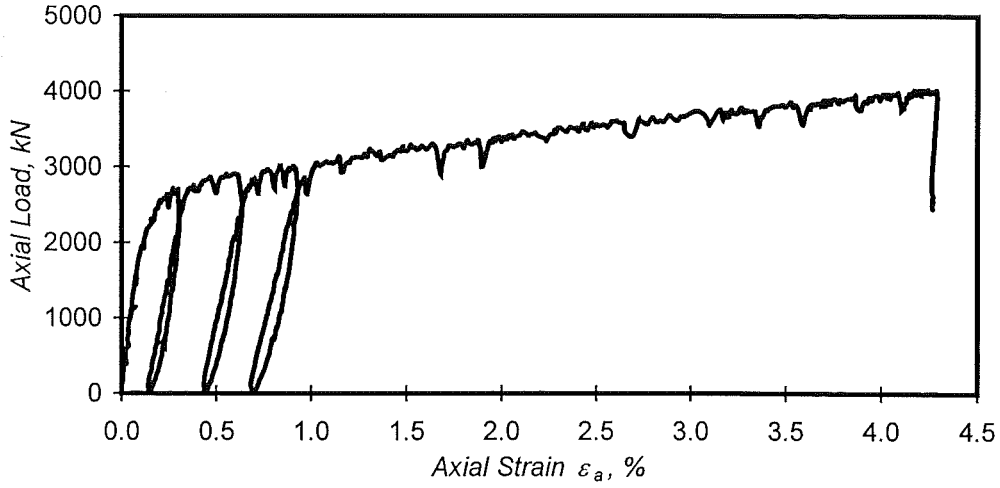

(a) Overall Response

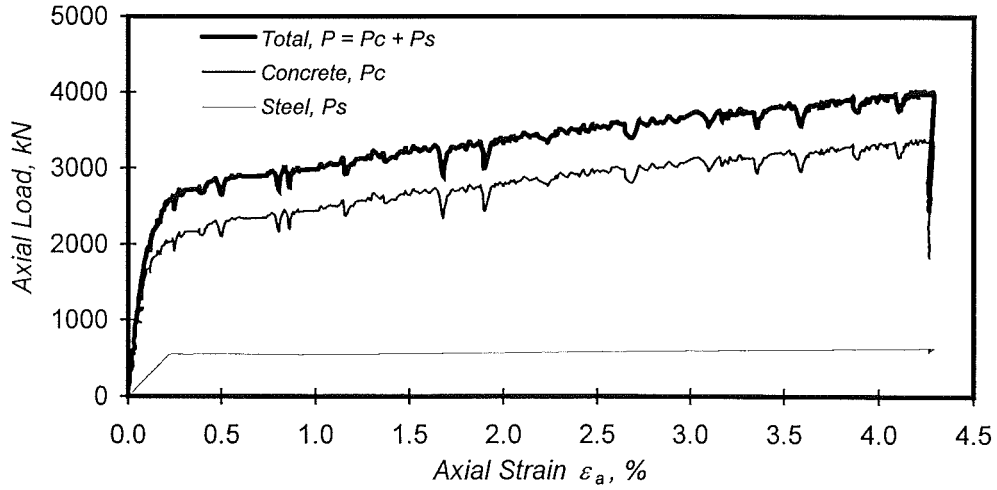

(b) Monotonic Loading Components

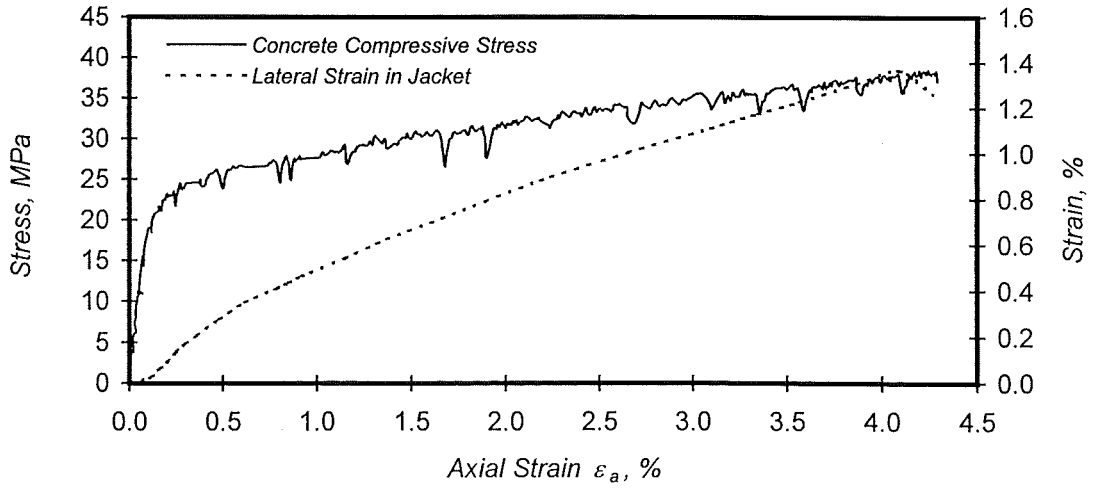

(c) Stress-Strain Relationship

Figure 8.10 Experimental Results of Unit CS6

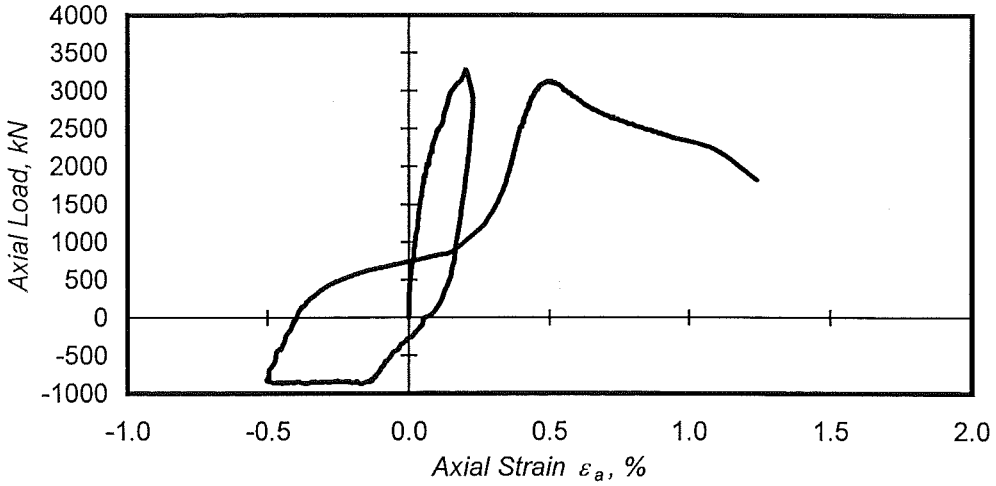

(a) Overall Response

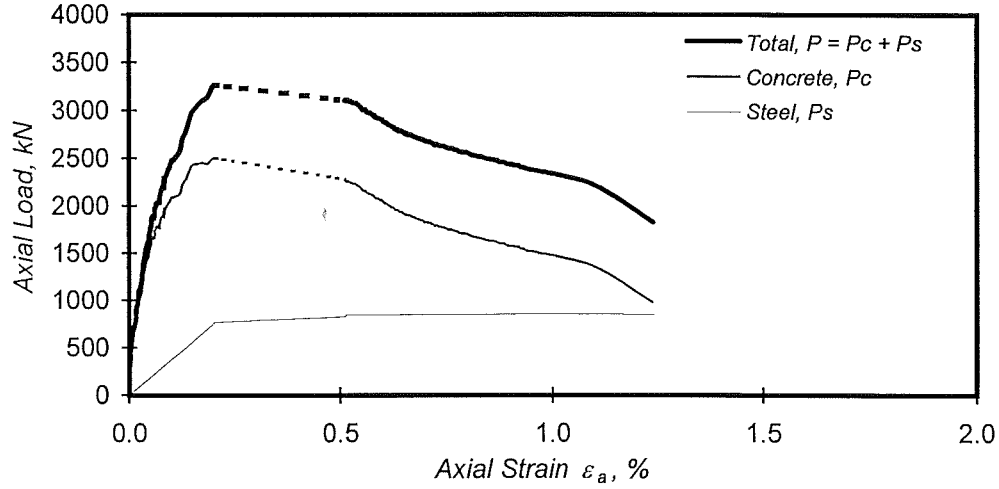

(b) Monotonic Loading Components

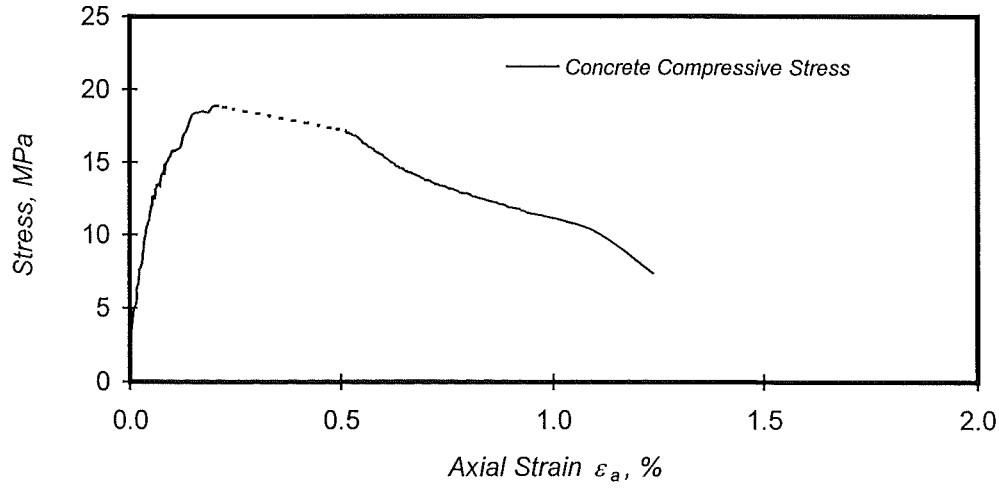

(c) Stress-Strain Relationship

Figure 8.11 Experimental Results of Unit CR0

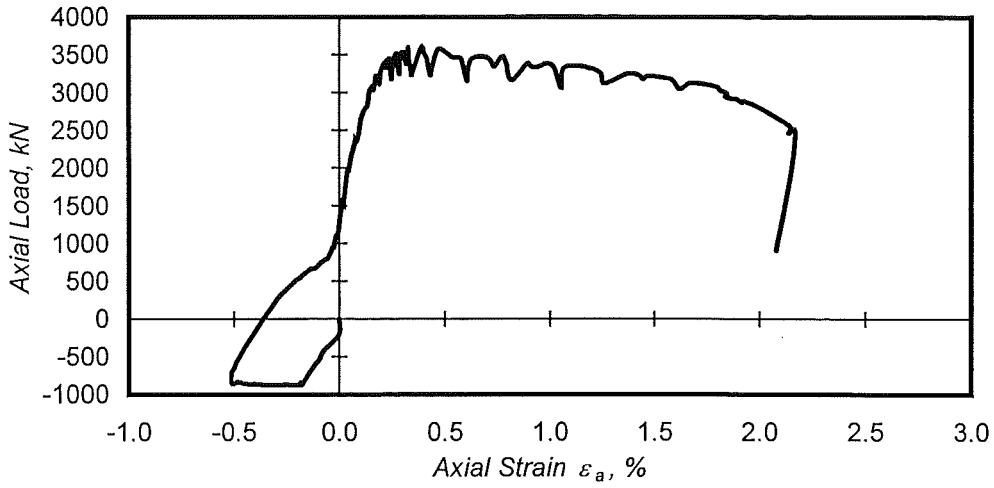

(a) Overall Response

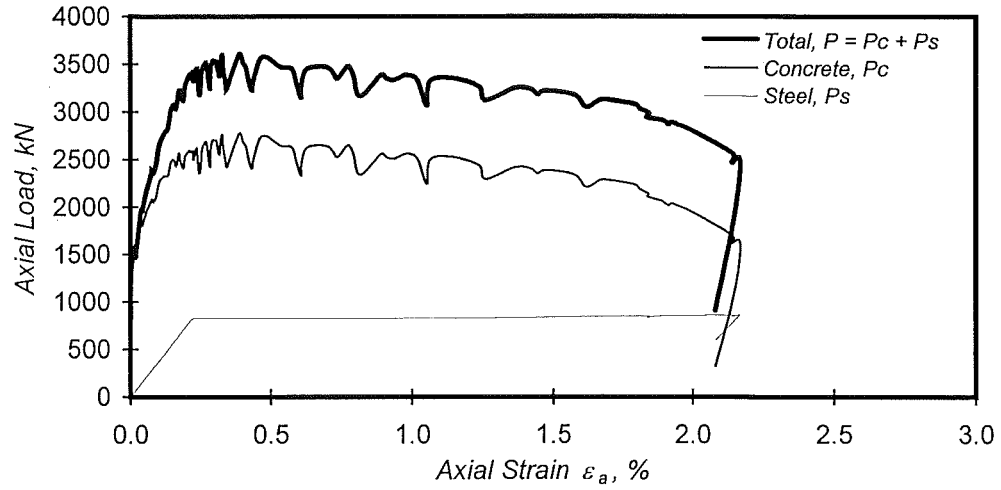

(b) Monotonic Loading Components

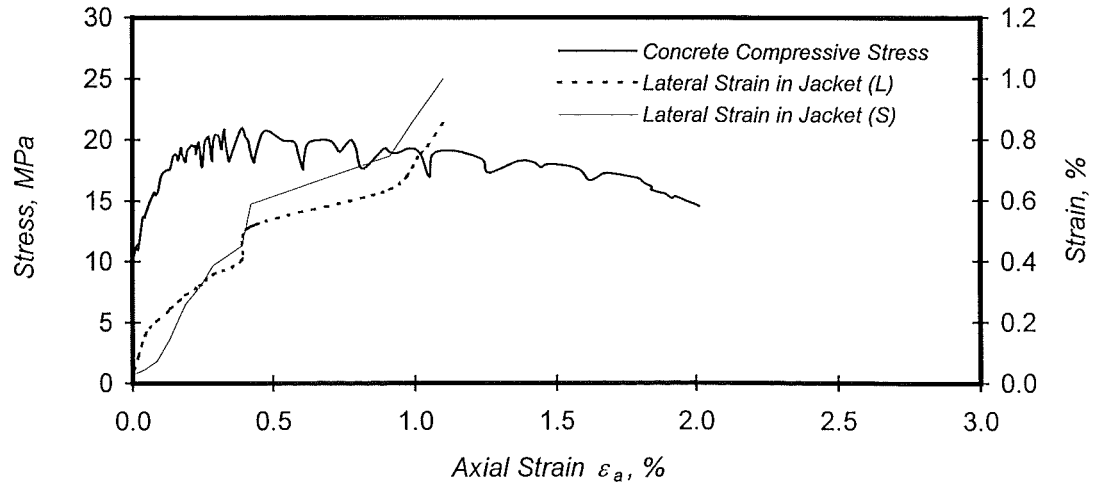

(c) Stress-Strain Relationship

Figure 8.12 Experimental Results of Unit CR2

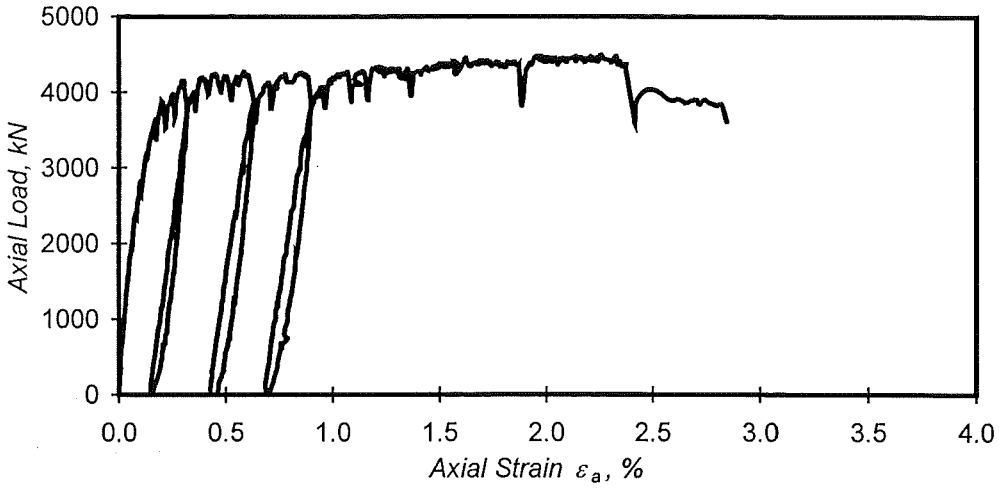

(a) Overall Response

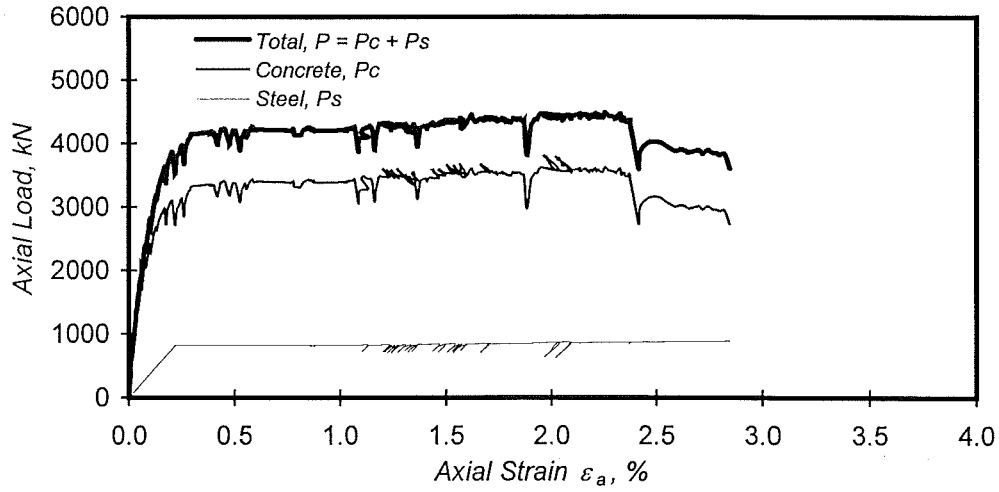

(b) Monotonic Loading Components

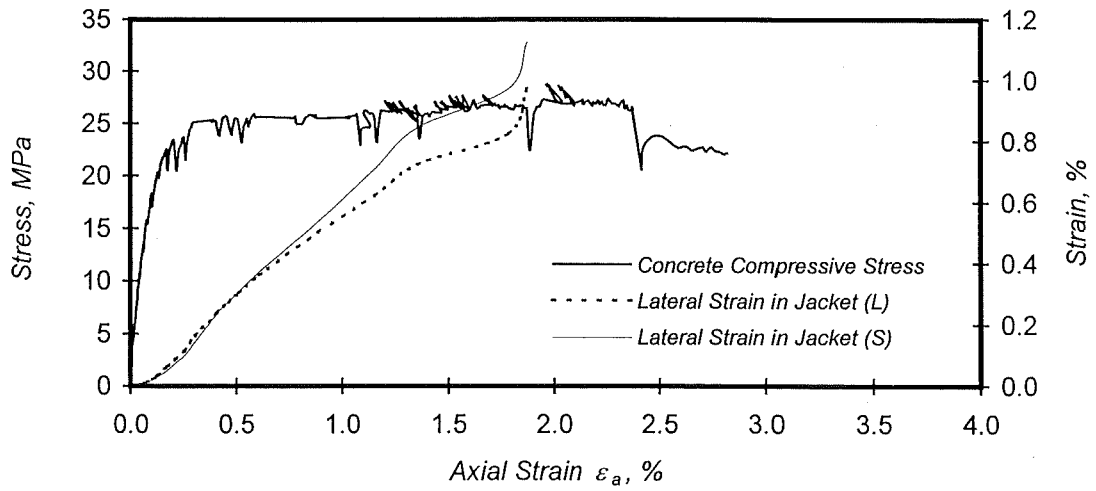

(c) Stress-Strain Relationship

Figure 8.13 Experimental Results of Unit CR6

For Units CS0 and CR0, the longitudinal reinforcement force could not be determined from the stress-strain model for steel proposed by Dodd and Restrepo since this model does not account for buckling. The force was experimentally determined from a test at a 10 mm diameter reinforcement coupon subjected to the same axial strain history as the columns themselves. The aspect ratio of the test coupon, $s/d_b = 9$, is the same as that of the HD20 tied to the hoops at 180 mm spacing in these columns. **Figure 8.14** shows the test set-up and the test results. The test was performed according to a previous test programme described in Restrepo et al. [R12]. It was found in the test results that the inelastic buckling of the steel reinforcing bar commenced when the axial compressive strain reached about 6-time yield strain of the bar. The observed response of the test coupon shown in **Figure 8.14** was normalised in terms of the yield stress and yield strain. The normalised values were then multiplied by the yield stress and yield strain of HD24 bars used in columns, CS0 and CR0. It is important to mention here that the axial strain in the longitudinal reinforcement in the region where the bars buckled was not obtained. The axial strain measured over 450 mm gauge length was assumed to be equal to the strain of the bars in this region. This assumption will somehow underestimate the actual bar strain after buckling occurs.

Finally, the confinement effect of the ACM jackets on increasing the concrete compressive strength was evaluated by subtracting the load carried by the longitudinal column bars. The confinement effect of the steel hoops on the concrete strength is also included in the strength enhancement of concrete but it is small due to the large space of the steel hoops. Note in some of the figures that the response is jagged due to stress relaxation in the steel and the concrete during the lapse when manual DEMEC gauge reading were taken.

(c) The concrete compressive stress and measured lateral strain on jacket.

The concrete compressive stress is obtained by dividing the force sustained by concrete by the concrete area of the column section.

The lateral strain measured using DEMEC gauges was performed in the jacketed columns. As mentioned previously, the lateral strain on the jacket and the transverse strain on the concrete surface are assumed identical. In the figures of rectangular columns

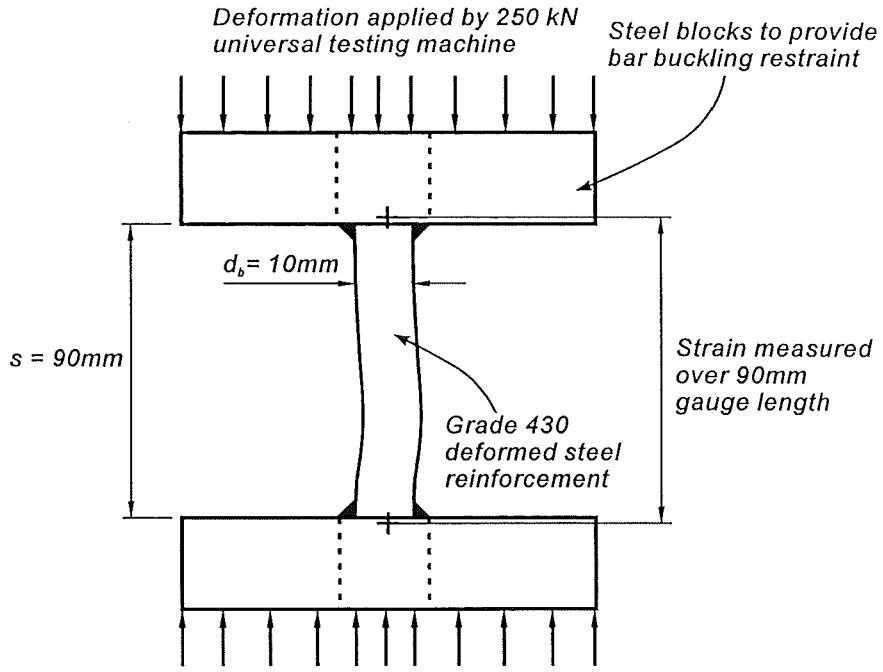

(a) Test Set-up Diagram

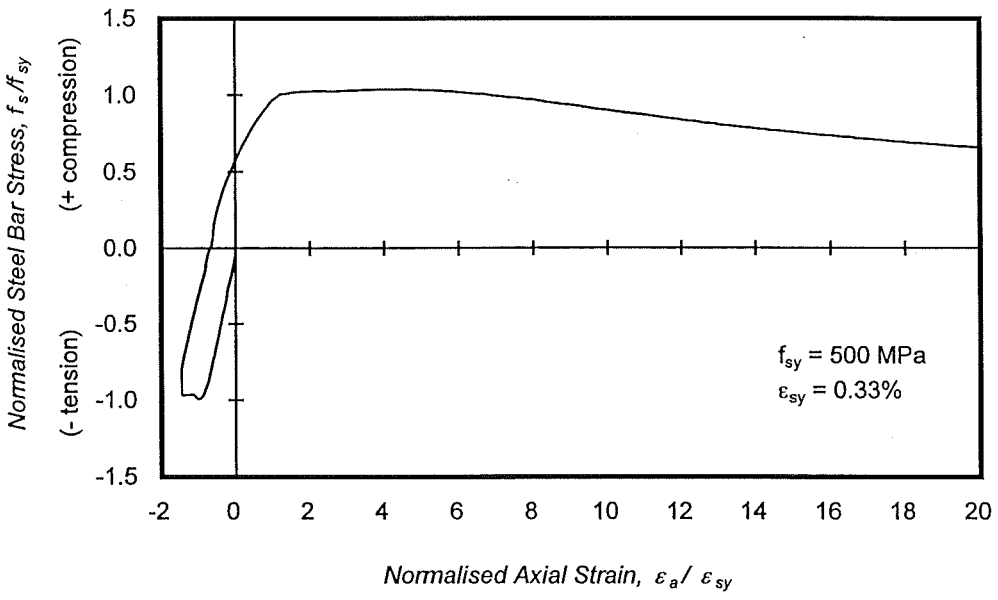

(b) Test Results

Figure 8.14 Inelastic Buckling Behaviour of a Grade 430 Deformed Reinforcing Bar with a Aspect Ratio s/d_b= 9

CR2 and CR6, notation L and S indicate the lateral strain measured in the long and short side of the column, respectively. The short side lateral strain was attained as a result of average value of two sides whereas the long side one was obtained by only the side without overlapping of the jacket ends. The result of lateral strain in Columns CS2 and CS6 was determined by the mean value in three sides of the column, discarding the reading in the side with overlapping of the jacket ends.

The following descriptions are based on the test results obtained in the above.

8.9.1 General Observations

Tests on Square Columns

Figures 8.8 to **8.10** and **Figure 8.15(a)** show the concentric load versus axial strain behaviour of test units CS0, CS2 and CS6. The envelope of the compressive load is shown in bold for clarity. It is evident in this figure that both the strength and the deformation capacity of the columns increase when increasing the jacket thickness.

The longitudinal bars in Column CS0 buckled upon reversing from the tensile strain excursion and induced spalling of the concrete cover. The compressive axial load decreased rapidly beyond a compressive strain of 0.2%. This column showed limited deformation capacity. **Figure 8.16(a)** shows this column at the end of the test.

The test in Column CS2 demonstrated the efficiency of the jacket in preventing early buckling of the longitudinal reinforcement from occurring. The load was maintained up to a compressive strain of 2%. The mode of failure was by delamination of the wraps. Delamination of the jacket commenced at a compressive strain of 0.8% and slowly progressed until it became unrestricted at a strain of 2%. **Figure 8.16(b)** shows this column at the end of the test.

Column CS6 showed remarkable behaviour. The concentric load was not only maintained but continuously increased to almost double the load of the benchmark unit, Column CS0. Failure occurred when the jacket split one of the corners at a strain of 4.3%. **Figure 8.16(c)** illustrates this column after the end of the test.

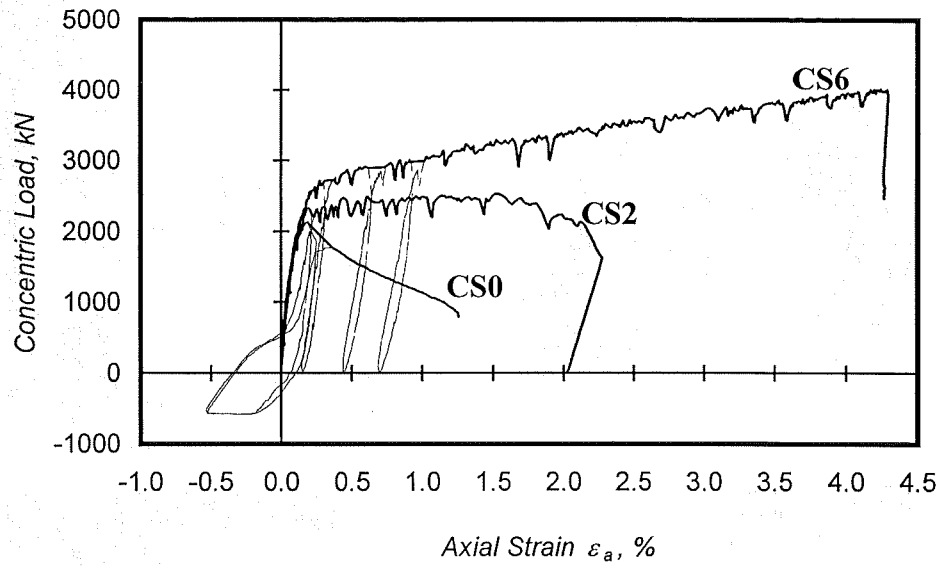

(a) Tests on Square Columns

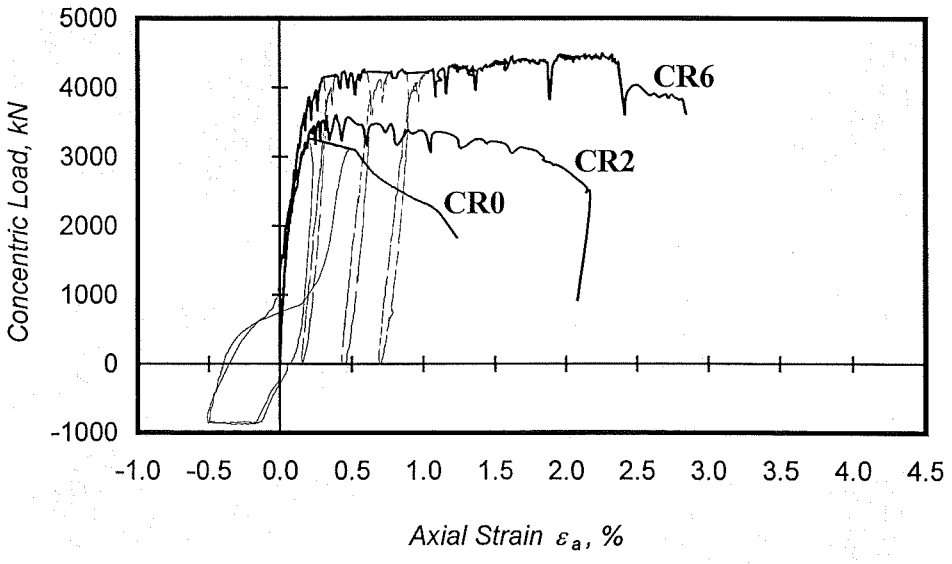

(b) Tests on Rectangular Columns

Figure 8.15 Observed Concentric Load - Axial Strain Response of the Test Units

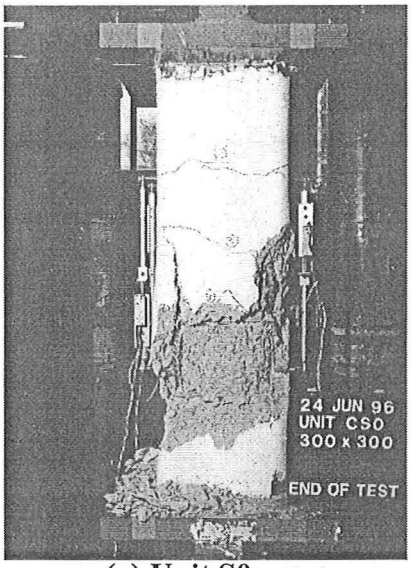

(a) Unit S0

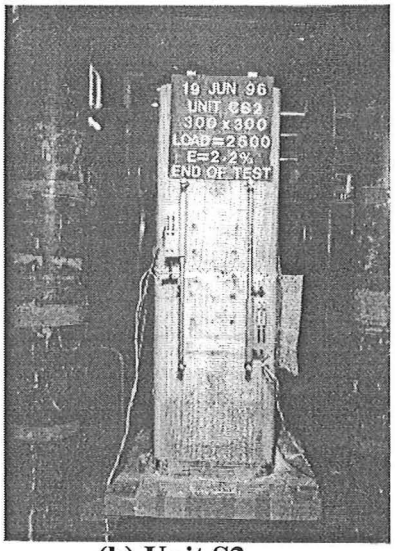

(b) Unit S2

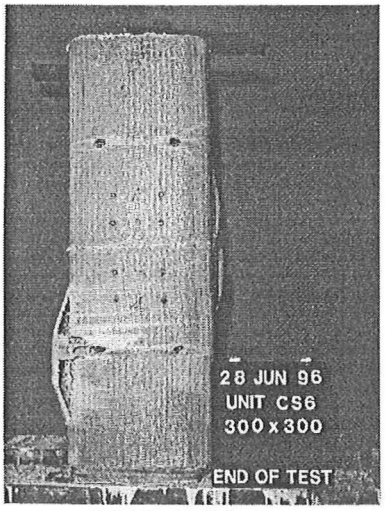

(c) Unit S6

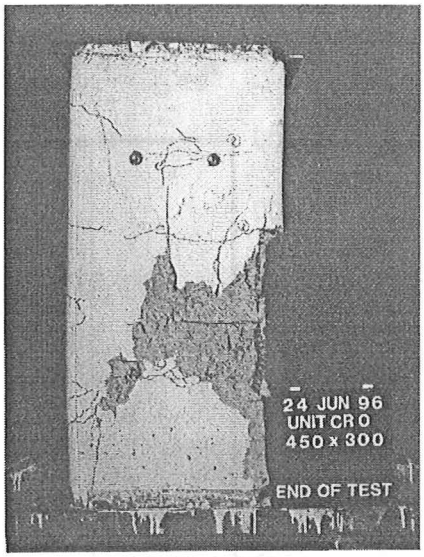

(d) Unit R0

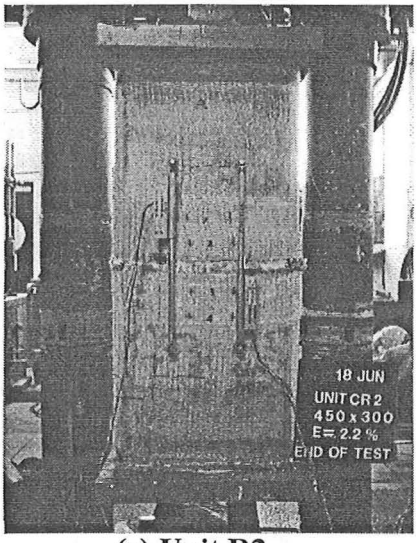

(e) Unit R2

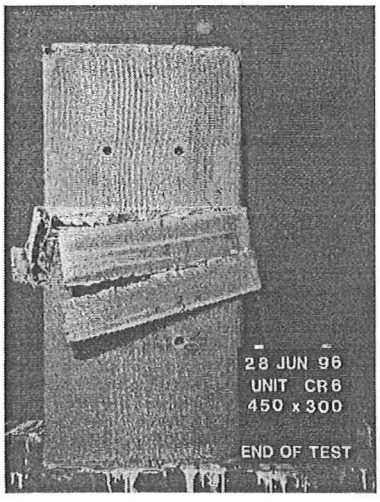

(f) Unit R6

Figure 8.16 Extent of Damage in the Units at the End of the Test

Tests on Rectangular Columns

The tests on the oblong columns showed similar trends and behaviour as the tests on square columns. **Figures 8.11** to **8.13** and **Figure 8.15(b)** plot the concentric axial load versus axial strain response for Columns CR0, CR2 and CR6 while **Figure 8.16(d)** to **(f)** illustrate the extent of damage of Columns CR0, CR2 and CR6 at the end of the test, respectively.

The response of Column CR2 shows a slight difference from Column CS2. The concentric compressive load was not maintained after the peak load occurred at about axial strain of 0.2%. Nevertheless, the load carrying capacity gradually decreased up to a compressive strain of 2% as seen in **Figure 8.15(b)**. The mode of failure was by delamination of the wraps in the longer side of the column. Delamination of the jacket commenced at a compressive strain of 0.6% and slowly progressed until it became unrestricted at a strain of 2%.

Column CR6 did not show the same increase in strength as Column CS6 but maintained the load carrying capacity until failure occurred. This column failed by splitting of the jacket at a compressive strain of 2.8%. The main reason for the difference in behaviour is due to the poorer confinement effect exerted by the wraps in oblong columns, as is analytically shown in Chapter 7.

8.9.2 Confining Effectiveness

Effective Poisson's Ratio

To examine the confining effectiveness of the jacketed columns, the volume change and dilation rate of the confined concrete were calculated. In a triaxial state of stress, the volumetric strain ε_v (or dilatation) is defined as the volume change per unit volume, see Eq.2.23. In this equation, tensile strains and dilatation are considered negative. A positive ε_v represents volume reduction (contraction) whereas a negative ε_v indicates volume expansion (dilation). The tangential Poisson's ratio, υ_t, is defined as the

rate change of lateral strains with respect to the axial strain, see Eq.2.24. **Figure 8.17** shows the normalised axial stress-volumetric strain curves for the jacketed columns whereas **Figure 8.18** illustrates the tangential Poisson's ratio – axial strain for these units. In these figures, the typical response of unconfined concrete is plotted for comparison [C8].

For plain concrete, a volume reduction occurs until the compressive stress reaches $0.90f'_c$ and then the direction of volume change is reversed and dilation is finally observed. Beyond the peak strength, an unrestricted expansion occurs in plain concrete [C8]. Similarly in the tangential Poisson's ratio curve, the rate of unconfined concrete begins at a value corresponding to Poisson's ratio of concrete, $\upsilon = 0.2$, and then increases rapidly with the development of microcracks, and tends to infinity near its peak strength.

Among the results in test on the jacketed columns, the volumetric strain in columns CS2 and CR2 is similar to that of plain concrete, but the expansion of the concrete volume is slightly different from the plain concrete (see **Figure 8.17**). This is because the confining effectiveness developed by the two layers of glass ACM jackets causes a small amount of passive lateral confining pressure onto the concrete and results in maintaining the confining stress without failing during the concrete dilation.

The behaviour of columns CR6 and CS6 in **Figure 8.17** reveal a completely different trend. Volume expansion occurs near and immediately past the peak stress but then the volume begins to decrease again and continues to do so until the end of tests. This phenomena can especially be observed in column CS6, which is the square column confined with six layers of glass ACM jackets corresponding to the reinforcement ratio ρ_{jx} or $\rho_{jx} = 0.051$.

In **Figure 8.18**, the dilation response of ACM-confined concrete consists of three regions. The initial rate of dilation is about the same as the Poisson's ratio of unconfined concrete. In the first stage, the tangential Poisson's ratio remains constant during the early stages of loading when concrete behaves elastically. As microcracking develops, the ratio begins to increase (the second stage). Then in the final stage when the ratio of the confined concrete reaches a peak value of $\upsilon_{t,\,max}$, the ratio decreases

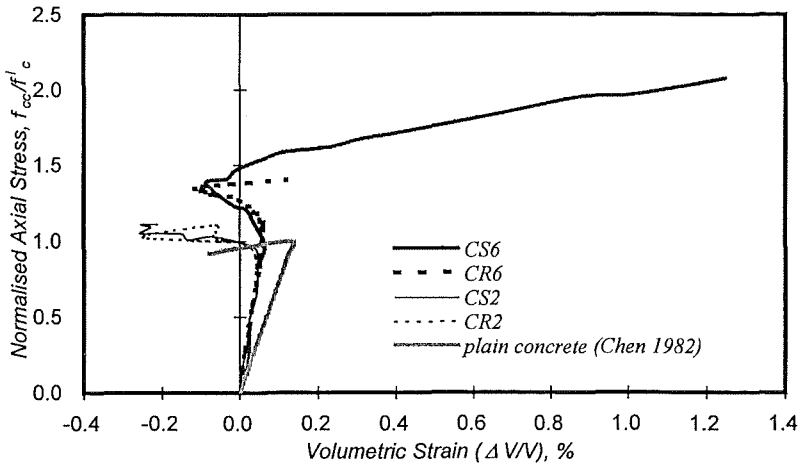

Figure 8.17 Volumetric Response for the Jacketed Columns

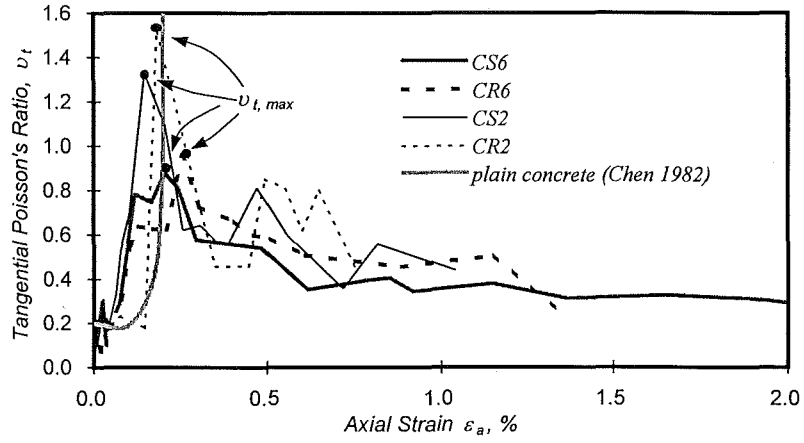

Figure 8.18 Tangential Poisson's Ratio of the Jacketed Columns

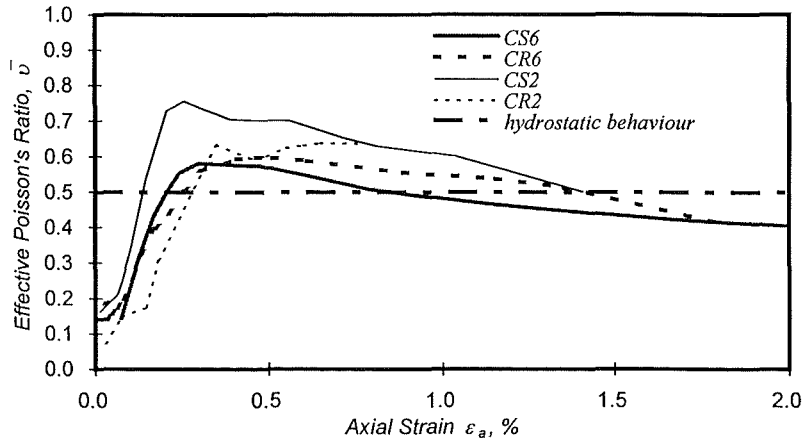

Figure 8.19 Effective Poisson's Ratio of the Jacketed Columns

asymptotically to a constant value. The thicker jacket results in a lower value of $\upsilon_{t,\,max}$.

The observed behaviour suggests that the relationship between axial and lateral strain for the confined concrete is not constant and depends on the stiffness of the elastic ACM wrapping. Hence, a better way for describing the axial-lateral strain relationship of the jacketed columns is to use an effective Poisson's ratio, defined as

$$\bar{\upsilon} = \frac{\int_0^{\varepsilon_a} \upsilon_t(\varepsilon_a)\, d\varepsilon_a}{\varepsilon_a} \tag{8.1}$$

Figure 8.19 shows the value of $\bar{\upsilon}$ versus the axial strain ε_a for the wrapped columns. Also plotted in this figure is $\bar{\upsilon}$=0.5, which assumes no volume change, that is, a hydrostatic behaviour. The value of $\bar{\upsilon}$ obtained from the tests are closer or greater than $\bar{\upsilon}$=0.5 for most of the range of axial strains. The use of $\bar{\upsilon}$=0.5 for axial strains beyond 0.2% results in a conservative and simple approach that can be incorporated into a design equation when strength is defined as the load between 0.3 and 1.5% axial strain.

Concrete Arching

As mentioned in Section 2.3.1, originally the model of confined concrete stress-strain proposed by Mander et al. [M11] is adopted and refined in this study. In this model, two parameters are required. They are the ratio R, see Eq.2.7, and the initial angle θ of arching of the concrete, see Section 2.3.2. R depends on the characteristic properties of unconfined and confined concrete whereas θ relates to the concrete arching action onto the confined materials. In Mander's model for the normal concrete confined by steel lateral hoops, R=5 is adopted and the initial angle θ of concrete arching is assumed to be equal to 45 degrees. It is assumed in the proposed analytical model that R is equal to 5. In practice in conventional columns, where confinement is provided by closely spaced hoops and ties, any variation in the angle θ leads to a small change. This is not the case in columns with ACM jackets and therefore such angle needs to be derived for practical use. Thus, the initial arching θ is evaluated in this section.

Figure 8.20 to **8.23** shows the prediction is performed for different values of the initial angle θ. The optimum angle for each column wrapped with different layers of glass ACM jacket is given in **Table 8.4**. Note that to eliminate the effect of accurate prediction on concrete confining behaviour, the observed relationship between axial and lateral strain is used in the analysis. It is clear that θ decreases as the confinement ratio increases. According to results shown in **Table 8.4**, θ ranges between 42 degrees and 47 degrees. In average, 45 degree can be adopted for use in analysis and design.

8.9.3 Comparison between Experimental and Analytical Results

The result of the theoretical analysis proposed in the previous chapter is discussed in this section. By means of comparison with experimental results, the proposed model can be revised to provide the design application of concentrically loaded columns wrapped with glass ACM jackets.

Simple Analytical Model

To simplify the analytical prediction, the following assumptions can be made,

- The longitudinal steel bars are assumed to be an elasto-plastic material for the prediction of the column subjected to monotonically axial loading.

- Poisson's ratio is constant up to the failure of the column. Poisson's ratio varies with the column axial load and depends on the stiffness of the elastic confining materials. Based on the test results depicted in **Figure 8.19**, the ratio $\upsilon = 0.5$ is conservative yet close to the measured values. **Figure 8.24** compares the experimental and assumed axial versus lateral strain for the jacketed columns tested in this programme. An advantage of assuming a constant value for υ is that the transverse strain found from the model is made independent from the stiffness of the elastic confining materials.

- The constant R and angle θ are assumed constant and equal to 5 and 45 degrees, respectively.

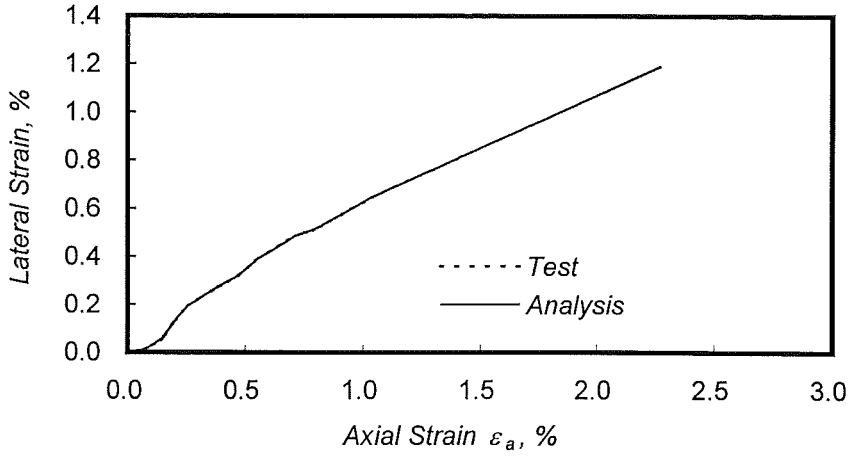

(a) Axial Strain v.s. Lateral Strain

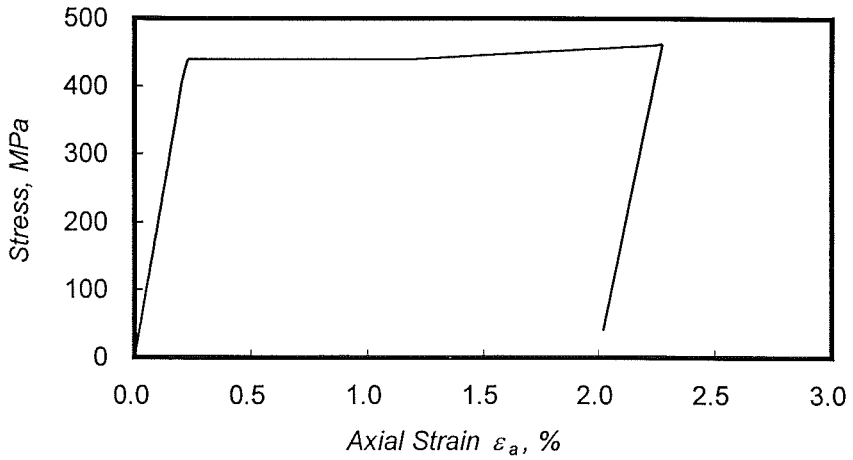

(b) Stress-Strain of Longitudinal Steel Bar HD20

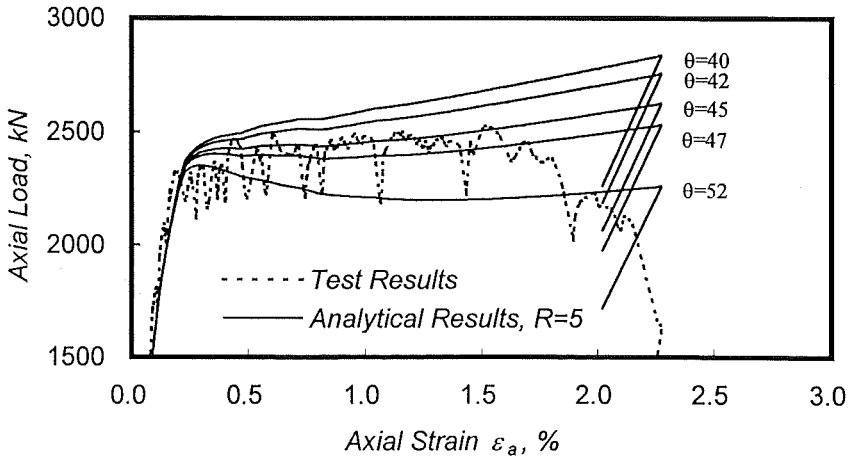

(c) Analytical Results with Variable θ

Figure 8.20 Comparison between Test and Analytical Results of CS2

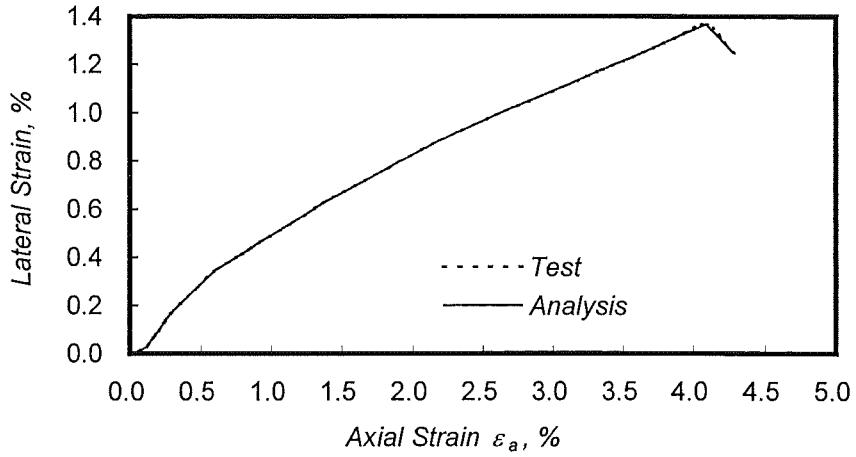

(a) Axial Strain v.s. Lateral Strain

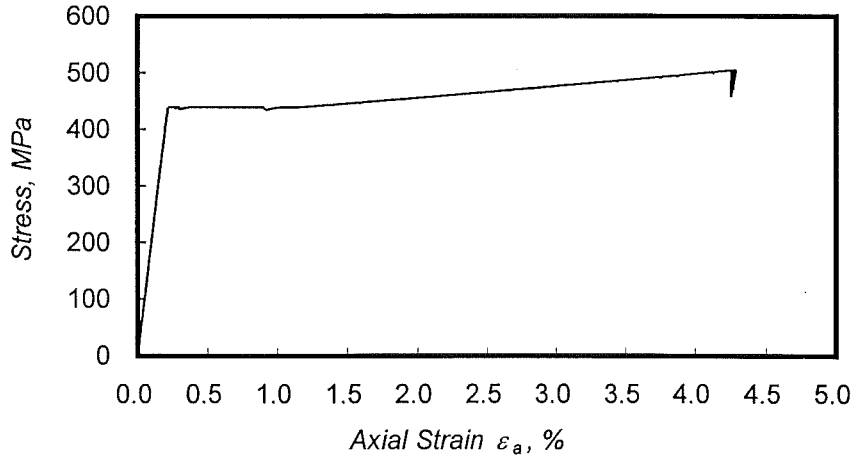

(b) Stress-Strain of Longitudinal Steel Bar HD20

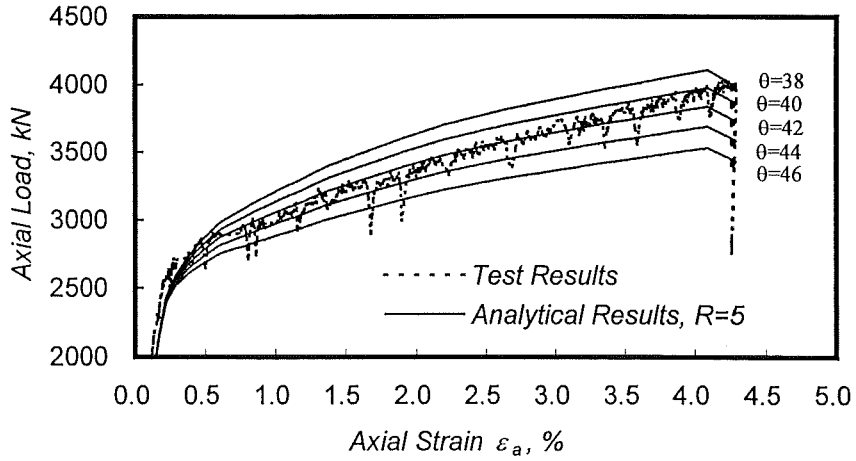

(c) Analytical Results with Variable θ

Figure 8.21 Comparison between Test and Analytical Results of CS6

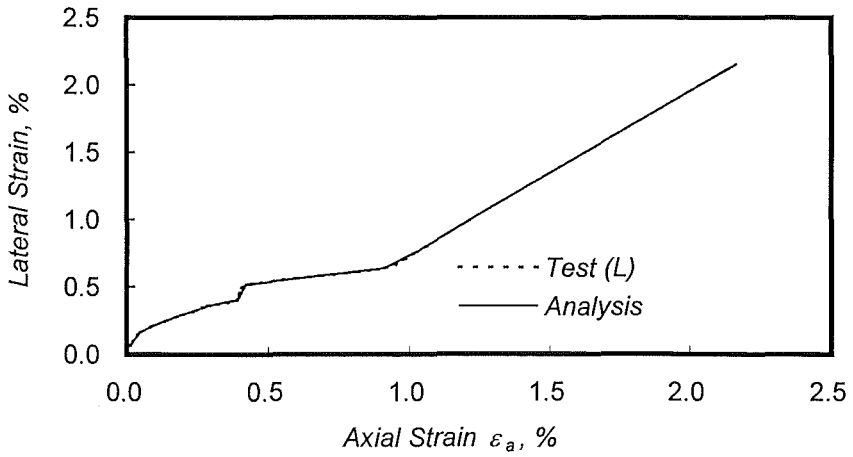

(a) Axial Strain v.s. Lateral Strain

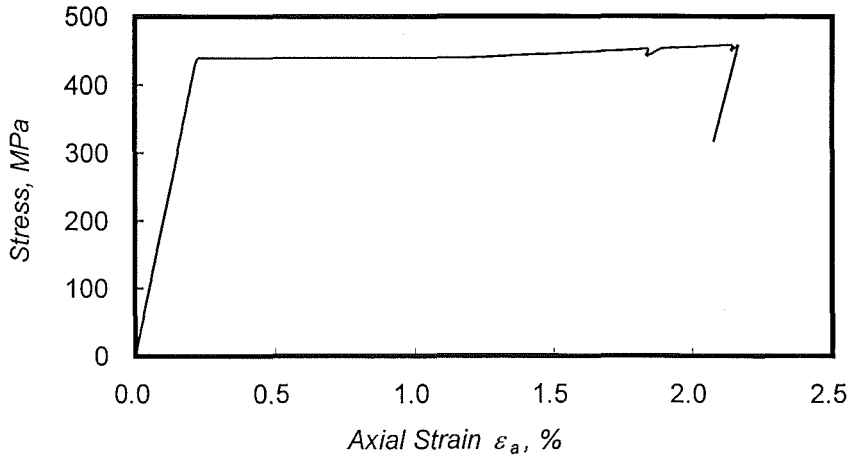

(b) Stress-Strain of Longitudinal Steel Bar HD20

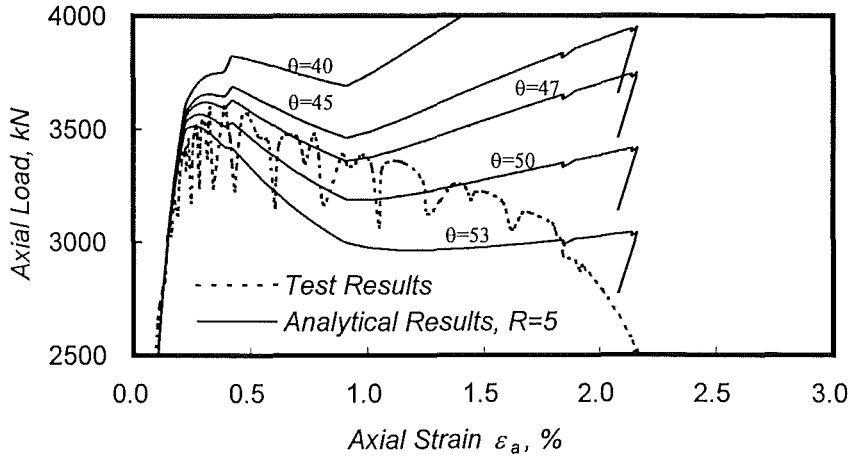

(c) Analytical Results with Variable θ

Figure 8.22 Comparison between Test and Analytical Results of CR2

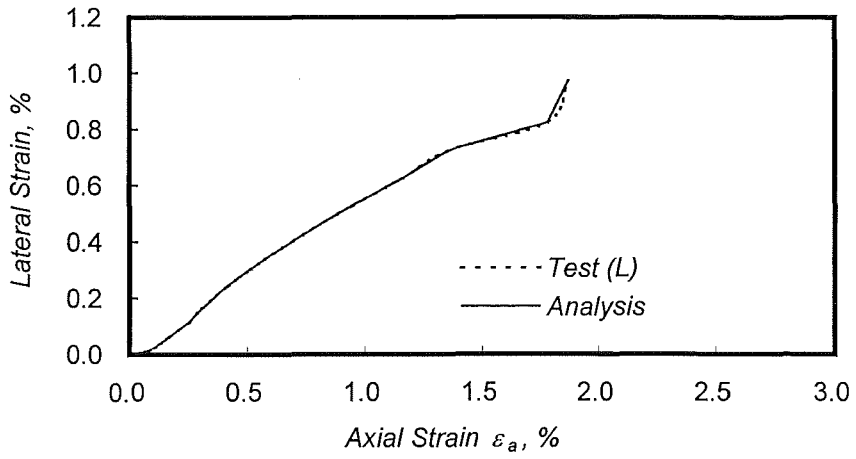

(a) Axial Strain v.s. Lateral Strain

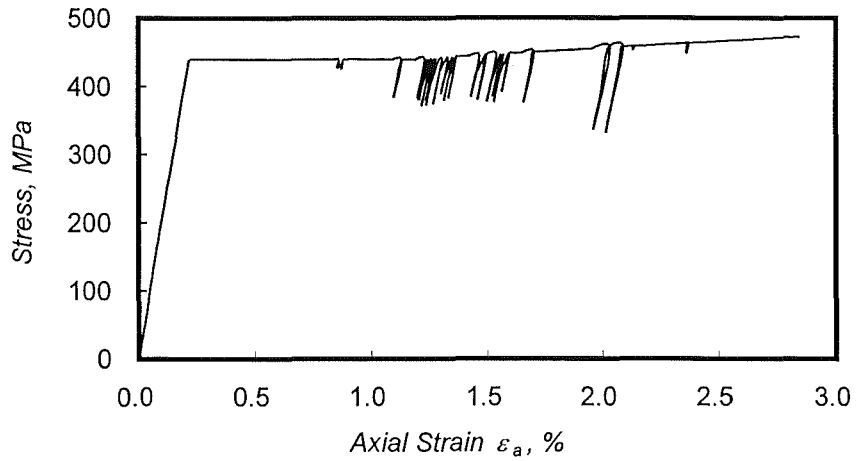

(b) Stress-Strain of Longitudinal Steel Bar HD20

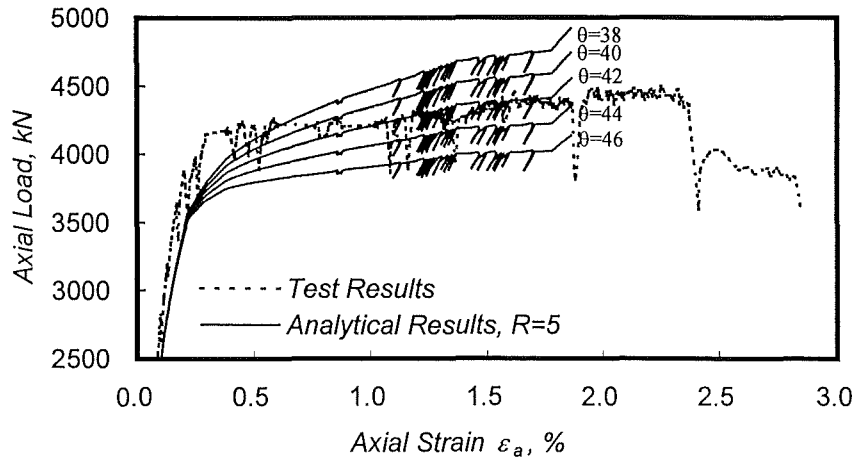

(c) Analytical Results with Variable θ

Figure 8.23 Comparison between Test and Analytical Results of CR6

Table 8.4 The Optimum Tangential Angles of Concrete Arching Action due to the Confinement of ACM Jackets

Cross section	Number of plies	t_j (mm)	ρ_{jx}	ρ_{jy}	ρ_j ($=\rho_{jx} + \rho_{jy}$)	Specimen number	$\theta^{(1)}$ (degrees)	$R^{(2)}$
Square (300 x 300 mm) f'_c = 18.9 MPa	2	2.54	0.017	0.017	0.034	CS2	45	5
	6	7.62	0.051	0.051	0.102	CS6	42	5
Rectangular (450^L x 300^S mm) f'_c = 18.9 MPa	2	2.54	0.017	0.011	0.028	CR2	47	5
	6	7.62	0.051	0.034	0.085	CR6	42	5

Notes: (1) θ is the initial tangent slope in a second-degree parabola of concrete arching.

(2) R is the ratio of strain increase to stress increase at the peak strength of confined concrete, see Eq.2.7.

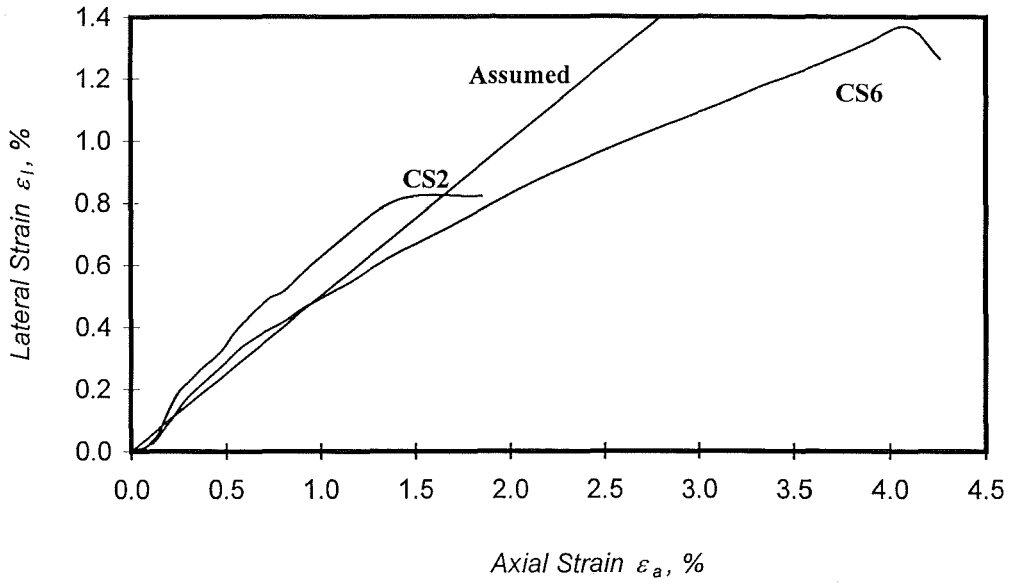

(a) Square Columns

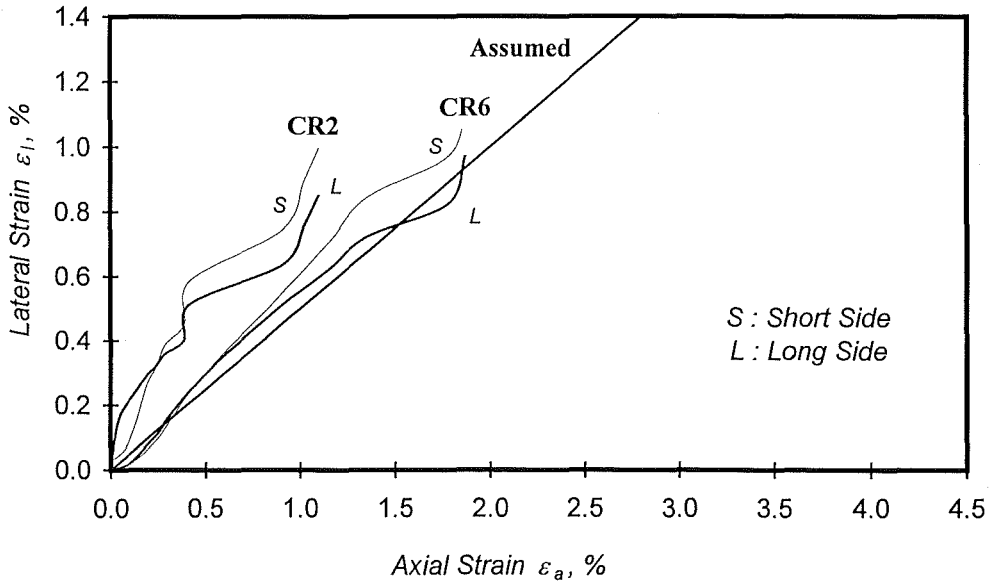

(b) Rectangular Columns

Figure 8.24 Axial Strain - Lateral Strain Measured in the Columns

Figures 8.25 to **8.28** compares the measured and predicted behaviour using the simple model. In square columns CS2 and CS6, the prediction of the confined concrete strength f'_{cc} and its corresponding strain ε_{cc}, proposed by SEQAD [S15] (see Eqs.2.21 and 2.22), is also plotted. It is obvious that the prediction curves agree with experimental results very well for the ACM-wrapped columns except column CR6. This implies the prediction of well-confined ACM-wrapped rectangular columns assuming $\theta = 45$ degrees is underestimated.

SEQAD prediction of the concrete confining strength and its corresponding strain of square columns, shows the calculated value is lower than the value determined by the proposed model and the test results. That means the concrete confining strength predicted by SEQAD's proposed equations is conservative, especially for the well-confined columns such as column CS6.

Verification of the Model

The model proposed in Chapter 7 and calibrated using the data found in the present experimental work shows excellent correlation. However, in order to prove the validity of the model a prediction is made for the response of tests conducted elsewhere [S15].

Table 8.5 gives details of the specimens tested by SEQAD [S15]. In this test series eight 207 mm square by 610 mm high unreinforced concrete prisms were wrapped with glass ACM jackets. The concrete compressive strength, measured on two plain concrete prisms, was 37 MPa. The corners of the square section were rounded to 20 mm. The elastic modulus of the ACM jacket was 23 GPa.

Three types of jacketed concrete prisms are selected here for comparison purpose. **Table 8.5** and **Figure 8.29** show the comparison between experimental and analytical results. It can be found the predicted and measured response fit very well.

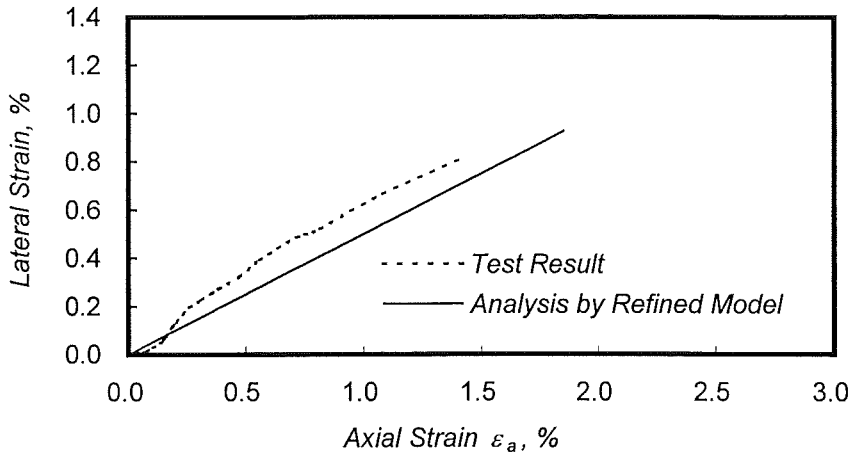

(a) Axial Strain v.s. Lateral Strain

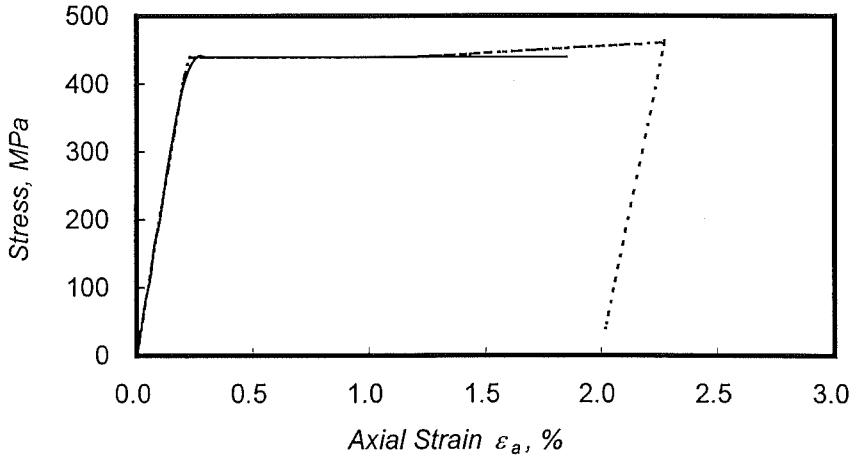

(b) Stress-Strain of Longitudinal Steel Bar HD20

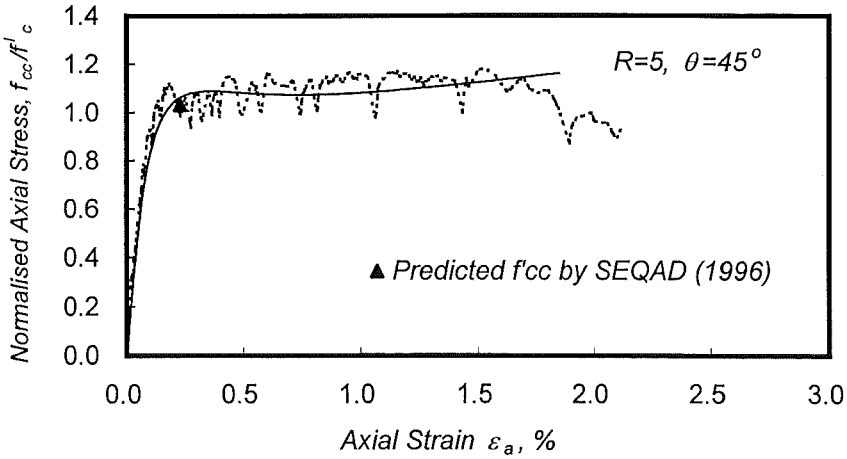

(c) Axial Stress-Strain Curves

Figure 8.25 Prediction on Axial Strength of Confined Concrete Using Refined Model, CS2

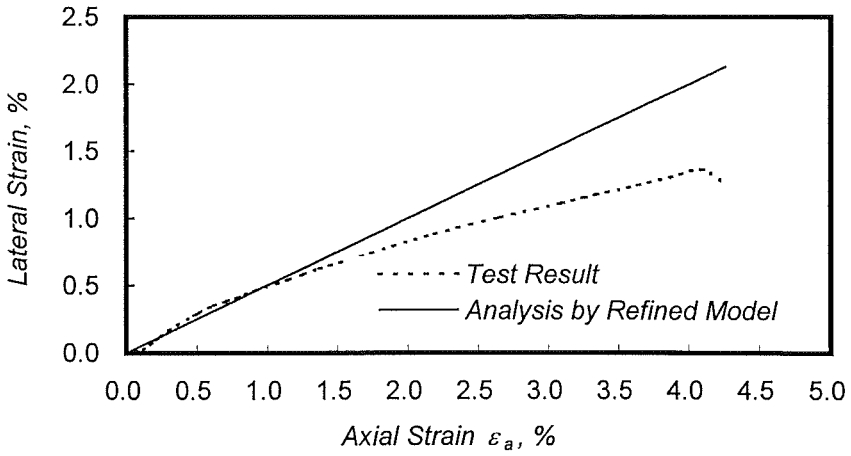

(a) Axial Strain v.s. Lateral Strain

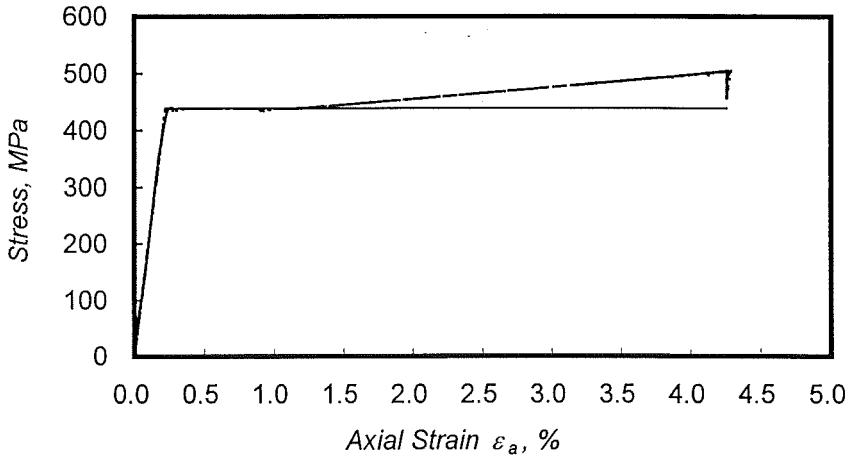

(b) Stress-Strain of Longitudinal Steel Bar HD20

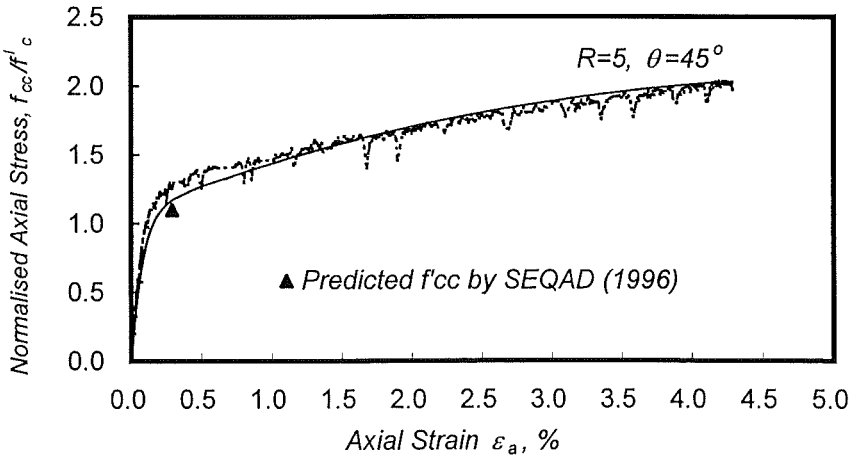

(c) Axial Stress-Strain Curves

Figure 8.26 Prediction on Axial Strength of Confined Concrete Using Refined Model, CS6

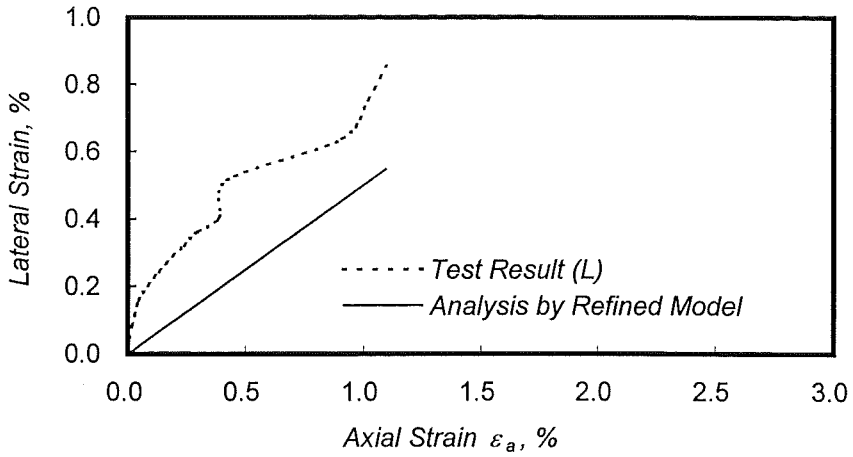

(a) Axial Strain v.s. Lateral Strain

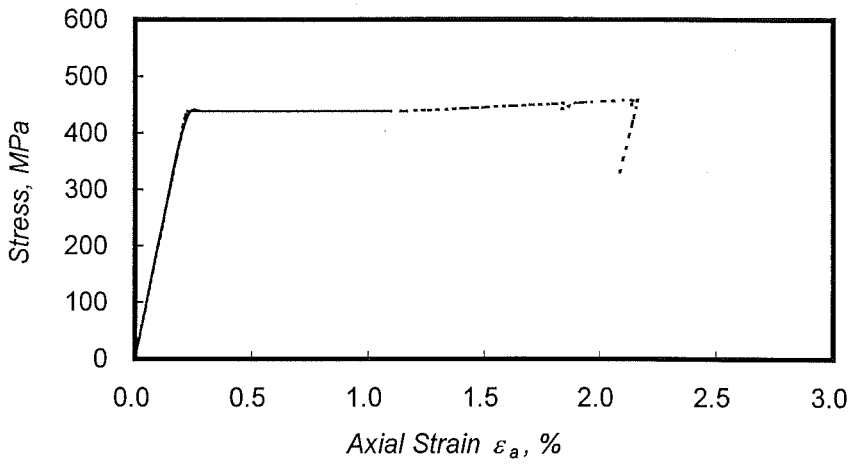

(b) Stress-Strain of Longitudinal Steel Bar HD20

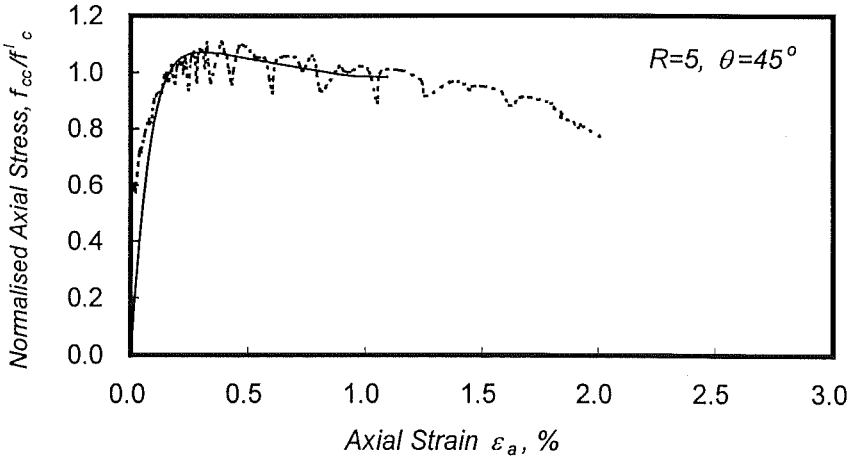

(c) Axial Stress-Strain Curves

Figure 8.27 Prediction on Axial Strength of Confined Concrete Using Refined Model, CR2

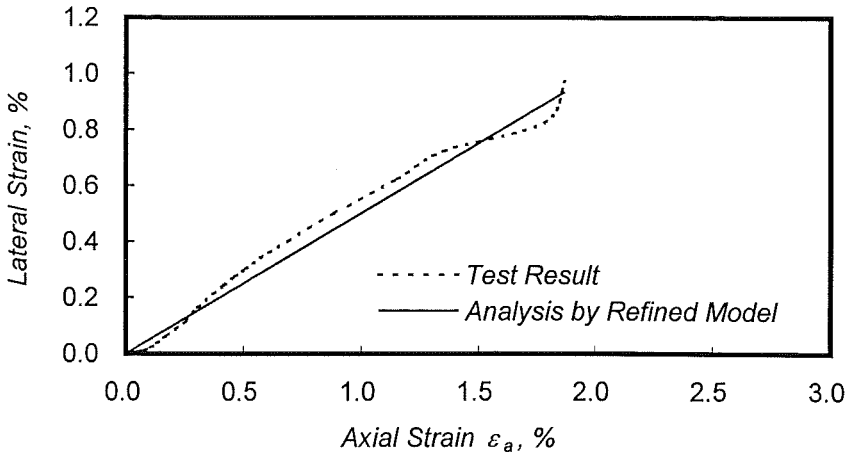

(a) Axial Strain v.s. Lateral Strain

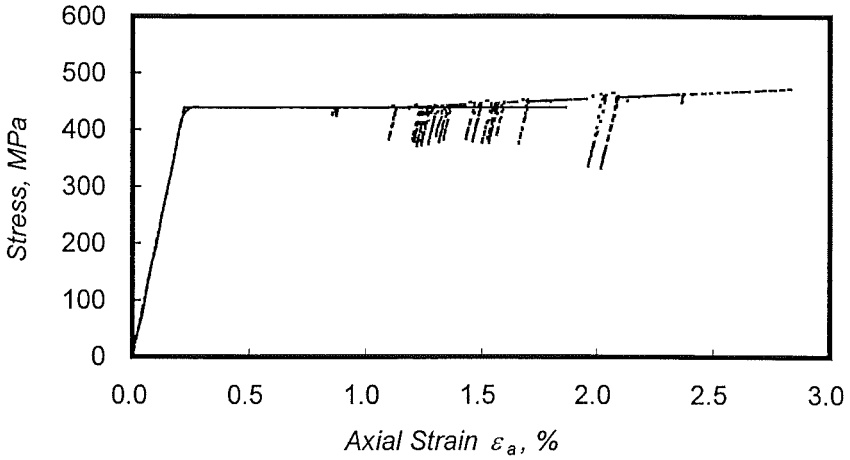

(b) Stress-Strain of Longitudinal Steel Bar HD20

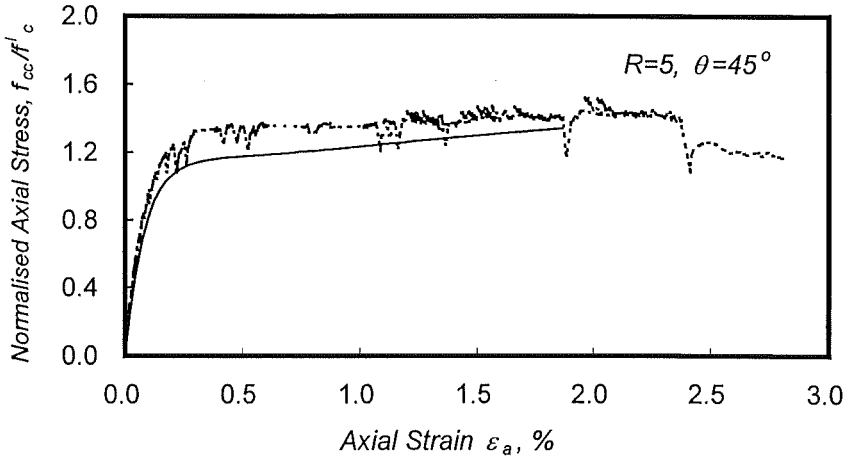

(c) Axial Stress-Strain Curves

Figure 8.28 Prediction on Axial Strength of Confined Concrete Using Refined Model, CR6

Table 8.5 Concrete Prism Details and Test Results Performed by SEQAD [S15]

Description of test [1]	Wraps of GFRP jacket	t_j (mm)	ρ_j ($= \rho_{jx} + \rho_{jy}$)	Test results		Ratio, f'_{cc}/f'_c	
				Ultimate Load (kN)	Ultimate Stress f'_{cc} (MPa)	Measured	Predicted[2]
• Tested 10 concrete prisms. • Dimensions (mm): 207 x 207 x 610 high • $f'_c = 37$ MPa, $E_p = 23$ GPa • Radius of the sectional corner is 20 mm.	1	1.27	0.025	1680	39.2	1.06	1.03
	2	2.54	0.050	1731	40.4	1.09	1.05
	4	5.08	0.100	1828	42.7	1.15	1.12

Notes: (1) The original report is provided by US customary units.

(2) The value is predicted using the simple analytical model presented in Section 8.9.3.

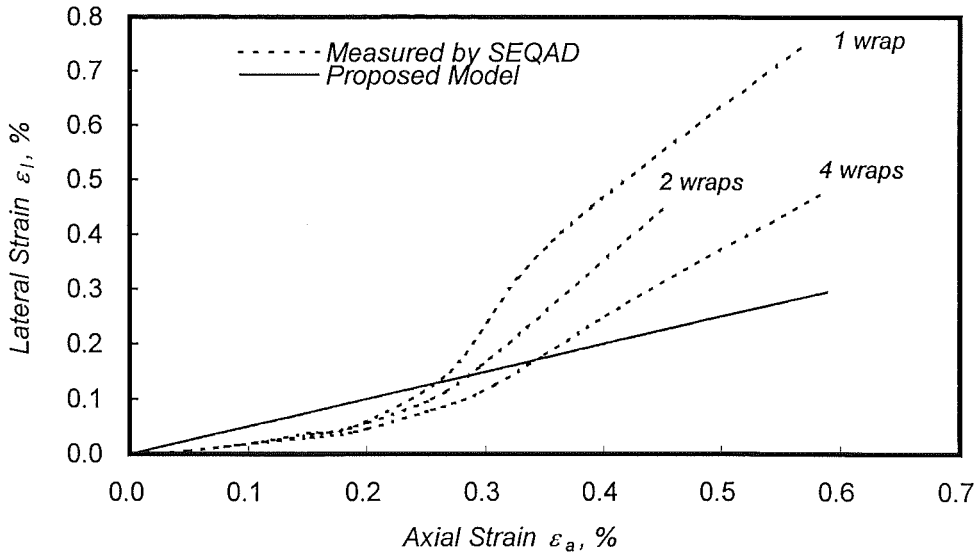

(a) Axial Strain v.s. Lateral Strain

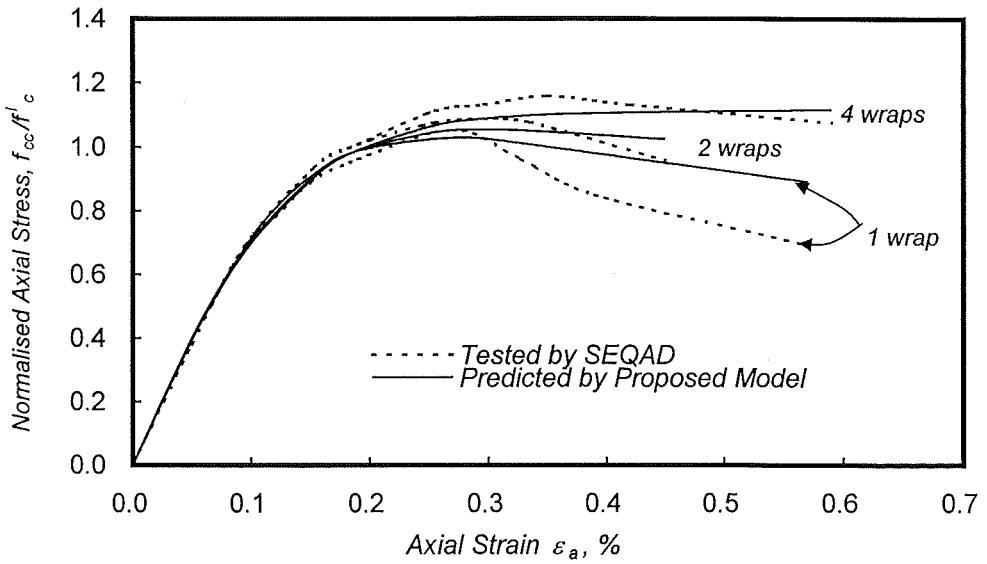

(b) Axial Stress-Strain Curves

Figure 8.29 Tests on Jacketed Prisms Conducted by SEQAD [S15]

8.10 Corner Radii in Jacketed Square and Rectangular Columns

Based on the test observation, the 30 mm radius at the corners had little effect on the overall response of the test units, at least for the normally expected range of longitudinal strains. This observation suggests that in small columns of buildings, the current recommendation of using a 51 mm radius [S16] for applying ACM jackets to columns seems unduly conservative.

8.11 Conclusions

1. Experimental work was conducted on six square and rectangular columns. Fibreglass/epoxy ACM jackets were applied to four columns. The other two columns were tested in their "as built' condition. The columns were tested under concentric loading, including load reversals in the tensile strain domain. The results from the tests confirm that ACM jackets provide excellent confinement in rectangular and square reinforced concrete columns, increasing both the ultimate strength and strain. Compressive strains of at least about 2% were measured without significant loss of the load carrying capacity in tests on columns with a minimum of two wraps. It was also observed that the ACM jackets are remarkably effective in precluding premature buckling of the longitudinal reinforcing bars in the columns. Larger strains were recorded when the number of wraps were increased from two to six.

2. The study shows a unique characteristic of confinement with ACMs in that the fibreglass/epoxy jacket hampers the dilation tendency of concrete, as it reverses the direction of volumetric strains in columns with large confining reinforcement ratios.

3. Columns jacketed with two glass ACM wraps failed by delamination of the jacket whereas columns jacketed with six wraps failed by splitting of the jacket at the rounded corners of the columns. Both failure types occurred at large axial strain levels. Using rounded corners with 30 mm radius had no adverse effect on the behaviour of the columns.

4. The analytical model built on the work by Mander et al. [M10, M11] and discussed in Chapter 7 was calibrated using the test results. It was concluded that when using R =5, $\theta = 45°$, and an effective Poisson's ratio for concrete $\upsilon = 0.5$, an excellent agreement with the results conducted in the present experimental work and other similar test is obtained. The proposed model can be easily incorporated for the analysis and design of the axially loaded columns retrofitted with ACM jackets.

CHAPTER 9

DESIGN RECOMMENDATIONS FOR PART III

9.1 General

Chapter 7 dealt with the derivation of equations to analyse the stress-strain behaviour of short columns wrapped with ACM jackets under concentric short term loads. The equations were calibrated using the results from the experimental work described in Chapter 8. In this chapter, the analytical model is modified for use in design.

9.2 Assumptions

The nominal concentric compressive strength of a short concrete column, P_n, is from Eq.7.1,

$$P_n = P_{cn} + P_{sn} \tag{9.1}$$

where P_{cn} and P_{sn} are the nominal compressive strength carried by the concrete and the longitudinal reinforcing steel bars, respectively, when the axial compression reaches the ultimate state of the column. It is assumed in this study that the ultimate limit state in a concentrically loaded column is associated with 1% axial strain. With Poisson's ratio assumed equal to $\upsilon = 0.5$, the transverse strain at 1% axial strain is equal to 0.5%.

It is assumed the reinforcing steel behaves as an elasto-plastic material. The nominal compressive strength carried by the concrete, P_{cn}, results from the stresses in three distinct regions shown in **Figure 7.1**. At 1% axial strain the unconfined concrete has reached its peak strength, f'_c, and has degraded to a residual strength to $0.3f'_c$ [P1]. Now from Eq.7.1c with $f_{c0} = 0.3f'_c$,

$$P_{cn} = 0.3f'_c A_{cu} + f'_{cc,j} A_{cj} + f'_{cc,js} A_{cjs} \tag{9.2}$$

$$P_{sn} = f_{sy} A_s \tag{9.3}$$

where $f'_{cc,j}$ and $f'_{cc,js}$ are the confined concrete compressive strength due to the single confinement of the external jacket and the dual confinement of the jacket and steel hoops, respectively. A_{cu}, A_{cj}, and A_{cjs} are the confined area with respect to different confining regions, which are defined by Eqs.7.2 to 7.4. f_{sy} is the yield strength of longitudinal reinforcement and A_s is the area of longitudinal reinforcement.

For design purposes it is necessary to reduce the nominal concentric strength given in Eq.9.1, to account for variations in the materials properties, scatter in the design equation, bending of the columns, nature and consequences of failure and reduction in load carrying capacity under long-term loads. This reduction results in a dependable concentric strength, ϕP_n, for short column given by,

$$\phi P_n = \phi_c P_{cn} + \phi_s P_{sn} \tag{9.4}$$

Material strength reduction factors ϕ_c and ϕ_s may be found using reliability analysis if the concrete strength in both the outside shell and in the core of the column as well as the yield strength of the longitudinal and transverse steel can be established with some degree of certainty. Alternatively, code reduction factors may be adopted to obtain the strength reduction factor ϕ. For example, the ACI 318 Building Code [A12] requires for columns that the ultimate axial compressive load found from analysis shall not exceed ϕP_n calculated as,

$$\phi P_n = 0.80\phi(0.85P_{cn} + P_{sn}) \tag{9.5}$$

For the axial compression members with transverse hoops, the strength reduction factor ϕ is 0.7. Therefore, Eq.9.5 becomes,

$$\phi P_n = 0.476P_{cn} + 0.56P_{sn} \tag{9.6}$$

in which $\phi_c = 0.476$ and $\phi_s = 0.56$. Thus the design requirement is given as,

$$\phi P_n \geq P_u \tag{9.7}$$

where P_u is the design concentric axial load in the column.

9.3 Calculation of the Nominal Concentric Strength

This section deals with the evaluation of the nominal concentric strength carried by columns strengthened with ACM jackets. The detailed calculation procedure has been described in Chapter 7, in which the compressive strength of confined concrete f'_{cc} (see Section 7.3 and 7.4) is to be attained. Particularly, 0.5% transverse strain in the jacket and the yield strength of the hoops are provided in the determination of lateral confining stresses due to the jacket and steel hoops (see Eq.7.13 to 7.21) when the nominal compressive strength of the concrete at ultimate state is evaluated. At 0.5% transverse strain typical strength steel hoops are yielding in tension.

Once the compressive strengths of the confined concrete, $f'_{cc,j}$ and $f'_{cc,js}$, and the confined areas, A_{cu} A_{cj} and A_{cjs}, are computed, the nominal compressive strength carried by the concrete is then obtained using Eq.9.2. An example of the application of the design recommendations is given in Section 9.5 to demonstrate the detailed design procedure.

9.4 Practical Recommendations

The experimental programme demonstrated that the use of small round corners has no effect over the range of longitudinal strains expected to occur in practice. It is recommended in this study that the radius in the round corners of columns be at least 30 mm.

Under service load conditions, a column with high ultimate axial load will be subject to relatively low lateral strains. Large lateral strains occurring as a result of dilation of the concrete will only occur when the concrete reaches the unconfined

compressive strength. In practice jackets are applied to columns when they are loaded close to the service load. The error of applying the jackets before the tests of the columns is very small and should not have an important effect on the results of loaded columns of buildings.

9.5 Prediction of Test Results

Table 9.1 shows the measured concentric loads in the concentrically loaded columns tested in this investigation. The experimental work was discussed in detail in Chapter 8. **Table 9.1** also shows the predicted nominal concentric load using Eq.9.2, 0.5% transverse strain, $\upsilon = 0.5$, and the measured material properties for the longitudinal and transverse reinforcement and for the glass ACM jackets. The concrete compressive strength used was obtained by averaging the stresses derived from the tests in Column CS0 and CR0 when loaded to 0.2% compressive strain.

Table 9.1 Measured and Predicted Compressive Loads

Unit	Compressive Load (kN)			
	Measured			Predicted[2]
	at 0.2% axial strain	at 0.5% transverse strain[1]	Maximum	
CS0	2,127		2,127	
CS2	(f'_c= 18.9 MPa)	2,335	2,525	2,355
CS6		2,978	4,025	2,949
CR0	3,268		3,268	
CR2	(f'_c= 18.9 MPa)	3,420	3,598	3,300
CR6		4,200	4,494	3,924

Notes: (1) Average of three sides. Ignores the transverse strain measured over the overlapped side.
(2) Using a jacket strain of 0.5%

The results in this table shows excellent agreement between the measured and predicted loads when the average transverse strain reaches 0.5%. No attempt is made to use higher transverse strains than 0.5% for the prediction of the ultimate strength, since more than 1% axial strain values are of little practical use. Note also that the transverse strain chosen in practice could be less than 0.5% as the sustained load characteristics of some ACM may control the design.

9.6 Design Example

The 670 mm by 380 mm rectangular column shown in **Figure 9.1** is to be confined with 14 layers of glass ACM jackets. The nominal thickness of one-layer jacket is 1.27 mm and elastic modulus of the jacket is 20 GPa. Find the ultimate concentric axial load that the jacketed column can sustain if the concrete cylinder compressive strength is 15 MPa, and the 5 percentile characteristic yield strengths of the longitudinal and transverse reinforcement are 430 MPa and 300 MPa, respectively. Find the dependable concentric compression load in the column using the ACI 318 Building Code approach assuming that 0.5% transverse strain is an acceptable value for design.

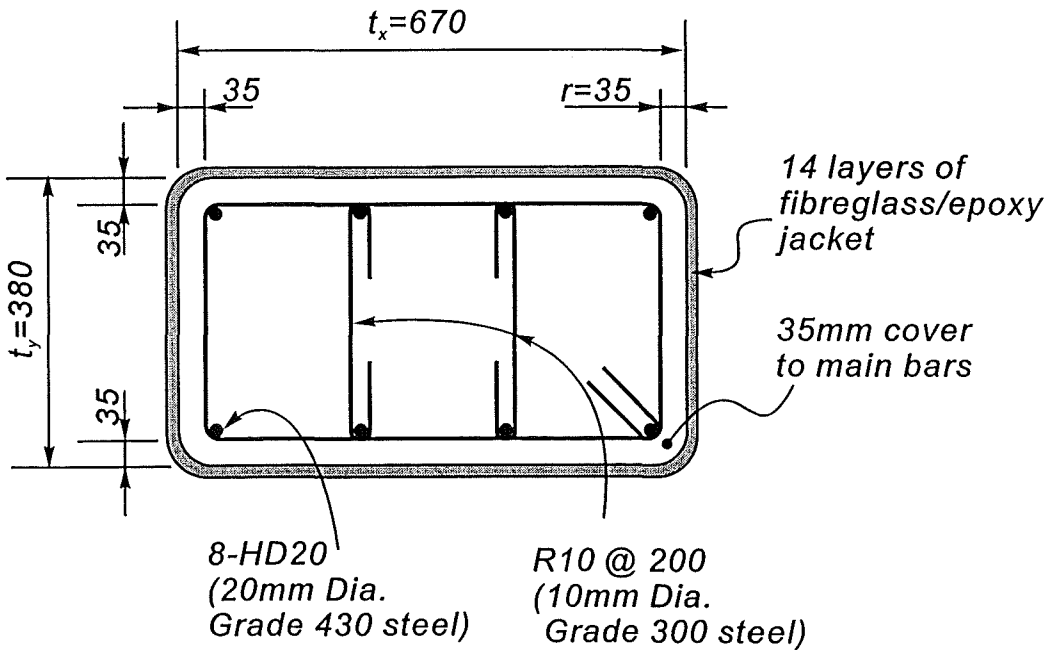

Figure 9.1 General Reinforcing Details of 670 mm by 380 mm Column

Solution

(1) Find the dependable axial compressive load carrying capacity of the "as-built" column using the unconfined concrete cylinder compressive strength.

from Eq.9.6,

$$\phi P_n = 0.476 \times (670 \times 380 - 2{,}512) \times 15 + 0.56 \times 2{,}512 \times 430 = 2{,}405\,\text{kN}$$

(2) Find the dependable concentric compressive load carrying capacity considering the confinement of the concrete.

(2.1) Confining pressure due to the transverse steel reinforcement only.

from Eq.7.18,

$A_{t,x} = 2 \times 78.5 = 157\ \text{mm}^2$ $A_{t,y} = 4 \times 78.5 = 314\ \text{mm}^2$

$d_x = 610$ mm $d_y = 320$ mm $s = 200$ mm $s' = 190$ mm

$$\rho_{sx} = \frac{157}{200 \times 320} = 0.00245$$

$$\rho_{sy} = \frac{314}{200 \times 610} = 0.00257$$

from Eq.7.17,

$$f_{l,sx} = 0.00245 \times 300 = 0.735$$

$$f_{l,sy} = 0.00257 \times 300 = 0.771$$

(2.2) Confining pressure provided by the jacket.

from Eq.7.14,

$$\rho_{jx} = 2 \times \frac{14 \times 1.27}{380} = 0.0936$$

$$\rho_{jy} = 2 \times \frac{14 \times 1.27}{670} = 0.0531$$

Use Eq.7.13 to predict the lateral confining stress due to the jacket at 0.5% lateral strain for ultimate state,

$$f_{l,jx} = 0.0936 \times (20{,}000 \times 0.005) = 9.36 \text{ MPa}$$

$$f_{l,jy} = 0.0531 \times (20{,}000 \times 0.005) = 5.31 \text{ MPa}$$

Use Eq.7.12 to calculate the compressive strength of the concrete,

$$F_l = \max.(f_{l,jx}, f_{l,jy}) = 9.36 \text{ MPa}$$

$$f_l = \min.(f_{l,jx}, f_{l,jy}) = 5.31 \text{ MPa}$$

$$\alpha_1 = 1.25\left(1.8\sqrt{1 + 7.94 \times \frac{9.36}{15}} - 1.6 \times \frac{9.36}{15} - 1\right) = 2.99$$

$$\alpha_2 = \left[1.4 \times \frac{5.31}{9.36} - 0.6 \times \left(\frac{5.31}{9.36}\right)^2 - 0.8\right]\sqrt{\frac{9.36}{15}} + 1 = 0.84$$

Now from Eqs.7.11 and 7.10,

$$k_c = 2.992 \times 0.843 = 2.52$$

$$f'_{cc,j} = 2.522 \times 15 = 37.83 \text{ MPa}$$

(2.3) Combined jacket and hoop confinement.

from Eq.7.21,

$$f_{l,x} = 0.735 + 9.36 = 10.1 \text{ MPa}$$

$$f_{l,x} = 0.771 + 5.31 = 6.1 \text{ MPa}$$

Use Eq.7.12 to calculate the compressive strength of the concrete,

$$F_l = \max.(f_{l,x}, f_{l,y}) = 10.1 \text{ MPa}$$

$$f_l = \min.(f_{l,x}, f_{l,y}) = 6.01 \text{ MPa}$$

$$\alpha_1 = 1.25\left(1.8\sqrt{1 + 7.94 \times \frac{10.095}{15}} - 1.6 \times \frac{10.095}{15} - 1\right) = 3.1$$

$$\alpha_2 = \left[1.4 \times \frac{6.081}{10.095} - 0.6 \times \left(\frac{6.081}{10.095}\right)^2 - 0.8\right]\sqrt{\frac{10.095}{15}} + 1 = 0.86$$

from Eqs.7.11 and 7.10,

$$k_c = 3.071 \times 0.857 = 2.63$$

$$f'_{cc,js} = 2.632 \times 15 = 39.5 \text{ MPa}$$

(3) Calculate the confined areas.

From **Figure 9.2,**

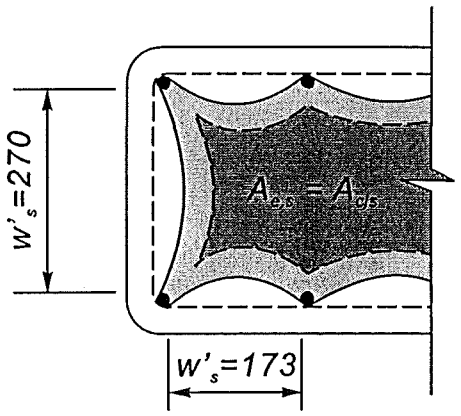

Figure 9.2 Effective Confined Area, $A_{cj,}$

In x-direction,

$$w'_s = (670 - 2\times 35 - 20\times 4)/3 = 173 \text{ mm}$$

In y-direction,

$$w'_s = 380 - 2\times 35 - 2\times 20 = 270 \text{ mm}$$

from Eq.7.7,

$$A_{e,s} = \left(610\times 320 - 6\times\frac{173^2}{6} - 2\times\frac{270^2}{6}\right)\left(1-0.5\times\frac{190}{610}\right)\left(1-0.5\times\frac{190}{320}\right)$$
$$= 83{,}683\text{mm}^2$$

From **Figure 9.3** and Eq.7.6, setting θ = 45°,

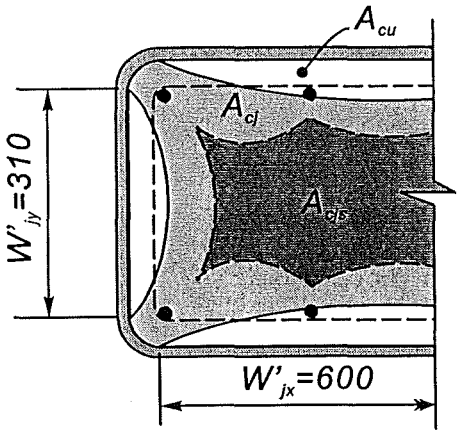

Figure 9.3 All Effective Confined Areas

$$A_{e,j} = 670\times 380 - \frac{600^2 + 310^2}{3}\tan 45^o - 2{,}512 - (4\times 35^2 - \pi\times 35^2)$$
$$= 99{,}003\text{mm}^2$$

from Eq.7.5,

$$A_{cc,J} = 670\times380 - 2{,}512 - (4\times35^2 - \pi\times35^2)$$
$$= 251{,}037\text{mm}^2$$

from Eqs.7.2 to 7.4,

$$A_{cu} = 251{,}037 - 99{,}003 = 152{,}034\text{mm}^2$$
$$A_{cj} = 99{,}003 - 83{,}683 = 15{,}320\text{mm}^2$$
$$A_{cjs} = 83{,}683\text{mm}^2$$

(4) Calculate the dependable axial compressive load carrying capacity of the jacketed column.

from Eqs.9.2, 9.3, and 9.6,

$$P_{cn} = 0.3\times15\times152{,}034 + 37.83\times15{,}320 + 39.48\times83{,}683 = 4{,}567\text{ kN}$$
$$P_{sn} = 430\times2{,}512 = 1{,}080\text{ kN}$$
$$\phi P_n = 0.476\times4{,}567 + 0.56\times1{,}080 = 2{,}779\text{ kN}$$

which represents an axial load increase of 16% from the original strength of the "as-built" column.

9.7 Conclusions

This chapter presents a design procedure to evaluate the nominal concentric strength carried by columns strengthened with ACM jackets. The assumptions are made using 1% axial strain as the ultimate limit state for the jacketed columns. An advantage of this design method is that the evaluation of the column axial compressive strength can be easily performed in practice. The predicted values resulting from the evaluation method also correlate the test results obtained in the experimental work discussed in Chapter 8 very well. A design example is discussed to show the application of the simple method.

PART IV

CONCLUSIONS AND RECOMMENDATIONS FOR FUTURE RESEARCH

PART Ⅳ

CONCLUSIONS AND RECOMMENDATIONS FOR FUTURE RESEARCH

1. General

Advanced composite materials (ACM), which were originally developed for the aerospace, are now widely used for retrofitting reinforced concrete members in buildings and bridges. A typical ACM laminate, Tyfo Fibrwrap System provided by FYFE Co. Ltd. in USA [F2], was selected to be strengthening materials for reinforced concrete beams and columns tested in the study.

This investigation began with reviewing previous research work on the use of ACM laminates and steel plates for strengthening reinforced concrete beams and columns, see Chapter 2 in Part Ⅰ. Three main studies were performed in the research programme. They are described in Parts Ⅱ and Ⅲ of this report.

The experimental programme discussed in Chapters 3 and 4 relate to the study on increasing the service live and the ultimate load of ACM-strengthened bridge girders. The retrofitting scheme of the beam using ACMs includes flexural, bond and shear strength enhancement. Ten half-scale simply supported ACM-strengthened T-beams were tested in the programme in three test series, namely Series-A, Series-B, and Series-C. Series-A and B included tests in which the carbon ACM (CACM) laminates were bonded to the full length on the soffit of the beams or were staggered. Six units were tested in Series-A to obtain information about the flexural strengthening of reinforced concrete beams with ACM laminates. Three units in Series-B were tested to observe the behaviour of the beams strengthened for both shear and flexure. One unit tested in Series-C was to study the fatigue behaviour of a beam. To simulate the traffic loading, repeated cyclic loading was applied in the service load range to all strengthened units. The repeated loading in Series-A and B tests were consisted in ten thousand cycles whereas that in Series-C consisted in one million cycles. The amplitude of the cycles was

such to induce 200 MPa stress range in the beam longitudinal reinforcement of mid-span. Then, these beams were monotonically loaded to failure to look at their performance and failure mode at the ultimate limit state.

Via this study, the mechanism of the CACM laminate debonding was found to occur in the tests in Series-A. The glass ACM (GACM) U-strips used in Series-B and C tests effectively precluded the laminate debonding and enhanced the shear strength. The analytical model proposed in Chapter 3 predicted accurately the observed behaviour of units. Design recommendations based on the results obtained in both tests and analyse is proposed in Chapter 6.

The test programme described in Chapter 5 investigated the seismic response of ACM-strengthened/retrofitted beams where the prototype beam had shear and bar curtailment deficiencies. This study was relative to seismic upgrading of reinforced concrete beams using ACM laminates. In this test, two full-scale T-section cantilever beams were built and tested under reversed cyclic loading. One unit was tested in its "as-built" condition until a flexure-shear failure developed at the curtailment point of the negative longitudinal reinforcement. The test unit was then repaired by applying GACM laminates across the top of the slab and to the sides of the beam in the damage region. It was again re-tested under reversed cyclic loading. The other unit was retrofitted before testing in the same manner as the previous damaged unit and then subjected to reverse cyclic loading. A seismic assessment on the prototype unit was proposed to provide a simple evaluation on the beam with deficiencies in flexural design of T-beam, shear, and longitudinal bar curtailment.

The analytical and experimental study presented in Chapters 7 to 9 proposed a method for evaluating the short-term axial load strength of rectangular and square reinforced compression members confined with an ACM jacket and steel hoops. The study was concentrated on the behaviour of ACM-wrapped columns subjected to the concentric axial load only. Three 300 mm square and three 300 mm by 450 mm short reinforced columns were concentrically loaded first in tension, then in compression to failure. Either two or six layers of GACM jackets were applied to four of these columns. Two control units were tested in order to evaluate the enhancement of the axial load carrying capacity and to observe whether the ACM jackets were able to preclude

premature buckling of the longitudinal reinforcement in the wrapped columns. The analytical model proposed was used to validate the test results. Design equations in close form were derived based on the calibration of the analytical model to provide a design of ACM-wrapped reinforced concrete column subjected to the concentric axial load.

The main conclusions and recommendations are made according to the three study topics mentioned above.

2. Conclusions

2.1 Conclusions for the Study on the Behaviour of RC Beams with Bonded ACM Laminates

The analytical model proposed in Chapter 3 and the experimental study presented in Chapter 4 are concluded together in the following items:

(1) The analytical discrete segment model presented in Chapter 3 was used to predict the response of the T-beams externally strengthened with epoxy-bonded ACM laminates. In the model each segment with ACM laminates bonded to the tension face and the side took into account the interaction between moment and shear using moment curvature analysis and modified compression field theory (MCFT). Thus, the interface bond characteristic between concrete and ACM laminates and the failure mode of the beams strengthened with ACM laminates was predicted.

(2) The predicted and observed CACM laminate longitudinal strain agreed the test results very well. That is, the analytical model can be used to study the strength and failure mode of reinforced concrete beams strengthened with full-length or staggered ACM laminates bonded to their soffit and sides. Furthermore, the analytical results showed that the beams strengthened with staggered ACM laminates bonded to their tension faces could be used more efficiently than the beams bonded with full-length ACM laminates.

(3) The strain measurement on bottom concrete face and carbon ACM laminate indicate that the assumption of no slip between concrete surface and ACM laminate described in the theoretical study is acceptable.

(4) It was found, by test and analysis data on the beams strengthened with CACM laminates bonded to their soffit, that the laminate debonding has a relationship with the beam shear strength. This is because the ACM laminate will separate suddenly due to a large shear kinking when the shear is applied near the beam shear strength. Moreover, an attention must be paid to the prototype beam with curtailed steel reinforcement that the flexure-shear crack in the vicinity of steel bar cut-off can cause the shear strength of the beam lower and poorly influence the response of a beam retrofitted with ACM laminates.

(5) The shear kinking was a main reason causing the ACM delamination failure observed in the most of Series-A units as discussed in the experimental study of Chapter 4. This phenomena was specially found in the test of Unit F3 which is the beam strengthened with three full-length layers of CACM laminates bonded to the beam soffit and with two GACM U-side strips bonded to the laminate ends.

(6) The beam with staggered CACM laminates was studied for the benefits of the structural response and a cost saving. Based on test results, the beams with full-length ACM laminates bonded to their soffit and the beams with staggered ACM laminates behave in a similar manner at the service load range and the ultimate limit state.

(7) According to the test results represented in the Series-B test of Chapter 4, GACM U-side strips with fibre-anchor can improve the bond strength of the ACM laminates bonded to the soffit of the beams and enhance the beam shear strength. The effective transverse strain of 0.4% can be used for the design of GACM U-side strips with mechanical anchors. The fibreglass Tyfo-anchors used in the test show very effective in preventing delamination of the U-side

strips and can be considered to be fully effective in 120 mm wide U-side strips.

(8) Test results on the unit tested in Series-C, which was subjected to one million cycles of repeated loading, shows that the behaviour of the beam strengthened with carbon and glass ACM laminates resembles the behaviour of the same type of beams subjected to the monotonic loading at service load range.

(9) For the general conclusion on the study, the ACM laminate for flexural strengthening in ultimate limit state can be used to increase the service live load capacity. The ACM U-side strips with effective mechanical anchors for shear enhancement can not only increase the beam shear strength but also prevent the unexpected failure mode such as the laminate debonding from occurring. The ACM laminates bonded to both the tension face and the side of the beam show an excellent performance in the behaviour of fatigue resistance. However, due to an economic point of view, the staggered layers of ACM laminates bonded to the beam soffit can be alternatively considered in the retrofit scheme design if they are designed adequately when the full-length laminates are used all the time.

2.2 Conclusions for the Study on the Use of Composite Plates for the Seismic Retrofitting of RC Beams with Shear and Bar Curtailment Deficiencies

The "as-built" structural assessment and experimental observation for the seismic upgrading of the existing RC beams in an old building, discussed in Chapter 5, are summarised as follow:

(1) A simple assessment on the existing reinforced concrete beams with longitudinal bar curtailment was carried out using a concept of tension shift adopting a variable angle truss model to identify the failure mechanism of the as-built beam. The assessment results revealed that beams of moment resisting frames designed to earlier seismic design codes might show inadequate performance due to the presence of the slab reinforcement. Slab reinforcement may be a cause for poor development of the beam negative flexural reinforcement and may push the formation of the plastic hinges away from the column faces into a region not detailed for ductility. This deficiency may result in an unexpected flexure-shear

failure of the beam at the shifted critical location, such as the region in the curtailment of longitudinal reinforcement.

(2) Experimental work conducted on full-scale beam/slab assemblies showed that ACM laminates, acting as additional negative beam reinforcement, could successfully be used to relocate the negative plastic hinges to the column face. To ensure the adequate performance of the retrofit scheme, shear deformations in the beam must be kept to a minimum to reduce the kinking effect and potential delamination of the composite material plate.

(3) The retrofitting design in flexural enhancement is to ensure that the strain limit of 0.4% imposed on the GACM laminate may be used to enhance the flexural strength at the beam bar cut-off points.

(4) To minimise the shear kinking effect causing eventually delamination of the ACM laminate, U-shaped ACM strips with anchors at the strip ends are recommended. In the test programme, a continuous type of U-shaped GACM strips bonded to the sides of a beam without any anchors at their ends were ineffective in resisting shear. The loss of the side strips caused shear distortion of the beam and led to kinking and delamination of the longitudinal GACM laminates at larger shear distortion angles.

2.3 Conclusions for the Design Recommendation on the RC Beams Retrofitted with ACM Laminates

A design approach for reinforced concrete T-beams strengthened with externally bonded ACM laminates being cut off is proposed. One important factor associated in the design is that not only the ultimate limit state requirement but also the serviceability limitation should be satisfied. A staggered ACM laminates bonded to the tension face of the beam is suggested for an economic design.

The concept of the laminate development length is adopted to the design guideline. ACM U-side strips with mechanical anchors are recommended in the case of the requirements in both the longitudinal ACM bond strength increase and the beam shear

strength enhancement. The design method also suggests that the debonding failure of the ACM laminate bonded to the beam soffit could be avoided with the incorporation of ACM U-side strips. U-side strips can also be used to resist shear providing that a shear failure originating between below the flange of a T-beam and the anchoring point of the side strips does not occur. Shear design recommendations based on a modified shear friction concept are given.

Finally, the design concept for seismic retrofit of beams with longitudinal bar cut-off deficiencies is proposed. The method uses GACM or CACM longitudinal laminates and U-side strips for both flexural and shear enhancement to shift the plastic hinge from the deficient region to the beam end.

2.4 Conclusions for the Study on the Strength Enhancement of Concentrically Loaded Reinforced Concrete Columns Using ACM Jackets

The work presented in Chapters 7 to 9 led to the following conclusions:

(1) A theoretical approach for evaluating the full response of the axial load and deformation of the columns by means of confined ACM jackets was proposed to predict and compare the tested columns. The analytical model was calibrated using the test results. It was concluded that when using the theoretical stress-strain model proposed by Mander et al. with R =5, θ = 45°, and an effective Poisson's ratio for concrete υ = 0.5, an excellent agreement with the results conducted in the experimental programme and other similar test was obtained.

(2) The results from the test on full-scale square and rectangular cross sections of reinforced concrete columns confined with two to six layers of fibreglass/epoxy ACM jackets, showed compressive strains of at least 2% were attained without significant loss of the load carrying capacity in tests on columns with a minimum of two ACM wraps. Larger strains were recorded when the number of wraps was increased from two to six. The results demonstrated the effectiveness of the ACM jackets in enhancing the ultimate strain (ductility) and strength of concrete and their ability to prevent buckling of the longitudinal reinforcement.

(3) Columns jacketed with two GACM wraps failed by delamination of the jacket whereas columns jacketed with six wraps failed by splitting of the jacket at the rounded corners of the columns. Both failure types occurred at large axial strain levels. Using rounded corners with 30 mm radius had no adverse effect on the overall behaviour of the columns.

(4) The study shows a unique characteristic of confinement with fibre composites in that ACM jacket hampers the dilation tendency of concrete, as it reverses the direction of volumetric strains in columns with large confining reinforcement ratios.

(5) A design procedure to evaluate the nominal concentric strength carried by columns strengthened with ACM jackets was finally built up. The assumptions were made using 1% axial strain and 0.5% transverse strain as the ultimate limit state for the jacketed columns. The predicted values resulting from the design method correlated the test results very well.

3. Main Contributions Obtained from This Research

The following items described are the main contributions originating from this research:

Study on RC Beams Retrofitted with ACM Laminates

(1) Staggered ACM laminates bonded to the soffit of the beam was originally considered in the research. Resulting from analytical and experimental works, the staggered laminates are very effective in the structural behaviour and in an economic point of view.

(2) The proposed analytical segment model, refined from the analytical discrete model [A9] which only considered the effect of bending moment, additionally takes into account the influence of shear diagonal cracking in each analytical

segment. This allows the prediction on the ACM-strengthened beams using the proposed segment model is more practical than that using the analytical discrete model.

(3) A factor causing the laminate debonding of the ACM-bonded beams was found experimentally due to the shear kinking effect. It has proven by means of the comparison between the analytical and experimental results that the shear kinking occurs when the applied shear force reaches near the theoretical beam shear strength.

(4) An evaluation method was developed for flanged beams in which the beam flange is in tension using a concept of tension shift and shear lag adopting a variable angle truss model.

(5) An incorrect design concept used in the past pointed out in the study on the beams of moment resisting frames designed for seismic resistance is highlighted. This design deficiency is due to the fact that the contribution of the slab reinforcements in a T- beam is not considered in the overall seismic response of the beam.

(6) A design guideline for the beam strengthened with ACM laminates was proposed considering both the enhancement of the service load ability and the strength increase in ultimate limit state.

Study on Axially Loaded RC Columns Confined with ACM Jackets

(1) A theoretical model for evaluating the enhancement of the axial compression load of columns by means of ACM jackets was developed with success from a model used for determining the compressive strength of concrete columns confined by steel hoops only.

(2) The experimental work is conducted to show the effects of ACM jackets in confining the concrete core of full scale square and rectangular columns and in preventing premature buckling of the column longitudinal reinforcement, which

can hardly be proven by the theoretical model.

(3) A fundamental research on the behaviour of confined concrete can be better understood using the present study on axially loaded concrete columns confined with ACM jackets.

(4) A design approach proposed to evaluate the nominal concentric strength carried by columns strengthened with ACM jackets can be easily performed in practice, which is different from other design methods.

4. Recommendations for Future Research

As in every research project the author believes that the study described here is far from complete. Future research should address both analytically and experimentally the issues mentioned below:

4.1 RC Beams Strengthened with ACM Laminates

(1) When the prediction on the beams strengthened with ACM laminates bonded to their tension face is performed, the nominal flexural strength envelope is needed. Due to lack of previous research on the development length of the externally bonded ACM laminates, it is assumed that the laminate development length can be approximated as shown in Eq.4.2. It is necessary to study the development length of the ACM laminate in an experimental manner.

(2) The scenario of shear kinking in the ACM laminate bonded to the beam soffit was observed in the test. However, quantifying the effect on the laminate debonding is required as the further theoretical and experimental studies.

(3) The analytical segment model described in Chapter 3 has proven its validity using the test results mentioned in Chapter 4. However, the calculated laminate stress using the approximate solution of the modified compression field theory (MCFT) for evaluating the shear cracking seems unlikely to converge very well

as the decrease in the segment length. It is necessary to study this furthermore such as the convergent trend always discussed in finite element analysis. Perhaps, the analytical segment model with more accurate solution of the MCFT like dual-section analysis [C4] or with other methods for shear cracking evaluation can solve this problem.

(4) Unlike electrical type of strain gauges, the mechanical type of DEMEC gauge is recommended for the strain measurement on the ACM laminate. This allows very stable reading to be obtained. However, it seems not to be possibly carried out using the DEMEC gauge measurement when the test load reaches near the beam failure. An alternative measured method for working out the disadvantage is necessary.

(5) The full-scale beams retrofitted with ACM laminates using the design guideline that were proposed in Chapter 6 need to be experimentally verified. A future study can be performed using the design method to look at the long-term behaviour of the retrofitted beam. Some factors such as the creep and fatigue of the bonded ACM laminate, material reduction factors in the design method, and the cost efficiency analysis can also be obtained.

(6) A shear friction failure developing in the web between the flange and the end of the ACM U-side strips has been taken into account in the design recommendation of the beam retrofitted with ACM laminates. However, this failure mode not observed in the present test programme can be investigated further.

(7) An interesting subject comprises the investigation into the use of different mechanical anchors to the U-side ACM strip. A special attention when choosing suitable anchors for testing should be paid to the practical use. Meanwhile, a cross section aspect ratio b_w/d, for the consideration of the anchor rod crossing the full beam web, can be studied further.

(8) Other important issues correlated to the beams strengthened with ACM composites have to be investigated such as:

- the effect of different concrete surface roughening methods on the interface bond strength between concrete and ACM laminate;
- the effect of the temperature changes because concrete and ACM have different temperature expansion coefficients;
- the influences of the existing cracks and the initial loading of the beam at the time when the retrofitting is carried out.

4.2 RC Columns Confined with ACM Jackets

The study on the RC columns with ACM jackets in the thesis was focused on the RC columns subjected to axial compressive load. The excellent performance for the experimental and analytical works had been achieved as presented in Part Ⅲ. However, some topics, presented in the following, are needed to be studied further:

(1) A theoretical study on the relationship of moment and curvature of the RC columns confined with ACM jackets can be developed using the stress-strain behaviour of the confined concrete columns tested and predicted by the present project.

(2) An experimental work should be performed to verify the above analytical model. The ACM-confined columns will be tested under axial compression and lateral reversed cyclic loading.

(3) Due to the columns subjected to the long-term compression, a research on the time-dependent creep characteristics of the ACM material should be carried out. This study will recommend safe stress value to avoid the creep failure.

(4) The ACM-strengthened reinforced concrete column designed using the proposed method needs more experimental verification particularly under combined axial load, bending and shear.

REFERENCES

[A1] ACI Committee 440, 1996, State-of-the-Art Report on Fiber Reinforced Plastic (FRP) Reinforcement for Concrete Structures.

[A2] ASTM D 3039, 1995, Standard Test Method for Tensile Properties of Polymer Matrix Composite Materials.

[A3] ASTM D 4258-83, 1992, Practice for surface cleaning concrete for coating.

[A4] ASTM D 4259-83, 1992, Practice for abrading concrete.

[A5] ASTM D 5295-83, 1992, Standard guide for preparation of concrete surfaces foe adhered (Bonded) membrane water proofing systems.

[A6] An, W., Saadatmanesh, H., and Ehsani, M.R., 1991, RC beams strengthened with GFRP plates Ⅱ : analysis and parametric study, Journal of Structural Engineering, ASCE, V.117, No.11, pp.3434-3455.

[A7] Arduini, M., D'Ambrisi, A., and Di Tommaso, A., 1994, Shear failure of concrete beams reinforced with FRP plates, Infrastructure: New Materials and Methods of Repair, Proceedings of the Third Materials Engineering Conference, Nov., San Diego, California, pp.123-130.

[A8] Arduini, M., Di Tommaso, A., and Nanni, A., 1997, Brittle failure in FRP plate and sheet bonded beams, ACI Structural Journal, V.94, No.4, July-Aug., pp.363-370.

[A9] Arduini, M., and Nanni, A., 1997, Parametric study of beams with externally bonded FRP reinforcement, ACI Structural Journal, V.94, No.5, Sep.-Oct., pp.493-501.

[A10] Arduini, M., and Nanni, A., 1997, Behavior of precracked RC beams strengthened

with carbon FRP sheets, Journal of Composite for Construction, ASCE, V.1, No.2, May, pp.63-70.

[A11] American Concrete Institute, 1971, Building Code Requirements for Reinforced Concrete ACI 318-71, Detroit, Michigan.

[A12] American Concrete Institute, 1995, Building Code Requirements for Reinforced Concrete (ACI 318-95) and Commentary (ACI 318R-95), Detroit, Michigan.

[A13] AASHTO, 1977 and 1989, Standard Specifications for Highway Bridges, 12nd and 14th editions, Washington D.C.

[B1] Branson, D.E., 1977, Deformation of Concrete Structures, McGraw-Hill, USA, 546pp.

[B2] Batchelar, M.L., 1973, Epoxy Resin Materials as Structural Adhesives, M.S. Thesis, University of Canterbury, New Zealand, 101pp.

[B3] Bresson, J., 1971, Nouvelles recherches et applications concernant I'utillisation des collages dans les structures, Annales de I'ITBTB, serie BBA/116.

[B4] Beukel, A. van den, 1978, Composite Beams, HERON, Research Report, V.23, N.2, Department of Civil Engineering, Delft University of Technology, Delft, The Netherlands.

[C1] Cheung, P.C., Paulay, T., and Park, R., 1991, Seismic Design of Reinforced Concrete Beam-column Joints with Floor Slab, Research Report 91-4, Department of Civil Engineering, University of Canterbury, Christchurch, 328pp.

[C2] Chana, P.S., 1987, Investigation of the mechanism of shear failure of reinforced concrete beams, Magazine of Concrete Research, V.39, No.141, Cement and Concrete Association, England, pp.196-204.

[C3] Chajes, M. J., Januszka, T. F., Mertz, D. R., Thomson, T. A. Jr., and Finch, W. W. Jr., 1995, Shear strengthening of reinforced concrete beams using externally applied composite fabrics, ACI Structural Journal, V.92 No.3, pp.295-303.

[C4] Collins, M.P., and Mitchell, D., 1991, Prestressed Concrete Structures, Prentice Hall, New Jersey, 766pp.

[C5] Construction Techniques Group Ltd., 1997, Design Manual – Performance Enhancement of Concrete, Mansonry, and Timber Structures Using Tyfo Composite Materials, New Zealand.

[C6] Charles, H.H., and Scott, A.O., 1997, Cleaning and preparing concrete before repair, Concrete International, ACI, pp.60-63.

[C7] Cusens, A.R., and Smith, D.W., 1980, A study of epoxy resin adhesive joints in shear, The Structural Engineer, V.58A, No.1, pp.13-18.

[C8] Chen, W.F., 1982, Plasticity in Reinforced Concrete, McGraw-Hill Book Co., New York, 474pp.

[D1] Dale, J.T., 1983, The shear strength of partially prestressed concrete beams, Report No.317, Depart. of Civil Eng., Univ. of Auckland, New Zealand, 351 pp.

[D2] Dodd, L., 1992, The Dynamic Behaviour of Reinforced-Concrete Bridge Piers Subjected to New Zealand Seismicity, Ph.D. Thesis, Department of Civil Engineering, University of Canterbury, Christchurch, New Zealand, 460 pp.

[D3] Dodd, L.L., and Restrepo-Posada, J.I., 1995, Model for predicting cyclic behavior of reinforcing steel, Journal of Structural Engineering, ASCE, V.121, No.3, pp.433-445.

[E1] Elwi, A.A., and Murray, D.W., 1979, A 3D hypoelastic concrete constitutive relationship, Journal of Engineering Mechanics Division, ASCE, V.105, No.EM4, pp.623-641.

[F1] Fenwick, R.C., Tankut, C.W., and Thom, C.W., 1981, The Deformation of

Reinforced Concrete Beams Subjected to Inelastic Cyclic Loading - Experimental Results, Report No.268, Depart. of Civil Eng., Univ. of Auckland, New Zealand, 72 pp.

[F2] Fyfe Co. LLC, 1988, Design Manual for Tyfo Fibrwrap System – Rev.1, Feb., USA.

[F3] Fleming, C.J., and King, G.E.M., 1967, The development of structural adhesives for three original uses in South Africa, RILEM International Symposium, Synthetic Resins in Building Construction, Paris, pp.75-92.

[F4] Fyfe, E.R., Gee, D.J., and Milligan, P.B., 1998, Composite systems for seismic applications, Concrete International, ACI, June, pp.31-33.

[G1] Guess, T.R., Allred, R.E., and Gerstle Jr., F.P., 1977, Comparison of cap shear test specimens, Jounal of Testing and Evaluation, V.5, No.3, Mar., pp.84-93.

[G2] Gemert, D.V., 1980, Force transfer in epoxy bonded steel/concrete joints, International Journal Adhesion and Adhesives, pp.67-73.

[G3] Goland, M., and Reissner, E., 1944, The stresses in cemented joints, Journal of Applied Mechanics, No.66.

[H1] Hakuto, S., Park, R., and Tanaka, H., 1995, Retrofitting of Reinforced Concrete Moment Resisting Frame, Research Report 95-4, Department of Civil Engineering, University of Canterbury, Christchurch, 390pp.

[J1] Jones, R, Swamy, R.N., and Charif, A., 1988, Plate separation and anchorage of reinforced concrete beams strengthened by epoxy-bonded steel plates, The Structural Engineer, March, V.66, No.5, pp.85-94.

[K1] Kaiser, H. P., 1989, Strengthening of Reinforced Concrete with Epoxy-Bonded Carbon Fibre Plastics, Doctoral Thesis, Diss. ETH Nr.8918, ETH Zurich, CH-8092 Zurich/Swizerland (in German), 224pp.

[K2] Katsumata, H., Kobatake, Y., and Takeda, T., 1988, Study with carbon fiber for

earthquake-resistant capacity of existing reinforced concrete columns, Proceedings of the Ninth World Conference on Earthquake Engineering, Tokyo, V.7, pp.517-522.

[L1] Ladner, M., 1983, Reinforced concrete members with subsequently bonded steel sheets, printed in Strengthening of Building Structures – Diagnosis and Therapy, IABSE Symposium, pp.203-210.

[L2] L'hermite, R.L., and Bresson, J., 1967, Beton arme par collage des armatures, RILEM International Symposium, Synthetic Resins in Building Construction, Paris, pp.175-203.

[L3] Li, B., Park, R., and Tanaka, H., 1995, Strength and Ductility of Reinforced Concrete Members and Frames Constructed Using High Strength Concrete, Research Report 94-5, Department of Civil Engineering, University of Canterbury, Christchurch, New Zealand, 373pp.

[M1] Ma, S.M., Bertero, V.V., and Popov, E.P., 1976, Experimental and Analytical Studies on Hysteretic Behavior of Reinforced Concrete Rectangular and T-Beams, Report EERC 76-2, Earthquake Engineering Research Center, Univ. of California, Berkeley, California.

[M2] Meier, U., 1992, Carbon fibre-reinforced polymers: modern materials in bridge engineering, Structural Engineering International, V.2, pp.7-12.

[M3] Meier, U., 1995, Strengthening of structures using carbon fibre/epoxy composites, Construction and Building Materials, V.9, No.6, pp.341-351.

[M4] Meier, U., and Kaiser, H., 1991, Strengthening of structures with CFRP laminates, reprinted from Advanced Composites Materials in Civil Engineering Structures Proceedings, MT Div./ASCE/Las Vegas, pp.224-232.

[M5] Macdonald, M.D., 1978, The flexural behaviour of concrete beams with bonded external reinforcement, TRRL Supplementary Report 415.

[M6] Mohamed Ali, M.S., and Oehlers, D.J., 1997, Preventing debonding through shear

of tension face plated concrete beams, Conference on the Mechanics of Structures and Materials, Grzebieta, Al-Mahaidi & Wilson, Australia, 1997, pp.123-127.

[M7] Mukhopadhyaya, P., Swamy, N., and Lynsdale, C., 1998, Optimizing structural response of beams strengthened with GFRP plates, Journal of Composites for Construction, ASCE, V.2, No.2, May, pp.87-95.

[M8] Macdonald, M.D., and Calder, A.J.J., 1982, Bonded steel plating for strengthening concrete structures, International Journal of Adhesion and Adhesives, pp.119-127.

[M9] Morsch, E., 1908, Der Eisenbetonbau (Reinforced Concrete Construction), Verlag von Konard Wittwer, Stuttgart, West Germany.

[M10] Mander, J.B., Priestley, M.J.N., and Park, R., 1984, Seismic Design of Bridge Piers, Research Report 84-2, Department of Civil Engineering, University of Canterbury, Christchurch, New Zealand, 442 pp.

[M11] Mander, J.B., Priestley, M.J.N., and Park, R., 1988, Theoretical stress-strain model for confined concrete, Journal of Structural Division, ASCE, V.107, No.ST11, pp.2227-2244.

[M12] Mirmiran, A., and Shahawy, M., 1997, Behavior of concrete columns confined by fiber composites, Journal of Structural Engineering, ASCE, V.123, No.5, pp.583-590.

[M13] Mirmiran, A., Shahawy, M., Samaan, M., Echary, H.E., Mastrapa, J.C., and Pico, O., 1998, Effect of column parameters on FRP-confined concrete, Journal of Composites for Construction, ASCE, V.2, No.4, pp.175-185.

[M14] Mays, G.C., and Hutchinson, A.R., 1992, Adhesives in Civil Engineering, the Press Syndicate of the University of Cambridge, England, 333pp.

[M15] Mattock, A.H., 1976, Design proposals for reinforced concrete corbels, PCI Journal,

V.21, No.3, May-June, pp.18-42.

[N1] Nilson, A.H., and Winter, G., 1986, Design of Concrete Structures, McGraw-Hill, New York, 730pp.

[N2] Nanni, A., 1997, New technology becomes mainstream – CFRP strengthening, Concrete International, ACI, June, pp.19-23.

[N3] Norris, T., Saadatmanesh, H., and Ehsani, M.R., 1997, Shear and flexural strengthening of R/C beams with carbon fiber sheets, Journal of Structural Engineering, ASCE, V.123, No.7, July, pp.903-911.

[N4] NZS 3101: Part 1 and 2, 1995, New Zealand Concrete Structures Standard, Part 1- The Design of Concrete Structures and Part 2- Commentary on The Design of Concrete Structures.

[N5] NZS 3112: Methods of Test for Concrete, 1986, Part 2: Tests Relating to the Determination of Strength of Concrete.

[O1] Oehlers, D.J., 1988, Reinforced Concrete Beams with Steel Plates Glued to Their Soffits: Prevention of Plate Separation Induced By Flexural Peeling, Report No.R80, Department of Civil Engineering, The University of Adelaide, Australia.

[O2] Oehlers, D.J., and Moran, J.P., 1990, Premature failure of externally plated reinforced concrete beams, Journal of Structural Engineering, ASCE, V.116, No.4, pp.978-995.

[O3] Oehlers, D.J., 1992, Reinforced concrete beams with plates glued to their soffits, Journal of Structural Engineering, ASCE, V.118, No.8, pp.2023-2038.

[O4] Oehlers, D.J., Mohamed Ali, M.S., and Luo, W., 1998, Upgrading continuous reinforced concrete beams by gluing steel plates to their tension faces, Journal of Structural Engineering, ASCE, V.124, No.3, pp.224-232.

[O5] Orr, D.M.F., and Lynch, C., 1993, Design of externally bonded flexural and shear

reinforcement for strengthening reinforced concrete T-beams, Proceedings of 13th Australasian Conference on the Mechanics of Structures and Materials, University of Wollongong, pp.651-656.

[P1] Park, R., and Paulay, T., 1975, Reinforced Concrete Structures, John Wiley & Sons, New York, 769pp.

[P2] Park, R., 1989, Evaluation of Ductility of Structures and Structural Assemblages from Laboratory Testing, Bulletin of the New Zealand National Society for Earthquake Engineering, V.22, No.3, New Zealand, pp.155-166.

[P3] Priestley, M.J.N., Seible, F., and Fyfe, E., 1992, Column Seismic Retrofit Using Fibreglass/Epoxy Jackets, Proc., 1st International Conference on Advanced Composite Materials in Bridges and Structures, pp.287-298.

[P4] Paulay, T., and Priestley, M.J.N., 1992, Seismic Design of Reinforced Concrete and Masonry Building, John Wiley & Sons, New York, 744pp.

[P5] Plevris, N., Triantafillou, T.C., and Veneziano, D., 1995, Reliability of RC members strengthened with CFRP laminates, Journal of Structural Engineering, V.121, No.7, July, pp.1037-1044.

[P6] Priestley, M.J.N., Seible, F., and Calvi, G.M., 1996, Seismic Design and Retrofit of Bridges, John Wiley & Sons, New York, 686pp.

[P7] Priestley, M.J.N., 1995, Displacement based seismic assessment of existing reinforced concrete moment resisting frames, Proceedings of pacific Conference on Earthquake Engineering, V.2, Melbourne, Australia, pp.225-244.

[P8] Popovics, S., 1973, A numerical approach to the complete stress-strain curves for concrete, Cement and Concrete Research, V.3, No.5, pp.583-599.

[P9] Priestley, M.J.N., and Seible, F., 1991, Design of Seismic Retrofit Measures for Concrete Bridges, Report SSRP 91-03, University of California, San Diego.

[Q1] Quantrill, R.J., Hollaway, L.C., and Thorne, A.M., 1996, Experimental and analytical investigation of FRP strengthened beam response: Part Ⅰ, Magazine of Concrete Research, V.48, No.177, Dec., pp.331-342.

[Q2] Quantrill, R.J., Hollaway, L.C., and Thorne, A.M., 1996, Predictions of the maximum plate end stresses of FRP strengthened beams: Part Ⅱ, Magazine of Concrete Research, V.48, No.177, Dec., pp.343-351.

[R1] Restrepo-Posada, J.I., 1992, Seismic Behaviour of Connections Between Precast Concrete Elements, PhD thesis, Department of Civil Engineering, University of Canterbury, Christchurch, New Zealand, 385pp.

[R2] Restrepo, J.I., Park, R., and Buchanan, A.H., 1995, Design of connections of earthquake resisting precast reinforced concrete perimeter frames, PCI Journal, V.40, No.5, Sep.-Oct., pp.68-80.

[R3] Restrepo, J.I., and DeVino, B., 1996, Enhancement of the axial load carrying capacity of reinforced concrete columns by means of fiberglass-epoxy jackets, 2nd Conference on Advanced Composite Materials in Bridges and Structures, Montreal, Canada, pp.547-553.

[R4] Rochette, P., and Labossiere, P., 1996, A plasticity approach for concrete columns confined with composite materials, 2nd Conference on Advanced Composite Materials in Bridges and Structures, Montreal, Canada, pp.359-366.

[R5] Ritchie, P.A., Thomas, D.A., Lu, L., and Connelly, G.M., 1991, Eternal reinforcement of concrete beams using fiber reinforced plastics, ACI Structural Journal, V.88, No.4, July-Aug., pp.490-500.

[R6] Roberts, T.M., 1988, Plate separation and anchorage of reinforced concrete beams strengthened by epoxy-bonded steel plate, The Structural Engineer, V.67, No.12, June, pp.187-188.

[R7] Roberts, T.M., 1989, Approximate analysis of shear and normal stress concentrations in the adhesive layer of plated RC beams, The Structural Engineer, V.67, No.12/20, June, pp.229-233.

[R8] Ranisch, E.H., and Rostasy, F.S., 1986, Bonded steel plates for the reduction of fatigue stresses of couple tendons in multispan bridges, Proc. International Symp. on Adhesive Between Polymers and Concrete, RILEM, ed. H.R. Sasse, Chapman & Hall, London, pp.561-570.

[R9] Richart, F.E., Brandtzaeg, A., and Brown, R.L., 1928, A study of the failure of concrete under combined compressive stresses. Bulletin No.185, Engineering Experimental Station, University of Illinois, 104 pp.

[R10] Richart, F.E. and Staehle, G.C., 1931, Column tests at the University of Illinois, ACI Journal, V.27, pp.731-761.

[R12] Restrepo-Posada, J.I., Dodd, L.L., Park, R., and Cooke, N., 1994, Variables affecting cyclic behavior of reinforcing steel, Journal of Structural Engineering, ASCE, V.120, No.11, pp.3178-3195.

[S1] Schickert, G., and Winkler, H., 1979, Result of tests concerning strength and strain of concrete subjected to multiaxial compressive stresses, Deutscher Ausschuss fur Stahlbeton, Heft 277, Berlin, west Germany, 1977.

[S2] Saadatmanesh, H., and Ehsani, M.R., 1990, Fibre composite plates can strengthen beams, Concrete International, ACI, Mar., pp.65-71.

[S3] Saadatmanesh, H., and Ehsani, M.R., 1996, Experimental study of concrete girders retrofitted with epoxy-bonded composites laminates, ACI SP-165, ed. by R.N. Swamy and R. Gaul, pp.205-234.

[S4] Silfwerbrand, J., 1997, Improving concrete bond in repaired bridge decks, printed in Bridged Repair and Rehabilitation, ACI Compilation 29, pp.7-12.

[S5] Swamy, R.N., Jones, R, and Charif, A., 1986, Shear adhesion properties of epoxy resin adhesives, printed in Adhesion between Polymer and Concrete, RILEM ISAP86, pp.741-755, 1986.

[S6] Swamy, R.N., Jones, R, and Bloxham, J.W., 1987, Structural behaviour of

reinforced concrete beams strengthened by epoxy-bonded steel plates, The Structural Engineer, V.65A, No.2, pp.59-68.

[S7] Swamy, R.N., Jones, R, and Charif, A., 1988, Plate separation and anchorage of reinforced concrete beams strengthened by epoxy-bonded steel plates, The Structural Engineer, V.66, No.5, pp.85-94.

[S8] Swamy, R.N., Jones, R, and Charif, A., 1989, The effect of external plate reinforcement on the strengthening of structurally damaged RC beams, The Structural Engineer, V.67, No.3, pp.45-56.

[S9] Sharif, A., Al-Sulaimani, G.J., Basunbul, I.A., Balucn, M.H., and Husain, M., 1995, Strengthening of shear-damaged RC beams by external bonding of steel plates, Magazine of Concrete Research, V.47, No.173, pp.329-334.

[S10] Sharif, A., Al-Sulaimani, G.J., Basunbul, I.A., Balucn, M.H., and Chaleb, B.N., 1994, Strengthening of initially loaded reinforced concrete beams using FRP plates, ACI Structural Journal, V.91, No.2, Mar.-Apr., pp.160-168.

[S11] Saadatmanesh, H., and Ehsani, M.R., 1991, RC beams strengthened with GFRP plates I : Experimental Study, Journal of Structural Engineering, ASCE, V.117, No.11, pp.3417-3433.

[S12] Sheikh, S.A., and Uzumeri, S.M., 1980, Strength and ductility of tied concrete columns, Journal of Structural Division, ASCE, ST5, pp.1079-1102.

[S13] Sheikh, S.A., and Uzumeri, S.M., 1982, Analytical model for concrete confinement in tied columns, Journal of Structural Division, ASCE, ST12, pp.2703-2721.

[S14] Saadatmanesh, H., Ehsani, M.R., and Li, M.W., 1994, Strength and ductility of concrete columns externally reinforced with fiber composite straps, ACI Structural Journal, V.91, No.4, pp.434-447.

[S15] SEQAD Consulting Engineers, 1996, Axial Load Characteristics of Rectangular Columns Wrapped with TYFO-S Jackets, Report Prepared for HEXCELL FYFE INC., Report No.96/04.

[S16] SEQAD Consulting Engineers, 1993, Seismic Retrofit of Bridge Columns Using High Strength Fiberglass/Epoxy Jackets, Report, Solana Beach, California.

[S17] Samaan, M., Mirmiran, A., and Shahawy, M., 1998, Model of concrete confined by fiber composites, Journal of Structural Engineering, ASCE, V.124, No.10, pp.1025-1031.

[S18] Shaikh, A.F., 1978, Proposed revisions to shear friction provisions, PCI Journal, V.23, No.2, Mar.-Apr., pp.12-21.

[T1] Triantafillou, T.C., and Gibson, L.J., 1989, Debonding in foam-core sandwich panels, Materials and Structures, V.22, pp.64-69.

[T2] Triantafillou, T.C., and Deskovic, N., 1991, Innovative prestressing with FRP sheets: mechanics of short-term behavior, Journal of Engineering Mechanics, ASCE, V.117, No.7, pp.1652-1672.

[T3] Triantafillou, T.C., and Plevris, N., 1991, Post-strengthening of R/C beams with epoxy-bonded fiber composite materials, Proceedings of the Speciality Conference on Advanced Composites materials in Civil Engineering Structures, ASCE, pp.245-256.

[T4] Triantafillou, T.C., Deskovic, N., and Deuring, M., 1992, Strengthening of concrete structures with prestressed fiber reinforced plastic sheets, ACI Structural Journal, V.89, No.3, May-June, pp.235-244.

[T5] Triantafillou, T.C., and Plevris, N., 1992, Strengthening of RC beams with epoxy-bonded fibre-composite materials, Materials and Structures, V.25, pp.201-211.

[V1] VanGemert, D., 1980, Force transfer in epoxy bonded steel/concrete joints, International Journal of Adhesion and Adhesives, V.1, pp.67-72.

[V2] VanGemert, D., and VandenBosch, M., 1985, Repair and strengthening of reinforced concrete structures by means of epoxy bonded steel plates, International Conference on Deterioration, Bahrain, pp.181-192.

[W1] Willam, K.J., and Warnke, E.P., 1975, Constitutive model for the triaxial behaviour of concrete, International Association for Bridge and Structural Engineering, Proceedings, V.19.

[W2] Walraven, J., Frenay, J., and Pruijssers, A., 1987, Influence of concrete strength and load history on the shear friction capacity of concrete members, PCI Journal, V.32, No.1, Jan.-Feb., pp.66-84.